Permafrost changes along the Alaska Highway Corridor, Southern Yukon, from ground temperature measurements and DC Electrical Resistivity Tomography

Maxime Arsène Duguay

uOttawa

Thesis submitted to the
Faculty of Graduate and Postdoctoral Studies
In partial fulfillment of the requirements
For the Master of Science degree in Geography

Supervisor: Dr. Antoni Lewkowicz
Department of Geography, University of Ottawa

Co-Supervisor Dr. Sharon Smith
Geological Survey of Canada, Natural Resources Canada

Department of Geography
Faculty of Arts
University of Ottawa

Abstract

Permafrost temperatures were measured by the Geological Survey of Canada (GSC) in 1977-1981 at boreholes along a proposed pipeline route in the southern Yukon. Analysis of climate station records indicate that mean annual air temperatures in the region have since increased by 0.5-1.0˚C. Renewed interest in the pipeline and the need to develop adaptation strategies for existing highway infrastructure have meant that information on permafrost and geotechnical conditions must be updated.

To accomplish this goal, a total of eight GSC boreholes ranging in depth from 5-9 m were located, unblocked of ice and instrumented with thermistor cables and data-loggers to permit renewed ground temperature monitoring. Manual temperature measurements were also taken at four other shallow boreholes. Electrical resistivity tomography (ERT) surveys were conducted at each site.

MAGTs below 1 m at permafrost sites in the study area range from -0.2˚C to -1.5˚C with permafrost depths greater than 25 m. The permafrost at the study sites can be classified as sporadic discontinuous and extensive discontinuous. Ground temperatures indicate that permafrost can persist under warmer climatic conditions as long as it remains protected by its ecosystem properties.

Thermal monitoring for 2011-2012 shows an average increase of 0.5-1.0˚C when compared to the original 1978-1981 ground temperatures. This slow rate of ground warming is mainly attributed to a combination of limited climate change, especially in the south of the study area, ground temperatures close to 0˚C, and the possible disturbance of sites from the removal of vegetation prior to the original measurements being made. ERT surveys conducted at most borehole sites show deeper thaw or taliks where the cleared cut-line used for geophysical work in the 1970s is crossed.

These results indicate the impacts of climate change and environmental change in the study area over the past three decades. They appear to match the relatively slow rates of ground warming observed elsewhere in northern Canada where permafrost temperatures are close to 0˚C and where warming also requires changes in latent heat due to internal thaw. TTOP equilibrium modelling suggests that if climate change is responsible for the ground warming, most of the change can be attributed to the step-like MAAT increase that occurred between 1975-1976.

Acknowledgements

It is with immense gratitude that I acknowledge and thank my two supervisors, Dr. Antoni G. Lewkowicz and Dr. Sharon L. Smith for their passion, guidance and support which has been indispensable to my growth as a scientist and as a person over these past two years. It has been a pleasure and an honour to work with two of the most renowned permafrost researchers in the world. I would like to express my deepest appreciation for the valuable time and energy they have spent helping me to improve myself and my work, and for inspiring me with their knowledge and enthusiasm on permafrost sciences.

Toni was the first to open the door for me in northern research back in 2009, granting me a CRYO-EX scholarship to study the Nordic periglacial environment for six months at the University of Oslo in Norway. From that moment on, I was hooked for life. I am also privileged to have conducted field research in some of the most isolated and beautiful places in the world such as Norway, Svalbard, Iceland, British Columbia, Alaska and the Yukon which would have been only a dream without Toni. I will be forever thankful for all the opportunities you have given me and I hope to be able to work with you again in the future regardless of the career path I choose.

This research would not have been possible without the financial support provided by the University of Ottawa, the Geological Survey of Canada, the Natural Sciences and Engineering Research Council of Canada and the Program for Energy Research and Development of Natural Resources Canada. It gives me great pleasure to acknowledge the friendly staff at the Arctic Institution of North America for their hospitality and for making our stay on the shores of Kluane Lake the most memorable. I would also like to express my appreciation to the Yukon Geological Survey and Yukon College for letting us store our equipment at their facilities.

I must acknowledge my field assistants, Christina Miceli, Zoe Kuntz, Alex Bevington "Big Al", Ellorie McKnight, and Mark Ednie. I was fortunate to have helpful and competent individuals whose company I enjoyed very much during the over 100 days I spent in the Yukon wilderness. Together we have shared so much and lived unforgettable adventures which we will cherish for the rest of our lives. Even getting charged at by a grizzly bear with Mark seems like a cool story to tell. I am indebted to Lance Goodwin "The Man of the Yukon" for always being

there for me and for inspiring me to create my pressure cooker steaming rig which was at the core of the borehole rehabilitation process used in this thesis.

I would like to thank my amazing family and friends for always being supportive of my goals and dreams. Without their love and support, I would not be where I am today, and for that I must say thank you from the bottom of my heart. Finally, I would like acknowledge all the wonderful and friendly people I have met along my way during my adventures in the great white north. Thanks for being a part of my journey!

TABLE OF CONTENTS

List of Figures

List of Tables

Definitions and Symbols

A – Amplitude
$\mathbf{A_{ZAA}}$ – Amplitude at zero annual amplitude, or 0.1˚C
$\mathbf{A_{(z)}}$ – Amplitude at *z* depth
BH – Borehole
DC Resistivity – Direct-current resistivity
$\mathbf{D_{ZAA}}$ – Depth of zero-annual amplitude
ECCS – Environment Canada Climate Station
ERT – Electrical resistivity tomography
FDD – Freezing degree-days (˚C day)
$\mathbf{FDD_a}$ – Freezing degree-days of the air (˚C day)
$\mathbf{FDD_s}$ – Freezing degree-days of the ground surface (˚C day)
GT – Ground temperature
$\boldsymbol{K}$ – Apparent thermal diffusivity
MAAT – Mean annual air temperature
MAGST – Mean annual ground surface temperature
MAGT – Mean annual ground temperature
MMGT – Mean monthly ground temperature
$\mathbf{max}\boldsymbol{T}$ – Maximum annual temperature at *Z* depth
$\mathbf{min}\boldsymbol{T}$ – minimum annual temperature at *Z* depth
$\mathbf{n_f}$ – Freezing n-factor
$\mathbf{n_t}$ – Thawing n-factor
P – Period
SDD – Snow-depth days (cm day)
SAA – Specific Surface Area
TDD – Thawing degree-days (˚C day)
$\mathbf{TDD_a}$ – Thawing degree-days of the air (˚C day)
$\mathbf{TDD_s}$ – Thawing degree-days of the ground surface (˚C day)
TOP – Depth to the top of permafrost (m)
TTOP – Temperature at the top of permafrost
Z – Depth
ZAA – Zero-annual amplitude
$\mathbf{Z_{ZAA}}$ – Depth of zero-annual amplitude (m)

SECTION 1: INTRODUCTION AND OBJECTIVES

1.0 INTRODUCTION AND OBJECTIVES

1.1 Introduction

Permafrost distribution and characteristics are broadly controlled by the climate system (Smith and Riseborough, 1996; Lewkowicz et al., 2012; Throop et al., 2012). The climate warming expected over the next century, due to the enhanced greenhouse effect, has significant implications for the permafrost environment, with land poleward of 60^{o} N experiencing greater warming due to feedback processes (Smith and Riseborough., 1996; Arctic Climate Impact Assessment [ACIA], 2005; Arctic Monitoring and Assessment Programme [AMAP], 2012). Permafrost is predicted to warm and diminish in extent with rising air temperatures (ACIA, 2005; Intergovernmental Panel on Climate Change [IPCC], 2007; AMAP, 2012). Hydrological processes at the base of aquatic and terrestrial ecosystems will be affected, and possibly change due to warming and thawing of permafrost, impacting the traditional lifestyles of northerners (ACIA, 2005; AMAP, 2012). Degrading permafrost can have significant impacts on ecosystems and also have implications for structural integrity of northern infrastructure (ACIA, 2005; AMAP, 2012).

Changes in permafrost have been underway for some time, as revealed by a northward migration of the southern boundary of permafrost (James, 2010), warming ground temperatures throughout most of the permafrost regions (Lachenbruch and Marshall, 1986; Osterkamp and Romanovsky, 1999; Oskerkamp, 2005; Smith at al., 2005; Isaksen et al., 2007; Romanovsky et al., 2010; Smith at al., 2010; Christiansen et al., 2012; Lewkowicz et al., 2012; Throop et al., 2012), increases in active layer thickness, and permafrost degradation (Jorgensen et al., 2001; Jorgenson et al., 2006; Pullman et al., 2007; Fortier et al., 2011). Permafrost degradation in the Yukon has already caused serious negative effects on the structural integrity of vertical infrastructure (Laxton and Coates, 2011) and transportation routes such as highways, roads and airstrips (Lepage and Doré, 2010).

Understanding the distribution and dynamics of permafrost is essential for infrastructure design in permafrost environments, including major linear infrastructure such as pipelines and highways. A great deal of information was collected to describe subsurface conditions including thermal conditions in the 1970s in support of a proposed gas pipeline project along the Alaska

Highway Corridor (Figure 1.1). For example, ground temperatures were measured in a suite of boreholes by the Geological Survey of Canada between 1978 and 1981 (Burgess et al., 1982). However, little recent information exists for the corridor. Renewed interest in the pipeline proposal and the need to develop adaptation strategies for existing highway infrastructure has stimulated a need for updated information on baseline permafrost conditions and how these are changing.

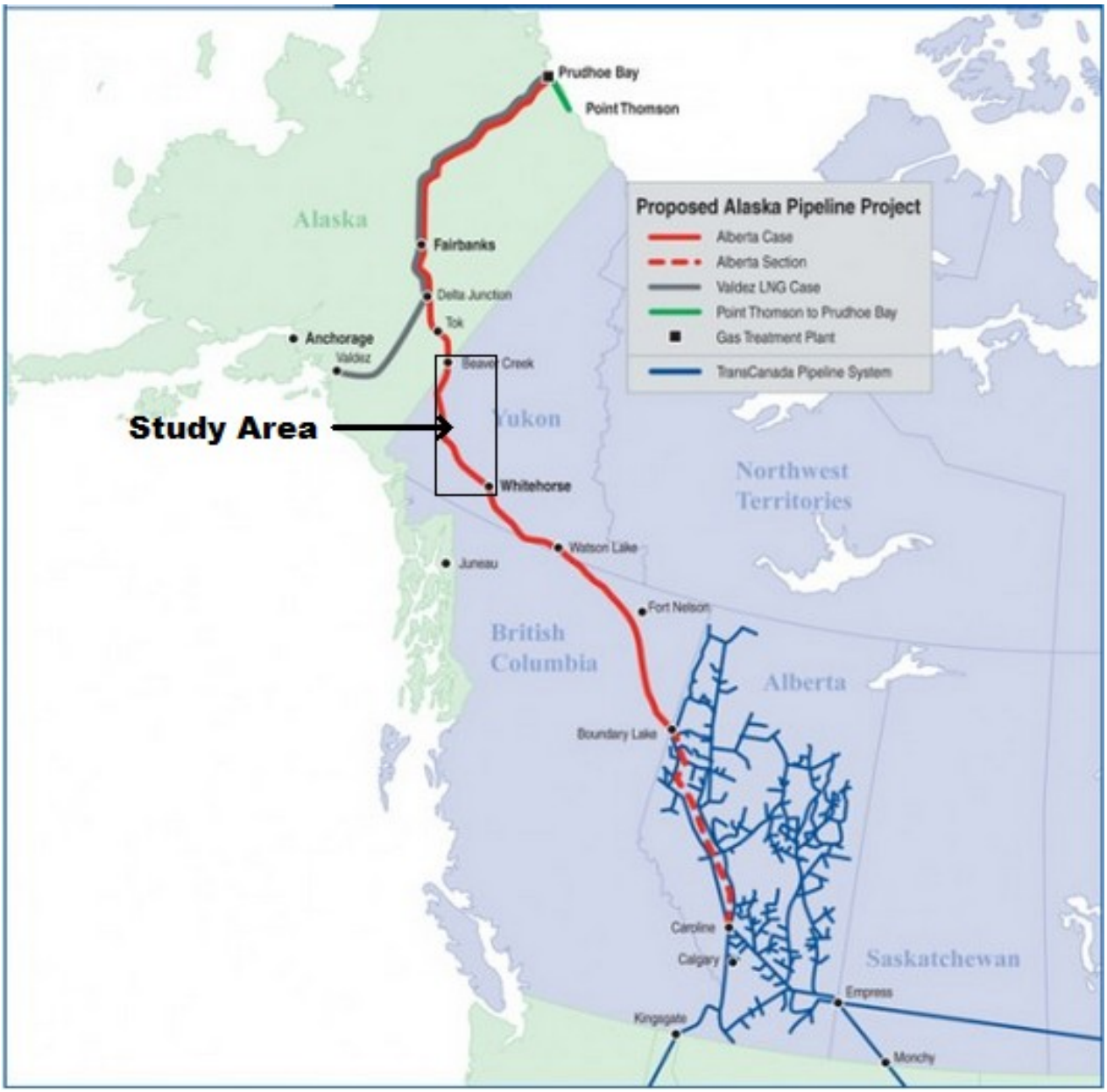

Figure 1.1: Proposed Alaska Pipeline Project route showing the study area along the Alaska Highway Corridor, Southern Yukon (Pipelines International, 2010).

1.2 Research Objectives

The central objective of this research is to use renewed ground temperature monitoring and DC Electrical Resistivity Tomography (ERT) profiling to evaluate the impacts of multi-decadal climate change and environmental change on permafrost conditions at borehole sites along an approximately 457 km length of the Alaska Highway Corridor from Whitehorse to Beaver Creek, YT (Figure 1.2). This research forms part of a longer term project with goals of increasing our understanding of the distribution and dynamics of permafrost in the Yukon. The steps necessary to achieve the research objective were:

- Analyze climate records from Environment Canada climate stations in communities along the 457 km transect in an effort to link change in permafrost conditions to recent climate change.
- Re-locate, unblock of ice and install temperature sensors for renewed thermal monitoring in boreholes drilled in the 1970s during geotechnical investigations for the proposed Alaska Highway Gas Pipeline and where the GSC had previously collected ground temperature data to evaluate multi-decadal differences.
- Perform ERT surveys at each borehole site and over the regrown cut-line used for previous geophysical work in the 1970s to further examine permafrost subsurface conditions and to investigate the effects of environmental change in the corridor.

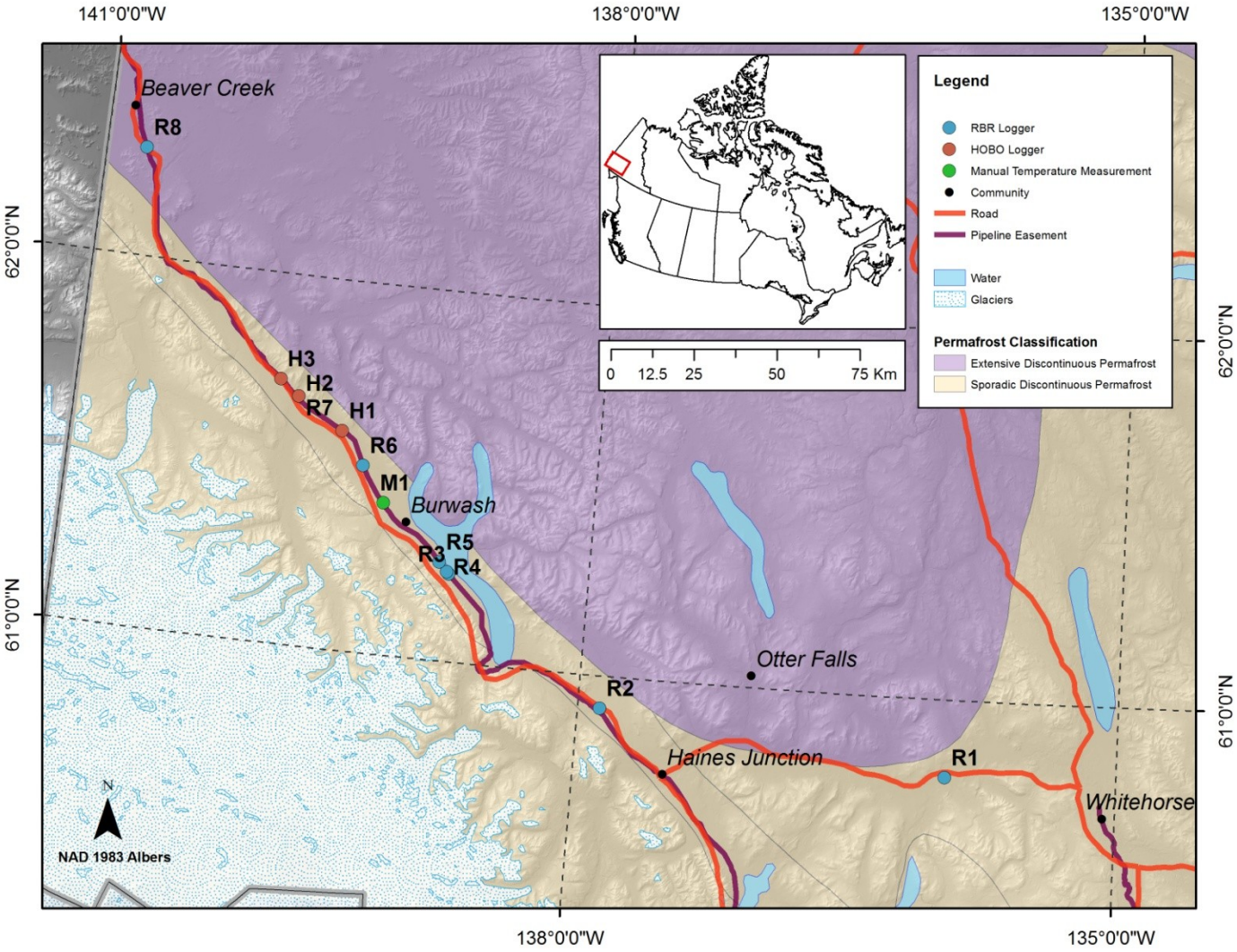

Figure 1.2: Map of the study area showing the borehole monitoring sites. Permafrost zones are from Heginbottom et al., (1995).

1.3 Structure of the Thesis

The thesis is divided into the following seven sections:

Section One	-	Introduction and Objectives	Provides a general overview.
Section Two	-	Background	Outlines the background literature on permafrost dynamics and ERT monitoring.
Section Three	-	Study Area	Describes the study area and the specific climate and environmental characteristics.
Section Four	-	Methodology	Describes the methodology and analytical methods used to conduct the research project.
Section Five	-	Results	Presents site descriptions and comprehensive results of the research for each site.
Section Six	-	Discussion	Discusses and analyzes the data collected.
Section Seven	-	Conclusion	Presents the conclusion of the research.

SECTION 2: BACKGROUND

2.0 BACKGROUND

2.1 A Changing Climate

The international scientific community has agreed that Earth's climate is changing at a rapid pace and that global temperatures are becoming warmer in most locations around the world (IPCC, 2007). These changes in global climate include changes in temperature, precipitation, and oceanic and atmospheric circulation which have been partially attributed to the increased atmospheric concentrations of anthropogenic greenhouse gases caused by human activity (ACIA, 2005; Anisimov and Nelson, 1997; IPCC, 2007). Since the start of the industrial revolution (1750), atmospheric greenhouse gases have increased at an unparalleled rate: CO_2 by 31 %, CH_4 by 150 %, NO_2 by 16% and CFCs by 100 % (IPCC, 2007). An increase of 0.74˚C ± 0.18˚C in global mean surface temperatures occurred from 1906-2005 and the rate of warming over the last 50 years was almost double that of the last 100 years (IPCC, 2007). A global surface temperature increase of 1.1^{o}C to 6.4^{o}C has been projected for the 21st century, with land north of 60^{o} latitude experiencing warming of approximately twice the global mean, mostly due to pronounced changes in feedback process from melting arctic sea ice (ACIA, 2005; IPCC, 2007). This warming is expected to occur predominately during winter, and mean annual surface temperatures are projected to increase by 4^{o}C to 7^{o}C over the next 100 years in Arctic regions according to the A2 climate scenario, with a major impact on all elements of the cryosphere (ACIA, 2005; IPCC, 2007; AMAP, 2012) (Figure 2.1).

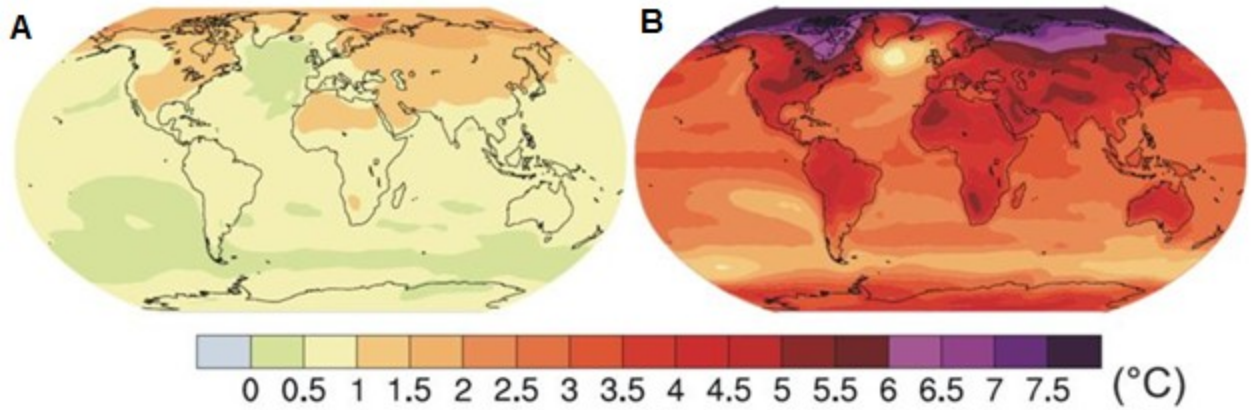

Figure 2.1: Projected surface temperature changes for the early 21st century (A: 2020-2029) and the late 21st century (B: 2090-2099). The map shows the multi-AOGCM average projection for the A2 scenario. Temperature changes are relative to the period 1980-1999 (source: IPCC, 2007).

2.2 Permafrost Classification

Permafrost is defined as ground (soil, rock and organic material) that remains at or below $0^{o}C$ for two or more consecutive years (although most permafrost has existed for centuries to thousands of years) (Muller; 1943; Brown and Péwé, 1973; Van Everdingen, 1976; Kudryavtsev, 1978; IPCC, 2007). The active layer is the upper layer of the ground that seasonally experiences positive temperatures (Burn, 1988) and seasonal freeze-thaw cycles (Van Everdingen, 1976; IPCC, 2007; French, 2007). Permafrost ranges in thickness from a few metres to hundreds of metres and in temperature from close to $0^{o}C$ to much lower than $-10^{o}C$ and is generally found in areas where the mean annual air temperature (MAAT) is below $0^{o}C$ (Romanovsky et al., 2010). Permafrost occurs not only at high latitudes but also at high elevations, underlying approximately 23-25 % of the world's land surface, with about 15 % of all permafrost occurring within Canada (Baranov, 1959). More than 50 % of the Canadian landmass falls into a permafrost zone (Heginbottom et al., 1995; NRCan, 2007).

Many different classification schemes have been proposed for permafrost distribution based on proportion of land underlain by permafrost (IPCC, 2007). A typical classification recognizes continuous permafrost as underlying 90-100 % of the landscape with only rivers and water bodies not underlain (Heginbottom et al., 1995; ACIA, 2005; French, 2007; UNEP, 2007). The majority of this permafrost was formed during or before the last glaciation (UNEP, 2007). The International Permafrost Association (IPA, 2011) classifies discontinuous permafrost as underlying 50-90 % of the landscape and sporadic permafrost as underlying 0-50 %. Discontinuous permafrost is normally found to be much younger than continuous permafrost, as it generally formed after the last glacial period (UNEP, 2007). Heginbottom et al., (1995) sub-classify the discontinuous permafrost zone into extensive discontinuous permafrost (50-90 %) and sporadic discontinuous permafrost (10-50 %). However, the sporadic discontinuous zone is classified as 10-30 % by the ACIA (2005). Areas with permafrost occupying 0-10 % of the landscape are classified as isolated patches (Heginbottom et al., 1995; ACIA, 2005; UNEP, 2007). Zoltai (1971) and French and Egorov (1998) have used the term "localised" in areas where permafrost is only present in small islands of peaty or silty soil. However, the identification and localisation of these isolated patches is difficult without specific field testing (French and Egorov, 1998).

Permafrost is often viewed as a product of climate (Kudryavtsev, 1954). Climate in an area can be favourable, neutral, or unfavourable to permafrost (Shur and Jorgenson, 2007). However, in most situations, the impact of climate change on permafrost is indirect because permafrost is a component of a complex geo-ecological system and its existence also depends on other environmental factors including vegetation and soil properties (Shur and Jorgenson, 2007). Climate can also vary temporally so that an area that was once favorable can now be neutral or unfavourable resulting in permafrost disappearing, or remaining in the landscape due to other environmental factors (Shur and Jorgenson, 2007).

Shur and Jorgenson (2007) proposed a classification system that identifies different types of interactions between climate and ecosystems that affect formation of permafrost and its long-term stability. They classify permafrost into five categories: (1) *climate-driven*; (2) *climate-driven, ecosystem-modified*; (3) *climate-driven, ecosystem protected*; (4) *ecosystem-driven*; and (5) *ecosystem protected* (Figure 2.2). *Climate-driven* permafrost forms independently of vegetation in cold and very cold areas. Factors other than climate are not involved in permafrost formation at its initial stage. *Climate-driven, ecosystem-modified* permafrost is initially formed under a favourable cold climate and becomes less reliant on climate as ecological succession modifies the upper part of the permafrost and its sensitivity to degradation. *Climate-driven, ecosystem-protected* permafrost was formed under a favourable past cold climate and can survive under warmer climatic conditions as long as it remains protected by its ecosystem properties. These areas are normally covered by mosses and peat, and are generally permafrost neutral. *Ecosystem-driven* permafrost forms in areas where climate alone is insufficient to cause permafrost formation. Complex interactions of biophysical factors taking place under significant ecosystem influence, such as north-facing slopes and peat lands, play an important role in permafrost formation and persistence. Disturbance from human activity or forest fire would permanently thaw these areas. Lastly, *Ecosystem-protected* permafrost has similar characteristics to *Ecosystem-driven* permafrost, but occurs under climates where MAATs are approximately 2^{o}C to -2^{o}C. It can persist in undisturbed late-successional ecosystems, but cannot re-develop after disturbance.

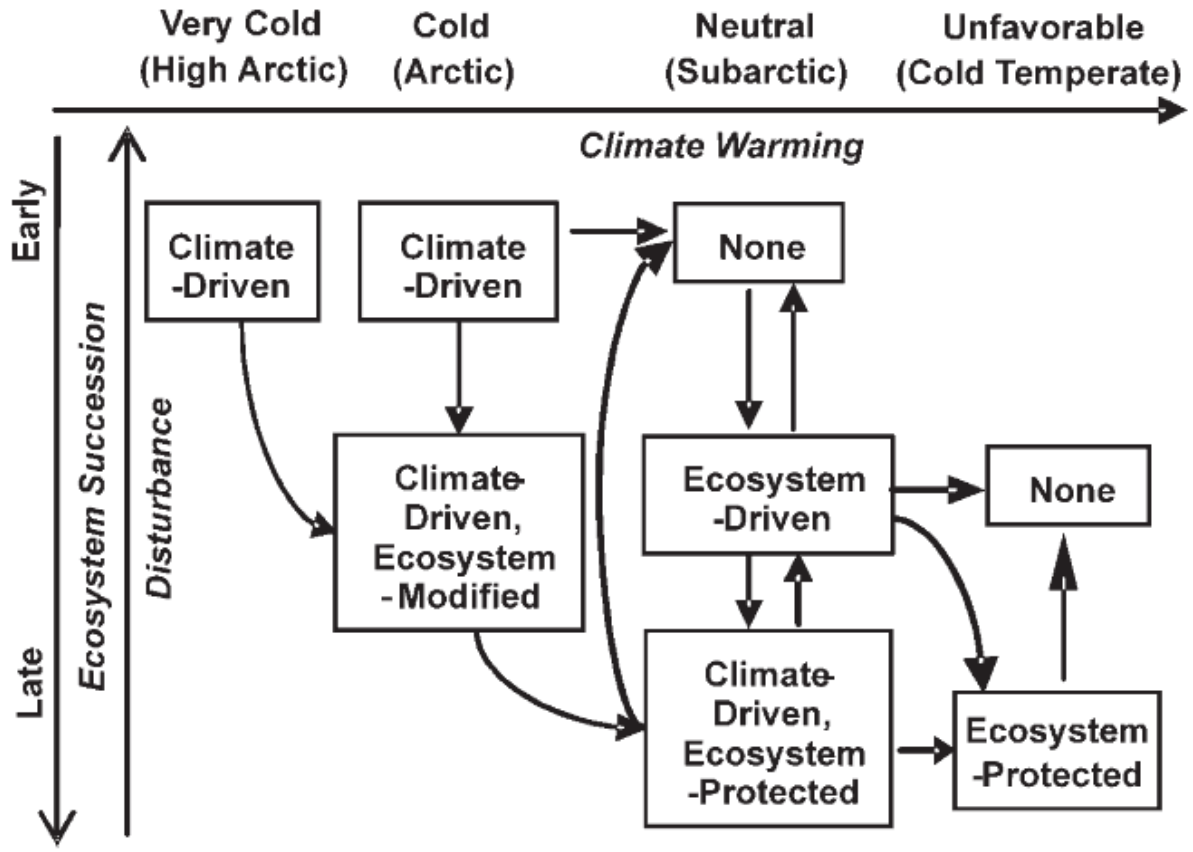

Figure 2.2: Permafrost conditions in relation to climate, ecological succession and disturbance (*from* Shur and Jorgenson, 2007).

2.3 Thermal Dynamics of Permafrost

The IPCC (2007) has advocated that research should be directed towards understanding the physical relationship between permafrost temperatures and air temperatures as climate exerts the strongest control on permafrost existence at the macro-scale. Recent studies by Lewkowicz et al. (2012) and Throop et al. (2012) confirm this strong climate-permafrost relationship at the macro-scale. However, numerous papers have shown that the relationship between permafrost and climate is not altogether simple (e.g. Smith and Riseborough, 2002).

The key parameters used to describe the permafrost-climate relationships are the mean annual air temperature (MAAT), the mean annual ground surface temperature (MAGST), the mean annual ground temperature at any depth below the surface (MAGT) and the mean temperature at the top of permafrost (TTOP) (Smith and Riseborough., 1996, 2002). Under equilibrium conditions, the presence and thickness of permafrost is dictated by the temperatures at each of these four levels and by the differences between the levels (Figure 2.3). As a general rule, the temperature at each of these levels will differ on a mean annual basis, according to the influences of surface cover and ground thermal properties (Smith and Riseborough, 2002).

The MAAT measured at a given permafrost monitoring site represents the point of linkage between regional climate and the local micro-climate (Smith and Riseborough, 1996). In contrast, the MAGST, MAGT and the TTOP incorporate local environmental factors, area characteristics and lithological conditions (Smith and Riseborough, 1996, 2002). The MAGST is representative of the interference between the atmosphere and the surface of the snowpack in winter or the vegetated layer in the summer (Smith and Riseborough, 1996). Heat transfer processes occurring at this interface and within the buffer layer are complex, involving radiative influxes, turbulence, conduction, evaporation, and transpiration of living vegetation (Smith and Riseborough, 1996). The MAGST is in most cases warmer than the MAAT since the insulation due to winter snowcover is generally greater than the shading due to vegetation in the summer (Smith and Riseborough, 1996).

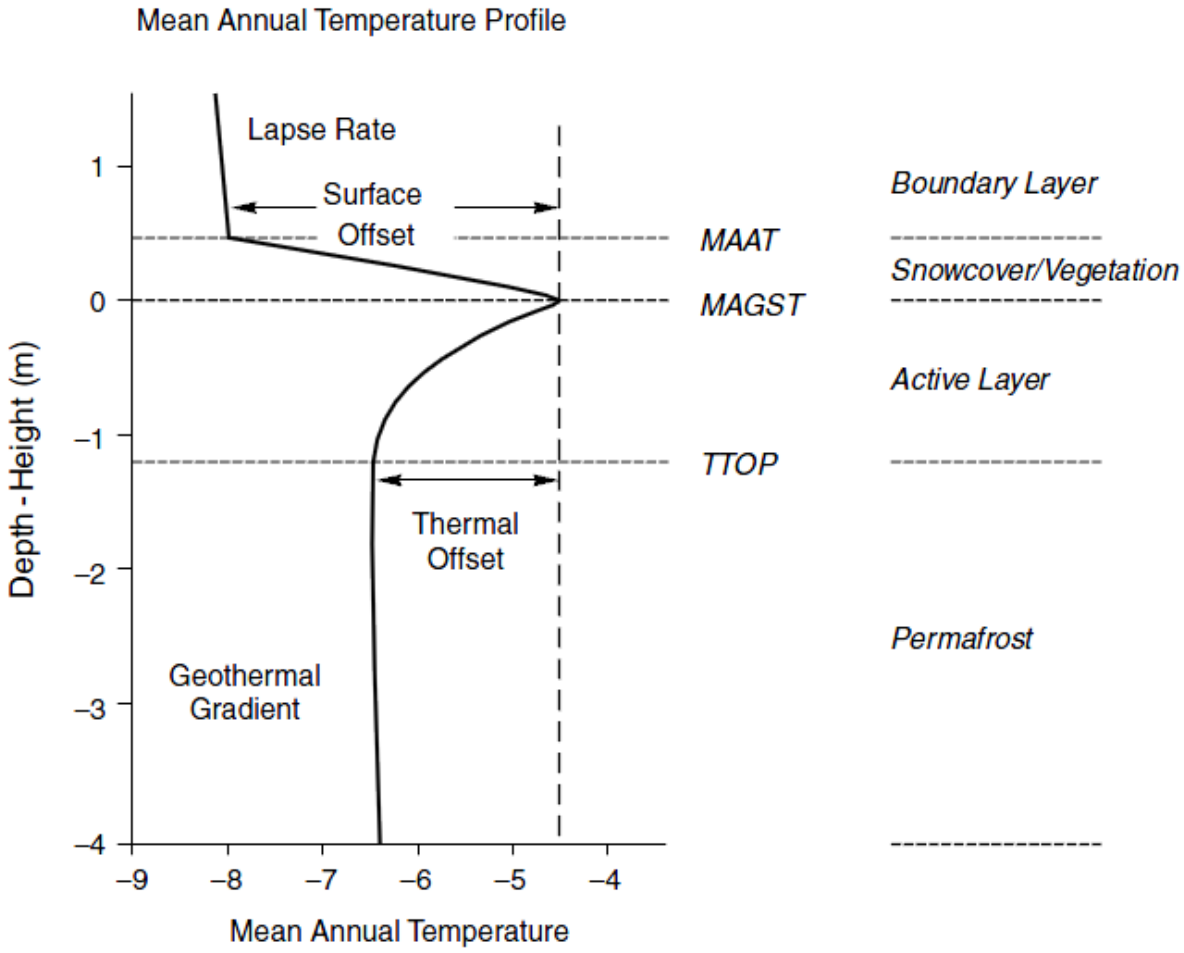

Figure 2.3: Schematic mean annual temperature profile through the surface boundary layer, showing the relation between air temperature and permafrost temperature. Note that the MAGT can be calculated at any depth below the ground surface. (*from* Smith and Riseborough, 2002).

The TTOP is measured at the top of permafrost, independent of active layer thickness (Smith and Riseborough, 2002). Mean TTOP values remain fairly constant intra-annually since the ground below the active layer does not undergo significant phase change (Smith and Riseborough, 1999). This characteristic keeps the soil thermal properties constant, therefore keeping the temperature fairly consistent over time. An increase in active layer thickness due to climate warming is not an indicator of TTOP change and does not necessarily mean an increase in permafrost temperatures (Smith and Riseborough, 1996).

The MAGT which is measured at the depth of zero annual amplitude (D_{ZAA}) is another common parameter used to describe permafrost characteristics (Smith and Riseborough, 2002). The D_{ZAA} is discussed in Section 2.6.4.

2.4 Interactions between the Air and Ground Surface

2.4.1 Surface Offset

Local microclimatic factors commonly override the influence of larger scale macroclimatic factors on ground thermal conditions, leading to a measureable surface offset (Smith and Riseborough, 2002). The surface offset is defined as:

$$\text{Surface Offset} = \text{MAGST} - \text{MAAT} \quad (1)$$

The size of the surface offset is dependent on ground surface conditions which act as a buffer between the atmosphere and the ground surface (Smith and Riseborough, 2002). The three main factors that control the surface offset are: (1) the snow cover that insulates the ground and restricts the loss of heat during winter; (2) the vegetation cover that shades the ground surface from direct insolation during the summer (Williams and Smith, 1989; Smith and Riseborough, 2002); and (3) the presence or absence of permafrost (Karunaratne and Burn, 2004).

Snow cover is a very effective insulator by comparison with most natural ground surface materials due to its low thermal conductivity, and therefore has a strong influence on the thermal regime of the ground (Goodrich, 1982; Williams and Smith, 1989; Smith and Riseborough, 2002). In general, a thicker snowpack restricts heat loss from the ground to a greater extent during the coldest part of the year, thus limiting the magnitude of ground cooling (Goodrich, 1978; Smith and Riseborough, 2002). Greater ground cooling due to greater heat lost is typically observed where the snow cover is thin or absent (Ishikawa, 2002).

The net effect of snow cover over a year is to raise mean annual ground temperatures, often by several degrees (Goodrich, 1982). As a result, local and regional spatial variability in snow cover due to topography, vegetation and drift patterns is the largest single factor accounting for variations in the ground surface temperature during the winter months (Desrochers and Granberg, 1988; Smith and Riseborough, 2002). In addition, inter-annual

variability of the snowpack leads to an augmented inter-annual variability in the temperature of the ground, beyond that due simply to variation in air temperatures (Smith and Riseborough, 2002).

The ground thermal regime is significantly influenced by the timing of the first accumulation of snow on the surface, the duration of the snow cover, and the maximum thickness reached during the winter (Goodrich, 1982). Early snowfall or early snow melt can increase ground temperatures, while late snowfall or late snowmelt has the opposite effect, so the timing of the arrival and departure of snow can be significant (Ling and Zhang 2003: Morse and Burn, 2010). Snow begins to melt once air temperatures rise above 0˚C in the spring but the near-surface temperatures only begin to rise once snow has melted (Woo et al., 2007). The lag time between air temperatures rising above 0°C and ground surface temperatures rising above 0°C can be used to represent the duration of the snowmelt (Woo et al., 2007). The annual depth and duration of snow cover can be measured with a single value using snow depth-days (SDD), which is a cumulative total of daily average snow depths over the winter (Karunaratne and Burn, 2003).

Vegetation cover is an effective buffer in the summer, reducing the amount of solar radiation reaching the ground surface, consequently causing ground temperatures to be cooler than the air (Smith and Riseborough, 2002). The interception of precipitation and transpiration by the canopy influences the ground thermal regime through the water balance (Smith and Riseborough, 2002). The snow-holding capacity of vegetation critically influences ground temperatures and is controlled by vegetation structure (Kokelj et al., 2007; Morse and Burn, 2010). Snow cover is thin at upland tundra surfaces where the snow-holding capacity of low shrubs is minimal. The wind redistributes snow to drifts that accumulate where there are taller shrubs, or to lee slopes, valley bottoms, and topographic concavities (Kokelj et al., 2007; Morse and Burn, 2010). Overall, vegetation leads to smaller amplitudes of ground temperature waves (Karunaratne and Burn, 2004).

2.4.2 Thawing and Freezing Degree Days

Degree days are useful indices for examining temperature ranges at a particular site through a seasonal perspective (Kwong and Gan, 1994). Thawing degree-days (TDD) are the sum of daily mean temperatures above 0˚C during the thawing season while freezing degree-days (FDD) are the sum of daily mean temperatures below 0˚C during the freezing season (Klene et al., 2001). TDD and FDD can be calculated for both the air (TDD_a; FDD_a) and ground surface (TTD_s; FDD_s) and are used to indicate temporal changes in air-to-ground surface temperature relations, as well as for seasonal analysis and comparisons among sites (Klene et al., 2001).

2.4.3 N-factors

Lunardini (1978) and Jorgensen and Kreig (1988) used *N*-factors as transfer functions between the air temperature and the ground surface temperature for both the thawing and the freezing seasons, to account for the local influence of vegetation and snow cover. N-factors are ratios of the seasonal ground surface temperature index to the seasonal air temperature index for both thawing and freezing seasons. The thawing n-factor (n_t) and freezing n-factor (n_f) are calculated using Eq. (2) and Eq. (3) respectively:

$$n_t = \frac{TDD_s}{TDD_a} \tag{2}$$

$$n_f = \frac{FDD_s}{FDD_a} \tag{3}$$

Klene et al. (2001) and Karunaratne and Burn (2003) define the start and the end of the freezing and thawing seasons using the ground surface temperature. Others however (e.g. Lewkowicz et al., 2012) have determined the start and end of the freezing and thawing seasons independently for the air and ground surface to better investigate the impact of snow cover. The closer the value of n_t or n_f is to 1.0, the more similar the air temperature index is to the ground surface index, and the lower the value, the greater the buffering between the air and the surface (Taylor, 1995).

The summer (thawing) n-factor incorporates all microclimatic effects (radiation, convection, evapotranspiration, shading, etc.) due to vegetation cover (Smith and Riseborough, 1996). High values of n_t suggest direct exposure to sun and an open area, resulting in higher ground surface temperatures than air temperatures while low values of n_t suggest significant shading from vegetation such as in a forest, resulting in lower ground surface temperatures than air temperatures (Taylor, 1995). Heat penetration is directly related to a soil's thermal diffusivity, so soil with high thermal diffusivity will have a higher n_t (French, 2007).

The freezing n-factor is dominated by the influence of snow cover as the low thermal conductivity of snow restricts the loss of heat from the ground during the coldest parts of the year (Smith and Riseborough, 1996). Vegetation plays an important role in trapping blowing snow in the winter, allowing a thicker snow cover to accumulate in some areas (Smith and Riseborough, 1996) Low values of n_f suggest a thick insulating snow cover, resulting in higher ground surface temperatures than air while higher values of n_f suggest a thin snow cover, resulting in more similar temperatures for the air and the ground surface (French, 2007). The n_f increases as the MAAT decreases for any snow depth (Smith and Riseborough, 1996).

2.4.4 TTOP Model

Smith and Riseborough (1996) have presented an explicit formulation of the climate-permafrost system that provides a functional framework for analyzing the influence of climate, terrain and lithological factors on the temperature condition and distribution of permafrost (TTOP model). The TTOP model links ground temperatures to the atmospheric temperature regime through the use of seasonal n-factors (Lunardini, 1981), which provide a highly simplified representation of the influence of the buffer layer in modulating heat exchange between the atmosphere and the ground surface (Wright et al., 2003). The model assumes a homogeneous substrate and that a state of thermal equilibrium exists (on a year to year basis) between the atmosphere and the ground thermal regime (Wright et al., 2003). The TTOP relation is shown in Eq. (4) with frozen and thawed conductivity values for various terrain units (Wright et al., 2003):

$$TTOP = \frac{\frac{Kt}{Kf}(nt \cdot DDT - nf \cdot DDF)}{P} \quad (4)$$

Where:

TTOP = Temperature at the top of permafrost
K_t = Thermal conductivity of unfrozen ground
K_f = Thermal conductivity of frozen ground
DDT = Air thawing index (degree days)
DDF = Air freezing index (degree days)
n_t = Thawing n-factor
n_f = Freezing n-factor
P = Annual period (365 days)

Surficial unit	Dry Density Kg/m^3	K_t W/m/°C	K_f W/m/°C
Colluvial	1400	1.15–1.54	1.61–2.69
Lacustrine	1475	1.21–1.62	1.82–2.74
Aeolian	1500	1.39–1.60	1.63–2.47
Glaciofluvial	1550	1.26–1.66	1.65–2.50
Alluvial	1600	1.30–1.72	1.59–2.53
Glacial till	1750	1.41–1.98	1.68–2.92
Organic	300	0.52	1.70

2.5 Ground Surface and Permafrost Interactions

2.5.1 Thermal Offset and Thermal Conductivity

It was shown by Goodrich (1978) that the mean annual ground temperature (MAGT) profile is not constant but is generally offset to progressively lower values at depth within the active layer, with the lowest MAGT occurring at the base of the active layer, or at the top of permafrost. This thermal offset is defined as (Smith and Riseborough, 2002):

$$\text{Thermal Offset} = TTOP - MAGST \quad (5)$$

The thermal offset arises because the thermal conductivity of a soil is substantially greater when frozen than when thawed resulting in seasonal variability in heat transfer by conduction between the ground surface and the top of permafrost (Smith and Riseborough, 1996; Taylor et al., 2000). The difference is due to the thermal conductivity of ice being four times that of water (Smith and Riseborough, 2002).

The thermal conductivity (λ) is the property of a material to conduct heat as described in Fourier's Law for heat conduction (Burn, 2012). Heat transfer through materials of high thermal conductivity occurs at a higher rate than across materials of low thermal conductivity (Burn 2012). Within permafrost, heat flow is dominated by conduction, since pore spaces are generally blocked by ice and the critical property is the thermal conductivity (λ, W/m/˚C) (Osterkamp and Burn, 2003; Burn, 2012). The thermal conductivity of water (0.65 W/m/˚C) increases to about (2.2 W/m/˚C) when frozen resulting in high λ in saturated frozen sand and peat when compared with thawed soil (Burn, 2012).

As a result of the thermal offset, permafrost can develop even where the MAGST is above 0˚C (Burn and Smith, 1988; Romanovsky and Osterkamp, 1995; Smith and Riseborough, 2002). Minor seasonal changes in thermal conductivity occur at sites with bedrock and dry earth materials where moisture content is limited, resulting in negligible to no thermal offset (Burn and Smith, 1988; Romanovsky and Osterkamp, 1995; Smith and Riseborough, 2002). Since the thermal offset can vary significantly between sites, the MAGST cannot alone be used to define the characteristics of permafrost (Burn and Smith, 1988).

The occurrence of permafrost in peatlands at the southern margins of the discontinuous permafrost zone has commonly been attributed to the difference in λ between frozen and unfrozen peat (Burn, 2012). In the summer, the low λ of dry peat reduces the flow of heat into the ground while the high λ of saturated frozen peat assists cooling in the winter (Burn, 2012) Noticeable difference in λ between the thawed and frozen states of the active layer of mineral soil also play a significant role in the thermal state of permafrost (Burn, 2012).

2.5.2 Unfrozen Water in Frozen Soils

Seasonally frozen ground and permafrost contain unfrozen water (Figure 2.4) and ice in equilibrium at temperatures below 0˚C as a result of the differential effects of soil particles and solutes (Osterkamp and Burn, 2003). In the absence of solutes, temperature and the soil's specific surface area are the primary determinants of the amount of unfrozen water content (Osterkamp and Burn, 2003).

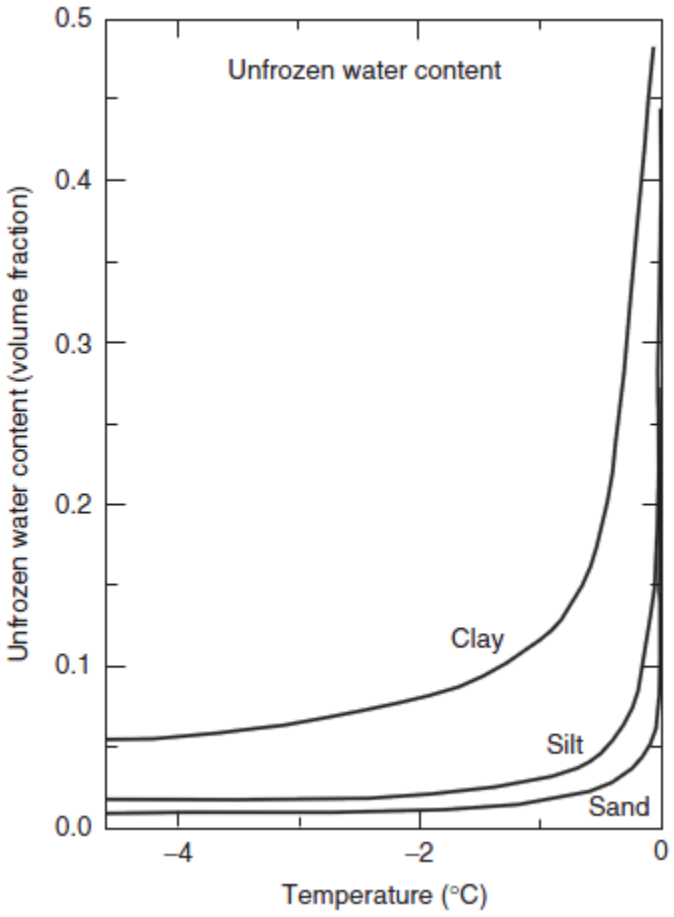

Figure 2.4: Representative values for the temperature dependence of unfrozen water contents in sand, silt and clay. Unfrozen water contents typically increase with temperature and finer grained soil (Osterkamp and Burn, 2003). Note that these curves could be shifted if solutes caused substantial freezing point depression (Anderson and Morgenstern, 1973). This was not generally observed at the field sites (see Chapter 5)

Finer-grained soils, such as clays and silts, have the highest specific surface area (SSA) and porosity while coarser soils such as gravel have the lowest (Osterkamp and Burn, 2003; Williams and Smith, 1989). Bulk water exists in the middle of the pores of these fine-grained soils as well as water attracted to soil particles due to adsorption and capillarity (Anderson and Morgenstern, 1973; Sloan and Van Everdingen, 1988). Capillarity is the physical process that relates to the molecular forces that exist between phases when the interfaces are confined and it increases as the soil particles become smaller (Anderson and Morgenstern, 1973).

During freezing of fine-grained soil, the purest water within the centre of the pore space freezes first. This results in water being confined progressively in smaller spaces as it migrates to the freezing zone, which is referred to as cryosuction (Williams and Smith, 1989). The free energy of the water falls accordingly as freezing takes place and this is most apparent in fine-grained sediments (Williams and Smith, 1989). Temperatures below 0˚C are required for the remaining unfrozen moisture to change phase explaining how unfrozen water can exist in permafrost (Williams and Smith, 1989).

The presence of dissolved solutes and minerals has the effect of lowering the initial freezing point of water (Anderson and Morgenstern, 1973; Sloan and Van Everdingen, 1988). This freezing point depression is most prominent in soils with high SSA due to unfrozen water remaining bonded to the soil particles under high tension (Anderson and Morgenstern, 1973; Sloan and Van Everdingen, 1988). The thin mono-layers of water are strongly bound to the individual soil particles, reducing the ability of the water to freely migrate in permafrost (Sloan and Van Everdingen, 1988). The thickness of the water films decreases when temperatures fall below the initial freezing point of the soil water (Sloan and Van Everdingen, 1988)

Poorly drained silty soils usually possess some of the highest water or ice contents and are termed “frost susceptible” while coarse, free-drained sediments are termed “non-frost-susceptible” (Williams and Smith, 1989). Soils with smaller pore spaces will have higher unfrozen moisture contents than those with larger pore spaces at the same temperature (Williams and Smith, 1989; Anderson and Morgenstern, 1973; Osterkamp and Burn, 2003).

2.5.3 Latent Heat and the Zero-Curtain Effect

Latent heat is the amount of energy released or absorbed by a substance during a phase change (e.g. solid to liquid or liquid to gas) (French, 2007). In autumn, as the ground begins to freeze, the freezing front progresses from the ground surface downwards through the active layer (French, 2007). As moisture in the ground freezes at the freezing front, latent heat is released and flows upwards along the thermal gradient (French, 2007). When temperatures within the active layer approach 0˚C, they remain constant for as long as sufficient unfrozen moisture is present to release enough latent heat to satisfy the thermal gradient and thermal conductivity (French, 2007). This phenomenon is known as the zero-curtain effect (Williams and Smith, 1989; French, 2007). When ice formation decreases due to a reduced supply of unfrozen moisture, less latent heat is released and the soil cools down below 0˚C at a higher rate, allowing the freezing front to advance once again (Williams and Smith, 1989; French, 2007).

In the spring, a similar zero-curtain effect pattern is observed when ice present within the active layer thaws (Outcalt and Hinkel, 1996). As ground temperatures rise in the active layer and approach 0˚C, they remain constant until the latent heat necessary for phase change of ice to water has been satisfied. Once the ground has thawed, the soil can warm at a higher rate, allowing the thawing front to advance once again (Outcalt and Hinkel, 1996).

Studying zero-curtain effects at borehole sites can be useful in determining the amount of frozen or unfrozen moisture content in the active layer spatially and temporally over time (Throop et al., 2012). An extended zero-curtain indicates a significant amount of frozen or unfrozen moisture present in the active layer or that the thermal gradient is weak (Isaksen et al., 2007). Inter-annual variability in zero-curtains can give an indication of how much moisture conditions change at a site and can be used to examine more extreme climatic events such as exceptional amounts of rainfall prior to freeze-back (Isaksen et al., 2007).

2.6 Thermal State of Permafrost

2.6.1 Amplitude of Annual Temperature Wave

The amplitude of the annual ground temperature wave is half of the difference between the maximum and minimum temperature fluctuation at a given depth (Williams and Smith, 1989):

$$A_{(z)} = \frac{\max T - \min T}{2} \tag{6}$$

Where $A_{(z)}$ is the amplitude at z depth, max$T$ and min$T$ are the maximum and minimum temperatures reached over one year at z depth, respectively (Williams and Smith, 1989). The amplitude is attenuated with depth until seasonal fluctuations are no longer detectable at the D_{ZAA} and only long-term changes occur (Williams and Smith, 1989).

2.6.2 Thermal Diffusivity

The thermal diffusivity is the rate at which temperature changes are able to propagate with depth (Williams and Smith, 1989). The thermal diffusivity is driven by temperature gradients and is dependent upon the ratio between the thermal conductivity and heat capacity of the substrate (Hinkel, 1997). The thermal diffusivity can be calculated at sites with a sinusoidal temperature wave using:

$$\kappa = \frac{\pi}{P}\left(\frac{z_2 - z_1}{\ln A_1 / A_2}\right)^2 \tag{7}$$

Where k is the thermal diffusivity (m^2s^{-1}) and P is the period of the wave, usually in seconds, either over one day (86400 s) or over one year (3.15×10^7) depending on the period which the amplitude represents; A_1 and A_2 are the calculated amplitudes at the two depths of measurements Z_1 and Z_2, Z_2 being the greater depth (Williams and Smith, 1989). This calculated value for thermal diffusivity is considered "apparent" because it includes non-conductive heat transfer within the soil such as latent heat effects related to phase change (Williams and Smith, 1989).

Obtaining a value for the apparent thermal diffusivity using this method can be problematic at sites where soil moisture contents fluctuate over time (William and Smith, 1989).

2.6.3 Depth of Zero Annual Amplitude

The depth of zero annual amplitude (D_{ZAA}) is the level at where annual temperature amplitudes diminish to less than 0.1˚C (Williams and Smith, 1989). Changes in ground temperature below this depth occur over multiple years or decades and are normally associated with climate change and environmental change (Williams and Smith, 1989). Temperature envelopes are a visual representation of the annual range of temperatures at each depth and can be used to estimate the D_{ZAA} (Brown, 1978).

The temperature at the D_{ZAA} relates directly to the TTOP and is generally observed to be greater in areas with cold surfaces and highly conductive substrates such as bedrock (Smith and Riseborough, 2002). The shallowest D_{ZAA} are observed in fined-grained soil close to 0˚C with high unfrozen moisture content where phase change is occurring (Riseborough, 1990). Surface temperatures propagate faster at sites where the ground is frozen compared to unfrozen sites, due to higher thermal diffusivities (Riseborough, 1990). Higher thermal diffusivities at frozen sites reduce the rate of attenuation of ground surface temperatures with depth, resulting in a greater D_{ZAA} (Riseborough, 1990). The opposite is true at unfrozen sites where the thermal diffusivities are generally lower due to high amounts of unfrozen moisture (Riseborough, 1990). In this case, the amplitude is rapidly dampened with depth and the D_{ZAA} is shallower (Riseborough, 1990). The MAGT is usually warmer than the TTOP value due to the geothermal gradient (Smith and Riseborough 2002).

The approximate D_{ZAA} of shallow boreholes can be calculated using the apparent thermal diffusivity. The D_{ZAA} is calculated using the deepest known apparent thermal diffusivity (K) in a borehole that is shallower than the D_{ZAA} (Williams and Smith, 1989). The depth of zero annual amplitude (D_{ZAA} or Z_{ZAA}) can be calculated using:

$$z_{ZAA} = \sqrt{\frac{\kappa P}{\pi}\left(\ln A_1 / A_{ZAA}\right)^2} + z_1 \qquad (8)$$

Where Z_{ZAA} is the D_{ZAA}, A_1 is the amplitude at the second deepest thermistor, and A_{ZAA} is the amplitude at D_{ZAA} or 0.1˚C (Williams and Smith, 1989). The amplitude at the second deepest thermistor is used because it will not be affected by phase changes that may occur within the active layer during the thawing and freezing periods (Williams and Smith, 1989).

2.6.4 Phase Lag

The apparent thermal diffusivity can also be used to calculate the phase lag of a temperature wave (Williams and Smith, 1989). The phase lag reflects the length of time it takes for a temperature wave to reach a particular depth (Williams and Smith, 1989). The phase lag (t) can be calculated using:

$$t = \frac{z}{2}\left(\frac{P}{\pi K}\right)^{1/2} \tag{9}$$

Where t is the lag of the wave with depth (z) (Williams and Smith, 1989). The period of the wave, P and the apparent thermal diffusivity, K are defined in section 2.6.2. Substrates with high thermal diffusivities such as bedrock propagate seasonal temperature fluctuations more rapidly downwards, producing shorter phase lags than material with low thermal diffusivities (Williams and Smith, 1989). Sites with high thermal diffusivities and short phase lags can attain depths of ZAA greater than 20 m (Williams and Smith, 1989).

2.6.5 Permafrost Thickness

The thickness of permafrost is controlled by factors that influence its heat balance and heat flow within it (Osterkamp and Burn, 2003). Heat balance and heat flow are mainly controlled by ground surface temperatures and conditions as well as the geothermal gradient and the thermal conductivity of the substrate (Osterkamp and Burn, 2003; French, 2007; Burn, 2012). The geothermal gradient is a result of heat from the centre of the earth flowing towards the surface, known as the geothermal heat flux (French, 2007). The geothermal flux is a geologic phenomenon, and changes little over human time scales (Burn, 2012). The geothermal gradient varies across space and is controlled by the thermal conductivity of the earth materials and the

geothermal heat flux (Judge, 1973). The flux is almost constant spatially over vast areas of Canada at approximately 0.05 W/m^2 (Burn, 2012). Permafrost is in equilibrium when the heat going into the ground is equal to the heat coming out of the ground (Burn, 2012). Thick permafrost should have a combination of low mean annual ground surface temperatures, high thermal conductivity, and low heat flow (Williams and Smith, 1989).

Equilibrium permafrost depths can be calculated using the surface temperature, heat flow, and the thermal conductivity of the ground (Burn, 2012) using:

$$z = \frac{\mathrm{Ts} \cdot \lambda_f}{Q} \tag{10}$$

Where Z is the depth of permafrost, Q is the geothermal heat flux, Ts is the temperature at the surface (MAGST), and λ_f is the average thermal conductivity value of the complete thickness of frozen ground (modified from Burn, 2012). A geothermal heat flux of 0.05 W/m^2 can be used in most geologically stable areas of Canada (Burn, 2012).

Another method used to estimate permafrost thickness is the downward extrapolation of the geothermal gradient from below the D_{ZAA} (Gruber et al., 2004). Ground temperatures generally follow the geothermal gradient to the base of permafrost below the D_{ZAA}, assuming that permafrost is in equilibrium with current climatic conditions (Burn, 2012). If the geothermal gradient is unknown, a general range of possible permafrost thickness can be derived with the assumption that the ground warms by 1˚C per 30-60 m (French, 2007). However, these methods can be problematic at sites where geothermal gradients vary regionally along with differences in geology and tectonics and at sites where ground temperatures are close to 0˚C due to the effects of unfrozen moisture and latent heat effects (Williams and Smith, 1989).

2.7 Permafrost and Global Warming

Efforts to characterize the thermal state of permafrost in northern North America were made during the Fourth International Polar Year (IPY) using ground temperature data collected from 350 boreholes (Smith et al., 2010). This study found that permafrost warming has occurred essentially continuously over the past 20-30 years in western North America (Smith et al., 2010).

The magnitude of these changes varied, being less in warmer permafrost (>-2^{o}C) than in colder permafrost (Smith et al., 2010). Based on the observed trends, it will take decades to centuries for colder permafrost to reach the thawing point while warmer permafrost is already undergoing internal thaw at temperatures below 0^{o}C (Smith et al., 2010).

Permafrost thaw due to climate change and environmental change can have profound effects in an area (UNEP, 2007; AMAP, 2011). Long-term permafrost degradation can result in increases in water drainage, resulting in shrinking of lakes and ponds while increasing dryness of soils (AMAP, 2011). These changes can affect aquatic ecosystems and place significant stress on vegetation (AMAP, 2011). Thawing of ice-rich permafrost can result in the replacement of boreal forests with wetlands, affecting wildlife habitats (AMAP, 2011). Potential impacts of thawing permafrost on Arctic infrastructure are also of increasing concern (AMAP, 2011). Warming and thawing of ice-rich permafrost can have impacts on infrastructure (e.g. community and infrastructure) integrity and human activity (UNEP, 2007). These impacts may be greater in warmer, discontinuous permafrost zones, where permafrost is already close to thawing (Ladanyi, 1995). In some cases, surface disturbance such as the removal of vegetation potentially outweighs the effect of climate warming in the first decades following disturbance, although climate warming may become important over longer time periods (Smith and Riseborough, 2010).

Thawing permafrost may lead to changes in the carbon cycle with feedbacks to the system (Kuhry et al., 2010). Tarnocai et al. (2009) estimate that approximately 1672 Pg C of soil organic carbon (SOC) is stored in perennially frozen ground of the northern hemisphere. Thawing permafrost could result in remobilization of the previously frozen SOC pools and the release of large amounts of greenhouse gases (Schuur et al., 2008). This is a positive feedback within the Earth System, as climate warming results in permafrost thawing that causes a further increase of atmospheric greenhouse gases (Schuur et al., 2008). Strong evidence suggests that SOC in permafrost terrain is already starting to be released (Kuhry et al., 2010). However, the IPCC has not considered soil organic carbon in its climate change scenarios (Kuhry et al., 2010).

2.8 Electrical Resistivity Tomography (ERT)

2.8.1 ERT in Permafrost Research

Since permafrost is a phenomenon primarily defined thermally, common observation techniques are based on thermal aspects of permafrost evolution (Nicholson and Granberg, 1973; Nicholson, 1978; Burgess, 1983; Desrochers, 1988; Hilbich et al., 2008). Although a borehole can provide detailed information on the thermal and physical conditions (including moisture and ice content) of the ground, information is only provided for a single point (Burgess, 1983; Desrochers, 1988; Vonder Muhll et al., 2002). Subsurface thermal regimes can vary spatially resulting in very complex distributions of frozen ground with large differences possible within short distances (Nicholson, 1978; Burgess, 1983; Desrochers, 1988; Harris and Vonder Muhll, 2001; Vonder Muhll et al., 2002). Surface and subsurface monitoring and investigations should therefore be extended from single point locations (boreholes) to two-dimensional and three-dimensional investigations of freezing and thawing processes (Hilbich et al., 2008).

Because a number of physical parameters change during phase transition from the unfrozen to the frozen state, geophysical measurements offer the possibility of identifying permafrost and determining its characteristics (Vonder Muhll et al., 2002). Geophysical techniques can be used to examine the spatial distribution of subsurface geophysical properties to delineate horizontally and vertically the active layer, permafrost and taliks (Kneisel et al., 2008). Spatial and temporal changes in subsurface geophysical properties due to cooling, warming, aggradation or degradation of permafrost can also be assessed through geophysical monitoring (Kneisel et al., 2008; Miceli, 2012).

Electrical resistivity is sensitive to phase changes between water and ice and is therefore directly associated with the ice and unfrozen water content of the subsurface material (Hilbich et al., 2008; Lewkowicz et al., 2011). During freezing, measured electrical resistivity rises exponentially as unfrozen water content within a substrate decreases (Hauck, 2002; Hilbich et al., 2011). The increase in resistivity with decreasing temperature is small and linear for temperatures above the freezing point and exponential for temperatures below (Hauck, 2002; Hilbich et al., 2011). Under the assumption that general conditions (lithology, pore space, electrode coupling, etc.) remain constant, measured changes in resistivity can be attributed to

changes in the unfrozen water content (Hilbich et al., 2008, 2011; Lewkowicz et al., 2011). These properties allow permafrost bodies to be identified and their ice content to be estimated without excavation (Kneisel et al., 2008).

Electrical Resistivity Tomography (ERT) relies heavily on the range of known resistivity values for different earth materials (Hauck and Kneisel, 2008; Locke, 2012). Subsurface conditions in an area can be determined based on resistivity values if the material can be identified (Hauck and Kneisel, 2008). However, different materials can have overlapping resistivity values, allowing for a range of interpretation (Table 2.1). A borehole logged along the ERT profile is an effective way of identifying the soil lithology and sub-surface materials (Hilbich et al., 2008)

Table 2.1: Resistivity values for different earth materials (Hauck and Kneisel, 2008).

Material	Range of resistivity (Ohm-m)
Organic matter	1-300
Clay	1-100
Sand	100-500 x 10^3
Gravel	100-400 x 10^2
Groundwater	10-300
Frozen sediments, Permafrost, Ground Ice	1 x 10^3-10^6
Air	infinity

Note: *The upper ends of the resistivity ranges for sand and gravel are observed under dry conditions.

Due to the great sensitivity of electrical resistivity to the transition from unfrozen to frozen materials, ERT surveys constitute an increasingly common geophysical method used for permafrost investigations (Kneisel et al., 2008). In the past few years, great progress has been achieved in permafrost applications of DC resistivity tomography methods and promising results have been achieved (Hauck and Vonder Muhll, 1999; Vonder Mull et al., 2000; Hauck et al., 2001; Fortier and Bolduc, 2008; Kneisel et al., 2008; Hilbich et al., 2011; Lewkowicz et al., 2011; Miceli, 2012).

2.8.2 ERT Basic Theory

ERT measurements are normally made by injecting current into the ground through two electrodes and measuring the voltage difference at two potential electrodes (Loke, 1999). From this measurement, the apparent resistivity (p_a) value is calculated as follows:

$$p_a = \frac{kV}{I} \tag{11}$$

Where V is voltage, I is current and K is the geometric factor (Loke, 1999). The calculated resistivity value is not the true resistivity of the subsurface, but an "apparent" value which represents the resistivity of homogeneous ground (Loke, 1999). The relationship between the "apparent" resistivity and "true" resistivity is complex and can be calculated by inversion techniques using a computer program (Loke, 1999).

A two dimensional (2-D) subsurface survey can be acquired when a series of electrodes measure resistivity along a transect (Hilbich et al., 2008). Two-dimension electrical imaging can take into account both horizontal and vertical changes in the subsurface (Locke, 2012). This allows for monitoring of permafrost evolution such as advancing and retreating freezing fronts on different timescales, i.e., short-term, seasonal, and inter-annual changes (Hauck, 2002; Hilbich et al., 2008; Miceli, 2012).

Electrodes can be placed in different arrays in order to effectively detect different subsurface structures (Loke, 1999). When constructing a 2-D electrical profile, it is assumed that resistivity does not change perpendicular to the survey line (Locke, 2012). This assumption is usually reasonable when monitoring permafrost bodies (Locke, 2012). Since all geological structures and permafrost bodies are 3-D in nature, a fully 3-D resistivity survey using a 3-D interpretation model yields the most accurate results (Locke, 2012). Although 3-D surveying is presently the subject of active research, it has not reached the level where it is routinely used (Locke, 2012). This is mainly due to higher costs and time constraints related to 3-D surveys (Locke, 2012).

2.8.3 Wenner Array

The Wenner array (Figure 2.4) has become widely accepted as the most effective in surveying permafrost bodies (Hauck et al., 2003; Hilbich et al., 2011; Lewkowicz et al., 2011). The Wenner array has almost horizontal contours beneath the centre of the array which makes it most sensitive to vertical resistivity changes (Figure 2.5) (Loke, 1999; Locke, 2012). This property makes it useful for identifying horizontal subsurface structures such as permafrost (Loke, 1999). Areas of low sensitivity near the surface of the plot (Figure 2.4) result in underestimations of resistivity values if a high resistivity body is present within this area (Locke, 2012). The opposite occurs in areas of high sensitivity (Locke, 2012).

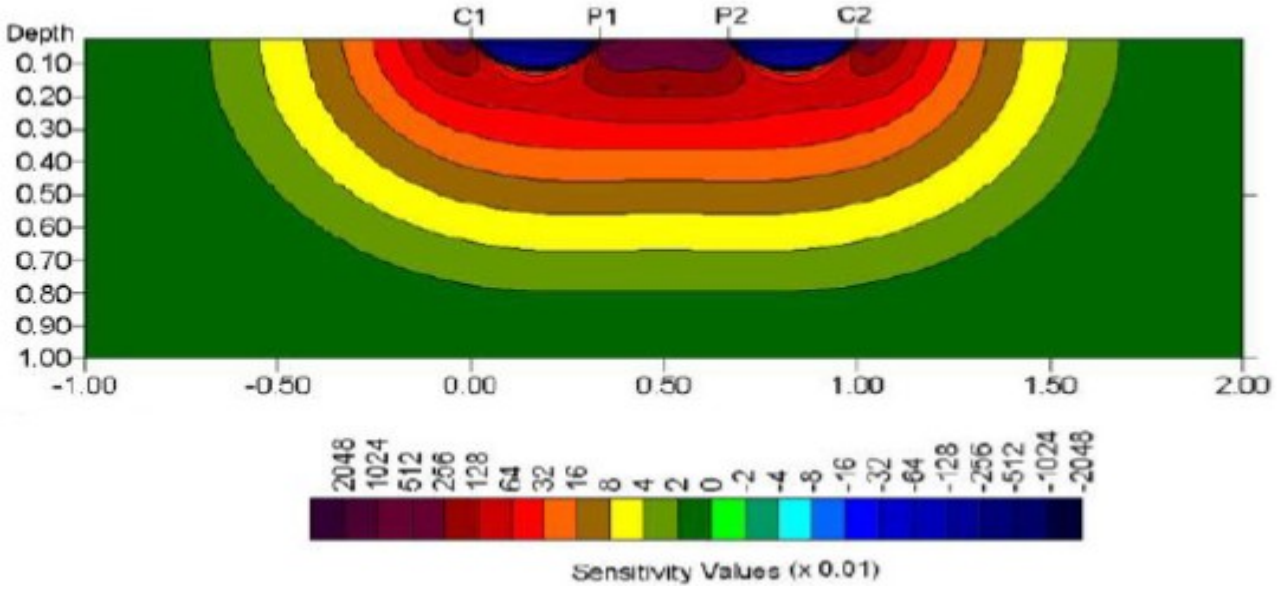

Figure 2.5: Wenner array sensitivity plot (Locke, 2012).

The Wenner array also has the smallest geometrical factor (2πa) of any other array (Hauck *et al*., 2003; Loke, 1999). The geometric factor is inversely proportional to the signal strength which gives it the strongest signal strength and the ability to penetrate the ground to greater depths (Loke, 1999). One disadvantage for this array for 2-D surveys is the relatively poor horizontal coverage as the electrode spacing is increased, because no data are collected in the lower areas near the edges of the array (Loke, 1999).

2.8.4 Resistivity Post Processing

In order to properly interpret resistivity results, the "apparent" resistivity data collected in the field needs to be converted to "true" resistivity values through a geoelectrical imaging computer software such as RES2DINV (Griffiths and Barker, 1993). The relationship between "apparent" and "true" resistivity is quite complex (Locke, 1999). Resistivity surveys are undertaken for various studies in a range of different fields meaning that most users are not knowledgeable in geophysical inversion theory (Locke, 1999). Programs such as RES2DINV attempt to simplify this process by allowing only minimal input by the user (Locke, 1999).

The apparent resistivity plot is first loaded into RES2DINV as a pseudosection which is only used for a preliminary view of the data (Locke, 2012). Before inverting the data, "apparent" resistivity values for each resistivity survey must be examined for bad data points which are eliminated (e.g. Figure 2.6).

When studying permafrost bodies, sharp boundaries are expected which calls for the use of the robust or blocky inversion method. Each inversion goes through multiple iterations (never more than 7 to avoid over-filtering) which result in progressively smaller RMS errors. The inversion normally must be run several times before satisfactory results are achieved, corresponding to an RMS error <5%. Lastly, topography can be added to a profile at study sites with noticeable relief to gain a better perspective on the subsurface characteristics (Hilbich et al., 2008).

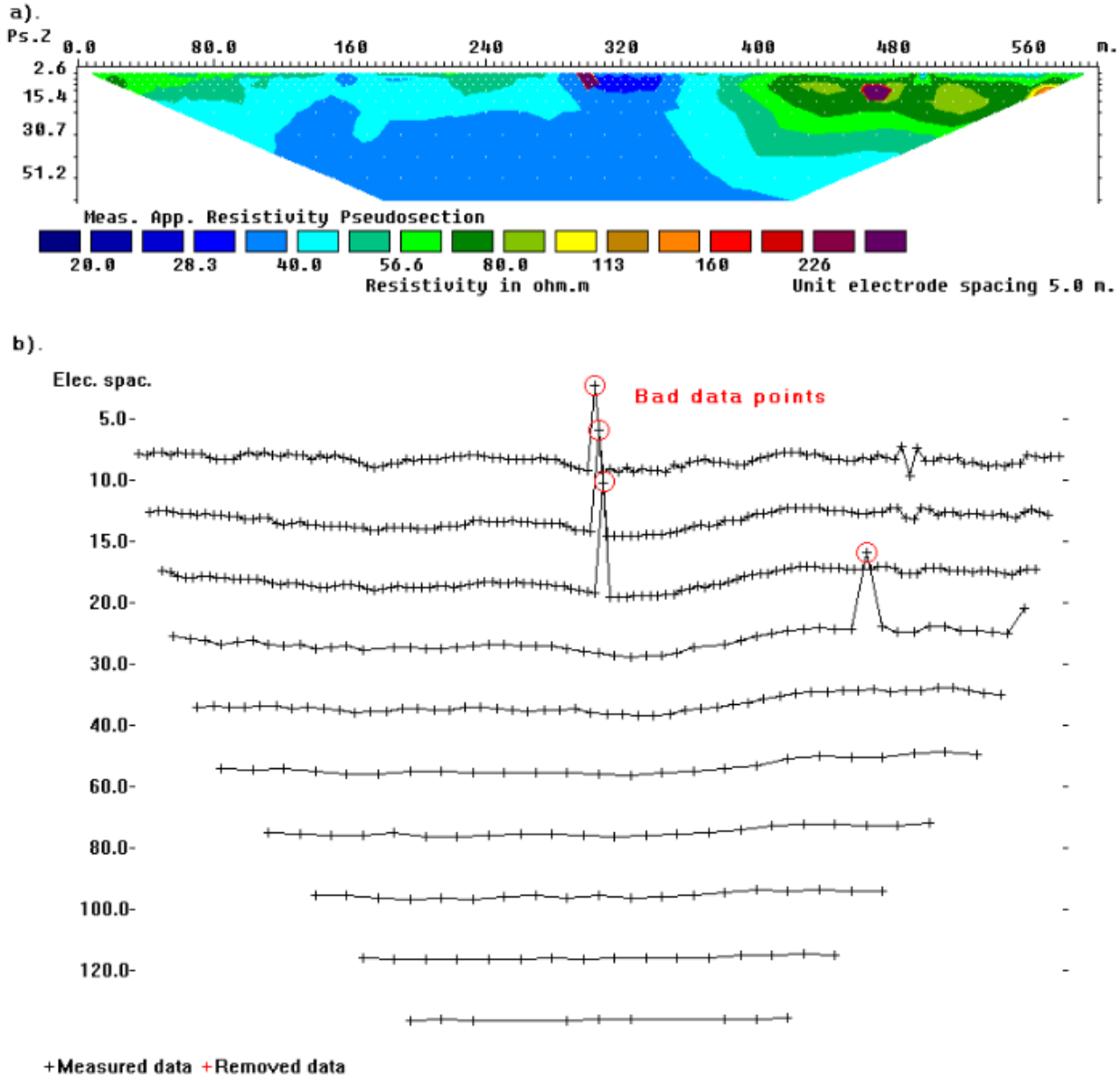

Figure 2.6: An example of a field data set with a few bad data points. The most obvious bad data points are located below the 300 metre and 470 metre marks. (a) The apparent resistivity data in pseudosection form and in (b) profile from (Locke, 1999).

2.8.5 ERT Weaknesses

ERT is a very useful tool used for permafrost investigation but it does have some weaknesses in the field (Vonder Muhll et al., 2002). Good electrical coupling between the electrodes and subsurface is essential (Hauck et al., 2003). Establishing reasonable electrical contact may be very difficult in dry, coarse, and rocky terrain such as rock glaciers which can affect the inversion results (Hauck et al., 2003). Another weakness is the effect of distance between electrodes on the survey's spatial resolution (Vonder Muhll et al., 2002). Surveys with large distances between electrodes are less effective at identifying small subsurface features or sharp transitions such as a thin active layer (Vonder Muhll et al., 2002).

Interpretation of ERT surveys during post-processing must be done carefully (Vonder Muhll et al., 2002). The relationship between "apparent" and "true" resistivity inverted by the computer software program is quite complex (Loke, 1999). Inversion of the field data can cause artefacts, which are areas of the resistivity profile with low accuracy (Hilbich et al., 2009). Additional geophysical methods (e.g., seismic tomography, EM methods, BTS) can be applied to reduce ambiguities (Vonder Muhll et al., 2002). Due to these weaknesses, ERT is not meant to replace conventional borehole investigations and thermal monitoring but rather complement them (Hilbich et al., 2008).

SECTION 3: STUDY AREA

3.0 STUDY AREA

3.1 Physical Location

The study area for this project is located along a 457 km length of the Alaska Highway between Whitehorse, YT (60^{o} 43' N, 135^{o} 03' W) and Beaver Creek, YT (62^{o} 23' 7" N, 140^{o} 53' 35" W). This area is within the sporadic discontinuous (10-50 %) and extensive discontinuous (50-90 %) permafrost zones (Heginbottom et al., 1995). Permafrost in this area is potentially vulnerable to the impacts of recent and predicted climate change (Smith et al., 2010). Figure 3.1 shows the permafrost monitoring sites and the major communities within the study area as well as the probability of permafrost occurrence as derived from Bonnaventure and Lewkowicz. (2012). All borehole field sites are located within 500 m of the highway, with the exception of borehole R8 which is located 1.2 km away from the highway.

3.2 Previous Research

In 1964, R.J.E. Brown undertook a permafrost investigation along the Alaska Highway between Fort St. John, British Columbia and Whitehorse, Yukon (north of 56^{o}N and south of 65^{o}N). Permafrost was found at 55 % of the sites visited, and was generally within poorly drained, north-facing slopes (Brown, 1967). In 2007 and 2008, James (2010) located 55 of the 86 sites Brown had identified as having permafrost. From 1965-2008, air temperature in the area had increased at a rate of 0.4-0.5^{o}C per decade, resulting in the loss of permafrost within 2 m of the ground surface at half of the sites (James, 2010). Most sites (81 %) that no longer had permafrost present were in the southern section of the study area between Fort Nelson and Fort St. John B.C. James (2010) concluded that the southern limit of permafrost in the study region had shifted approximately 75 km north.

An intensive geotechnical program, including ground temperature measurements took place along the Alaska Highway Corridor about a decade after Brown's 1964 permafrost investigation. The study was part of an initial assessment for a proposed gas pipeline in the area and over 1400 boreholes were drilled between 1977-1981 from Fort St. John, BC north to the Alaskan border near Beaver Creek, YT. The Geological Survey of Canada also measured ground temperatures in some of these boreholes (Burgess et al., 1982), the majority of which were

located between Whitehorse, YT and Beaver Creek, YT, within about 1 km of the road. Climate in the area has also warmed since the 1970s (Smith et al., 2010). However, permafrost conditions and thermal regimes along the route have not been re-examined in general since 1981 although work on permafrost distribution has been undertaken since 2008, largely related to vulnerability of the highway to climate change (Reimchen et al., 2009), and new boreholes were also established during the IPY (Smith et al., 2010).

3.3 Topography

The study area borders the Western Cordillera from southeast-northwest in southwest Yukon (Mathews, 1986; Wahl et al., 1987). The Alaska Highway corridor within this study area crosses the Teslin and Kluane Plateau over the Shakwak Trench and follows the Kluane Ranges which form a 30 to 60 kilometer wide belt of high relief often referred to as the foothills of the much higher St. Elias Mountains (Figure 3.2) (Gabrielse et al., 1991; Hulbert, 1997). Topography in the study area reflects this, with numerous mountains, valleys and plateaus (Figure 3.3) (Mathews, 1986; Wahl et al., 1987). The Alaska Highway corridor is less variable in elevation compared to the surrounding area. Elevation of the study sites ranged from 682 m (R1) to 941 m (M1). Local relief does not exceed a few meters within each study site.

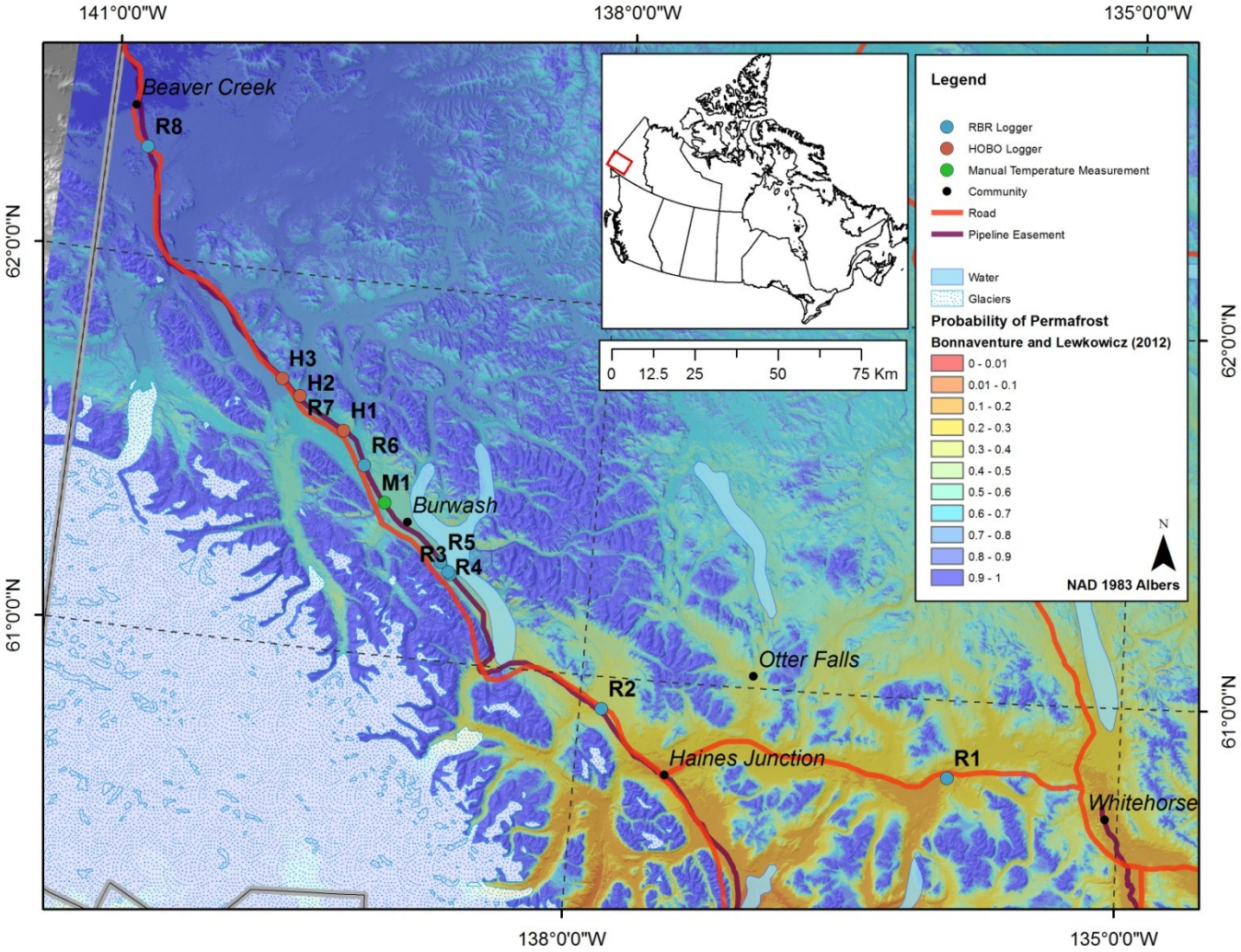

Figure 3.1: Map of the study area showing the borehole monitoring sites. Permafrost probability is from Bonnaventure and Lewkowicz. (2012).

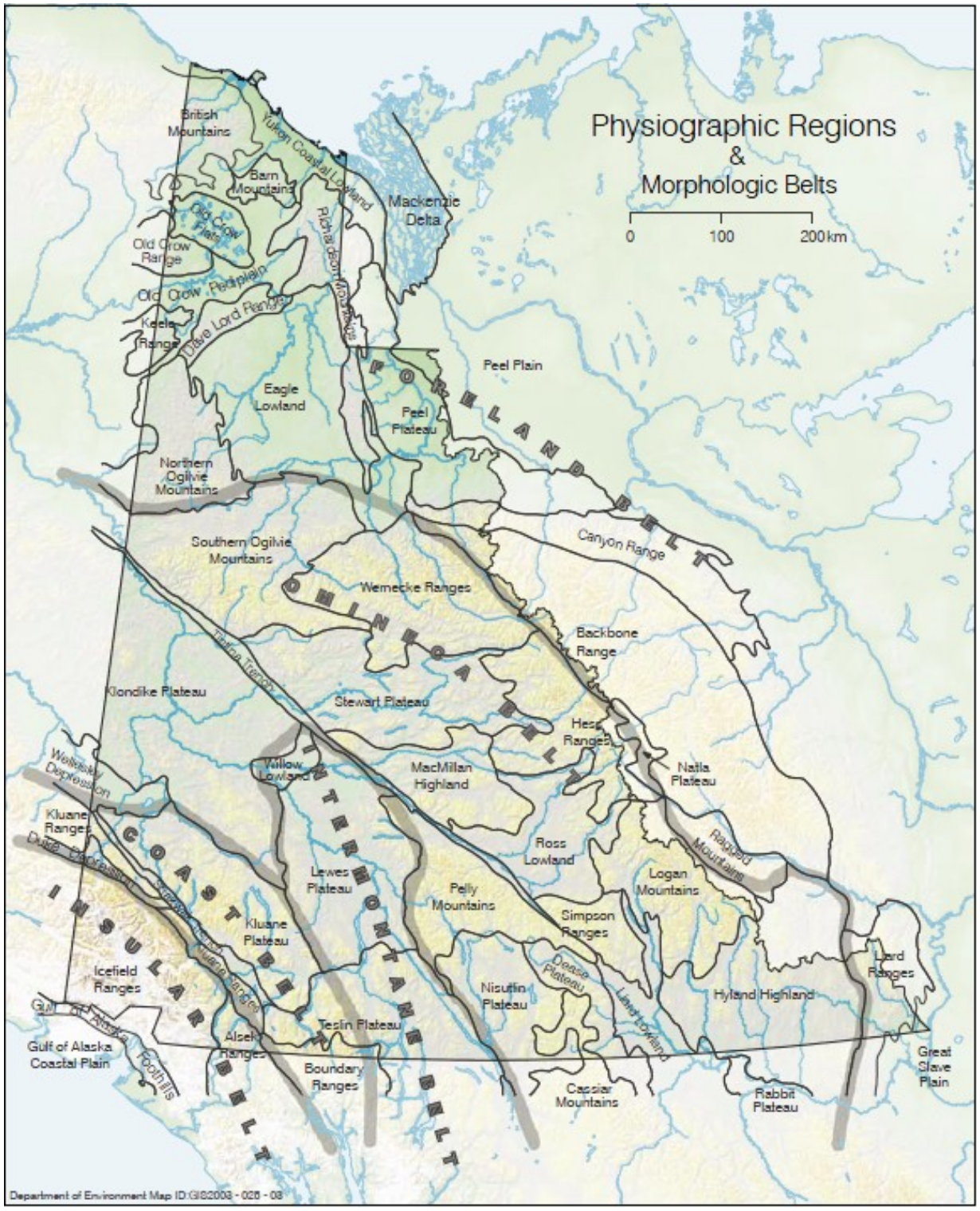

Figure 3.2: Physiographic regions and morphologic belts of the Yukon (Gabrielse et al., 1991).

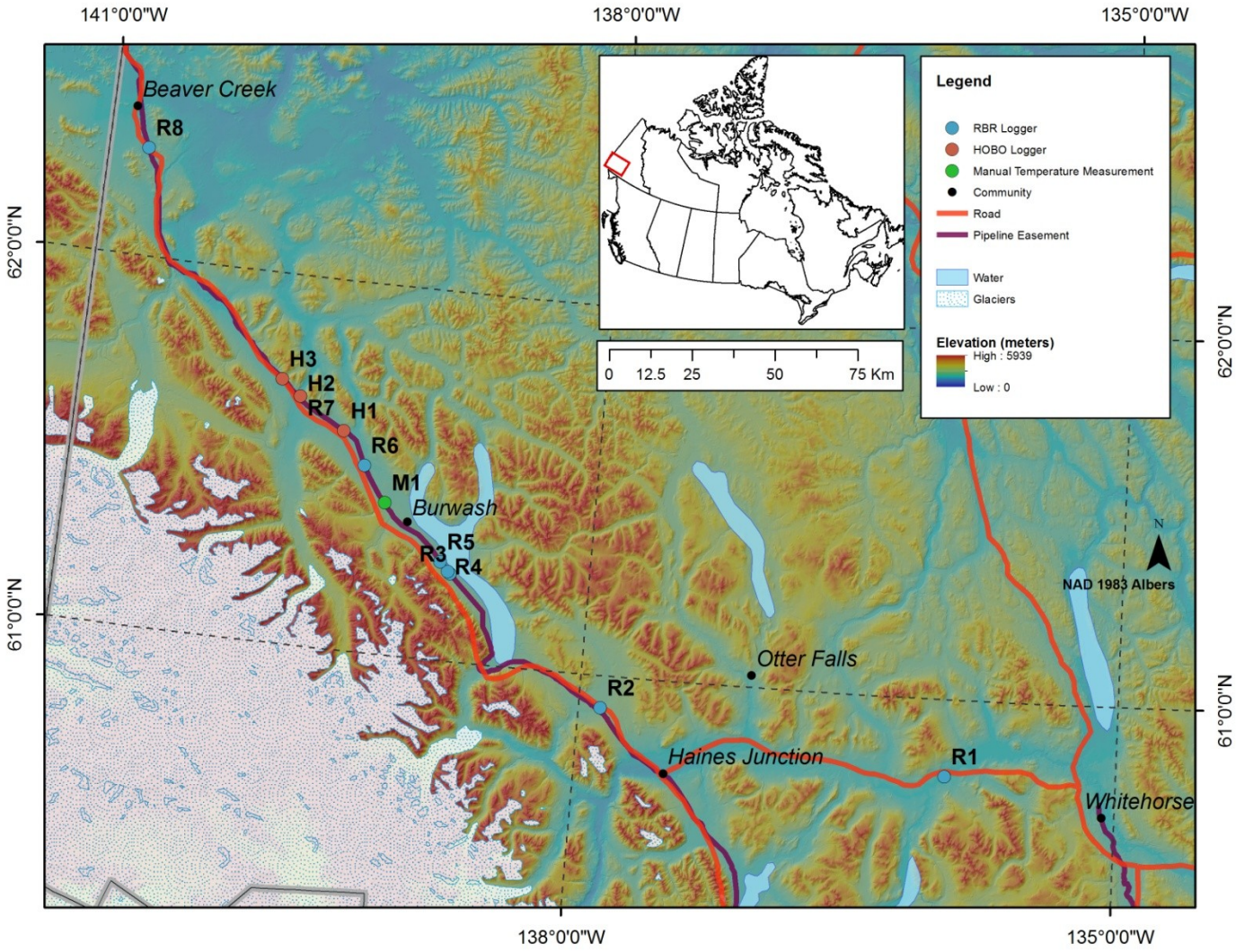

Figure 3.3: Digital Elevation Model (DEM) of the study transect and its surrounding area (Source: Geomatics Yukon DEM, 2012; Natural Resources Canada, 2012).

3.4 Quaternary History and Deposits

The study area was last glaciated during the Wisconsinan, approximately 80 ka to 10 ka years ago (Bond, 2004). The area now traversed by the Alaska Highway from Whitehorse to Beaver Creek was covered by the Cordilleran Ice Sheet advancing from the west (Fulton, 1989). Glacial limits and ice flow direction are shown in Figure 3.4 (Duk-Rodkin, 1999). Ice accumulations in the Coast Mountains of southwestern Yukon and the Cassiar Mountains of south-central Yukon during the late Wisconsinan were responsible for glaciation of the study area (Bond, 2004). The first glaciers that advanced out of the mountain valleys were likely supported by cirques in the Coast Mountains (Bond, 2004). Topographically unconstrained ice flow trending northwest over most of the study area occurred during the glacial maximum (Bond, 2004). Ice thickness over the city of Whitehorse exceeded 1350 m during full glacial conditions (Bond, 2004).

Deglaciation of the area was characterised by multiple changes in ice flow, glacial retreats, glacial re-advances, periods of dynamic equilibrium and glacial lake development (Bond, 2004). By 11 ka, glacial extent in the Cordillera was no greater than at the end of the 20th century (Menounos et al., 2009) and air temperatures were similar to those of today (ACIA, 2005). The magnitude of those recurring events shaped the landscape of southwestern Yukon (Brahney, 2007).

Geological evidence indicates that the level and size of Kluane Lake both fluctuated markedly throughout the Holocene resulting in the probable deposition of glaciolacustrine sediments in adjacent areas (Bostock 1969; Rampton and Shearer 1978a: Clague et al., 2006). The most recent rise in the level of Kluane Lake to its +12 m highstand occurred in the 17th century during the Little Ice Age advance of Kaskawulsh Glacier (Clague et al., 2006). Areas along the Alaska Highway near Haines Junction and in the Alsek Valley are also rich in glaciolacustrine deposits as they were submerged under “Neoglacial Lake Alsek” (Lipovsky, 2011). The Lowell Glacier has surged as far as Goatherd Mountain at least five times in the past 3000 years, damming the Alsek River and impounding a large lake that extended up the Alsek River valley to Haines Junction and into the Dezadeash River valley (Lipovsky, 2011). The last time Neoglacial Lake Alsek formed was around 1850, at the end of the Little Ice Age (Lipovsky, 2011). The glacial history at the northwestern portion of the study area, around the community of

Beaver Creek is not clear, partly because the glacial history of the Nutzotin Mountains in adjacent Alaska is unknown (Rampton, 1969). However, extensive moraines and till underlain by glaciofluvial deposits found in the area point to a dynamic glacial history (Rampton, 1969, 1971). According to Rampton (1971), the Macauley Glaciation began in the area at around 40,000 BP and lasted until 13,500 BP. Glacial ice was largely derived from a piedmont glacier complex that emanated from the Nutzotin Mountains and portions of this area escaped the direct effects of ice but nevertheless were exposed to extreme glacial influences (Rampton, 1971). Deglaciation appears to have been relatively complete by 11,000 BP, as shown by radiocarbon dating on organic materials directly overlying glacial till near the White River Bridge (Rampton, 1971). In 1993, during a highway upgrading project, Pleistocene faunal remains were recovered in the unglaciated area just north of the community of Beaver Creek (MacIntosh, 1997).

Soils in the study area vary from coarse-grained sands, to gravels, to fine-grained material such as silts and clay (Fulton, 1989; Fuller and Jackson, 2009). The coarse-grained soils are associated with till and moraine deposits, while the fine-grained ones are associated with alluvial and lacustrine deposits (Fulton, 1989). Large areas of poorly drained land are also commonly covered by peaty soils (<5 m thick) (Fulton, 1989). The distribution of surficial geological material for the Yukon is given in Figure 3.5.

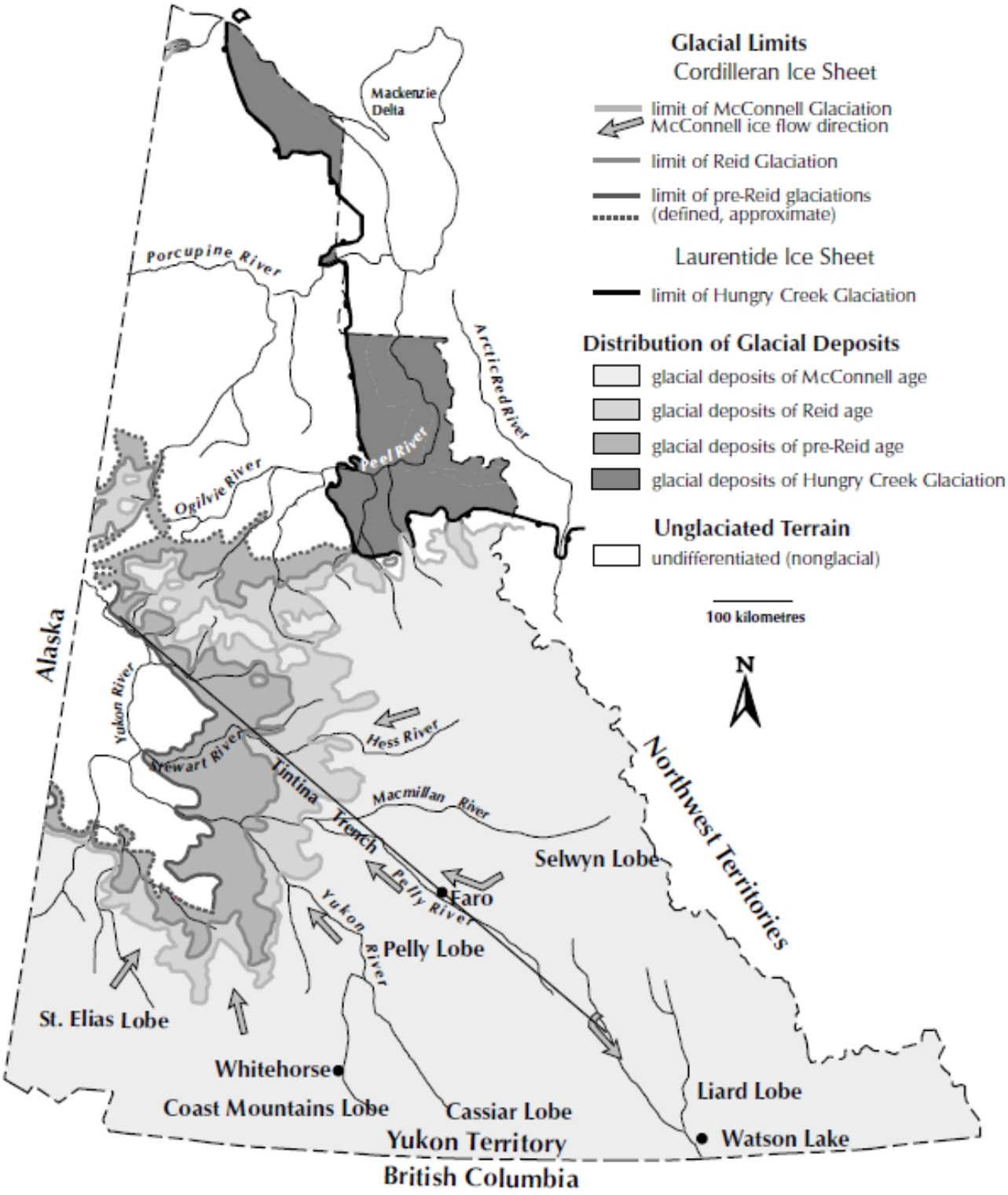

Figure 3.4: Glacial limits map of Yukon (Duk-Rodin, 1999).

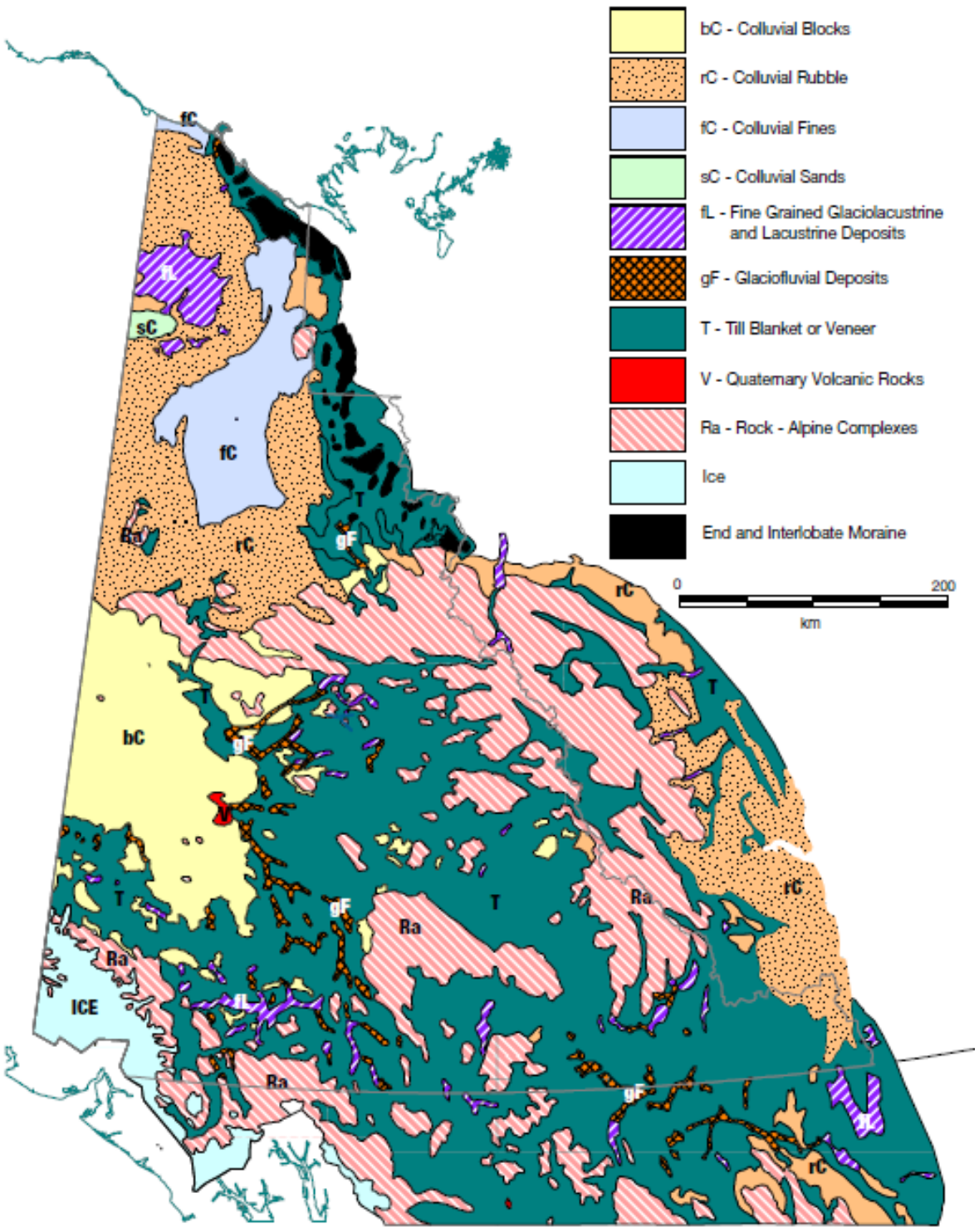

Figure 3.5: Distribution of surficial deposits (Fulton, 1989).

3.5 Climate

Yukon climate is the most variable in North America (Wahl et al., 1987). It is typified by long cold winters and short warm summers, with the mean annual temperature below freezing (Scudder, 1997). January is usually the coldest month and July the warmest, although the highest maximum temperatures may occur in August (Scudder, 1997). The complexity of the terrain is reflected in the area's climate, with a great deal of local and regional variation (Wahl et al, 1987; Laxton et al., 1996; Scudder, 1997).

3.5.1 Climate Zones

The study area is within the Yukon/North BC Mountains climate region which encompasses the entire Yukon and has both mountain and lowland terrain (Taylor, 1997). This region is further subdivided by Wahl *et al*. (1987) into three climate zones (Figure 3.6): the Upper Yukon-Stikine Basin, the St Elias Coast Mountains and the Central Yukon Basin. However, most of the study area is situated within the Upper Yukon-Stikine Basin.

The Upper Yukon-Stikine region is characterized by alpine, sub-alpine and lowland terrain lying between the St Elias Coast Mountains and the Cassiar-Pelly Mountains (Scudder, 1997). There is a marked contrast between the climates on the southwest and northeast flanks of the St. Elias Mountains (Wahl et al, 1987; Laxton et al., 1996; Scudder, 1997). The mountains form a prominent topographic barrier between the northeast Pacific Ocean and northwest North America which not only provide a rain shadow on their lee slopes, but also effectively block the penetration of many maritime air masses into the Yukon, maintaining cool, anticyclonic conditions there in the winter (Wahl et al, 1987; Laxton et al., 1996; Scudder, 1997). Due to the complexity of its relief and to the storminess of the Gulf of Alaska, the St Ellias-Coast Mountains region which parallel most of the study area to the southwest, is one of the more climatically variable and extreme of Yukon (Wahl et al., 1987; Scudder, 1997). Total annual precipitation ranges from 1000 mm to near 4000 mm on the southwest flanks of the St Elias Mountains to a low of 200 mm in the rain shadow of the northeast flanks (Figure 3.7) (Wahl et al, 1987). The result is a semiarid, continental climate near Kluane Lake and in most of the study area, with cold winters and warm, albeit short, summers (Laxton et al., 1996). Winds are also considerably influenced by topography and are frequently the strongest in the southwestern

Yukon (Wahl et al, 1987). Burwash Landing, along the study area has historically recorded winds of destructive forces with gusts up to 171 km/hr (Wahl et al, 1987).

The central Yukon Basin is a northward extension of the Yukon-Stikine Basin with a lower average elevation (Wahl et al, 1987). The region has fairly different climatological characteristics than its southern neighbor due to its greater distance from the effects of the Gulf of Alaska and the St Elias Mountains (Wahl et al, 1987). Temperatures are more variable and extreme with warm summers and prolonged sometimes severe cold spells in the winter (Wahl et al, 1987). The central Yukon Basin holds the record on the North American continent for extreme low air temperature, - 62.8^{o}C, recorded on February 3, 1947 at Snag along the northern transect of the study area (Scudder, 1997). Precipitation is relatively moderate, 300 to 400 mm, mainly falling as summer rain showers and wind tends to be light with a high percentage of calm conditions in the winter (Wahl et al, 1987).

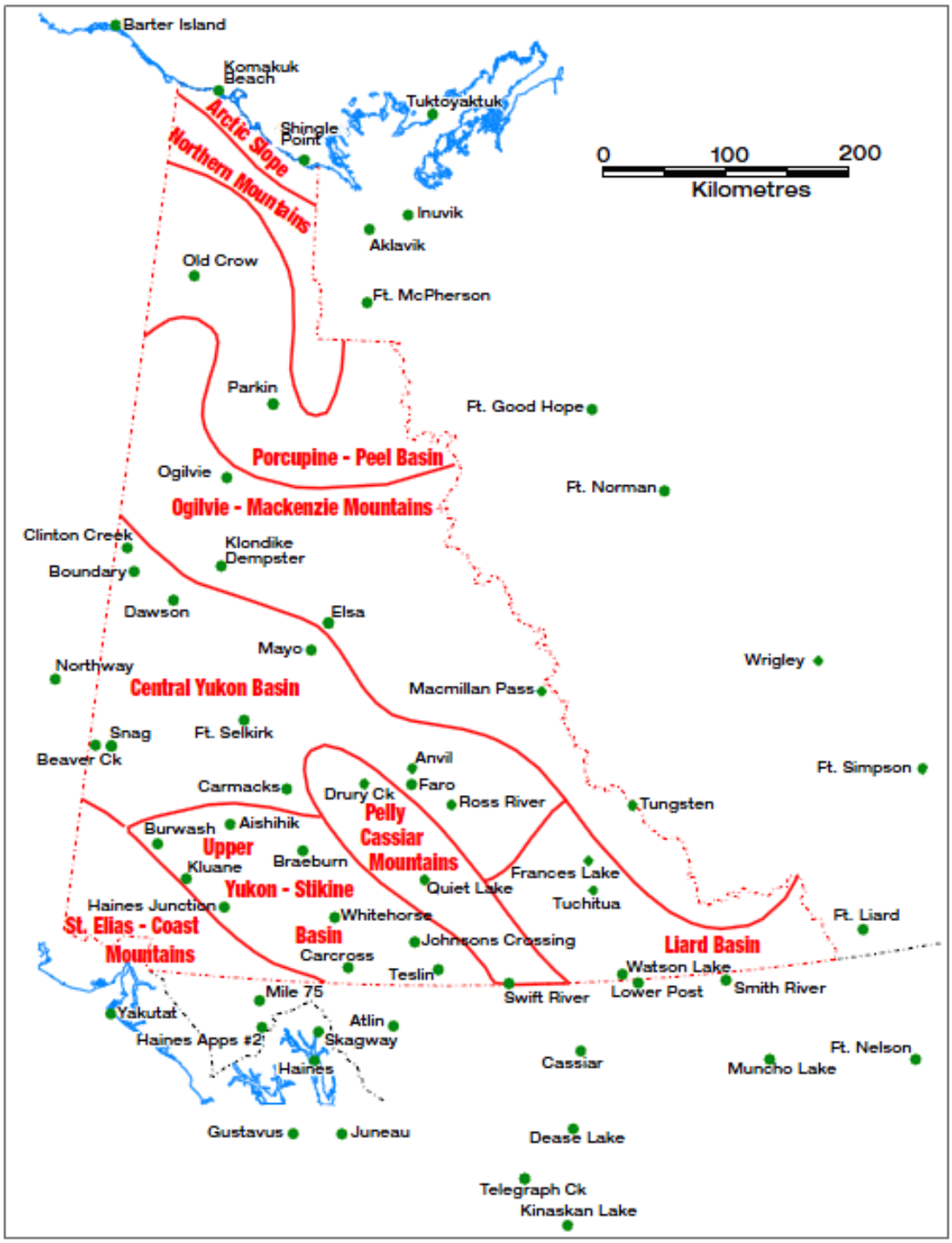

Figure 3.6: Climatic regions of the Yukon. The study area is located in the Upper Yukon-Stikine Basin, the St Elias Coast Mountains and the Central Yukon Basin. However, most of the study area is situated within the Upper Yukon-Stikine Basin (adapted from Wahl et al., 1987).

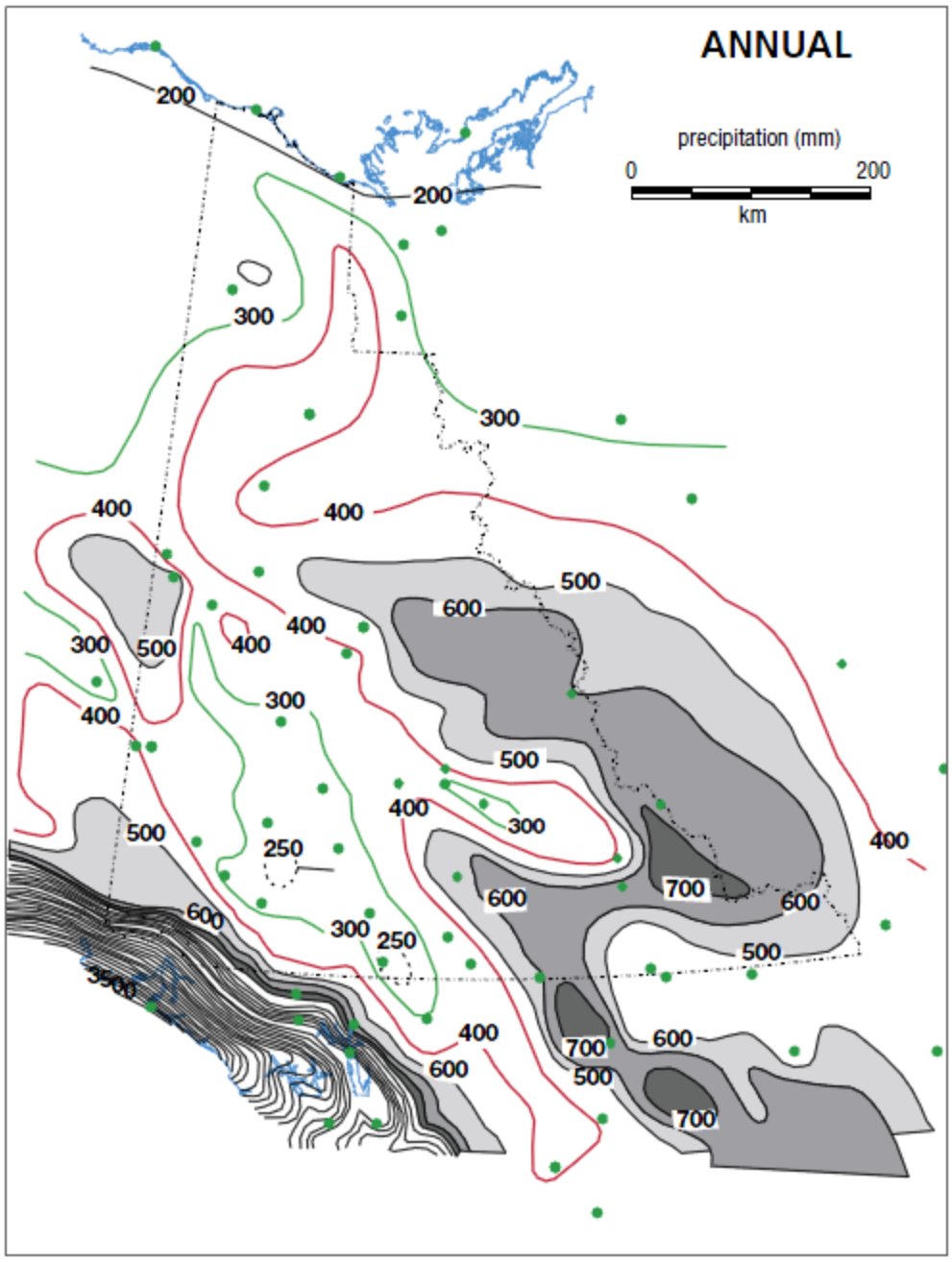

Figure 3.7: Mean total annual precipitation of the Yukon. Annual precipitation on coastal Alaska varies between 2 000 to 2 500 mm, whereas within the Yukon, low elevation valley floors receive only 250 to 300 mm. Over higher barriers within the Yukon, amounts are nearer 400 to 600 mm (adapted from Wahl et al., 1987).

3.5.2 Climate Normals and Recent Trends

MAGT is typically 1 to 6^{o}C warmer than the MAAT in northern Canada (Smith and Riseborough, 1996; Smith et al, 2010). Therefore, the southern limit of permafrost occurs at roughly the -1^{o}C mean annual isotherm (Smith and Riseborough, 1996). Table 3.1 displays the Mean Annual Climate Normals (1971-2000) for five Environment Canada climate stations in settlements along the study area from the southeast to the northwest. The data shown for Haines Junction is for the (1961-1990) time period.

Table 3.1: Mean Annual Climate Normals from 1971-2000 for communities along the study area (Environment Canada, 2012a).

Station *(Yukon Territory)*	**Location** *(Degrees, Minutes)*		**Elevation** *(m)*	**Mean Annual Air Temperature** *(^{o}C)*	**Mean Annual Precipitation** *(mm)*	**Mean Annual Rainfall** *(mm)*	**Mean Annual Snowfall** *(cm)*
	Latitude	**Longitude**					
Whitehorse	60^{o} 42’	135^{o} 04’	706	-0.7	267.4	163.1	145
Otter Falls**	61^{o} 02’	137^{o} 03’	830	-1.4	297.3	189.9	107.4
Haines Junction*	60^{o} 45’	137^{o} 30’	655	-2.9	305.7		
Burwash	61^{o} 22’	139^{o} 03’	806	-3.8	279.7	192.1	106.4
Beaver Creek	62^{o} 24’	140^{o} 52’	648	-5.5	416.3	295.7	123.1

Notes: *1961-1990 Normal; **Record starts in 1980.

Mean annual air temperature (MAAT) decreases along a south-east to north-west transect along the study area with MAAT ranging from -0.7˚C at Whitehorse to -5.5˚C at Beaver Creek (Table 3.1). This can also be observed in Figure 3.8 (Lewkowicz et al., 2012). Mean annual precipitation is the lowest at Whitehorse and the highest at Beaver Creek (Table 3.1) Mean annual rainfall follows the same pattern while Burwash holds the lowest mean annual snowfall and Whitehorse the highest (Table 3.1).

Long-term air temperature records show an evident cooling trend from 1943-1975 for Whitehorse and similar cooling at all other weather stations although their pre-1975 data records are not as complete (Figure 3.9). The Otter Falls climate record starts in 1980. Minimum MAAT were reached in 1975 for all the communities and temperatures have since been on the rise across the study area (Figure 3.9). This regime change slightly precedes the 1976/1977 Pacific Decadal

Oscillation shift from a cool climatic phase to a warm phase (Zhang et al., 1997) (Figure 3.10). The year 1975 also coincides with a La Niña that caused a cooler and snowier winter in most parts of Canada (Philip and Van Oldenborgh, 2006) (Figure 3.11). An in-depth analysis of long-term climate data along the study transect is presented in section 5.1.

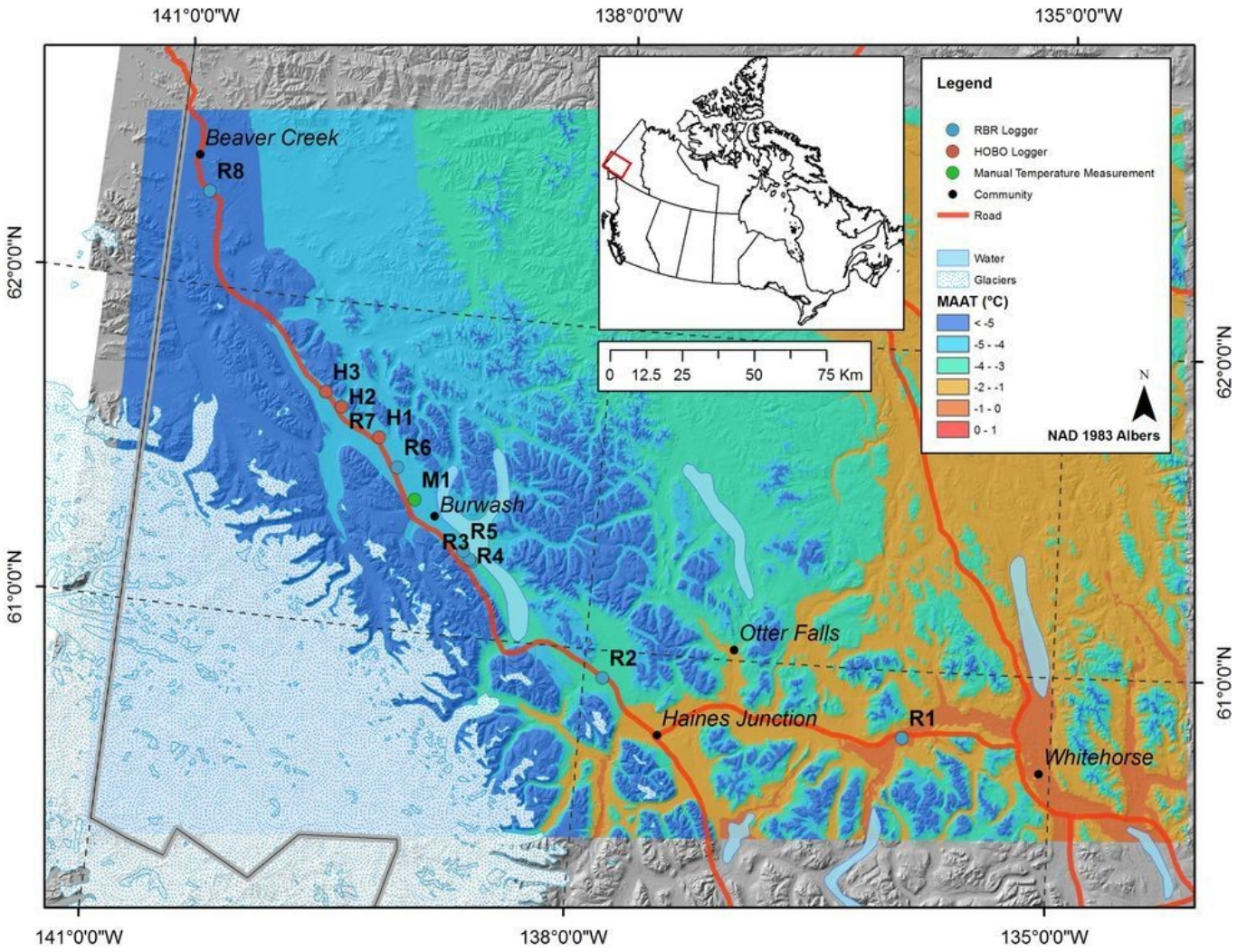

Figure 3.8: Modelled MAATs in the study area (Lewkowicz et al., 2012).

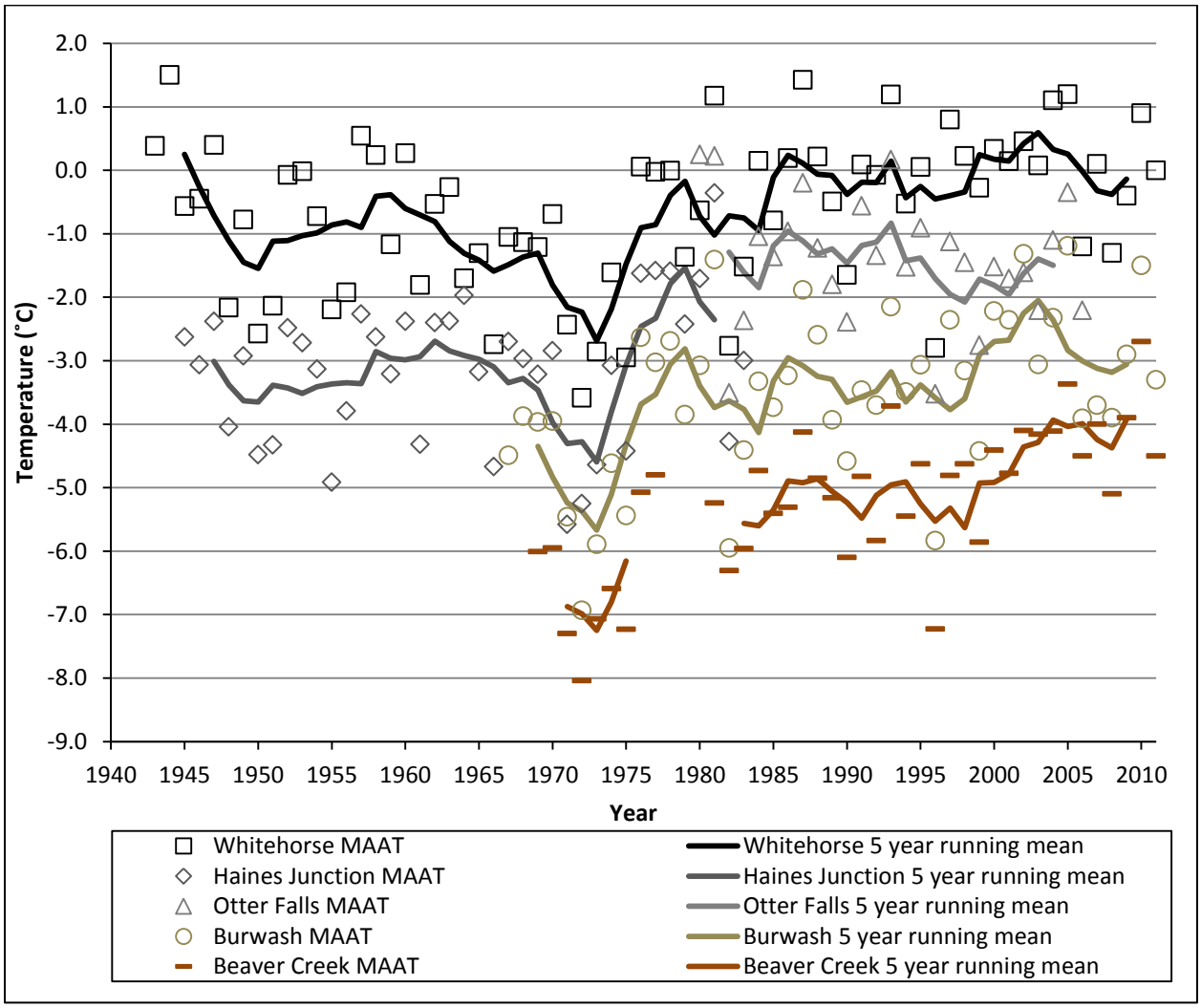

Figure 3.9: MAAT and five year running means for the major communities within the study area (Environment Canada 2012a). Note that many of the Environment Canada climate stations did not have data for the full 1943-2011 observed period.

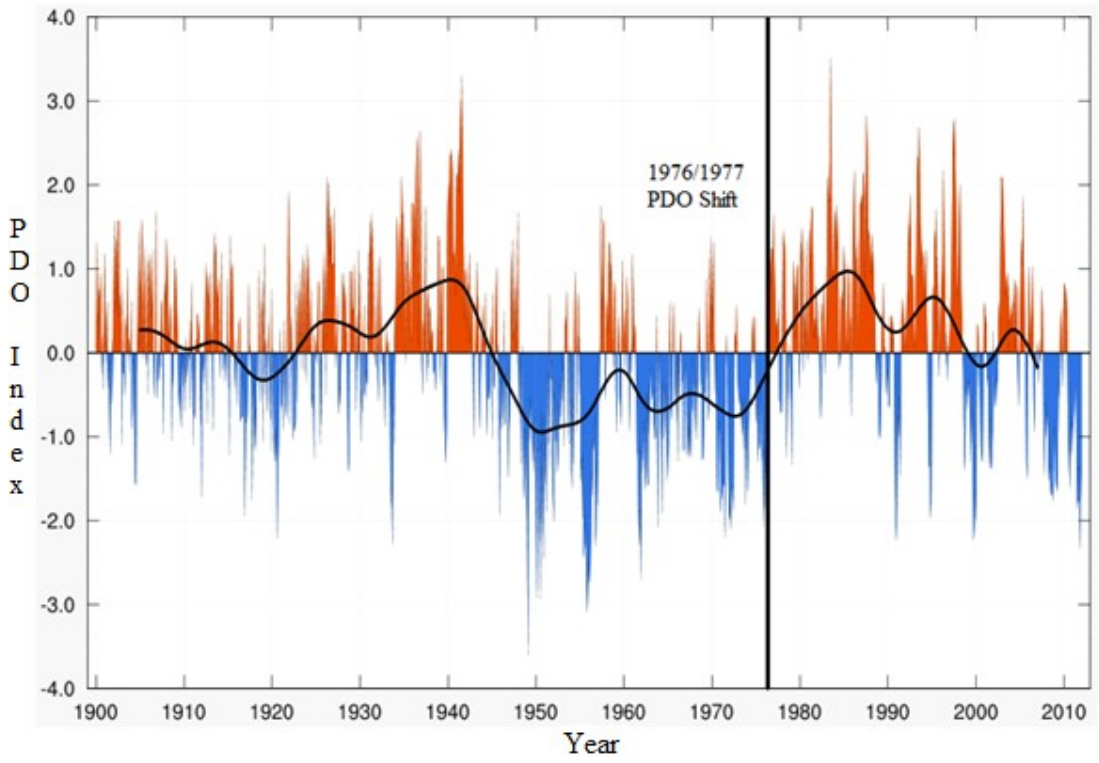

Figure 3.10: Monthly values for the Pacific Decadal Oscillation index, 1900-2011. (Source: PDO Index 2013). Retrieved January 18, 2013 from http://jisao.washington.edu/pdo/PDO.latest

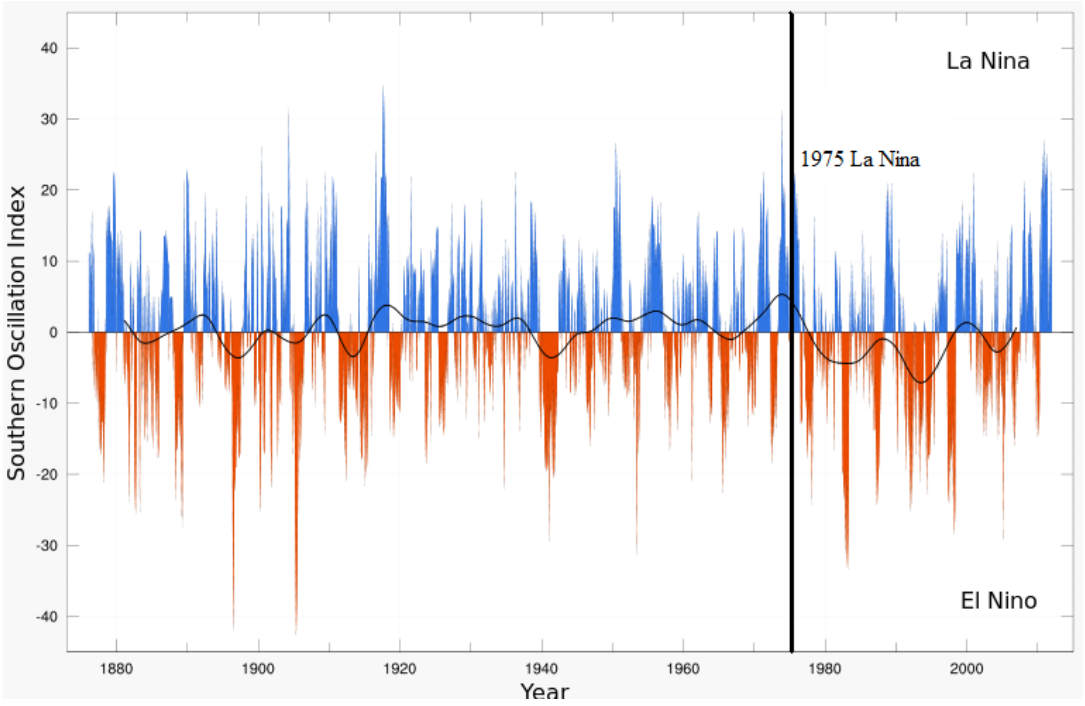

Figure 3.11: Southern Oscillation Index monthly data 1876-2011. Black line: 121 months smooth. (Source: SOI Index 2013). Retrieved January 18, 2013 from http://www.bom.gov.au/climate/current/soihtm1.shtml

3.6 Vegetation

The study area falls within the Boreal Cordillera Ecozone consisting of extensive mountains and valleys separated by wide lowlands (Rowe, 1972; Richie, 1984; Cody, 1996; Environment Canada, 2005). The region is subdivided into three separate ecoregions: the Yukon Southern Lakes, the Ruby Range and the Klondike Plateau (Figure 3.12) (Rowe, 1972; Richie, 1984; Cody, 1996). Each of these regions has similar tree species and vegetation is quite similar along the entire transect because the Alaska Highway corridor generally follows valleys with little variation in elevation.

Common species in the study area include white spruce (*Picea glauca*), black spruce (*Picea mariana*), lodgepole pine (*Pinus contorta*), jack pine (*Pinus banksiana*), aspen (*Populus tremuloides*), balsam poplar (*Polulus balsamifera*), tamarack (*Larix laricina*), paper bich (*Betula papyrifera*), and subalpine fir (*Abies lasiocarpa*) (Rowe, 1972; Richie, 1984; Cody, 1996). Low cover vegetation is mostly consistent throughout the study area with dwarf birch (*Betula nana*) and willow (*Salix spp*.) commonly observed in poorly drained low-lying areas (Rowe, 1972; Richie, 1984; Cody, 1996). Various mosses, lichens, sedges and Labrador Tea (*Rhododendron groenlandicum*) are common ground cover species (Rowe, 1972; Richie, 1984; Cody, 1996). Most sites show signs of vegetation succession after clearings were cut in the 1970s in relation to the proposed pipeline. Forest fires also have a profound impact in the study area, especially near Burwash Landing which burned in 1999. The effects of forest fires on permafrost vary according to the severity of the fire (Stocks et al., 2002). Ground temperatures normally increase due to the loss of vegetation which reduces shade and evaporation (Mackay, 1995; Burn, 2004) as well as a surface albedo reduced by up to 50 % (Yoshikawa et al., 2002).

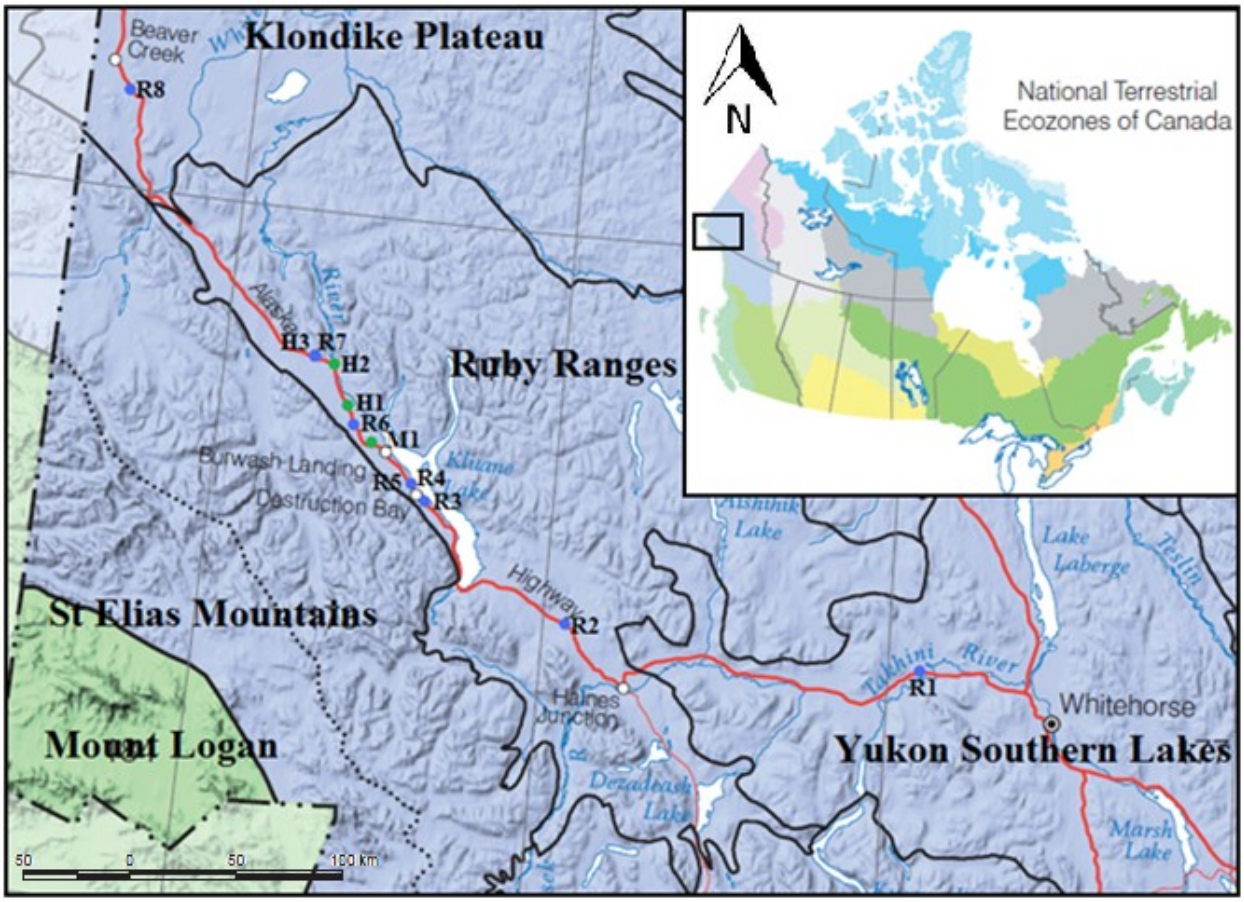

Figure 3.12: Ecoregions of the study area (Source: Ecological Stratification Working Group, 1995).

SECTION 4: METHODOLOGY

4.0 METHODOLOGY

This section contains an overview list of the major steps used to accomplish this research from field site selection, to initial installation of field equipment, execution of field work, and processing of collected data. The sections below outline each of these steps in detail.

The major steps were to:

1. Select boreholes in which the Geological Survey of Canada had previously measured ground temperatures between 1977-1981 (Burgess et al., 1982).
2. Re-locate old boreholes.
3. Rehabilitate boreholes blocked by ice using a custom-made portable steaming rig.
4. Install and maintain RBR temperature monitoring loggers in boreholes > 5 m in depth and install HOBO Micro Stations and perform manual temperature measurements in shallow boreholes (< 5 m).
5. Conduct ERT surveys at each borehole site to examine spatial variability in permafrost conditions and permafrost response to environmental changes such as clearing of the pipeline cut-line.
6. Probe active layer thickness and record vegetation characteristics at each point on each array in order to compare with ERT results.
7. Analyze climate records from communities along the 457 km study transect to permit comparisons of change in permafrost conditions and climate.
8. Install a climate monitoring station at BH R7 due to its considerable distance from standard climate stations.
9. Analyse borehole data in detail and determine the difference between 1977-1981 borehole ground temperatures and same day measurements from 2011-2012.
10. Analyse collected ERT surveys using RES2DINV software in order to determine permafrost boundaries at borehole sites and to complement thermal analysis.
11. Analyse borehole logs to better interpret modeled resistivity inverted results.

4.1 Field Site Selection

Information was compiled from Geological Survey of Canada (GSC) files and thermal data collection including Burgess et al. (1982) regarding boreholes in which the GSC had measured ground temperatures in the 1970s. A prioritized list of boreholes was prepared largely based on ease of access from the Alaska Highway (<500 m from road). Location information was utilized along with visual tools such as Google Earth, Arc Globe GIS and air photos from the National Air Photo Library to pin-point borehole locations and to assess evidence of recent changes in permafrost conditions.

4.2 Field Site Exploration

Site exploration began in May 2011 using a combination of coordinates (UTM, NAD 27) derived from engineering alignment sheets prepared in the 1970s, archived maps, aerial photographs, mile-post information, written descriptions, photos and other information from GSC files and a hand-held Global Positioning System (GPS). Ground searching grids were walked over areas of 200 m^2 that included the stated UTM coordinates as a mid-point in an effort to relocate the boreholes. Clues such as old regrown clearings from the passage of caterpillar (CAT) drilling rigs in the 1970s were also useful in some locations. A total of 22 boreholes were relocated during summer 2011, many of them as far as 150 m from their indicated coordinates. Boreholes were found to have exposed black or white 3" to 3.5" PVC pipes sticking out of the ground by 15 cm to 1.50 m. In most cases, the exposed casing was either damaged or broken.

4.3 Borehole Rehabilitation

Boreholes located in permafrost were found to be blocked by ice and had to be opened by steam using a custom-made portable rig (Figure 4.1). The steaming device was built in the field using a modified 15 L pressure cooker with an adaptation valve installed over the pressure release valve where a clip-on 12 m rubber steam hose could be attached. Water was heated in the pressure cooker to produce steam over a portable propane burner powered by a 20lb BBQ propane tank. A 30 L plastic water jug also had to be carried with all the equipment to sites with no nearby water sources.

Figure 4.1: Custom-made portable steaming rig used to unblock boreholes of ice during 2011.

Once steam was produced, the steam hose was taped to 1.25 m long by 1.5 inch wide connecting metal pipes for weight and to keep the entry straight when it was lowered in to the borehole. In most cases, the average borehole unblocking steaming rate was approximately 1 m/h in a 3" to 3.5" diameter hole. None of the unblocked boreholes were cased all the way down in the 1970s which limited our capacity to re-open them. Many boreholes were found to have collapsed at the end of the casing (<1 m) which made them impossible to steam and unsuitable for temperature measurement. In total, 8 boreholes ranging in depth between 5.00 m and 8.75 m were unblocked by steam and cased with 1.5 m pipe sections of 1.25" ABS plumbing pipes glued together with fitting connectors and capped at the bottom to prevent water leakage. In a few cases, one piece flexible black 1.25" PVC piping was used for borehole casing. The borehole rehabilitation process is shown in Figure 4.2.

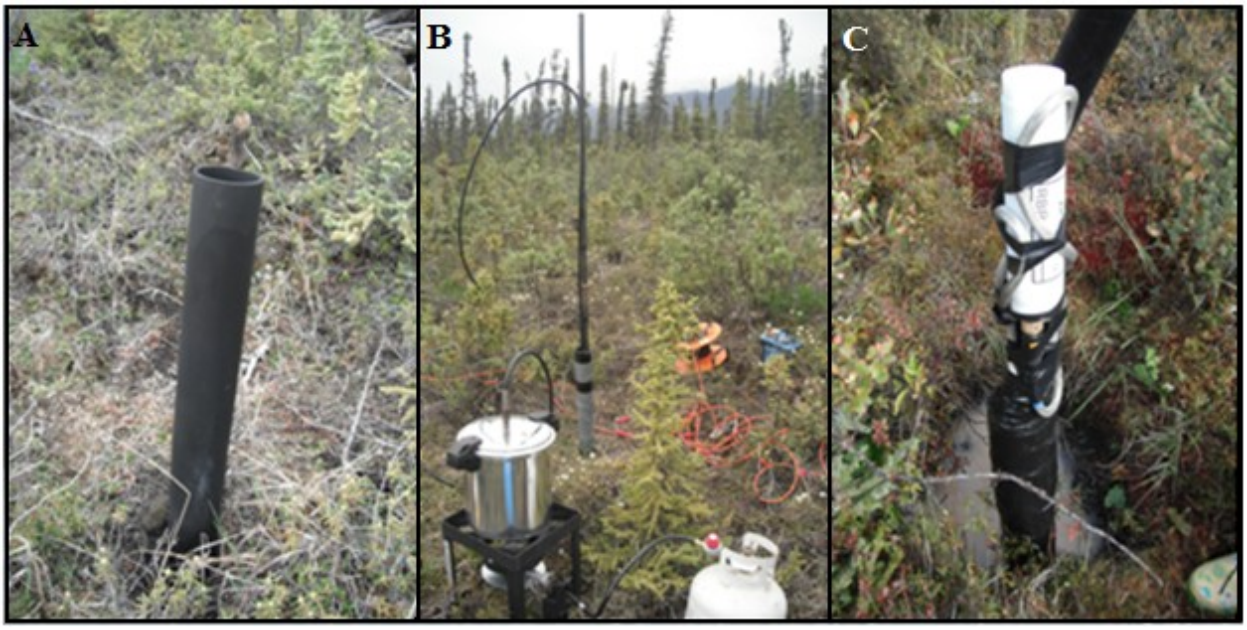

Figure 4.2: Borehole rehabilitation process: (A) 1970s borehole found in good condition; (B) borehole being unblocked with a portable steaming rig; (C) and an RBR data logger is installed for year-round ground temperature collection.

A mix of water-jet drilling (W-J-D) and steaming was used in areas where the borehole had collapsed at depth. Water-jet drilling uses a gas powered pump to pump water through a hose into a 20 mm diameter iron pipe. The heat and pressure of the water causes the pipe to penetrate the ice-rich ground making this method an inexpensive alternative for drilling in permafrost materials (e.g. Lewkowicz et al., 2011). A total of 4 collapsed boreholes were sequentially unblocked to depths of 2.0 m to 3.75 m using a combination of steam and water-jet drilling when a water source was available nearby (<60 m from borehole). These shallow boreholes were then cased and rehabilitated in the same way as the 8 deeper ones. The location of the 12 field sites (Figure 2.1) and related information is provided in Table 4.1. The dates of investigations and fieldwork executed are given in APPENDIX A.

Table 4.1: GPS Coordinates for Study Sites ("R" in the site name refers to deeper borehole sites where RBR loggers were installed, "H" refers to shallow borehole sites where HOBO Micro Station loggers were installed and "M" refers to shallow boreholes where only manual temperature measurements were taken). Boreholes are numbered sequentially from Whitehorse in the south-east to Beaver Creek in the north-west. The borehole unblocking method used, borehole depths and ERT profile information is also shown. The original borehole name is the name of the boreholes when they were first acquired by the GSC (Burgess et al., 1982).

Site Name	Original Borehole Name	Location *(Degrees, Minutes, Seconds)*		ERT profile Length *(m)*	Method Used for Borehole Unblocking	Borehole Depth *(m)*	
		Latitude	Longitude			Old	New
R1	79S-CS-5	60° 47' 31"	135 ° 56' 40"	1x 80	Not blocked	30.25	6.5
R2	78-A-71	60° 54' 50"	137 ° 52' 34"	1x 160	Not blocked	9.2	8.75
R3	78-A-64	61° 14' 17"	138 ° 46' 58"	1x 160	Steam	9.2	6.6
R4	78-A-63	61° 14' 39"	138 ° 47' 44"	1x 160	Steam	5.9	5.0
R5	78-A-62	61° 16' 04"	138 ° 50' 33"	1x160	Steam	9.2	8.0
M1	78-A-57	61° 24' 43"	139 ° 11' 20"	2x 80	Steam	6.55	2.8
R6	78-A-51	61° 30' 24"	139 ° 19' 32"	1x 160	Steam	8.5	5.15
H1	78-A-46	61° 35' 37"	139 ° 27' 46"	2x 80	Steam	9.0	3.0
H2	78-B-25	61° 40' 27"	139 ° 43' 48"	2x 80	W-J-D	6.7	2.0
R7	78-A-40	61° 42' 52"	139 ° 50' 25"	1x 160/1x 40	Steam	8.3	7.0
H3	78-A-39	61° 42' 54"	139 ° 50' 34"	1x 80	Steam	4.5	3.55
R8	78-A-8	62° 17' 31"	140 ° 46' 11"	1x 160	Steam	7.6	7.0

4.4 Borehole Temperature Monitoring

Eight rehabilitated boreholes (R1-R8, Table 4.1) ranging in depth from 5.00 m to 8.75 m were instrumented during the 2011 summer field season for renewed ground temperature collection with a multi-thermistor temperature cable connected to an eight-channel data logger manufactured by RBR Ltd (2009) (ex: Figure 4.3A). The time since drilling disturbance and ground temperature measurements is given in APPENDIX B. The RBR data loggers have a calibrated accuracy of ± 0.002°C and a sampling period of 8 h intervals (RBR, 2009). Thermistor spacing was generally 0.5 m in the upper 2 m with spacing increasing with depth. Logger information and thermistor position for the cable installed at each site is given in APPENDIX C. Depending on borehole depth, some cables had to be cut or folded. The exposed piping and RBR logger at the ground surface were covered with a removable 4" ABS cover for protection which was spray-painted white to increase albedo and lower thermal conduction of heat in the borehole (e.g. Smith et al., 2010; Lewkowicz et al., 2011).

Figure 4.3: Borehole temperature monitoring: (A) RBR logger instrumented borehole; (B) manual resistance borehole measurements; (C) and HOBO Micro Station logger instrumented borehole.

Manual resistance measurements were made during summer 2011 at 4 shallow (2.0 m to 3.75 m) rehabilitated boreholes (M1, H1, H2, H3) with an YSI 44033 Resistance 12 m long cable (ex: Figure 4.3B). One resistance reading (kΩ) was taken per minute for 15 minutes at depth increments of 0.5 m starting at ground surface (depth = 0 m). All recorded resistance measurements were then converted to temperature using a second order polynomial function calibrating the YSI thermistor to an accuracy of ± 0.02^{o}C for -5^{o}C to +7^{o}C. A time series plot was created for each depth increment and temperature was extrapolated to equilibrium (30 minutes) using a logarithmic trend line equation. Manual ground resistivity measurements and temperature conversions and equilibrium forecasting are given in APPENDIX D.

HOBO Micro Station H21-002 loggers were installed at 3 of the 4 shallow boreholes (H1, H2, H3) during the summer 2012 field season for renewed ground temperature monitoring (ex: Figure 4.3C). Each HOBO Micro Station is equipped with 4 HOBO 12-Bit 10 m temperature smart sensors which measure ground temperatures at varying depth increments from the surface (0 m) to the bottom of the borehole. The smart sensors have an accuracy of ± 0.2^{o}C and a sampling period of 4 h intervals (Onset Computer Corporation, 2012). The HOBO Micro Stations were mounted to metal pipes beside the borehole and protected with Tupperware plastic

covers. The exposed cables between the HOBO Micro Station and the borehole are protected by a metal screen.

4.5 Electrical Resistivity Tomography Surveys

ERT surveys were conducted at all twelve sites to better characterize the underlying permafrost bodies. The borehole was used as the mid-point for all ERT profiles. ERT surveys were generally 80 m or 160 m in length (Table 4.1) and roughly parallel to an existing cut-line that was associated with planning of a proposed pipeline in the 1970s. The ERT profiles were run perpendicular to the cut-line and crossed it at sites where it was in close proximity to the borehole in an attempt to evaluate the impacts of removal of the vegetation cover on permafrost conditions. Most surveys were conducted in August 2012 except for surveys conducted at R1, M1, H1, H2 and H3 in June 2011.

ERT surveys were executed with an ABEM Terrameter LS powered by a 12 volt rechargeable car battery using four ABEM Lund cable reels, each 40 m in length. The ABEM Terrameter LS was located at the profile mid-point for all surveys and a Wenner configuration was used in all cases. For 160 m profiles, four cable reels were used with two inner cables at 2 m electrode spacing and two peripheral cables at 4 m electrode spacing. Each cable take-out was attached using jumper cables to the electrodes (12” steel nails) which were inserted in the ground to a depth of 15-25 cm for proper contact. When conducting 80 m profiles, the electrode spacing for the outer two cables was at 2 m intervals while the two inner cables had an electrode spacing of 1 m. Two cables were used for the 40 m profile with 1 m electrode spacing. Figure 4.4 displays the distribution of steel electrodes for the 160 m, 80 m and 40 m profiles as well as the ABEM Geophysical equipment used for the surveys.

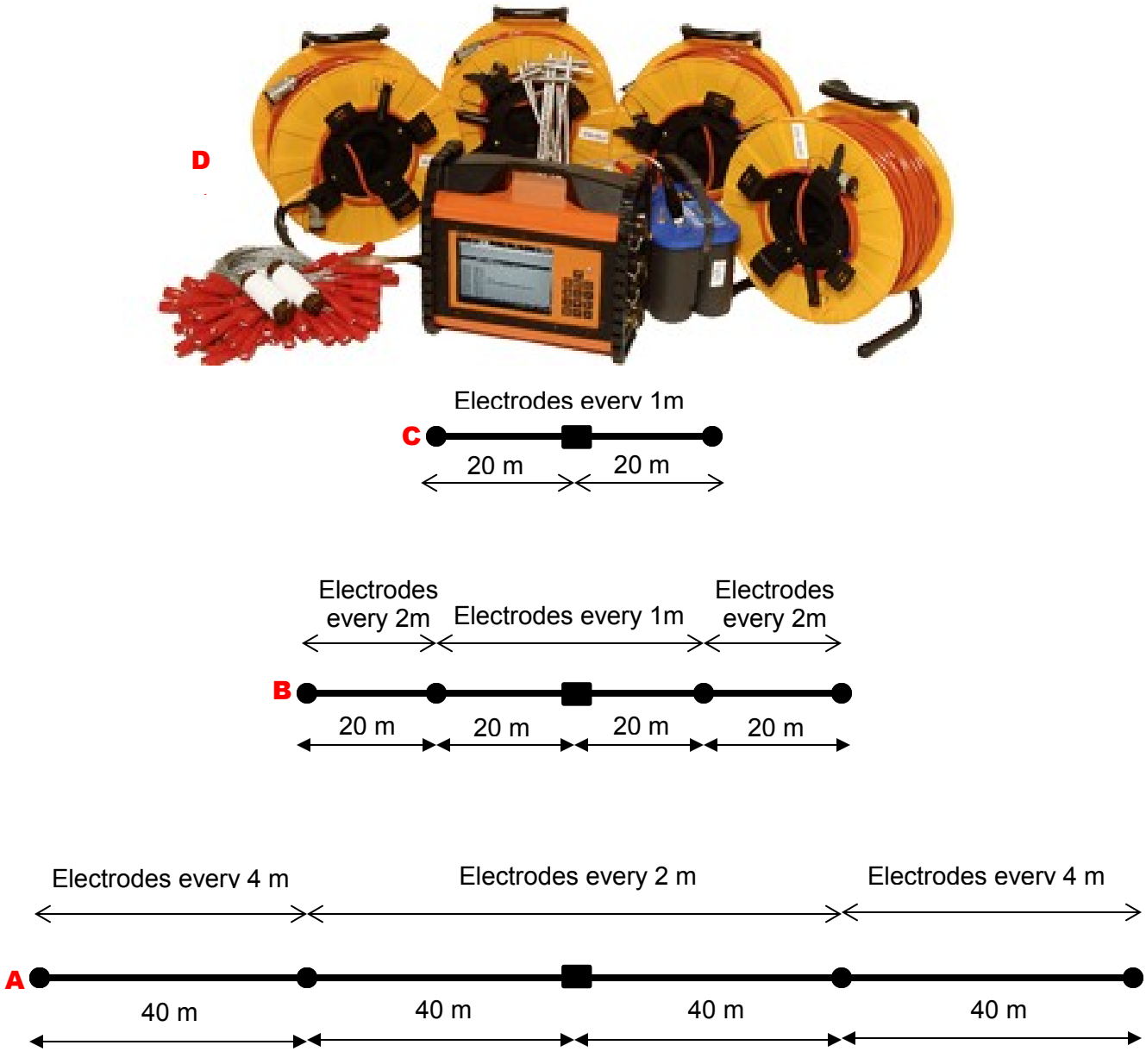

Figure 4.4: The distribution of electrodes for (A) 160 m surveys; (B) 80 m surveys and; (C) 40 m surveys. The rectangle in the middle represents the Terrameter at the mid-point of the profile while the circles represent the cable reels. The ABEM Geophysics equipment is shown in (D) and includes: the ABEM Terrameter LS, the four ABEM Lund cable reels, a 12 V battery, two cable connectors, steel electrodes and jumper cables.

The ERT surveys have maximum ground penetration depths of 25 m for 160 m profiles, 12.5 m for 80 m profiles and 6.5 m for 40 m profiles. The centre of the profile (two inner cables), with a higher distribution of electrodes, yields a higher resolution in the resistivity results.

In order to properly interpret the resistivity results collected at each sites, specific site information such as topography and active layer thickness were also measured. Relief was measured along the profile with an Abney level using the break-of-slope method. Each measurement was taken from a reference point on the field assistant who moved to each break-point in topography along the profile. This information is used during post-processing of the resistivity profiles.

Active layer thickness on the date of the ERT survey was measured manually at each electrode position along the profile using a 1.2 m long, 1 cm diameter titanium frost probe. In unfrozen areas where permafrost could not be identified by probing, the active layer thickness was recorded as > 120 cm. Such conditions or coarser material such as gravel which limited probing depth resulted in inaccuracies in mean active layer thickness estimates along most ERT profiles. Qualitative probing information on sub-surface characteristics such as (gravel, rock, clay, silt, wood) were also recorded. In addition, a detailed compilation of ground surface characteristics and vegetation was made along the ERT profiles. Photographs of all borehole sites and resistivity lines were taken at every stage of the research.

4.6 Climate Station Installation

To address a spatial gap in existing climate information, a climate station was installed at R7 in 2011 to measure air temperature, ground temperature and snow depth (Figure 4.5). Air temperature is measured hourly with the external thermistor of a HOBO Pro-8 logger installed 1.5 m above the ground within a solar radiation shield (accuracy ± 0.2^{o}C; precision 0,03^{o}C) (Onset Computer Corporation, 2012). Shallow ground temperature was measured hourly at depths of 0 cm and 20 cm with external probes from a cylindrical HOBO Pro V2 two-channel data logger with an accuracy of ± 0.2^{o}C and a precision of 0.03^{o}C (Onset Computer Corporation, 2012).

Snow depth is measured by utilizing a series of Thermochron iButton temperature loggers (accuracy ± 1^{o}C, Maxim Integrated Products, 2012) and the method described by Lewkowicz (2008). The iButtons are installed on a wooden stake at 5, 10, 20, 30, 40, 50, 60, 80 and 100 cm above ground surface. The snow depths at different times of year were inferred by analysing the temperature patterns at each height since there is a significant difference in temperatures above and within the snow pack.

Figure 4.5: Climate station installed at Borehole R7 during summer 2011. Note the white radiation shield for the air temperature thermistor.

4.7 Long Term Climate Data in the Study Area

Data collected from five Environment Canada climate stations located in communities along the study transect, were utilized to characterize the long-term climate conditions in the region. From the south-east to the north-west, these stations include; Whitehorse, Haines Junction, Otter Falls, Burwash Landing and Beaver Creek. Unfortunately, not all stations had complete records covering the period from the 1970s to the present. MAATs, TDDa, FDDa, total annual rainfall, total annual snowfall and total annual precipitation were examined and temporal trends were subjected to significance testing at a confidence level of 95%. Significance test results are given in APPENDIX E. The analysis of the climate series is split at 1975 due to a regime change in climate observed throughout the study area (refer to Section 3.5.2). Graphs are presented with 5-year running means and linear regressions for statistically significant trends.

4.8 Ground Temperature Analysis at Boreholes R1-R8

Ground temperature data are obtained from the RBR loggers in August 2012. For most sites, an almost complete one-year record of ground temperature is available. The specific dates of the annual record and the depth of the thermistors vary at each borehole site. This information as well as a summary of all the data used in the analysis of the boreholes is given in summary tables for each study site in Section 5. At BH R4, the equipment was damaged by a bear 12 days after installation and the logger at BH R8 did not properly operate so annual data records are unavailable for these sites. However, some useable data was recuperated from the loggers. In the earlier portion of some data records, ground temperatures may not have stabilized after borehole steaming, and these were not included in the analysis. All recognizable erroneous data were removed from the datasets before analysis began (e.g. missing values and obvious logger malfunction.

Ground temperatures measured manually with mutithermistor cables on different dates between 1979-1981 (Burgess et al., 1982) were used to estimate the precision of the original measurements (Table 4.2). The measurements were taken at the same increments below the D_{ZAA} at boreholes 79S-CS-5 (R1) and 79-CS-6 (Foothills CS-3) because these should not vary. Borehole 79-CS-6 is located within the study area and was re-located during field investigations in summer 2011 but could not be rehabilitated. The maximum range was 0.44˚C with an average

of 0.17˚C at borehole 79S-CS-5 (R1) and 0.33˚C with an average of 0.15˚C at borehole 79-CS-6 (Foothills CS-3). The maximum range or potential error for both sites is 0.44˚C with an average range of 0.16˚C and more than 50 % of the ranges being < 0.2˚C.

Table 4.2: Range of 1979-1981 manual ground temperature measurements below the depth of zero annual amplitude (D_{ZAA}).

Borehole 79S-CS-5 (R1)				
Depth (m)	Temperature (˚C) 26/10/1979	Temperature (˚C) 01/02/1980	Temperature (˚C) 28/04/1980	Temperature Range (˚C)
11.3	1.53	1.54	1.51	0.03
12.83	1.57	1.31	1.41	0.26
14.36	1.60	1.39	1.48	0.21
15.88	1.54	1.51	1.52	0.03
18.93	1.62	1.18	1.41	0.44
21.98	1.7	1.68	1.68	0.02
25.03	1.66	1.32	1.49	0.34
28.07	1.87	1.84	1.85	0.03
				$\bar{x}$ = 0.17

Borehole 78-CS-6 (Foothills CS-3)							
Depth (m)	T(˚C) 26/10/1979	T(˚C) 01/02/1980	T(˚C) 28/04/1980	T(˚C) 07/08/1980	T(˚C) 14/02/1981	T(˚C) 02/08/1981	T(˚C) Range
12.4	0.53	0.50	0.50	0.50	0.44	0.53	0.09
14.0	0.66	0.64	0.63	0.63	0.56	0.65	0.10
15.5	0.80	0.74	0.72	0.72	0.69	0.68	0.12
17.0	0.95	0.93	0.92	0.93	0.83	0.94	0.12
18.5	1.03	0.99	0.96	0.93	0.89	0.70	0.33
							$\bar{x}$ = 0.15

4.8.1 Annual Ground Temperature Cycle

Annual ground temperature records are available for 6 of the 8 RBR logger instrumented boreholes. Ground temperatures were measured at various depth increments and graphed over a one year period for each site. Efforts were made to measure ground surface temperatures at each site but this was not achieved in most cases as the priority was to reach the greatest possible depth with the thermistor cables. Records were individually analyzed to determine annual variability, time lag of temperature waves with depth and zero-curtain effects. The time lag of the freezing waves were accurately measured for each thermistor depth below surface by

calculating the number of days it takes for the temperature wave to propagate to depth (z). This was made by analysis of the raw annual data series in Microsoft Excel.

Zero-curtain effects for the freezing and thawing periods were calculated in Microsoft Excel by counting the number of days where ground temperatures were between 0.1˚C and -0.1˚C for a specific depth. Sites with long zero-curtain effects were interpreted as having high unfrozen moisture content resulting in the release of large amounts of latent heat to satisfy the thermal gradient and thermal conductivity (French, 2007).

4.8.2 Mean Monthly Ground Temperatures

Mean monthly ground temperatures were calculated for September 2011 to August 2012 and graphed for each site. The complete record for August 2012 was not available due to the timing of data collection. The August record was completed by utilizing data from August 2011. Mean monthly ground temperatures for August and September were in some cases affected by drilling at sites where borehole monitoring started before post-steaming ground temperature stabilization. The maximum and minimum mean monthly ground temperatures were determined for the shallowest and deepest thermistors.

4.8.3 Temperature Envelopes

Maximum and minimum temperatures for each measurement depth were determined at each borehole from the annual ground temperature record. Ground temperatures that had not yet stabilized following steaming were not included in the calculations. MAGTs were calculated from the raw data by averaging the daily temperature values at each depth for the entire year. The minimum, maximum and mean annual temperatures were then plotted to produce ground temperature envelopes (or trumpet curves). The annual temperature range for each depth was determined by calculating the difference between the maximum and minimum temperatures. The MAGT values plotted on this graph reveal the characteristics of the thermal profile. Negative MAGTs with depth were used to determine the occurrence of permafrost at borehole sites.

The D_{ZAA} was calculated by interpolating between the first MAGT that showed < 0.1˚C variations with its respective depth on the temperature envelope. The temperature at the D_{ZAA} was indicated for each site having a D_{ZAA} shallower than the borehole. The entire thermal year

was in most cases not encompassed in the annual record as the time between the maximum and minimum of the temperature waves was mostly longer than a single 12 month period. This made the mathematical calculation of deeper D_{ZAA} unreliable as the period of the annual ground temperature waves could not be precisely assessed. Thermal diffusivity calculations using Eq. 7 were also unreliable due to the ground temperature waves not being perfectly sinusoidal because of unfrozen moisture present in permafrost soils with MAGTs near 0˚C (Williams and Smith, 1989; French, 2007). This meant that original plans to calculate the amplitude, phase lags and permafrost depths could not be carried out (Williams and Smith, 1989).

The active layer thickness was determined by interpolating (assuming a linear gradiant) between the two depths where the maximum temperatures bracket 0˚C (Nelson and Hinkel, 2003; Throop et al., 2012). TTOP was calculated by interpolating between the MAGTs at these depths.

The surface offset and thermal offset were only calculated at sites where MAGSTs were available. The surface offset was calculated by subtracting the MAAT from the MAGST of the same year (Smith and Riseborough, 2002). The MAAT of the closest Environment Canada climate station was used in the calculation. BH R1 was located approximately mid-way between two ECCS so the average MAAT between the two stations was used. Positive values of the surface offset indicate that the ground surface is warmer than the air while negative values of the surface offset indicate the opposite (Smith and Riseborough, 2002). The thermal offset was calculated by subtracting the MAGST from the TTOP (Romanovsky and Osterkamp, 1995; Smith and Riseborough, 2002). The thermal offset is normally represented as a negative value, as the ground usually cools with depth within the active layer (Smith and Riseborough, 2002).

4.8.4 Ground Surface Climate interactions (BH R7)

Site-specific air temperature, ground surface temperature and snow depth were measured at the BH R7 climate station. The MAAT was calculated using hourly air temperatures measured on-site between August 15, 2011 and June 12, 2012. Daily air temperatures from the Beaver Creek ECCS between June 13, 2012 and August 15, 2012 were used the complete the air temperature record for MAAT calculation. The correlation coefficient between the two climate

stations for the available corresponding period is 0.85. Snow depths were inferred from ibutton measurements (refer to Section 4.6).

Snow depths were plotted against air and ground surface temperatures to investigate the lag between air and ground surface temperature changes, and to examine the effect that the timing of the snow's arrival and departure had on the length of the zero-curtain. Snow days were calculated by counting the number of days where snow was present on the ground. Snow depth days (SDD) were calculated by adding together each daily snow depth value through the season, taking into account both the depth and duration of snow accumulation (Karunaratne and Burn, 2003). TDD and FDD were calculated for both the air and the ground surface (refer to Section 2.4.2). N-factors for the thawing and freezing seasons were calculated using Eq. (2) and Eq. (3) respectively.

4.8.5 Multi-decadal Ground Temperature Differences

The analysis of multi-decadal ground temperature differences is an important part of this thesis as it reflects the effects of recent climate change and environmental change on the permafrost thermal regime in the study area. Ground temperature measurements made by the GSC between 1977 and 1981 (Burgess et al., 1982) were compared with same day temperatures acquired in 2011-2012. The original temperature logs collected by the GSC (Burgess et al., 1982) at boreholes R1-R8 and M1-H3 are given in APPENDIX F and APPENDIX G respectively. The multi-thermistor probes used by the GSC between 1977 and 1981 for manual temperature measurements were in general accurate to 0.2˚C (e.g. BH R1) while the single thermistor probes used at all the other boreholes is accurate to 0.01˚C (Burgess et al., 1982), comparable to that of the new equipment installed in the boreholes. The relative precision of the earlier GSC measurements varied from 0.03˚C – 0.44˚C with an average precision of 0.16˚C (refer to Section 4.8).

Long term statistically significant variations in MAAT and precipitation at the closest ECCS were used to partially explain the observed multi-decadal ground temperature differences. Variations in TDD and FDD for the immediate thawing and freezing season preceding the 1977-1981 and 2011-2012 ground temperature measurements were also analyzed to account for the effects of seasonal variations between both periods. TDD and FDD could not be analysed for

each site to due missing data at some ECCS. Site specific environmental change such as vegetation clearing for initial site access or geotechnical investigations in the 1970s was also examined and taken into consideration when trying to explain the causes of multi-decadal ground temperature differences.

4.9 Ground Temperature Analysis at Boreholes M1 and H1-H3

Manual resistance measurements were made during summer 2011 at 4 shallow (2.0 m to 3.75 m) rehabilitated boreholes (M1, H1, H2, H3) with an YSI 44033 Resistance 12 m long cable and converted to equilibrium temperatures as described in Section 4.4. Multi-decadal ground temperature differences were analyzed at BH H2 and H3 by comparing manual temperature measurement from August 2011 with manual temperature logs from November 1978. Variations in ground temperatures were explained using the same methodology explained in Section 4.8.5. 1970s temperature logs were not available for BH M1 and H1.

HOBO Micro Station H21-002 loggers were installed at 3 of the 4 shallow boreholes (H1, H2, H3) during the summer 2012 field season for renewed ground temperature monitoring as described in Section 4.4. Live readings were taken a day after installation in August 2012 to complement the 2011 temperature logs and the further help with the interpretation of ERT surveys.

4.10 Resistivity Post-Processing

In order to have consistent and accurate ERT data throughout the study area, each data set underwent the same post-processing procedures. The same ERT acquirement settings were also used in the field for each survey (APPENDIX H). Before inverting the data, "apparent" resistivity values for each survey were examined for bad data points which were eliminated (see Section 2.8.4). Due to the presence of permafrost bodies, sharp boundaries were expected within each survey which called for the use of the robust or blocky inversion method.

Each inversion went through multiple iterations (never more than 5 to avoid over-filtering) which resulted in progressively smaller root mean squared error (RMSE) errors. The inversions had to be run several times before satisfactory results were achieved, corresponding to an RMSE error <5%. Although the RMSE can continue to decrease after the 5th iteration, ERT

data is typically most accurate between 3-5 iterations (Hilbich et al., 2008). This is due to the fact that over fitting of the data can occur when using more than five iterations, leading to an increase in the maximum resistivity value within a profile (Hauck and Vonder Muhll, 2003).

Once the inversions were completed, with a corresponding RMS error <5% using the least-square inversion routine, the display settings were changed. The vertical display factor was set to 1.00 and a linear depth scale was used with logarithmic contour intervals. The same display setting parameters were used for each data set to ensure comparability.

Topography was taken into account during the inversion process for all study sites with noticeable relief. Topography was calculated using simple trigonometry from the Abney level break-of-slope measurements collected in the field. The calculated coordinates were added to the original DAT files before the inversion process.

The measured apparent resistivity pseudosection, calculated apparent resistivity pseudosection and inverse model resistivity pseudosection is given for each site in APPENDIX I for boreholes R1-R8 and in APPENDIX J for boreholes M1 and H1-H3.

Resistivity values for different earth materials (Table 2.1: Hauck and Kneisel, 2008) and ground ice content determined from geotechnical boreholes (from the 1970s) were used to better interpret the inverted ERT results. The full borehole logs used in the analysis include detailed soil descriptions and ground ice characteristics and are given in APPENDIX K. Ground temperatures acquired on the same day as the ERT survey at the centre point of each profile were also used to better characterize permafrost conditions. Active layer thicknesses were inferred from manual frost probe measurements at every electrode along the survey line (refer to Section 4.5). Intra-survey active layer variations were determined by the standard deviation of the measurements sample size.

Permafrost bodies and frozen/unfrozen interfaces were delineated by examining the resistivity gradients of each inverted model. The transition between unfrozen/frozen interfaces occurs around 500-900 Ohm-m at surveyed borehole sites in the study area based on the ERT results, probing and borehole temperatures (see Figure 6.4). This is similar to other results obtained in southwest Yukon (e.g. Lewkowicz et al., 2011; Miceli, 2012). Resistivity values in the 400-500 Ohm-m range were in most cases classified as ‘indeterminate’ ground by Miceli

(2012), meaning that this range of resistivities was unable to be identified conclusively as unfrozen or frozen (Figure 4.6). This 'indeterminate' range was found to be slightly lower than ERT results obtained for this thesis.

Finally, after analysing borehole ground temperatures and ERT inverted results, each study site was inferred to be in a one, two or three-layered state (Figure 4.7) (Sartorelli and French, 1982). In a one-layered state, the ground is unfrozen to the deepest effective exploration depth. A two-layered state means that permafrost is present under a thawed active layer to the deepest effective exploration depth. A three-layered system implies thin permafrost whose base falls within the depth of exploration. The lower boundary is based on the effective exploration depth and does not necessarily represent the base of permafrost.

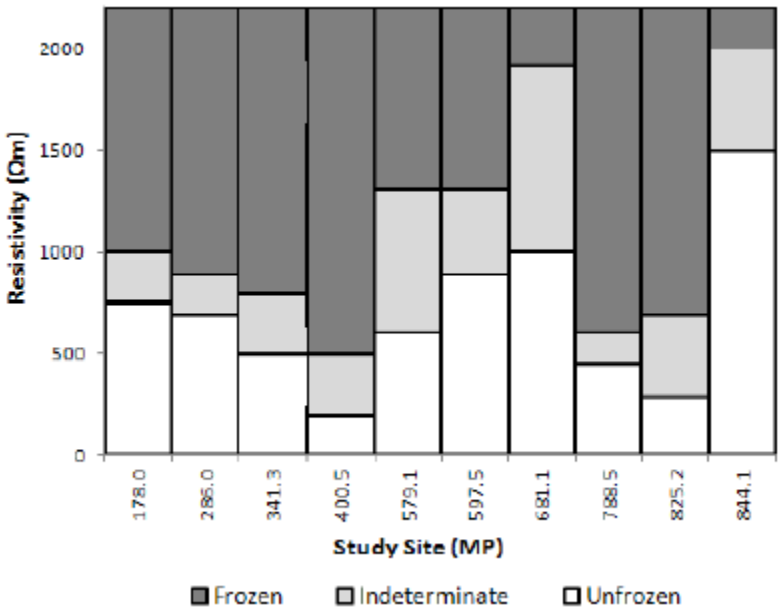

Figure 4.6: A bar graph displaying the upper and lower limits of each ERT classification from ten monitoring sites along the Alaska Highway Corridor from Whitehorse, YT to Fort Nelson, BC. Intermediate resistivity values were unable to be identified conclusively as unfrozen of frozen. (*from* Miceli, 2012).

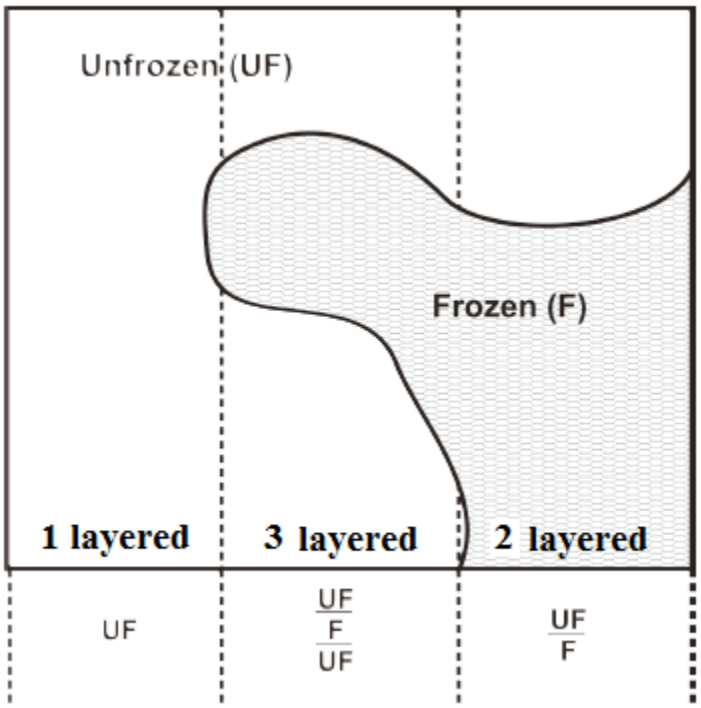

Figure 4.7: Model of layered terrain in summer (*modified* from Sartorelli and French, 1982).

SECTION 5: RESULTS

5.0 RESULTS

This section presents the results from the examination of each of the twelve study sites as well as analysis of past geotechnical and climatic data available along the study area. The results are presented in three main subsections:

1) Long term Climate Data in the Study Area
2) RBR Instrumented Boreholes
3) HOBO Instrumented Boreholes

The first section (5.1 Long term Climate Data in the Study Area) is a more detailed analysis of the long-term climate data from Environment Canada climate stations from five communities along the Alaska Highway from Whitehorse to Beaver Creek. In this section, the MAAT, TDDs, FDDs, total annual rainfall, total annual snowfall and total annual precipitation are examined and subjected to significance testing at a confidence level of 95%. Graphs are presented with 5-year running means and linear regressions for statistically significant trends.

The second section (5.2 RBR Instrumented Boreholes) is an in-depth intra-site analysis of all 8 borehole sites where RBR loggers were installed in summer 2011 (R-Boreholes) from R1 in the south-east to R8 in the north-west of the study transect. The results are presented for each site beginning with a site description which includes vegetation type, topography and an overview figure of the site before and after it was rehabilitated. A summary table presents important field work associated with each borehole and pertinent information used in the analysis. Next, soil type and ground ice descriptions from the 1978 geotechnical drilling program borehole logs are examined to complement the ERT surveys. ERT surveys were done at each site and are ether 160 m, 80 m or 40 m in length. The goal of the ERT surveys is to better characterise the underlying permafrost bodies horizontally and vertically in 2-dimensions. Frost probing results and borehole temperatures from the day of the survey also help in the interpretation. Thirdly, the thermal conditions within the permafrost are examined using full year ground temperature records, monthly average ground temperature envelopes, maximum/minimum/mean temperature envelopes, time lags, the temperature and depth of the ZAA and the thickness of the permafrost. The surface and thermal offset are determined at sites where the MAGST is available. The relationship between temperatures in the air and at the ground surface is examined at BH R7

through the on-site characteristics of snow, the surface offset and its controls, and the n-factors relating to the FDD and TDD of the air and the ground surface. Lastly, multi-decadal ground temperature differences are determined through comparison of manual temperature measurements taken between 1978-1981 by the GSC and same-date measurements from 2011 or 2012 extracted from the RBR logger record.

The third and last section (5.3 HOBO Instrumented boreholes) is an analysis of manual temperature measurements and HOBO Micro Station logger live readings taken at 4 shallower borehole sites (M1, H1, H2, H3). The results are presented in the same format as the previous section but only include single borehole measurement in 2011 and in 2012. Manual temperature profiles from 1978 were available for BH H2 and BH H3 for multi-decadal comparison with the recent ground temperature logs. Two 80 m ERT cross section surveys are presented for every borehole (except borehole H3 where only one 80 m ERT survey was performed) to better interpret vertical and horizontal permafrost distribution and characteristics.

5.1 Long term Climate Data in the Study Area

In order to examine whether ground temperature increases and apparent active layer deepening in the study area might have resulted from decadal to centennial-scale climate change, the available climate data series from five Environment Canada climate stations in communities along the study transect, were examined. From south-east to north-west, these stations were; Whitehorse, Haines Junction, Otter Falls, Burwash Landing and Beaver Creek. Unfortunately, not all records are complete. The MAATs in the study area follow a cooling trend from 1943 to 1975 followed by a warming trend to present day (refer to Section 3.5.2). The early manual temperature measurements by the GSC were recorded between 1977 and 1981 immediately following the abrupt step change increase in MAAT was observed across the study area (Figure 5.1).

MAATs were chosen for analysis because permafrost is a climatically controlled phenomenon, and is impacted by long-term changes in air temperature (ACIA, 2005; Smith and Riseborough, 2002). TDDa and FDDa were calculated for stations with available daily temperatures to examine temperature ranges and change through a seasonal perspective. The rate and the response of the ground temperature to changes in air temperatures is also directly affected by precipitation which impacts ground thermal conductivity, the surface offset, and active layer freezing and thawing time (Smith and Burgess, 1999). Variations in rainfall or snowfall are also highly relevant to ground temperature and the thermal regime. An increase in rainfall can result in active layer thickening while an increase in snowfall results in a buffering low conductivity insulating layer which lessens the impact of rising air temperatures in the winter (Smith and Burgess, 1999). Figures 5.1 to 5.4 show the climate data for the five stations. The significance test results are summarized in table 5.1, and appear in more detail in Appendix E.

Table 5.1: Slope coefficients resulting from the regression analysis of various climate data from weather stations in the study area (Environment Canada, 2012). Bolded values are statistically significant at a 95% confidence level. Refer to Appendix E for statistical test results.

Measured	Whitehorse		Haines Junction		
parameters	1943-1975	1976-2011	1945-1975	1993-2011	1993-2006
MAAT	**-0.066**	0.017	-0.029	0.010	N/A
TDDa	**-6.747**	2.367	0.920	N/A	N/A
FDDa	**18.530**	-1.490	6.310	N/A	N/A
Rainfall	0.277	0.711	-0.325	N/A	0.937
Snowfall	**1.447**	-0.102	1.131	N/A	-2.687
Precipitation	0.392	0.857	0.229	N/A	-0.893

Measured	Otter Falls	Burwash Landing	
parameters	1980-2006	1976-2011	1976-2007
MAAT	-0.025	0.019	N/A
TDDa	N/A	N/A	2.289
FDDa	N/A	N/A	-0.219
Rainfall	-0.068	N/A	0.372
Snowfall	-0.768	N/A	0.575
Precipitation	-0.650	N/A	0.225

Measured	Beaver Creek	
parameters	1980-2011	1981-2006
MAAT	**0.057**	N/A
TDDa	N/A	N/A
FDDa	N/A	N/A
Rainfall	N/A	1.857
Snowfall	N/A	-0.817
Precipitation	N/A	0.897

Note: Statistical testing of the pre-1975 climate data at Burwash Landing and Beaver Creek was not conducted due to the record being too short.

5.1.1 MAAT

MAAT varies spatially throughout the study area, with MAAT decreasing from Whitehorse to Beaver Creek (Figure 5.1A). The MAAT data recorded at Environment Canada climate stations in the study area also show a trend of declining MAATs from 1943 to 1975 for Whitehorse and a similar but weaker trend at Haines Junction, in part because the warm years of 1943 and 1944 are missing for the latter. The short records for Burwash Landing and Beaver Creek show the same pattern in the brief record prior to 1975 (Figure 5.1A). MAATs in the study area experienced an abrupt trend change in 1975 from a decreasing MAAT trend to an increasing MAAT trend (Figure 5.1A). Missing data for Otter Falls prior to 1980 make it impossible to determine if a similar trend shift also occurred (Figure 5.1A). The step-like rise in MAAT between 1975 and 1976 caused an abrupt MAAT increase of 3.1˚C in Whitehorse, 2.8˚C in Haines Junction and Burwash Landing, and 2.1˚C in Beaver Creek (Figure 5.1A). MAAT remained mainly stable afterwards between 1976 and 1978 with a variation of 0.1˚C in Whitehorse, 0.2˚C in Haines Junction and 0.3˚C in Burwash Landing (Figure 5.1A). Data is missing between 1978 and 1980 at Beaver Creek for comparison. Observable variation resumed after 1978 and a stable slight warming trend establishes afterwards (Figure 5.1A).

Whitehorse and Beaver Creek were the only ECCS to show statistically significant trends (Table 5.1 and Figure 5.1A). A statistically significant cooling trend of -0.66˚C/decade was observed in Whitehorse from 1943 to 1975 and a statistically significant warming trend of 0.57˚C/decade was observed in Beaver Creek between 1980 and 2011 (Figure 5.1A). Although not statistically significant, MAATs warmed by 0.6˚C and 0.18˚C in Whitehorse and Haines Junction respectively between 1976-2011 and by 0.67˚C in Burwash Landing between 1993-2011 (Figure 5.1A). MAATs cooled by -0.87˚C in Haines Junction between 1945-1975 and by -0.65˚C in Otter Falls between 1980-2006 (Figure 5.1A).

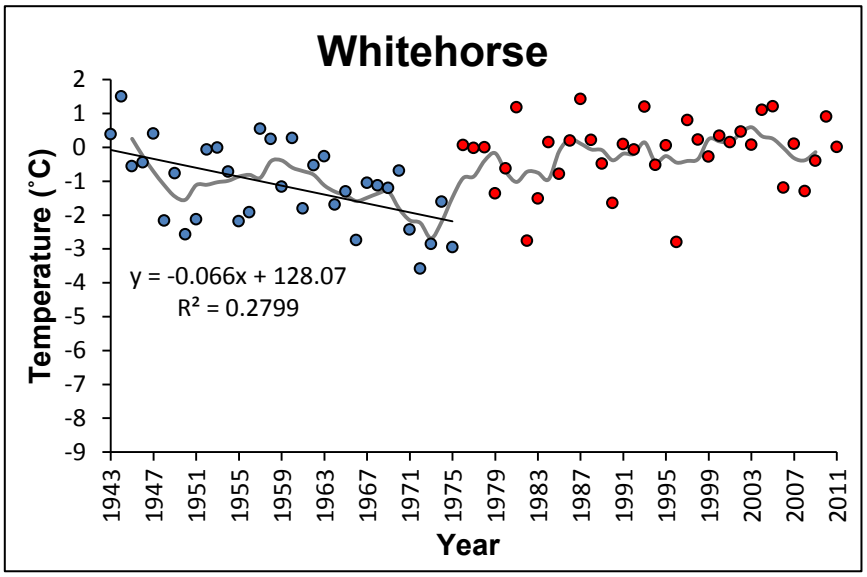
Whitehorse
Temperature (°C)
Year
y = -0.066x + 128.07
R² = 0.2799

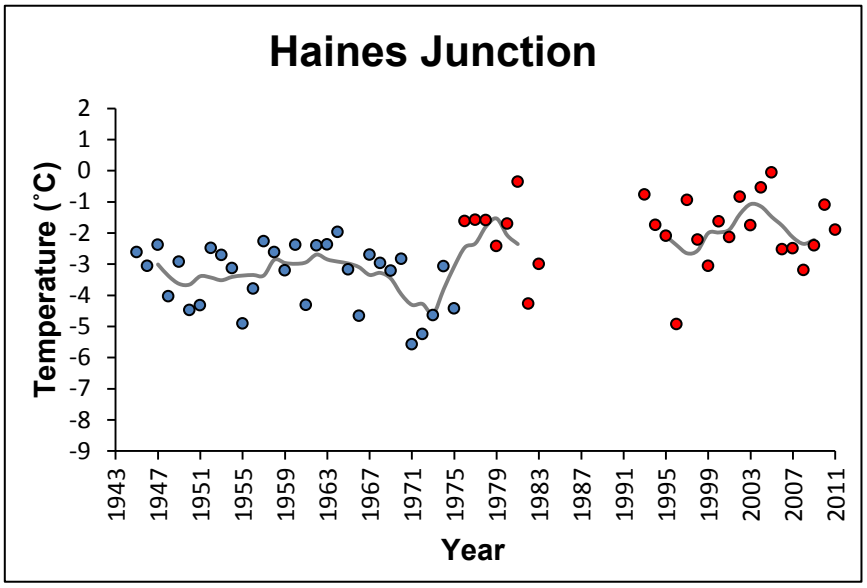
Haines Junction
Temperature (°C)
Year

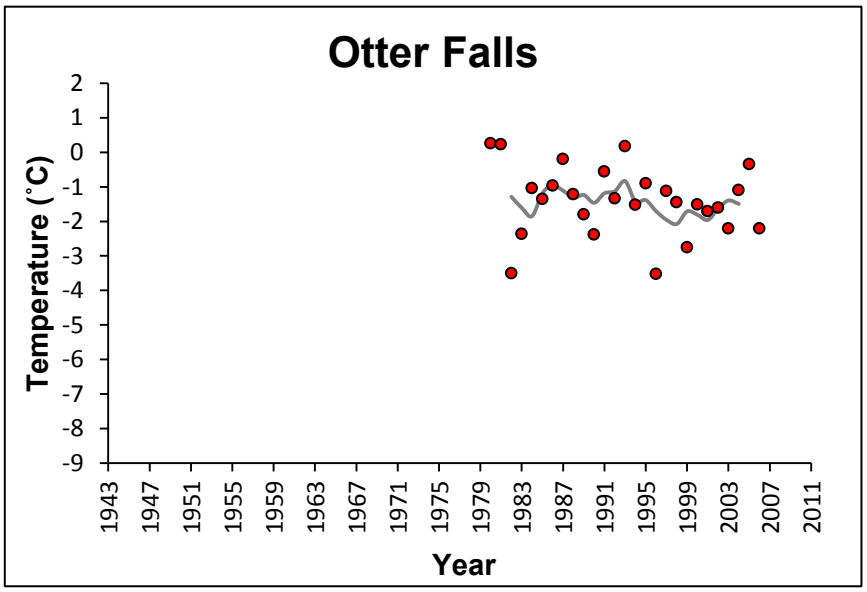
Otter Falls
Temperature (°C)
Year

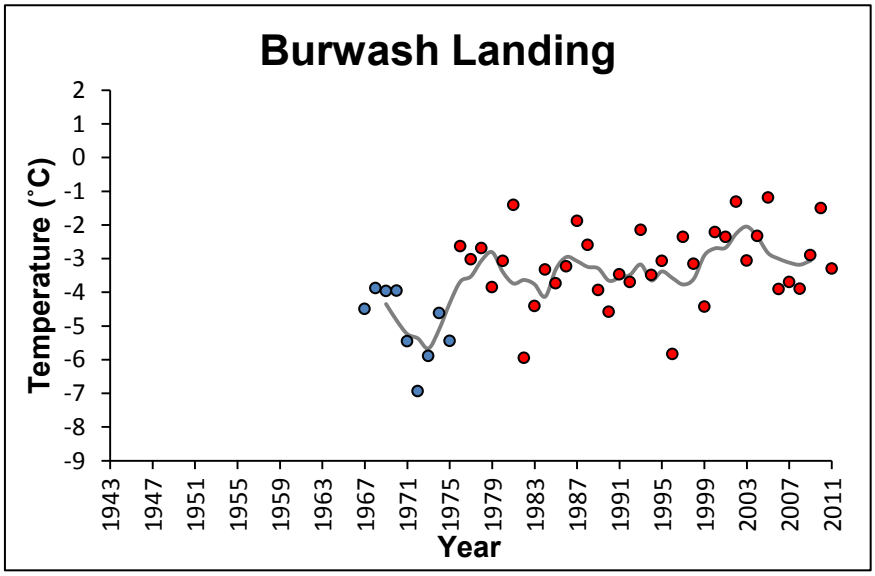

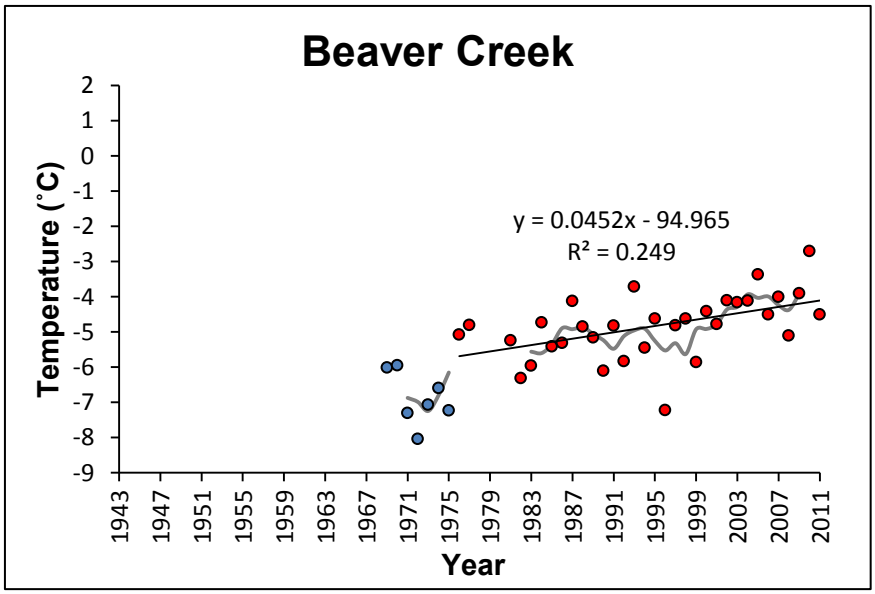

Figure 5.1A: Historical MAATs (ºC) from Environment Canada climate stations in the study area (Environment Canada, 2012). The blue markers are the available MAAT data between 1943 and 1975 while the red markers are the available MAAT data afterwards; the grey line is a 5-year running mean. The black line is a linear regression, and appears only on the charts of stations showing statistically significant changes in MAAT (using a 95% confidence limit). Linear regressions are calculated for all available data collected until 1975 and for all available data collected from 1976 onward. The figure also allows comparison of spatial temperature patterns along the studied part of the Alaskan Highway, with temperatures becoming colder from Whitehorse to Beaver Creek. Time series of available data varies between weather stations. Missing data for Haines Junction in the 1980s and 1990s and missing data for Beaver Creek in the 1970s and 1980s may have affected the results.

5.1.2 Thawing/Freezing Degree Days

Seasonal degree days vary spatially throughout the study area, following the MAAT trends observed in Figure 5.1A. TDDa and FDDa were calculated for the period preceding the 1975 step change in MAAT and the period following the step change for the Whitehorse ECCS (Figure 5.1B). Degree days were only calculated for the period preceding the step change for the Haines Junction ECCS and for the period following the step change for the Burwash ECCS due to the limited availability of daily mean temperatures. Daily mean temperature records were incomplete for the Otter Falls and Beaver Creek stations and degree days could not be calculated.

Statistically significant decreases of -67.5 TDDa/decade and increases of 185.3 FDDs/decade were observed in Whitehorse from 1943 to 1975 as the MAAT significantly decreased (Figures 5.1A and 5.1B). TDDa remained mainly stable afterwards while FDDa showed greater variation with no significant trend in place (Figure 5.1B).

Degree days remained fairly stable between 1943-1975 at Haines Junction and between 1976-2007 in Burwash with no statistically significant trend observed when the data was tested at a 95 % confidence level (Table 5.1; Figures 5.1C and 5.1D).

Overall, FDDa increases towards the northern end of the transect as MAATs decrease while TDDa remaining fairly constant (Figures 5.1A; 5.1B; 5.1C and 5.1D). FDDa also show high inter-annual variability in the study area while TDDa varies little on an annual basis. These trends indicate that winter is the most variable season spatially and temporally in the study area and the most responsive to recent climate change.

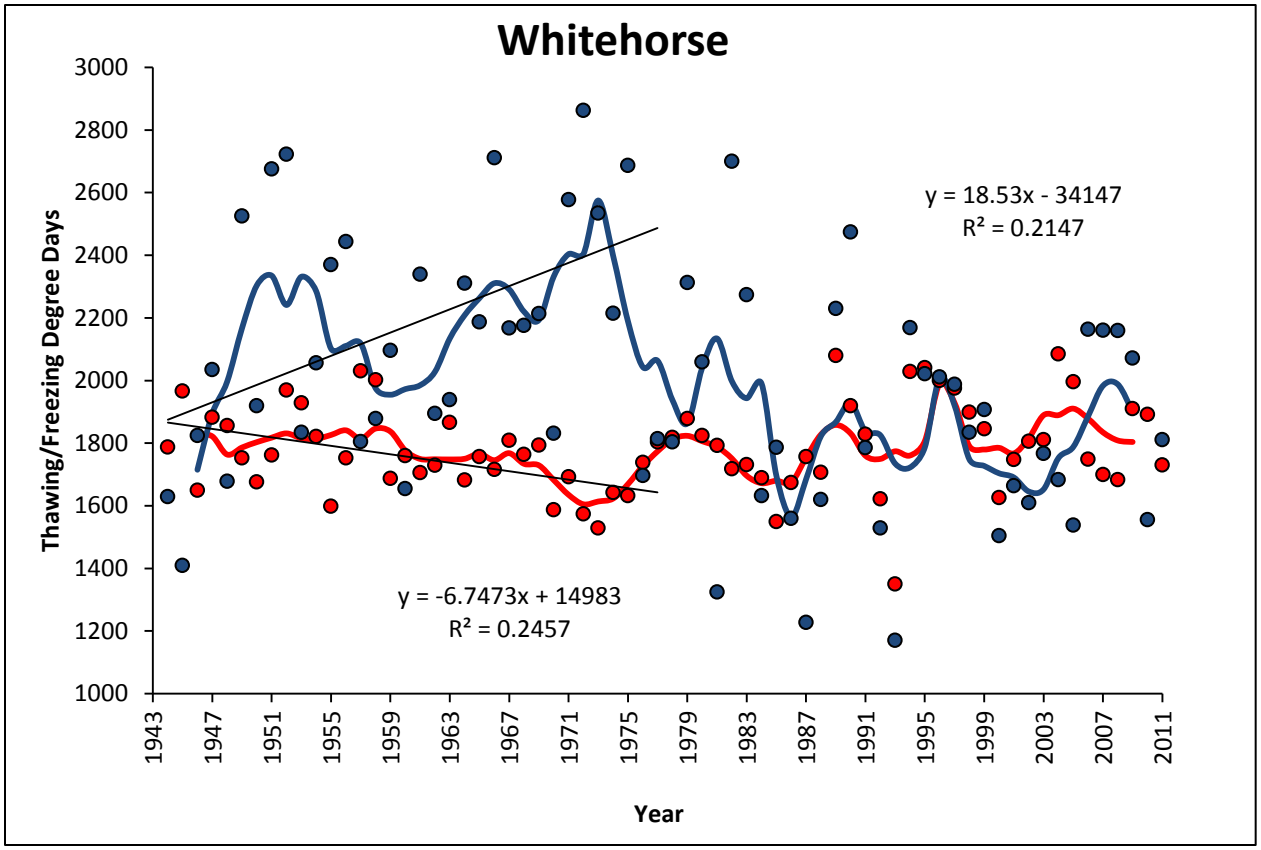

Figure 5.1B: Historical thawing degree days (TDDa) and freezing degree days (FDDa) from the Whitehorse Environment Canada weather station (Environment Canada, 2012). The blue markers are the available FDDa between 1943 and 2011 while the red markers are the available TTDa for the same time period. The blue and red lines are 5-year running means for the FDDa and TDDa respectively. The black lines are linear regressions and only appear on series showing statistically significant trends in FDDa and TDDa (FDDa: 1943-1975; TDDa: 1943-1975). Linear regressions are calculated for all available data collected until 1975 and for all available data collected from 1976 onward for both FDDa and TDDa series.

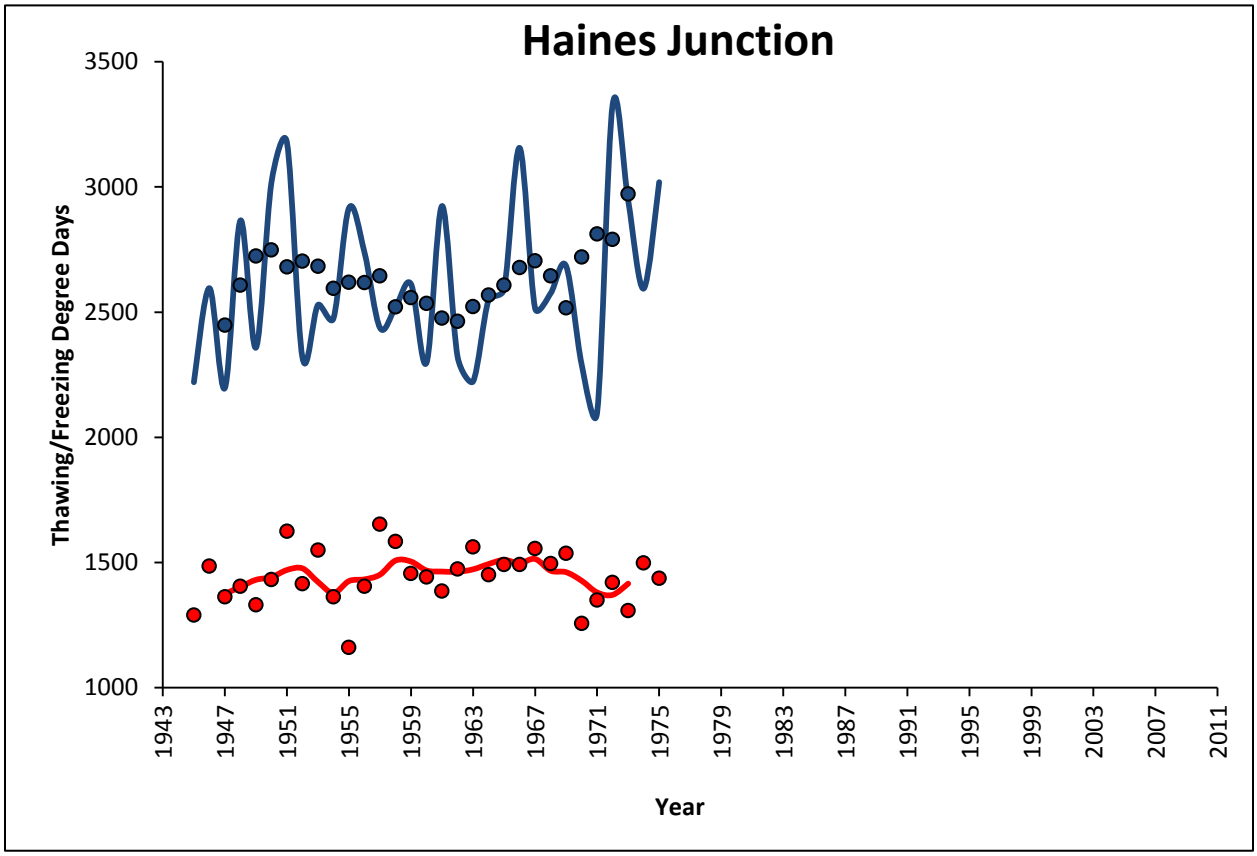

Figure 5.1C: Historical thawing degree days (TDDa) and freezing degree days (FDDa) from the Haines Junction Environment Canada weather station (Environment Canada, 2012). The blue markers are the available FDDa between 1945 and 1975 while the red markers are the available TTDa for the same time period. The blue and red lines are 5-year running means for the FDDa and TDDa respectively. No statistically significant changes in FDDa and TDDa are observed (using a 95% confidence limit).

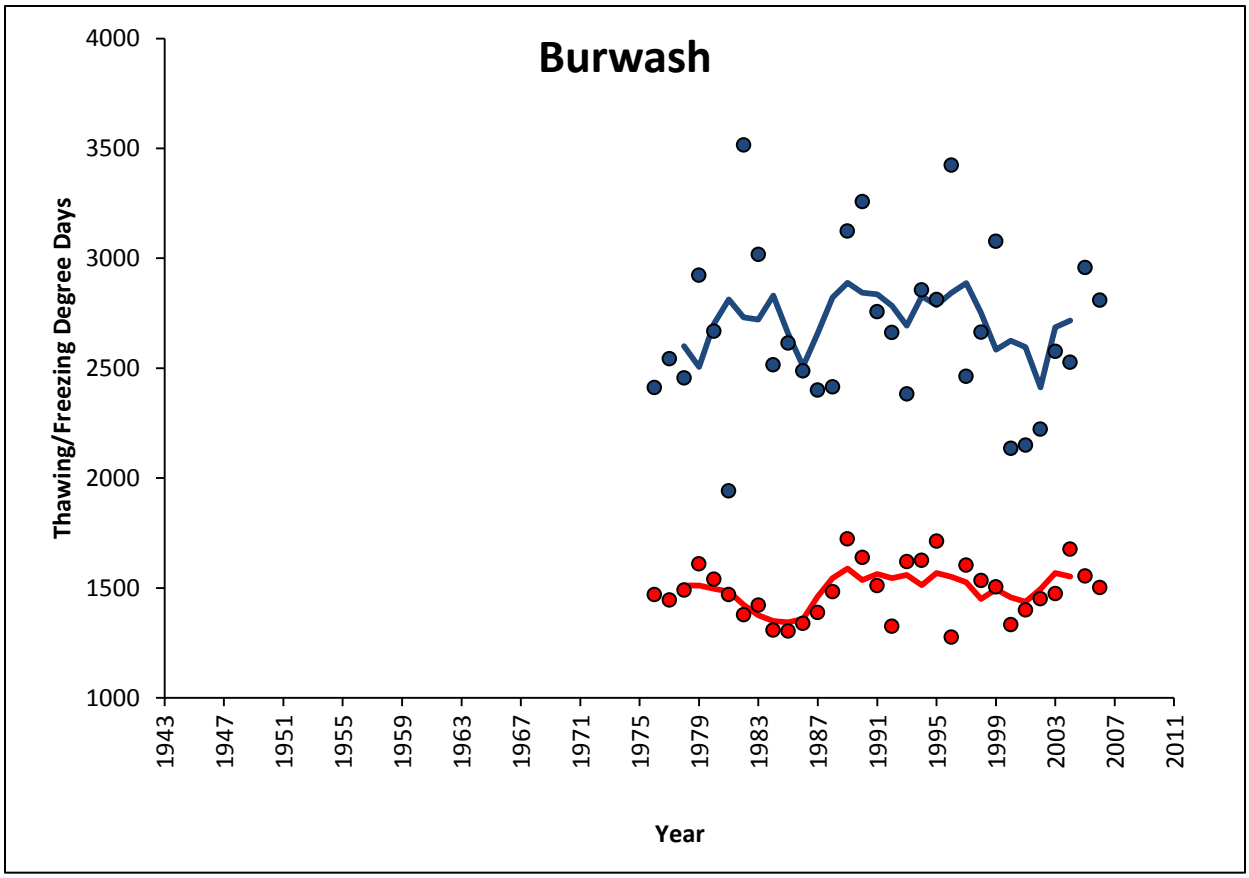

Figure 5.1D: Historical thawing degree days (TDDa) and freezing degree days (FDDa) from the Burwash Environment Canada weather station (Environment Canada, 2012). The blue markers are the available FDDa between 1976 and 2007 while the red markers are the available TTDa for the same time period. The blue and red lines are 5-year running means for the FDDa and TDDa respectively. No statistically significant changes in FDDa and TDDa are observed (using a 95% confidence limit).

5.1.3 Total Annual Rainfall

Total annual rainfall varies spatially throughout the study area, with rainfall increasing from Whitehorse to Beaver Creek (Figure 5.2). Regression analysis of total annual rainfall shows an increase in rainfall after 1975 at all ECCS except Otter Falls, where a decreasing trend is observed (Table 5.1 and Figure 5.2). Pre-1975 rainfall data shows an increasing trend in Whitehorse between 1943-1975 and a decreasing trend in Haines Junction between 1945-1975 (Figure 5.2). However, no total annual rainfall trends are statistically significant when tested at a 95% confidence level (Table 5.1).

Total annual rainfall remains mainly constant in Whitehorse from 1945 to 2011 with minimums observed in the 1950s and maximums in 1990 and 2011 (Figure 5.2). Haines Junction experienced high inter-annual variability in rainfall with minimums observed around 1949 and 1971 and maximums around 1955, 1967 and 1978 (Figure 5.2). Data is missing in the 1980s and 1990s but the available record for 1993-2006 shows no trend and high inter-annual variability (Figure 5.2). The 1980-2006 record at Otter Falls shows low inter-annual variability but some trends can be observed with rainfall increases in the 1980s and a steady decrease in the 1990s which stabilizes in the early 2000s (Figure 5.2). Burwash Landing shows no observable trends in total annual rainfall except a moderate inter-annual variability (Figure 5.2). Beaver Creek shows the highest inter-annual rainfall variability throughout the study area with an increasing variability from 1981 to 2006 (Figure 5.2).

Overall, the total annual precipitation trends observed in the study area follow the main MAAT trends with increases in rainfall observed when the MAAT increases at a site (Table 5.1 and Figure 5.2). The exception is Whitehorse, where an increase in rainfall occurred between 1943-1975 while a statistically significant cooling trend was observed (Table 5.1 and Figure 5.2).

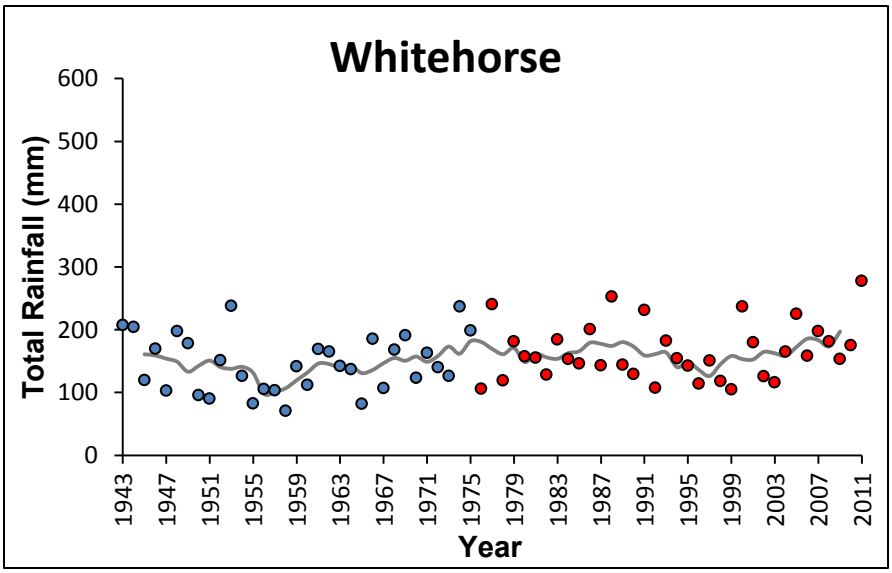
Whitehorse
Total Rainfall (mm)
600
500
400
300
200
100
0
1943
1947
1951
1955
1959
1963
1967
1971
1975
1979
1983
1987
1991
1995
1999
2003
2007
2011
Year

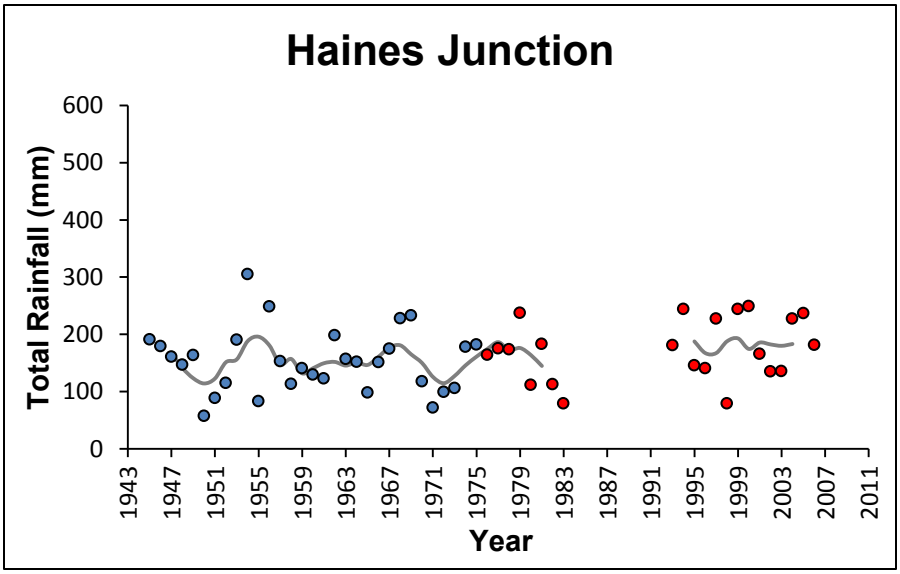
Haines Junction
Total Rainfall (mm)
600
500
400
300
200
100
0
1943
1947
1951
1955
1959
1963
1967
1971
1975
1979
1983
1987
1991
1995
1999
2003
2007
2011
Year

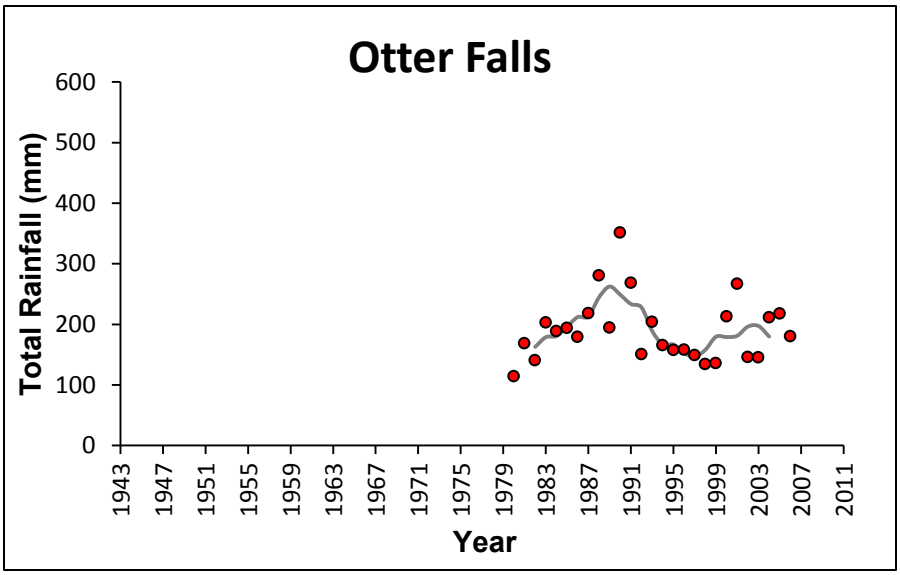
Otter Falls
Total Rainfall (mm)
600
500
400
300
200
100
0
1943
1947
1951
1955
1959
1963
1967
1971
1975
1979
1983
1987
1991
1995
1999
2003
2007
2011
Year

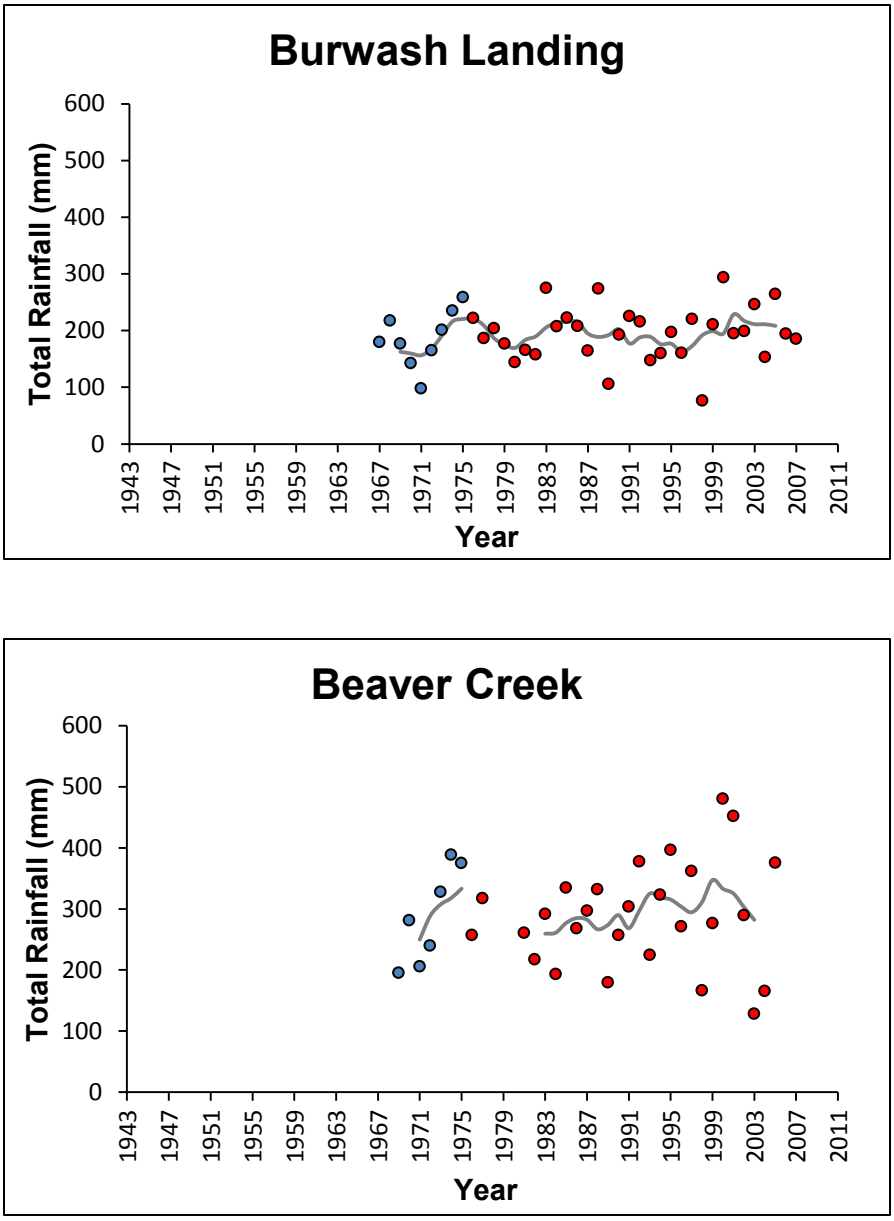

Figure 5.2: Historical total annual rainfall (mm) from Environment Canada climate stations in the study area (Environment Canada, 2012). The blue markers are the available total annual rainfall data between 1943 and 1975 while the red markers are the available total annual data afterwards; the grey line is a 5-year running mean. No station show statistically significant changes in total annual rainfall (using a 95% confidence limit). Linear regressions are calculated for all available data collected until 1975 and for all available data collected from 1976 onward. The figure also allows comparison of spatial total annual rainfall patterns along the studied part of the Alaskan Highway, with rainfall increasing from Whitehorse to Beaver Creek. Time series of available data varies between weather stations. Missing data for Haines Junction in the 1980s and 1990s and missing data for Beaver Creek in the 1970s and 1980s may have affected the results.

5.1.4 Total Annual Snowfall

Total annual snowfall varies spatially throughout the study area, with snowfall decreasing from Whitehorse to Beaver Creek (Figure 5.3). Snowfall trends were not consistent across climate stations for the time period examined (Figure 5.3). The only statistically significant snowfall trend in the study area was observed in Whitehorse between 1943-1975 where snowfall increased by 14.5 cm/decade for a total increase of 46.30 cm (Table 5.1 and Figure 5.3). This increase in snowfall occurred while MAATs were significantly declining in Whitehorse (Table 5.1 and Figure 5.3). An observable peak in snowfall occurred in 1992 before the establishment of a falling trend with a 1997 minimum (Figure 5.3). Total annual snowfall has since been on the rise in Whitehorse (Figure 5.3).

Haines Junction experienced a rise in snowfall in the late 1950s and early 1960s followed by a decreasing trend with a minimum in 1971 and an increase afterwards to 1983 (Figure 5.3). Data is missing between 1983-1992. Inter-annual snowfall variation in Haines Junction from 1993 to 2011 was the highest of all stations in the study area (Figure 5.3). Otter Falls experienced a moderate increase in snowfall from 1980 to 1992, decreasing thereafter to the end of the measurement period in 2006 (Figure 5.3). No snowfall data is available prior to 1980 for this community. Burwash Landing saw peaks in snowfall in the late 1960s and early 1970s as well as around the year 1990 with minimums in the late 1970s and early 1980s (Figure 5.3). An observable decrease in snowfall occurred in Beaver Creek between 1969-1975 with high inter-annual variability (Figure 5.3). Total annual snowfall remained mostly constant between 1981-2006 with exceptions of a small decrease around 1995 and a small increase around 1999 (Figure 5.3).

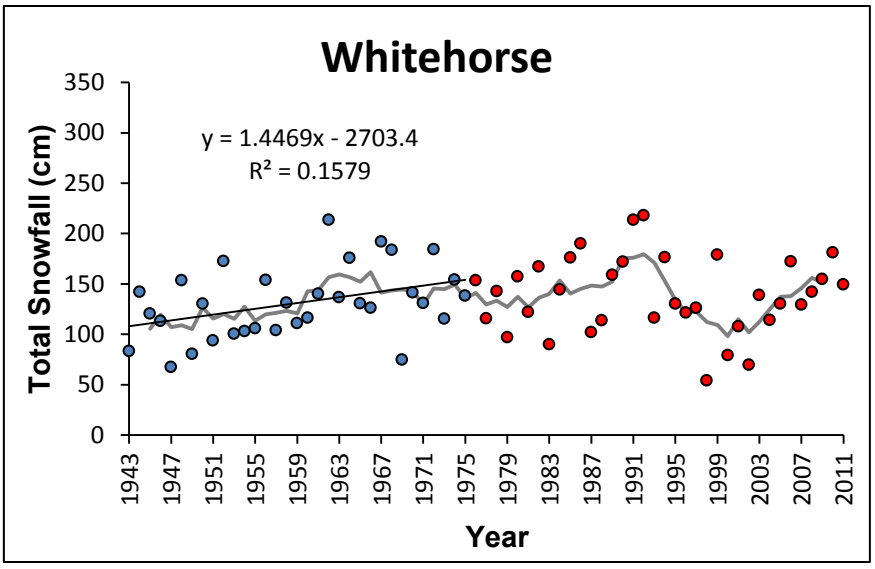
Whitehorse
y = 1.4469x - 2703.4
R² = 0.1579
Total Snowfall (cm)
Year

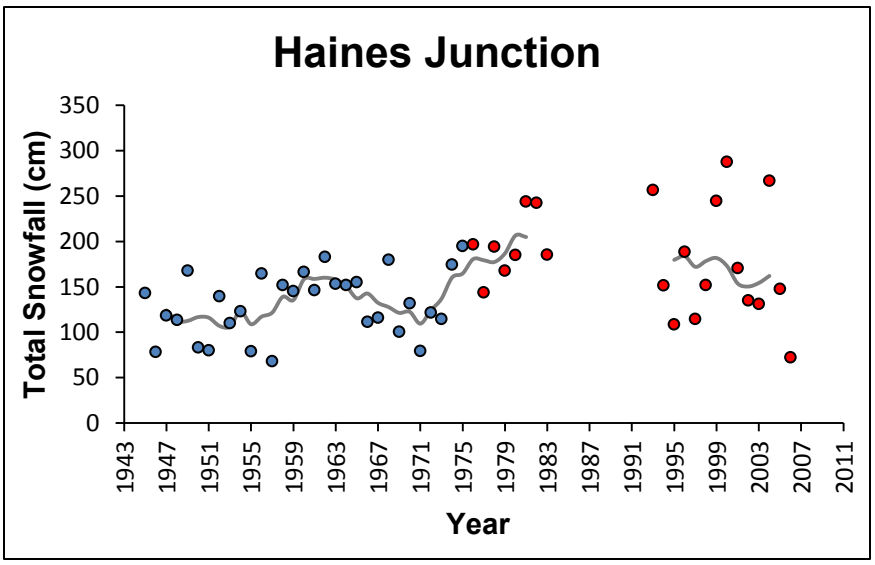
Haines Junction
Total Snowfall (cm)
Year

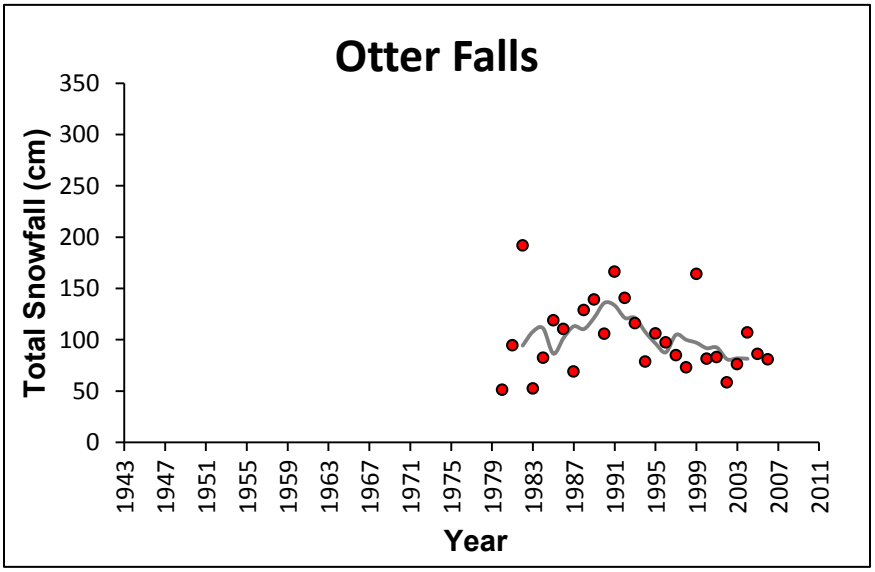
Otter Falls
Total Snowfall (cm)
Year

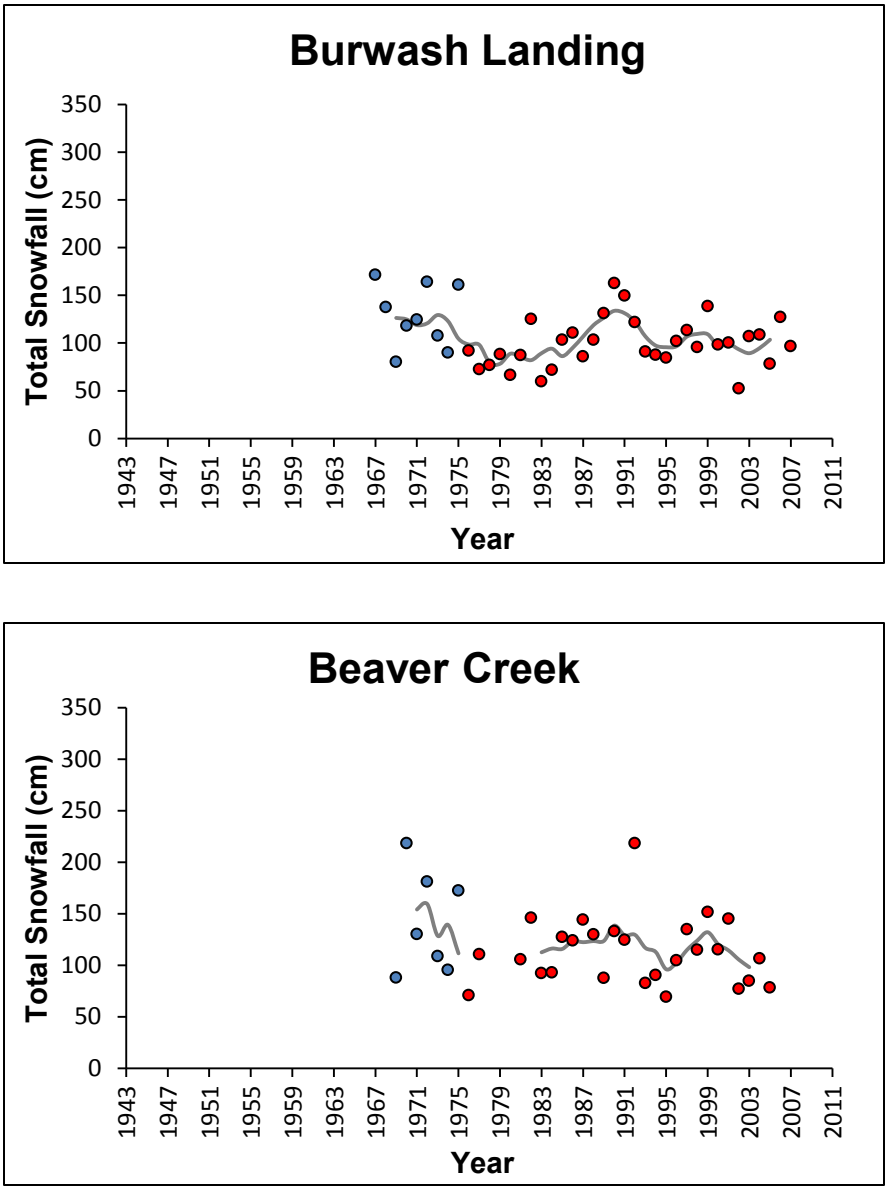

Figure 5.3: Historical total annual snowfall (cm) from Environment Canada climate stations in the study area (Environment Canada, 2012). The blue markers are the available total annual snowfall data between 1943 and 1975 while the red markers are the available total annual snowfall data afterwards; the grey line is a 5-year running mean. The black line is a linear regression, and appears only on the charts of stations showing statistically significant changes in total annual snowfall (using a 95% confidence limit). Linear regressions are calculated for all available data collected until 1975 and for all available data collected from 1976 onward. The figure also allows comparison of spatial total annual snowfall patterns along the studied part of the Alaskan Highway, with snowfall decreasing from Whitehorse to Beaver Creek. Time series of available data varies between weather stations. Missing data for Haines Junction in the 1980s and 1990s and missing data for Beaver Creek in the 1970s and 1980s may have affected the results.

5.1.5 Total Annual Precipitation

Total annual precipitation measured at the five ECCS did not exhibit a consistent pattern along the study route (Figure 5.4). No precipitation series prior to 1975 and post 1975 showed significant trends when subjected to statistically significant testing at a confidence level of 95% (Table 5.1). No noticeable trends in precipitation were seen in Whitehorse and the inter-annual variability in total annual precipitation was the lowest of all five communities studied (Figure 5.4).

The 5-year running mean at Haines Junction reaches a visible precipitation minimum in 1972 followed by a step-like rise in precipitation afterwards (Figure 5.4). Precipitation data is missing between 1984-1992 (Figure 5.4). Available data from 1993 to 2006 show a higher total annual precipitation and inter-annual variability than the start of the record (Figure 5.4).

The available total annual precipitation record for Otter Falls spans from 1980 to 2006 and shows an observable increasing trend in precipitation in the 1980s with a declining trend in the 1990s that stabilizes in the early 2000s (Figure 5.4). An overall increase in precipitation occurred in Beaver Creek from 1981 to 2004 (Figure 5.4). The Beaver Creek total annual precipitation record also shows the highest inter-annual variability in the study area (Figure 5.4).

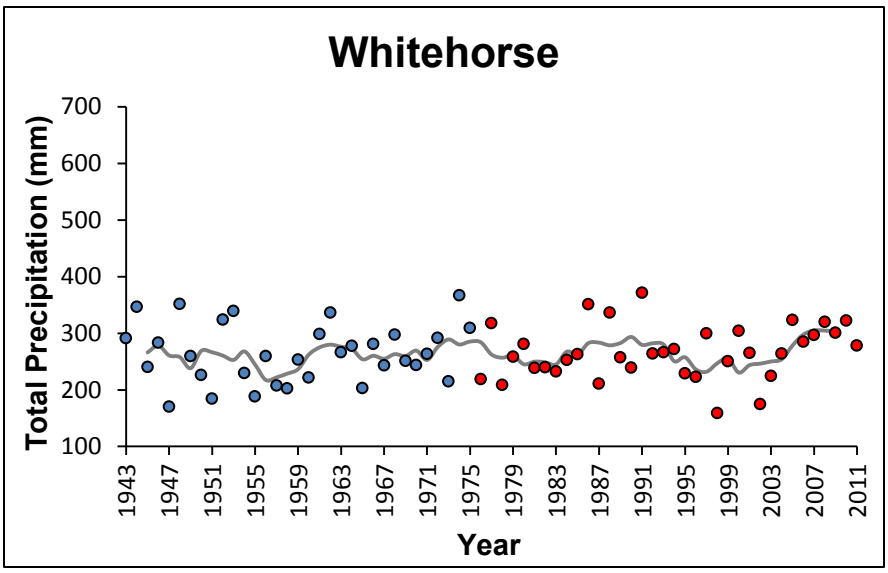
Whitehorse
Total Precipitation (mm)
700
600
500
400
300
200
100
1943
1947
1951
1955
1959
1963
1967
1971
1975
1979
1983
1987
1991
1995
1999
2003
2007
2011
Year

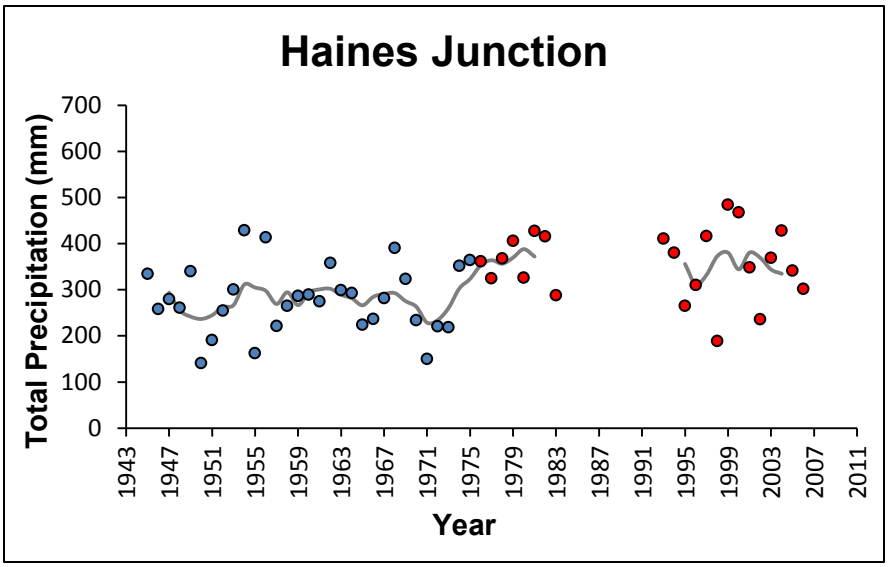
Haines Junction
Total Precipitation (mm)
700
600
500
400
300
200
100
0
1943
1947
1951
1955
1959
1963
1967
1971
1975
1979
1983
1987
1991
1995
1999
2003
2007
2011
Year

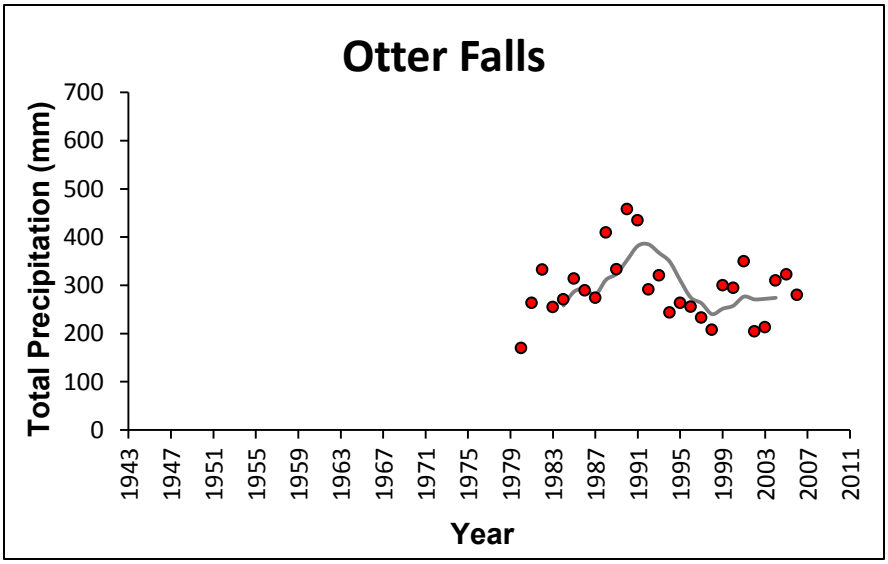
Otter Falls
Total Precipitation (mm)
700
600
500
400
300
200
100
0
1943
1947
1951
1955
1959
1963
1967
1971
1975
1979
1983
1987
1991
1995
1999
2003
2007
2011
Year

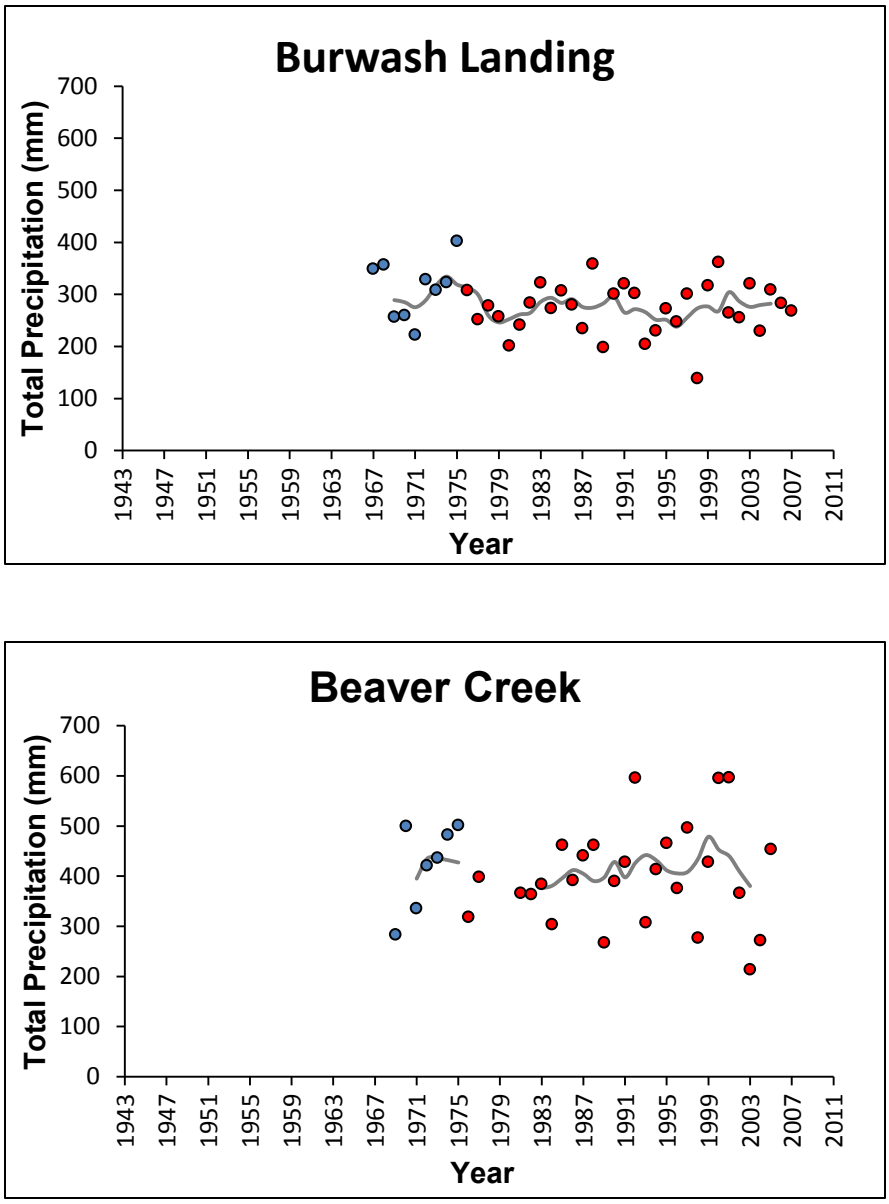

Figure 5.4: Historical total annual precipitation (mm) from Environment Canada weather stations in the study area (Environment Canada, 2012). The blue markers are the available total precipitation data between 1943 and 1975 while the red markers are the available total precipitation data afterwards; the grey line is a 5-year running mean. No station show statistically significant changes in total precipitation (using a 95% confidence limit). Linear regressions are calculated for all available data collected until 1975 and for all available data collected from 1976 onward. The figure also allows comparison of spatial total annual precipitation patterns along the studied part of the Alaskan Highway, with precipitation increasing from Whitehorse to Beaver Creek. Time series of available data varies between weather stations. Missing data for Haines Junction in the 1980s and 1990s and missing data for Beaver Creek in the 1970s and 1980s may have affected the results.

5.2 RBR Instrumented Boreholes

5.2.1 Borehole R1 (79S-CS-5)

The permafrost thermal monitoring site at borehole R1 is located in the sporadic discontinuous permafrost zone of the Yukon Territory at 60˚ 47’ 31” N and 135˚ 56’ 40” W and

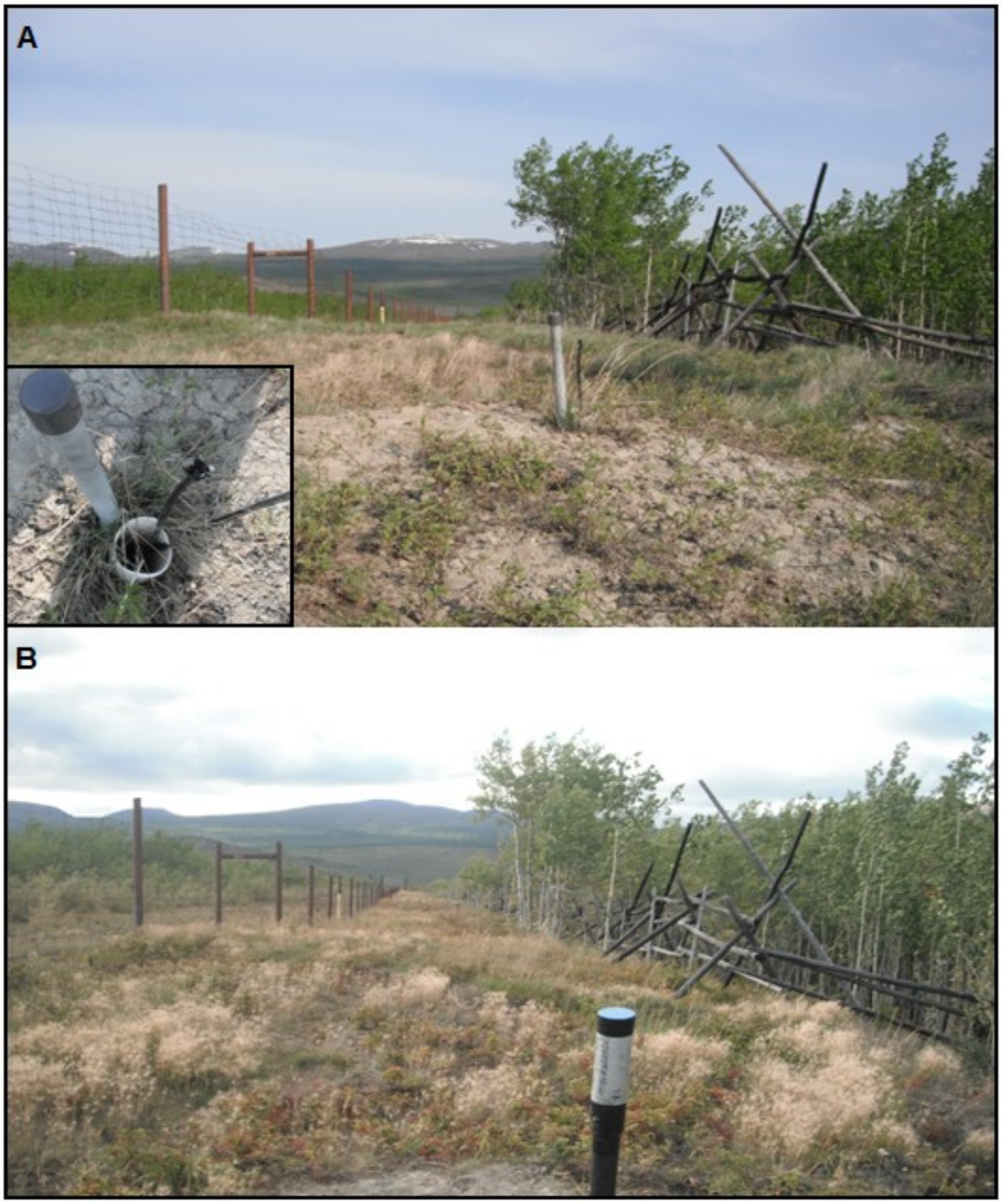

Figure 5.5: (A) Borehole R1 as it was found during the summer 2011 borehole exploration; (B) and borehole R1 after it was rehabilitated and cased.

at 686 m elevation (Figure 5.5). This site is located on a cleared cut-line which also serves as a trail along the boundary fences of the La Prairie Bison Ranch (Figure 5.5). The borehole site is exposed and consists mainly of dry clay covered with grasses on a relatively flat relief (Figure 5.5). The borehole was drilled to a depth of 30 m on August 8th and 9th 1979. Soil type and ground ice characteristics from the borehole log indicate the presence of unfrozen clay to a depth of 30 m. The borehole was rehabilitated on August 24, 2011 and a RBR logger with a multithermistor string was installed to a depth of 6.5 m. The maximum depth of 30 m could not be reached as the borehole had collapsed at 6.5 m. The length of the current ground thermal monitoring record as well as other related field work associated with borehole R1 and pertinent information is summarized in Table 5.2.

Table 5.2: Summary table of the data used in the analysis of borehole R1 and the depths of the thermistors from the surface. Note that more detailed field work and RBR logger information is given in Appendix C.

Borehole R1	
Closest ECCS Station and Distance	Whitehorse (49 km), Haines Junction (84 km)
Dates of 1979 drilling	August 8-9, 1979
Manual Temperature Measurements Available	October 10, 1979; February 01, 1980; April 28, 1980; August 07, 1980; July 30, 1981
Original Borehole Depth	30 m
New Rehabilitated Borehole Depth	6.5 m
Borehole Unblocking Method	Not blocked by ice (borehole cased)
RBR Logger Data	August 24, 2011 – August 22, 2012
Thermistor Depths (m)	0, 0.5, 1.0, 2.0, 4.0, 6.5
Length and Date of ERT Survey	80 m (June 10, 2011)

The thermal profile from June 10, 2012 at Borehole R1 (Figure 5.6) was extracted from the RBR logger data record for comparison with the June 10, 2011 ERT profile (Figures 5.7 and 5.8). Results from the daily ground temperature record show unfrozen conditions at the ground surface and 1 m depths, a temperature of -0.6˚C at 2 m, and positive temperatures at 4.0 m and 6.5 m (Figure 5.6). The 1979 borehole log indicates unfrozen conditions on August 8, 1979. Therefore, the frozen layer that was present on June 10, 2012 is interpreted as being due to seasonal frost. Linear interpolation between the thermistors indicates this layer may have extended from 1.8 m to 2.9 m but the spacing of the sensors means that the precision of the top and bottom of the frozen layer is low (Figure 5.6).

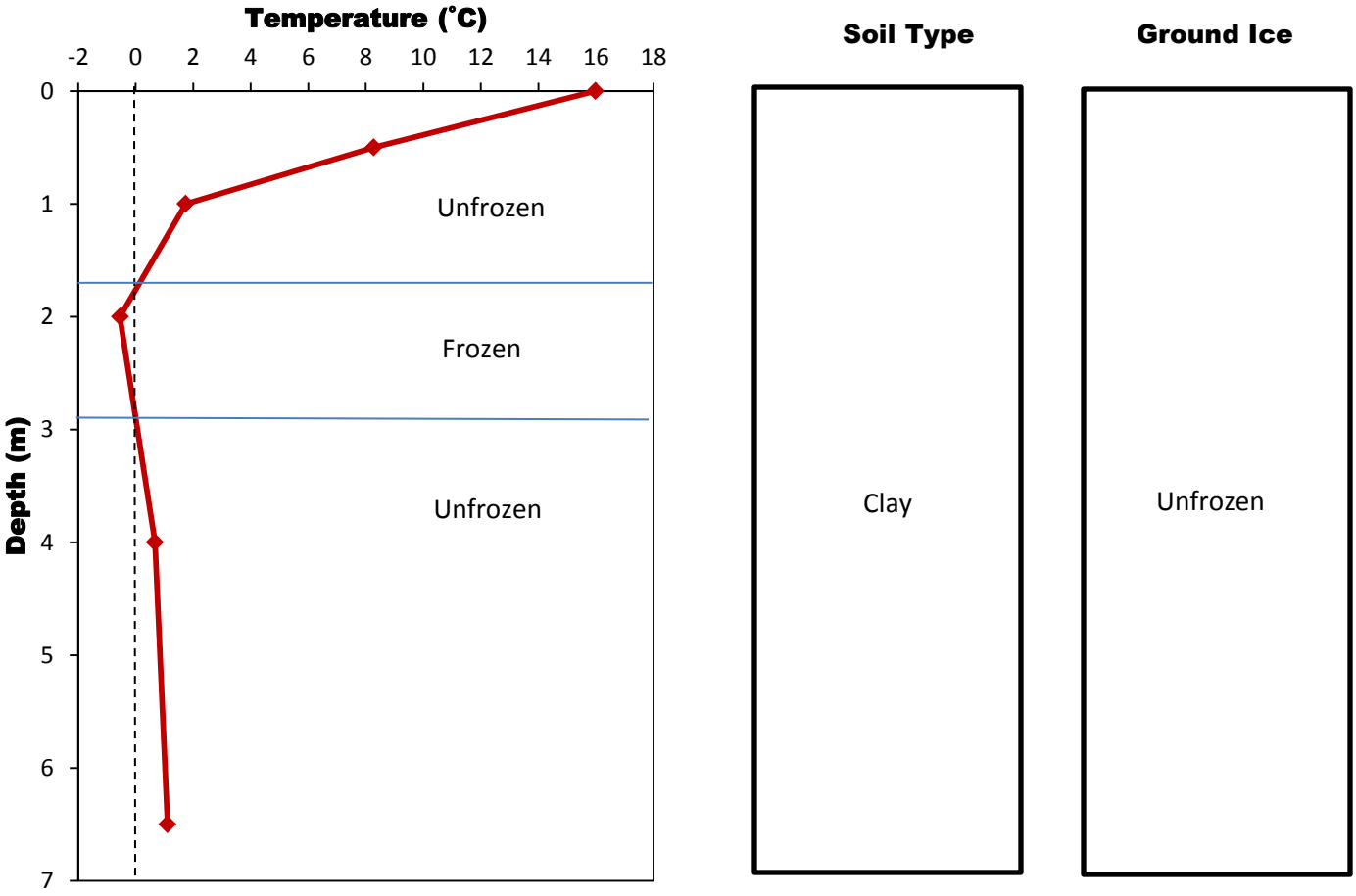

Figure 5.6: Borehole R1 average daily temperature measurements taken from the RBR logger on June 10, 2012. The diamonds represent the points of temperature measurement. Soil type and ground ice conditions taken from an August 8, 1979 borehole log are shown on the right hand side. Complete descriptions of the borehole log and ground ice classification to a depth of 30 m are found in Appendix K. Note that the ERT survey was conducted on June 10, 2011.

The 80 m ERT survey runs directly on a cleared access trail parallel to the boundary fence of the La Prairie Bison Ranch from a north-east, south-west orientation with the borehole located at the mid-point of the transect (Figures 5.7 and 5.8). The ERT survey shows low resistivity values less than 100 Ohm-m to an approximate depth of 1.5 m which can be interpreted as unfrozen conditions (Figure 5.8). Probing results gave a mean depth to resistance of 7 cm with a low standard deviation (N=61, SD=2) and did not reach a frost table. The top of the soil probed was mostly soft loose clay underlain by harder dry clay which could not be penetrated (Figure 5.8). The ERT results also show a higher horizontal resistivity layer between approximately 2 m and 4 m in depth ranging from approximately 150-600 Ohm-m. The upper resistivity values from this range are interpreted as seasonally frozen ground in the process of thawing (Figure 5.8), as shown by the borehole temperature of -0.6˚C at 2.0 m depth (Figure 5.6) that thawed later in the summer (Figure 5.9).

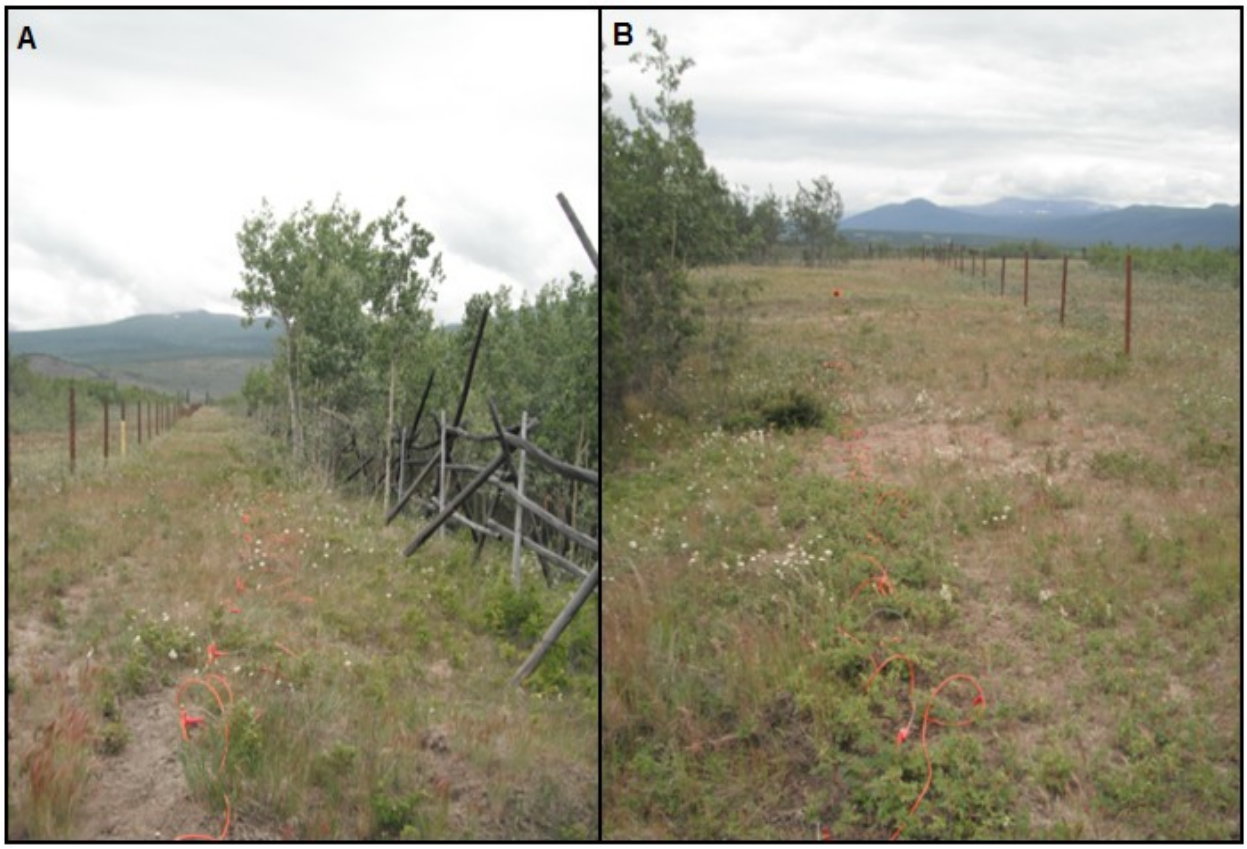

Figure 5.7: Resistivity transect of the 80 m NE-SW survey at borehole R1 on June 10, 2011. (A) Picture taken from the borehole at the mid-point looking north-east; (B) picture taken from the borehole at the mid-point looking south-west.

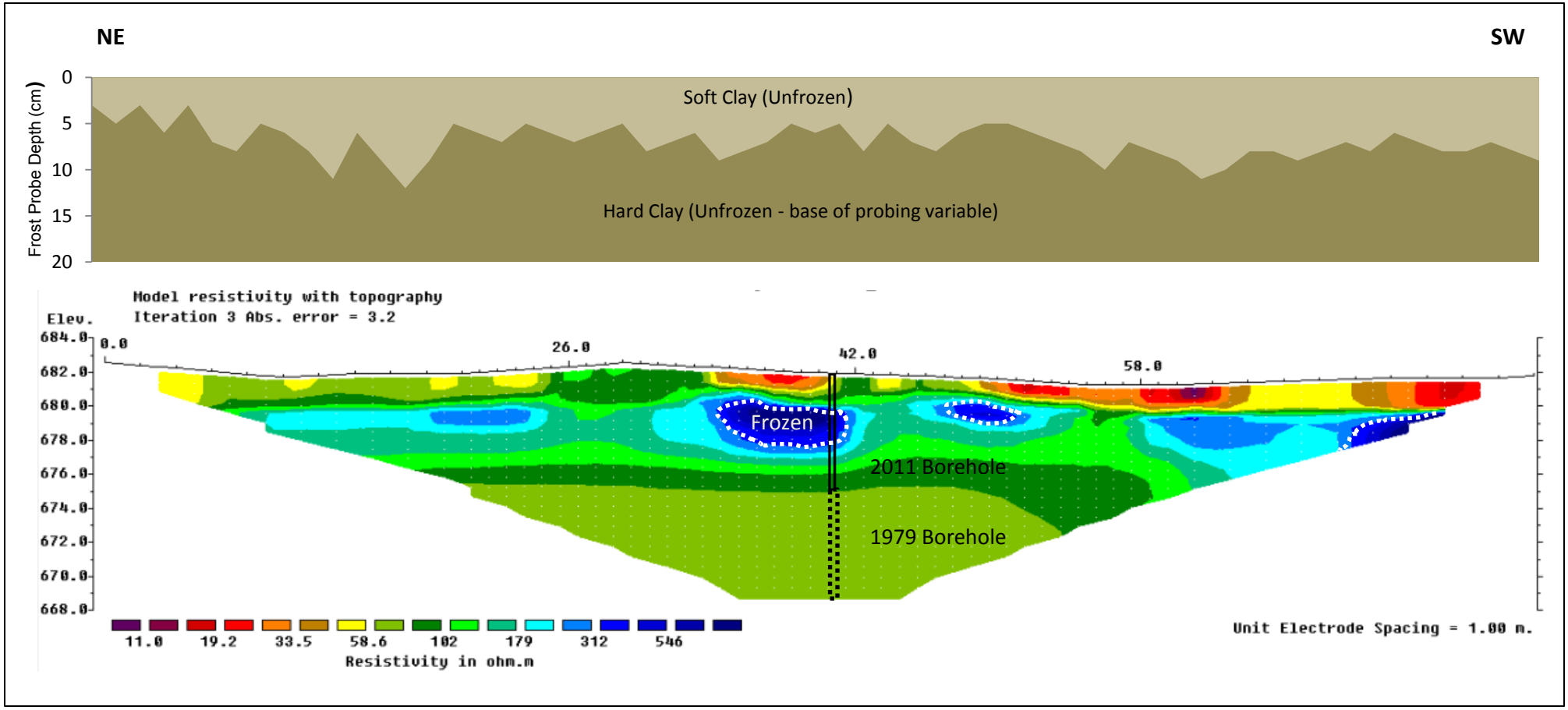

Figure 5.8: Borehole R1 NE-SW 80 m resistivity profile and frost probe chart from June 10, 2011. Vertical exaggeration in model section display = 1.00. Based on 323 data points (22 removed from original survey). The solid black lines indicates the location and depth of the 2011 borehole on the survey while the black dash lines indicate the original depth of the borehole in 1979. The white dashed circles indicates ground condition interpreted as seasonally frozen.

The full ground temperature record from borehole R1 shows high annual variability at the ground surface and is shorter than a year by 2 days (Figure 5.9). The 2011-2012 ground temperatures at BH R1 are below 0˚C between October 20 - April 10 at the surface, between November 5 - April 25 at 0.5 m, between December 3 - May 31 at 1.0 m and between February 24 – July 8 at 2.0 m. Ground temperatures did not fall below 0˚C at 4.0 m and 6.5 m (Figures 5.9 and 5.10). The time lag between freezing at the ground surface and 2.0 m was approximately 127 days and zero-curtain effects are largely weak or absent (Figures 5.9 and 5.10).

Mean monthly ground surface temperatures (MMGST) results for BH R1 show a maximum MMGST of 16.6˚C reached in July 2012 and a minimum MMGST of -19.0 in January 2012 (Figure 5.10). The mean monthly ground temperature (MMGT) for the deepest thermistor at 6.5 m reaches a maximum of 1.3˚C in February 2012 and a minimum of 0.9˚C in September 2011 (Figure 5.10).

The maximum ground surface temperature was 31.8˚C on July 27, 2012 and the minimum of -32.7˚C was reached on January 30, 2012 (Figures 5.9 and 5.12). The maximum ground temperature at the deepest measurement point of 6.5 m was 1.3˚C on February 18, 2012 and the minimum ground temperature was 0.8˚C on September 8, 2011 (Figures 5.9 and 5.12). The range in temperatures at the ground surface is about 64˚C, which is reduced to 0.5˚C at 6.5 m (Figure 5.12). The MAGST was 1.0˚C and MAGTs warmed with depth to 2 m with a recorded MAGT of 1.5˚C at 0.5 m and 1.7˚C at 2.0 m, cooling thereafter to 1.1˚C at 6.5 m (Figure 5.12). The depth of ZAA was not reached in BH R1 and is therefore deeper than 6.5 m. MAGTs are all greater than 0˚C which confirm that permafrost is not present at this site (Figure 5.12). An average between the MAAT recorded between August 24, 2011 and August 21, 2012 at ECCS weather stations in Whitehorse (-0.7˚C) and Haines Junction (-2.9˚C) was used to calculate the surface offset of 2.8˚C. The surface offset is also controlled by a minimal vegetation cover around the borehole as well as the possibility of the site being windblown of snow during the winter due to its open exposure (Williams and Smith 1989; Smith and Riseborough, 2002).

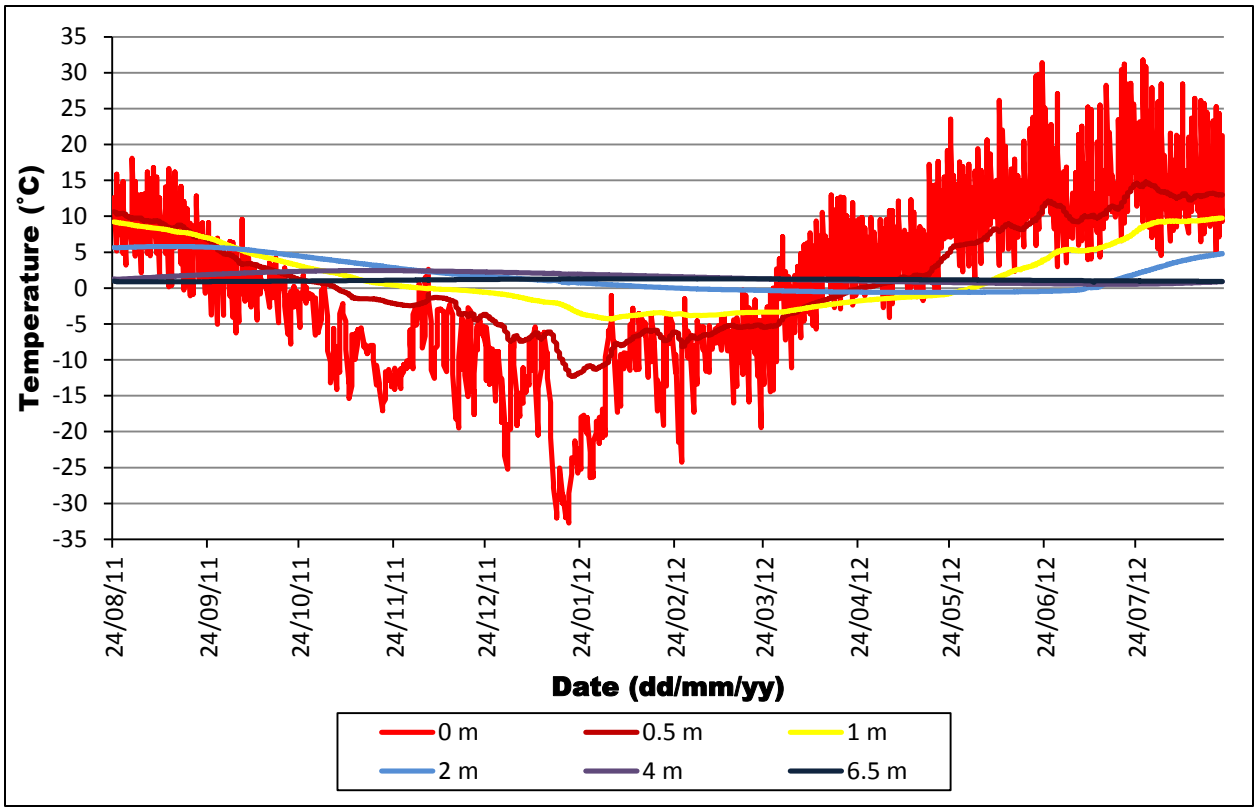

Figure 5.9: Full ground temperature series at Borehole R1 between August 24, 2011 and August 21, 2012. Note that 2 days are missing for a complete annual record.

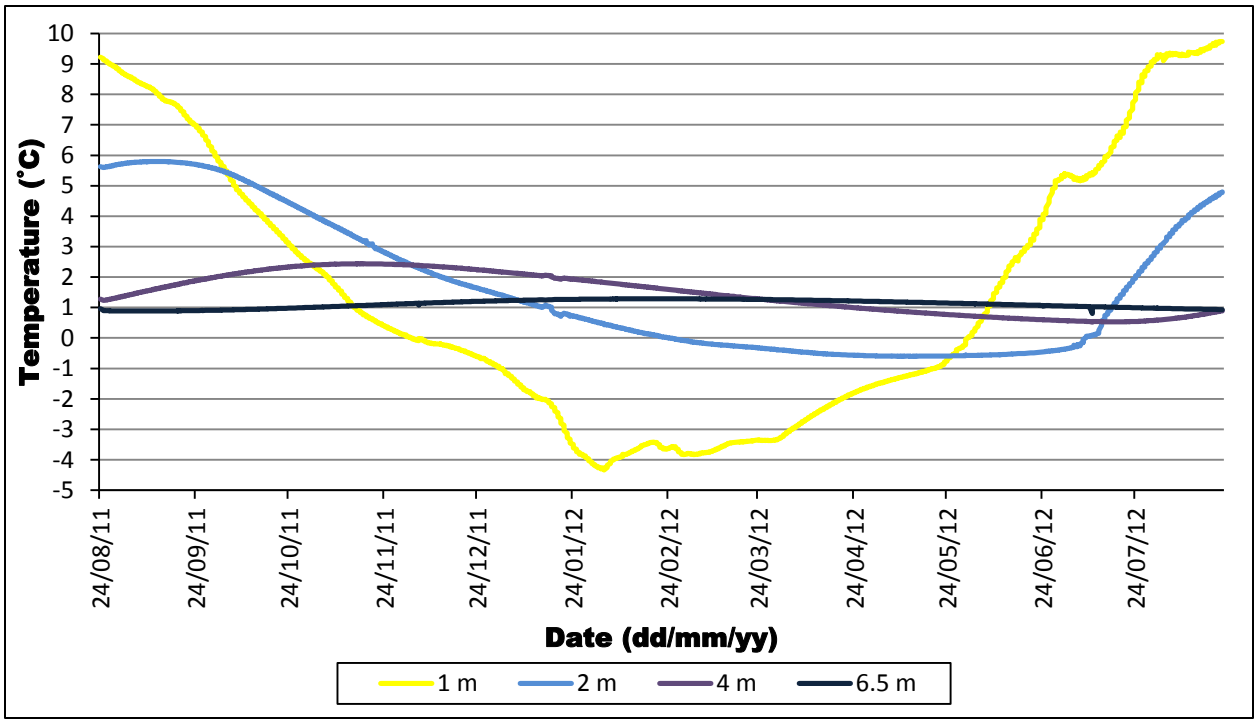

Figure 5.10: Deeper ground temperature series at Borehole R1 between August 24, 2011 and August 21, 2012. Note that 2 days are missing for a complete annual record.

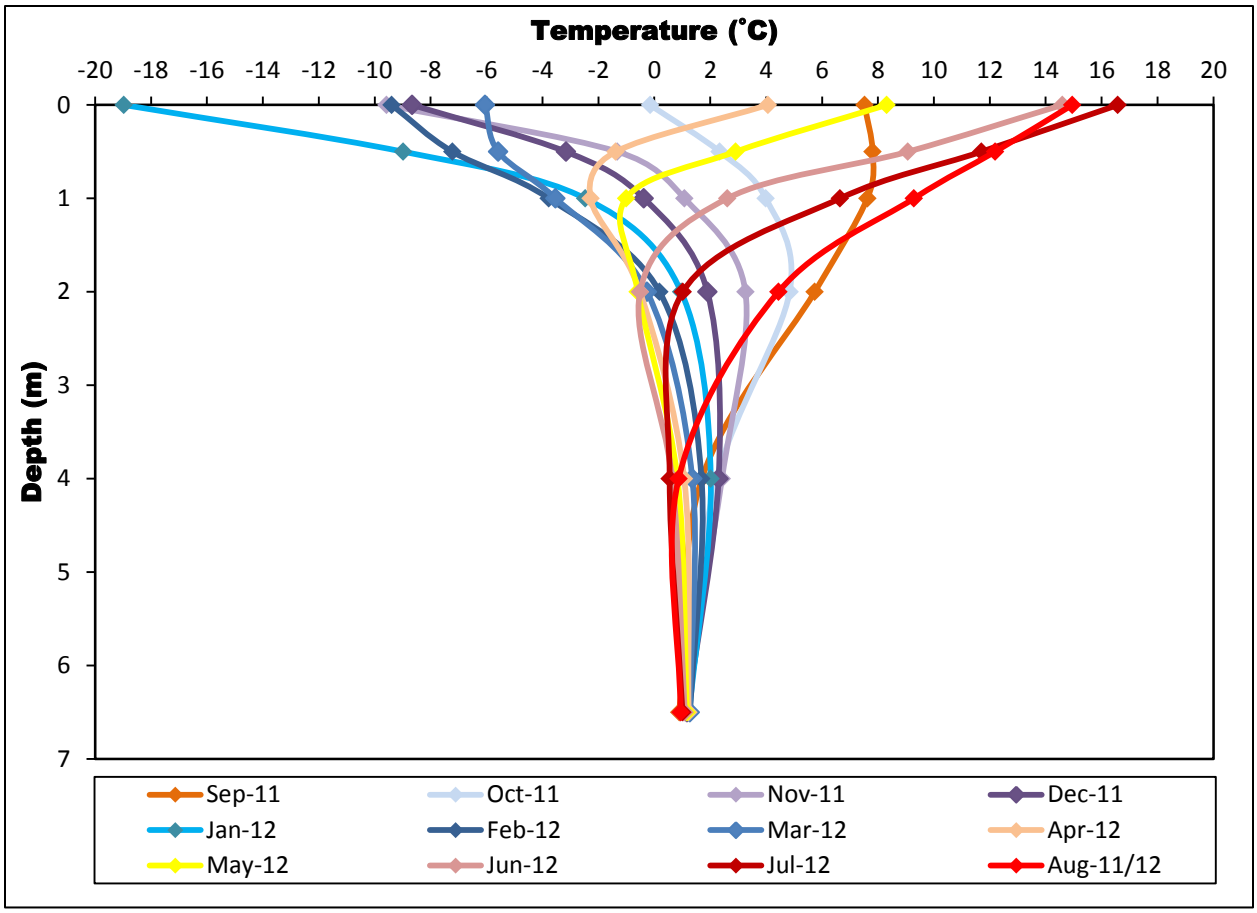

Figure 5.11: Monthly average ground temperature profiles from September 2011 to August 2012.

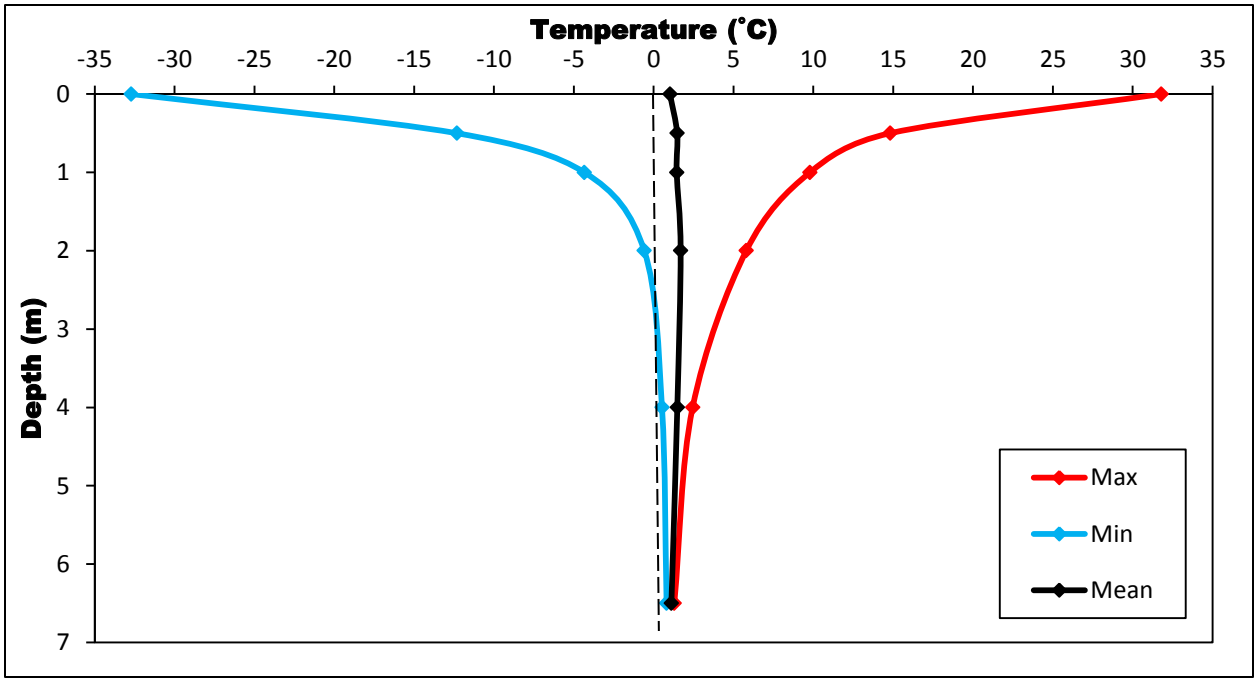

Figure 5.12: Temperature envelope at Borehole R1 for the 2011-2012 year. Mean values included two additional simulated days in which August 22 values were repeated to obtain a full year of data.

Comparisons between manual ground temperature logs from the late 1970s and early 1980s to the exact dates of measurement from 2011-2012 reveal no obvious long term ground temperature difference (Figure 5.13). Ground surface temperatures were not recorded between 1979-1981 and first measurements were taken from 2.1 m downwards at varying increments to a maximum depth of 28.1 m. The 2011-2012 record starts at the ground surface with consistent measurement depth taken at 0.5 m, 1.0 m, 2.0 m, 4.0 m and 6.5 m. Variations in TDDs and FDDs between specific periods in the 1979-1981 and 2011-2011 climate record at the Whitehorse ECCS weather station were examined to better interpret ground temperature variations (Table 5.3).

Table 5.3: TDDs and FDDs comparison at Whitehorse ECCS weather station between 1979-1981 and 2011-2012. This table relates to the immediate thawing and freezing season preceding the ground temperature measurements in Figure 5.13.

Figure 5.13A			
Thawing 01/01/1979 – 26/10/1979	Thawing 01/01/2011 – 26/10/2011	Freezing Fall 1979 – 26/10/1979	Freezing Fall 2011 – 26/10/2011
1643 TDD	1427 TDD	13 FDD	30 FDD
Figure 5.13B			
		Freezing Fall 1979 – 01/02/1980	Freezing Fall 2011 – 01/02/2012
		1469 FDD	1445 FDD
Figure 5.13C			
		Freezing Fall 1979 – 28/04/1980	Freezing Fall 2011 – 28/04/2012
		1925 FDD	1965 FDD
Figure 5.13D			
Thawing 01/01/1980 – 07/08/1980	Thawing 01/01/2012 – 07/08/2012	Freezing Fall 1979 – 07/08/1980	Freezing Fall 2011 – 07/08/2012
1064 TDD	970 TDD	1925 FDD	1966 FDD
Figure 5.13E			
Thawing 01/01/1981 – 30/07/1981	Thawing 01/01/2012 – 30/07/2012	Freezing Fall 1980 – 30/07/1981	Freezing Fall 2012 – 30/07/2012
867 TDD	877 TDD	1870 FDD	1966 FDD

Ground temperatures were 0.6˚C – 0.7˚C warmer at 6.5 m for the 1979-1981 manual ground temperature measurements than the same dates in 2011-2012 (Figure 5.13). Other depths of measurements showed variations between the two time periods. There were 216 TDDs more in the thawing season preceding the October 26, 1979 temperature measurements than in 2011

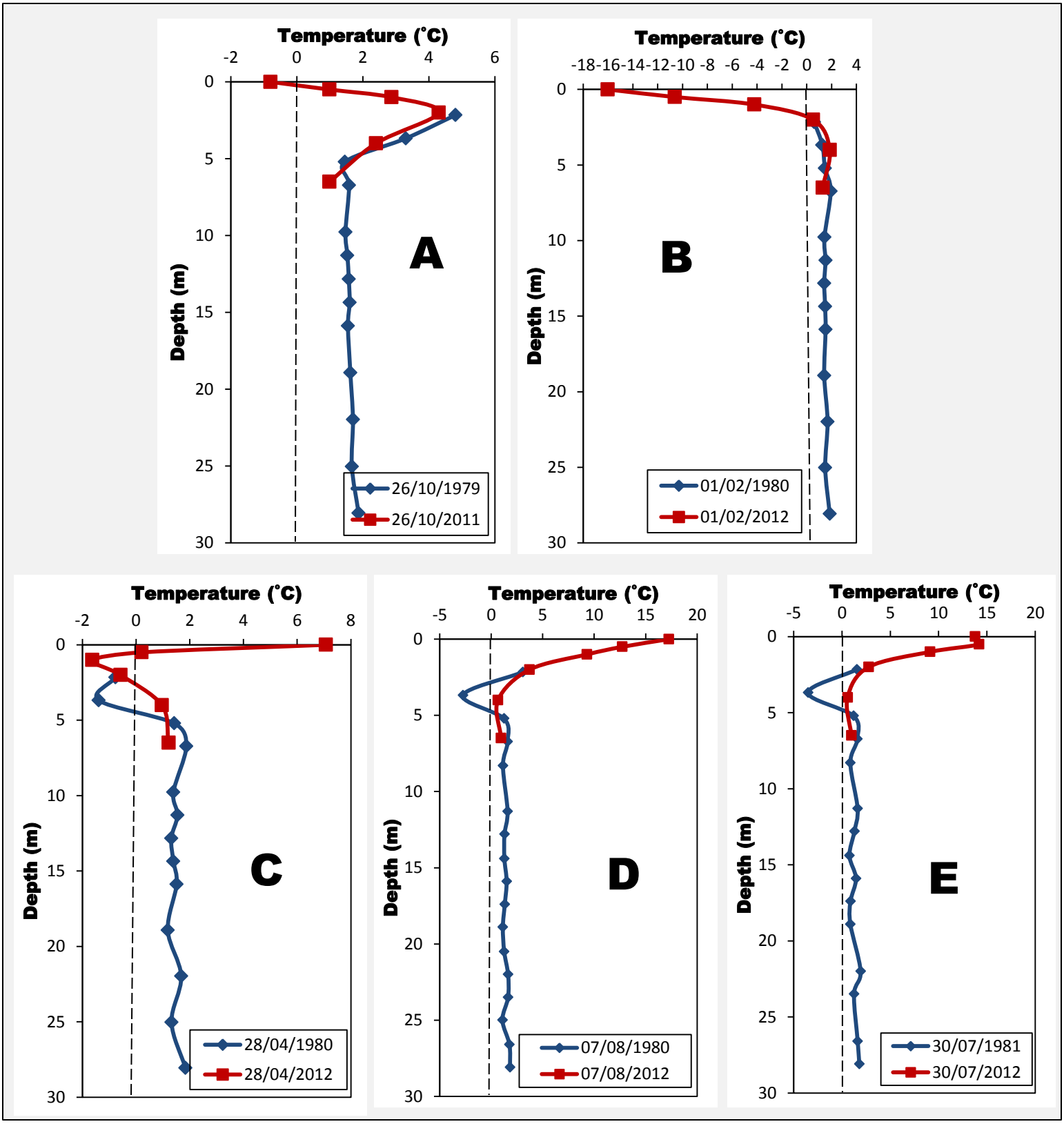

Figure 5.13: Ground temperature differences at borehole R1. (A) 26/10/1979 vs 26/10/2011; (B) 01/02/1980 vs 01/02/2012; (C) 28/04/1980 vs 28/04/2012; (D) 07/08/1980 vs 07/08/2012; and (E) 30/07/1981 vs 30/07/2012.

which could explain the slightly warmer temperatures between 2-5 m in 1979 (Table 5.3 and Figure 5.13A). The freezing season preceding the February 1 measurements of 1980 and 2012 only had a 24 FDD difference which may explain the similarity in their ground temperature values (Table 5.3 and Figure 5.13B). The small variations in TDDs and FDDs from Whitehorse between the 1980-1981 and 2012 measurement periods do not by themselves suggest an explanation for the 2.4˚C – 4.1˚C colder 1980-1981 ground temperature values at 4.0 m when compared to the same dates in 2012 (Figures 5.13C, 5.13D and 5.13E). The difference may relate to the effect of soil moisture conditions on freezing depth. Site specific climatic conditions at borehole R1 might also have varied from the nearest ECCS weather stations affecting the interpretation of TDD and FDD. It is concluded that this non permafrost site did not show multi decadal change in its ground temperature regime.

5.2.2 Borehole R2 (78-A-71)

The permafrost thermal monitoring site at borehole R2 is located in the sporadic discontinuous permafrost zone of the Yukon Territory at 60˚ 54’ 50’’ N and 137˚ 52’ 34’’ W and at 840 m elevation (Figure 5.14). This site is located approximately 500 m from the Alaska Highway and about 1 km south-east of the Jarvas River. The borehole site was cleared for

Figure 5.14: (A) Borehole R2 as it was found during the summer 2011 borehole exploration; (B) and borehole R2 after it was rehabilitated and cased.

drilling in August 1978 and was still mostly exposed with scattered shrubs averaging 2 m in height during the 2011-2012 field seasons (Figure 5.14). The relief at the site is relatively flat (Figure 5.14). The borehole was drilled to a depth of 9.2 m in August 1978. Soil type and ground ice conditions from the August 1978 borehole log indicate a gravel layer at the surface to a depth of 1.2 m underlain by a layer of clay to 5.3 m, a gravel layer between 5.3 m and 6.2 m and a layer of sand from 6.2 m to the bottom of the borehole at 9.2 m (Figure 5.15). The borehole was unfrozen throughout (Figure 5.15). The borehole was rehabilitated and cased on June 30, 2011 and a RBR logger with a multithermistor string was installed to a depth of 8.75 m on August 14, 2011. The borehole did not need to be steamed as it was not blocked by ice. The length of the current ground thermal monitoring record as well as other related field work associated with borehole R2 and pertinent information is summarized in Table 5.4.

Table 5.4: Summary table of the data used in the analysis of borehole R2 and the depths of the thermistors from the surface. Note that more detailed field work and RBR logger information is given in Appendix C.

Borehole R2	
Closest ECCS Station and Distance	Haines Junction (25 km), Otter Falls (55 km)
Date of 1978 drilling	August 1978
Manual Temperature Measurements Available	November 26, 1978
Original Borehole Depth	9.2 m
New Rehabilitated Borehole Depth	8.75 m
Borehole Unblocking Method	Not blocked by ice (borehole cased)
RBR Logger Data	August 15, 2011 – August 15, 2012
Thermistor Depths (m)	0.25, 0.75, 1.75, 3.75, 8.75, (6.25 failed)
Length and Date of ERT Survey	160 m (August 7, 2012)

The thermal profile from August 7, 2012 at borehole R2 (Figure 5.15) was extracted from the RBR logger data record for comparison with the August 7, 2012 ERT results (Figures 5.16 and 5.17). Results from the daily ground temperature record show unfrozen conditions from the ground surface to the maximum depth of measurement of 8.75 m (Figure 5.15). The absence of frozen conditions in the August 1978 borehole log confirms that permafrost is not present at borehole R2 (Figure 5.15). However, a more horizontal view of ground conditions from the 160 m ERT survey suggest the possible presence of isolated patches of frozen ground (Figure 5.17).

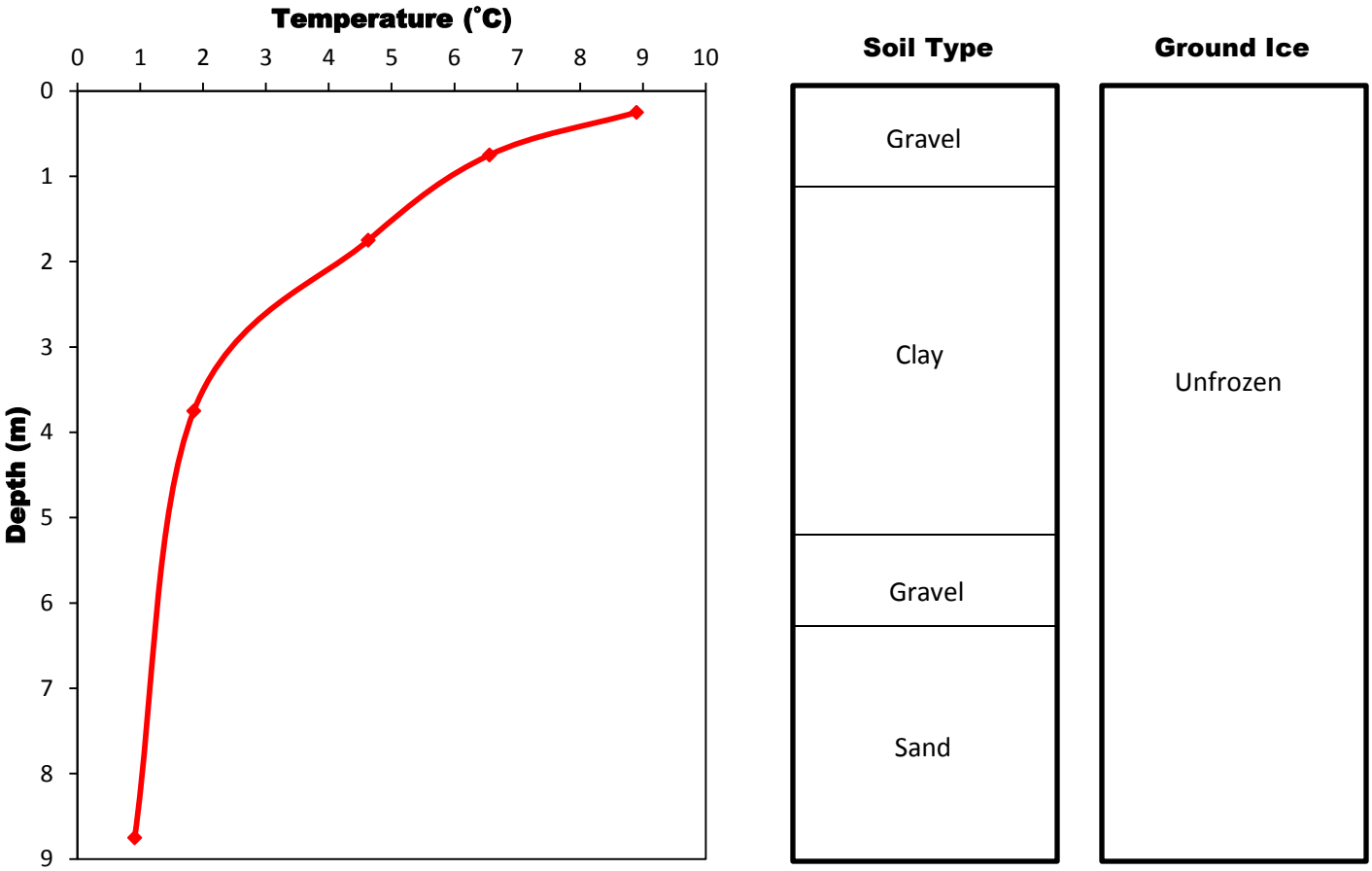

Figure 5.15: Borehole R2 average daily temperature measurements taken from the RBR logger on the same day as the ERT survey of August 7, 2012. The diamonds represent the points of temperature measurement. Soil type and ground ice conditions taken from an August 1978 borehole log are shown on the right hand side. Complete descriptions of the borehole log and ground ice classification are found in Appendix K.

The ERT survey runs from a north-east, south-west orientation with the borehole located at the mid-point of the profile (Figures 5.16 and 5.17). The 160 m ERT transect runs through small clearings with scattered shrubs averaging 2.0 m in height as well as areas with full grown spruce trees (Figure 5.16). The ground surface along the survey was consistently dry, with dry grasses and dry organic matter (Figure 5.16).

The ERT survey shows a horizontal higher resistivity layer from the surface down to about 7.5 m ranging from approximately 150-600 Ohm-m underlain by a lower resistivity layer in the 100-150 Ohm-m range from approximately 7.5 m down to the bottom of the survey at 25 m. Probing results were highly variable, giving a mean depth of 29 cm with a relatively high standard deviation (N=61, SD=10) and did not reach a frost table. The top of the soil probed was mostly dry organic matter and soft loose clay underlain by harder dry clay and gravel which could not be penetrated (Figure 5.17). The observed horizontal resistivity layering of the ERT modelled pseudosection may be associated with the stratigraphic contrast which can be seen from the borehole log (Figures 5.15 and 5.17). The stratigraphy could be producing the higher resistivity values for the upper layer or they may be due to lateral differences in frozen ground conditions (Figures 5.15 and 5.17). Negative ground temperatures measured at approximately the same depth in Borehole R1 in the same material (clay) with similar resistivity values support the possible presence of isolated patches of frozen ground in the process of thawing (Figure 5.17). However, the ERT survey at borehole R1 was conducted in June when seasonally frozen ground is more likely to be present. Relatively uniform resistivity values below the 9.2 m borehole log to the bottom of the profile at 25 m suggest a consistent lithology with sand and gravel (Figures 5.15 and 5.17).

Figure 5.16: Resistivity transect of the 160 m NE-SW survey at borehole R2 on August 7, 2012. (A) Picture taken from the 40 m point looking north-east towards the start of the transect; (B) picture taken from the borehole at the 80 m mid-point looking north-east; (C) picture taken from the borehole at the 80 m mid-point looking south-west; and (D) picture taken from the 120 m point looking south-west towards the end of the survey line.

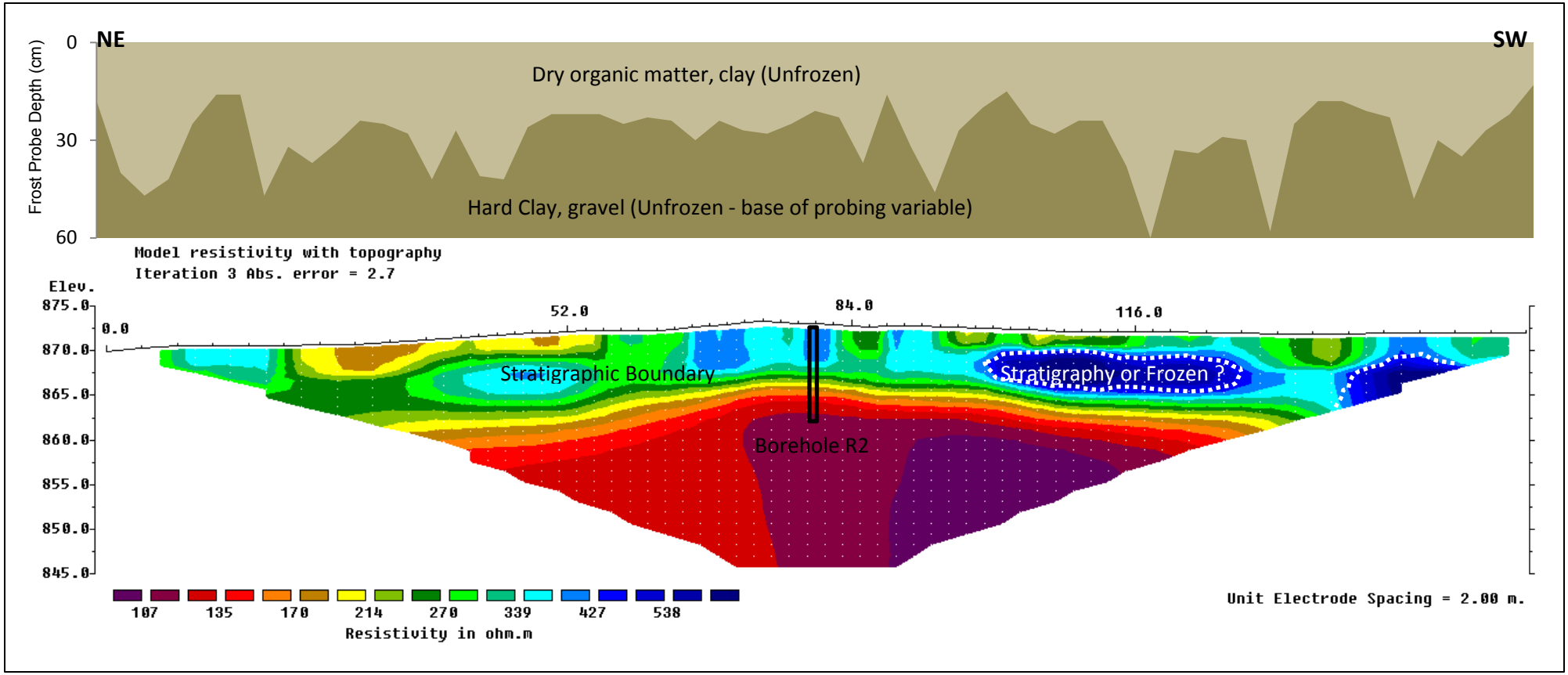

Figure 5.17: Borehole R2 NE-SW 160 m resistivity profile and frost probe chart from August 7, 2012. Vertical exaggeration in model section display = 1.00. Based on 317 data points (28 removed from original survey). The solid black lines indicates the location and depth of the 2011 borehole on the survey. The interior of the white dashed circles indicates ground conditions interpreted as possibly being frozen.

The ground temperature record from borehole R2 represents a full year of measurements between August 15, 2011 and August 15, 2012 (Figure 5.18). The 2011-2012 record shows ground temperature values below 0˚C between October 14 – May 19 at 0.25 m and between December 15 – May 24 at 0.75 m (Figures 5.18 and 5.19). Ground temperatures did not fall below 0˚C at 1.75 m, 3.75 m or 8.75 m (Figures 5.18 and 5.19). The time lag between freezing at 0.25 m and 0.75 m was approximately 62 days (Figures 5.18 and 5.19). Zero curtain effects are seen during freeze-up at 0.75 m between December 6 and December 28 for a total of 22 days and for 37 days during the spring thawing season between April 18 and May 25 (Figure 5.19). Ground temperatures reached 0.1˚C at 1.75 m but did not fall below 0˚C because of the time taken to freeze the overlying layers (Figure 5.19).

Mean monthly ground temperature (MMGT) results for BH R2 show a maximum MMGT of 8.4˚C for the first thermistor at 0.25 m reached in July 2012 and a minimum MMGT of -1.7˚C in January 2012 (Figure 5.20). MMGT for the deepest measured thermistor at 8.75 m reaches a maximum of 1.3˚C in January 2012 and a minimum of 0.9˚C in August 2012 (Figure 5.20).

The maximum ground temperature at 0.25 m was 10.2˚C on July 28, 2012 and the minimum of -4.3˚C was reached on November 25, 2011 (Figures 5.18 and 5.21). The maximum ground temperature at the deepest measurement point of 8.75 m was 1.3˚C on January 3, 2012 and the minimum ground temperature was 0.9˚C on August 18, 2012 (Figures 5.18 and 5.21). The range in temperatures at 0.25 m is about 15.2˚C, which is reduced to approximately 0.4˚C at 8.75 m (Figures 5.18 and 5.21). The mean annual ground temperature was 1.8˚C at 0.25 m and the MAGT warmed to 1.9˚C at 0.75 m, cooling thereafter to 1.1˚C at 8.75 m (Figure 5.21). The depth of ZAA was not reached in BH R2 and is therefore deeper than 8.75 m. MAGTs are all greater than 0˚C which confirms that permafrost is not present at the borehole site (Figure 5.21).

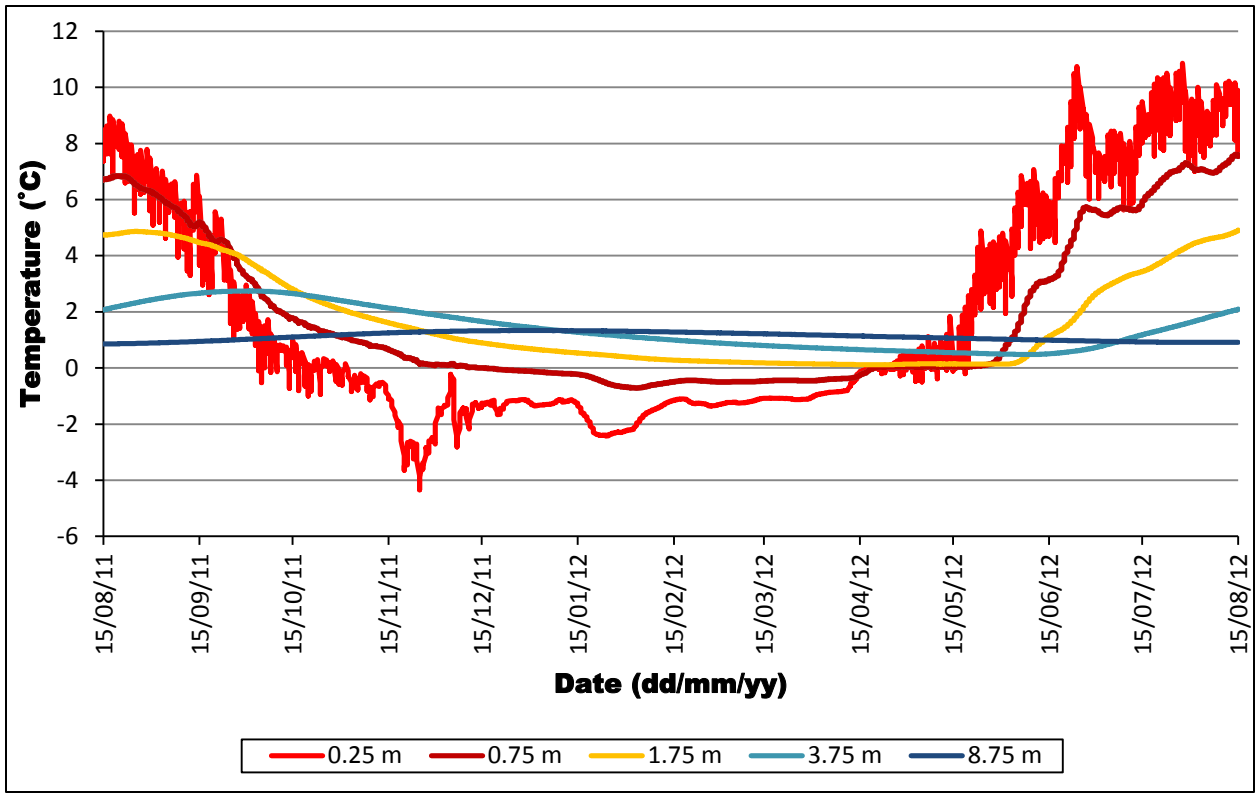

Figure 5.18: Full ground temperature series at Borehole R2 between August 15, 2011 and August 15, 2012.

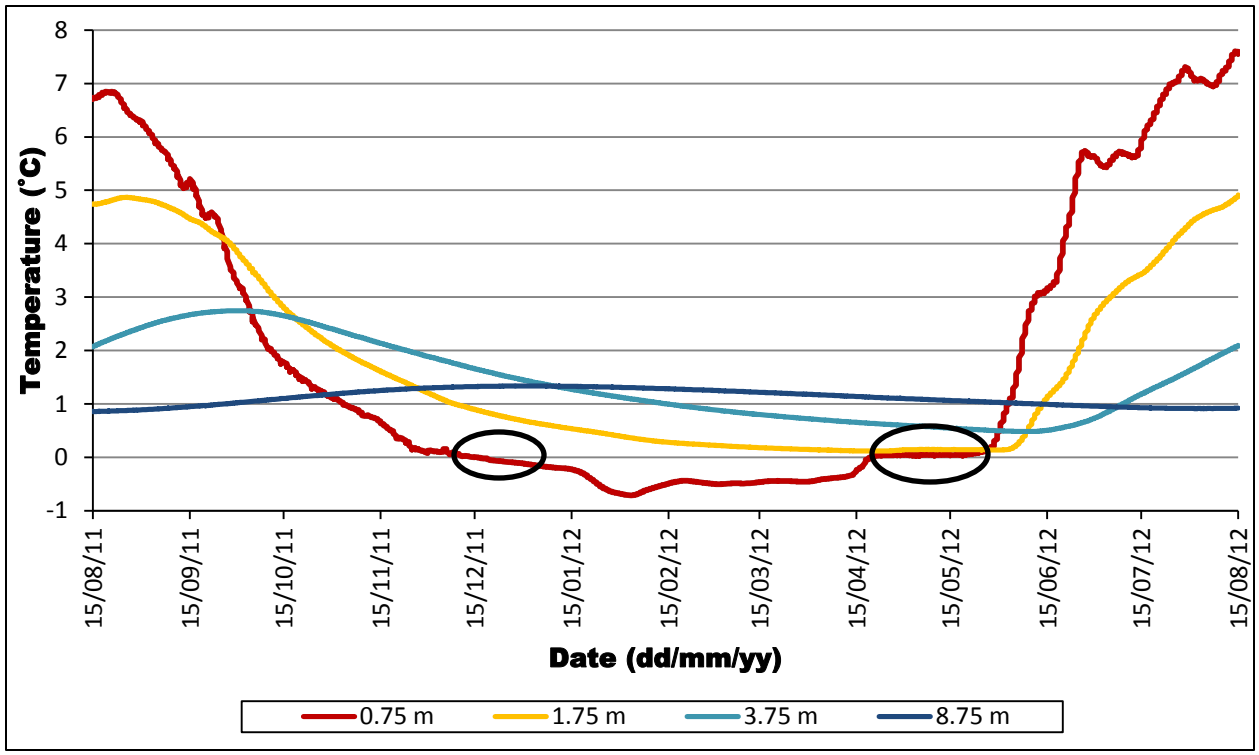

Figure 5.19: Deeper ground temperature series at Borehole R2 between August 15, 2011 and August 15, 2012. The black circles indicate zero curtain effects during freezing and thawing.

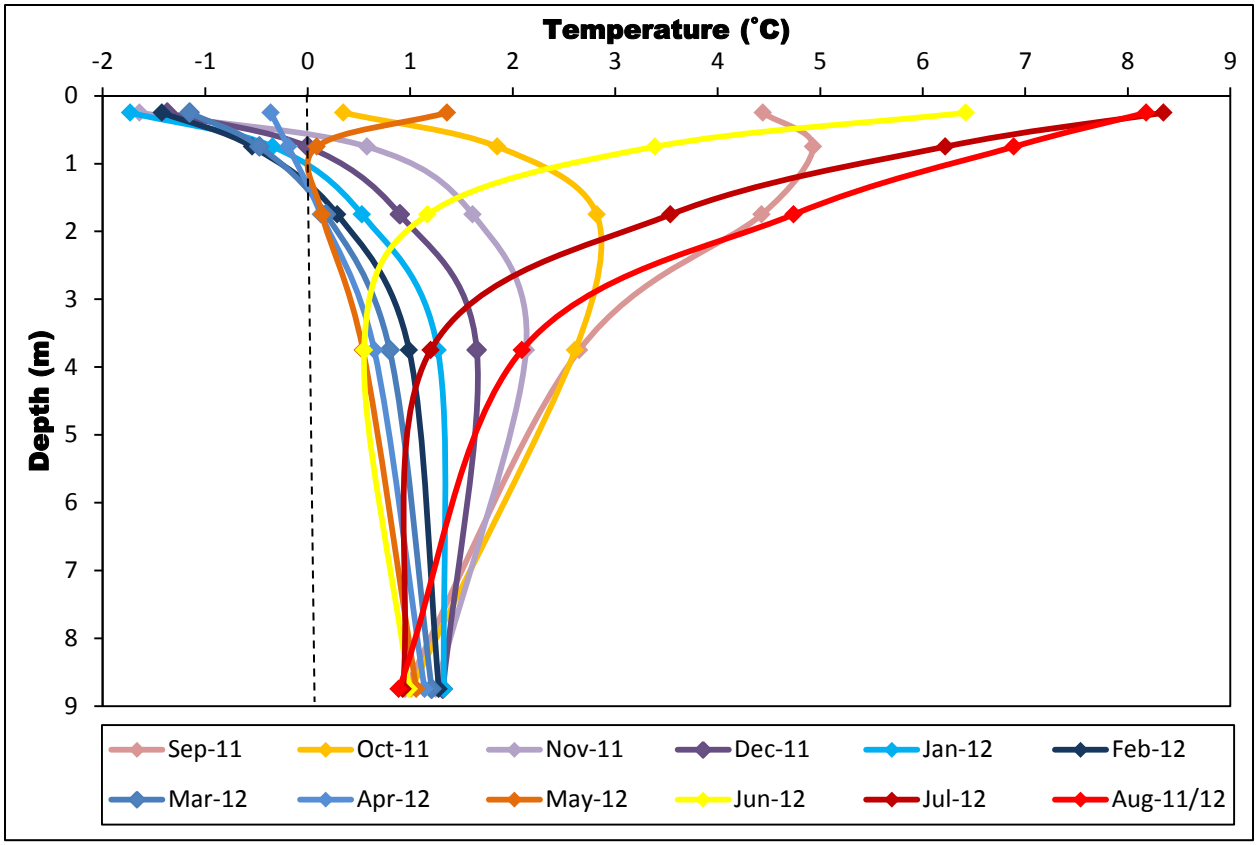

Figure 5.20: Monthly average ground temperature profiles at Borehole R2 from September 2011 to August 2012.

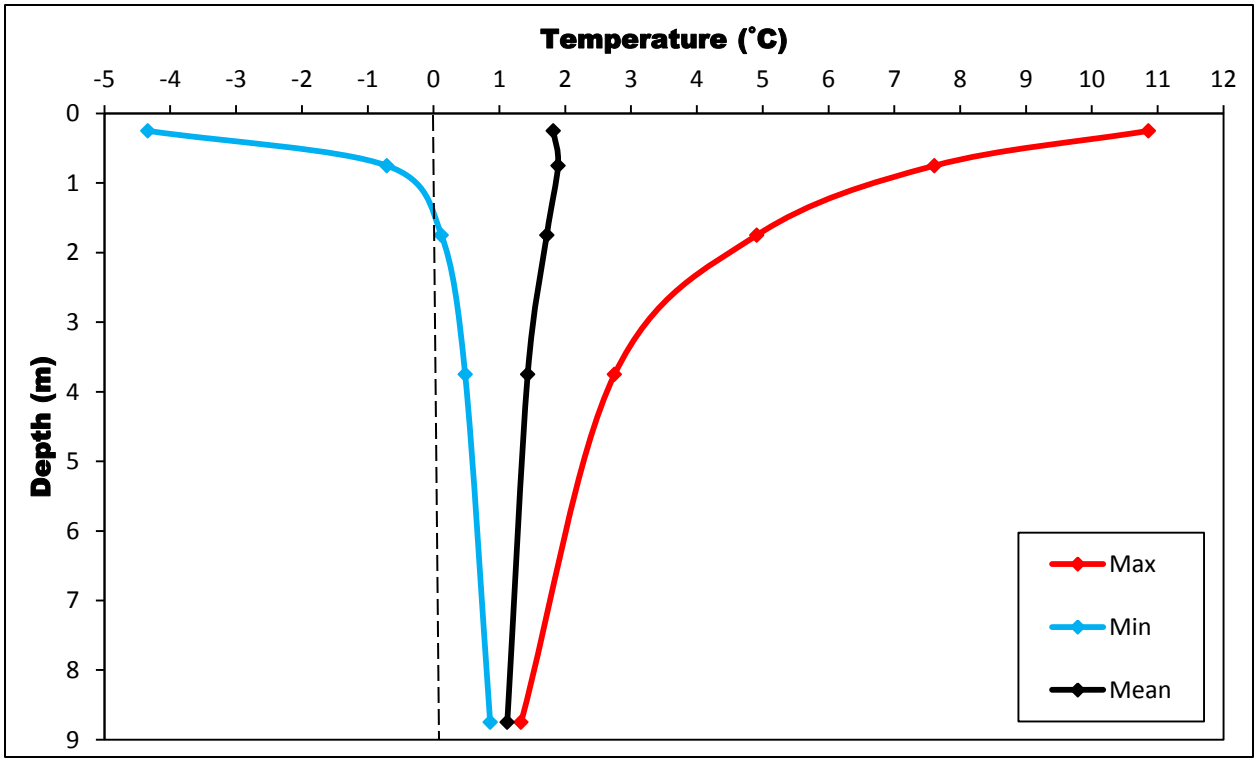

Figure 5.21: Temperature envelope at Borehole R2 for the 2011-2012 year.

Comparisons between manual ground temperature measurements from November 26, 1978 to November 26, 2011 show pronounced long term ground temperature warming for all depths (Figure 5.22). Ground temperatures were approximately 1.1˚C warmer at 1.75 m, 1.8˚C warmer at 3.75 m and 1.1˚C warmer at 8.75 m on November 26, 2011 than on the same day in 1978 (Figure 5.22). These changes are significantly greater than potential measurement errors and therefore the ground has warmed over the three decade interval.

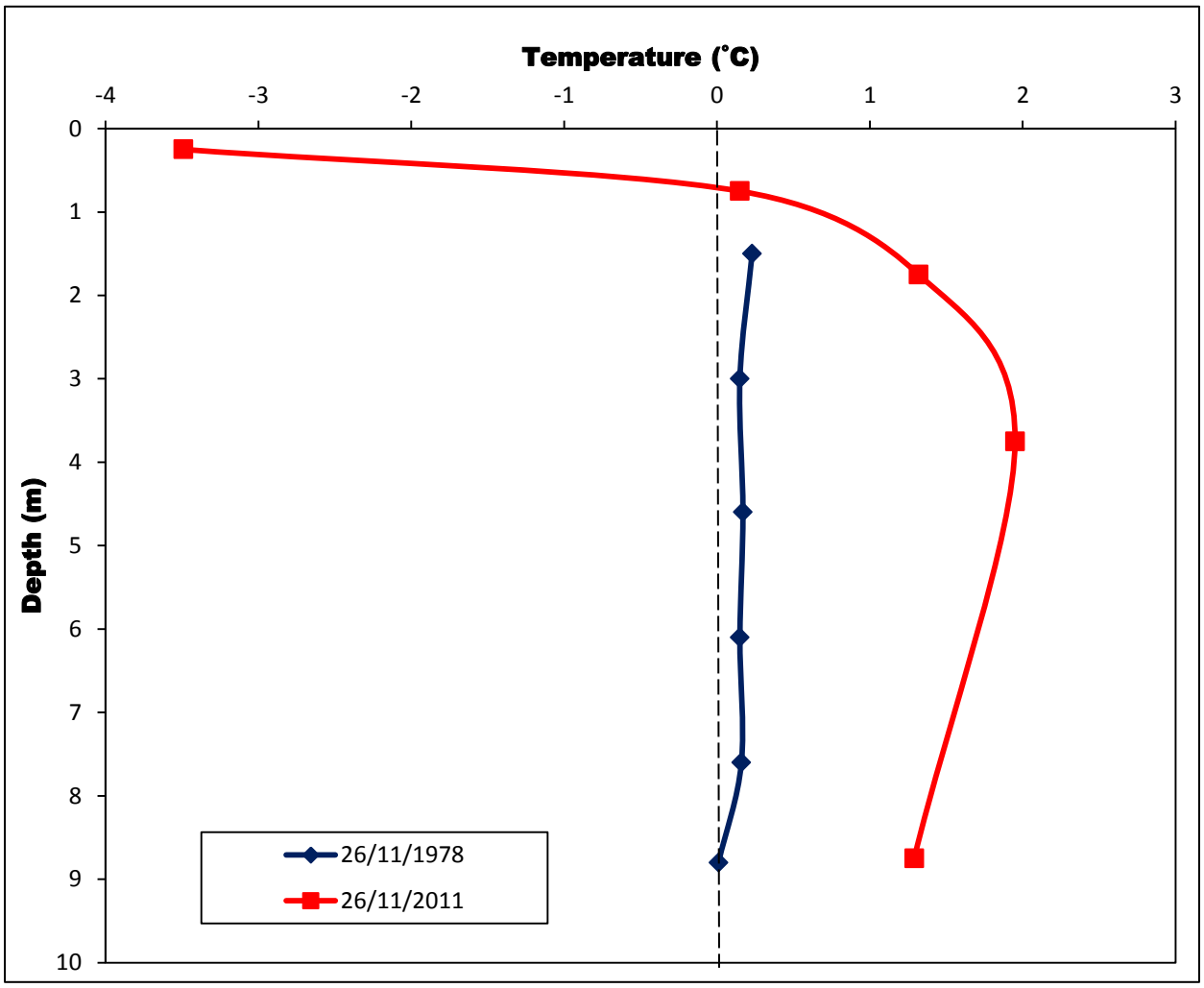

Figure 5.22: Ground temperature differences at borehole R2 between November 26, 1978 and November 26, 2011.

Variations in TDDs and FDDs between specific periods in the 1978 and 2011 climate record at the Haines Junction ECCS weather station were examined to better interpret ground temperature variations (Table 5.5). The thawing season preceding the November 26, 1978 manual ground temperature measurements had 171 TDD more than the thawing season preceding the November 26, 2011 measurements while the fall freezing period immediately preceding the November 26, 1978 measurements had 148 FDD less than the same period in 2011 (Table 5.5). The lower TDD and higher FDD observed in 2011 show that 2011 was cooler than 1978 and this could have slightly decreased the long term ground temperature difference in the near surface (Table 5.5). This suggest that the 1.1˚C – 1.8˚C warmer ground temperatures measured in 2011 are probably due to long term climate warming and environmental changes such as clearing of the site for drilling.

Table 5.5: TDDs and FDDS comparison at Haines Junction ECCS weather station between 1978 and 2011. This table relates to the immediate thawing and freezing season preceding the ground temperature measurements from Figure 5.20.

Thawing 01/01/1978 – 26/11/1978	Thawing 01/01/2011 – 26/11/1978	Freezing Fall 1978 – 26/11/1978	Freezing Fall 2011 – 26/11/2011
1600 TDD	1429 TDD	334 FDD	482 FDD

5.2.3 Borehole R3 (78-A-64)

The permafrost thermal monitoring site at borehole R3 is located in the sporadic discontinuous permafrost zone of the Yukon Territory at 61˚ 14’ 17’’ N and 138˚ 46’ 52’’ W and at 845 m elevation (Figure 5.23). The field site is located approximately 1.3 km from the south-west shore of Kluane Lake at about 230 m from the Alaska Highway and 22 m from a regrown cut-line used for previous geophysical work in the 1970s. The borehole site had already been cleared in the past before drilling. Vegetation at the BH R3 site had re-grown by the time of the 2011-2012 field work visits and consisted mainly of shrubs and small spruce trees averaging 1.5 m to 3 m in height (Figures 5.23). The borehole was drilled to a depth of 9.2 m on August 20, 1978. Soil type and ground ice conditions from the August 20, 1978 borehole log indicate a thin layer of peat at the surface to a depth of 0.6 m underlain by a layer of clay to 1.1 m, a layer of sand between 1.1 m and 4.8 m and a layer of clay from 4.8 m to the bottom of the borehole at 9.2 m (Figure 5.24).

Figure 5.23: (A) Borehole R3 as it was found during the summer 2011 borehole exploration; (B) and borehole R3 after it was rehabilitated and cased.

When it was drilled, the soil was unfrozen from the surface down to 0.7 m in the peat layer, with visible individual ice crystals or inclusions (Vx) between 0.7 m and 3.5 m and un-specified frozen conditions from 3.5 m to the bottom of the borehole log at 9.2 m (Figure 5.24). The borehole was unblocked of ice by steam and cased on August 16, 2011 and a RBR logger with a multithermistor string was installed to a depth of 6.6 m on the same day. The length of the current ground thermal monitoring record as well as other related field work associated with borehole R3 and pertinent information is summarized in Table 5.6.

Table 5.6: Summary table of the data used in the analysis of borehole R3 and the depths of the thermistors from the surface. Note that more detailed field work and RBR logger information is given in Appendix C.

Borehole R3	
Closest ECCS Station and Distance	Burwash (17 km)
Date of 1978 drilling	August 20,1978
Manual Temperature Measurements Available	November 22, 1978 ; July 26, 1979
Original Borehole Depth	9.2 m
New Rehabilitated Borehole Depth	6.6 m
Borehole Unblocking Method	Steaming (borehole cased)
Borehole Unblocking Date	August 16, 2011
RBR Logger Data	August 17, 2011 – August 17, 2012
Thermistor Depths (m)	0.1, 0.6, 1.1, 2.1, 4.1, 6.6
Length and Date of ERT Survey	160 m (August 8, 2012)

The thermal profile from August 8, 2012 at borehole R3 (Figure 5.24) was extracted from the RBR logger data record for comparison with the August 8, 2012 ERT results (Figures 5.25 and 5.26). Results from the daily ground temperature record show frozen conditions to the maximum depth of measurement of 6.6 m with an interpolated active layer approximately 0.9 m in thickness (Figure 5.24). The thickness of the active layer was estimated by linear interpolation between the thermistors and the 0˚C bracket but the spacing of the sensors means that the precision of the estimate is low (Figure 5.24). The 1978 borehole log indicates a thawed layer from the surface down to 0.7 m on August 20, 1978 which is indicative of an increase in active layer thickness of about 0.2 m when compared to the same period in 2012 (Figure 5.24).

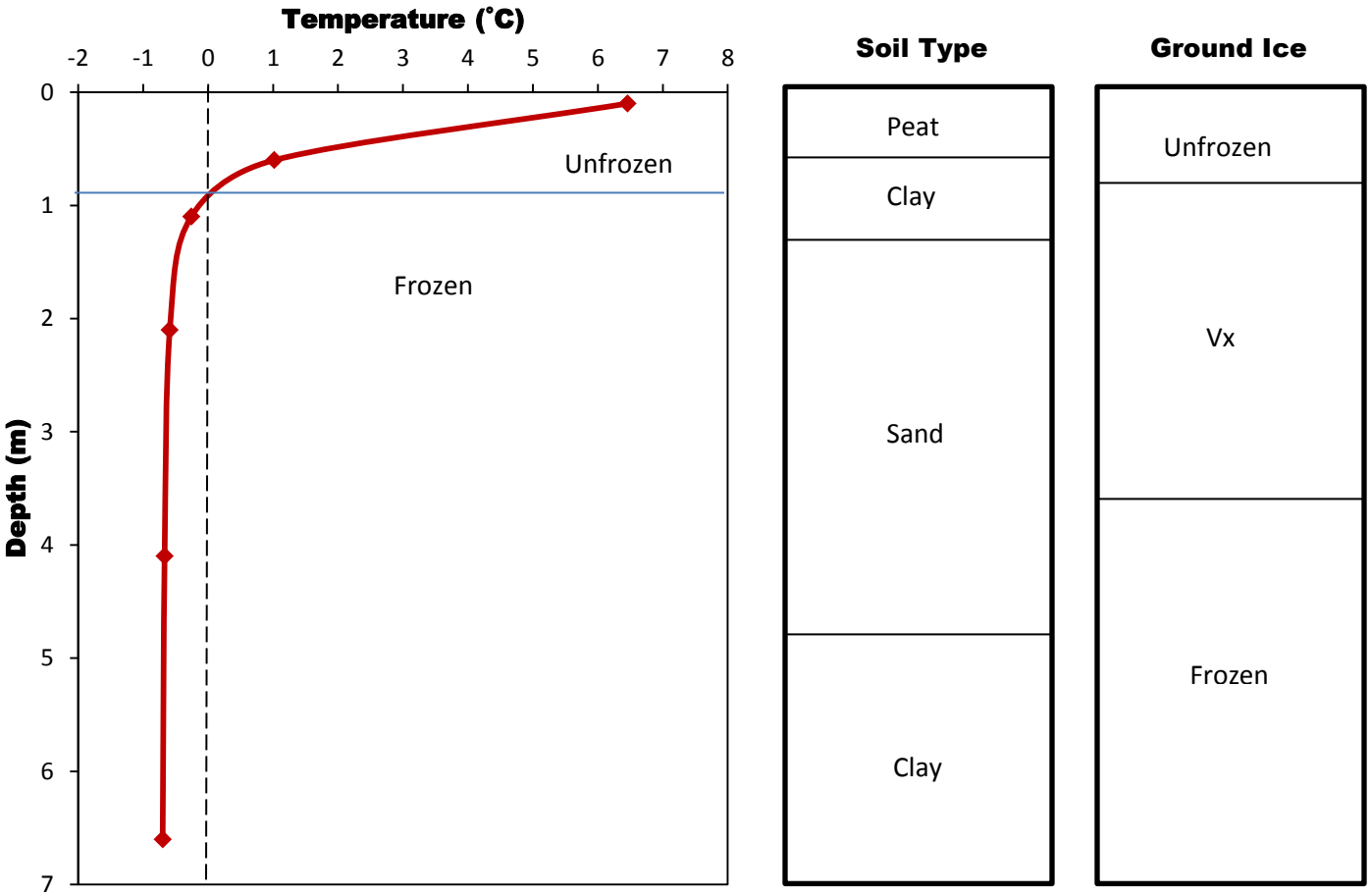

Figure 5.24: Borehole R3 average daily temperature measurements taken from the RBR logger on the same day as the ERT survey of August 8, 2012. The diamonds represent the points of temperature measurement. Soil type and ground ice conditions taken from an August 20, 1978 borehole log are shown on the right hand side. Complete descriptions of the borehole log and ground ice classification to a depth of 9.2 m are found in Appendix K.

The 160 m ERT profile at BH R3 runs from a north-east, south-west direction, crossing a regrown cut-line used for previous geophysical work in the 1970s between 54 m and 68 m (Figures 5.25 and 5.26). The ERT survey runs through a mature spruce forest with areas with dense shrubs with a ground surface consisting mainly of dry mosses and dry organic matter (Figure 5.25). The terrain rises by approximately 13 m from the start to the end of the survey (Figure 5.26).

Probing results along the survey line were highly variable, giving a mean thaw depth of 69 cm with a high standard deviation (N=61, SD=23) (Figure 5.26). A frost table could not be reached (active layer > 120 cm) at the start of the survey from 0 m to 8 m and around the borehole casing between 76 m to 82 m along the survey line (Figure 5.26). These areas of unfrozen ground are represented on the modelled ERT pseudosection as lower resistivity areas in the range of 200 Ohm-m to 250 Ohm-m (Figure 5.26). This interpretation of the resistivity results is supported by an interpolated portion of the frost table at a depth of 0.9 m at BH R3 on the day of the ERT survey (Figure 5.24). Shallower active layers are not identifiable on the modelled resistivity plot due the fact that the inversion routine cannot cope with extremely high resistivity contrast in the near surface at the unfrozen/frozen interface (Hilbich et al., 2008; Miceli, 2012). The regrown cut-line used for previous geophysical work in the 1970s does not seem to have resulted in significant differences in vertical resistivity and frost probe results do not suggest deeper thaw. However, compact clay limited probing on the cut-line and active layers may be thicker.

High resistivity values (>20 000 Ohm-m) from 0.7 m down to the bottom of the borehole at 6.6 m matched with negative temperatures recorded on the day of the survey are indicative of permafrost at this site (Figures 5.24 and 5.26). Stratigraphic layering from the 1978 borehole log and changes in unfrozen moisture content between clay and sand may have produced the layers on the resistivity plot where the sand layer between 1.4 m and 4.8 m shows significantly higher resistivity values than the overlying and underlying clay layers (Hauck and Kneisel, 2008) (Figures 5.24 and 5.26). Negative ground temperatures around -1˚C in the sand layer also suggest low unfrozen water content which subsequently translates into higher resistivity values (Osterkamp and Burn, 2003) (Figures 5.24 and 5.26). Resistivity values greater than 2000 Ohm-

m down to the bottom of the resistivity plot suggest permafrost deeper than 25 m at borehole R3 (Figure 5.26).

Figure 5.25: Resistivity transect of the 160 m NE-SW survey at borehole R3 on August 8, 2012. (A) Picture taken from the 40 m point looking north-east towards the start of the transect; (B) picture of the survey crossing the regrown cut-line between 54 m and 68 m; (C) picture taken from the borehole at the 80 m mid-point looking north-east; (D) picture taken from the borehole at the 80 m mid-point looking south-west; and (E) picture taken from the 120 m point looking south-west towards the end of the survey line.

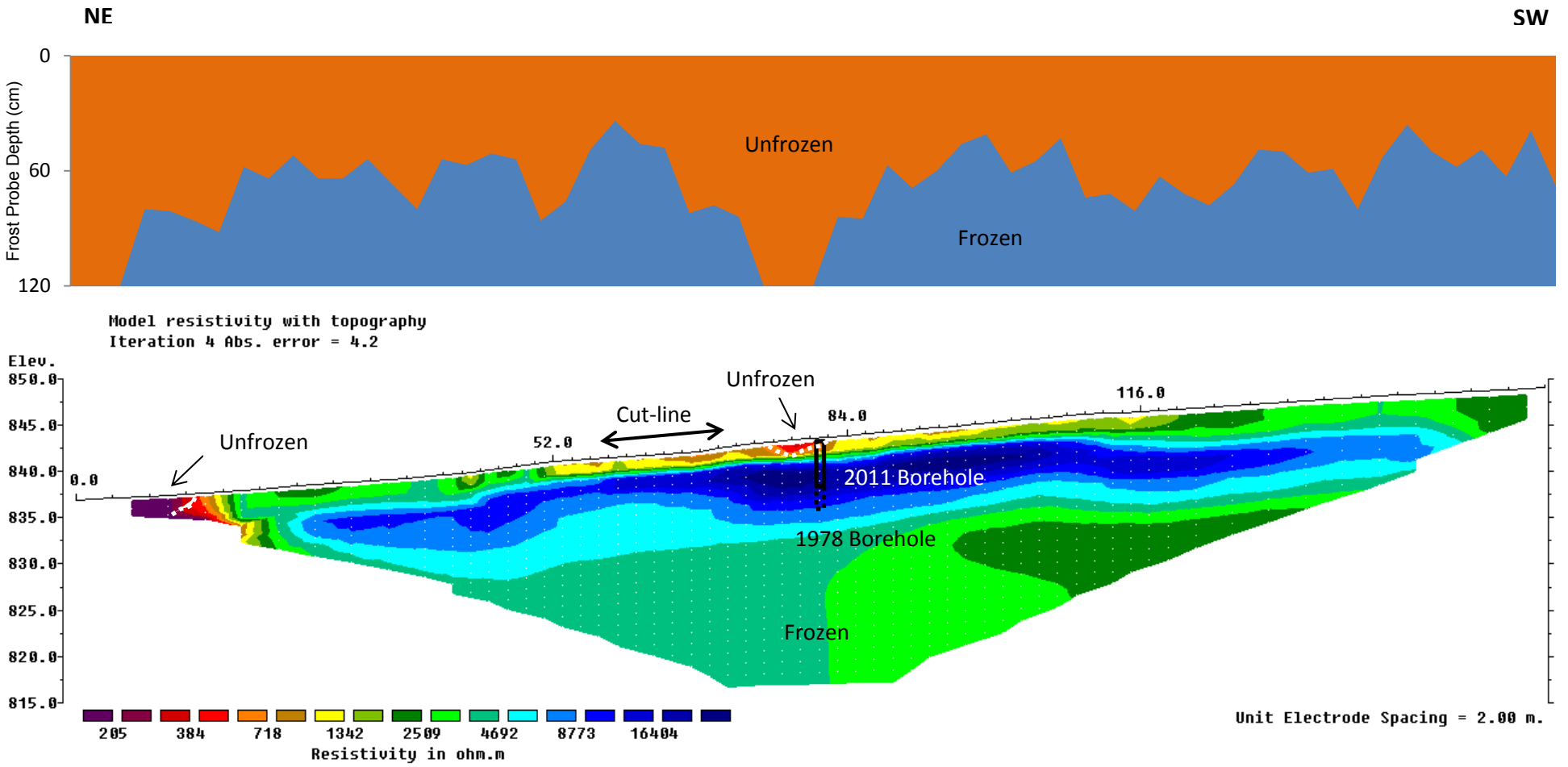

Figure 5.26: Borehole R3 NE-SW 160 m resistivity profile and frost probe chart from August 8, 2012. Vertical exaggeration in model section display = 1.00. Based on 337 data points (8 removed from original survey). The solid black lines indicates the location and depth of the 2011 borehole on the survey while the black dash lines indicate the original depth of the borehole in 1978.

The ground temperature record from borehole R3 represents a full year of measurements between August 17, 2011 and August 17, 2012 (Figure 5.27). Recovery following drilling did not occur until approximately September 20, 2011. The 2011-2012 record shows ground temperature values below 0˚C between September 25 – May 14 at 0.1 m and between October 5 – June 30 at 0.6 m (Figures 5.27 and 5.28). Ground temperatures remained below 0˚C for the entire year at 1.1 m, 2.1 m, 4.1 m and 6.6 m depths (Figures 5.27 and 5.28). The time lag between freezing at 0.1 m and 0.6 m was approximately 125 days (Figures 5.27 and 5.28). Zero curtain effects are seen during freeze-up at 0.6 m between October 5 and January 28 for a total of 125 days and for 14 days during the spring thawing season between June 30 and July 13 (Figure 5.28). The long zero curtain effect observed during freeze-up at 0.6 m may be due to the high water content present in the active layer after drilling.

MMGT results for BH R3 show a maximum MMGT of 5.8˚C for the first thermistor at 0.1 m reached in August 2012 and a minimum MMGT of -3.7˚C in November, 2011 (Figure 5.29). The maximum ground temperature at 0.1 m was 8.6˚C on July 27, 2012 and the minimum of -6.7˚C was reached on November 20, 2012 (Figures 5.27 and 5.30). The range in ground temperatures at 0.1 m is about 15.4˚C which is reduced to approximately 0.4˚C at 2.1 m (Figures 5.27 and 5.30). Ground temperatures at 4.1 m and 6.6 m remain constant throughout the year at approximately -0.7˚C with minimal variations < 0.1˚C indicating the D_{ZAA} to occur around 4.1 m at borehole R3 (Figure 5.30). The MAGT at the D_{ZAA} is approximately -0.7˚C. The mean annual ground temperature was -0.1˚C at 0.1 m cooling thereafter to -0.7˚C at 6.6 m (Figure 5.30). The MAGT at 0.6 m is slightly warmer than it should be which may be due to a longer freeze-up after water percolation during drilling (Figure 5.30). MAGTs are all below 0˚C which confirms that permafrost is present at this site (Figure 5.30).

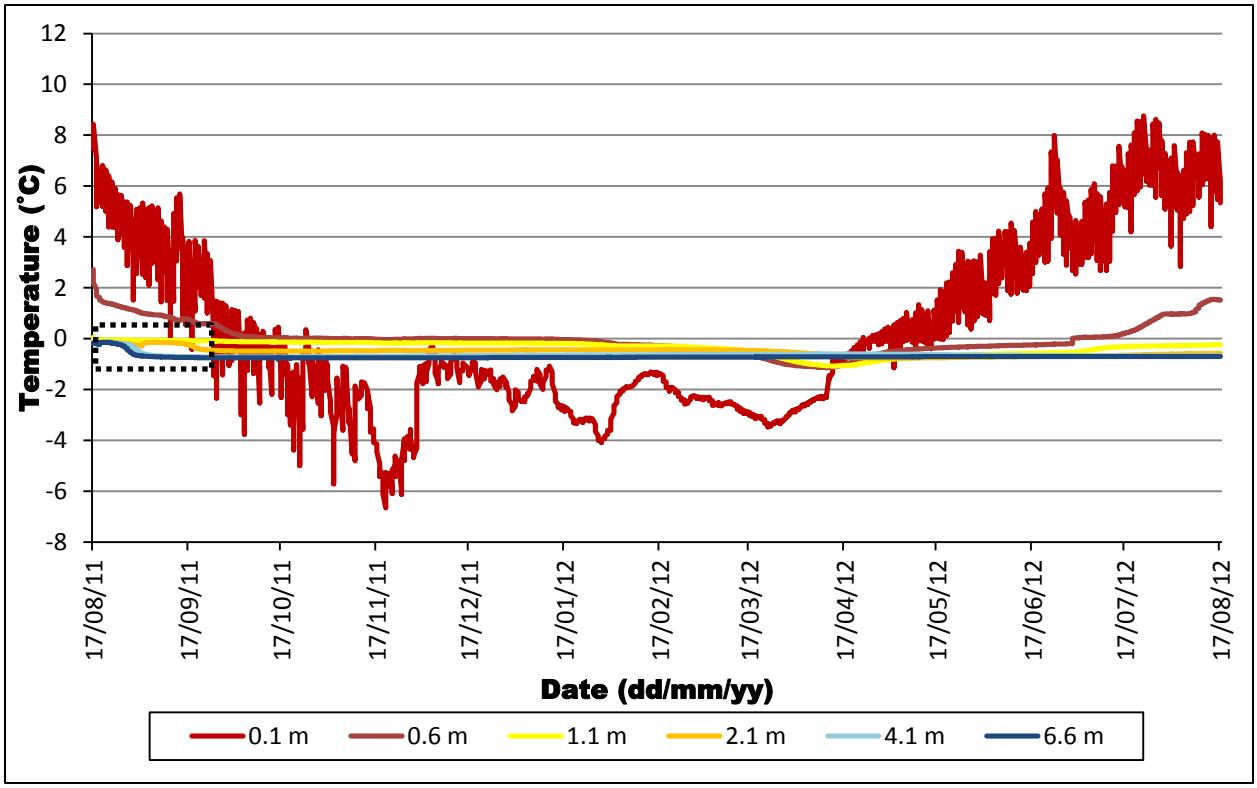

Figure 5.27: Full ground temperature series at Borehole R3 between August 17, 2011 and August 17, 2012. Note that deeper thermistors do not recover after drilling before September 20, 2011 (dashed box).

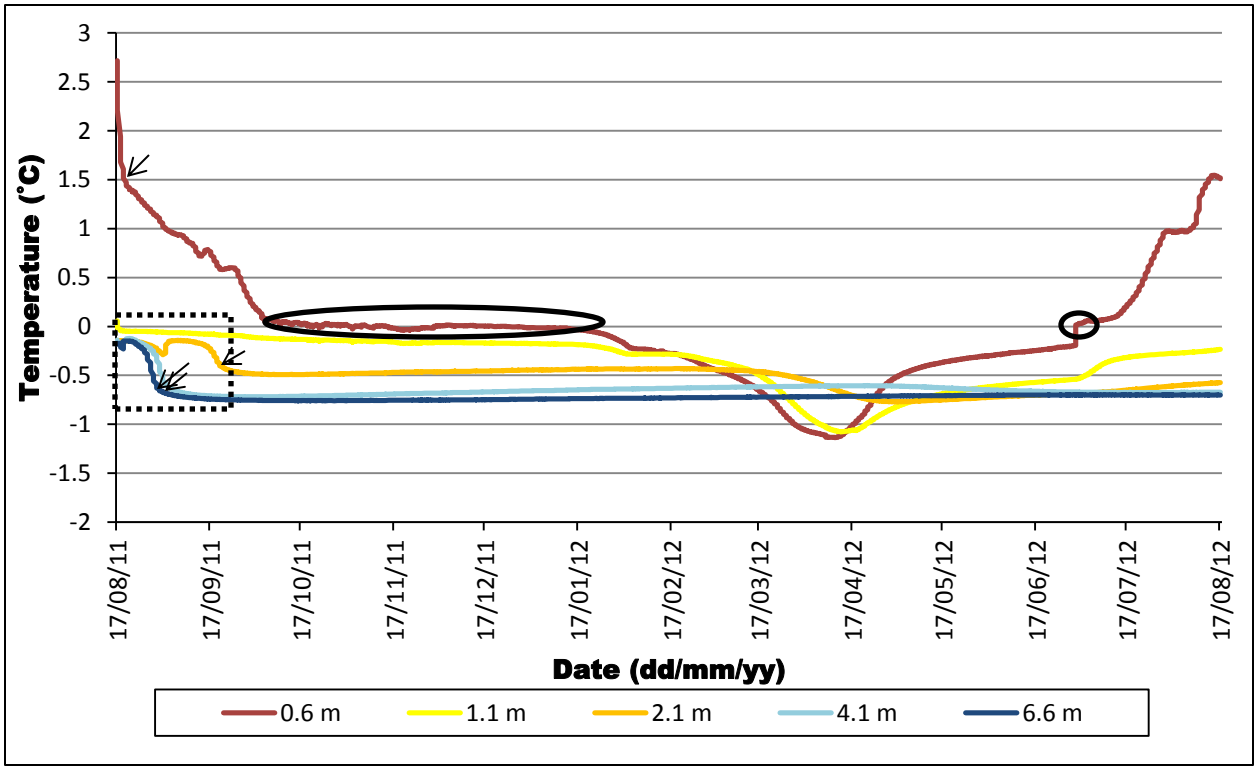

Figure 5.28: Deeper ground temperature series at Borehole R3 between August 17, 2011 and August 17, 2012. Note that deeper thermistors do not recover after drilling before September 20, 2011 (dashed box). The arrows indicate the approximate post-drilling recovery dates. The black circles indicate zero curtain effects during freezing and thawing.

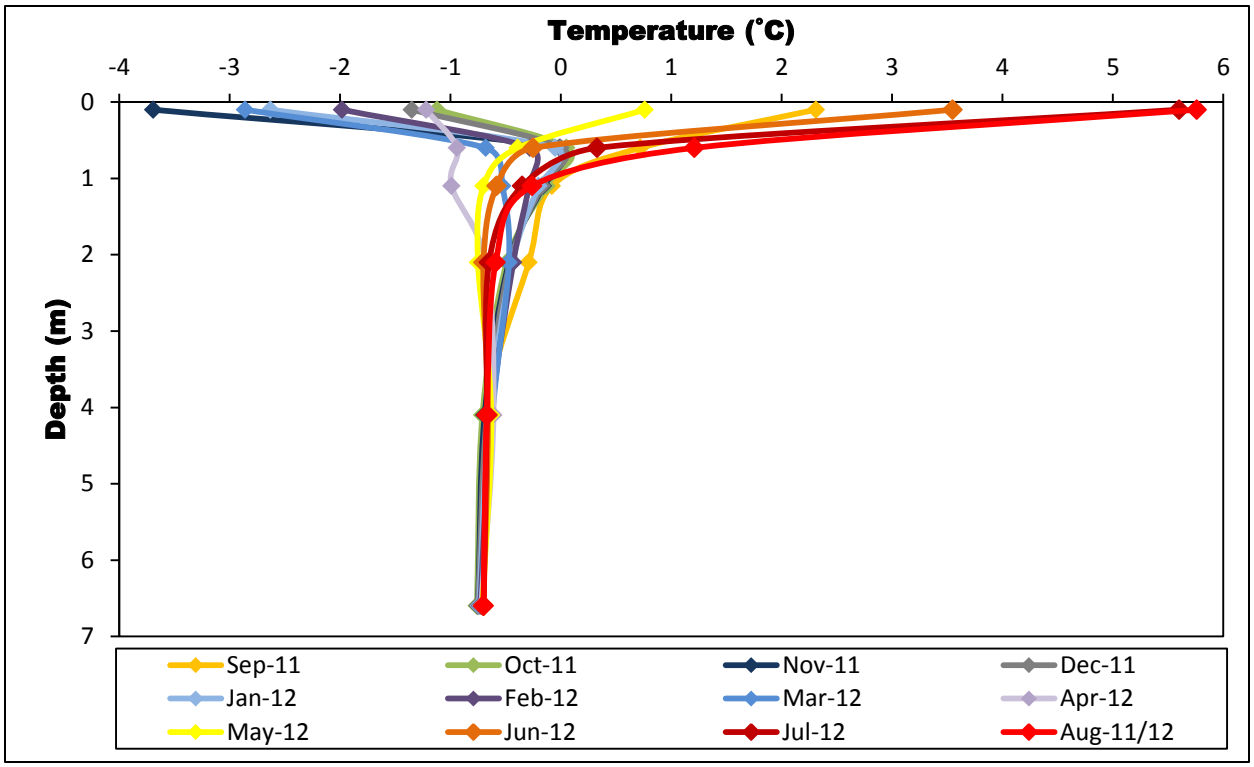

Figure 5.29: Monthly average ground temperature profiles at Borehole R3 from September 2011 to August 2012.

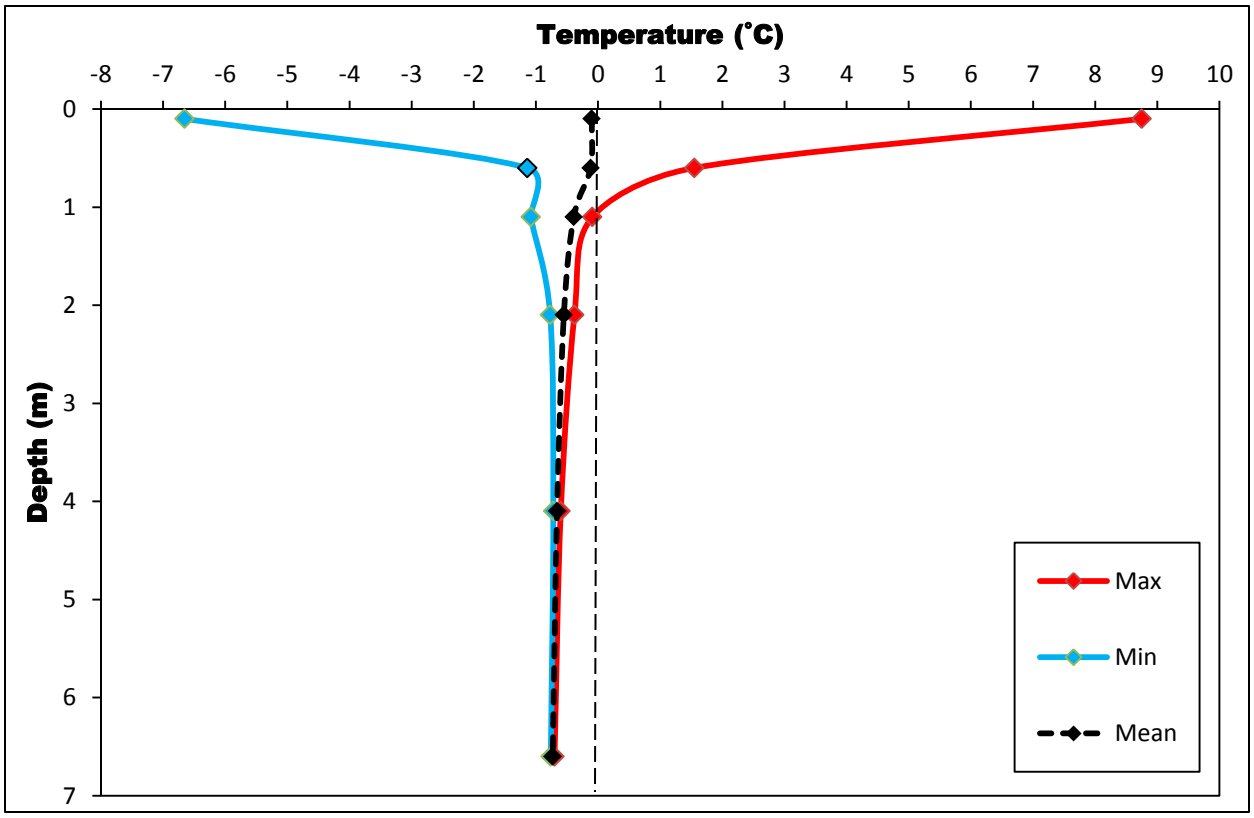

Figure 5.30: Temperature envelope at Borehole R3 for the 2011-2012 year. Note that data from August 17, 2011 to September 20, 2011 were not included in the calculations as post drilling equilibrium temperatures were not yet achieved.

Comparisons between manual ground temperature measurements from November 22, 1978 to November 22, 2011 and between July 26, 1979 to July 26, 2012 show an increase in the ground temperatures measured at borehole R3, but the change is within the margin of potential error for the manual measurements (Figure 5.31). Ground temperature were approximately 0.8˚C warmer at 2.1 m, 0.2˚C warmer at 4.1 m and 0.1˚C warmer at 6.6 m on November 22, 2011 than on the same day in 1978 (Figure 5.31A). Measured ground temperatures between July 26, 1979 and July 26, 2012 showed virtually no change (<0.1˚C) at 4.1 m while warming by about 0.2˚C at 6.6 m (Figure 5.31B). Warmer ground temperatures measured in 2011 may be due to long term climate warming and environmental changes such as the original clearing of the site for drilling.

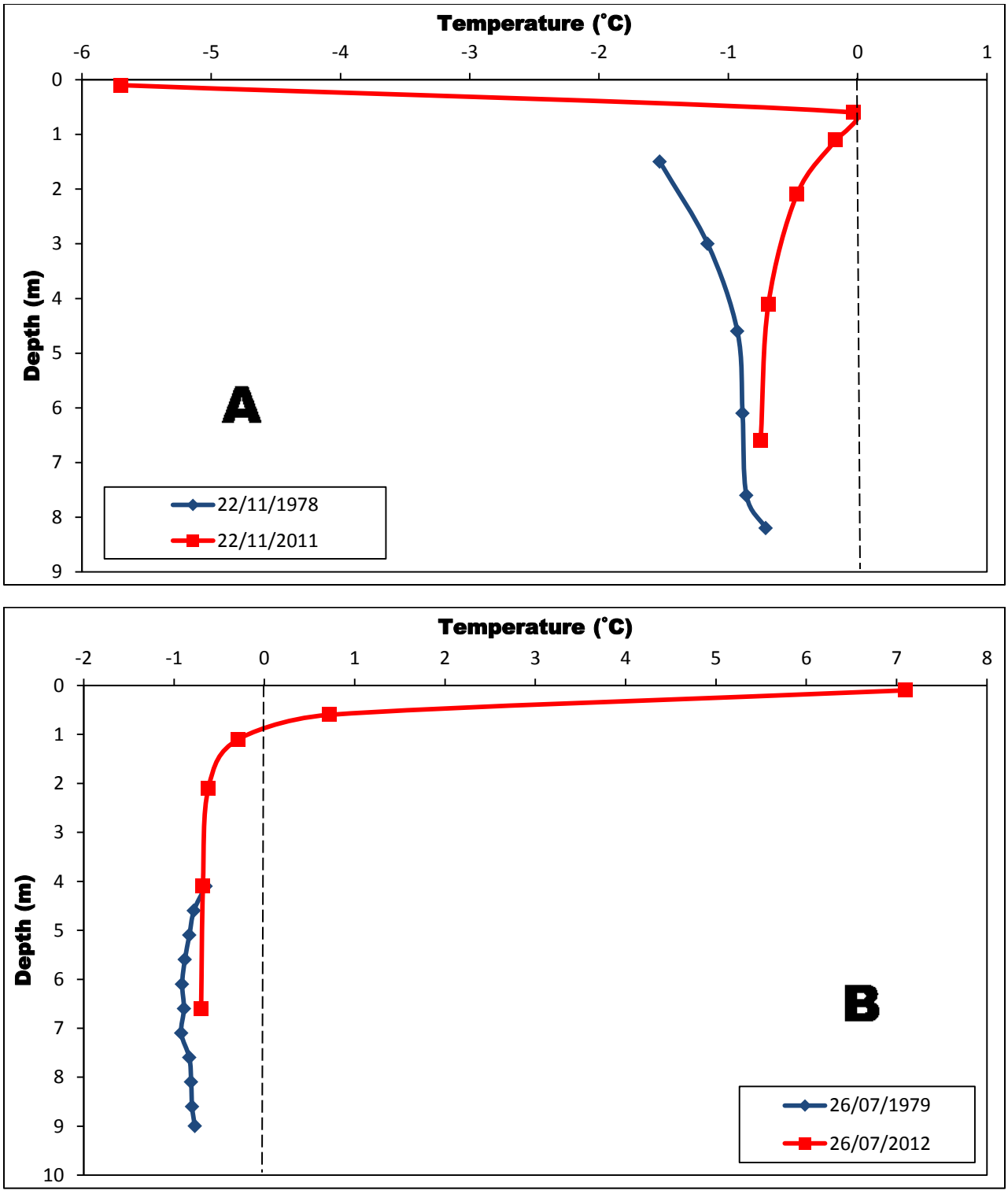

Figure 5.31: Ground temperature differences at borehole R3 between; (A) November 22, 1978 and November 22, 2011 and (B) July 26 1979 and July 26, 2012.

5.2.4 Borehole R4 (78-A-63)

The permafrost thermal monitoring site at borehole R4 is located in the sporadic discontinuous permafrost zone of the Yukon Territory at 61˚ 14’ 39’’ N and 138˚ 47’ 44’’ W and at 823 m elevation (Figure 5.32). The field site is located approximately 1.1 km from the south-west shore of Kluane Lake at about 250 m from the Alaska Highway and 28 m from a regrown cut-line used for previous geophysical work in the 1970s. The borehole was drilling in August 1978 to a depth of 5.9 m and the site was cleared before drilling. Soil type and ground ice conditions from an August 1978 borehole log indicate a layer of silt at the surface to a depth of 0.4 m underlain by a layer of clay to 1.6 m, a layer of sand between 1.6 m and 5.0 m and bedrock from 5.0 m to the bottom of the borehole at 5.9 m (Figure 5.33). Unfrozen conditions were present from the surface down to 1.8 m, with visible stratified or oriented ice (Vs) and visible individual ice crystals or inclusions (Vx) at 6% between 1.8 m and 2.6 m and not visible well bonded materials (Nbn) from 2.6 m to the bottom of the borehole log at 5.9 m (Figure 5.33).

Figure 5.32: (A) Borehole R4 as it was found during the summer 2011 borehole exploration; (B) and borehole R4 after it was rehabilitated and cased.

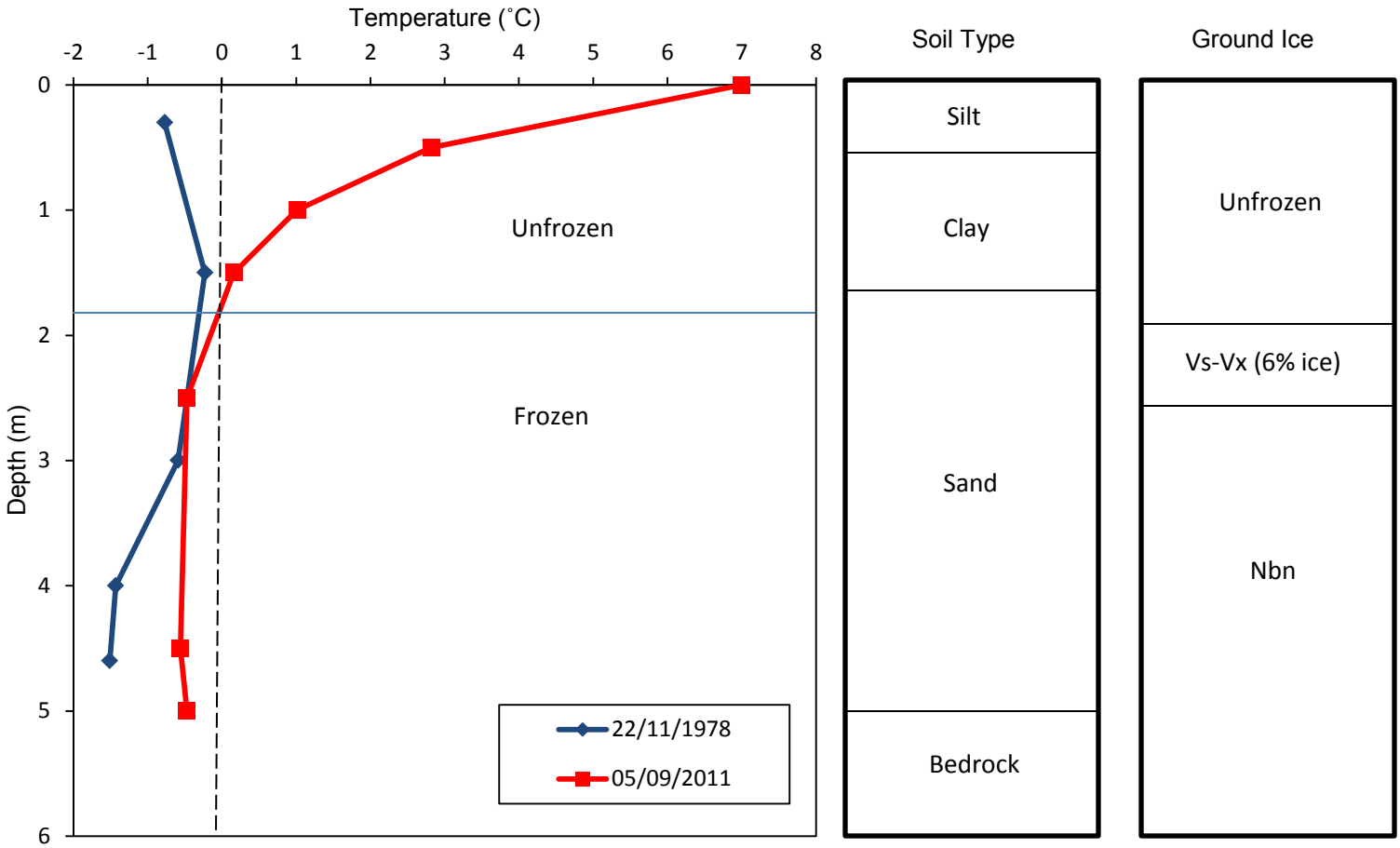

Figure 5.33: Ground temperature differences at borehole R4 between November 22, 1978 and September 5, 2011. Soil type and ground ice conditions taken from an August 1978 borehole log are shown on the right hand side. Complete descriptions of the borehole log and ground ice classification are found in Appendix K. Note that the temperature measurements were not taken on exactly the same day due to logger failure. The ERT survey was conducted on August 7, 2012.

The borehole was unblocked of ice by steam and cased on August 19, 2011 and a RBR logger with a multithermistor string was installed to a depth of 5.0 m on August 24, 2011. The borehole was found to have been destroyed by a bear when visited on June 6, 2012 and could not be repaired during the summer 2012 field season as the damaged thermistor string had frozen in the borehole and could not be removed (Figure 5.34). Data recuperated from the RBR logger show that it failed on September 5, 2011. Vegetation at the BH R4 site had re-grown by the time of the 2011-2012 field work visits and consisted mainly of scattered spruce trees and shrubs averaging 1.5 m to 3 m in height (Figures 5.32 and 5.35). Ground surface conditions around the borehole were composed of dried organic matter.

Figure 5.34: Borehole R4 on June 6, 2012. The borehole was found chewed by a bear and could not be repaired. The RBR logger record shows that the borehole was damaged on September 5, 2011.

The length of the current ground thermal monitoring record as well as other related fieldwork associated with borehole R4 and pertinent information is summarized in Table 5.7.

Table 5.7: Summary table of the data used in the analysis of borehole R4 and the depths of the thermistors from the surface. Note that more detailed field work and RBR logger information is given in Appendix C.

Borehole R4	
Closest ECCS Station and Distance	Burwash (16.5 km)
Date of 1978 drilling	August 1978
Manual Temperature Measurements Available	November 22, 1978
Original Borehole Depth	5.9 m
New Rehabilitated Borehole Depth	5.0 m
Borehole Unblocking Method	Steaming (borehole cased)
Borehole Unblocking Date	August 19, 2011
RBR Logger Data	August 24, 2011 – September 5, 2011
Thermistor Depths (m)	0, 0.5, 1.0, 1.5, 2.5, 4.5, 5.0
Length and Date of ERT Survey	160 m (August 7, 2012)

The thermal profile from September 5, 2011 at borehole R4 (Figure 5.33) was extracted from the RBR logger on the last day of record before it failed, for comparison with the November 22, 1978 manual ground temperature measurements. The September 5 measurements were taken 17 days after the borehole was steamed, so the deeper thermistors should have recovered after drilling. The active layer was estimated to be approximately 1.7 m thick on September 5, 2011 by linear interpolation between the thermistors bracketing 0˚C but the spacing of the sensors means that the precision of the estimate of the top of the frozen layer is low (Figure 5.33). This interpretation is similar the active layer measured in the August 1978 borehole log (Figure 5.33). Comparisons between November 22, 1978 manual ground temperature measurements to September 5, 2011 show long term ground temperature warming ranging from 1.0˚C to 1.1˚C between 4.0 m and 5.0 m which should be close to the D_{ZAA} based on observations at borehole R3 (Figure 5.33).

The 160 m ERT profile at BH R4 runs from a north-east, south-west direction, crossing a regrown cut-line used for previous geophysical work in the 1970s between 36 m and 52 m (Figures 5.35 and 5.36). The ERT survey runs through a mature spruce forest with areas of scattered spruce trees and dense shrubs averaging 1.5 m to 3.0 m in height (Figure 5.35). The ground surface consists of mainly dry organic matter with the exception of the last 40 m of the

survey which is in a wet marshy area (Figure 5.35). The terrain is relatively flat along the survey line with topographic variations of less than 2 m.

Probing results along the survey line were highly variable, giving a mean depth of 64 cm with a high standard deviation (N=61, SD=24) and did not reach a frost table in most cases (Figure 5.35). A frost table was only reached by probing at the start of the survey between 0 m and 24 m (Figure 5.35). Probing was variable between 42 m and 132 m and the penetration depth was limited by unfrozen hard clay and organic matter (Figure 5.35). Probing depths were all greater than 120 cm in the wet marshy area at the end of the survey line between 132 m and 160 m (Figures 5.34 and 5.35).

The areas of unfrozen ground determined by probing are represented on the modelled ERT pseudosection as low resistivity areas in the range of 90 Ohm-m to 500 Ohm-m in the uppermost 1.5 m to 2.5 m of the ground with an indeterminate zone between 500-900 Ohm-m where it is not certain if the ground is unfrozen or frozen (Figure 5.35). This can be interpreted as deep active layers which are supported by positive ground temperatures measured to a depth of 1.8 m on September 5, 2011 (Figure 5.32). The regrown cut-line between 36 m and 52 m shows low resistivity values in the range of 90 Ohm-m to 300 Ohm-m, suggesting thawed ground and the presence of a talik to a depth greater than 20 m due to environmental change (Figure 5.35).

High resistivity values from 1.8 m down to the bottom of the borehole at 5.0 m matched with negative temperatures recorded on September 5, 2011 and are indicative of permafrost at this site (Figures 5.33 and 5.36). Resistivity values in the range of 400 Ohm-m to 500 Ohm-m directly under the borehole to the bottom of the survey suggest that permafrost is present under borehole R4. However, this resistivity range is in the indeterminate zone and cannot be interpreted as frozen or unfrozen with certainty (Figure 5.36). A gradual decrease in resistivity values from the adjacent permafrost body towards the thawed cut-line indicates that the permafrost beneath BH R4, if still present, may be warming and degrading internally due to environmental change (Figure 5.36). Higher resistivity values up to 30 000 Ohm-m below the active layer to the bottom of the resistivity plot in the second half of the survey suggests colder and probably deeper permafrost that has not been affected by the surface disturbance (Figure 5.36).

Figure 5.35: Resistivity transect of the 160 m NE-SW survey at borehole R4 on August 7, 2012. (A) Picture taken from the 40 m point looking north-east towards the start of the transect; (B) picture of the survey line crossing the regrown cut-line between 36 m and 52 m; (C) picture taken from the borehole at the 80 m mid-point looking north-east; (D) picture taken from the borehole at the 80 m mid-point looking south-west; and (E) picture taken from the 120 m point looking south-west towards the end of the survey line.

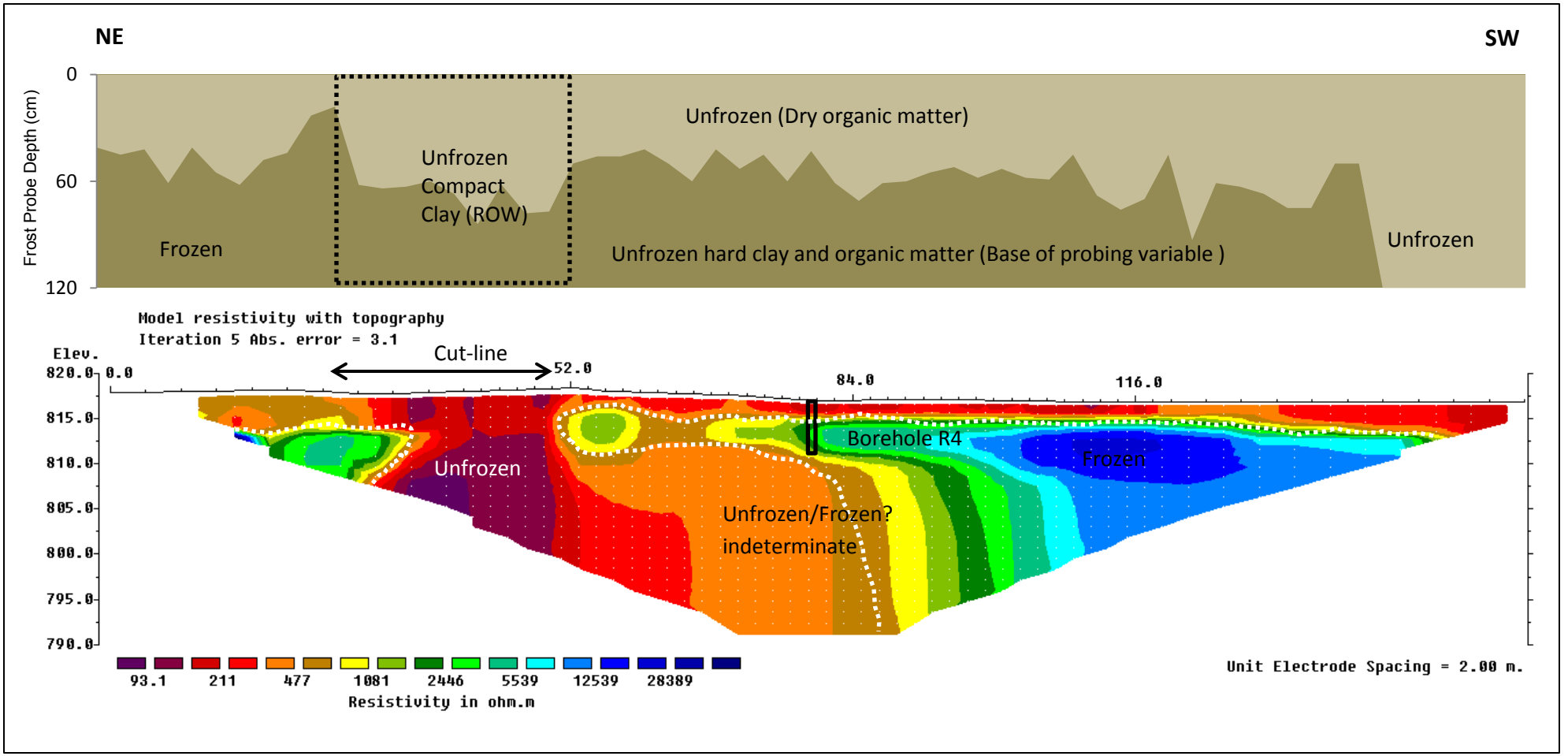

Figure 5.36: Borehole R4 NE-SW 160 m resistivity profile and frost probe chart from August 7, 2012. Vertical exaggeration in model section display = 1.00. Based on 338 data points (7 removed from original survey). The solid black lines indicates the location and depth of the 2011 borehole on the survey. The white dashed lines indicate the interface between frozen and unfrozen conditions.

5.2.5 Borehole R5 (78-A-62)

The permafrost thermal monitoring site at borehole R5 is located in the sporadic discontinuous permafrost zone of the Yukon Territory at 61˚ 16’ 04’’ N and 138˚ 50’ 33’’ W and at 844 m elevation (Figure 5.37). The field site is located in a hummocky clearance with scattered spruce trees and shrubs averaging between 1 m and 3 m in height (Figure 5.37). It is situated approximately 740 m from the south-west shore of Kluane Lake at about 150 m from the Alaska Highway and 68 m from a regrown cut-line used for previous geophysical work in the 1970s. The borehole site was cleared for drilling and drilled to a depth of 9.2 m on August 19, 1978. Soil type and ground ice conditions from the August 19, 1978 borehole log indicate a layer of organic silt at the surface to a depth of 0.5 m, underlain by a layer of clay to 1.8 m, a layer of silt between 1.8 m and 3.2 m, a mixed layer of sand and gravel between 3.2 and 3.8 m, a layer of sand between 3.8 m and 6.2 m and a layer of clay from 6.2 m to the bottom of the borehole at 9.2 m (Figure 5.38).

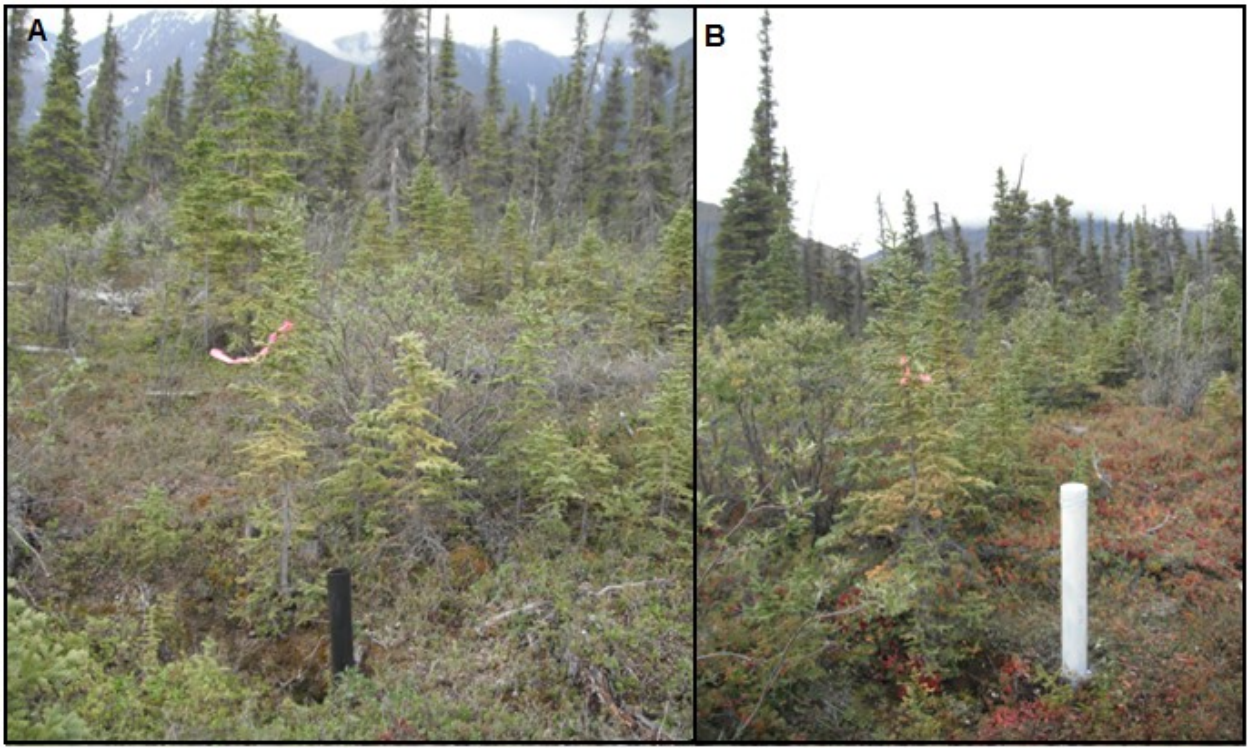

Figure 5.37: (A) Borehole R5 as it was found during the summer 2011 borehole exploration; (B) and borehole R5 after it was rehabilitated and cased.

Unfrozen conditions were present from the surface down to 0.4 m in the organic silt layer, with visible stratified or oriented ice at 10-20% observed between 0.4 m and 0.5 m and visible individual ice crystals or inclusions (Vx) and visible ice with random or irregular orientations (Vr) at 40% between 0.5 m and 2.3 m and at 20-30% between 2.3 m and 2.8 m. Visible stratified or oriented ice (Vs) and visible individual ice crystals or inclusions (Vx) 15-20% were observed between 2.8 m and 3.2 m, underlain by visible ice with random or irregular orientations (Vr) and visible individual ice crystals or inclusions (Vx) at 20 % between 3.2 m and 4.9 m, decreasing in ice content to 10-20% between 4.9 m and 6.4 m, to 5-10% between 6.4 m and 7.9 m and to 15% from 7.9 m to the bottom of the borehole log at 9.2 m (Figure 5.38). The borehole was unblocked of ice by steam and cased on August 19, 2011 and a RBR logger with a multithermistor string was installed to a depth of 8.0 m on August 24, 2011. A HOBO Pro-8 logger was installed to measure ground surface temperatures at 0 m and at 50 cm but failed and data could not be retrieved during field visits in August 2012. The length of the current ground thermal monitoring record as well as other related field work associated with borehole R5 and pertinent information is summarized in Table 5.8.

Table 5.8: Summary table of the data used in the analysis of borehole R5 and the depths of the thermistors from the surface. Note that more detailed field work and RBR logger information is given in Appendix C.

Borehole R5	
Closest ECCS Station and Distance	Burwash (13 km)
Date of 1978 drilling	August 19,1978
Manual Temperature Measurements Available	November 22, 1978 ; July 26, 1979
Original Borehole Depth	9.2 m
New Rehabilitated Borehole Depth	8.0 m
Borehole Unblocking Method	Steaming (borehole cased)
Borehole Unblocking Date	August 19, 2011
RBR Logger Data	August 25, 2011 – August 20, 2012
Thermistor Depths (m)	1.0, 1.5, 2.0, 2.5, 3.5, 5.5, 8.0
Length and Date of ERT Survey	160 m (August 8, 2012)

The temperature profile from August 8, 2012 at borehole R5 (Figure 5.38) was extracted from the RBR logger data record for comparison with the August 8, 2012 ERT results (Figures 5.39 and 5.40). Results from the daily ground temperature record show frozen conditions from 1.0 m to the bottom of the borehole at 8.0 m on the day of the ERT survey (Figure 5.38)

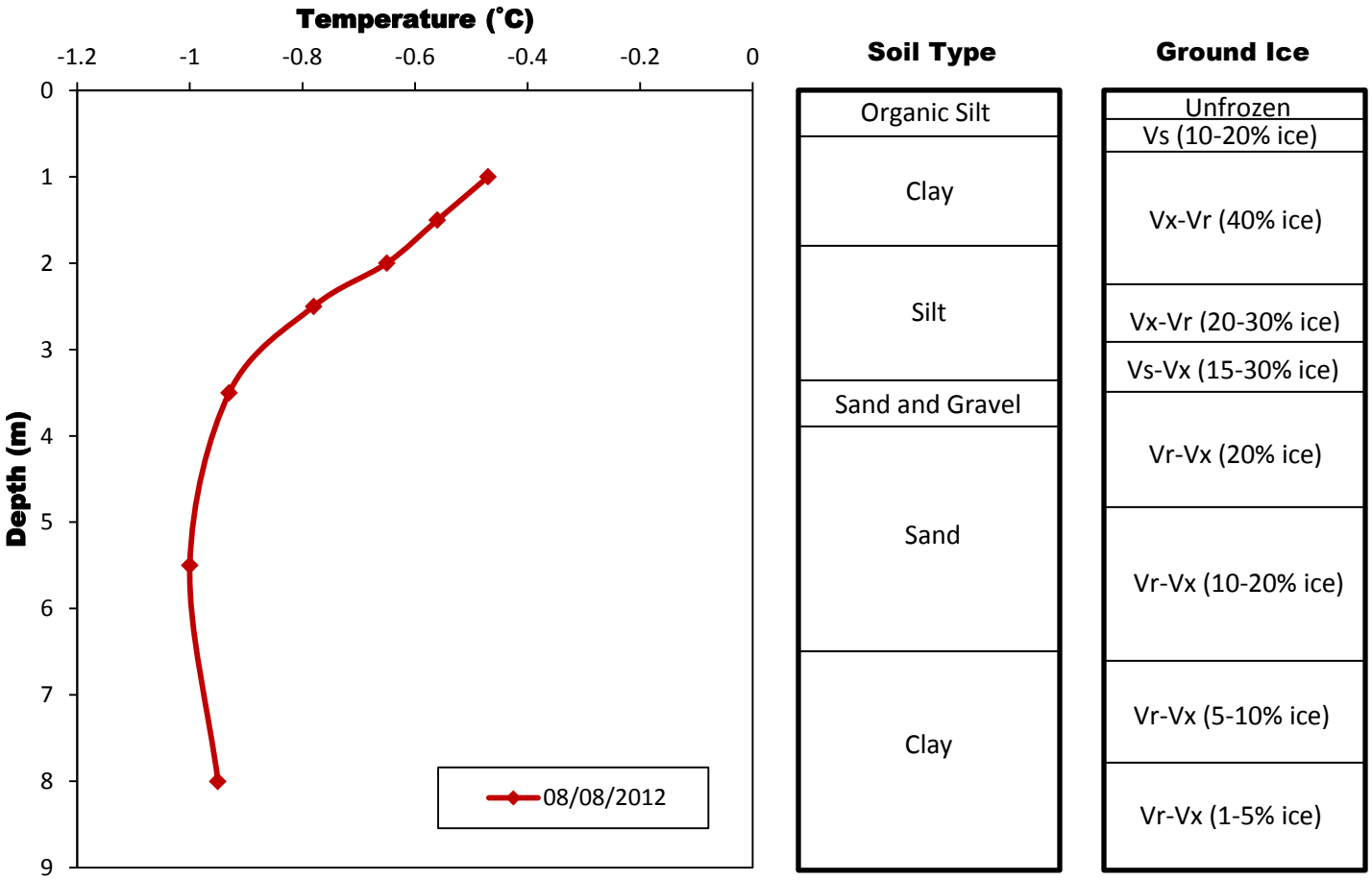

Figure 5.38: Borehole R5 average daily temperature measurements taken from the RBR logger on the same day as the 160 m ERT survey of August 8, 2012. The diamonds represent the points of temperature measurement. Soil type and ground ice conditions taken from an August 14, 1978 borehole log are shown on the right hand side. Complete descriptions of the borehole log and ground ice classification are found in Appendix K.

The 160 m ERT profile at BH R5 runs from north-east to south-west, crossing a regrown cut-line used for previous geophysical work in the 1970s between 8 m and 12 m (Figures 5.39 and 5.40). The ERT survey runs through a scattered spruce forest with many dead trees and a hummocky mossy ground surface (Figure 5.39). The terrain rises by approximately 8 m from the start to the end of the survey (Figure 5.40).

Probing results along the survey line showed low variability, giving a mean depth of 49 cm (N=61, SD=21) (Figure 5.40). A frost table could not be reached (active layer > 120 cm) at the start of the survey from 0 m to 8 m, which includes a portion of the survey that crosses the regrown cut-line. Deeper than average frost probe results for the survey (~65 cm) around the borehole can be attributed to standing water present around the black PVC pipe when it was first relocated in the summer of 2011 (Figures 5.37 and 5.40). The active layer is therefore interpreted as being approximately 0.65 m at BH R5 on August 8, 2012. These areas of unfrozen ground are represented on the modelled ERT pseudosection as low resistivity areas in the range of 150 Ohm-m to 500 Ohm-m (Figure 5.40). Shallow active layers are not identifiable on the modelled resistivity plot due the fact that the inversion routine cannot cope with extremely high resistivity contrast in the near surface at the unfrozen/frozen interface (Hilbich et al., 2008; Miceli, 2012).

High resistivity values in the range of 5000 Ohm-m to 20 000 Ohm-m from 1.0 m down to the bottom of the borehole at 8.0 m matched with negative temperatures recorded on the day of the survey are indicative of permafrost at this site (Figures 5.38 and 5.40). A steep decrease in resistivity values at the bottom of the borehole could be due to the stratigraphic transition between higher resistivity sand to lower resistivity clay as well as a decrease in ice content with depth observed in the 1978 borehole log (Figures 5.38 and 5.40) (Hauck and Kneisel, 2008, Hilbich et al., 2008). Resistivity values greater than 3000 Ohm-m down to the bottom of the resistivity plot suggest permafrost deeper than 25 m at borehole R5 (Figure 5.40).

Figure 5.39: Resistivity transect of the NE-SW 160 m survey at borehole R5 on August 8, 2012. (A) Picture taken from the 40 m point looking north-east towards the start of the transect; (B) picture of the survey line crossing a regrown cut-line between 8 m and 12 m; (C) picture taken from the borehole at the 80 m mid-point looking north-east; (D) picture taken from the borehole at the 80 m mid-point looking south-west; and (E) picture taken from the 120 m point looking south-west towards the end of the survey line.

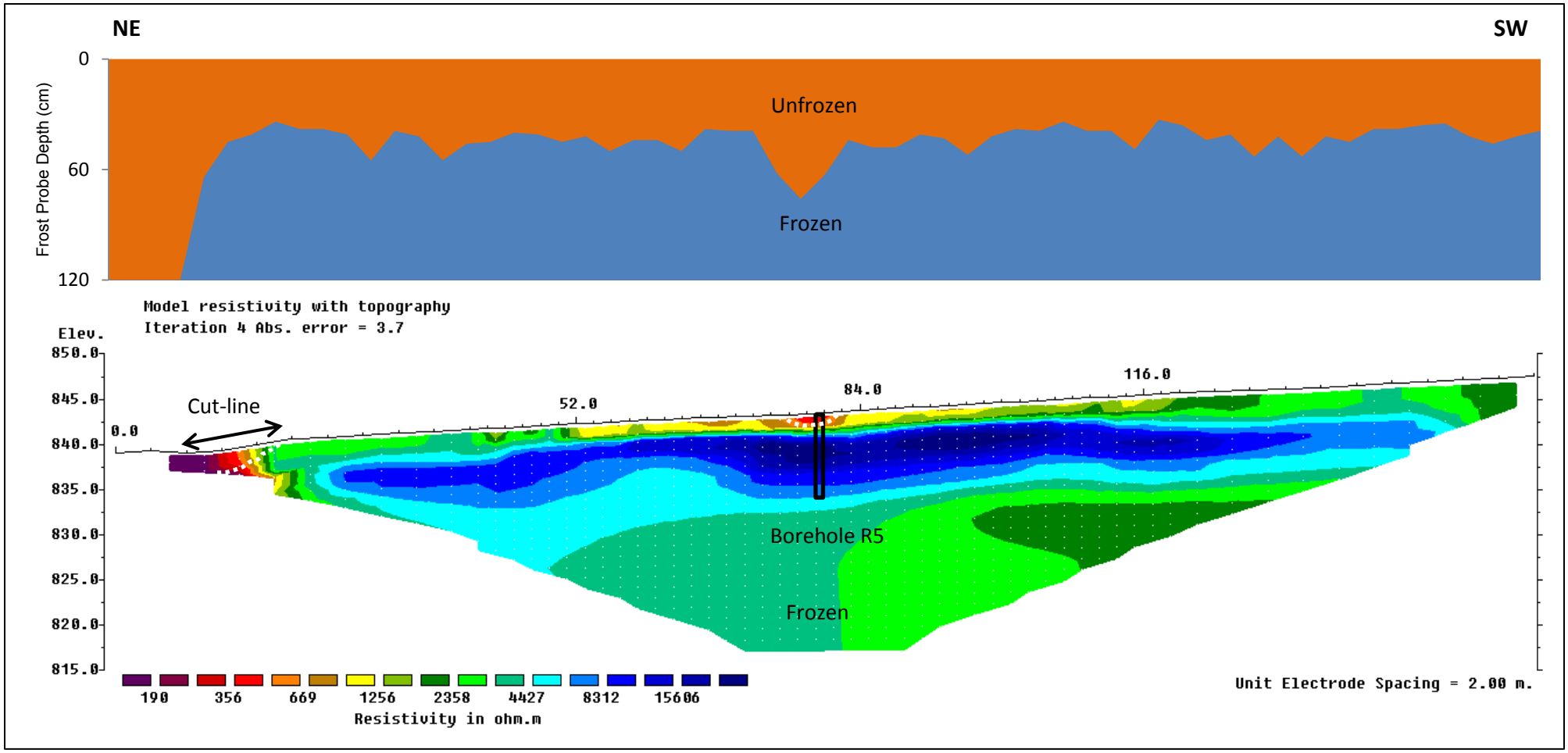

Figure 5.40: Borehole R5 NE-SW 160 m resistivity profile and frost probe chart from August 9, 2012. Vertical exaggeration in model section display = 1.00. Based on 339 data points (6 removed from original survey). The solid black lines indicates the location and depth of the borehole on the survey. The upper parts of the white dashed lines indicate ground condition interpreted as beeeing unfrozen.

The ground temperature record from borehole R5 represents slightly less than one year of measurements between August 25, 2011 and August 20, 2012 (Figure 5.41). Recovery following drilling did not occur until approximately September 25, 2011 (Figure 5.41). The 2011-2012 record shows ground temperature values below 0˚C for the entire year from 1.0 m to the bottom of the borehole at 8.0 m (Figures 5.41 and 5.42). The high variability in ground temperatures at 1.0 m and 1.5 m observed between August 25, 2011 and May 1, 2012 may be attributed to a winter with periods of prolonged cooling separated by warmer periods (Figure 5.41). The variability is substantially reduced after snowmelt in spring 2012 (Figure 5.41).

MMGT results from BH R5 show a maximum MMGT of -0.3˚C for the first thermistor at 1.0 m reached in September 2011 and a minimum MMGT of -1.3 in November, 2011 (Figure 5.43) The September maximum MMGT at 1.0 m has been slightly affected by drilling and should theoretically be cooler. MMGT for the deepest measured thermistor at 8.0 m stays around -1.0˚C for the entire year with variations of 0.1˚C with a colder MMGT in September and warmer MMGTs in May, June and July 2012 (Figure 5.43).

The maximum ground temperature at 1.0 m was -0.2˚C on September 25, 2011 and the minimum of -2.0˚C was reached on November 25, 2012 (Figures 5.41 and 5.44). The range in ground temperatures at 1.0 m is about 2.2˚C which is reduced to less than 0.1˚C at 8.0 m (Figures 5.41 and 5.44). MAGTs at shallower depth damped out quickly due to high ice contents in fine grained soil (Figure 5.44). The D_{ZAA} occurs around 6.0 m where MAGT show minimal variations < 0.1˚C downwards. The MAGT at the D_{ZAA} is about -1.0˚C. The mean annual ground temperature was -0.8˚C at 1.0 m cooling thereafter to approximately -1.0˚C at 8.0 m (Figure 5.44). MAGTs are all below 0˚C which confirms that permafrost is present at this site (Figure 5.44).

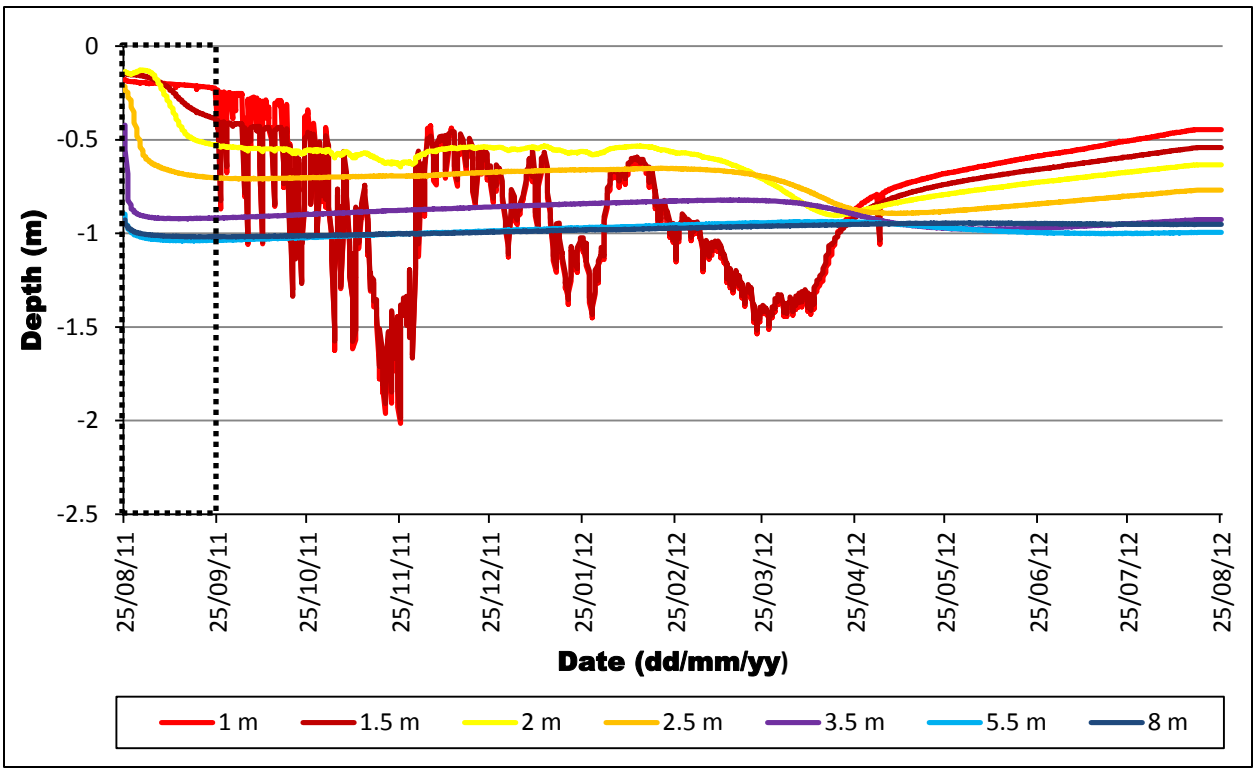

Figure 5.41: Full ground temperature series at Borehole R5 between August 25, 2011 and August 20 2012. Note that deeper thermistors do not recover after drilling until September 25, 2011 (dashed box). Note that 5 days are missing for a complete annual record.

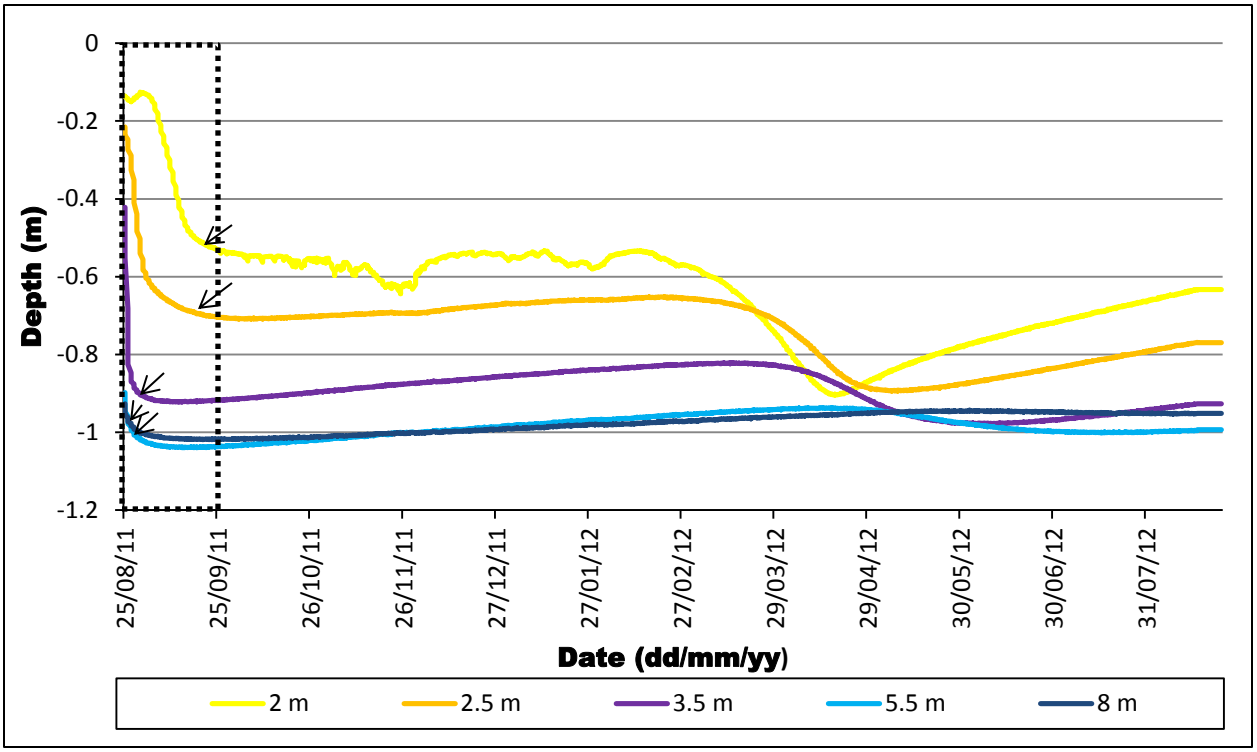

Figure 5.42: Deeper ground temperature series at Borehole R5 between August 25, 2011 and August 25, 2012. Note that deeper thermistors do not recover after drilling until September 25, 2011 (dashed box). The arrows indicate the approximate date of post-drilling recovery. Note that 5 days are missing for a complete annual record.

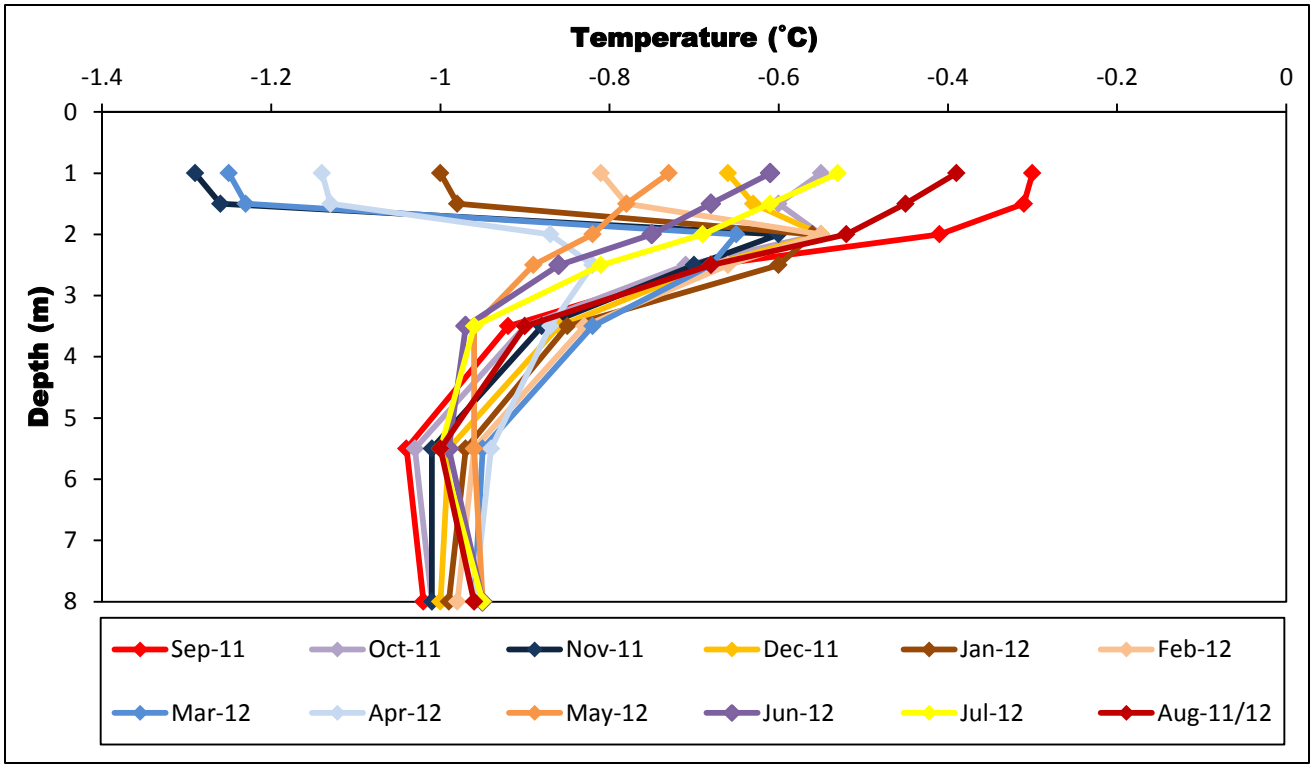

Figure 5.43: Monthly average ground temperature profiles from September 2011 to August 2012. Note that September 2011 is affected by the drilling.

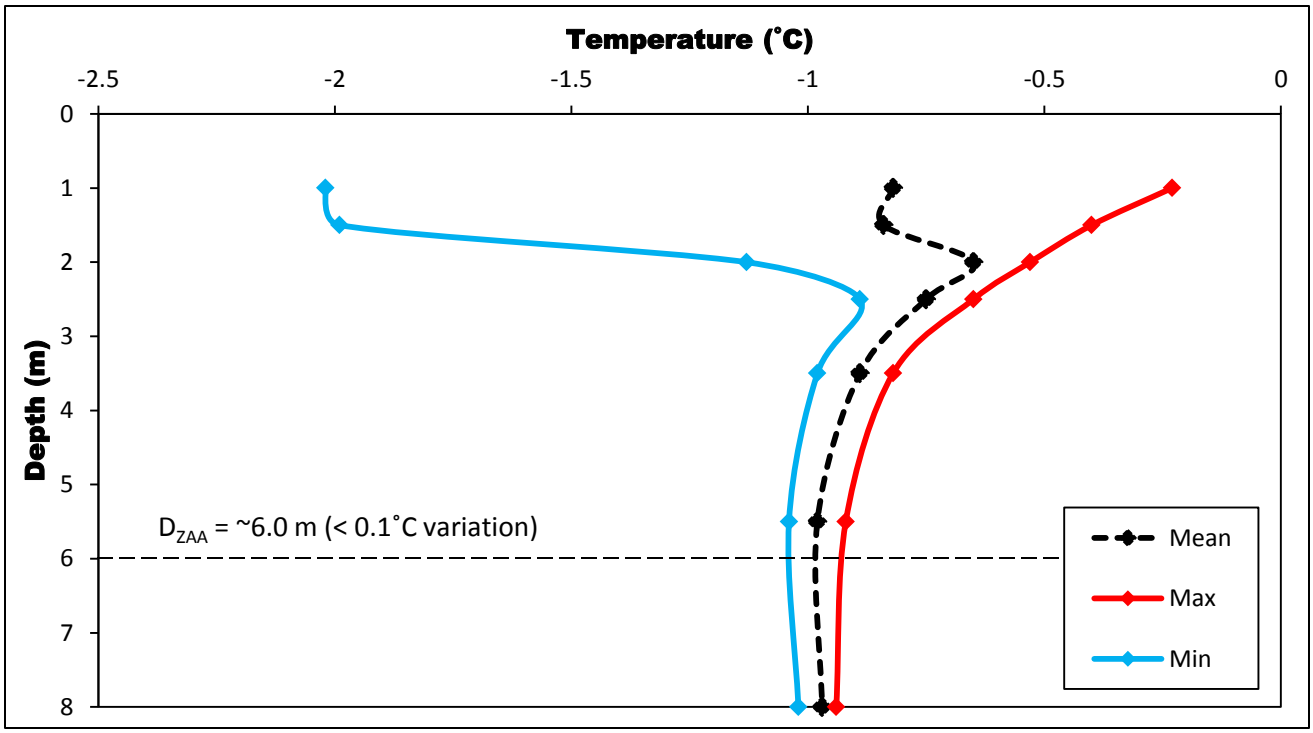

Figure 5.44: Temperature envelope at Borehole R5 for the 2011-2012 year. Note that data from August 25, 2011 to September 25, 2011 were not included in the calculations as post drilling equilibrium temperatures were not yet achieved. The D_{ZAA} occurs around 6.0 m.

Comparisons between manual ground temperature measurements from November 22, 1978 to November 22, 2011 and between July 26, 1979 to July 26, 2012 show ground temperature warming at borehole R5 (Figure 5.45). The 1978 temperature measurements were taken at varying depths between 1.5 m and 7.3 m while the 1979 temperature measurements were taken at varying depths between 1.0 m and 9.0 m (Figure 5.45). Temperature measurements for 2011 and 2012 were taken at varying depths between 1.0 m and 8.0 m (Figure 5.45). Ground temperatures were approximately 0.5˚C warmer at 3.0 m and 5.5 m and 0.7˚C warmer at 8.0 m on November 22, 2011 than on the same day in 1978 (Figure 5.45A). However, the November 22, 1978 ground temperature at 1.5 m was about 0.3˚C warmer than in 2011 (Figure 5.45A). Missing daily climate data for 2011-2012 at the Burwash ECCS make it impossible to compare TDDs and FDDs with 1978-1979 to explore the possibility of seasonal anomalies as a cause for the colder near surface ground temperatures in November 2011. Comparison of ground temperatures between July 26, 1979 and July 26, 2012 also show warming in the latter (Figure 5.45B). Ground temperatures were approximately 0.4˚C warmer at 1.0 m, 0.6˚C warmer at 3.5 m, 0.8˚C warmer at 5.5 m and 0.9˚C warmer at 8.0 m on July 26, 2012 (Figure 5.45B). Ground temperatures at 1.5 m showed insignificant change (<0.1˚C) (Figure 5.45B). Overall, there was an increase in temperature rise with depth between 1978-1979 and 2011-2012 (Figure 5.45). The deepest thermistors show ground temperature warming greater than the potential margin of error for the 1978 and 1979 manual temperature measurements. The observed warming may be due to long term climate warming and environmental change such as the clearing of the site for drilling.

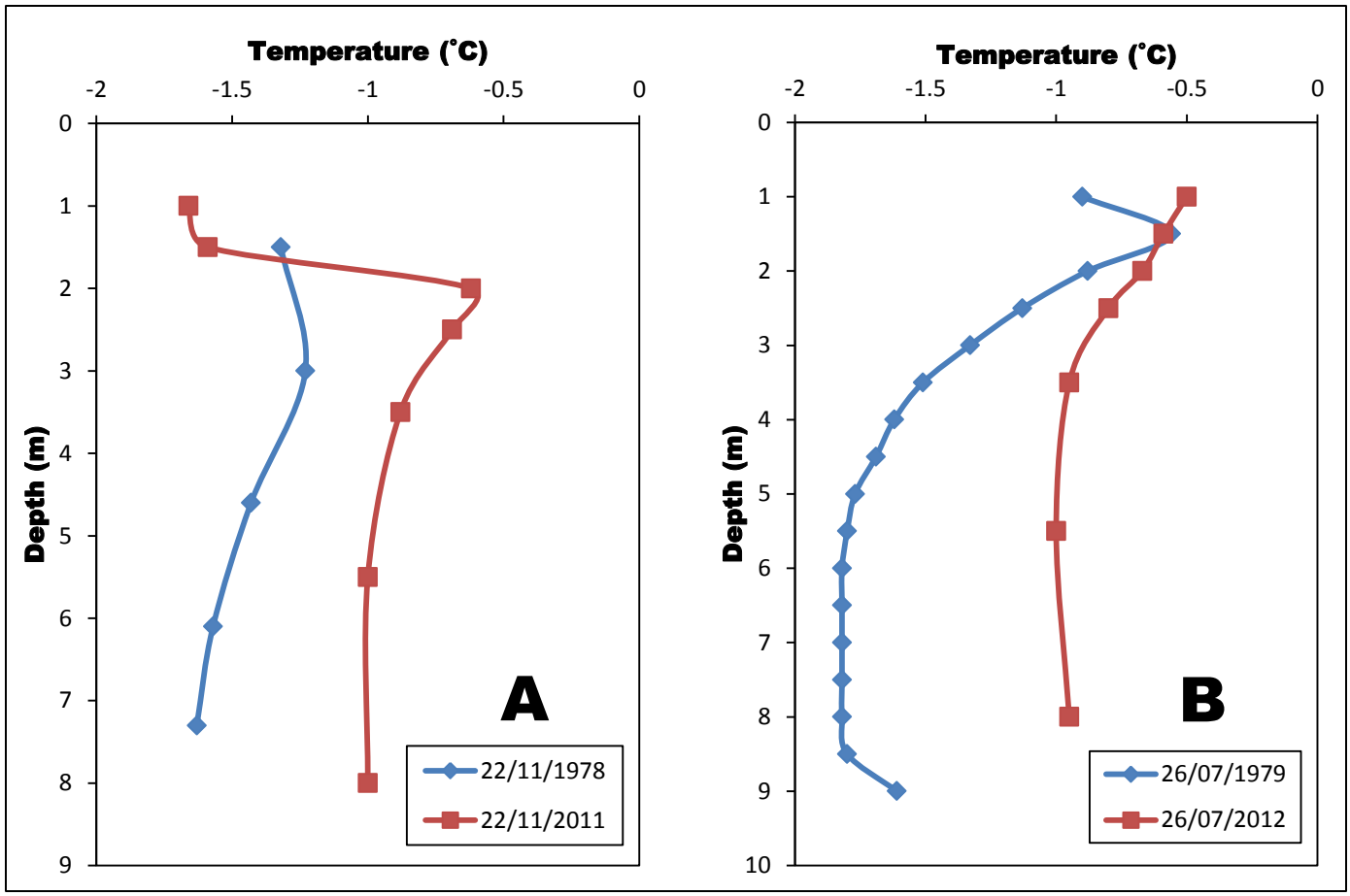

Figure 5.45: Ground temperature differences at Borehole R5 between; (A) November 22, 1978 and November 22, 2011 and (B) July 26, 1979 and July 26, 2012.

5.2.6 Borehole R6 (78-A-51)

The permafrost thermal monitoring site at borehole R6 is located in the sporadic discontinuous permafrost zone of the Yukon Territory at 61˚ 30’ 24’’ N and 139˚ 19’ 32’’ W and at 777 m elevation (Figure 5.46). The field site is located in an open dry hummocky clearance with scattered spruce trees and low-lying shrubs averaging between 1 m to 3 m in height (Figure 5.46). The borehole is situated approximately 40 m from an unnamed lake, 20 m from an ATV trail and is accessible by a dirt road from the Alaska Highway (~600 m). The site is about 18 km northwest of the northern end of Kluane Lake. The borehole site was cleared for drilling and drilled to a depth of 8.5 m in August 1978. Soil type and ground ice conditions from the August 1978 borehole log indicate a layer of peat at the surface to a depth of 0.1 m, underlain by a layer of sand to 0.2 m, a layer of volcanic ash between 0.2 m and 0.3 m, a layer of silt between 0.3 m and 0.8 m, a layer of clay between 0.8 m and 3.8 m, a layer of sand between 3.8 m and 4.6 m and a layer of clay from 4.6 m to the bottom of the borehole at 8.5 m (5.47).

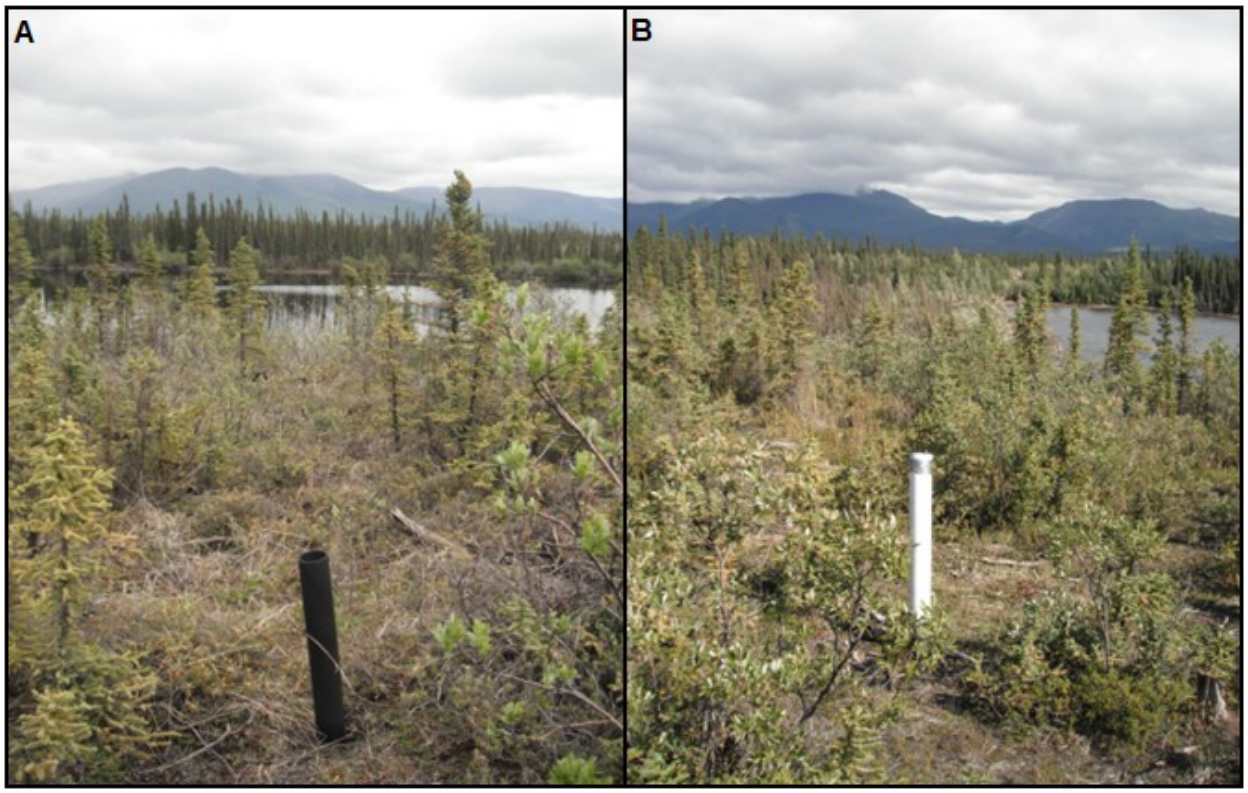

Figure 5.46: (A) Borehole R6 as it was found during the summer 2011 borehole exploration; (B) and borehole R6 after it was rehabilitated and cased.

The borehole was unfrozen from the surface down to 0.3 m when drilled, with visible ice crystals or inclusions (Vx) observed between 0.3 m and 0.6 m, no visible ice but well bonded sediments (Nb) between 0.6 m and 1.5 m, visible stratified or oriented ice (Vs) at 50-60% between 1.5 m and 2.2 m and at 30-40% between 2.2 m and 3.2 m. Visible ice crystals or inclusions (Vx) and visible stratified or oriented ice (Vs) at 1-5% was observed between 3.2 m and 6.2 m as well as unspecified frozen conditions from 6.2 m to the bottom of the borehole at 8.5 m (Figure 5.47). The borehole was unblocked of ice by steam and cased on June 21, 2011 and a RBR logger with a multithermistor string was installed to a depth of 5.15 m on August 8, 2011. The length of the current ground thermal monitoring record as well as other related field work associated with borehole R6 and pertinent information is summarized in Table 5.9.

Table 5.9: Summary table of the data used in the analysis of borehole R6 and the depths of the thermistors from the surface. Note that more detailed field work and RBR logger information is given in Appendix C.

Borehole R6	
Closest ECCS Station and Distance	Burwash (24 km)
Date of 1978 drilling	August 1978
Manual Temperature Measurements Available	November 23, 1978
Original Borehole Depth	8.5 m
New Rehabilitated Borehole Depth	5.15 m
Borehole Unblocking Method	Steaming (borehole cased)
Borehole Unblocking Date	June 21, 2011
RBR Logger Data	August 15, 2011 – August 15, 2012
Thermistor Depths (m)	0.65, 1.15, 1.65, 2.15, 2.65, 3.15, 4.15, 5.15
Length and Date of ERT Survey	160 m (August 7, 2012)

The thermal profile from August 8, 2012 at borehole R6 (Figure 5.47) was extracted from the RBR logger data record for comparison with the August 8, 2012 ERT results (Figures 5.48 and 5.49). Results from the daily ground temperature record show frozen conditions to the maximum depth of measurement of 5.15 m with an interpolated active layer of approximately 1.1 m (Figure 5.47). The spacing of the sensors used for the interpolation means that the precision of the top of the frozen layer is low. The 1978 borehole log indicates a thawed layer from the surface down to 0.3 m in August 1978 which suggests an approximate increase in active layer thickness of about 0.8 m when compared to the same period in 2012 (Figure 5.47).

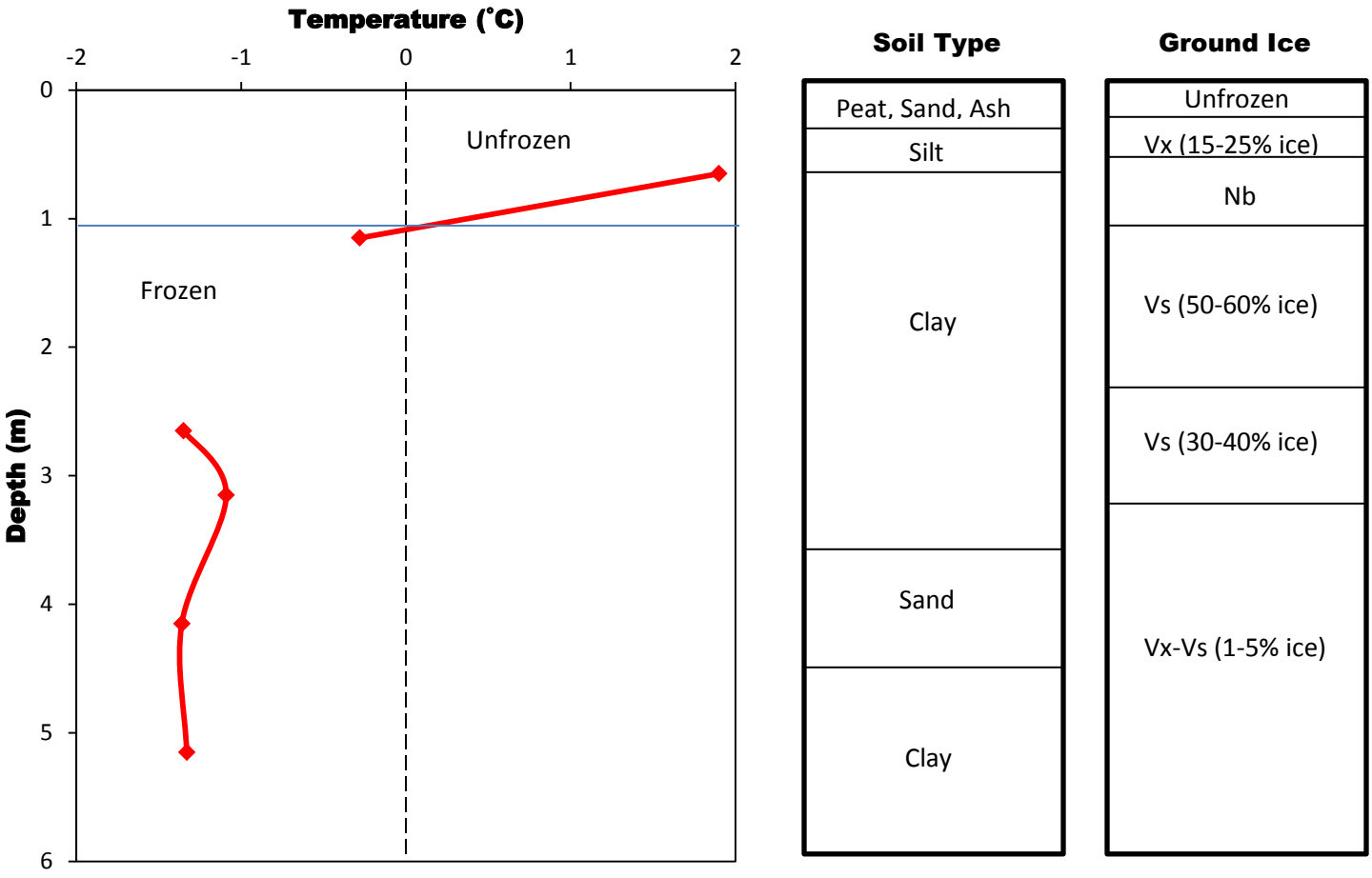

Figure 5.47: Borehole R6 average daily temperature measurements taken from the RBR logger on the same day as the ERT survey of August 7, 2012. The diamonds represent the points of temperature measurements. Soil type and ground ice conditions taken from an August 1978 borehole log are shown on the right hand side. Complete descriptions of the borehole log and ground ice classification to a depth of 8.2 m are found in Appendix K. Note that the thermistors at 1.65 m and 2.15 m failed on May 10, 2012.

The 160 m ERT profile at BH R6 runs from north-west to south-east, through a dry scattered spruce forest with areas showing signs of past forest fire (Figures 5.48 and 5.49). The ground surface consists mainly of mosses and organic matter which were dry at the time of the survey (Figure 5.48). The terrain rises by approximately 5 m from the start to the end of the survey (Figure 5.49).

Probing results along the survey line were highly variable, giving a mean depth of 61 cm with a high standard deviation (N=61; SD=21) (Figure 5.49). A frost table could not be reached (active layer > 120 cm) at the start of the survey from 0 m to 4 m and around the borehole casing between 78 m to 82 m along the survey line (Figure 5.49). These areas of unfrozen ground are represented on the modelled ERT pseudosection as low resistivity areas in the range of 400 Ohm-m to 500 Ohm-m (Figure 5.49). This interpretation of the resistivity results is supported by positive ground temperatures to a depth of 1.1 m at BH R6 on the day of the ERT survey (Figure 5.47). Shallower active layers are not identifiable on the modelled resistivity plot due the fact that the inversion routine cannot cope with extremely high resistivity contrast in the near surface at the unfrozen/frozen interface (Hilbich et al., 2008; Miceli, 2012).

High resistivity values in the range of 1000 Ohm-m to 8 000 Ohm-m from approximately 1.5 m down to the bottom of the borehole at 5.15 m matched with negative borehole temperatures recorded on the day of the survey, are indicative of permafrost at this site (Figures 5.47 and 5.49). Resistivity values in the range of 6000-8000 Ohm-m between approximately 3 m and 10 m in depth suggest the presence of a permafrost body with a high ice content which is supported by the ground ice descriptions of the borehole log (Figures 5.47 and 5.49). A transition to resistivity values as low as 400 Ohm-m at depth may represent the base of permafrost as these values match with low near surface resistivity values previously interpreted as unfrozen conditions by probing and positive borehole temperatures (Figures 5.47 and 5.49). This interpretation indicates the presence of a three layered permafrost body at BH R6 with the base of permafrost situated at a depth of approximately 20 m (Figure 5.49). However, these resistivity values are in the “indeterminate” zone defined as resistivity values that were unable to be identified conclusively as frozen or unfrozen (see Figure 6.4). Thus, it is uncertain whether the base of permafrost is reached in the profile or if it is deeper than 25 m. The geothermal gradient

would have to be really high if the base of permafrost was at 20 m given measured ground temperatures of -1.2˚C at 5 m, which seems fairly unlikely.

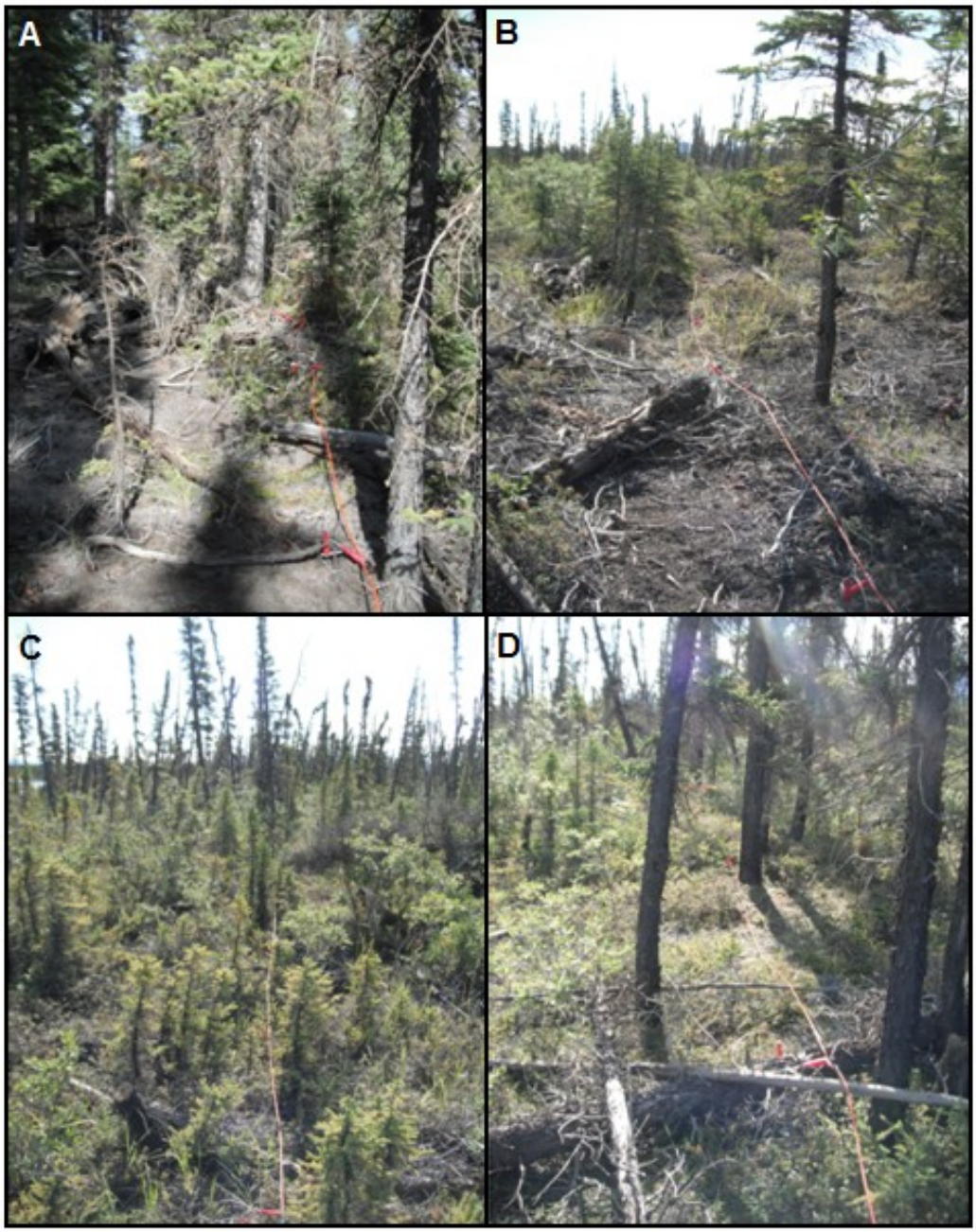

Figure 5.48: Resistivity transect of the 160 m NW-SE survey at borehole R6 on August 7, 2012. (A) Picture taken from the 40 m point looking north-west towards the start of the transect; (B) picture taken from the borehole at the 80 m mid-point looking north-west; (D) picture taken from the borehole at the 80 m mid-point looking south-east; and (E) picture taken from the 120 m point looking south-east towards the end of the survey line.

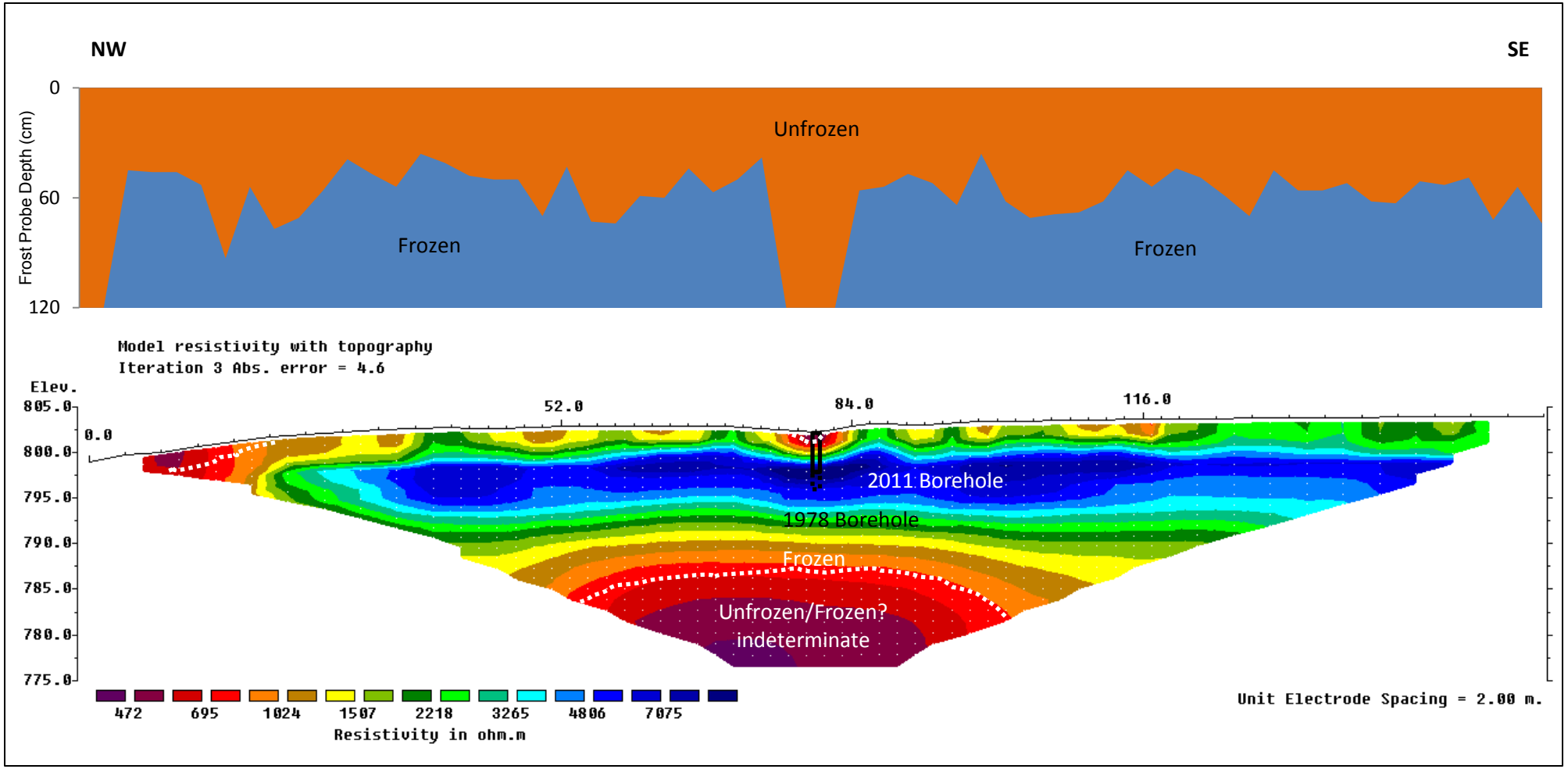

Figure 5.49: Borehole R6 NW-SE 160 m resistivity profile and frost probe chart from August 7, 2012. Vertical exaggeration in model section display = 1.00. Based on 322 data points (23 removed from original survey). The solid black lines indicates the location and depth of the 2011 borehole on the survey while the black dash lines indicate the original depth of the borehole in 1978. The white dashed lines delimits the boundary between frozen and unfrozen ground.

The ground temperature record from borehole R2 represents a full year of measurements between August 15, 2011 and August 15, 2012 (Figure 5.50). Temperature measurements start 56 days after the borehole was steamed and there is no evidence that ground temperatures had not fully recovered before the start of monitoring. The 2011-2012 record shows ground temperature values below 0˚C between September 26, 2011 and May 8, 2012 at 0.65 m and negative values for the entire year at all measured depths from 1.15 m to the bottom of the borehole at 5.15 m (Figures 5.50 and 5.51). Zero curtain effects are not observed at BH R6 (Figure 5.50). Thermistors at 1.65 m and 2.15 m both failed on May 10, 2012 (Figure 5.50).

MMGT results from BH R6 show a maximum MMGT of 2.0˚C for the first thermistor at 0.65 m reached in August 2012 and a minimum MMGT of -4.5˚C in March, 2012 (Figure 5.52). The deepest measured thermistor at 5.15 m reached a maximum mean monthly ground temperature (MMGT) of -1.1˚C in February 2012 and a minimum MMGT of -1.5˚C in May 2012 (Figure 5.52).

The maximum ground temperature at 0.65 m was 2.6˚C on August 10, 2012 and the minimum of -5.1˚C was reached on March 23, 2012 (Figures 5.50 and 5.53). The maximum ground temperature at the deepest measurement depth of 5.15 m was -1.0 on February 7, 2012 while the minimum of -1.5˚C was reached on May 16, 2012 (Figures 5.50 and 5.53). The unusual minimum profile from 0.65 m to 1.65 m may not be easily explainable but doesn't seem to be an error in the measurements (Figure 5.53). MAGTs at shallower depths damped out quickly due to high ice contents in fine grained sand (Figure 5.53). The range in ground temperatures at 0.65 m is about 7.7˚C which is reduced to 0.4˚C at 5.15 m indicating that the D_{ZAA} is deeper than 5.15 m (Figure 5.53). The mean annual ground temperature was -1.0˚C at 0.65 m cooling thereafter to approximately -1.2˚C at 5.15 m (Figure 5.53). MAGTs are all below 0˚C which confirms that permafrost is present at this site (Figure 5.52).

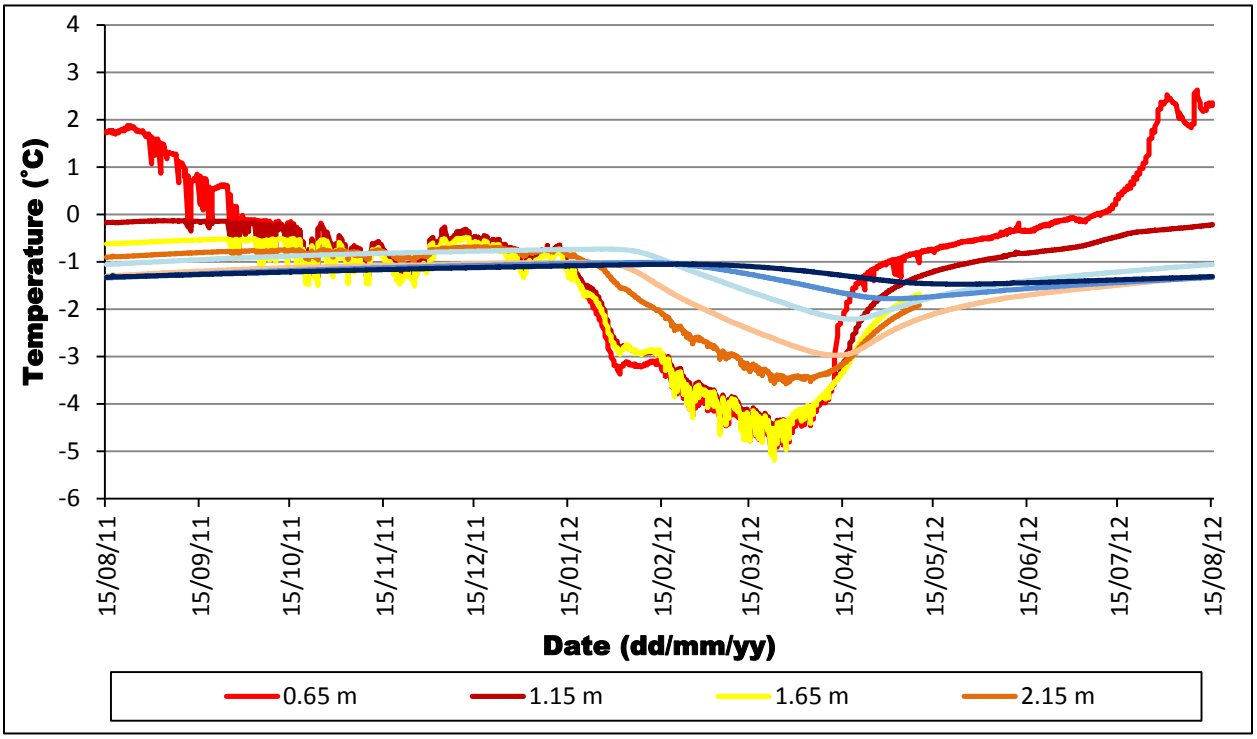

Figure 5.50: Full ground temperature series at Borehole R6 between August 15, 2011 and August 15, 2012. Note that thermistors at 1.65 m and 2.15 m failed on May 10, 2012.

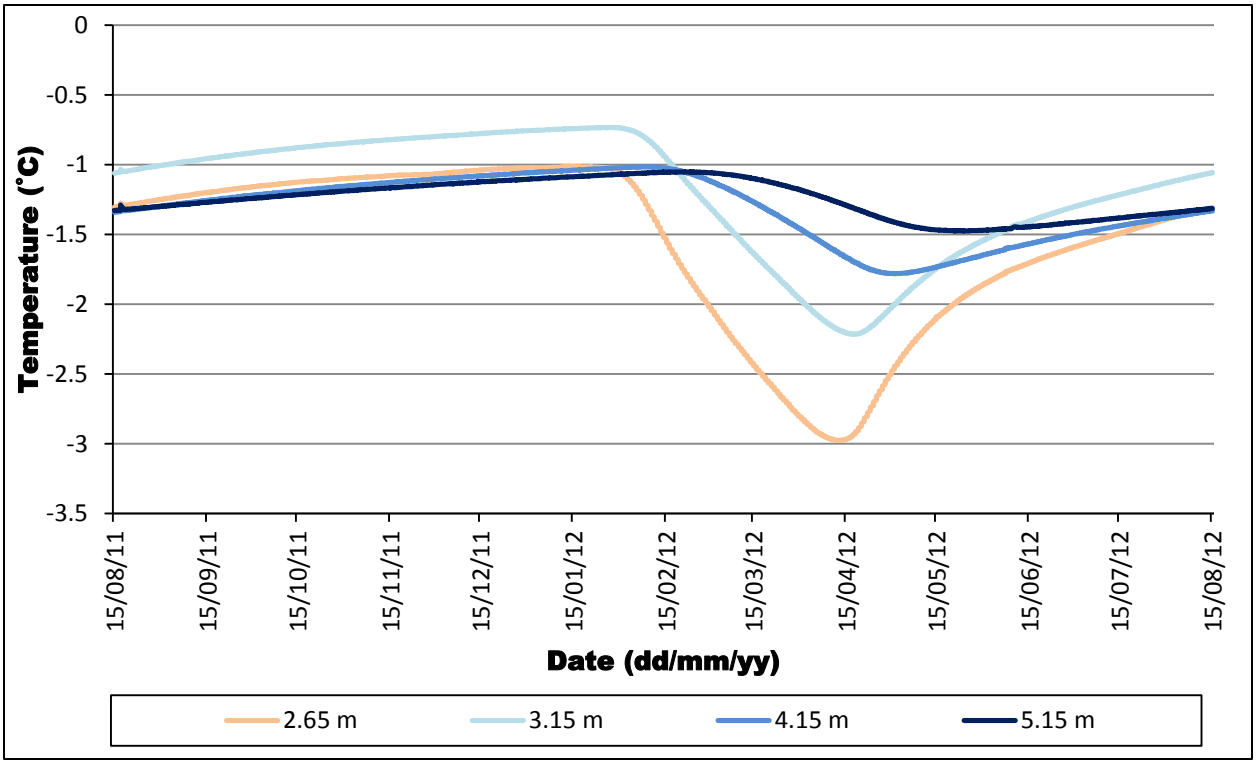

Figure 5.51: Deeper ground temperature series at Borehole R6 between August 15, 2011 and August 15, 2012.

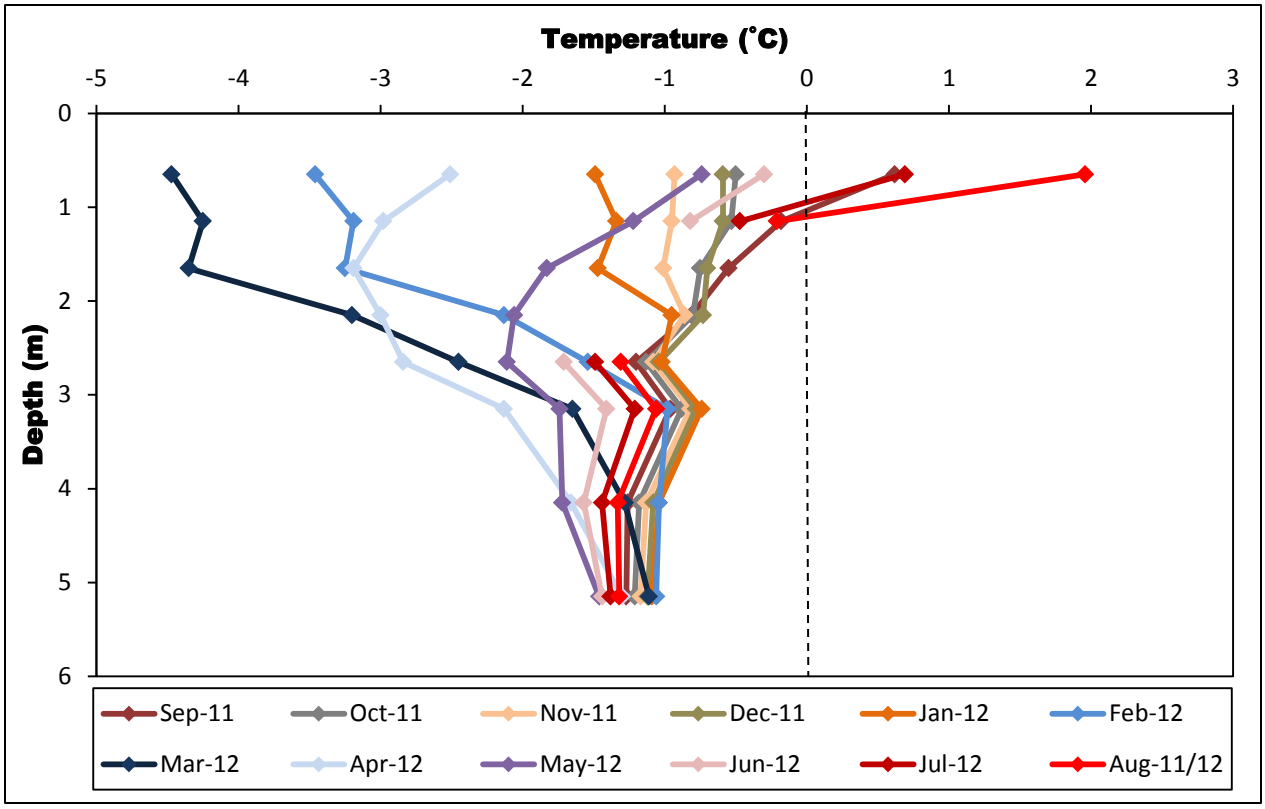

Figure 5.52: Monthly average ground temperature profiles at Borehole R6 from September 2011 to August 2012. Note that thermistors at 1.65 m and 2.15 m failed on May 10, 2012.

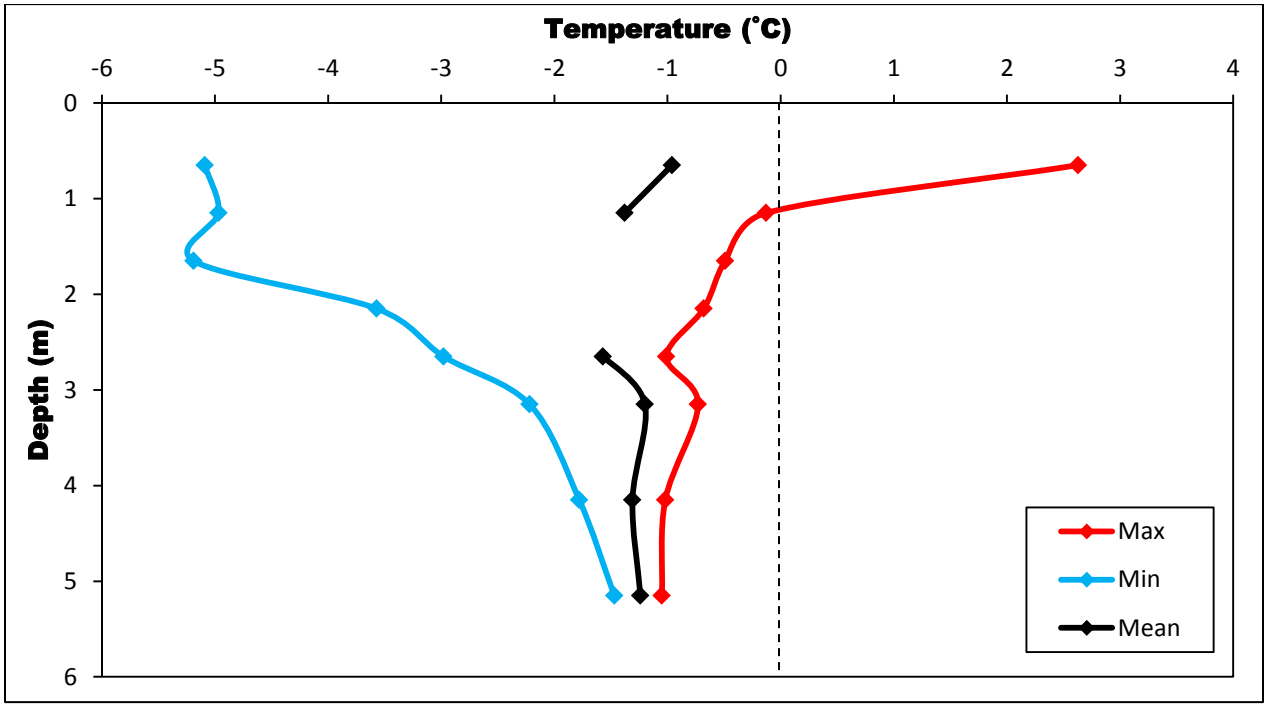

Figure 5.53: Temperature envelope at Borehole R6 for the 2011-2012 year. Note that thermistors at 1.65 m and 2.15 m failed on May 10, 2012 and MAGTs were not calculated at these depths.

Comparison between ground temperature measurements from November 23, 1978 and November 23, 2011 shows colder near surface temperatures and warmer deeper ground temperatures in 2011 (Figure 5.54). Ground temperatures were approximately 0.4˚C colder at 1.15 m, with temperature variations negligible (<0.01˚C) at 2.15 m and 0.2˚C colder at 2.65 m on November 23, 2011 than on the same day in 1978 (Figure 5.54). However, the November 23, 2011 ground temperature was about 0.1˚C warmer at 3.15 m, 0.8˚C warmer at 4.15 m and 1.4˚C warmer at 5.15 m than on November 23, 1978 (Figure 5.54). Missing daily climate data for 2011-2012 at the Burwash ECCS make it impossible to compare TDDs and FDDs with 1978-1979 to explore the possibility of seasonal anomalies as a cause for colder near surface ground temperatures in November 2011. The deepest thermistors show significant ground temperature warming greater than the potential margin of error for the 1978 manual temperature measurements. The observed warming may be due to long term climate warming and environmental change such as the clearing of the site for drilling.

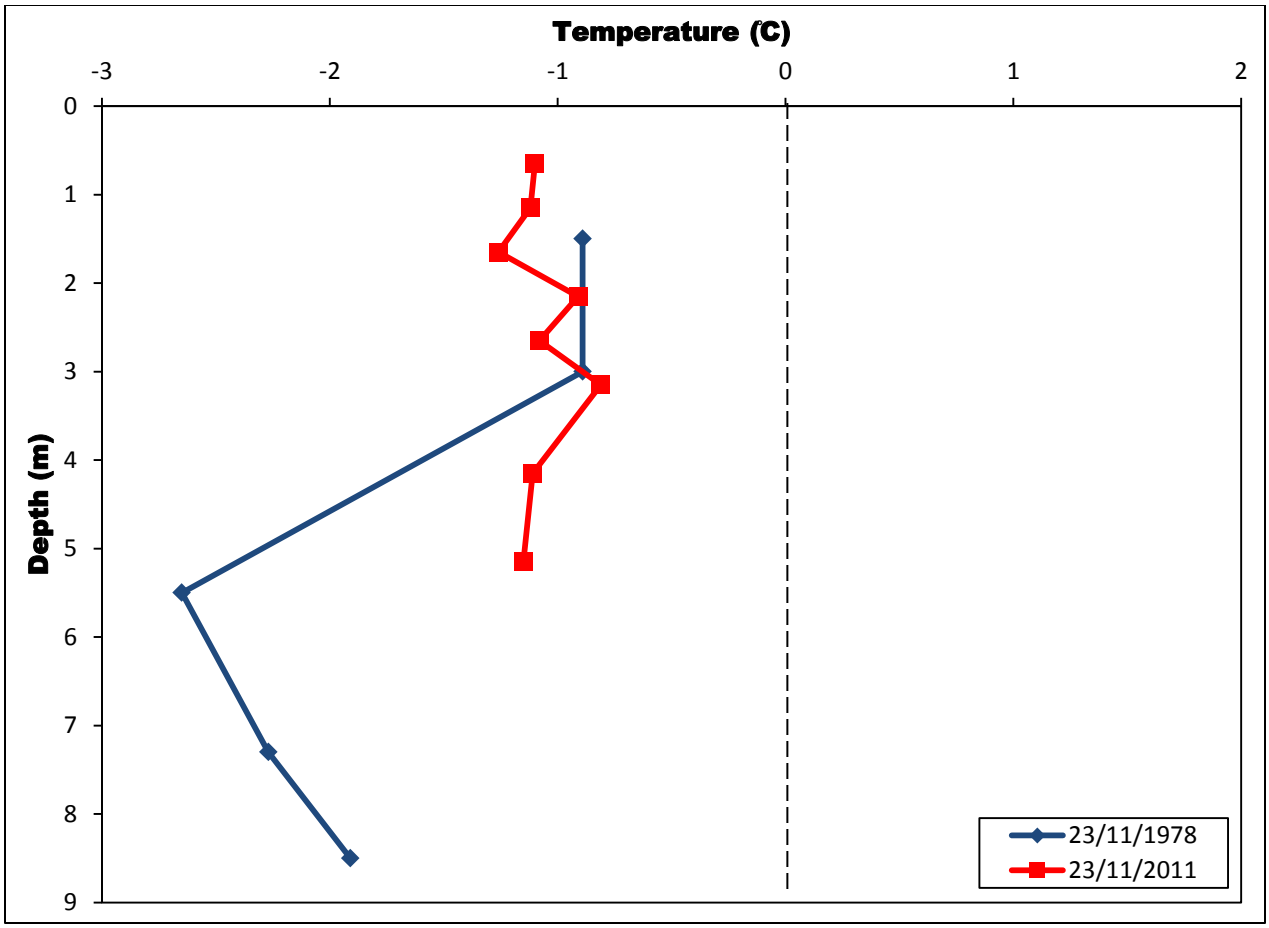

Figure 5.54: Ground temperature differences at borehole R6 between November 23, 1978 and November 23, 2011.

5.2.7 Borehole R7 (78-A-40)

The permafrost thermal monitoring site at borehole R7 is located in the sporadic discontinuous permafrost zone of the Yukon Territory at 61˚ 42’ 52’’ N and 139˚ 50’ 25’’ W and at 780 m elevation (Figure 5.55). The borehole is located in a small clearing undergoing

Figure 5.55: (A) Borehole R7 as it was found during the summer 2011 borehole exploration; (B) and borehole R7 after it was rehabilitated and cased.

regrowth surrounded by spruce and birch trees with low lying shrubs and is approximately 20 m from the Alaska Highway and 8 m from a regrown cut-line used for previous geophysical work in the 1970s (Figure 5.55). The borehole site was cleared in the past before drilling and drilled to a depth of 8.3 m in August 1978. The August 1978 borehole log indicates a layer of peat and volcanic ash from the surface down to a depth of 0.3 m, underlain by a layer of volcanic ash and sand to 0.9 m, underlain by alternating thin layers of peat and silt from 0.9 m to the bottom of the borehole log at 8.3 m (Figure 5.56). Unfrozen conditions were present from the surface down to 0.6 m, with visible ice with ice coating on particles (Vc) at 5-10% observed between 0.6 m and 1.1 m, visible stratified or oriented ice (Vs) at 15% between 1.1 m and 2.6 m, visible ice with random or irregular orientation (Vr) and visible stratified or oriented ice (Vs) at 10-50% between 2.6 m and 3.1 m. Visible stratified or oriented ice (Vs) at 20-30% was observed between 3.1 m and 4.9 m and at 5-15% between 4.9 m to the bottom of the borehole log at 8.3 m (Figure 5.56).

The borehole was unblocked of ice by steam on June 24, 2011 and cased on June 25, 2011. A RBR logger with a multithermistor string was installed to a depth of 7.0 m on August 5, 2011. A climate station monitoring air temperature, ground temperature and snow depth was also installed to provide site-specific measurements at borehole R7 on August 21, 2011 due to its distance from the closest ECCS (Figure 5.55). The length of the current ground thermal monitoring record as well as other related field work associated with borehole R7 and pertinent information is summarized in Table 5.10.

Table 5.10: Summary table of the data used in the analysis of borehole R7 and the depths of the thermistors from the surface. Note that more detailed field work and RBR logger information is given in Appendix C.

Borehole R7	
Closest ECCS Station and Distance	Burwash (60 km), Beaver Creek (93 km)
Dates of 1978 drilling	August 1978
Manual Temperature Measurements Available	November 23, 1978
Original Borehole Depth	8.3 m
New Rehabilitated Borehole Depth	7.0 m
Borehole Unblocking Method	Steam
Borehole Unblocking Date	June 24, 2011
RBR Logger Data	Aug 15, 2011 – Aug 15, 2012
Thermistor Depths (m)	0, 0.5, 1.0, 1.5, 2.5, 4.5, 7.0
Length and Date of ERT Survey	40 m (June 24, 2011), 160 m (August 5, 2012)
Weather station climate record	August 15, 2011 – June 12, 2012

The thermal profiles from June 24, 2012 and August 5, 2012 at Borehole R7 (Figure 5.56) were extracted from the RBR logger data record for comparison with the June 24, 2011 and August 5, 2012 ERT results (Figures 5.57, 5.58, 5.59 and 5.60). Frozen conditions exist to the maximum depth of measurement with an interpolated thawed layer of approximately 0.9 m on June 24, 2012 and 1.1 m on August 5, 2012 (Figure 5.56). The 1978 borehole log indicates a thawed layer from the surface down to 0.6 m in August 1978 which suggests an increase in active layer thickness of about 0.3 m when compared to the same date in 2012 (Figure 5.56).

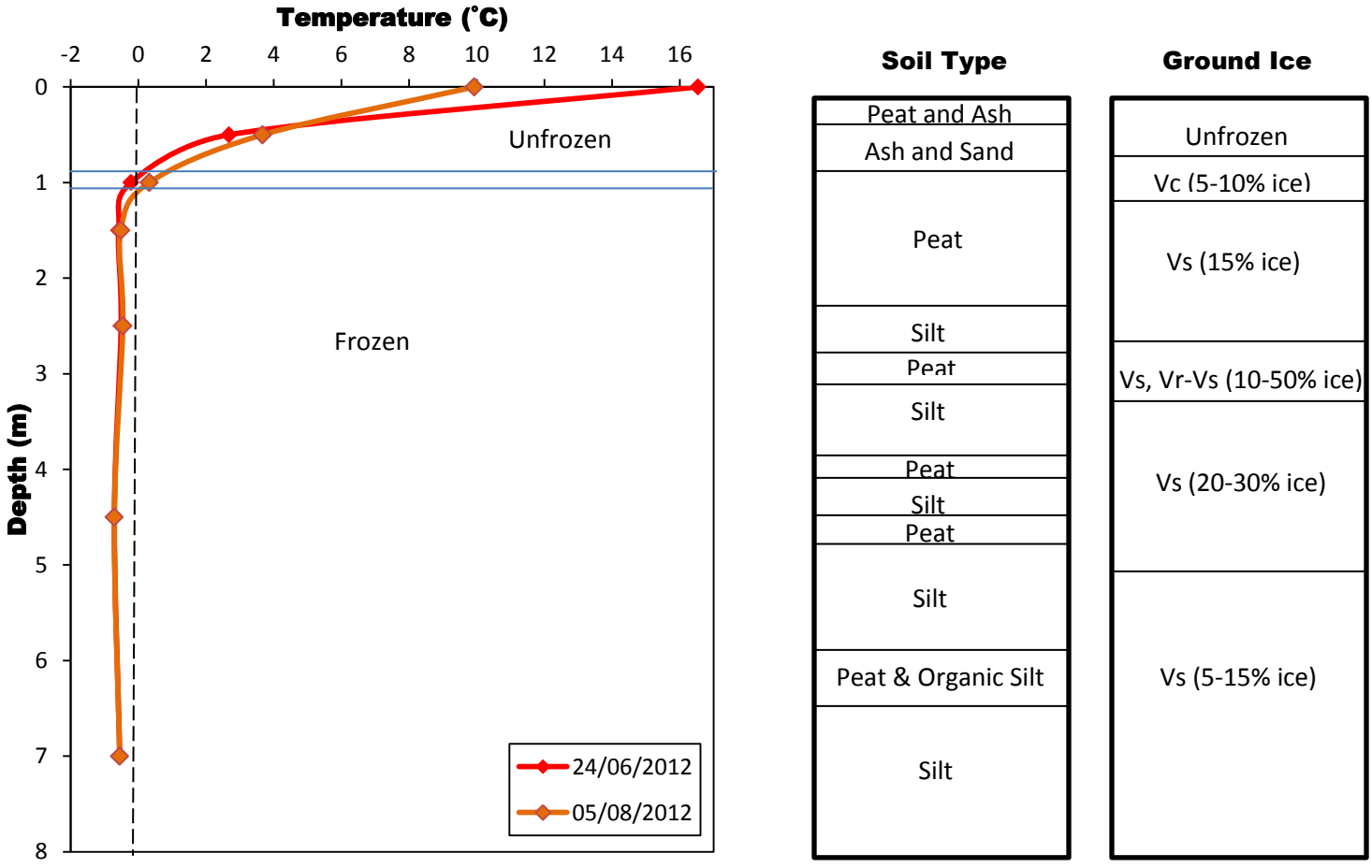

Figure 5.56: Borehole R7 average daily temperature measurements taken from the RBR logger on the same day as the 160 m ERT survey of August 5, 2012. Ground temperatures from June 24, 2012 are shown for comparisons with the 40 m ERT survey of June 24, 2011. The diamonds represent the points of temperature measurement. Soil type and ground ice conditions taken from an August 1978 borehole log are shown on the right hand side. Complete descriptions of the borehole log and ground ice classification are found in Appendix K.

The 160 m ERT profile at BH R7 was done on August 5, 2012 and runs from a south-east, north-west direction, through a dense spruce forest and clearances with smaller spruce trees and scattered low lying shrubs (Figure 5.57). The ground surface was covered by mosses in wetter areas and grasses in dryer ones. The terrain is relatively flat, with less than 2 m variation from the start to the end of the survey (Figures 5.57 and 5.58).

Probing results along the survey line were variable (N=61; SD=18), giving a mean depth of 71 cm (Figure 5.58). A frost table could not be reached (active layer > 120 cm) in a wet area from 46 m to 60 m with standing and flowing along the survey line (Figure 5.57A). This area of unfrozen ground is represented on the modelled ERT profile as a low resistivity area in the range of 80 Ohm-m to 250 Ohm-m to an approximate depth of 3 m (Figure 5.58). Resistivity values in the 500-900 Ohm-m range from the surface down to about 10 m depth at the end of the survey (130-160 m) could represent unfrozen or frozen conditions as this is the indeterminate range (see Figure 6.4). Shallower active layers are not identifiable on the modelled resistivity plot due the fact that the inversion routine cannot cope with extremely high resistivity contrast in the near surface at the unfrozen/frozen interface (Hilbich et al., 2008; Miceli, 2012). Positive borehole temperatures to an interpolated depth of approximately 1.1 m on August 5, 2012 suggests that the probing results averaging 75 cm around the borehole might not be accurate and that gravel might have been misinterpreted as the frost table, or that the borehole itself was slightly warmer than the surrounding ground.

Higher resistivity values in the range of 700 Ohm-m to 5000 Ohm-m from the near surface down to the bottom of the borehole at 7.0 m matched with negative temperatures recorded on the day of the survey are indicative of permafrost at this site (Figures 5.56 and 5.58). Resistivity values in the 4000 Ohm-m to 5000 Ohm-m range at the bottom of the resistivity plot suggest permafrost deeper than 25 m at BH R7 (Figure 5.58).

Figure 5.57: Resistivity transect of the 160 m SE-NW survey at borehole R7 on August 8, 2012. (A) Picture taken from the 40 m point looking south-east towards the start of the transect; (B) picture taken from the borehole at the 80 m mid-point looking south-east; (D) picture taken from the borehole at the 80 m mid-point looking north-west; and (E) picture taken from the 120 m point looking north-west towards the end of the survey line.

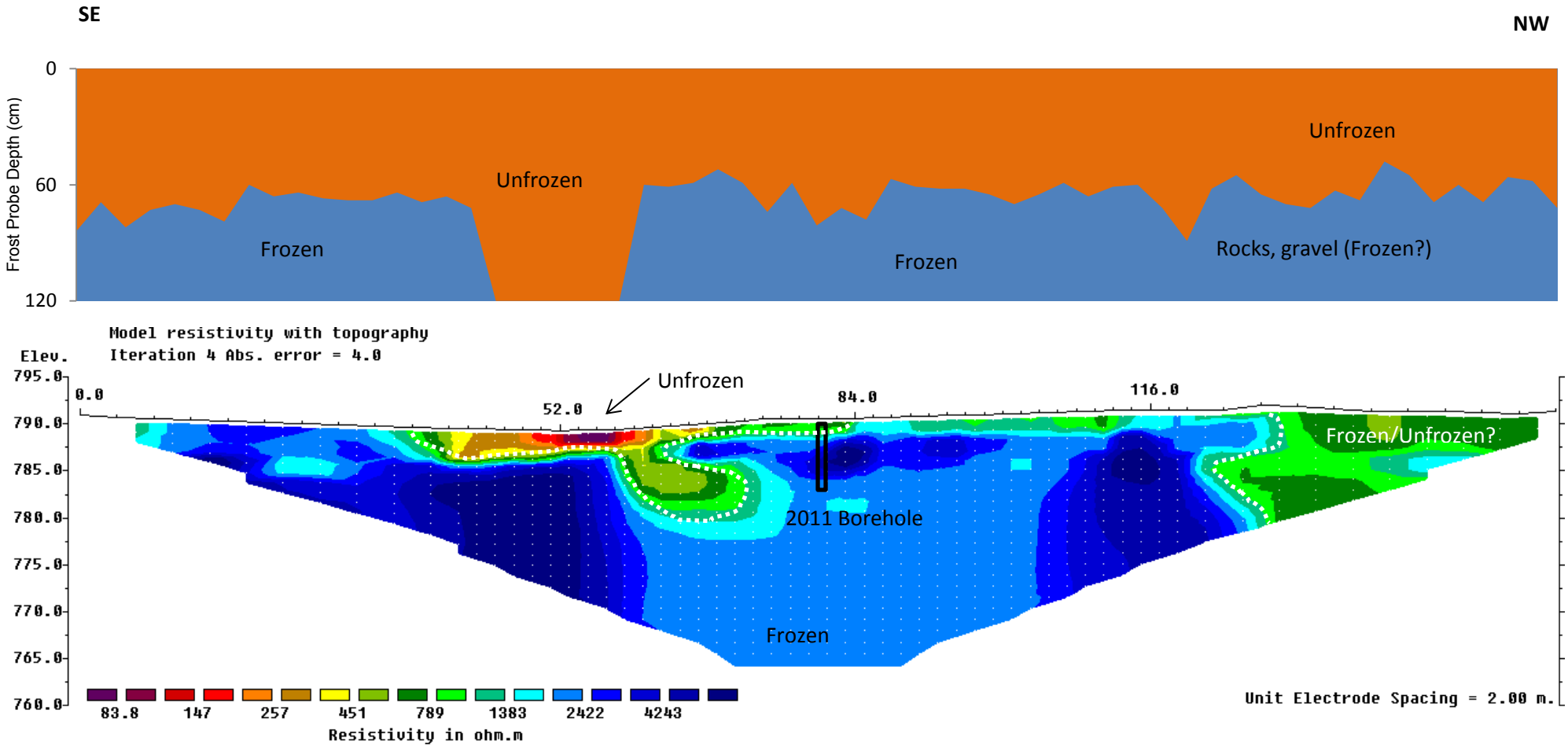

Figure 5.58: Borehole R7 SE-NW 160 m resistivity profile and frost probe chart from August 5, 2012. Vertical exaggeration in model section display = 1.00. Based on 342 data points (3 removed from original survey). The solid black lines indicates the location and depth of the 2011 borehole on the survey while the white dashed lines indicates the interpreted boundary between frozen and unfrozen ground.

The 40 m ERT profile at BH R7 was done on June 24, 2011 and runs from a north-east, south-west direction (Figures 5.59 and 5.60). The ERT survey starts on the gravel shoulder of the Alaska Highway (0 m to 6 m) and crosses a regrown cut-line used for previous geophysical work in the 1970s between 27 m and 35 m (Figure 5.59). The terrain decreases by approximately 1.5 m from the start to the end of the survey and is relatively hummocky (Figure 5.60).

Probing results along the survey line showed high variability, with a mean depth of 52 cm a high standard deviation (N=41, SD=38) (Figure 5.60). The first 6 m of the survey was on the gravel highway shoulder and could not be probed due to coarse gravel and rocks (Figures 5.59 and 5.60). The highway shoulder shows resistivity values in the range of 300 Ohm-m to 500 Ohm on the modelled ERT profile which can be interpreted as unfrozen ground (Figure 5.60). A frost table could not be reached (active layer > 120 cm) from 27 m to 35 m, where the survey crosses the regrown cut-line. This area of unfrozen ground determined by probing is represented as a low resistivity area in the range of 50 Ohm-m to 300 Ohm to a depth of approximately 3 m on the resistivity plot and represents a possible talik (Figure 5.60). The resistivity values directly under this area are around 500-600 Ohm-m which is in the "indeterminate" zone, representing values that were unable to be identified conclusively as frozen or unfrozen (see Figure 6.4). Thus, it is not certain if the thawed layer exceeded the depth of the profile of approximately 4 m. The borehole temperature measurements show positive temperatures to an interpolated depth of about 0.9 m on the day of the ERT survey which is represented as resistivity values around 600 Ohm-m on the resistivity plot (Figure 5.56). However, this range of resistivity values cannot be used as an unfrozen condition guideline for the entire plot because of near surface uncertainties in the modelled resistivity results. This is due to the fact that the inversion routine cannot cope with extremely high resistivity contrast in the near surface at the unfrozen/frozen interface (Hilbich et al., 2008; Miceli, 2012).

High resistivity values in the range of 8000 Ohm-m to more than 50 000 Ohm-m are observed at approximately 3 m in depth between 10 m and 20 m along the survey line (Figure 5.60). These resistivity values are much higher than the ones from the perpendicular 160 m ERT survey (Figure 5.58) which could be indicative of permafrost with a substantially lower unfrozen

moisture content or a different soil lithology (Figure 5.60) (Hilbich et al., 2008). However, it may also be an artefact of the inversion.

Figure 5.59: Resistivity transect of the 40 m NE-SW survey at borehole R7 on June 24, 2011. (A) Picture taken from the 20 m mid-point looking north-east towards the highway; (B) picture taken from the borehole at the 20 m mid-point looking south-west across the regrown cut-line.

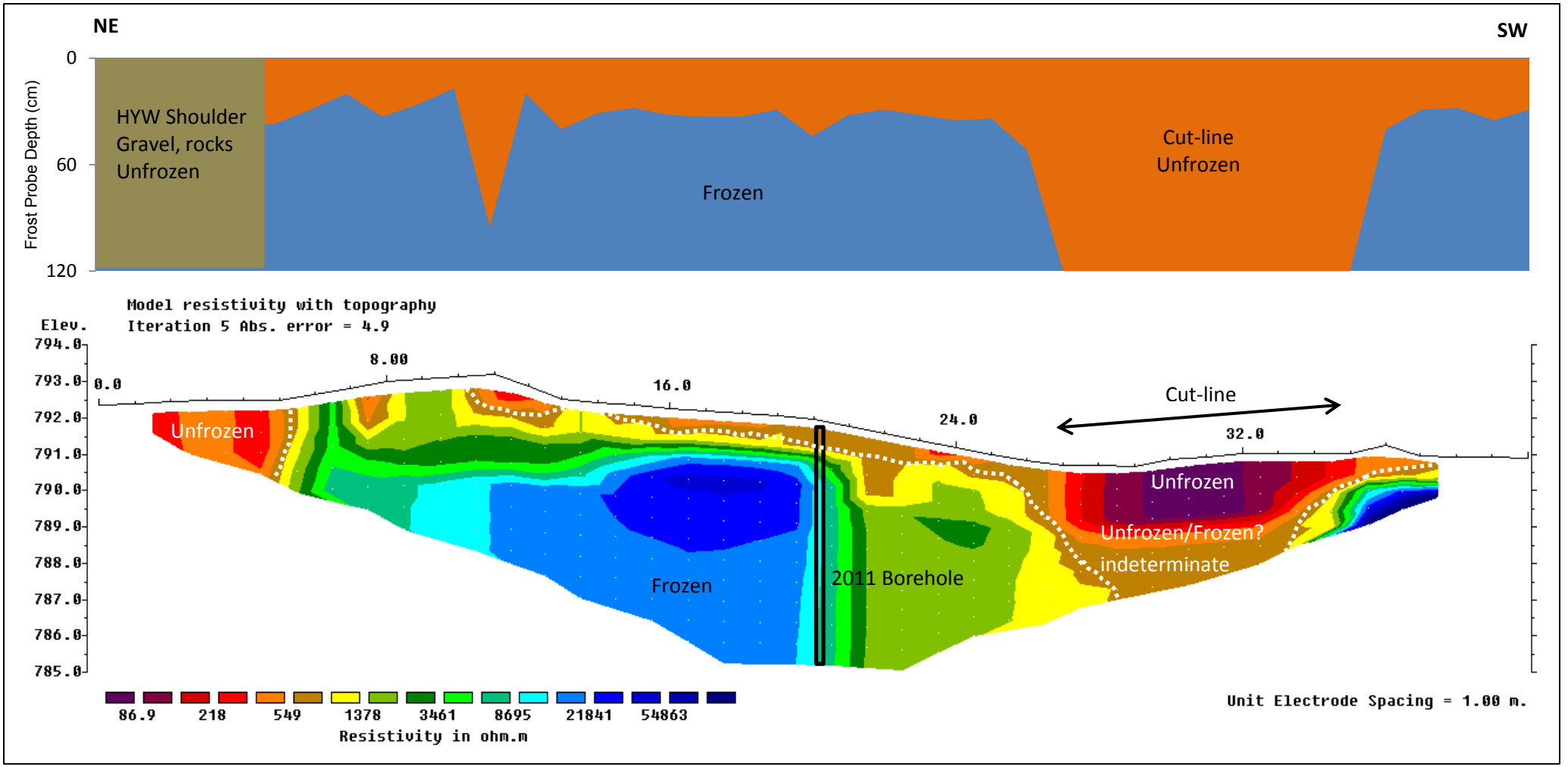

Figure 5.60: Borehole R7 NE-SW 40 m resistivity profile and frost probe chart from June 24, 2011. Vertical exaggeration in model section display = 1.00. Based on 182 data points (8 removed from original survey). The solid black lines indicates the location and depth of the 2011 borehole on the survey while the white dashed lines indicates the interpreted boundary between frozen and unfrozen ground.

The ground temperature record from borehole R7 represents a full year of measurements between August 15, 2011 and August 15, 2012 (Figure 5.61). Temperature measurements start 53 days after the borehole was steamed. Even so, the temperatures recorded at depth at the beginning of the period were warmer than those at the end which suggests that recovery following drilling was probably not complete. Ground temperatures were below 0˚C between September 24 – April 5 at the ground surface, between October 27 – May 10 at 0.5 m and between October 7 – July 22 at 1.0 m (Figures 5.61 and 5.62). Ground temperatures stayed below 0˚C for the entire year from the 1.5 m depth to the bottom of the borehole at 7.0 m (Figure 5.62). Ground temperatures at 1.0 m fell below 0˚C 10 days earlier than at 0.5 m which may be due to measurement accuracy or stratigraphy (Figures 5.56; 5.61 and 5.62) Zero-curtain effects are seen during freeze-up at 0.5 m between October 15 and December 20 for a total of 66 days and at 1 m between October 5 and February 15, for a total of 97 days (Figures 5.61 and 5.62). The long zero-curtains observed during freeze-up at the near surface may be due to presence of unfrozen moisture after drilling which required the extraction of latent heat for phase change.

Ground surface temperatures follow the cooling and warming trends measured by the weather station air temperature thermistor (Figure 5.61). Interpretation from the weather station ibuttons suggest that snow was on the ground from October 29, 2011 to April 25, 2012, with a maximum snow depth of approximately 30 cm between November 17, 2011 and March 30, 2012 (Figure 5.61). The MAAT from the R7 weather station was -2.9˚C and the MAGST was 0.1˚C between August 15, 2011 and August 15, 2012 (Figure 5.61). The MAGST was taken at 0.5 m in the borehole due to the 0 m sensor being affected by surface air temperatures. This means that the MAGST, resulting offsets and n-factors are less accurate. There were totals of 1527 TDD_a and 315 TDD_s during the thawing season and a total of 2597 FDD_a and 275 FDD_s during the freezing season (Figure 5.61). The thawing n-factor (n_t) was approximately 0.2 while the freezing n-factor (n_f) was about 0.1. A low n_t of 0.2 at BH R7 suggests significant shading from the surrounding vegetation, resulting in lower ground surface temperatures than air temperatures (Taylor, 1995). The low nf of 0.1 can be explained by a total of 180 snow days with 135 days having more than 30 cm of snow. The buffering effects of the snow cover results in higher ground surface temperatures than air (Taylor, 1995).

Mean monthly ground surface temperatures (MMGST) results for BH R7 show a maximum MMGST of 13.6˚C reached in July 2012 and a minimum MMGST of -12.5˚C in January 2012 (Figure 5.63). The MMGT for the deepest measured thermistor at 7.0 m stayed around -0.6˚C for the entire year with no observable variation (Figure 5.63). The maximum temperature recorded at the ground surface was 29.7˚C on July 21, 2012 and the minimum of -18.5˚C was reached on January 28, 2012 (Figure 5.64). The range in ground temperatures at the surface was about 26˚C which fell to less than 0.1˚C at 7.0 m (Figure 5.64). The MAGST was 0.2˚C and MAGTs cooled with depth to 1.15 m, with a MAGT of 0.1˚C at 0.5 m, -0.2˚C at 1.0 m and -0.5˚C at 1.5 m (Figures 5.64 and 5.65). MAGTs then warmed to -0.4˚C at 2.5 m before cooling to -0.7˚C at 4.5 m and warming to -0.6˚C at the deepest thermistor at 7.0 m (Figures 5.64 and 5.65). Mean temperatures at 1.5 m and 2.5 m may have been affected by the borehole steaming (Figures 5.64 and 5.64). The D_{ZAA} occurs around 4.0 m where the MAGT shows minimal variations < 0.1˚C downwards (Figures 5.64 and 5.65). MAGTs are all below 0˚C from approximately 1.0 m downwards which confirms that permafrost is present at this site (Figures 5.64 and 5.65). Hourly air temperature data collected at the R7 weather station between August 15, 2011 and June 12, 2012 as well as daily air temperatures from the ECCS Beaver Creek weather station between June 13, 2012 and August 15, 2012 were used to calculate the MAAT of -2.9˚C. The correlation coefficient between the two climate stations for the available corresponding period is 0.85. The resulting surface offset is approximately -3˚C and the thermal offset is about -0.4˚C considering a MAGST of 0.1˚C and a TTOP of -0.3˚C (Figures 5.64 and 5.65).

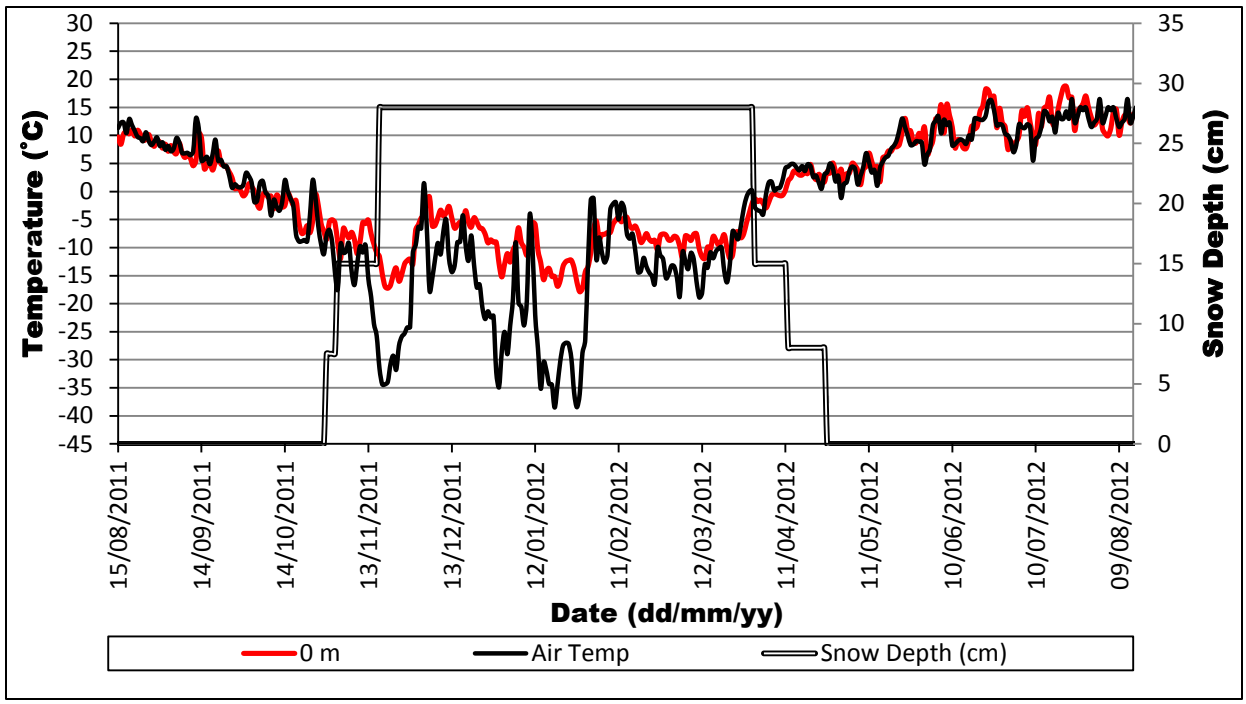

Figure 5.61: Full ground temperature series at Borehole R7 between August 15, 2011 and August 15, 2012. Daily temperatures from the R7 weather station between August 15, 2011 and June 12, 2012 are also shown with daily air temperatures from the Beaver Creek ECCS weather station between June 13, 2012 and August 15, 2012. The correlation coefficient between the two climate stations for the available corresponding period is 0.85. Snow depths from ibutton measurements are also shown.

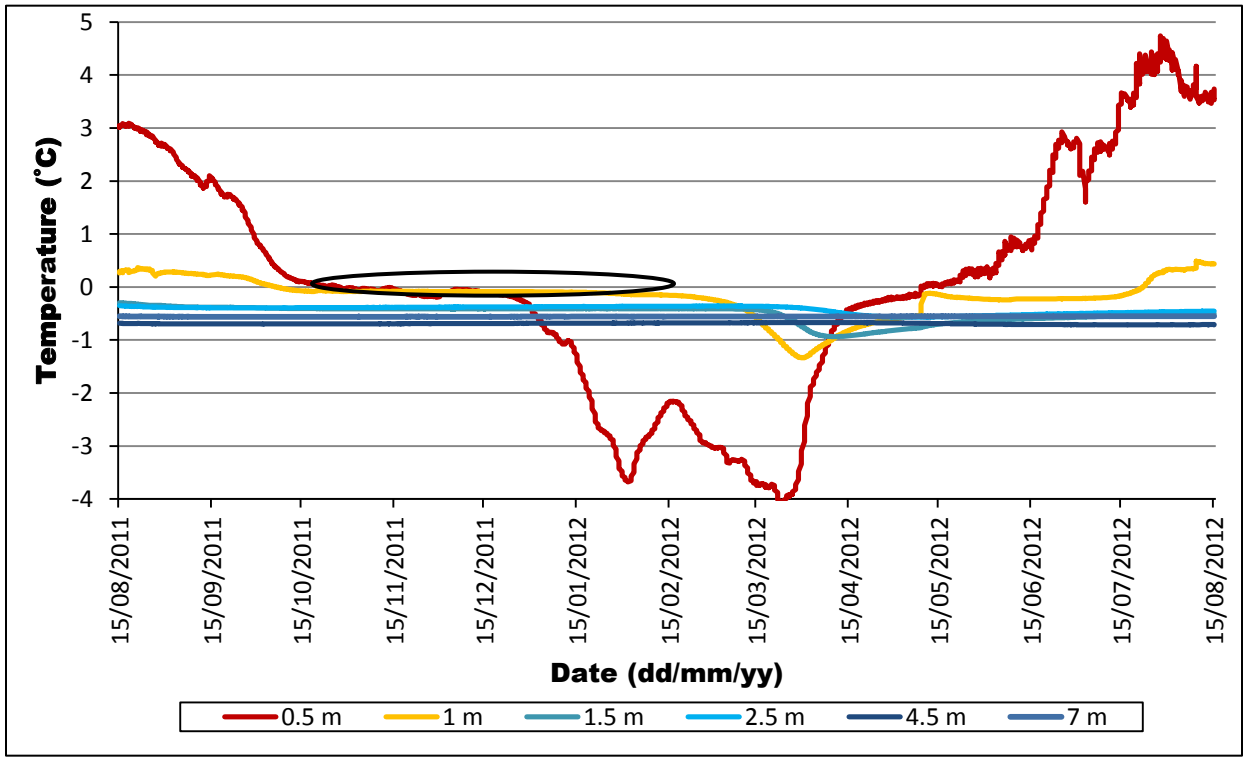

Figure 5.62: Deeper ground temperature series at Borehole R7 between August 15, 2011 and August 15, 2012. Note the long zero-curtains at 0.5 m and 1.0 m during freeze-up. The black circle indicates the zero curtain effects during thawing at 0.5 m and 1 m.

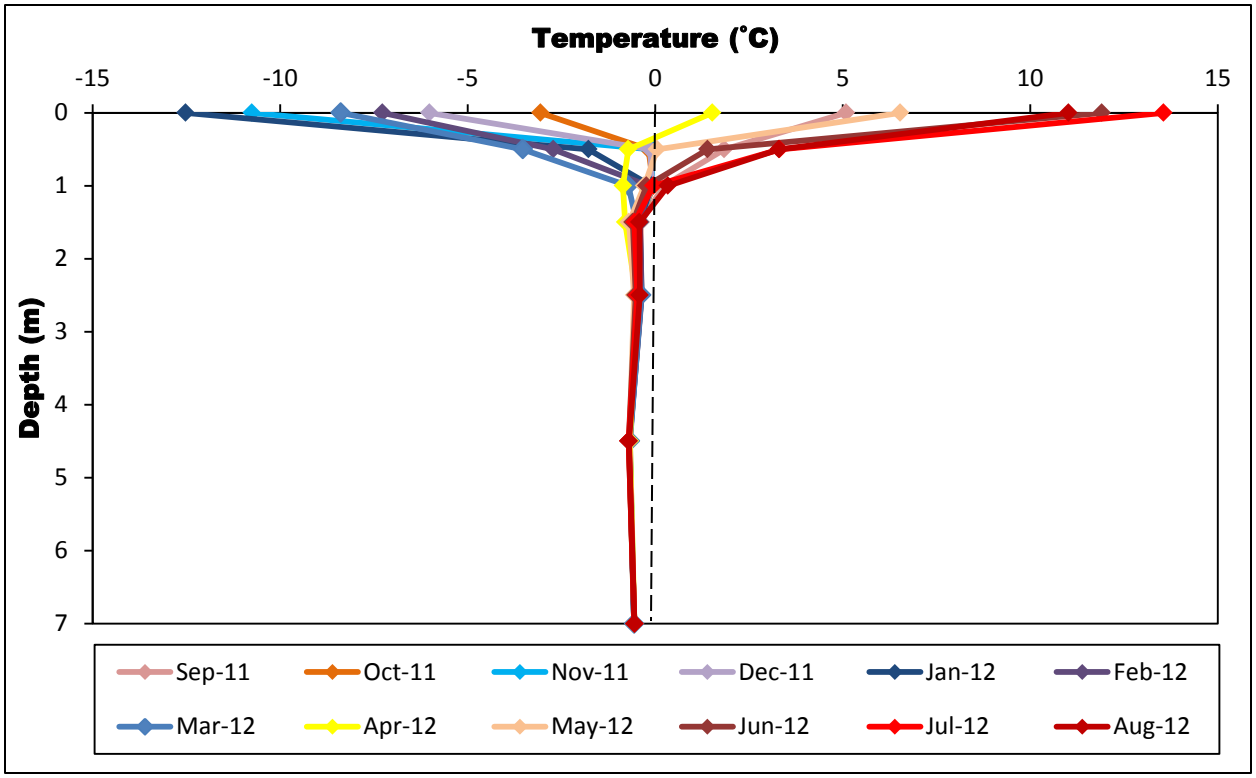

Figure 5.63: Monthly average ground temperature profiles for Borehole R7 from September 2011 to August 2012.

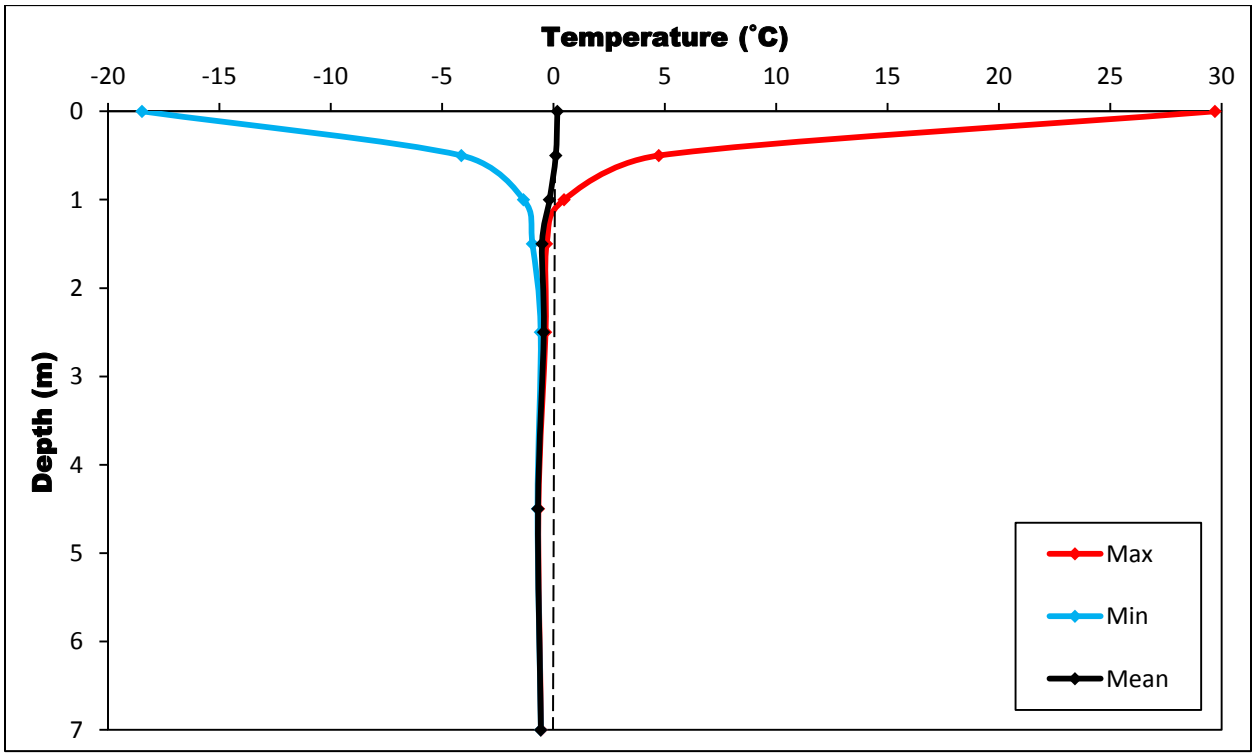

Figure 5.64: Temperature envelope at Borehole R7 for the 2011-2012 year.

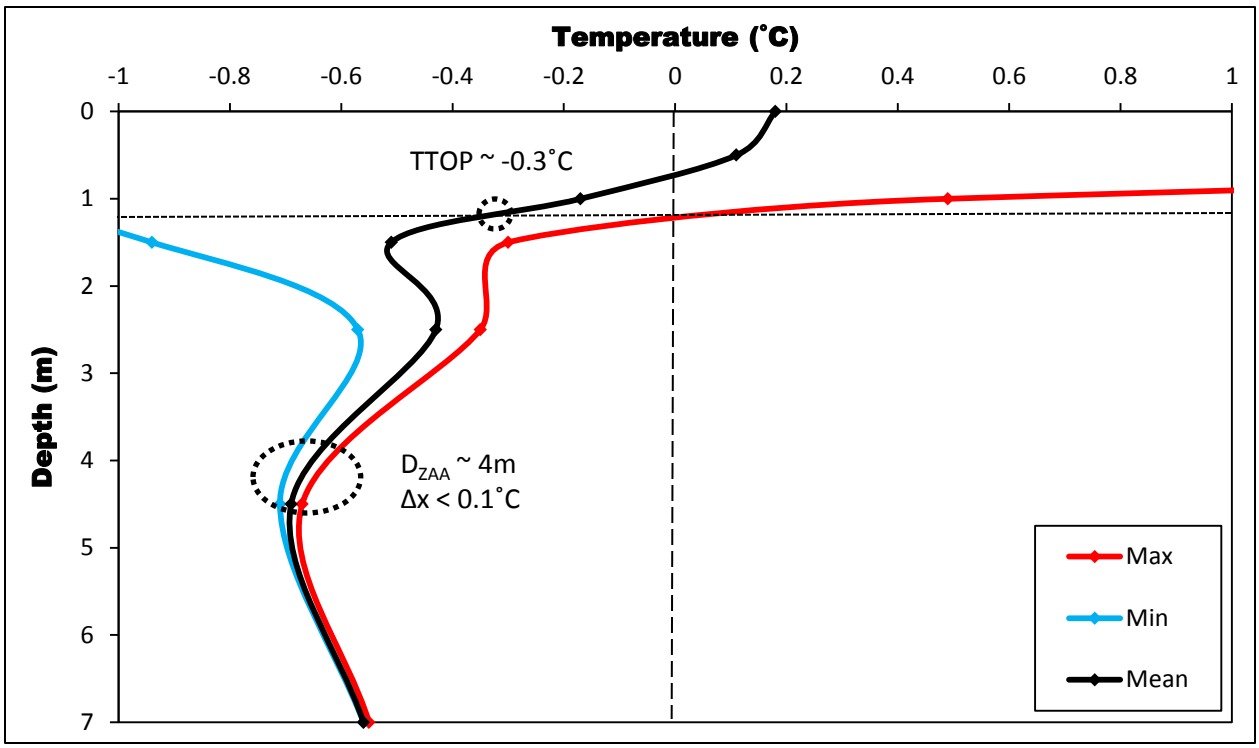

Figure 5.65: Details of temperature envelope at Borehole R7 for the 2011-2012 year showing the approximate depth of zero annual amplitude and TTOP. Ground temperatures at 1.5 m and 2.5 m are affected by non-equilibrium temperatures at the start of the monitoring period.

Comparisons of manual ground temperature measurements from November 23, 1978 and November 23, 2011 suggest warming has occurred (Figure 5.66). Ground temperatures were approximately 0.1˚C warmer at 1.5 m and 3.0 m and 0.9˚C warmer at the deepest measurement of 7.0 m on November 23, 2011 than on the same day in 1978 (Figure 5.66). However, the November 23, 2011 ground temperature at 4.5 m was about 0.1˚C cooler than in 1978 (Figure 5.66). The deepest thermistor shows ground temperature warming significantly greater than the potential margin of error for the 1978 manual temperature measurements, especially as this is below the depth of zero annual amplitude

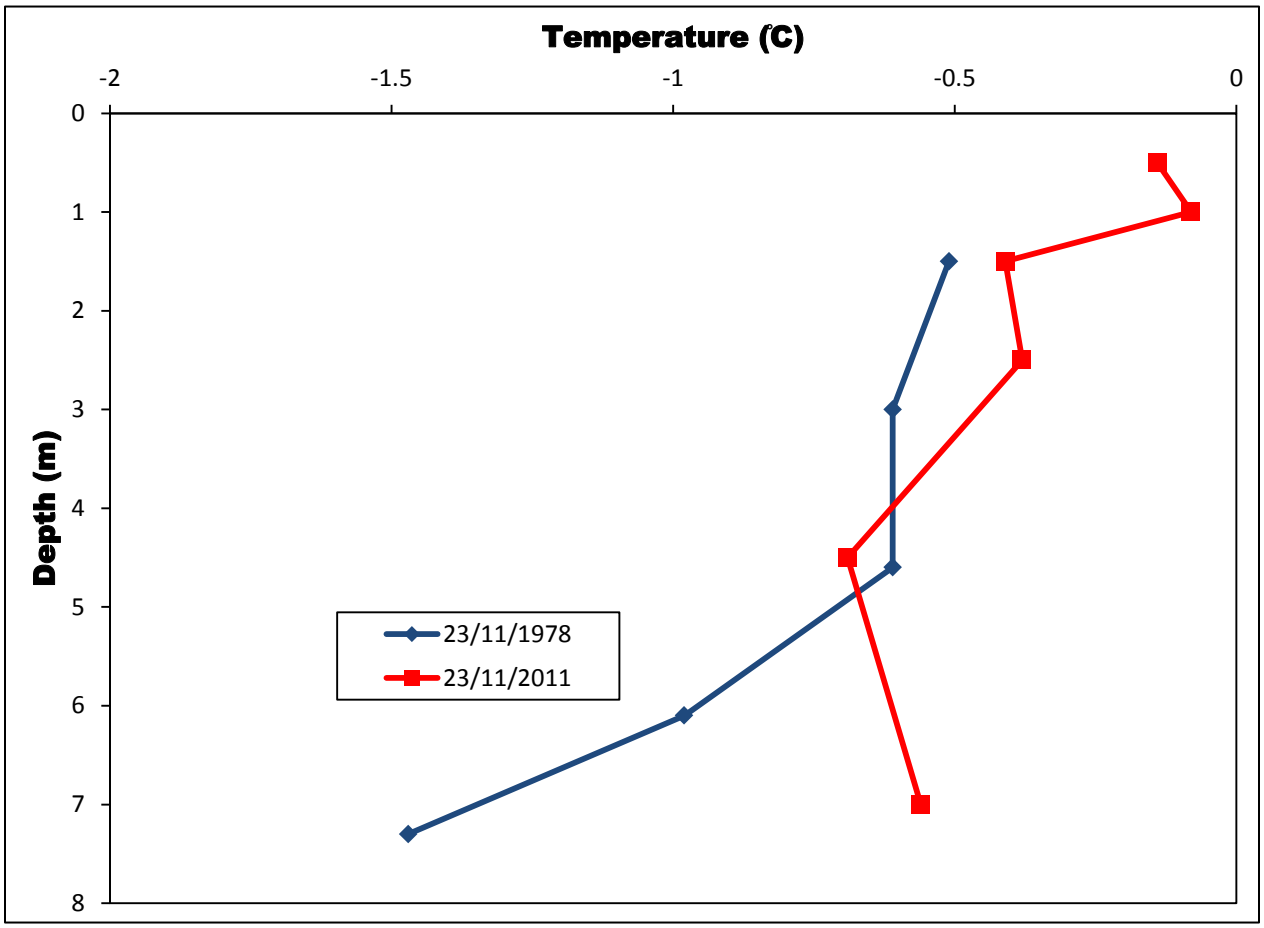

Figure 5.66: Ground temperature differences at borehole R7 between November 23, 1978 and November 23, 2011.

5.2.8 Borehole R8 (78-A-8)

The permafrost thermal monitoring site at borehole R8 is located in the extensive discontinuous permafrost zone of the Yukon Territory at 62˚ 17’ 31’’ N and 140˚ 46’ 11’’ W and at 747 m elevation (Figure 5.67). The field site is located in a hummocky clearing with scattered spruce trees and low-lying shrubs averaging between 1 m and 3 m in height (Figure 5.67). The borehole is situated approximately 22 m from a regrown cut-line used for previous geophysical work in the 1970s and is a 1.2 km walk from the Alaska Highway. The field site is about 11 km south of Beaver Creek. The borehole site was cleared for drilling and drilled to a depth of 7.6 m on August 5, 1978. Soil type and ground ice conditions from the August 1978 borehole log indicate a layer of peat from the ground surface to a depth of 0.3 m, underlain by a silt layer from 0.3 m to the bottom of the borehole at 7.6 m (Figure 5.68).

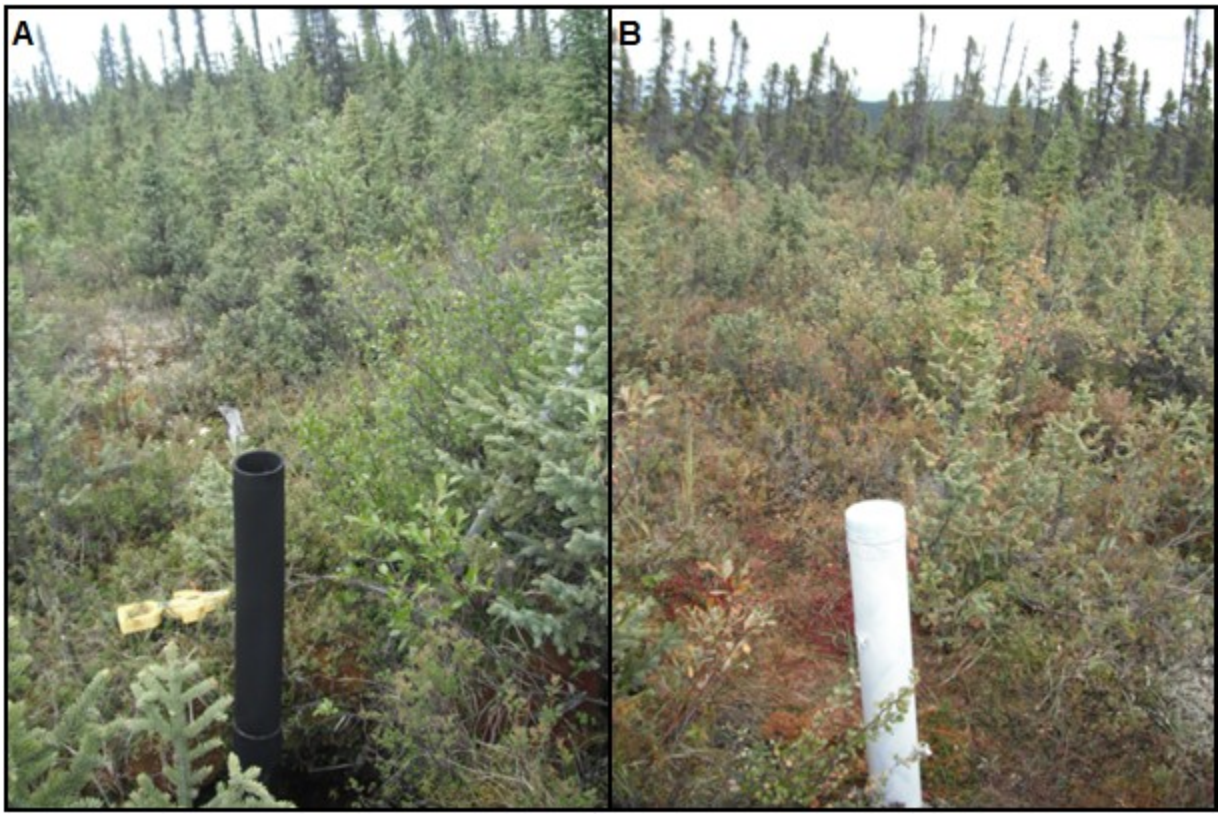

Figure 5.67: (A) Borehole R8 as it was found during the summer 2011 borehole exploration; (B) and borehole R8 after it was rehabilitated and cased.

The borehole was unfrozen from the ground surface down to 0.2 m when drilled, with visible stratified or oriented ice (Vs) and visible random or irregular oriented ice (Vr) at 20-95% observed between 0.2 m and 0.6 m, visible stratified or oriented ice (Vs) at 10-95% between 0.6 m and 1.1 m, at 15-60% between 1.1 m and 1.7 m, at 15% between 1.7 m and 2.1 m, at 1-2 % between 2.1 m and 3.6 m and at 20% between 3.6 m and 4.7 m (Figure 5.68). Visible stratified or oriented ice (Vs) and visible random or irregular oriented ice (Vr) at 40% was observed between 4.7 m and 5.5 m, with visible stratified or oriented ice (Vs) at 10 % between 5.5 m and 5.9 m and well bonded sediments without visible ice (Nbn) from 5.9 m to the bottom of the borehole at 7.6 m (Figure 5.68).

The borehole was unblocked of ice by steam and cased on August 20, 2011 and a RBR logger with a multithermistor string was installed to a depth of 7.0 m on the same day. Field visits during June 2012 revealed that the cable had failed right after installation and no data could be retrieved. The RBR logger was replaced on June 12, 2012. The length of the current ground thermal monitoring record as well as other related field work associated with borehole R8 and pertinent information is summarized in Table 5.11.

Table 5.11: Summary table of the data used in the analysis of borehole R8 and the depths of the thermistors from the surface. Note that more detailed field work and RBR logger information is given in Appendix C.

Borehole R8	
Closest ECCS Station and Distance	Beaver Creek (14 km)
Dates of 1978 drilling	August 5, 1978
Manual Temperature Measurements	November 25, 1978; July 25, 1979
Original Borehole Depth	7.6 m
New Rehabilitated Borehole Depth	7.0 m
Borehole Unblocking Method	Steam
RBR Logger Data	June 12, 2012 – August 5, 2012
Thermistor Depths (m)	0.15, 0.65, 1.15, 1.65, 2.65, 4.65, 7.15
Length and Date of ERT Survey	160 m (August 5, 2012)

The thermal profile from August 5, 2012 at borehole R8 (Figure 5.68) was extracted from the RBR logger data record for comparison with the August 5, 2012 ERT results (Figures 5.69 and 5.70). Results from the daily ground temperature record show frozen conditions to the maximum depth of measurement of 7.0 m with an interpolated active layer of approximately 0.55 m (Figure 5.68). The 1978 borehole log indicates an active layer from the surface down to

0.2 m on August 5, 1978 which suggests an increase in active layer thickness of about 0.35 m when compared to the same period in 2012 (Figure 5.68).

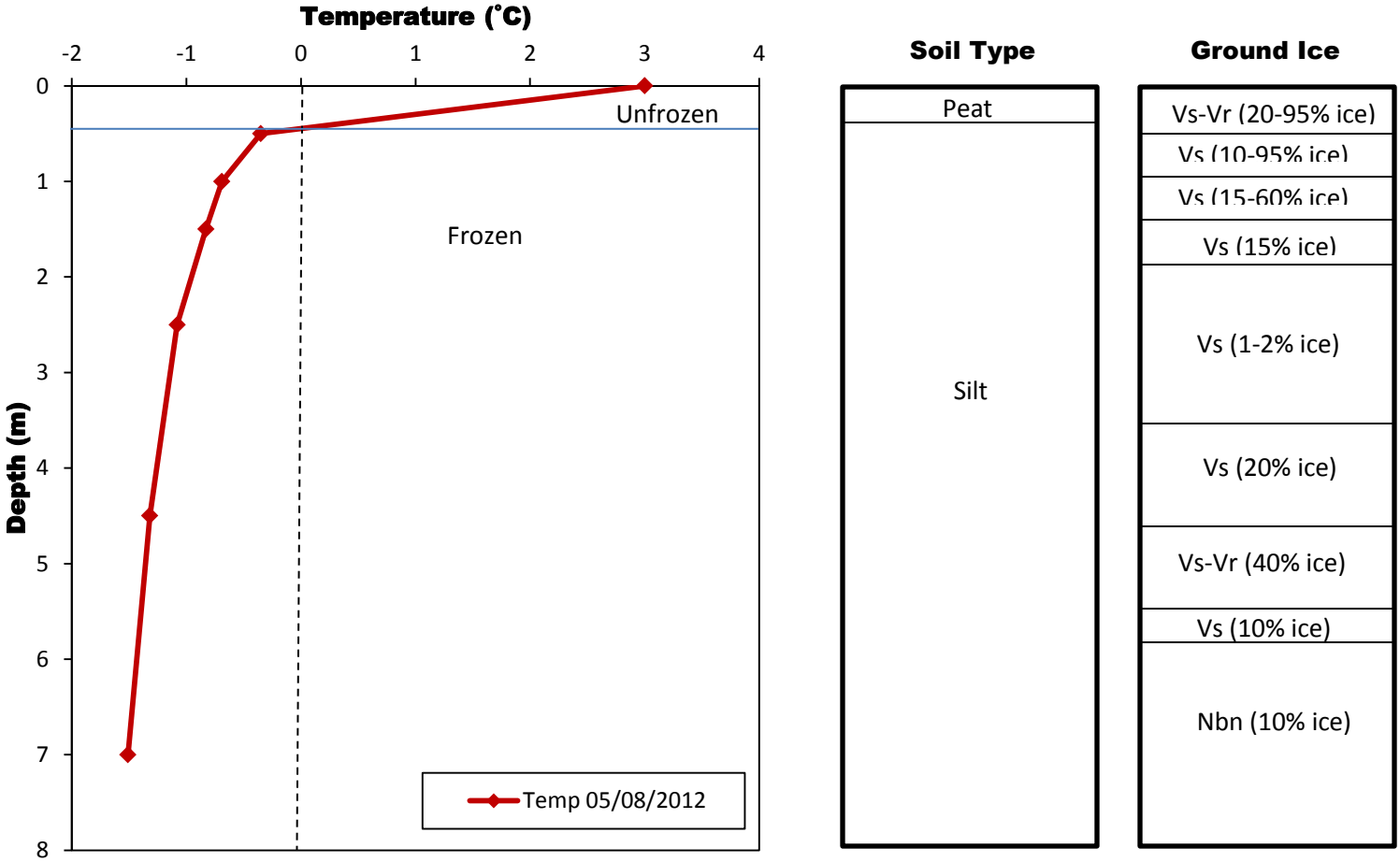

Figure 5.68: Borehole R8 average daily temperature measurements taken from the RBR logger on the same day as the 160 m ERT survey of August 5, 2012. The diamonds represent the points of temperature measurement. Soil type and ground ice conditions taken from an August 5, 1978 borehole log are shown on the right hand side. Complete descriptions of the borehole log and ground ice classification are found in Appendix K. Note that the 1978 borehole log shows unfrozen conditions in the top 0.2 m which is not indicated on the figure.

The 160 m ERT profile at BH R8 runs south-west, to north-east, through a scattered spruce forest and crosses a regrown cut-line used for previous geophysical work in the 1970s between 48 m and 58 m (Figures 5.69 and 5.70). The ground surface consists mainly of hummocky wet mosses and Labrador tea (Figure 5.69). The terrain decreases by approximately 5 m from the start to the end of the survey (Figure 5.70).

Probing results along the survey line were variable, giving a mean depth of 42 cm (N=61; SD=11) (Figure 5.70). The deepest active layers were probed where the survey crosses the regrown cut-line and measured between 65 cm and 82 cm (Figure 5.70). Shallower active layers are not identifiable on the modelled resistivity plot because the inversion routine cannot cope with extremely high resistivity contrast in the near surface at the unfrozen/frozen interface (Hilbich et al., 2008; Miceli, 2012).

Resistivity values along the survey line range from 1000 Ohm-m to more than 15 000 Ohm-m (Figure 5.70). High resistivity values from the ground surface down to the bottom of the borehole at 7.0 m matched with negative temperatures recorded on the day of the survey and are indicative of permafrost at this site (Figures 5.68 and 5.70). The low end of the resistivity values is mainly situated at the near surface around the borehole, where the site was cleared in August 1978 as well as under the regrown cut-line (Figure 5.70). Although extensive thawing is not observed under the cut-line, substantially lower resistivity values suggest that the permafrost is warmer with higher unfrozen moisture content due to environmental change (Figure 5.70). The high end horizontally layered resistivity values present between depths of 1 m and 5 m suggest permafrost with low unfrozen moisture content and high ice content as shown in the borehole log (Figure 5.68) (Osterkamp and Burn, 2003) (Figure 5.70). Resistivity values greater than 7000 Ohm-m down to the bottom of the resistivity plot indicate permafrost deeper than 25 m at borehole R8 (Figure 5.70).

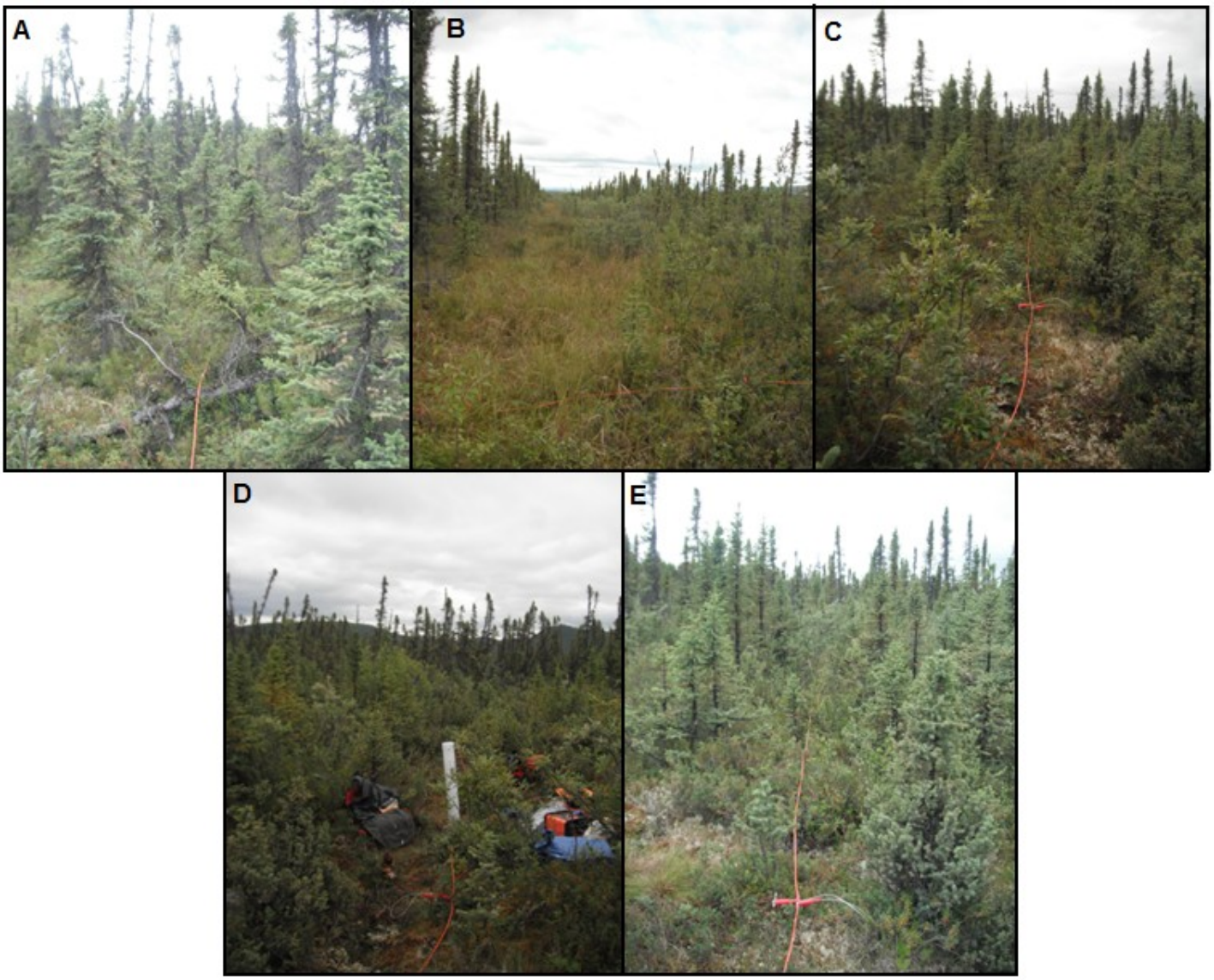

Figure 5.69: Resistivity transect of the 160 m SW-NE survey at borehole R8 on August 5, 2012. (A) Picture taken from the 40 m point looking south-west towards the start of the transect; (B) picture of the survey line crossing the regrown cut-line between 48 m and 58 m; (C) picture taken from the borehole at the 80 m mid-point looking south-west; (D) picture taken from the borehole at the 80 m mid-point looking north-east; and (E) picture taken from the 120 m point looking north-east towards the end of the survey line.

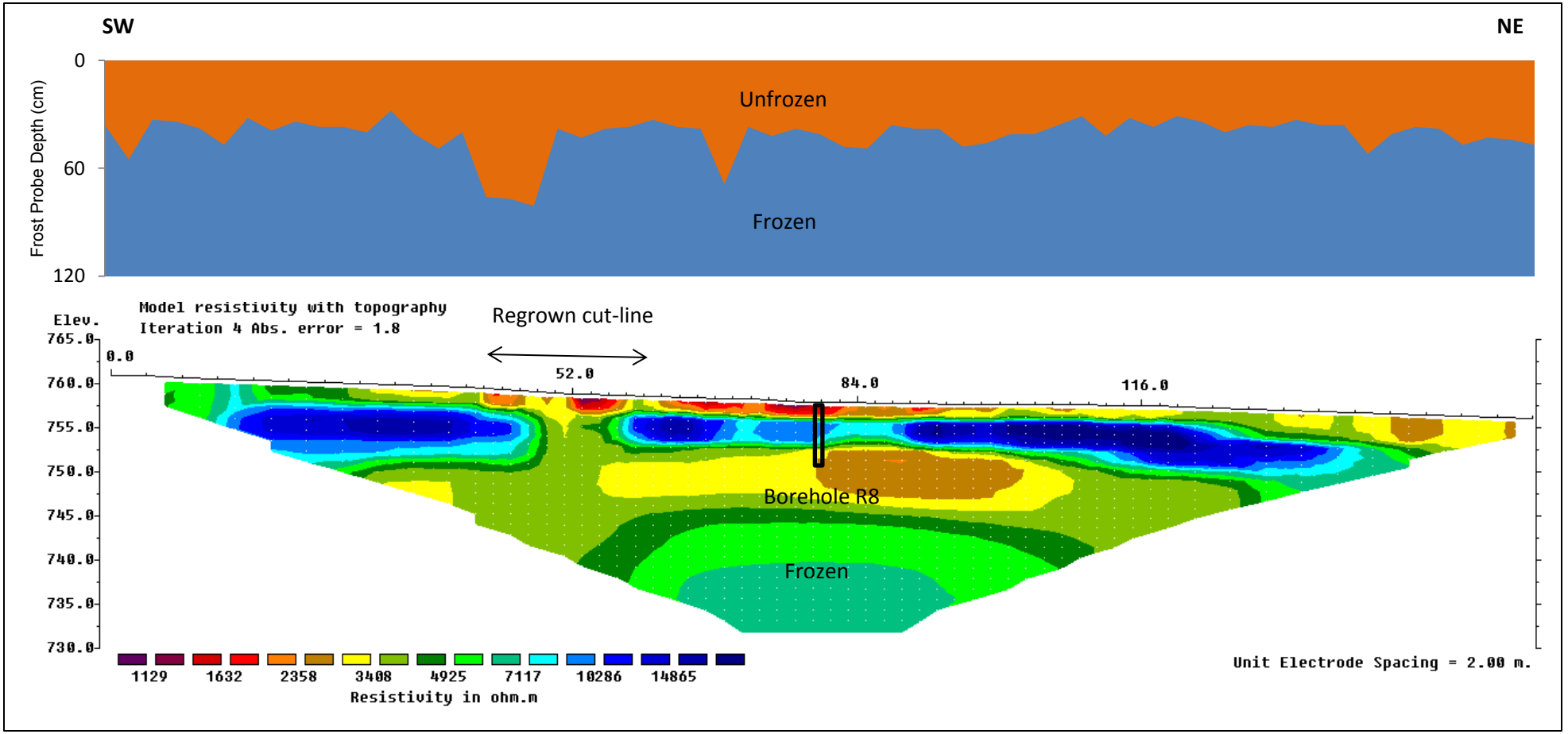

Figure 5.70: Borehole R8 SW-NE 160 m resistivity profile and frost probe chart from August 5, 2012. Vertical exaggeration in model section display = 1.00. Based on 314 data points (31 removed from original survey). The solid black lines indicates the location and depth of the 2011 borehole on the survey.

Comparisons between ground temperature measurements from July 25, 1979 and July 25, 2012 show an increase in the ground temperatures measured at borehole R8 (Figure 5.71). Ground temperatures were also measured on November 25, 1978 (Figure 5.71). Ground temperatures showed insignificant change (<0.1˚C) at 1.5 m and were approximately 0.2˚C warmer at 2.5 m , 0.7˚C warmer at 4.5 m and 0.6˚C warmer at 7.0 m on July 25, 2012 than on the same day in 1979 (Figure 5.71). The deepest thermistors show ground temperature warming significantly greater than the potential margin of error for the 1978 manual temperature measurements. Measurements at 7.0 m were approximately 0.4˚C warmer on July 25, 2012 than on November 25, 1978 (Figure 5.71). Comparison between measured ground temperatures at 7.0 m on July 25, 1979 and November 25, 1978 show a 0.2˚C difference which suggest that the D_{ZAA} was not reached at 7.0 m during 1978-1979 unless the observed difference was due to measurement error as this is within the accuracy for the manual temperature measurements (Figure 5.71). However, the 55 day RBR logger record between June 12, 2012 and August 5, 2012 shows ground temperature variations of 0.05˚C at 7.0 m which suggest further variations during the year and consequentially, a D_{ZAA} deeper than but close to 7.0 m at BH R8.

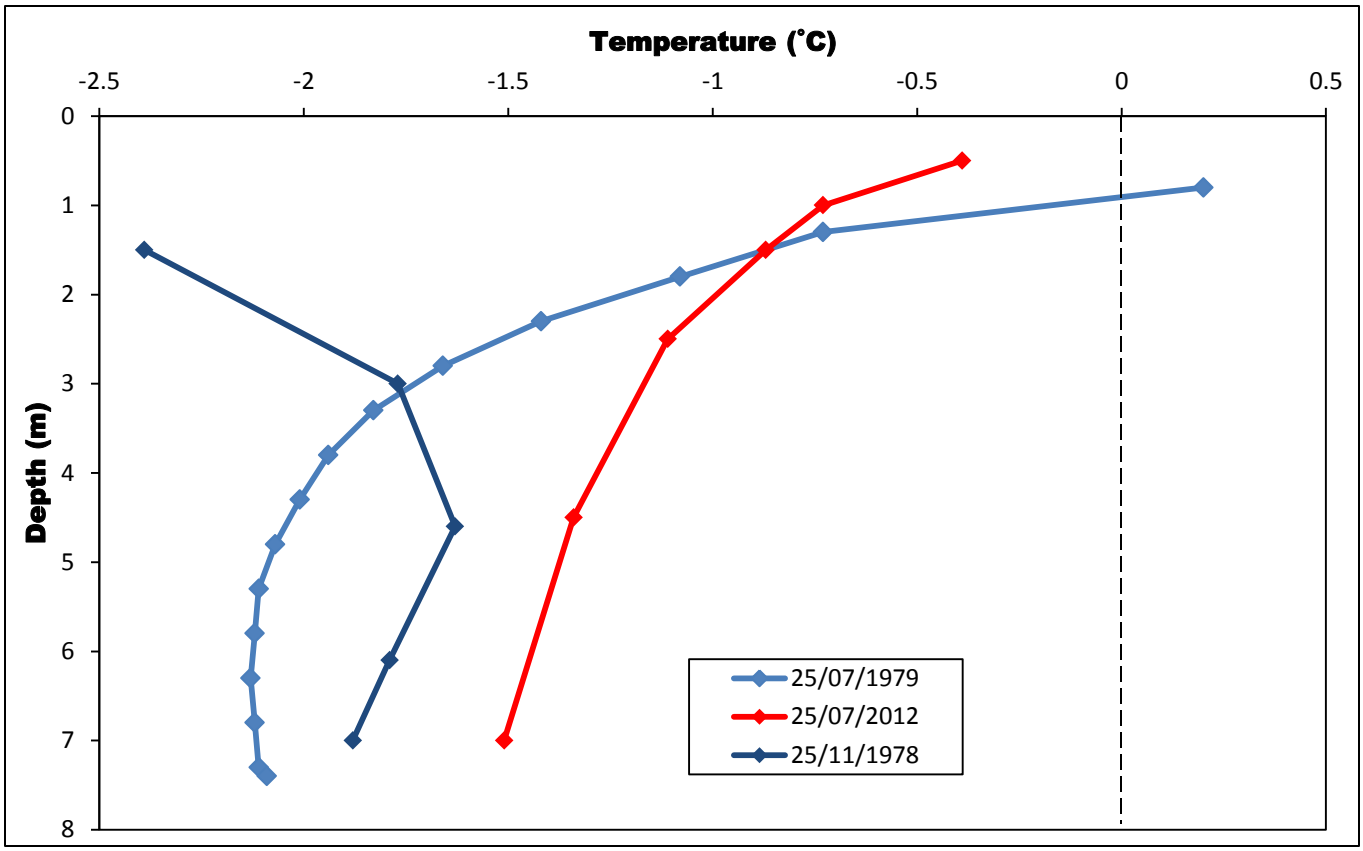

Figure 5.71: Ground temperature differences at borehole R8 between July 25, 2012 and July 25, 1979. Manual ground temperature measurements from November 11, 1978 are also shown.

5.3 HOBO Instrumented Boreholes

5.3.1 BH M1 (78-A-57)

The permafrost thermal monitoring site at borehole M1 is located in the sporadic discontinuous permafrost zone of the Yukon Territory at 61^{o} 24’ 43” N and 139 ^{o} 11’ 20” W and at 829 m elevation (Figure 5.72). The site is located in an open marsh land about 100 m from the Alaska Highway where a cut-line used for previous geophysical work in the 1970s crosses the bog at about 30 m from the borehole. The terrain at this site is mainly flat within 200 m of the borehole (Figure 5.72). The bog had an average water depth of 10-60 cm during the site visits and is interspersed with small spruce trees typically 1.0 m to 3.0 m in height. Spruce trees become taller as the marsh approaches the drier forest about 200 m to the south-east and north-west of the borehole. Other common vegetation at this site includes sphagnum mosses, Labrador tea, grasses and sedges (Figure 5.72). Signs of past forest fires were present in the area.

Figure 5.72: Borehole M1 as it was found during the summer 2011 borehole exploration. Note that this borehole was not cased. The old casing and wood stake show burn marks which could possibly indicate the passage of a forest fire since the 1970s.

The borehole was drilled to a depth of 6.55 m in August 1978. No temperature measurements were collected at this site during the 1970s but soil type and ground ice characteristics are available from the 1978 borehole log (Figure 5.73). The borehole log indicates a layer of peat and organic silts to a depth of 1.0 m, a silt layer between 1.0 m and 1.3 m and a layer of gravel from 1.3 m to the bottom of the borehole at 6.55 m. The borehole was unfrozen from the surface down to 1.0 m, with visible stratified or oriented ice (Vs) at 10-30% between 1.0 m and 1.4 m and visible stratified/oriented ice (Vs) and individual ice crystals or inclusions at 5-15% from 1.4 m to the bottom of the borehole at 6.55 m (Figure 5.73). Relatively high ice content (Vs at 10-30%) directly below the active layer is indicative of the top of permafrost (Shur et al., 2005; French and Shur, 2010) at around 1.0 m during 1978 (Figure 5.73).

The borehole was unblocked by steam on June 29, 2011 to a depth of 2.8 m but the original depth could not be reached because the borehole had collapsed. The borehole was not instrumented nor cased due to unfrozen conditions with water down to the new depth of 2.8 m in August 2011 and 2012. Other related field work associated with borehole M1 and pertinent information is summarized in Table 5.12.

Table 5.12: Summary table of the data used in the analysis of borehole M1. Note that more detailed field work information is given in Appendix C.

Borehole M1	
Closest ECCS Station and Distance	Burwash (12 km)
Date of 1978 drilling	August 1978
Manual Temperature Measurements Available	August 17, 2011
Original Borehole Depth	6.55 m
New Rehabilitated Borehole Depth	2.8 m
Borehole Unblocking Method	Steaming
Borehole Unblocking Date	June 29, 2011
Length and Date of ERT Survey	2 x 80 m cross-section (June 29, 2011)

The manual temperature measurements from August 17, 2011 (Figure 5.73) were taken for comparison with the June 29, 2011 ERT results. Results show unfrozen conditions from the ground surface to the bottom of the borehole at approximately 2.8 m where temperatures fall below 0˚C (Figure 5.73). Probing the ground around the borehole did not reach a frost table (active layer > 120 cm) on August 17, 2012 and the lowering of a weighted string in the borehole revealed unfrozen conditions with water down to 2.8 m. These observations suggest an increase of approximately 1.8 m in active layer thickness between 1978 and 2011 which may be due to the effects of the highway on drainage, which has probably raised water levels in the marsh (Figure 5.73).

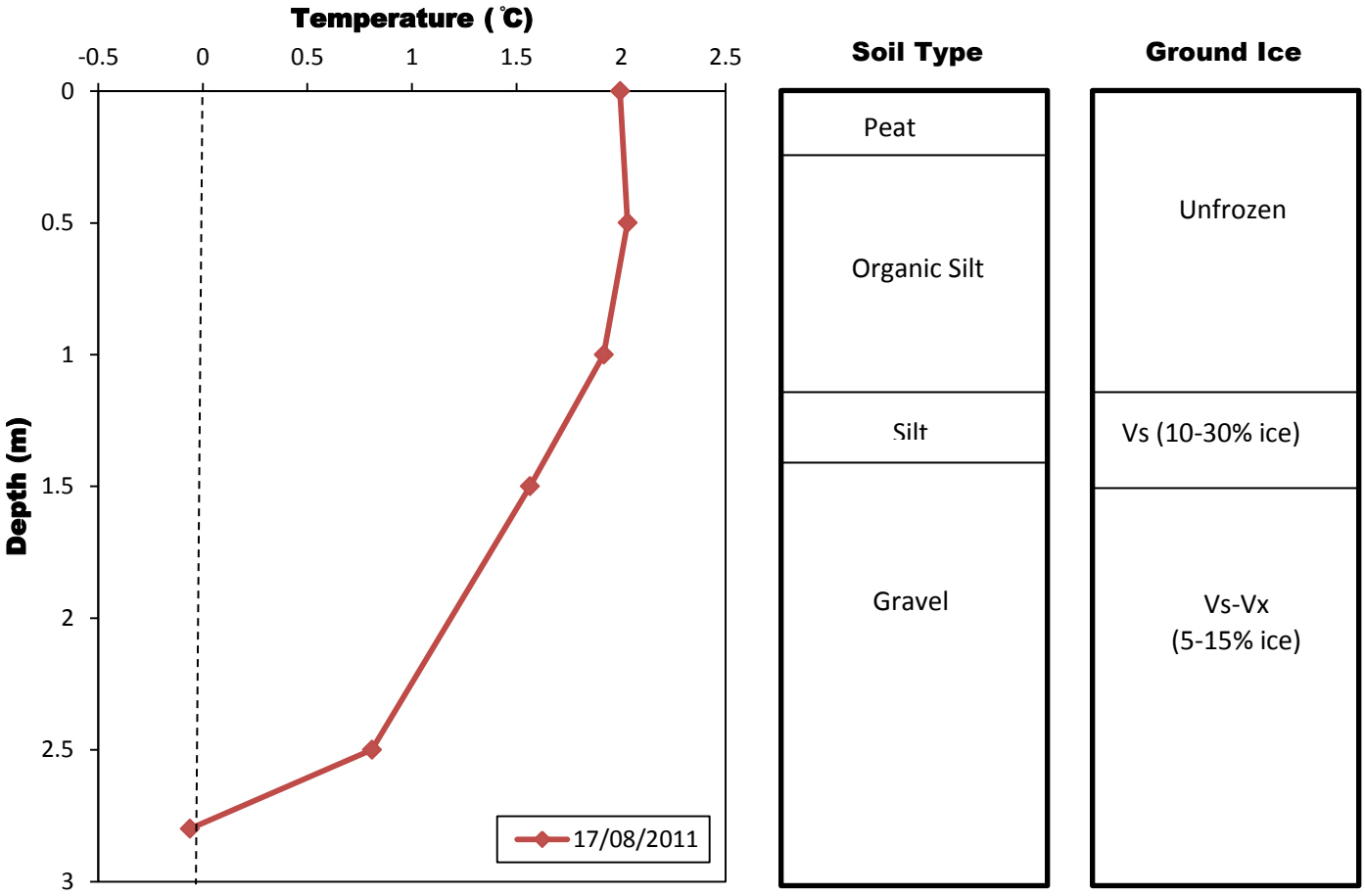

Figure 5.73: Borehole M1 manual ground temperature measurements taken on August 17, 2011. The diamonds represent the points of temperature measurement. Soil type and ground ice conditions taken from a 1978 borehole log are shown on the right hand side. Detailed descriptions of the borehole log and ground ice classification to a depth of 6.55 m are found in Appendix K. Note that ground temperature measurements were not available for 1978.

Two 80 m ERT perpendicular cross-section surveys were conducted on June 29, 2011, 40 days before the manual temperature measurements were undertaken with the mid-point at borehole M1 to better interpret vertical and horizontal permafrost characteristics and distribution (Figures 5.74, 5.75, 5.76 and 5.77). Both surveys show resistivity values less than 300 Ohm-m to a depth of about 1.5 m at the borehole which matched with positive manual ground temperatures measured on August 17, 2011 (Figures 5.75 and 5.77).

The 80 m SE-NW ERT profile runs through a wet marsh with a relatively flat relief (Figure 5.74). Probing results along the survey line were variable, giving a mean depth of 54 cm (N=61, SD=9) and it was uncertain in most case if a frost table was reached due to widespread gravel under the organic surface layer which interfered with probing (Figure 5.75). The presence of silt and gravel from 0.4 m downwards is confirmed by the 1978 borehole log (Figure 5.73). However, the fact that the mean depth of both profiles is similar suggests that a frost table was reached (Figures 5.75 and 5.77). Probing the ground around the borehole again on August 17, 2012 did not reach a frost table (active layer > 120 cm) (Figures 5.75 and 5.77). These measurements support the interpretation of deep active layers seen as a horizontal layer with resistivities less than 380 Ohm-m from the surface down to about 1.0 m to 1.5 m between 17 m to 60 m along the transect in the open marsh (Figure 5.75). Horizontal extremities of this survey show higher resistivity values in excess of 691 Ohm-m where the survey traverses scattered spruce on drier terrain, so the thin thawed layers measured during frost probing were not identifiable at the profile ends due to the larger electrode spacing (Figure 5.75)

High resistivity values up to 8 000 Ohm-m from 2.8 m down to the bottom of the ERT plot can be interpreted as permafrost deeper than 12.5 m with a thick active layer in the marsh. Frozen conditions were measured at 2.8 m in the borehole on August 17, 2011 (Figure 5.73).

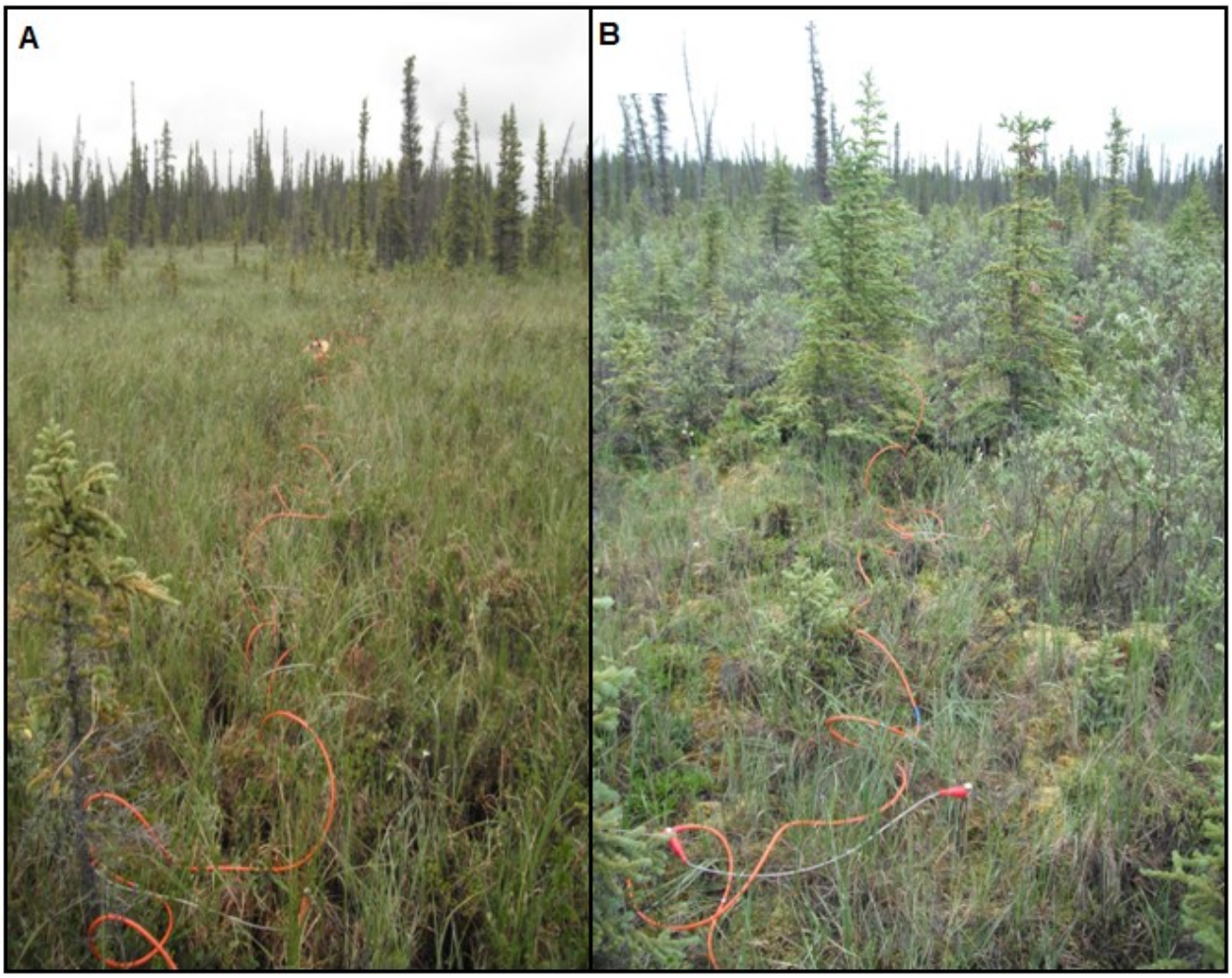

Figure 5.74: Borehole M1 resistivity transect of the 80 m SE-NW survey. (A) Picture taken from the borehole at the mid-point looking south-east; (B) picture taken from the borehole at the mid-point looking north-west.

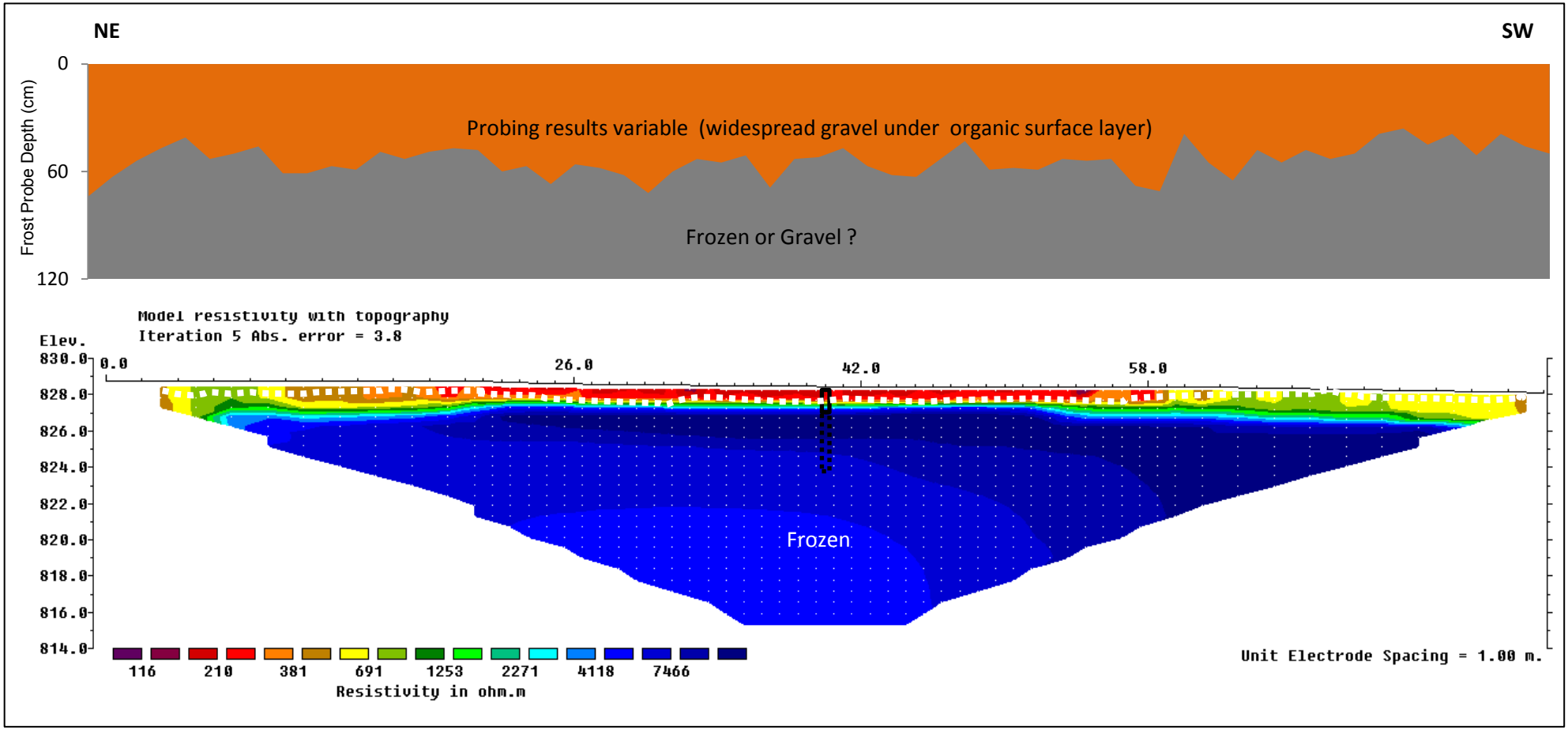

Figure 5.75: Borehole M1 SE-NW 80 m resistivity profile and frost probe chart from June 29, 2011. Vertical exaggeration in model section display = 1.00. Based on 341 data points (4 removed from original survey). The solid black lines indicates the location and depth of the 2011 borehole on the survey while the black dashed lines indicate the original depth of the 1978 borehole. The white dashed lines indicate the interface between frozen and unfrozen conditions.

The 80 m NE-SW ERT profile shows similar results as the SE-NW profile with a low horizontal resistivity layer in the range of 300-400 Ohm-m from the surface down to about 1.0 m to 2.0 m along the transect interpreted as unfrozen ground (Figures 5.76 and 5.77). A homogeneous vegetation cover with scattered low lying spruce in a wet marsh was present along the whole transect (Figure 5.76). Probing results along the survey line were variable, giving a mean depth of 52 cm (N=61, SD=8) (Figure 5.77).

Higher resistivity values are seen on the horizontal extremities of the survey in excess of 700 Ohm-m and can be interpreted as permafrost with a shallow thawed layer measured by probing which cannot be identified in the resistivity plot due to the greater electrode spacing (Figure 5.77). The north-east end of the transect shows lower resistivity values at the surface than at the south-west end of the transect (Figure 5.77) which may be due to higher unfrozen moisture content in the top of the permafrost at the start of the survey and less at the end (Hilbich et al., 2008; Lewkowicz et al., 2011). Resistivity values are as high as 6000 Ohm-m under the thawed layer to the bottom of the survey suggesting permafrost deeper than 12.5 m (Figure 5.77).

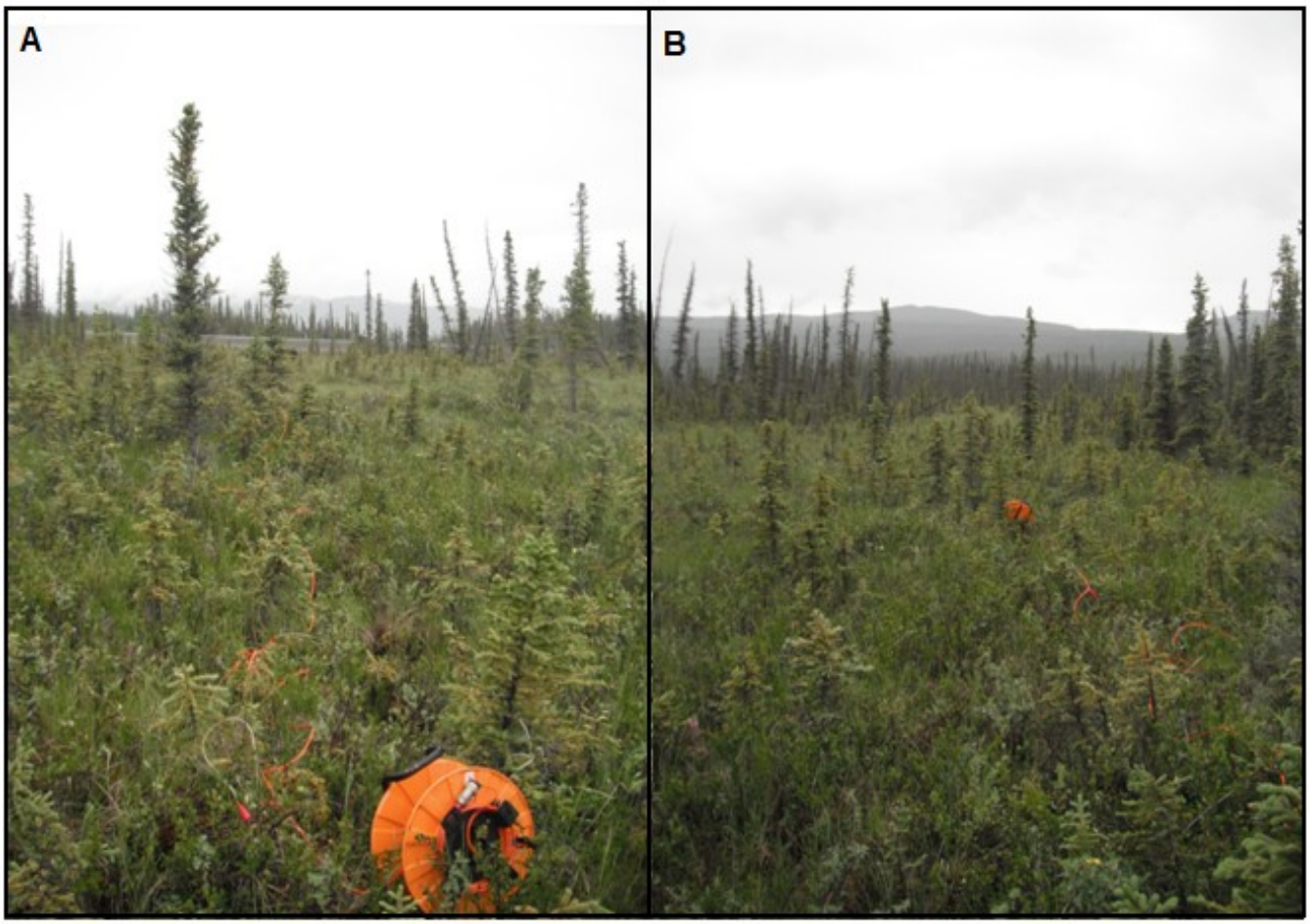

Figure 5.76: Borehole M1 resistivity transect of the 80 m NE-SW survey. (A) Picture taken from the borehole at the mid-point looking north-east; (B) picture taken from the borehole at the mid-point looking south-west.

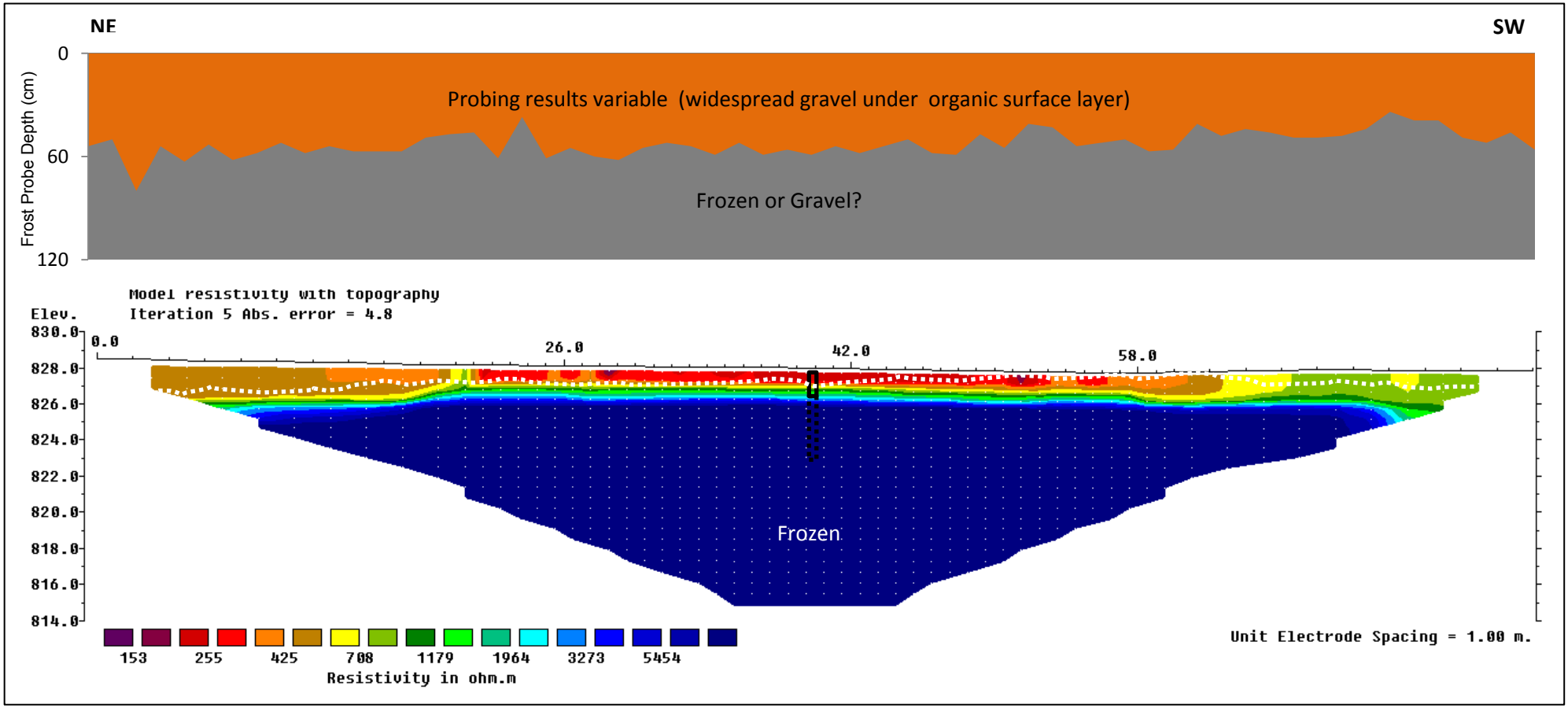

Figure 5.77: Borehole M1 NE-SW 80 m resistivity profile and frost probe chart from June 29, 2011. Vertical exaggeration in model section display = 1.00. Based on 345 data points (0 removed from original survey). The solid black lines indicates the location and depth of the 2011 borehole on the survey while the blck dashed lines indicate the original depth of the 1978 borehole. The white dashed lines indicate the interface between frozen and unfrozen conditions.

5.3.2 BH H1 (78-A-46)

The permafrost thermal monitoring site at borehole H1 is located in the sporadic discontinuous permafrost zone of the Yukon Territory at 61^{o} 35’ 37” N and 139 ^{o} 27’ 46” W and at 759 m elevation (Figure 5.78). The borehole is located on a cut-line used for previous geophysical work in the 1970s in an open bog land about 60 m from the Alaska Highway (Figure 5.78). The terrain is relatively flat within a 500 m radius of the borehole, excluding the highway. The bog had an average water depth of 10-30 cm during site visits in late June 2011 and mid-August 2011 and 2012 and has scattered spruce trees averaging 1.0 m to 5.0 m in height and low shrubs. Tall spruce forest dominates the extremities of the bog. Other common vegetation at this site includes sphagnum moss, Labrador tea, grasses and sedges.

Figure 5.78: (A) Borehole H1 after it was water-jet drilled and cased in summer 2011; (B) and Borehole H1 after it was instrumented with a HOBO H21-002 Micro station in August 2012.

The borehole was drilled to a depth of 8.8 m in August 1978. No temperature measurements were collected at this site during the 1970s but soil type and ground ice characteristics are available from the 1978 borehole log (Figure 5.79). The borehole log indicates a peat layer at the surface to a depth of 0.2 m underlain by a layer of volcanic ash to 0.4 m, an organic silt layer between 0.4 m and 2.1 m, a gravel layer between 2.1 m and 3.2 m, a layer of clay between 3.2 m and 3.5 m, and a layer of sand and gravel from 3.5 m to the bottom of the borehole at 8.8 m. Unfrozen conditions were present from the surface down to 0.2 m in the peat layer, with visible individual ice crystals or inclusions (Vx) and visible stratified or orientated ice (Vs) at 5% between 0.2 m and 1.3 m, well bonded sediments with excess ice (Nbe) between 1.3 m to 2.6 m and individual ice crystals or inclusions (Vx) at 5% from 2.6 m to the bottom of the borehole at 8.8 m.

The borehole was re-opened using a combination of water-jet drilling and steam on June 28, 2011 to a depth of 3.0 m. The original depth of 9.0 m could not be reached because the borehole had collapsed at the surface. The borehole was cased on June 28, 2011 and manual temperature measurements were made on August 19, 2011. BH H1 was instrumented with a HOBO H21-002 Micro Station on August 16, 2012 (Figure 5.78). The length of the current ground thermal monitoring record as well as other related field work associated with borehole H1 and pertinent information is summarized in Table 5.13.

Table 5.13: Summary table of the data used in the analysis of borehole H1 and the depths of the thermistors from the surface. Note that more detailed field work and RBR logger information is given in Appendix C.

Borehole H1	
Closest ECCS Station and Distance	Burwash (36 km)
Date of 1978 drilling	August 1978
Manual Temperature Measurements Available	August 19, 2011
Original Borehole Depth	8.8 m
New Rehabilitated Borehole Depth	3.0 m (2011); 2.87 m (2012)
Borehole Unblocking Method	Water-Jet Drilling/Steaming (borehole cased)
Borehole Unblocking Date	June 28, 2011
HOBO H21-002 Micro Station Data	August 19, 2012 (Live Reading) Logging since August 16, 2012
Thermistor Depths (m)	0.5, 1.0, 1.75, 2.87
Length and Date of ERT Survey	2 x 80 m (June 28, 2011)

The thermal profile at Borehole H1 was measured manually 53 days after steaming and water-jet drilling on August 19, 2011 and given the timing, shows that permafrost is present at this site (Figure 5.79). Results show temperatures below 0ºC from the 1.2 m measurement depth downwards, reaching a minimum of -0.5ºC at the deepest measurement point of 3.0 m (Figure 5.79). Live readings from the HOBO H21-002 Mico Station on August 19, 2012 indicate temperatures below 0˚C from the 1.8 m sensor downwards, reaching a minimum of -0.5˚C at the deepest measurement point of 2.87 m (Figure 5.79). The interpolated active layer thickness varies from approximately 1.1 m on August 19, 2011 to 1.7 m on the same day in 2012 (Figure 5.79). However, the spacing of the sensors means that the precision of the top of the freezing layer is low. No significant ground temperature difference was observed at the deepest measurement point which shows that the manual temperature measurement method used in 2011 was adequate (Figure 5.79). Variations in near surface temperatures may be attributed to seasonal variations and variations in standing water around the borehole.

Probing the ground around the borehole on August 19, 2012 did not reach a frost table (active layer > 120 cm) and the lowering of weighted string in the borehole revealed unfrozen conditions down to 1.7 m. These observations suggest an increase of approximately 1.5 m in active layer thickness between 1978 and 2012 which may be due to an increase in standing water in the bog surrounding the borehole, perhaps affected by the nearby highway embankment.

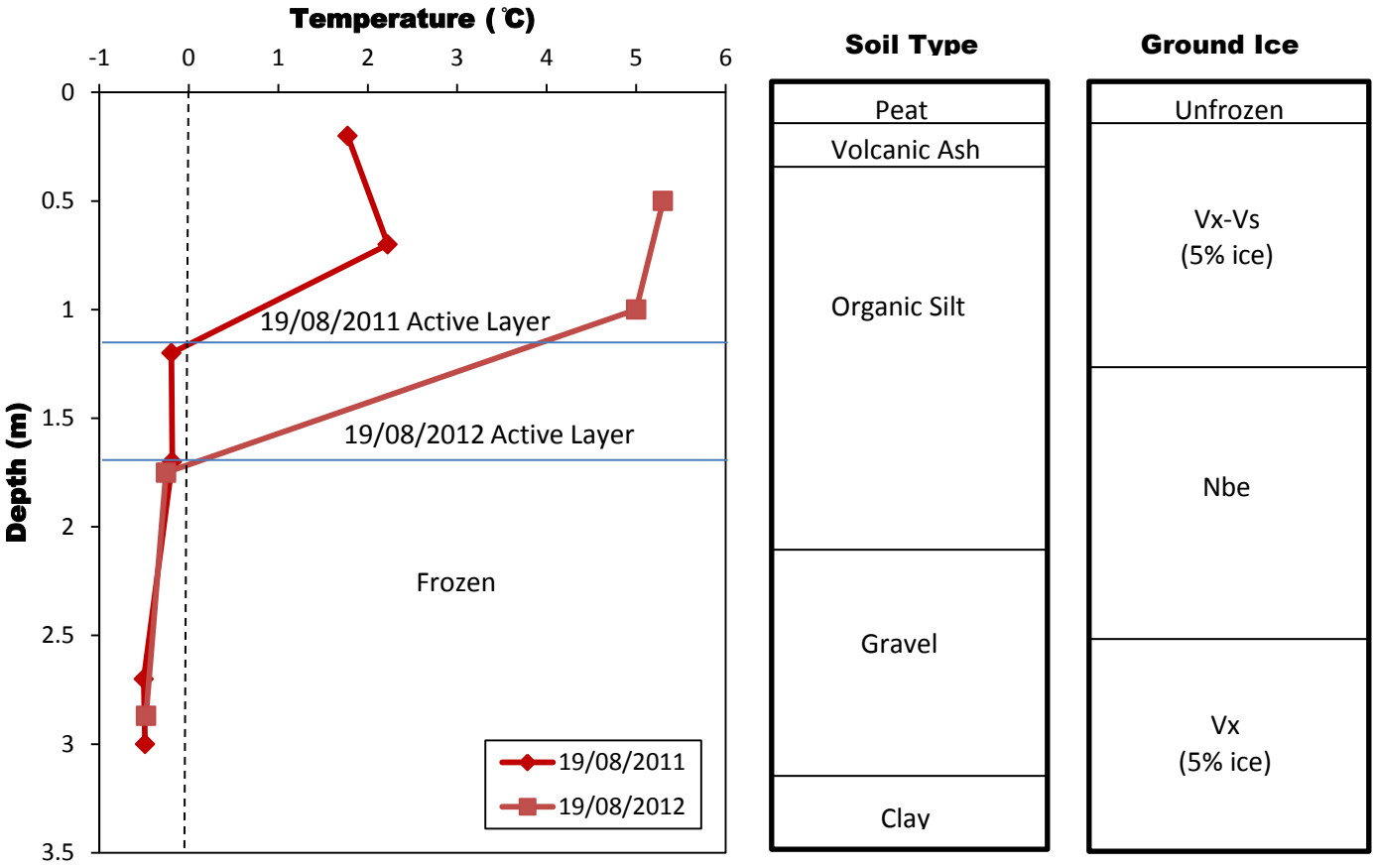

Figure 5.79: Borehole H1 manual ground temperature measurements taken on August 19, 2011 and August 19, 2012. The 2011 measurements were taken by manual temperature string logs while the 2012 measurements are live reading from the HOBO H21-002 Micro Station. The diamonds and squares represent the points of temperature measurement. Soil type and ground ice conditions taken from a 1978 borehole log are shown on the right hand side. Detailed descriptions of the borehole log and ground ice classification to a depth of 8.8 m are found in Appendix K. Note that ground temperature measurements were not available for 1978.

Two 80 m ERT perpendicular cross-section surveys were conducted on June 28, 2011, 39 days before the manual temperature measurements with the mid-point at borehole H1 to better interpret vertical and horizontal permafrost characteristics and distribution (Figures 5.80, 5.81, 5.82 and 5.83). Both surveys show resistivity values between 50-250 Ohm-m to a depth of about 1.0 m to 1.5 m at the borehole (Figures 5.81 and 5.83). This matches with positive manual ground temperatures measured in the borehole at that depth on August 19, 2011 and August 19, 2012 (Figure 5.79).

The 80 m SE-NW ERT profile runs through the bog with no real relief (Figure 5.80). Probing results along the survey line gave a mean depth of 51 cm (N=61, SD=12) and it was uncertain in most case if a frost table was reached due to widespread gravel under the organic surface layer which interfered with probing (Figure 5.81). The presence of silt and gravel at 0.4 m downwards is confirmed by the 1978 borehole log (Figure 5.79). Probing the ground around the borehole again on August 19, 2012 did not reach a frost table (active layer > 120 cm) (Figure 5.79). These measurements support the interpretation of a thawed layer seen as a low resistivity horizontal layer under 500 Ohm-m from the surface down to about 1.0 m to 2.0 m on the resistivity plot (Figure 5.81). However, it is very likely that frost tables were reached during probing because the electrode spacing and the wet conditions created a deeper and more uniformed low resistivity layer at the surface (Figure 5.81).

Resistivity values are as high as 10 000 Ohm-m beneath the thawed layer to the bottom of the survey which is interpreted as permafrost deeper than 12.5 m (Figure 5.81). Homogeneous resistivity values from the bottom of the 2011 borehole to the bottom of the ERT resistivity plot suggest a homogeneous soil lithology with minimal vertical variations in unfrozen moisture content in the permafrost body (Figure 5.81). The 1978 borehole logs shows frozen sand and gravel from 3.5 m to 8.8 m and this may extend to the bottom of the resistivity plot (Figures 5.79 and 5.81).

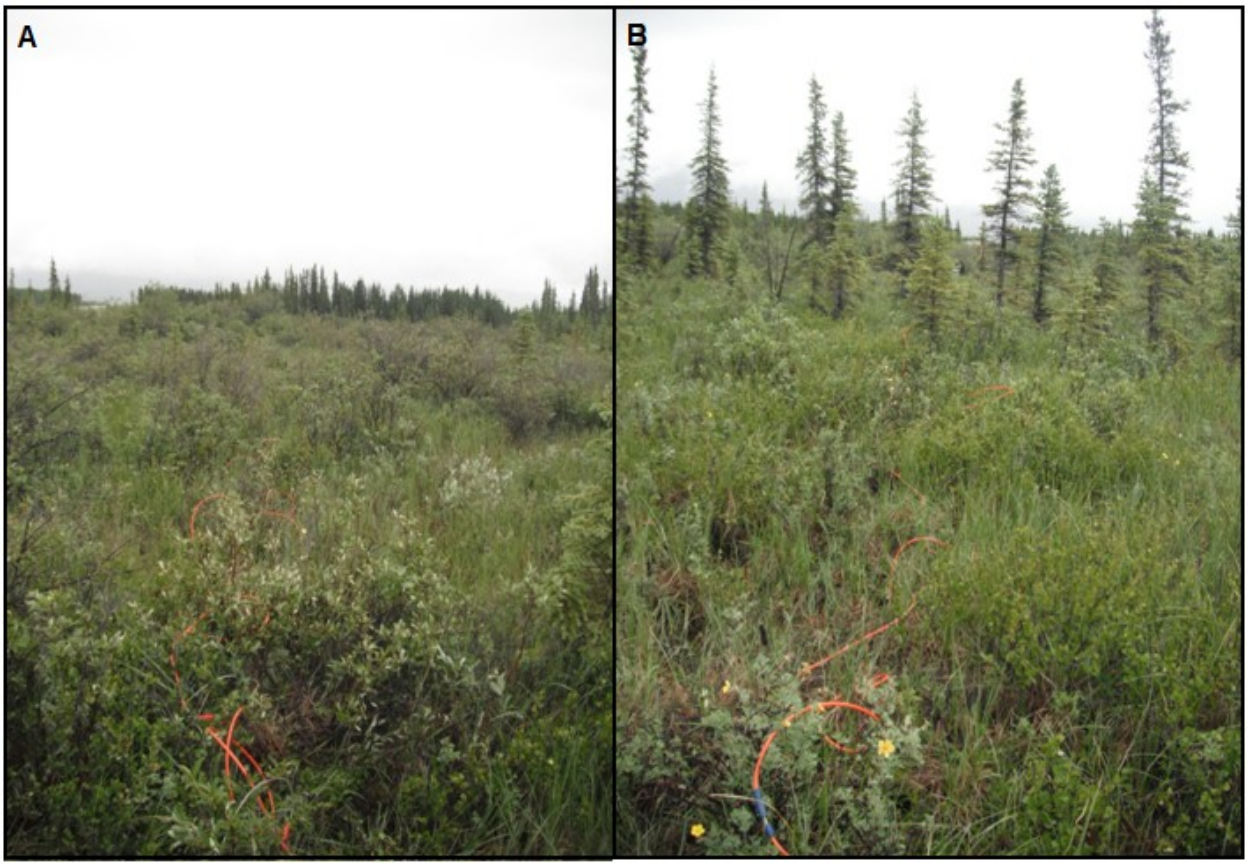

Figure 5.80: Borehole H1 resistivity transect of the SE-NW survey. (A) Picture taken from the borehole at the mid-point looking south-east; (B) picture taken from the borehole at the mid-point looking north-west.

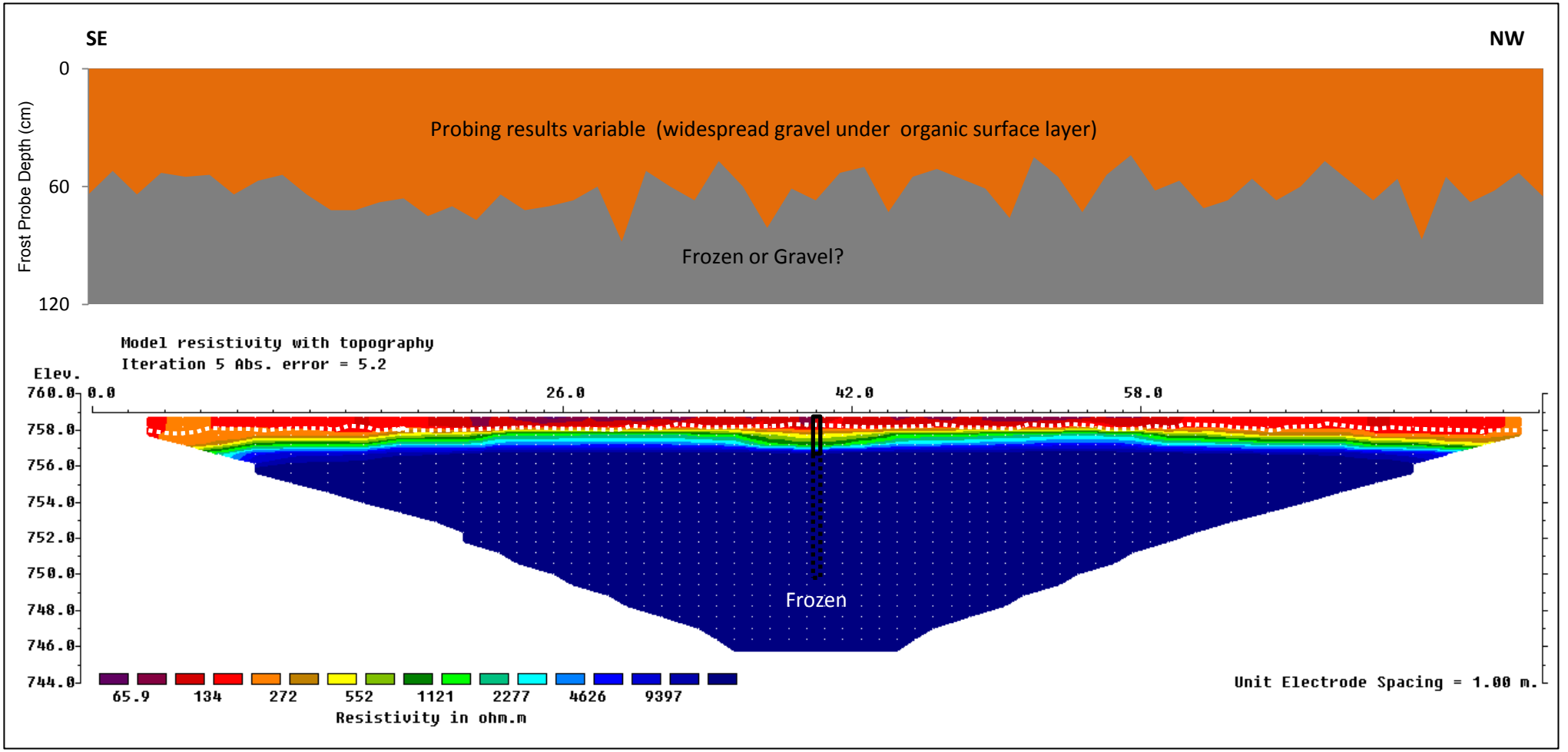

Figure 5.81: Borehole H1 SE-NW 80 m resistivity profile and frost probe chart from June 28, 2011. Vertical exaggeration in model section display = 1.00. Based on 345 data points (0 removed from original survey). The solid black lines indicates the location and depth of the 2011 borehole on the survey while the black dashed lines indicate the original depth of the 1978 borehole. The white dashed lines indicate the interface between frozen and unfrozen conditions.

The 80 m NE-SW ERT profile shows similar results as the SE-NW profile with a horizontal low resistivity layer in the range of 50-500 Ohm-m from the surface down to about 1.0 m to 2.0 m (Figure 5.83). The start of the ERT survey is on a grassy regrown section of the old Alaska Highway which slopes down to a wet marsh with scattered low lying spruce trees (Figure 5.82). The elevation decreases approximately 3.0 m from the start to the end of the survey (Figure 5.82).

Probing results along the survey line were variable, giving a mean depth of 52 cm (N=61, SD=10) and it was uncertain in most case if a frost table was reached due to widespread gravel under the organic surface layer which interfered with probing (Figure 5.83). The low resistivity horizontal layer under 500 Ohm-m from the surface down to about 1.0 m to 2.0 m along the transect is interpreted as deep active layers (Figure 5.83). However, similarly to Figure 5.81, it is very likely that frost tables were reached during probing because the electrode spacing and the wet conditions created a deeper and more uniformed low resistivity layer at the surface (Figure 5.83).

Higher resistivity values are observed at the start of the survey from 0 m to 10 m, where the profile overlays the old Alaska Highway (Figure 5.83). An underlying layer of gravel and crushed rocks may explain the higher resistivity values at the near surface. The south-west end of the transect also shows higher resistivity values at the surface than at the middle of the transect (Figure 5.83) which may be due to lower unfrozen moisture content in the top of the permafrost at the end of the profile (Hilbich et al., 2008; Lewkowicz et al., 2011). The ground was also observed to be drier towards the end of the profile (Figure 5.82). Resistivity values are as high as 8000 Ohm-m under the thawed layer to the bottom of the survey which suggests permafrost deeper than 12.5 m (Figure 5.83). Homogeneous resistivity values similar to the SE-NW survey from the bottom of the 2011 borehole to the bottom of the ERT resistivity plot suggest a homogeneous soil lithology with minimal vertical variations in unfrozen moisture content in the permafrost body (Figure 5.83). The 1978 borehole logs shows frozen sand and gravel from 3.5 m to 8.8 m and this may extend to the bottom of the resistivity plot (Figures 5.79 and 5.81).

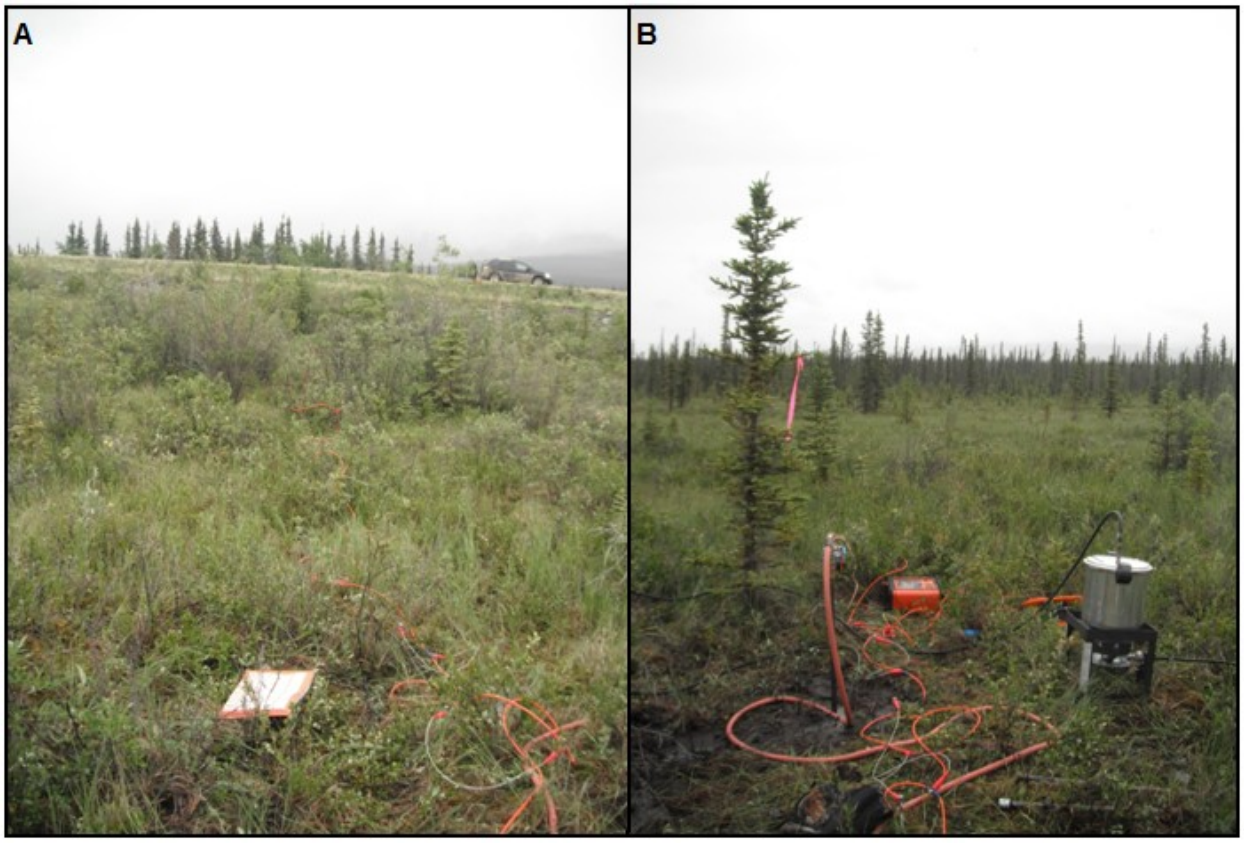

Figure 5.82: Borehole H1 resistivity transect of the NE-SW survey. (A) Picture taken from the borehole at the mid-point looking north-east; (B) picture taken from the borehole at the mid-point looking south-west.

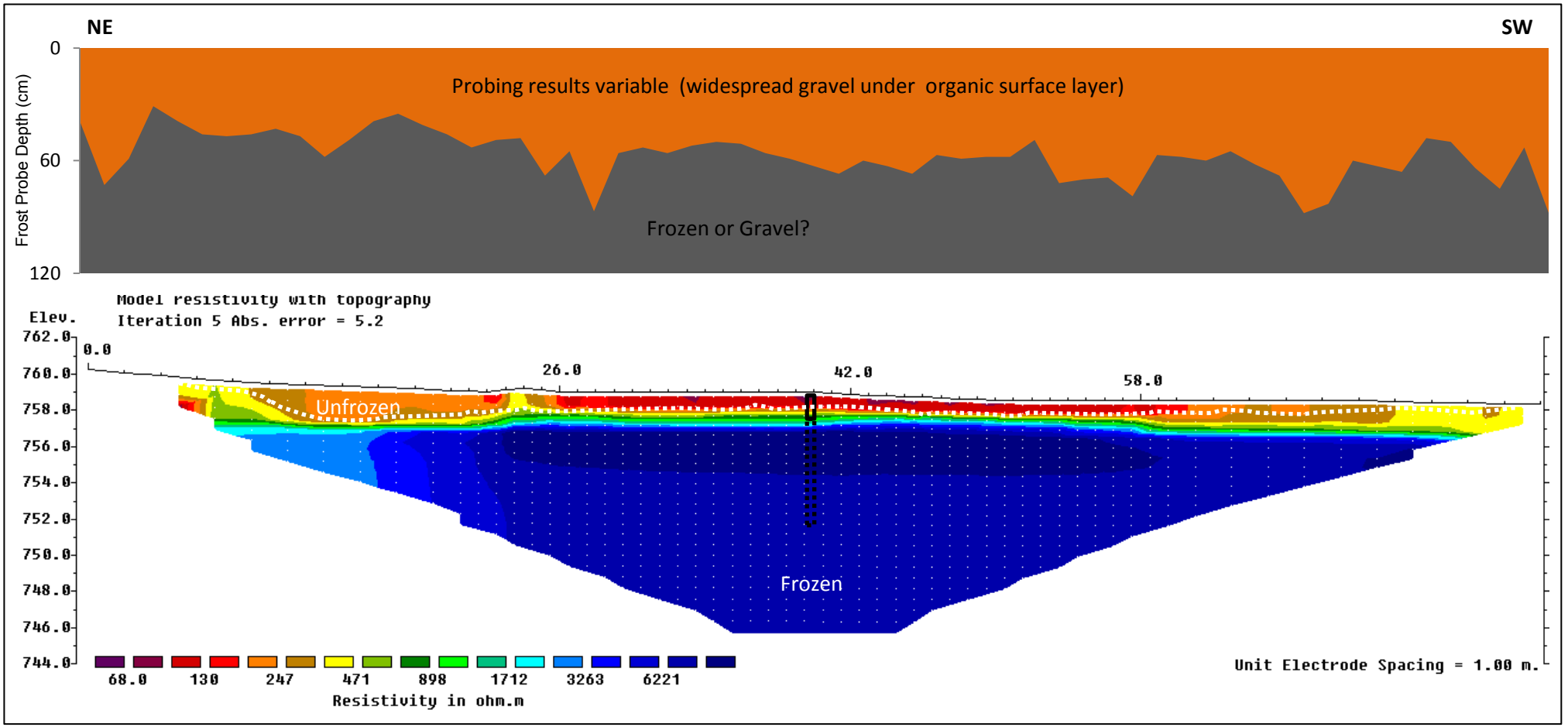

Figure 5.83: Borehole H1 NE-SW 80 m resistivity profile and frost probe chart from June 28, 2011. Vertical exaggeration in model section display = 1.00. Based on 330 data points (15 removed from original survey). The solid black lines indicates the location and depth of the 2011 borehole on the survey while the black dashed lines indicate the original depth of the 1978 borehole. The white dashed lines indicate the interface between frozen and unfrozen conditions.

5.3.3 BH H2 (78-B-25)

The permafrost thermal monitoring site at borehole H2 is located in the sporadic discontinuous permafrost zone of the Yukon Territory at 61° 40' 27" N and 139 ° 43' 48" W and at 713 m elevation (Figure 5.84). The borehole is located in a regrown clearing about 200 m from the Alaska Highway, 800 m south-east of the Donjek River and 80 m from a regrown cut-line used for geophysical work in the 1970s (Figure 5.84). The terrain is hummocky with elevation differences of about 2.0 m within a 40 m radius of the borehole. Some areas around the borehole were found to have standing water with maximum depths of 30 cm. Vegetation in proximity of the borehole mainly consists of low shrubs and spruce averaging 2.0 to 4.0 m in height, as well as aspen, paper birch, sphagnum mosses, lichens, Labrador tea and grasses. A mature spruce forest surrounds this clearing at about 40 m from the borehole. Scattered dead and burned trees indicate the past passage of a forest fire in the area but the timing is unknown.

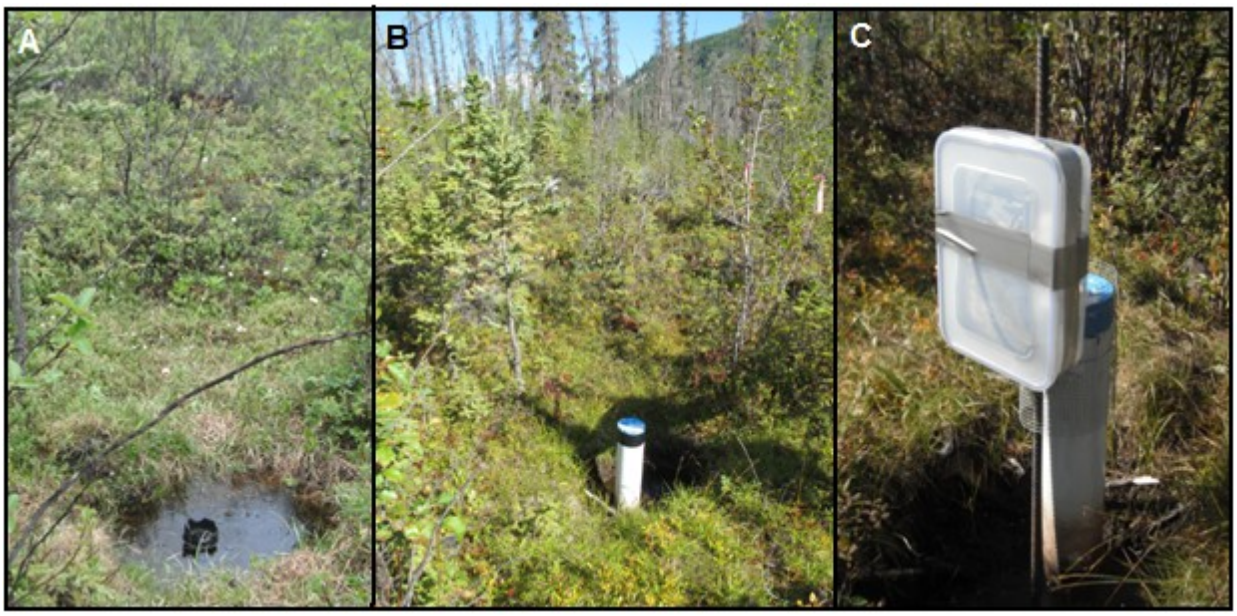

Figure 5.84: (A) Borehole H2 as it was found during the summer 2011 borehole exploration; (B) Borehole M3 after it was rehabilitated and cased in June 2011; (C) and Borehole H2 after it was instrumented with a HOBO H21-002 Micro Station in August 2012.

The borehole was drilled to a depth of 6.7 m in August 1978. The 1978 borehole log indicates a layer of peat from the surface down to 0.15 m underlain by a layer of sand to 0.3 m, a gravel layer from 0.3 m to 2.3 m, a sand layer from 2.3 m to 4.3 m, a silt layer from 4.3 m to 4.6 m and a layer of gravel mixed with sand from 4.6 m to the bottom of the borehole log at 6.0 m (Figure 5.85). The borehole was unfrozen in the top 0.2 m, with well bonded sediments and excess ice (Nbe) from 0.2 m to 1.4 m, individual visible ice crystals or inclusions (Vx) at 5-10% between 1.4 m to 2.7 m and individual visible ice crystals and inclusions (Vx) mixed with visible random or irregularly orientated ice (Vr) at 15-20 % from 2.7 m down to the bottom of the borehole log at 6.0 m (Figure 5.85).

The borehole was unblocked of ice to a depth of 2.0 m using a combination of water-jet drilling and steam on June 25, 2011. The original depth of 6.7 m could not be reached because the borehole had collapsed. The borehole was cased on June 26, 2011 and manual ground temperatures were measured on August 21, 2011. BH H2 was instrumented with a HOBO H21-002 Micro Station on August 16, 2012. The length of the current ground thermal monitoring record as well as other related field work associated with borehole H2 and pertinent information is summarized in Table 5.14.

Table 5.14: Summary table of the data used in the analysis of borehole H2 and the depths of the thermistors from the surface. Note that more detailed field work and RBR logger information is given in Appendix C.

Borehole H2	
Closest ECCS Station and Distance	Burwash (52 km)
Date of 1978 drilling	August 1978
Manual Temperature Measurements Available	November 23, 1978; August 21, 2011
Original Borehole Depth	6.7 m
New Rehabilitated Borehole Depth	2.0 m (2011); 2.0 m (2012)
Borehole Unblocking Method	Water-Jet Drilling/Steaming (borehole cased)
Borehole Unblocking Date	June 25, 2011 and June 26, 2011
HOBO H21-002 Micro Station Data	August 19, 2012 (Live Reading) Logging since August 16, 2012
Thermistor Depths (m)	0.5, 1.0, 1.75, 2.00
Length and Date of ERT Survey	2 x 80 m (June 25, 2011)

Manual ground temperature measurements to a depth of 2.0 m were conducted 58 days after borehole steaming, on August 21, 2011 (Figure 5.85). Results show temperatures of 0.2ºC at a depth of 2.0 m which is about 1.7ºC warmer than the manual temperature measurement taken on November 23, 1978 at the same depth (Figure 5.85). No significant ground temperature variation was observed at the deepest measurement point between the August 21, 2011 manual temperature measurements and the August 19, 2012 HOBO H21-002 Micro Station live readings (Figure 5.85). This shows that the manual temperature measurement method used in 2011 was adequate (Figure 5.85).Variations in near surface temperatures can be attributed to seasonal variations in climate and variations in standing water around the borehole. The 1978 temperature measurements extended to a depth of 4.9 m where temperatures were -1.0˚C. However, it should be noted that the 1978 temperature measurements were done 3 months later in the year than in 2011 and 2012.

Probing the ground around the borehole did not reach a frost table (active layer > 120 cm) on August 19, 2012 and positive ground temperatures were measured to a depth of 2.0 m (Figure 5.85). These observations suggest an increase of approximately 1.8 m in active layer thickness between 1978 and 2012 which may be due to the original clearing of vegetation before drilling in 1978. This left the borehole in a depression causing the formation of standing water as observed during field visits in summer 2011 and 2012.

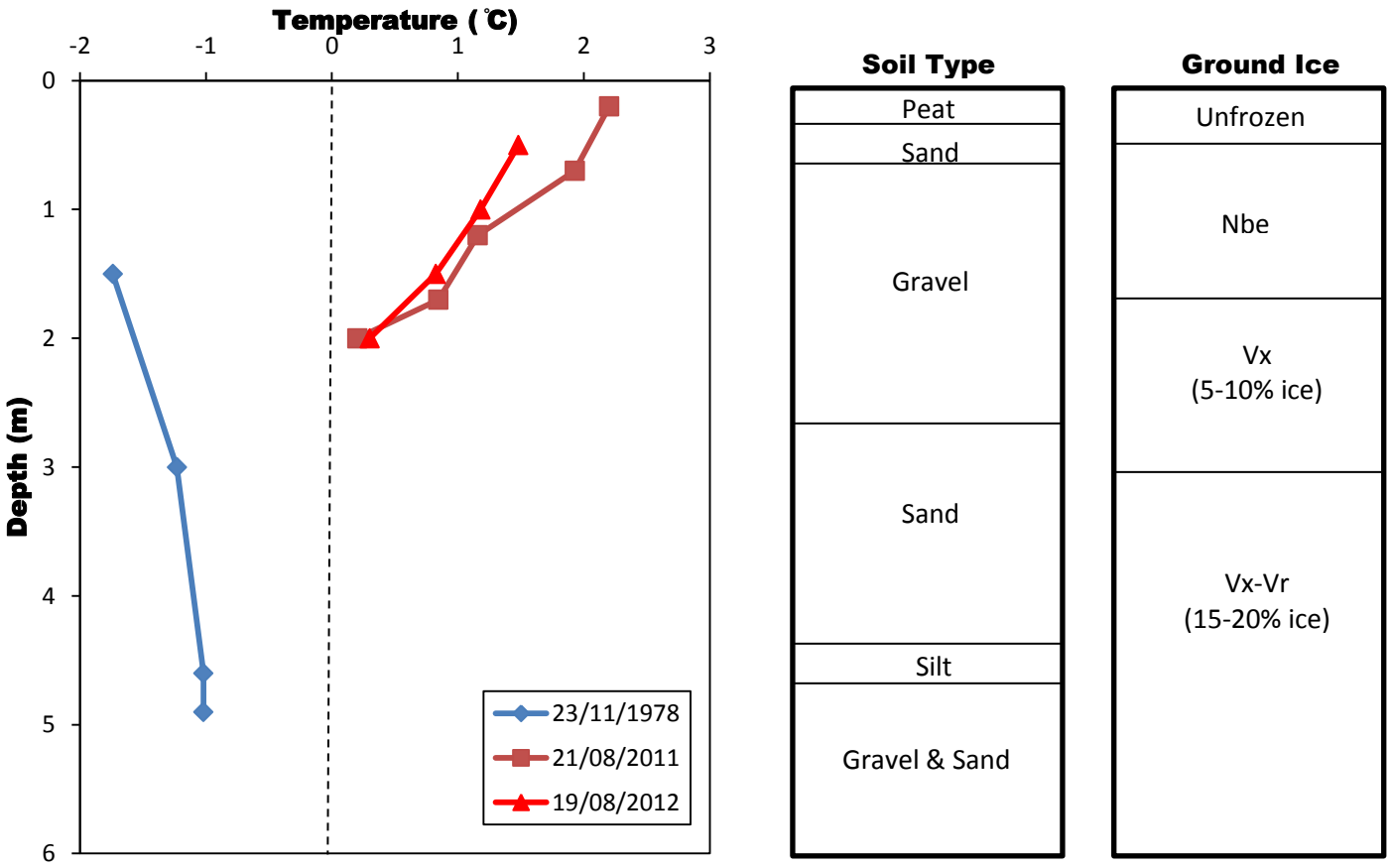

Figure 5.85: Borehole H2 manual ground temperature measurements variations between November 23, 1978, August 19, 2011 and August 19, 2012. The 1978 and 2011 measurements were taken by manual temperature string logs while the 2012 measurements are live reading from the HOBO H21-002 Micro Station. The diamonds, triangles and squares represent the points of temperature measurement. Soil type and ground ice conditions taken from a 1978 borehole log are shown on the right hand side. Detailed descriptions of the borehole log and ground ice classification to a depth of 6.7 m are found in Appendix K.

Two 80 m ERT perpendicular cross-section surveys were conducted on June 25, 2011, 36 days before the manual temperature measurements with the mid-point at borehole H2 (Figures 5.86, 5.87, 5.88 and 5.89). Both surveys show resistivity values between 50-300 Ohm-m to a depth of about 1.0 m to 1.5 m at the borehole. (Figures 5.87 and 5.89) This matches with positive ground temperatures measured in the borehole at that depth on August 21, 2011 and August 19, 2012 (Figures 5.87 and 5.89). The deep active layer around the borehole can be attributed to a post 1978 drilling depression around the borehole PVC pipe which has resulted in the long term accumulation of standing water during the annual thawing seasons (Figure 5.84).

The 80 m NE-SW ERT profile runs through a poorly drained area interspersed with drier spots with low shrubs and small spruce trees ranging from 1 m to 3 m in height (Figure 5.86). The terrain rises by approximately 2.0 m from the start to the end of the survey. Probing results along the survey line were highly variable, giving a mean depth of 66 cm (N=61, SD=38). Frost tables were measured to be around 80 cm in depth from about 21 m to 28 along the profile, where the survey crossed a pool of standing water. No frost table was reached around the borehole (thawed layer > 120 cm) and from about 50 m to 70 m along the profile where the survey crosses a stream with flowing water (Figures 5.86 and 5.87). These measurements support the interpretation of deep active layers which are seen as a resistivity layer < 500 Ohm-m from the surface down to about 2.0 m on the resistivity plot (Figure 5.87). Lower resistivity values extend to greater depths beneath the stream, which suggest thawed ground down to about 4 m (Figure 5.87).

Resistivity values as high as 35 000 Ohm-m are present beneath the thawed layer to the bottom of the survey and are interpreted as permafrost deeper than 12.5 m (Figure 5.87). Homogeneous resistivity values from the bottom of the 2011 borehole to the bottom of the ERT resistivity plot suggest a homogeneous soil lithology such as sand and gravel which yield higher resistivity values (Kneisel, 2008). This interpretation is supported by the 1978 borehole log (Figure 5.85) and the fact that the borehole is located on an old tributary of the Donjek River.

Figure 5.86: Borehole H2 resistivity transect of the SE-NW survey. (A) Picture taken from the borehole at the mid-point looking south-east; (B) picture taken from the borehole at the mid-point looking north-west.

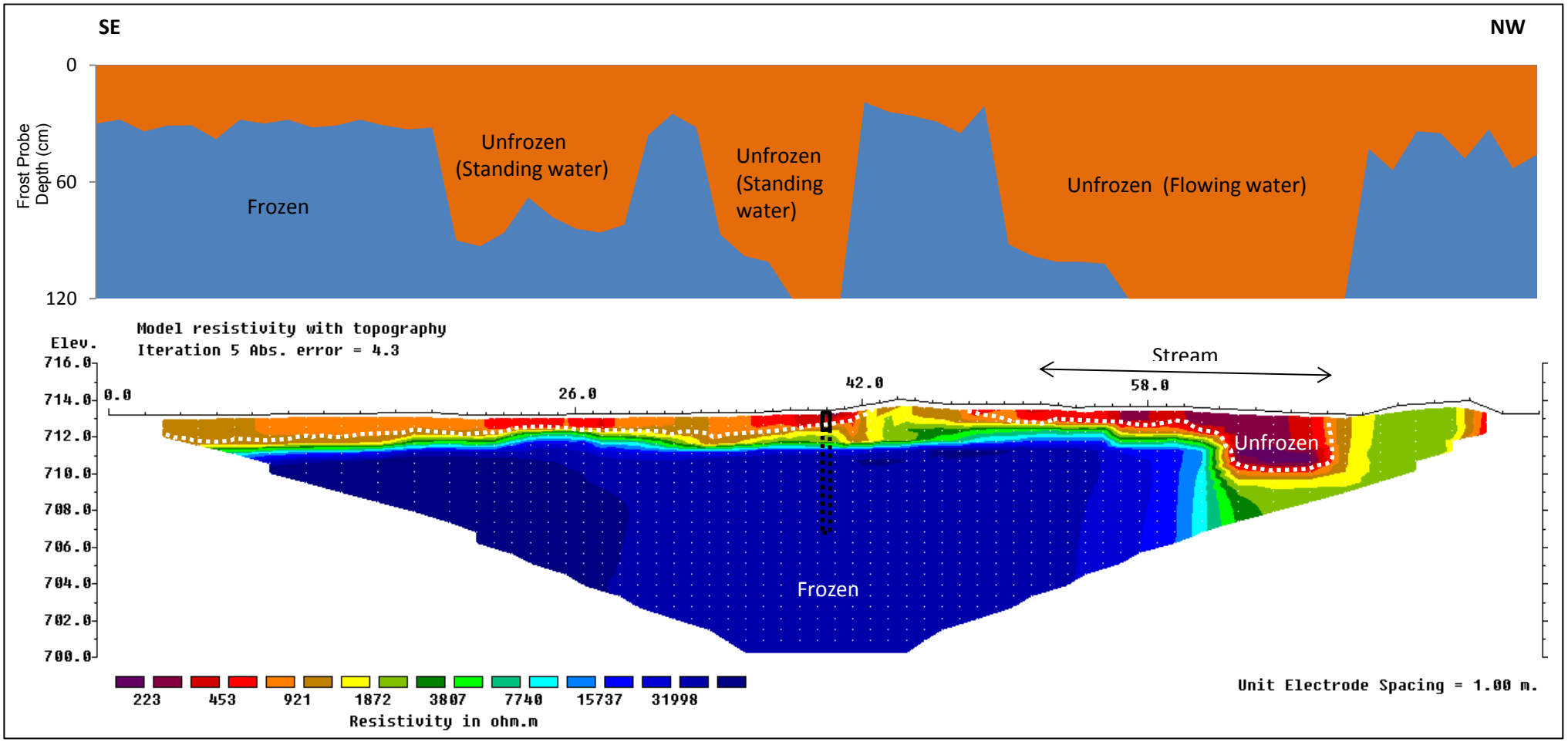

Figure 5.87: Borehole H2 SE-NW 80 m resistivity profile and frost probe chart from June 25, 2011. Vertical exaggeration in model section display = 1.00. Based on 326 data points (19 removed from original survey). The solid black lines indicates the location and depth of the 2011 borehole on the survey while the black dashed lines indicate the original depth of the 1978 borehole. The white dashed lines indicate the interface between frozen and unfrozen conditions.

The 80 m NE-SW ERT profile shows similar results as the SE-NW profile with a resistivity layer in the range of 50-400 Ohm-m from the surface down to about 1.0 m to 2.0 m in areas with standing water interspersed with shallower active layers in dryer areas (Figures 5.88 and 5.89). The start of the ERT survey is in a poorly drained area which becomes a scattered spruce forest towards the end of the survey (Figure 5.88). The terrain rises by approximately 2.0 m from the start to the end of the survey (Figure 5.88).

Probing results along the survey line were highly variable, giving a mean depth of 80 cm (N=61, SD=41). Frost tables were not reached (active layer > 120 cm) where the survey crossed a wet marsh with standing water from the start of the profile to about 26 m (Figures 5.88 and 5.89). No frost table was reached around the borehole and towards the end of the profile where standing water was also present (Figures 5.88 and 5.89). These measurements matched with measured positive ground temperatures in August 2011 and 2012 to a depth of 2.0 m support the interpretation of deep thawed layers down to about 1.0 m to 2.0 m on the resistivity plot (Figure 5.89). Drier areas along the survey line yielded shallower active layers during probing (Figures 5.88 and 5.89).

Resistivity values increase as high as 400 000 Ohm-m under the active layer to the bottom of the survey which is interpreted as permafrost deeper than 12.5 m (Figure 5.89). Homogeneous resistivity values from the bottom of the 2011 borehole to the bottom of the ERT resistivity plot suggest a homogeneous soil lithology such as sand and gravel which yield high resistivity values when frozen (Kneisel, 2008). This interpretation is supported by the 1978 borehole log and the fact that the borehole is located on an old tributary of the Donjek River.

Figure 5.88: Borehole H2 resistivity transect of the NE-SW survey. (A) Picture taken from the borehole at the mid-point looking north-east; (B) picture taken from the borehole at the mid-point looking south-west.

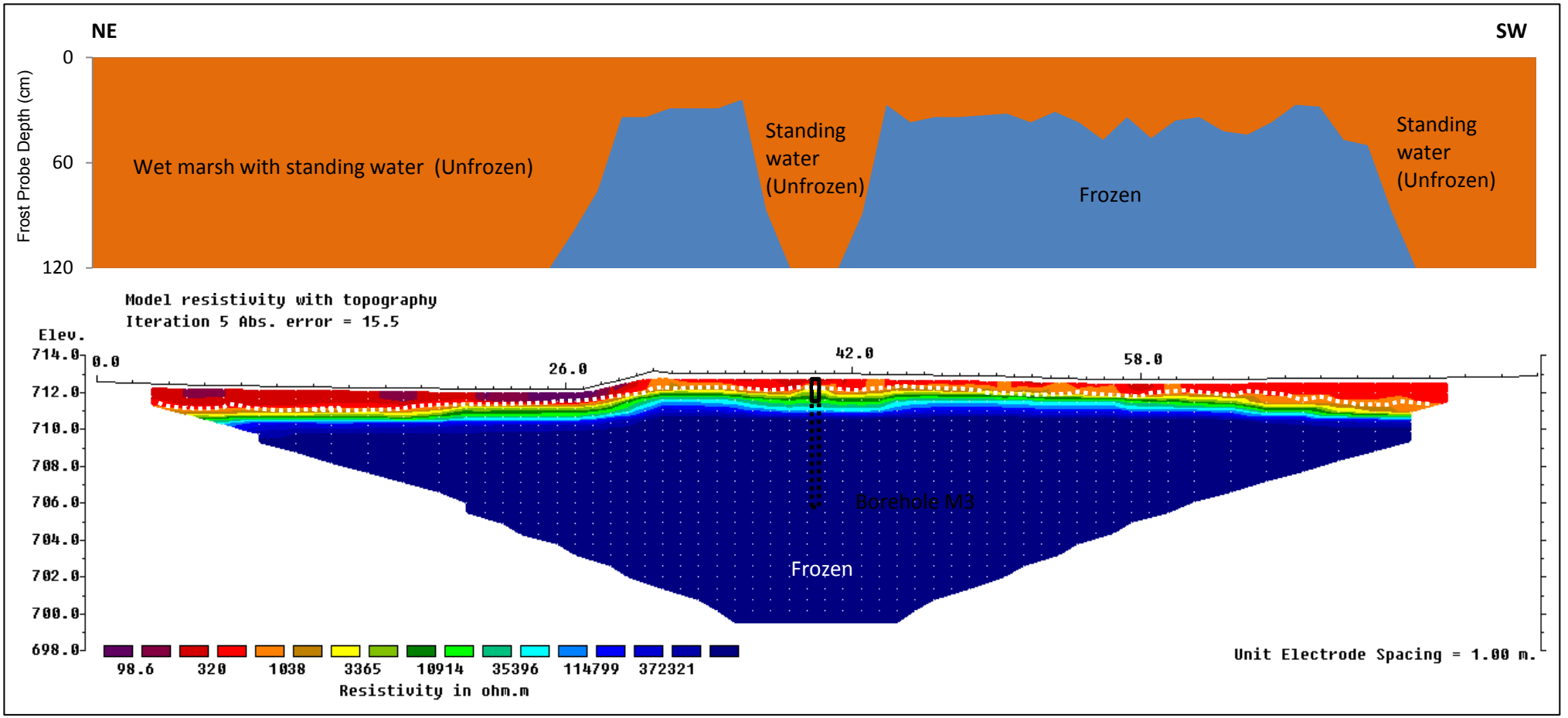

Figure 5.89: Borehole H2 NE-SW 80 m resistivity profile and frost probe chart from June 25, 2011. Vertical exaggeration in model section display = 1.00. Based on 331 data points (14 removed from original survey). The solid black lines indicates the location and depth of the 2011 borehole on the survey while the black dashed lines indicate the original depth of the 1978 borehole. The white dashed lines indicate the interface between frozen and unfrozen conditions. Note the abnormally high RMS error.

5.3.4 BH H3 (78-A-39)

The permafrost thermal monitoring site at borehole H3 is located in the sporadic discontinuous permafrost zone of the Yukon Territory at 61^{o} 42’ 54” N and 139 ^{o} 50’ 34” W and at 787 m elevation (Figure 5.90) The borehole is located on a regrown cut-line used for geophysical work in the 1970s at about 40 m from the Alaska Highway and is about 150 m from borehole R7 (Figure 5.90).

Figure 5.90: (A) Borehole H3 as it was found during the summer 2011 borehole exploration; (B) Borehole M4 after it was rehabilitated and cased in June 2011; (C) and Borehole H3 after it was instrumented with a HOBO H21-002 Micro Station in August 2012.

The topography on the cut-line is mainly flat with elevation differences of about 2.0 m from the south-east starting point of the ERT transect to the end of the transect at the north-west. Shallow flowing water was observed around the borehole to a depth of 50 cm (Figure 5.90). Vegetation on the cut-line includes low shrubs, sphagnum mosses, Labrador tea, grasses and sedges.

The borehole was drilled to a depth of 4.5 m in August 1978. The 1978 borehole log indicates a layer of peat from the surface down to 0.2 m, underlain by a layer of volcanic ash from 0.2 m to 0.8 m, another peat layer from 0.8 m to 1.0 m and a layer of clay from 1.0 m to the bottom of the borehole log at 4.0 m (Figure 5.91). The borehole was unfrozen in the top 0.7 m, with visible individual ice crystals or inclusions (Vx) at 1% from 0.7 m to 1.5 m, visible stratified or oriented ice (Vs) at 5% from 1.5 m to 1.8 m, visible individual ice crystals or inclusions (Vx) at 40% from 1.8 m to 2.9 m and at 10% from 2.9 m to the bottom of the borehole log at 4.0 m (Figure 5.91).

The borehole was unblocked of ice by steam to a depth of 3.55 m and cased on June 23, 2011. Manual temperature measurements were collected on August 21, 2011. BH H3 was instrumented with a HOBO H21-002 Micro Station on August 16, 2012. The length of the current ground thermal monitoring record as well as other related field work associated with borehole H3 and pertinent information are summarized in Table 5.15.

Table 5.15: Summary table of the data used in the analysis of borehole H3 and the depths of the thermistors from the surface. Note that more detailed field work and RBR logger information is given in Appendix C.

Borehole H3	
Closest ECCS Station and Distance	Burwash (60 km)
Date of 1978 drilling	August 1978
Manual Temperature Measurements Available	November 23, 1978; August 21, 2011
Original Borehole Depth	4.5 m
New Rehabilitated Borehole Depth	3.55 m (2011); 2.39 m (2012)
Borehole Unblocking Method	Steaming (borehole cased)
Borehole Unblocking Date	June 23, 2011
HOBO H21-002 Micro Station Data	August 17, 2012 (Live Reading) Logging since August 16, 2012
Thermistor Depths (m)	0.5, 1.0, 1.75, 2.39
Length and Date of ERT Survey	80 m (June 23, 2011)

Manual ground temperature measurements to a depth of 3.5 m were conducted 60 days after borehole steaming, on August 21, 2011 (Figure 5.91). Results show temperatures declining with depth and dropping below 0ºC at 2.6 m to a minimum of -0.3ºC at the deepest measurement point of 3.5 m. Linear interpolation show temperatures of approximately -0.1ºC at a depth of 3.0 m which is about 0.8ºC warmer than the manual temperature measurement of -0.9˚C taken on November 23, 1978 for the same depth (Figure 5.91). No significant ground temperature difference was observed at the deepest measurement points between the August 21, 2011 manual temperature measurements and the August 17, 2012 HOBO H21-002 Micro Station live readings (Figure 5.91). This shows that the manual temperature measurement method used in 2011 was adequate (Figure 5.91). Variations in near surface temperatures can be attributed to seasonal differences and variations in standing water around the borehole. Note that the 1978 temperature measurements were taken 3 months later in the year than in 2011 and 2012.

Probing the ground around the borehole on August 17, 2012 did not reach a frost table (active layer > 120 cm) and positive ground temperatures were measured to an interpolated depth of about 2.4 m. These observations indicate an increase of approximately 1.8 m in active layer thickness between 1978 and 2012 which is probably due to the accumulation of water around the borehole from a small stream flowing on the cut-line (Figures 5.90 and 5.92). However, spacing of the sensors means that the precision of the top of the freezing layer is low.

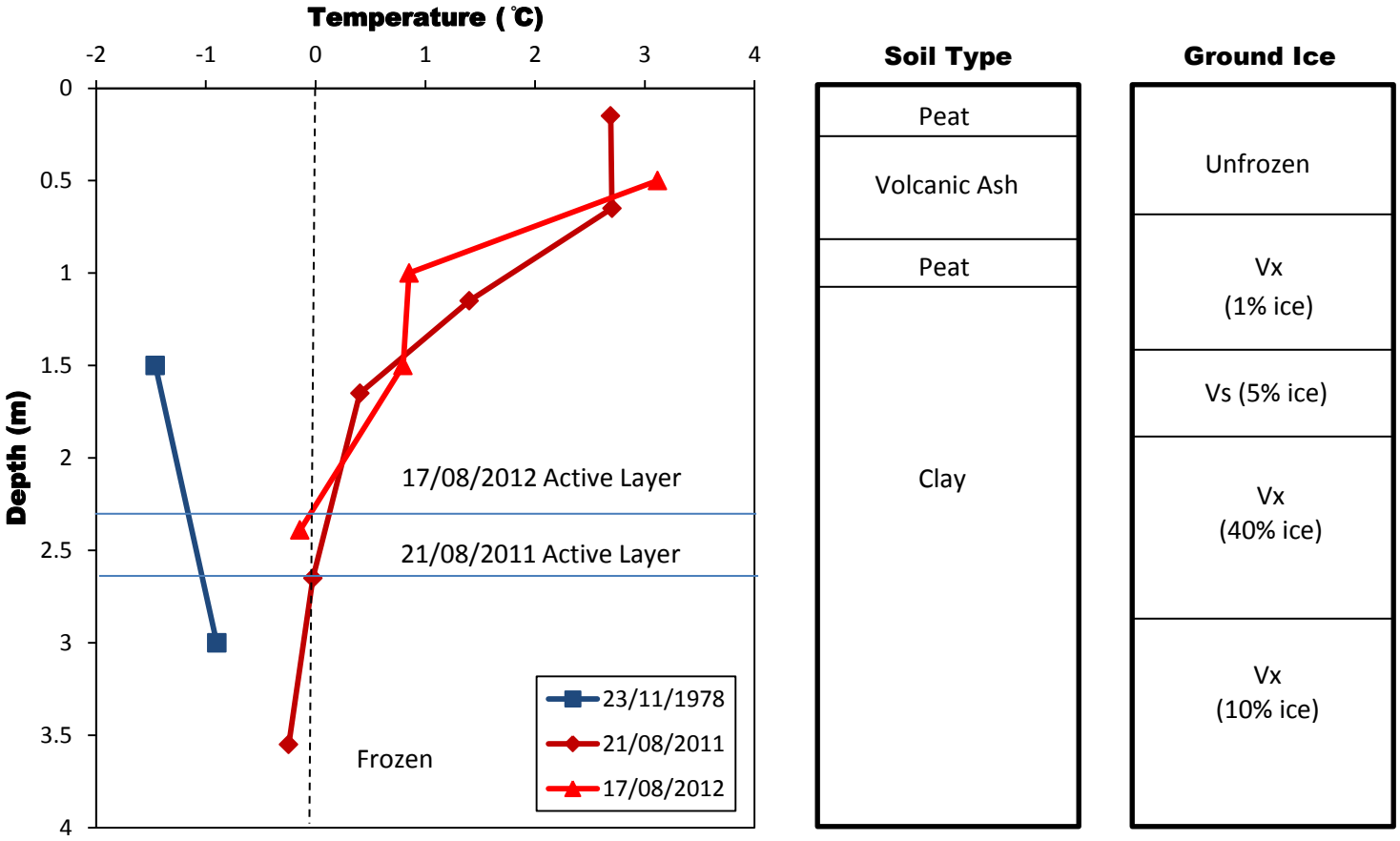

Figure 5.91: Borehole H3 manual ground temperature measurements variations between November 23, 1978, August 21, 2011 and August 17, 2012. The 1978 and 2011 measurements were taken by manual temperature string logs while the 2012 measurements are live reading from the HOBO H21-002 Micro Station. The diamonds, triangles and squares represent the points of temperature measurement. Soil type and ground ice conditions taken from a 1978 borehole log are shown on the right hand side. Detailed descriptions of the borehole log and ground ice classification to a depth of 4.5 m are found in Appendix K.

The 80 m ERT profile at borehole H3 runs along the regrown cut-line from a south-east to north-west orientation (Figures 5.92 and 5.93). The survey was conducted on June 23, 2011, 60 days before the manual temperature measurements with the mid-point at borehole H3 (Figures 5.92 and 5.93). Flowing water was present along the full length of the profile and the ground rose by approximately 2 m from the start to the end of the survey (Figures 5.92 and 5.93).

Probing results along the survey line were almost all > 120 cm, giving a mean depth of 114 cm (N=61, SD=18). The only measured frost tables were reached from 43 m to 50 m and from 68 m to 72 m along the profile. These measurements support the interpretation of deep thawed layers which are seen as a horizontal layer with resistivities less than 500 Ohm-m from the surface down to about 1.0 m to 2.5 m on the resistivity plot (Figure 5.93). Water running along the whole length of the profile may explain the abnormally deep thaw (Figures 5.92 and 5.93). The differences in near surface resistivities suggest variation in unfrozen moisture content along the profile with higher moisture content in areas with lower resistivities.

Resistivity values increased as high as 35 000 Ohm-m beneath the thawed layer to the bottom of the survey which suggests permafrost is deeper than 12.5 m (Figure 5.93). The borehole log also shows fairly high ice content in the upper parts of the permafrost body (Figure 5.91). Although the active layer may have deepened along the cut-line as the vegetation cover was removed in the late 1970s, permafrost has persisted at depth.

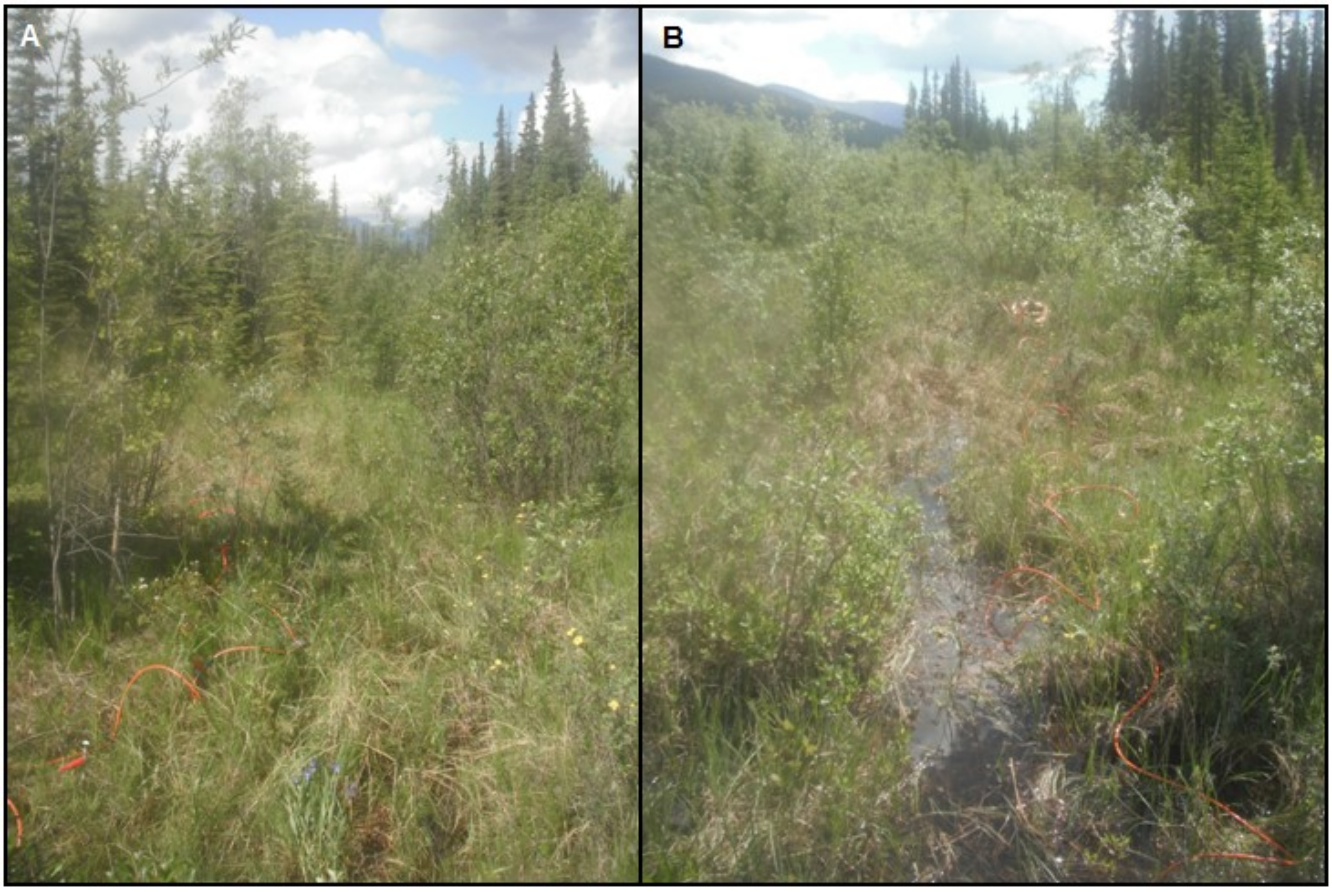

Figure 5.92: Borehole H3 resistivity transect of the SE-NW survey. (A) Picture taken from the borehole at the mid-point looking south-east; (B) picture taken from the borehole at the mid-point looking north-west.

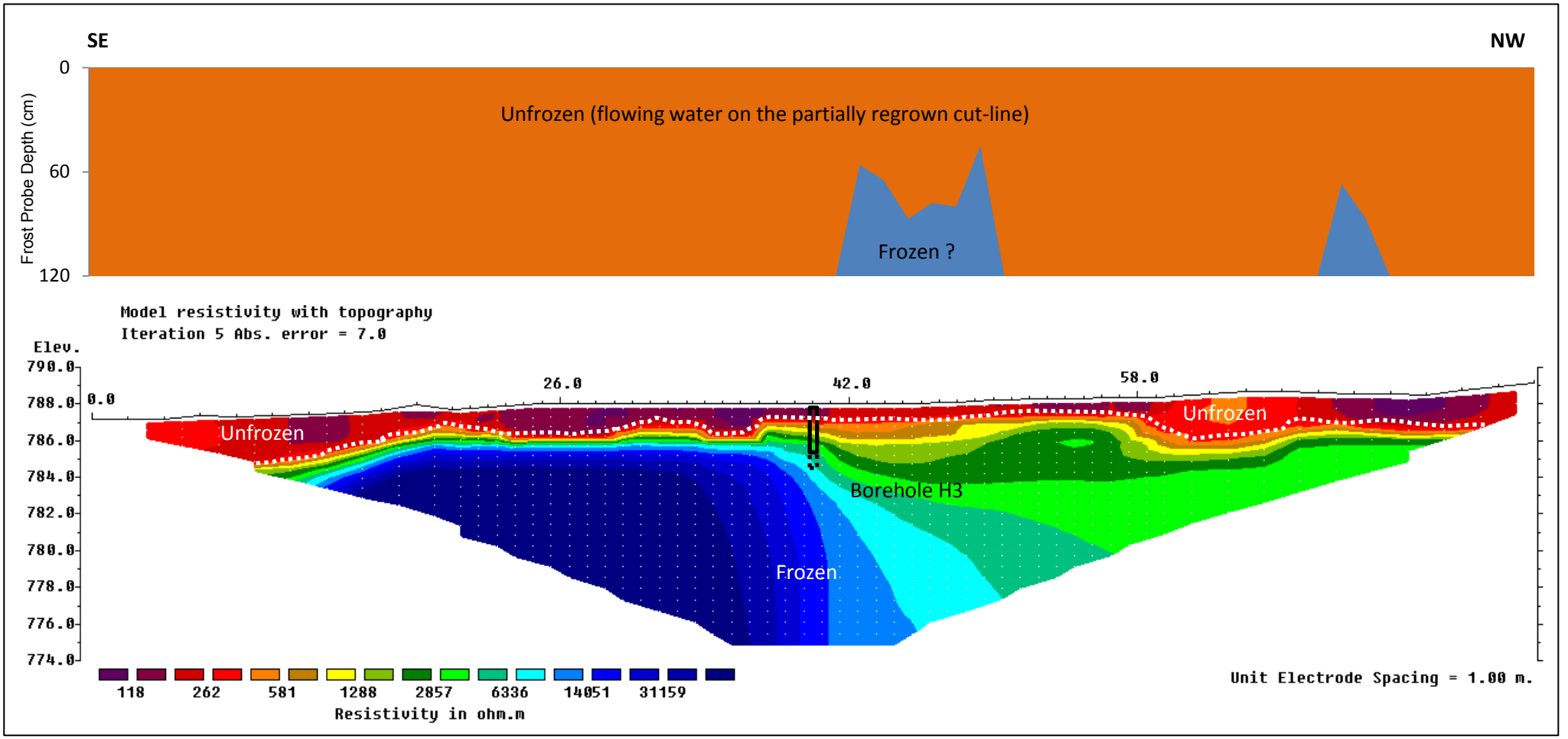

Figure 5.93: Borehole H3 SE-NW 80 m resistivity profile and frost probe chart from June 23, 2011. Vertical exaggeration in model section display = 1.00. Based on 338 data points (7 removed from original survey). The solid black lines indicates the location and depth of the 2011 borehole on the survey while the black dashed lines indicate the original depth of the 1978 borehole. The white dashed lines indicate the interface between frozen and unfrozen conditions.

SECTION 6: DISCUSSION

6.0 DISCUSSION

This section discusses: 1) inter-site comparisons of current permafrost conditions and characteristics derived from borehole ground temperature monitoring and ERT results in the context of major influences on permafrost, notably climate change and environmental change; 2) changes in ground temperatures and active layer depths since the late 1970s; 3) limitations of the study; 4) uncertainties; and 5) future research.

6.1 Inter-Site Comparison

6.1.1 Climate Change in the Study Area

Data from five Environment Canada climate stations in communities along the study area (Whitehorse, Haines Junction, Otter Falls, Burwash Landing and Beaver Creek) show a similar regime change between 1975 and 1976, from a long term cooling phase to an abrupt step-like increase in MAAT, followed by stability from 1976 to 1978 and moderate long-term warming thereafter. The step-like increase in MAAT between 1975 and 1976 caused an abrupt MAAT increase of 3.1˚C at Whitehorse, 2.8˚C at Haines Junction and Burwash Landing and, 2.1˚C at Beaver Creek. MAATs remained mainly stable afterwards between 1976 and 1978 with a variation of 0.1˚C in Whitehorse, 0.2˚C in Haines Junction and 0.3˚C in Burwash Landing. A slight warming trend established at most ECCS after 1979. FDDa show high inter-annual variability along the study area while TDDa varies little on an annual basis. These trends indicate that winter is the most variable season spatially and temporally in the study area and the most responsive to recent climate change.

The observed MAAT regime change in the study area slightly precedes the 1976/1977 Pacific Decadal Oscillation shift from a cool phase to a warm phase (Zhang et al., 1997). The year 1975 also coincides with a La Niña that caused a cooler and snowier winter in most parts of Canada (Philip and Van Oldenborgh, 2006). The original manual ground temperature measurements used in this thesis were collected by the Geological Survey of Canada between 1977 and 1981. The earlier measurements may still have been affected by the long term cooling trend while the measurements taken during the later years may already have experienced ground temperature warming from the 1975/1976 step-like increase in MAAT (see Section 6.4). Although permafrost is a climatically controlled phenomenon (Smith and Riseborough, 2002),

changes in temperature at the surface take time to impact permafrost at depth and this lag time may be in the order of years to decades for thin permafrost (ACIA, 2005).

Whitehorse and Beaver Creek were the only ECCS to show significant long-term trends in MAAT when subjected to significance testing at a confidence level of 95 %. A statistically significant cooling trend of -0.66˚C/decade was observed at Whitehorse from 1943 to 1975 and a warming trend of 0.57˚C/decade was observed at Beaver Creek between 1980 and 2011. Beaver Creek is located in the central Yukon Basin and has somewhat different climatological characteristics than its neighbouring stations to the southeast due to its greater distance from the effects of the Gulf of Alaska and the St Elias Mountains (Wahl et al., 1987). Similar changes occurred at the other communities but the trends are not statistically significant. The warming trends at the ECCS after 1975 coincide with an average Arctic warming of 0.4˚C/decade from 1966 to 2003, although the trend in the Yukon is less pronounced (ACIA, 2005). This warming occurred more in winter and spring than in summer (ACIA, 2005).

The rate and the response of ground temperatures to change in air temperatures is also affected by changes in precipitation which impact ground thermal conductivity, the surface offset, and active layer freezing and thawing timing and duration (Smith and Burgess, 1999). An increase in rainfall can result in active layer thickening while an increase in snowfall results in a buffering low conductivity insulating layer which lessens the impact of rising air temperatures in the winter (Smith and Burgess, 1999). Rainfall trends at most ECCS in the study area follow the main MAAT trends with increases in rainfall observed when the MAAT increases at a site. Total annual rainfall varies spatially throughout the study area, with rainfall increasing from Whitehorse to Beaver Creek. No statistically significant trends in rainfall were observed. Total annual snowfall decreases from Whitehorse to Beaver Creek and trends were more variable between sites. The only statistically significant snowfall trend was observed in Whitehorse between 1943-1975 where snowfall increased by 14.5cm/decade. Total annual precipitation did not show any statistically significant trends along the study route.

6.1.2 Environmental Change in the Study Area

Environmental change may be a confounding variable when trying to determine where permafrost has warmed or degraded due to climate warming between 1977-1981 and 2011-2012.

The dependence of the mostly warm sporadic discontinuous permafrost in the study area on favourable surface conditions make it vulnerable to thaw due to environmental changes such as surface disturbance (Shur and Jorgenson, 2007). A well-known mechanism of permafrost degradation occurs by the removal of near-surface protective insulating vegetation which exposes the permafrost to warmer temperatures (Shur and Jorgenson, 2007; Smith et al, 2008; Smith and Riseborough, 2010). In the summer months, shade from vegetation and a supply of soil moisture for evaporation are two significant site variables that reduce the ground surface temperature (Osterkamp and Burn, 2003; Smith et al, 2008; Smith and Riseborough, 2010). An organic layer at the ground surface commonly assists the persistence of permafrost (Osterkamp and Burn, 2003; Smith et al, 2008; Smith and Riseborough, 2010). Dry moss and peat have low thermal conductivities which reduce heat flow into the ground in summer. However, autumn rain characteristically increases the water content of the moss and peat, increasing their conductivity (particularly when frozen) and facilitating extraction of heat from the ground in winter (Osterkamp and Burn, 2003; Smith et al, 2008; Smith and Riseborough, 2010).

The borehole sites used in this thesis were all disturbed in the late 1970s during the initial drilling program (Burgess et al., 1982). Vegetation cover was removed in a 20 m radius of the borehole to permit the passage and drilling preparation of Caterpillar Drilling Rigs (Burgess et al., 1982). Temperatures measured shortly after the completion of drilling may still have been affected by the drilling process; usually the deeper the hole, the longer the drilling time, the greater the disturbance and the longer the time necessary for its dissipation (Burgess et al., 1982). No fluids were used during drilling which lessens the disturbance (Burgess et al., 1982). Most field sites used in this thesis have partially re-vegetated in the 3 decades following disturbance. Most relocated boreholes were found to be blocked with ice in summer 2011 and had to be opened using a portable custom made streaming rig. Recovery time after drilling was measured at borehole R5, where a RBR logger was installed and started recording ground temperatures 6 days after steaming (Figure 6.1). Deeper ground temperatures (3.5 m, 5.5 m and 8.0 m) recovered first, approximately 15-17 days after steaming, while shallower ground temperatures took about 24 days to recover at 2.5 m and 35 days at 2.0 m (Figure 6.1). The time lag between freezing at 0.1 m and 0.6 m was approximately 125 days due to a long zero-curtain effect that may be partially due to high unfrozen moisture content at the near surface due to borehole steaming. Other borehole sites show similar ground temperature recovery times. The time since

drilling disturbances in the 1970s and steaming in 2011 from the date of ground temperature measurements is outlined in APPENDIX B.

Ground temperatures measured in the 1970s should not have been heavily affected by initial borehole drilling as manual temperatures were all taken at least 65 days after drilling and in most cases hundreds of days after drilling. This delay is much longer than the ground temperature recovery times observed at borehole R5. However, all the sites were cleared of vegetation before drilling which may have affected near-surface temperature measurements. Ground temperatures that had been affected by borehole steaming in 2011 were not included in the analysis of the results. The possible effects of drilling and removal of vegetation on results are discussed in Section 6.4.

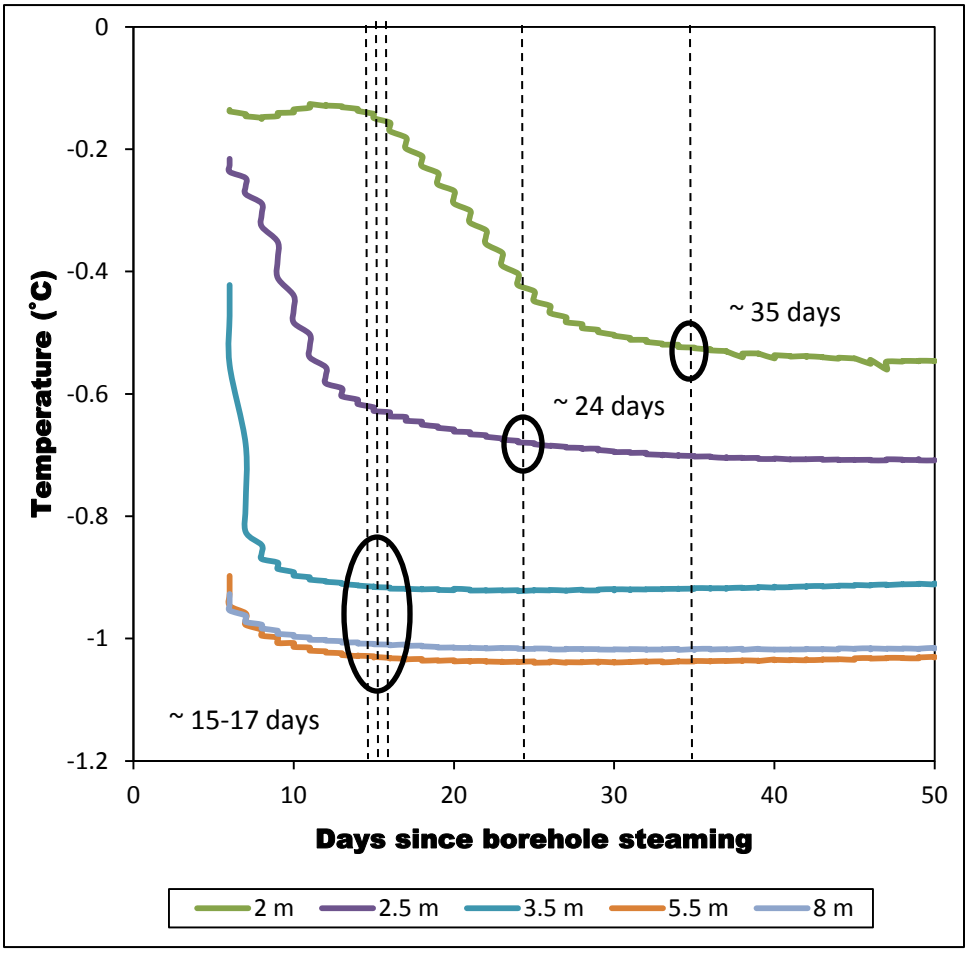

Figure 6.1: Time required for ground temperatures to recover at borehole R5 after borehole steaming on August 19, 2011. The RBR logger record starts 6 days after drilling.

Environmental change was also observed in the vicinity of the boreholes where a cut-line was cleared on the proposed pipe line right-of-way (ROW) in the 1970s for geophysical work. Smith and Riseborough (2010) described the thermal response of permafrost terrain to ROW disturbance and climate warming in the Norman Wells pipeline corridor since the early 1980s using results from both thermal monitoring and finite element modelling. Simulated results for warm permafrost (input: MAGT > -1.0˚C; 20 m thick) indicated that the combined effects of vegetation clearance and climate warming would likely result in permafrost degradation within 20 to 40 years (Smith and Riseborough, 2010). ROW disturbance effects might also extend outside the ROW under scenarios of climate warming due to a change in microclimate following vegetation clearing and surface organic layer disturbance (Smith and Riseborough, 2010). In colder and thicker permafrost (input: MAGT < -1˚C; 50 m thick), the combined effect of climate warming and ROW disturbance would not likely lead to talik formation within 50 years, although seasonal thaw penetration would increase (Smith and Riseborough, 2010). The effects of ROW disturbance potentially outweigh those associated with climate warming in the initial 10 to 15 years following disturbance, although climate warming becomes important over longer time periods (Smith and Riseborough, 2010).

Comparisons between ground temperature measurements in 1985 and 2007 show ground temperatures as much as 2˚C higher beneath the ROW at 4 m depth than those in the adjacent undisturbed terrain (Smith and Riseborough, 2010). Over the same monitoring period, thaw depths have increased by more than 2 m beneath the ROW near Norman Wells and more than 3 m in the warmer and thinner permafrost south of Fort Simpson (Smith and Riseborough, 2010). Similar results were obtained in the study area from 2011-2012 ERT surveys conducted over the partially regrown cut-line used for previous geophysical work near the boreholes in the 1970s. ERT results show deeper thaw (as much as 20 m) under the cut-line compared to the adjacent undisturbed terrain (Section 6.2.2).

6.2 Current Characteristics of Permafrost in the Study Area

Since the study area falls into the sporadic discontinuous and extensive discontinuous permafrost zones, it was not surprising to find both thin, warm permafrost and highly localized variations in active layer thickness and permafrost thickness (Heginbottom et al., 1995). This is consistent with previous research conducted in the area (James, 2010; Smith et al., 2010; Lewkowicz et al., 2011; Miceli, 2012).

6.2.1 Borehole Thermal Monitoring

The study sites in this thesis are considered to be located in a zone of "warm" permafrost which is classified by Wu et al. (2002) as permafrost having MAGTs warmer than -1.5˚C (Figure 6.2). The differentiation between "warm" and "cold" permafrost is important because they respond differently to changes in surface conditions (Wu et al., 2002). Warm permafrost is often influenced thermally by large amounts of unfrozen moisture and is more susceptible to thaw (Smith et al., 2010). Warm permafrost is usually within the discontinuous permafrost zone (Heginbottom et al., 1995), but can occasionally be located in the continuous zone where it is newly aggraded, or in areas of flooding or high snow cover (Smith et al., 2010). Cold permafrost is defined as having MAGTs lower than -1.5˚C (Wu et al., 2002), and tends to have little or no unfrozen moisture (Smith et al., 2010). Ground temperatures at cold permafrost sites are more responsive to changes in climate due to minimal amounts of unfrozen moisture (Smith et al., 2010) Cold permafrost is usually within the continuous permafrost zone, but does occasionally extend into the discontinuous zone (Smith et al., 2010).

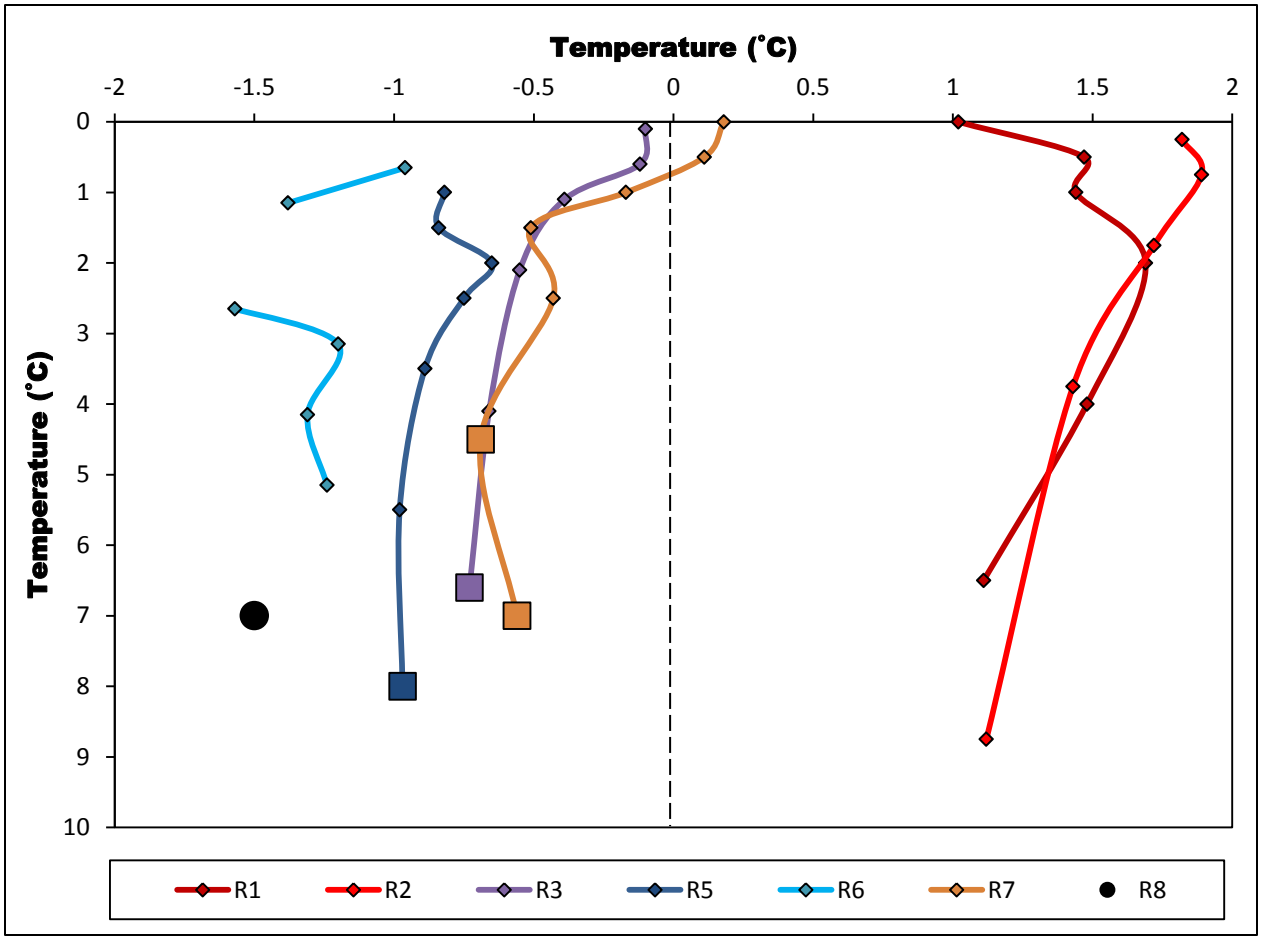

Figure 6.2: MAGT profiles for field sites along the study area. The diamonds represent the points of measurement while the larger squares are sensors located below the D_{ZAA}. Note that sensors at 1.65 m and 2.15 m at BH R6 failed mid-way in the annual record and were not included in MAGT calculations. Logger and cable failure at BH R4 and R8 made it impossible to calculate MAGTs at these sites. However, an estimate of MAGT at 7 m at R8 is shown as a circle, based on two months of records.

Four of the field sites showed in Figure 6.2 are located in the sporadic discontinuous permafrost zone (Heginbottom et al., 1995) and are classified as "warm" permafrost while R8 is in the extensive zone and may be "cold" permafrost. Permafrost was not present at boreholes R1 and R2 in the 1970s and positive MAGTs in 2001-2012 also indicate that it is now present now.

In general, MAGTs decrease from the southeast to the northwest, which reflects the trend in MAAT which decreases along a southeast to northwest transect from Whitehorse to Beaver Creek. The exception is borehole R7 which had warmer MAGTs than boreholes R3, R5 and R6. Soil lithology at borehole R7 consists mainly of peat and silts with mature surface vegetation while boreholes R3, R5 and R6 have thin surface organic layers with an underlying lithology consisting mainly of silt, clay and sand and are in clearings. The thawing n-factor was approximately 0.2 at borehole R7 while the freezing n-factor was about 0.1. A thawing n-factor of 0.2 at borehole R7 suggests significant shading from vegetation at the ground surface in the summer (Taylor, 1995), while the freezing n-factor of 0.1 can be explained by a total of 180 days with snow cover, and 135 days with more than 30 cm of snow. The resulting surface offset is approximately 3˚C which may partially explain why borehole R7 has warmer MAGTs than R3, R5 and R6 while being situated at the north end of the study area. However, this cannot be conclusively demonstrated as site specific climatic conditions were not collected at other borehole sites.

The only substantial zero curtain were observed during freeze-up at 0.6 m at borehole R3 and at 1 m at borehole R7 and lasted for approximately 125 days and 97 days respectively. The long zero-curtain was probably due to a greater than normal amount of unfrozen moisture present in the ground due to borehole steaming which required large amounts of latent heat to be extracted for phase change (French, 2007).

The annual temperature waves at the boreholes were not sinusoidal due to unfrozen moisture present in permafrost soils with MAGTs near 0˚C (Williams and Smith, 1989; French, 2007). This meant that original plans to calculate the thermal diffusivity, amplitude, the D_{ZAA}, phase lags and permafrost depths could not be carried out (Williams and Smith, 1989). The D_{ZAA} was only reached at boreholes R3, R5 and R7, with the shallowest D_{ZAA} observed at BH R7 around 4.5 m (Figure 6.3).

The absolute range in ground temperatures at 1 m, 3 m and 5 m depths at the studied boreholes is greatest at non permafrost sites (R1 and R2) and smallest at permafrost sites with MAGTs near 0˚C (R7) (Figure 6.3). The attenuation of temperature variation at near 0˚C permafrost sites is due to the presence of unfrozen moisture which requires changes in latent heat during cooling and warming (French, 2007). The absolute temperature range therefore increases as MAGTs decrease towards the north of the study area (Figure 6.3). The absolute temperature range also decreases with depth at every borehole as expected (Figure 6.3).

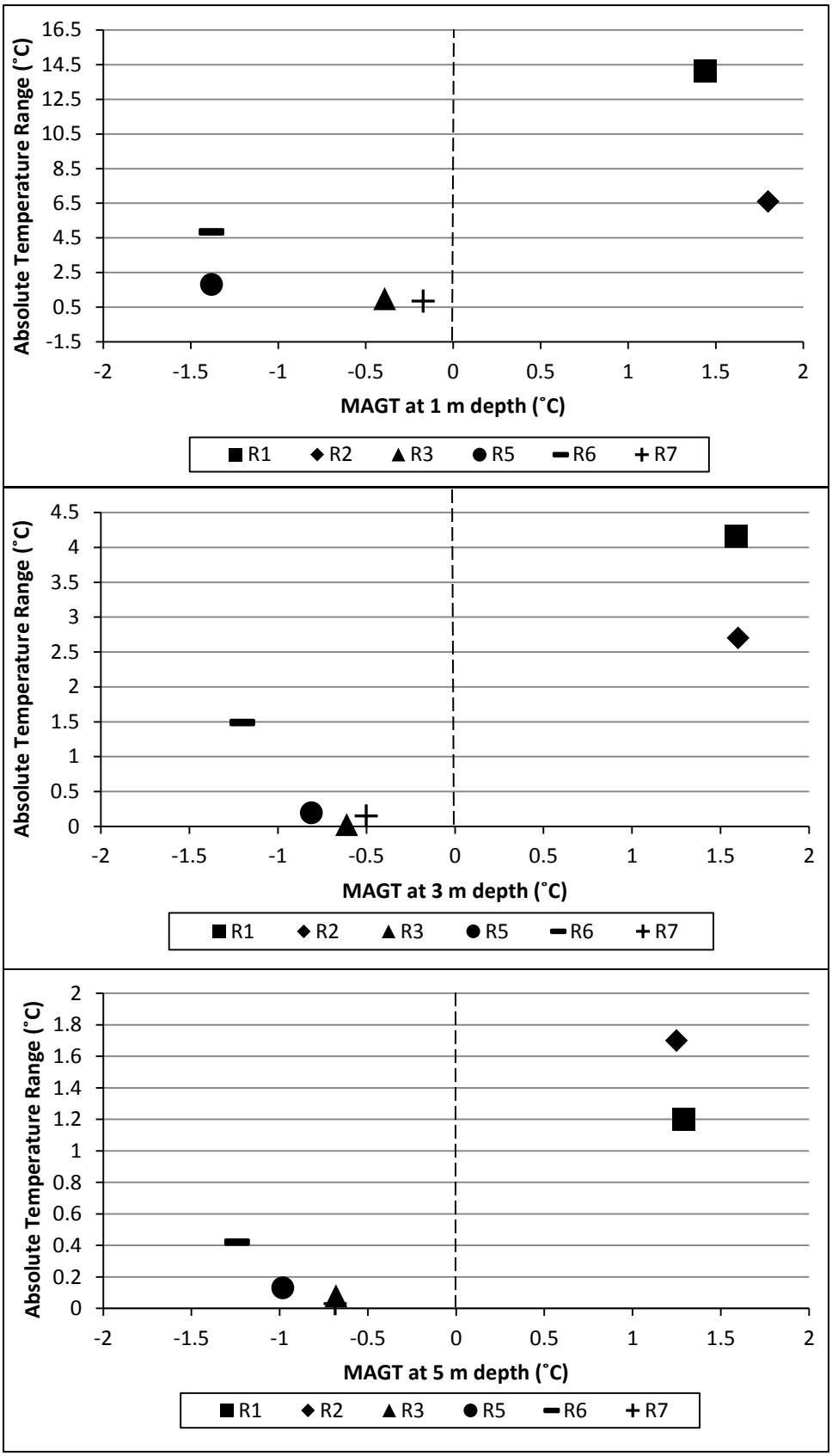

Figure 6.3: Absolute temperature range for MAGTs at 1 m, 3 m and 5 m depths from all the R-boreholes, with the exception of BH R4 and R8 due to logger failure. Note the different scales of the y-axes.

6.2.2 Electrical Resistivity Tomography Results

ERT surveys were conducted at each of the 12 borehole sites to complement thermal monitoring and in order to examine vertical and horizontal permafrost distribution and characteristics. Subsurface thermal regimes can change markedly from one place to another resulting in complex distributions of frozen ground with large differences possible over short distances (Vonder Muhll et al., 2002). Surface and subsurface monitoring techniques must therefore be extended from temperature monitoring at point locations (boreholes) to two-dimensional geophysical monitoring of freezing and thawing processes (Hilbich et al., 2008).

ERT results show a low resistivity layer at the surface of most surveys which matches a thawed surface layer (active layer) measured manually by probing. In some cases, thin thawed layers were not identifiable on the modelled resistivity plot even though they were present because the inversion routine cannot cope with extremely high resistivity contrast in the near-surface at the unfrozen/frozen interface (Hilbich et al., 2008; Miceli, 2012). Mean active layer thicknesses determined by probing varied from 49 cm at borehole R5 to 114 cm at borehole H3 (Table 6.1). Thicker active layers were observed at sites located in wetlands or in temporarily wet areas while thin active layers were found at drier sites. Mean active layer thicknesses could not be properly calculated at sites where probing was limited by gravel or hard clay and an active layer of 120 cm was used for the calculation of the mean when unfrozen conditions extended deeper than the length of the probe (Table 6.1). Mean active layer thicknesses should therefore be offset to higher but unknown values.

A statistically significant relationship at a confidence level of 95% is observed between negative borehole ground temperatures and ERT modelled resistivity values for all field sites with frozen sediments in the study area (Figure 6.4) The increase in resistivity with decreasing temperature is exponential for temperatures below 0˚C (Hauck, 2002; Hilbich et al., 2011) (Figure 6.4). The transition between frozen/unfrozen interfaces generally occurs around 500 Ohm-m at surveyed borehole sites in the study area based on the ERT results, probing and borehole temperatures. This is similar to other results obtained in the area (ex: Lewkowicz et al., 2011; Miceli, 2012). However, Figure 6.4 shows one positive temperature measurement with a resistivity value higher than 1000 Ohm-m. This is regarded as an outlier and may be due to the

fact that the modelled resistivities for areas below and above high resistivity bodies (in this case, the active layer) are less accurate (Hauck and Muhll, 2003).

Resistivity values in the 500-900 Ohm-m range are classified as 'indeterminate' ground, meaning that this range of resistivities cannot to be identified conclusively as unfrozen or frozen. This 'indeterminate' range was applied to the ERT results obtained in this thesis and is higher than the indeterminate zone of 400-500 Ohm-m described by Miceli (2012) south of the study area (see Figure 6.4).

Table 6.1: Summary of ERT results in the study area. The deepest ERT penetration depth is located vertically under the borehole at the mid-point of each survey. For sites with more than 1 ERT survey, only the longest one is shown. For sites with cross-sectional surveys of the same length, only the first one described in Section 5 is shown due to close similarity. Permafrost layering classification is from Sartorelli and French (1982).

BH	Permafrost Present (Y/N)	ERT Length (m)	ERT Penetration Depth (m)	Apparent Resistivity at deepest penetration depth (Ωm)
R1	N	80	12.5	60
R2	N	160	25	107
R3	Y	160	25	2500
R4	Y	160	25	400
R5	Y	160	25	2500
M1	Y	80	12.5	8000
R6	Y	160	25	400
H1	Y	80	12.5	10 000
H2	Y	80	12.5	35 000
R7	Y	160	25	5000
H3	Y	80	12.5	35 000
R8	Y	160	25	7000
BH	**Layering Classification**	**Mean Active Layer Thickness (cm)**	**Permafrost Depth (m)**	
R1	1 layered	N/A	N/A	
R2	1 layered	N/A	N/A	
R3	2 layered	69	>25	
R4	2 layered	? due to hard clay	>25?	
R5	2 layered	49	>25	
M1	2 layered	? due to gravel	>12.5	
R6	2 layered	61	>25?	
H1	2 layered	? due to gravel	>12.5	
H2	2 layered	66	>12.5	
R7	2 layered	71	>25	
H3	2 layered	114	>12.5	
R8	2 layered	42	>25	

*Note that different dry soils such as sand, gravels and bedrock can have overlapping resistivity values with permafrost. Thermal monitoring is needed to confirm the absence or presence of permafrost at any given site.

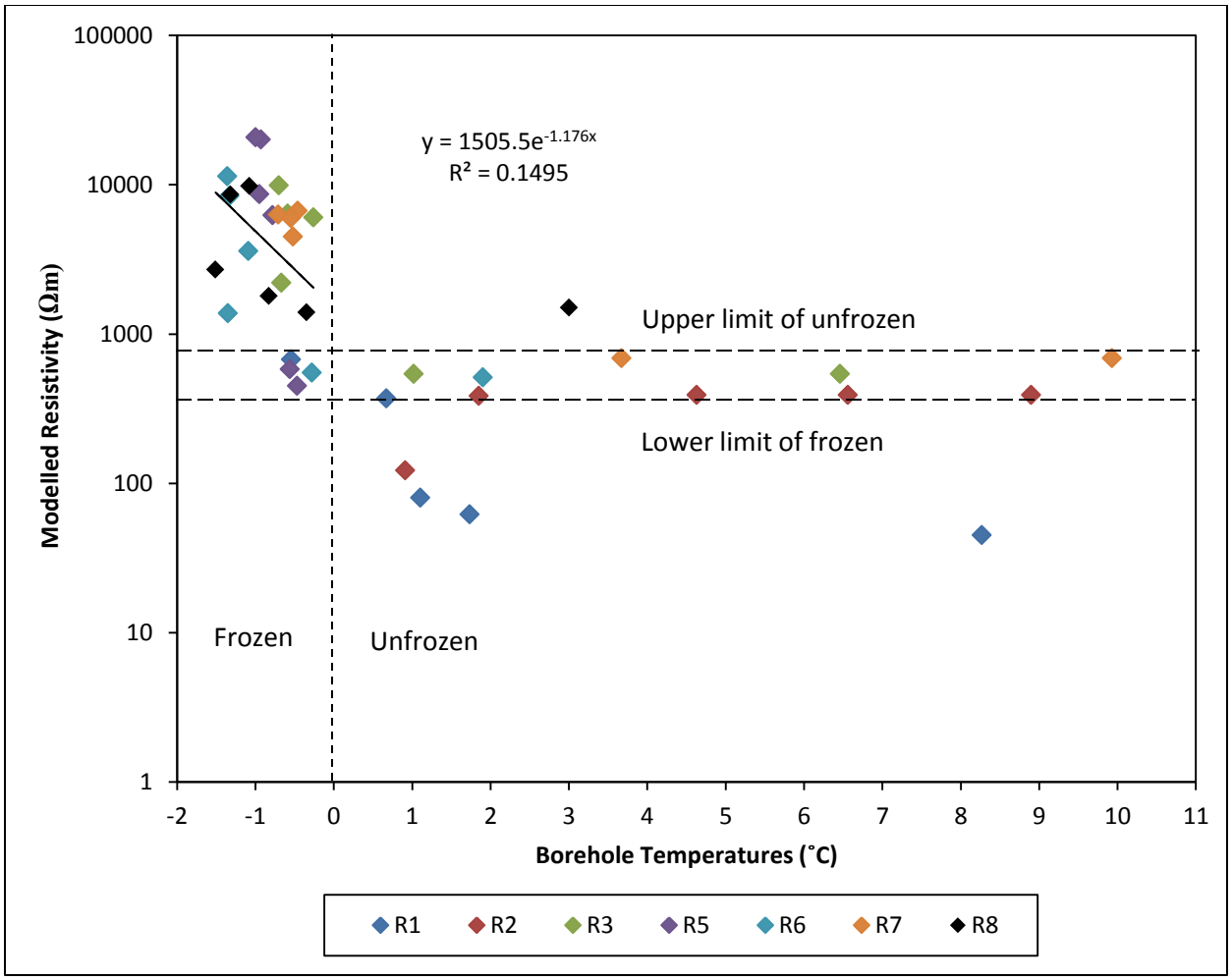

Figure 6.4: Relationship between measured ground temperatures and the modelled resistivity values (Ωm) for the same depth from all the R-boreholes, with the exception of R4 due to logger failure. The borehole temperatures and modelled resistivity values are from the same day as the ERT surveys in August 2012. The comparison at R1 is from June 2011. The black line represents a exponential regression with a $R^2 = 0.15$ for frozen borehole temperatures. The lower limit of frozen ground is represented by modelled resistivity values of approximately 600 Ωm while the upper limit is represented by modelled resistivity values of approximately 900 Ωm.

Thermal monitoring and ERT results indicate the presence of permafrost at every borehole site in the study area except for the two southern most ones; R1 and R2. ERT results at boreholes R3 to R8 show a two-layered state in summer meaning that permafrost is present under a thawed active layer to the deepest exploration depth (Table 6.1) (Satorelli and French., 1982). Boreholes R1 and R2 show a one-layered state as the ground is unfrozen to the deepest effective exploration depth (Sartorelli and French, 1982).

Those resistivity values that range from 2500 to 7000 Ohm at the bottom of the 160 m ERT surveys conducted at the RBR logger borehole sites indicate permafrost deeper than the deepest penetration depth of 25 m (Table 6.1). At boreholes R4 and R6, however, it is uncertain if permafrost is deeper than 25 m as resistivity values at the deepest penetration depth of 25 m are in the 'indeterminate' range. Also, it is well known that accuracy decreases in modelled values for areas below high resistivity bodies (Hauck and Muhll, 2003). ERT surveys at the manual temperature and HOBO instrumented boreholes were all 80 m in length and suggest permafrost deeper than the deepest penetration depth of 12.5 m at all sites with bottom resistivities ranging from 8 000 Ohm-m to 35 000 Ohm-m. These high resistivity values suggest that permafrost may also extend deeper than 25 m.

Based on the classification of Shur and Jorgenson (2007) the permafrost sites studied are likely climate driven, ecosystem-protected. The permafrost initially formed under a favourable past cold climate and can survive under warmer climatic conditions as long as it remains protected by its ecosystem properties. The exception is BH R8 at the northern end of the study area in the colder extensive discontinuous permafrost zone. Although permafrost sites in the study area have MAATs estimated to range from -2.5˚C to -5.5˚C, ERT results showed active layer thickening and probable talik development where surveys cross the regrown cut-line used for previous geophysical work in the 1970s (Figure 6.5). The removal of vegetation and organic matter compaction affected surface heat exchanges and created a warmer micro-climate. Permafrost appears to have thawed deeper than 20 m under the cut-line at borehole R4 (Figure 6.5). Further north at BH R8, in colder permafrost, lower resistivity values under the cut-line suggest internal warming and an increase in unfrozen moisture content (Figure 6.5). Permafrost has not thawed at this site after being exposed to solar radiation for more than 30 years which indicates that it can probably be classified as climate-driven permafrost based on the

classification of Shur and Jorgenson (2007). Permafrost at this site likely formed independently of vegetation due to a cold regional climate.

Permafrost degradation was also observed where the ERT survey crossed the cut-line at boreholes R3, R5 and R7. Similar effects of environmental change have been documented on the cleared pipeline right-of-way in the Norman Wells pipeline corridor (Smith and Riseborough, 2010) (Section 6.1.2).

Analysis of the modelled resistivities at the depth of various borehole temperature sensors in permafrost shows an observable relation between resistivity and the soil type logged in the boreholes (Figure 6.6). Finer grained materials such as clay and sand show generally lower resistivities than coarser grained soil such as sand and gravel (Figure 6.6). Modelled resistivity generally increases for both fined and coarse grained soils as temperatures decrease (Figure 6.6). However, the only statistically significant trend was observed on the coarser grained soil series when tested at a 95% confidence level (Figure 6.6). This matches with resistivity values outlined by Hauck and Kneisel (2008) for different earth materials. Lithological boundaries from the borehole logs were used to better interpret ERT plots.

Further analysis of modelled resistivities at the depth of various borehole temperature sensors in permafrost did not yield a relationship with volumetric ice content measured in the borehole logs from the 1970s (Figure 6.7). In theory, measured electrical resistivity rises exponentially as unfrozen water content within a substrate decreases (Hauck, 2002; Hilbich et al., 2011). Permafrost with higher ice content should yield higher resistitivity values (Hilbich et al., 2011). However, temperature sensors with high ice content (30-40 % and 40-50%) showed the lowest resistivity values (Figure 6.7). These areas of high resistivity are located at the top of permafrost, where ice content is generally higher and might be underestimated by the inversion routine which cannot cope with the extremely high contrast in resistivities at the near-surface (Miceli, 2012). It is also possible that volumetric ice content has changed since the 1970s and ground that had higher ice content 30 years ago might now have higher unfrozen moisture due to warming.

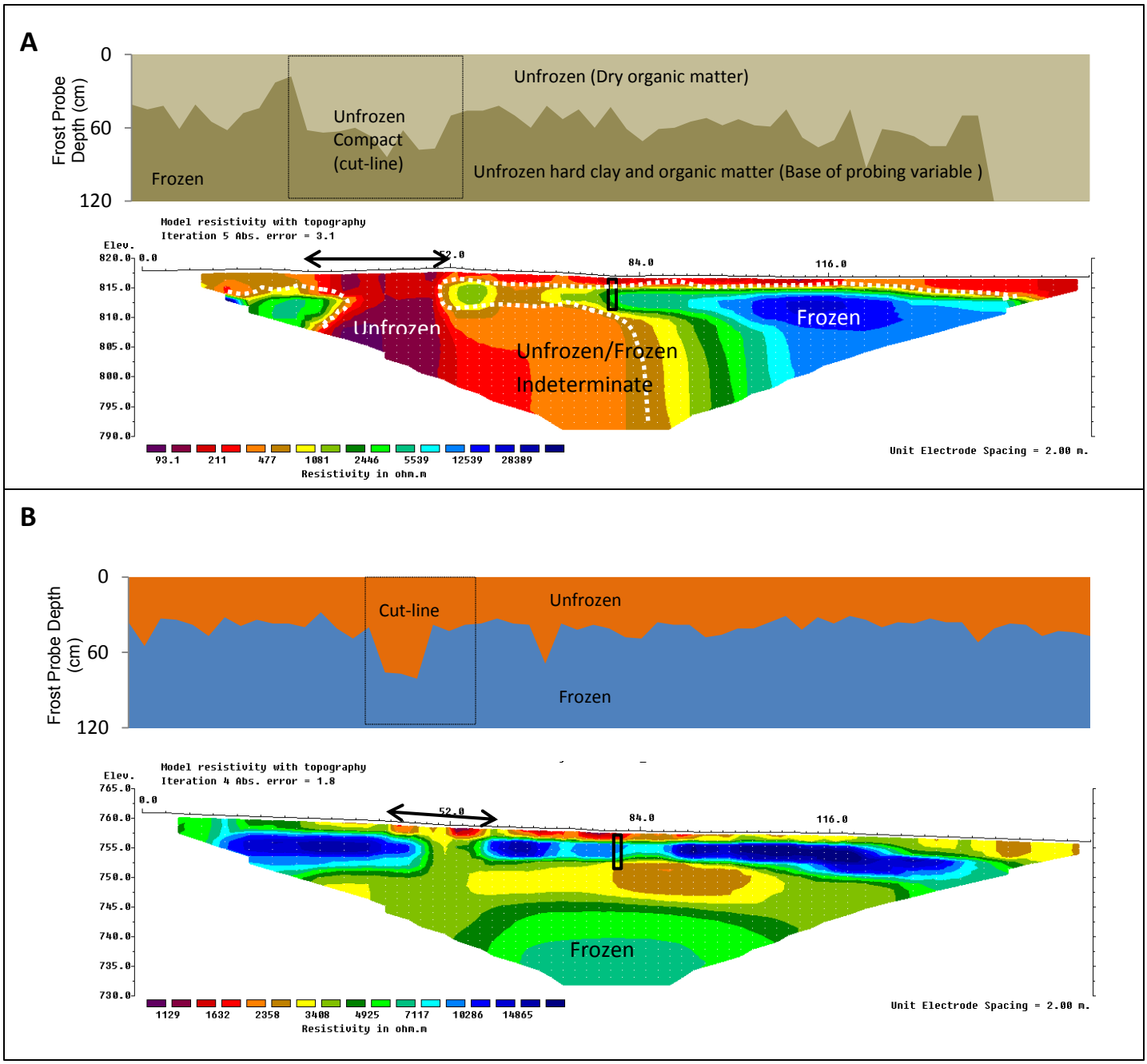

Figure 6.5: ERT surveys at (A) borehole R4 and (B) borehole R8 showing permafrost degradation due to environmental change under the regrown cut-line used for previous geophysical work in the 1970s.

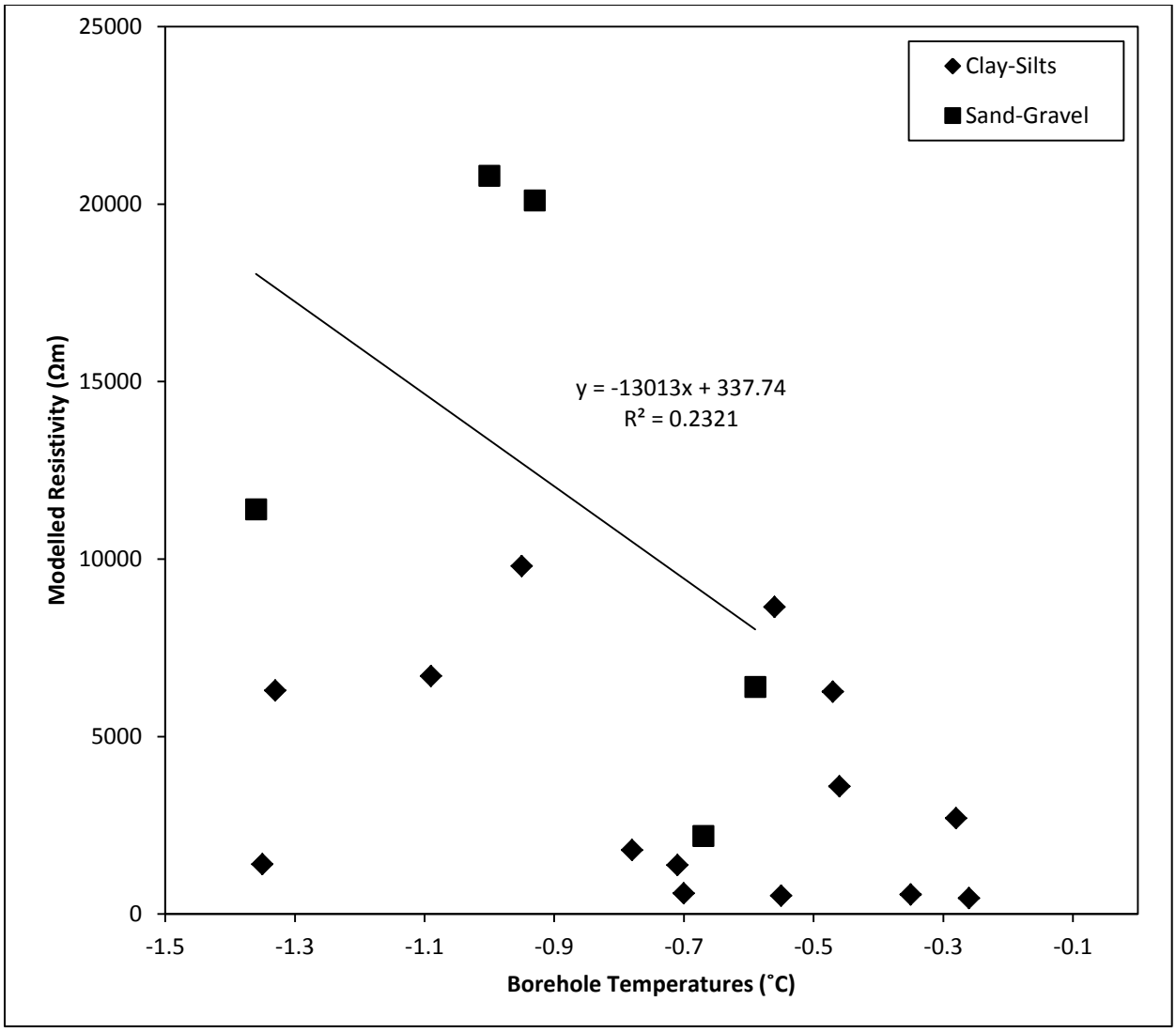

Figure 6.6: Relationship between soil type from the 1970s borehole logs and the modelled resistivity values (Ωm) for the measured temperatures (at the depth of the thermistors) from all the R-boreholes, with the exception of R4 due to logger failure. The borehole temperatures and modelled resistivity values are from the same day as the ERT surveys in August 2012. The black line indicates a statistically significant trend on the Sand-Gravel series (95% confidence level).

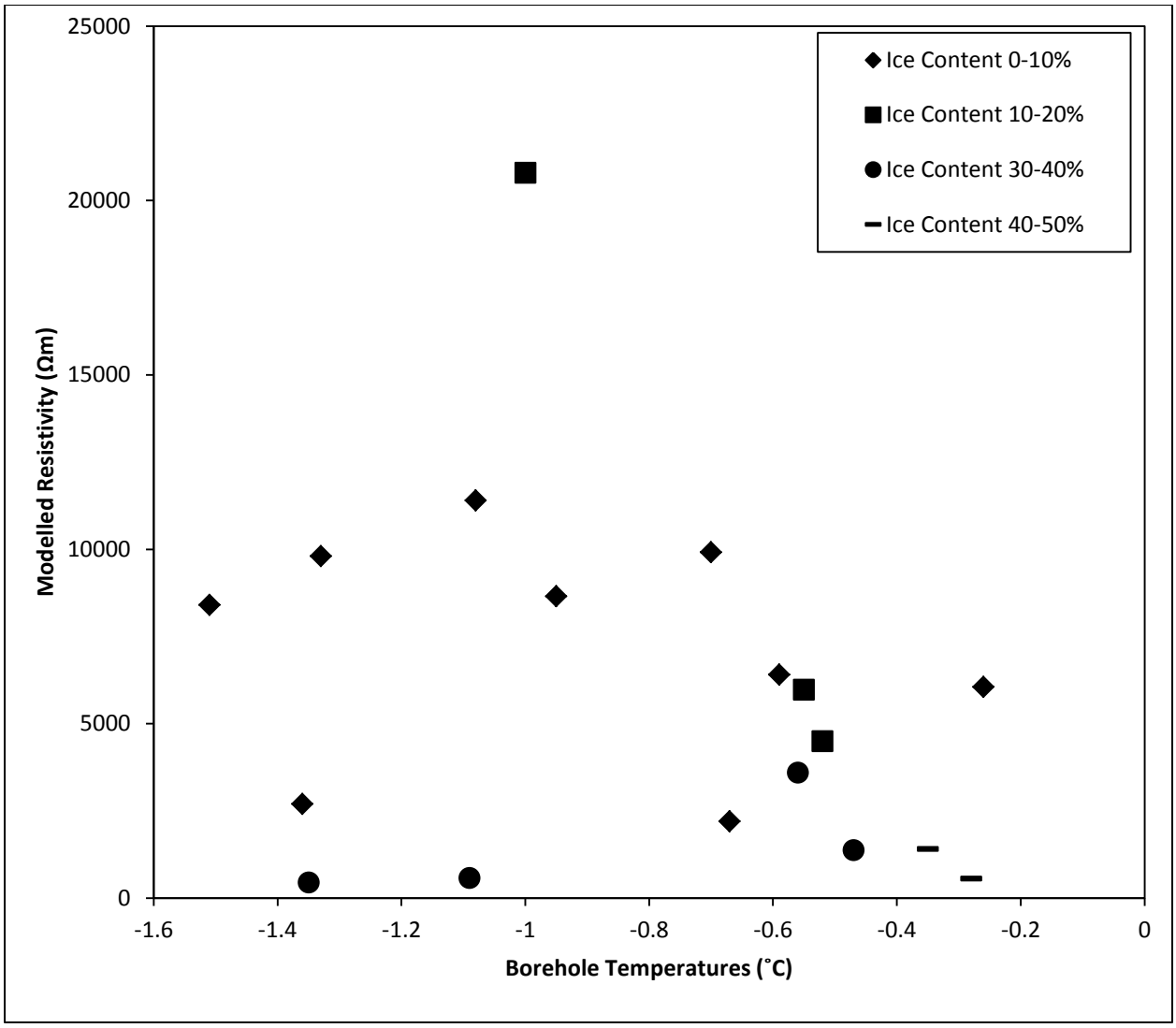

Figure 6.7: Relationship between the volumetric ice content from the 1970s borehole logs and the modelled resistivity values (Ωm) for the measured temperatures (at the depth of the thermistors) from all the R-boreholes, with the exception of R4 due to logger failure. The borehole temperatures and modelled resistivity values are from the same day as the ERT surveys in August 2012.

6.3 Changes over Time

6.3.1 Multi-Decadal Differences in Ground Temperatures

A combination of climate warming in the study area and environmental changes at the study sites has resulted in changes in ground temperatures between the original 1977-1981 manual temperature measurements and the 2011-2012 temperature measurements. A total of 54 ground temperature point measurements taken between 1977-1981 at depths ranging from 0.5 m to 8.0 m were compared to 2011-2012 temperature measurements taken at the same depths and on the same calendar date (Figure 6.6). More than 80% of these measurements are above the 1:1 line, indicating an increase in the measured ground temperatures since the 1970s (Figure 6.6). Conversely, almost 20% of the measurements are below the 1:1 line, indicating cooler ground temperatures in 2011-2012 when compared to 1977-1981 (Figure 6.6). However, all of the measurement points below the 1:1 line have a potential error extending over the 1:1 line, which suggest that these decreases may be due to measurement error (Figure 6.6). The manual temperature measurements conducted between 1977-1981 have a potential error of 0.44˚C (see Section 4.8). One-third of the measurements above 1:1 have a potential error extending below but the other two-thirds do not, indicating that they have experienced real temperature increase (Figure 6.6) Most of the field sites show overall ground temperature increases between 0.5-1.0˚C (Figures 6.6 and 6.7).

The results also show that ground layers that were cryotic between 1977-1981 were still cryotic between 2011-2012 except for two measurement points at borehole R1 (Figure 6.6). Thawed ground conditions between 1977-1981 remain thawed between 2011-2012 and no non-cryotic ground in the 1970s showed cryotic conditions in the most recent measurements. The greatest warming occurred at the thawed borehole sites of R1 and R2 and at the cooler permafrost sites such as boreholes R5, R6 and R8. Similar warming was observed at the deepest thermistor of borehole R7 while shallower depths did not warm much. The amount of warming is less at borehole sites with MAGTs approaching 0˚C due to the requirement of satisfying latent heat as unfrozen moisture increases (Smith et al., 2005; French, 2007; Burn, 2012) (Figures 6.2, 6.6 and 6.7).

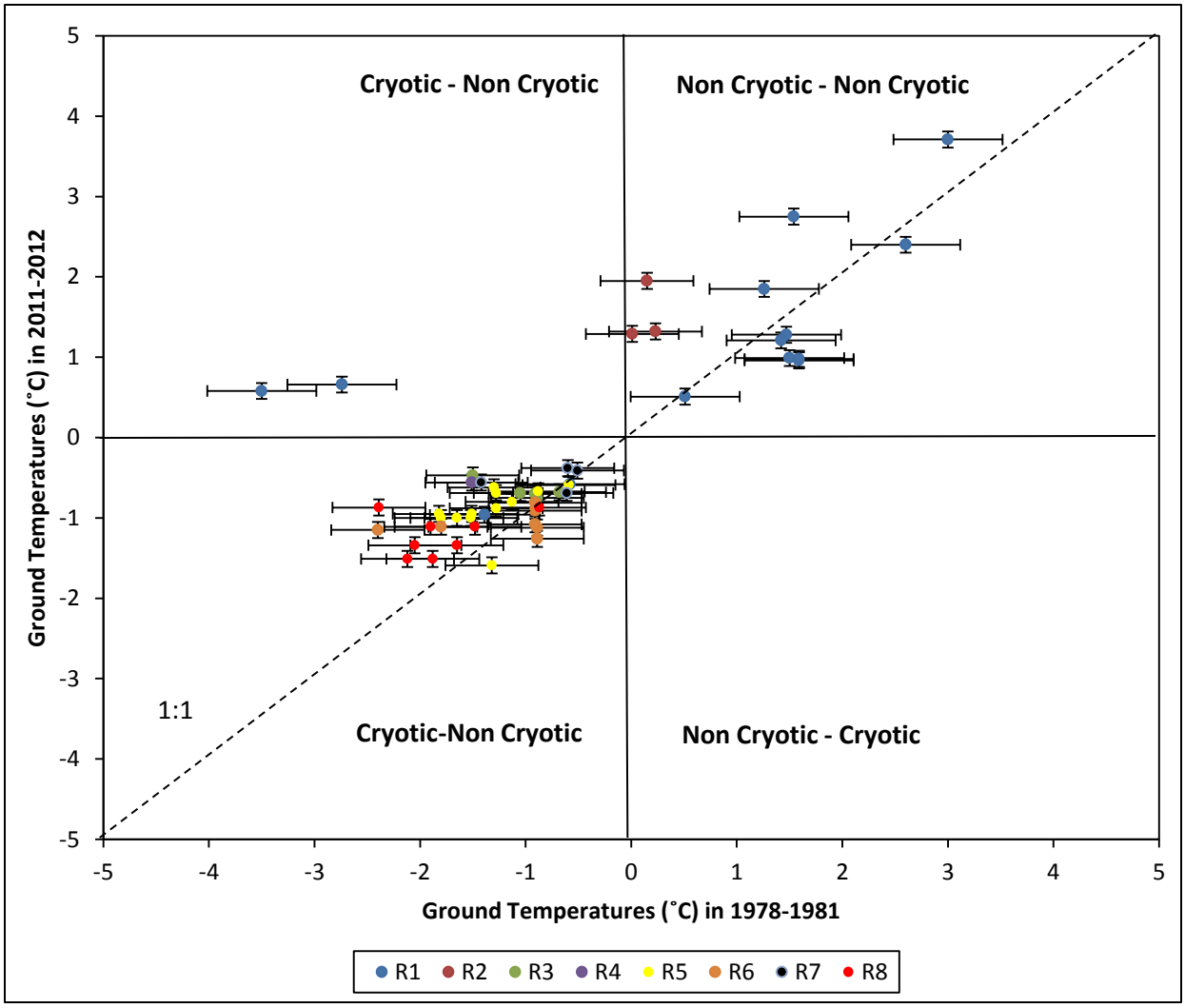

Figure 6.8: Relationship between the ground temperatures in 1978-1981 and the ground temperatures in 2011-2012 from all the R-boreholes measured on the same calendar day. Error bars for the 1978-1981 measurements represent a potential error of 0.44˚C for the manual temperature measurements while error bars for the 2011-2012 measurements represents an accuracy of 0.1˚C for the RBR data-loggers. The 1:1 line is shown. The four areas of the graph show conditions in the earlier period compared to those in the more recent one.

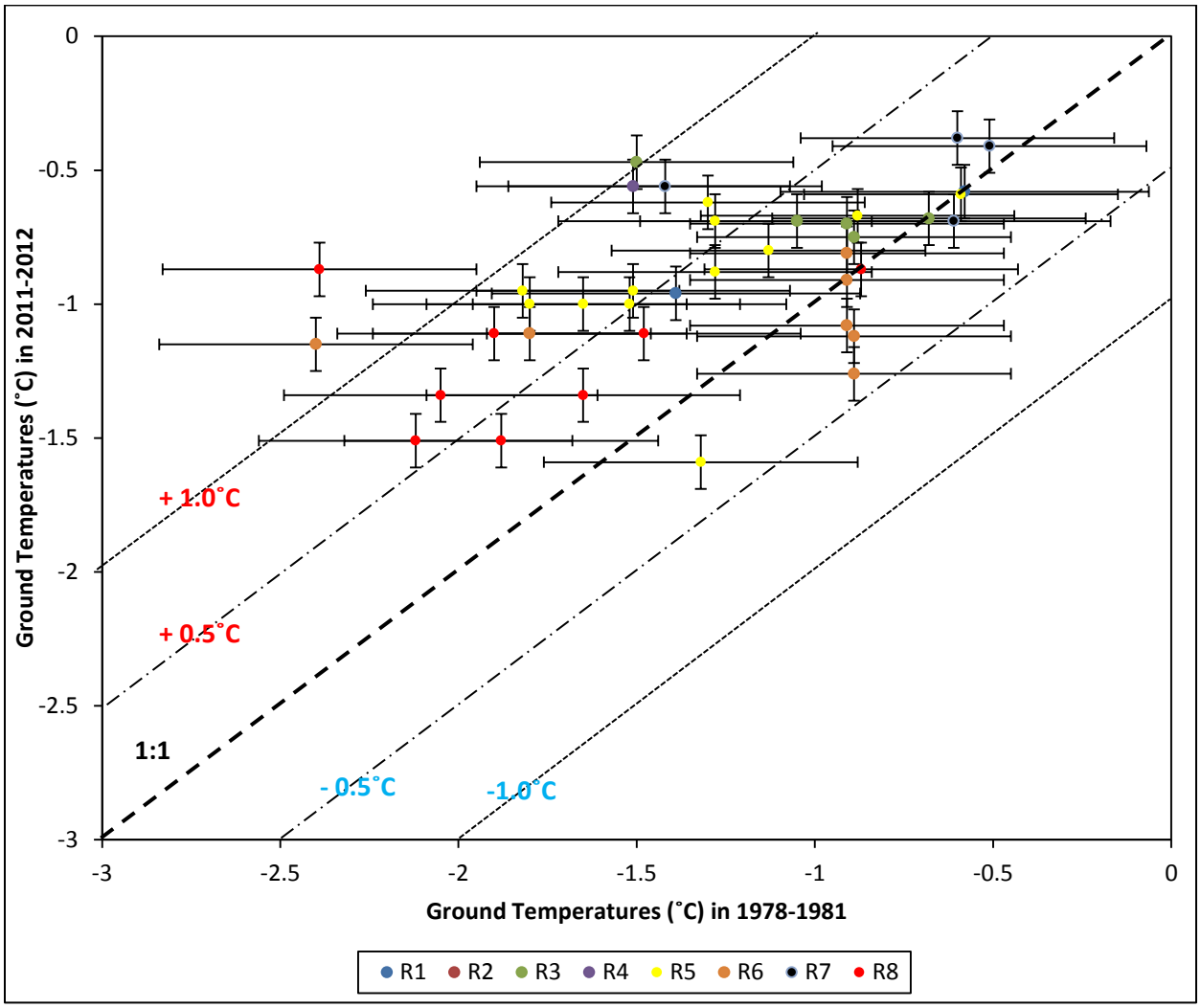

Figure 6.9: Relationship between negative ground temperatures in 2011-2012 and negative ground temperatures in 1978-1981 from all the R-boreholes. Points represent same calendar day comparisons between 2011-2012 and 1978-1981. Error bars for the 1978-1981 measurements represent a potential error of 0.44˚C for the manual temperature measurements while error bars for the 2011-2012 measurements represents an accuracy of 0.1˚C for the RBR data-loggers. The 1:1 line is shown with the +0.5:-0.5 line and the +1:-1 line.

The typical ground temperature increases of 0.5-1.0˚C from 1977-1981 to 2011-2012 meant that most of the original manual temperature measurements were cooler than the absolute minimum temperatures measured during 2011-2012 and were outside the current temperature envelope which is warmer (Figure 6.8). Moreover, only one measurement point from the 1977-1981 manual temperatures at R7 is warmer than the absolute maximum temperatures measured in 2011-2012 (Figure 6.8). No site showed significant cooling in the most recent measurements (Figure 6.8). Warming greater than 0.44˚C represents a significant change in ground temperatures as it falls out of the range of potential errors associated with the initial 1977-1981 manual temperature measurements.

Overall, increases exceeding the potential margin of error for the original manual temperature measurements were observed at most boreholes when comparing 2011-2012 measurements to same day temperature logs from 1977-1981 (Figures 6.8, 6.9 and 6.10). The relationship between the temperature change between 1978-1981 and 2011-2012 with depth shows possible seasonal effects at shallower depths for the non-cryotic sites R1 and R2 with positive changes as high as 4.2˚C observed at 4 m at R1 (Figures 6.9). Seasonal effects on temperature changes at shallow depths are also likely to have occurred at the permafrost sites, although not as pronounced (Figure 6.10). Most sites show greater temperature change at deeper thermistors than at the near surface. This might be due to ground temperatures having already responded to the 1975/1976 step change at shallower depths while warming had not yet fully propagated at deeper thermistors. Almost 90 % of measurement points in permafrost show a positive temperature change between 1978-1981 and 2011-2012 (Figure 6.10). No negative temperature change is observed below 4.5 m depth (Figure 6.10). The average ground temperature change at the deepest measurement depths for the boreholes in permafrost is 0.9˚C with a maximum change of 1.4˚C at R6 and a minimal change of 0.2˚C at R3 (Figure 6.10). These depths are below or near the DZAA and represent real long-term change.

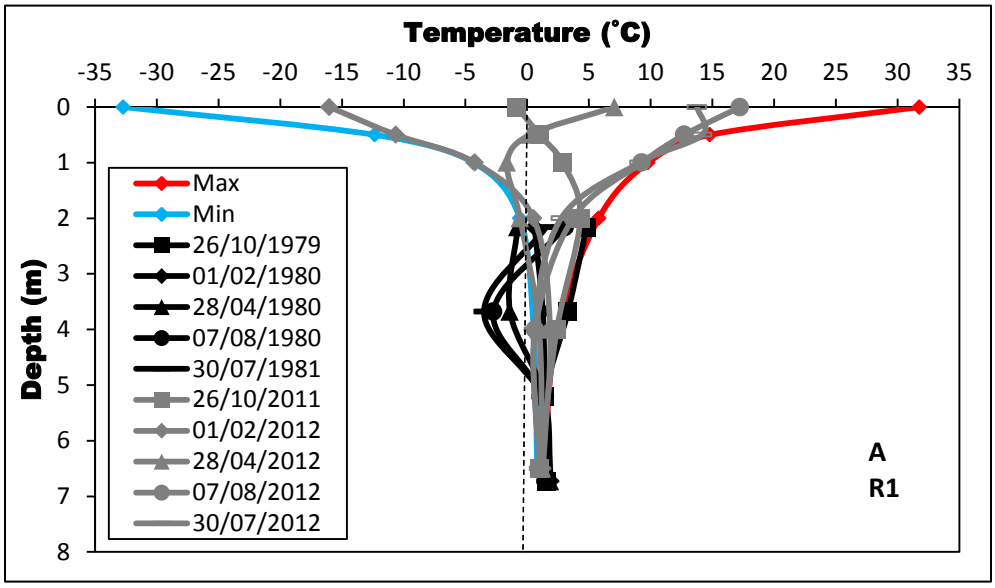
Temperature (˚C)
-35 -30 -25 -20 -15 -10 -5 0 5 10 15 20 25 30 35
Depth (m)
0 1 2 3 4 5 6 7 8
Max
Min
26/10/1979
01/02/1980
28/04/1980
07/08/1980
30/07/1981
26/10/2011
01/02/2012
28/04/2012
07/08/2012
30/07/2012
A
R1

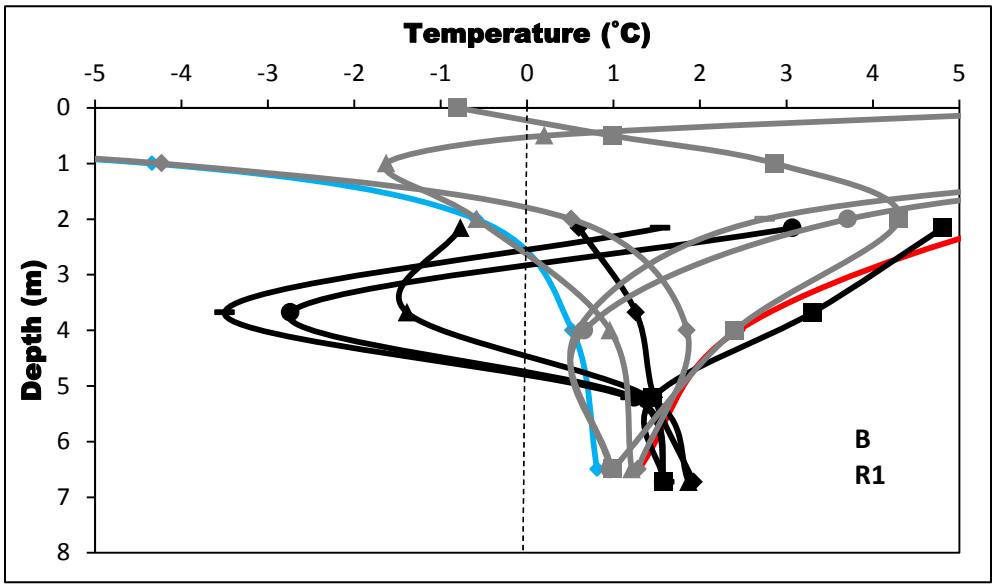
Temperature (˚C)
-5 -4 -3 -2 -1 0 1 2 3 4 5
Depth (m)
0 1 2 3 4 5 6 7 8
B
R1

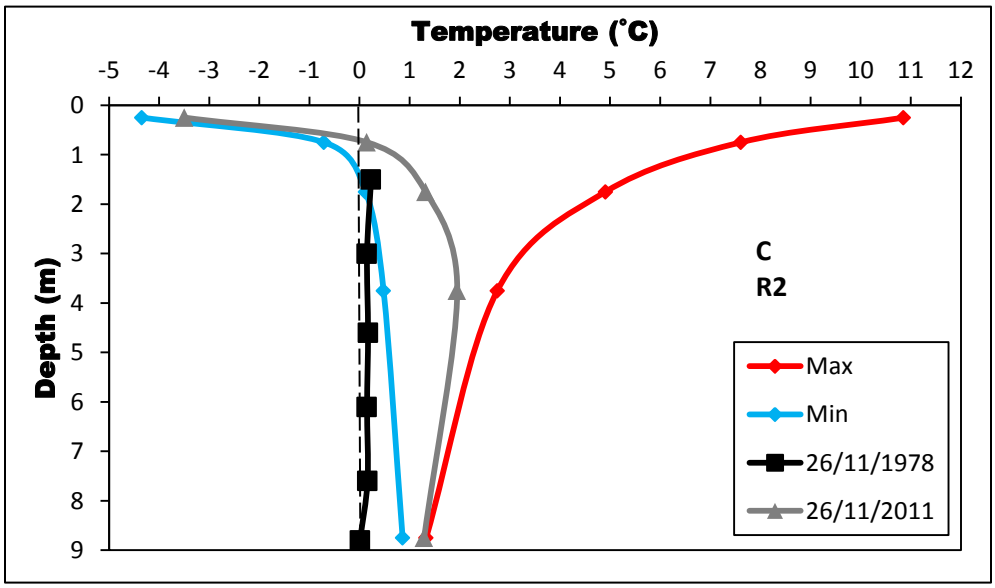
Temperature (˚C)
-5 -4 -3 -2 -1 0 1 2 3 4 5 6 7 8 9 10 11 12
Depth (m)
0 1 2 3 4 5 6 7 8 9
C
R2
Max
Min
26/11/1978
26/11/2011

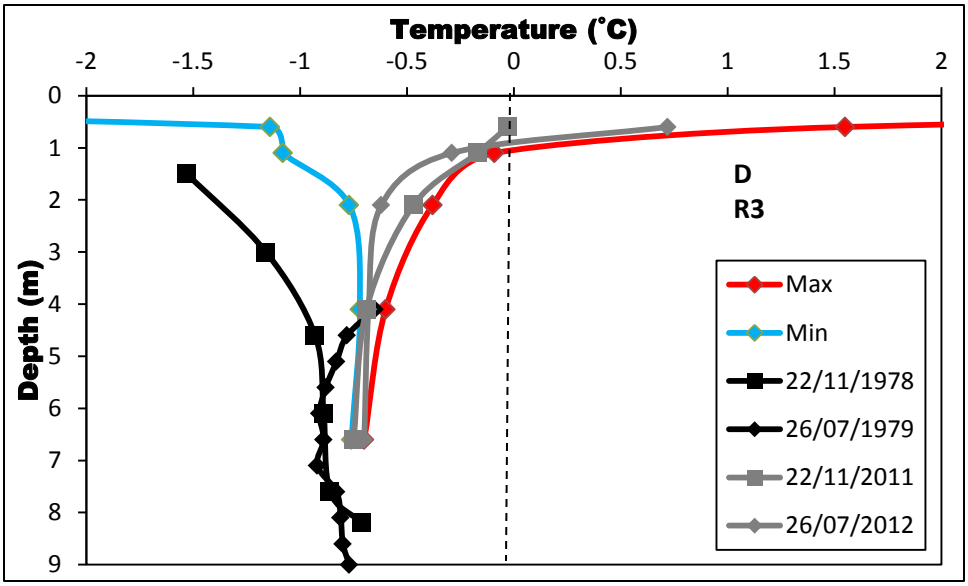
Temperature (˚C)
-2
-1.5
-1
-0.5
0
0.5
1
1.5
2
Depth (m)
0
1
2
3
4
5
6
7
8
9
D
R3
Max
Min
22/11/1978
26/07/1979
22/11/2011
26/07/2012

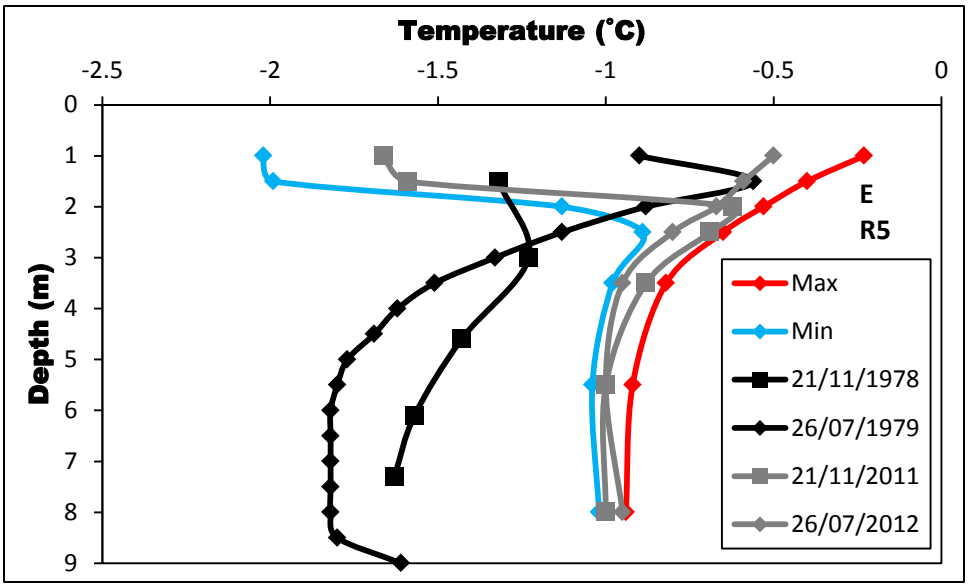
Temperature (˚C)
-2.5
-2
-1.5
-1
-0.5
0
Depth (m)
0
1
2
3
4
5
6
7
8
9
E
R5
Max
Min
21/11/1978
26/07/1979
21/11/2011
26/07/2012

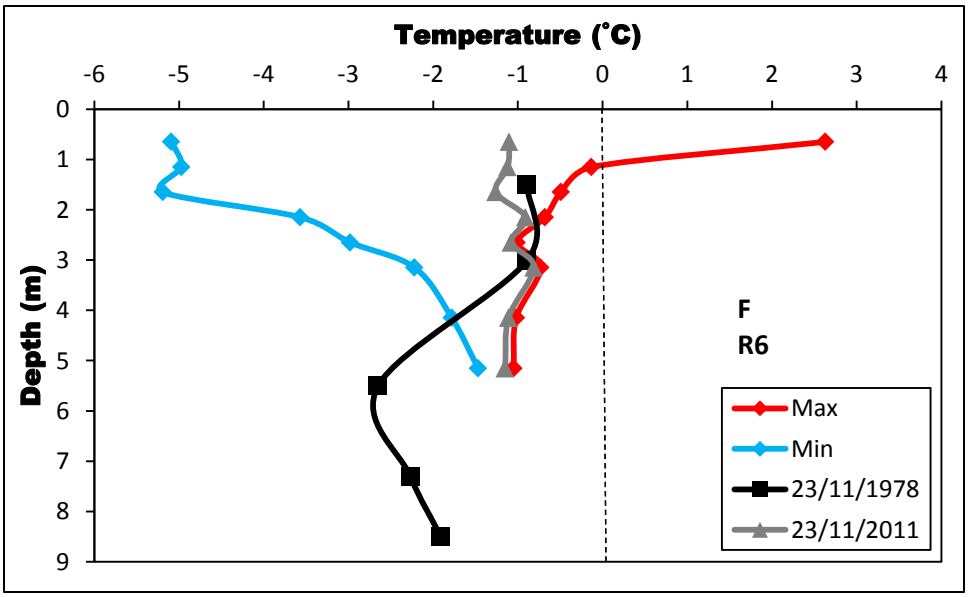
Temperature (˚C)
-6
-5
-4
-3
-2
-1
0
1
2
3
4
Depth (m)
0
1
2
3
4
5
6
7
8
9
F
R6
Max
Min
23/11/1978
23/11/2011

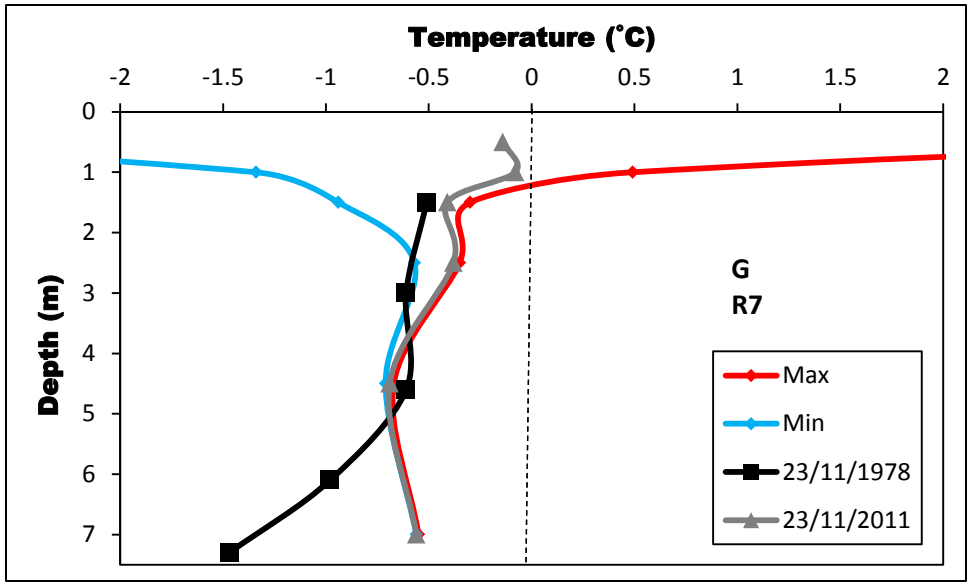

Figure 6.10: Temperature envelope for the 2011-2012 year showing the 1978-1981 manual temperature measurements and same day measurements from 2011-2012 for all the available R-boreholes. (A) R1; (B) R1; (C) R2; (D) R3; (E) R5; (F) R6; and (G) R7. Note changes in temperature scale between the sites.

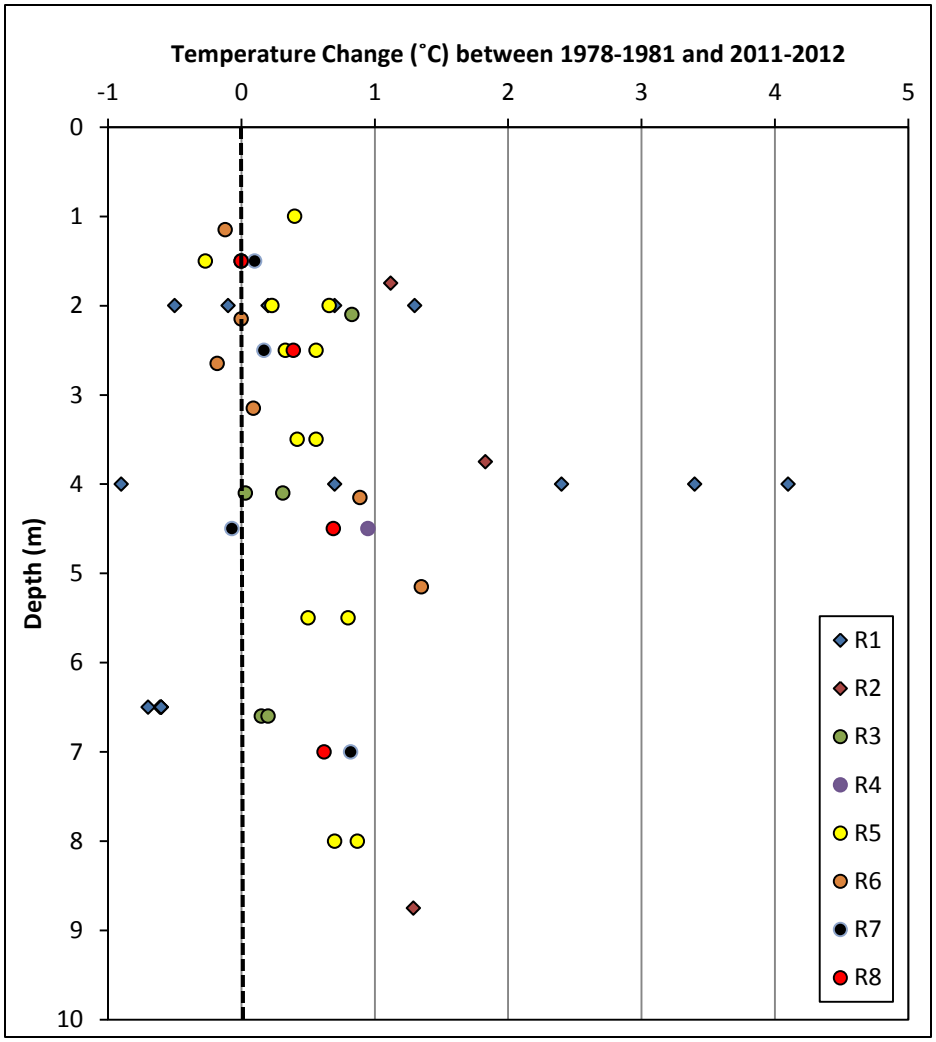

Figure 6.11: Relationship between the temperature change (˚C) between 1978-1981 and 2011-2012 with depth (m) from all the R-boreholes.

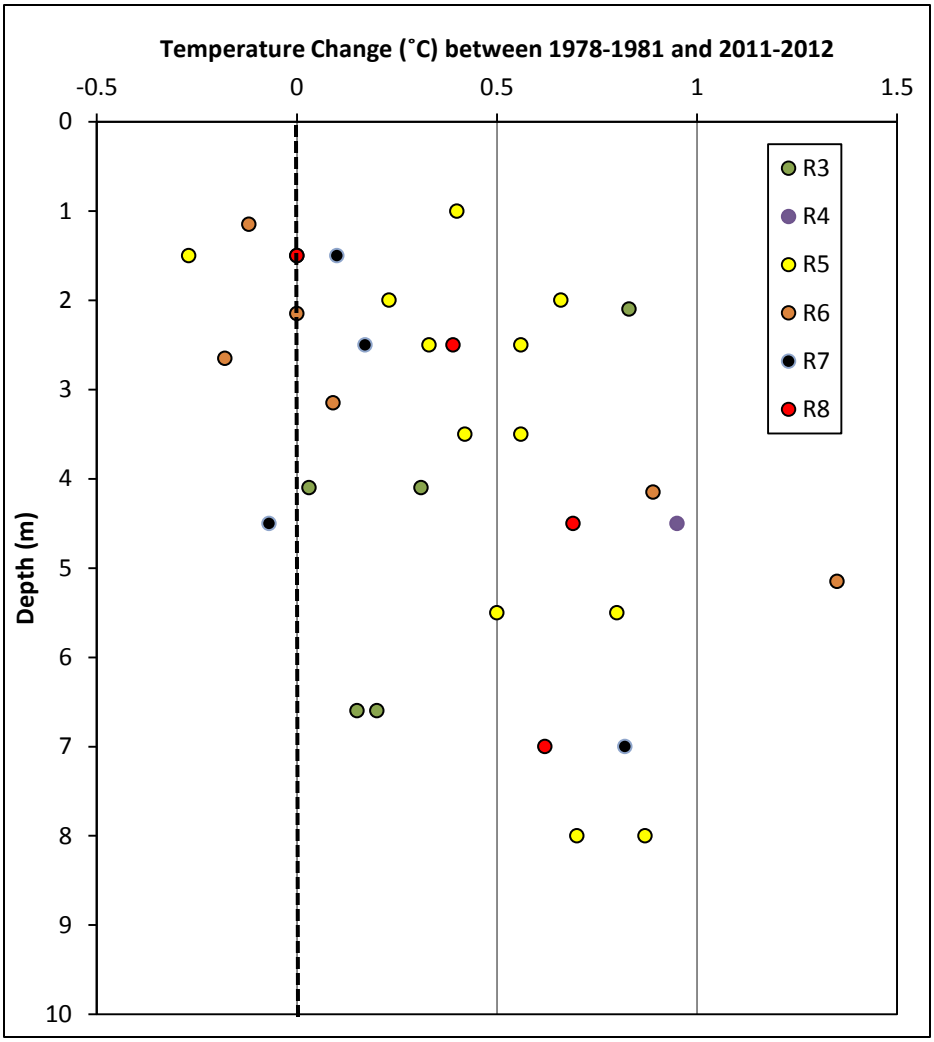

Figure 6.12: Relationship between the temperature change (˚C) between 1978-1981 and 2011-2012 with depth (m) from all the R-boreholes in permafrost.

Climate change and environmental change can explain the observed multi-decadal differences in ground temperatures between 1977-1981 and 2011-2012 (Figures 6.6, 6.7 and 6.8). An abrupt MAAT change occurred in the study area between 1975 and 1976, with an increase of 3.1˚C in Whitehorse, 2.8˚C in Haines Junction and Burwash Landing and, 2.1˚C in Beaver Creek. The observed MAAT regime change in the study area slightly precedes the 1976/1977 Pacific Decadal Oscillation shift from a cool phase to a warm phase (Zhang et al., 1997). The step-like increase in MAAT between 1975 and 1976 may be the main climate change forcing that affected much of the study area as MAATs have subsequently remained fairly stable. The amount of ground warming that may already have resulted from the MAAT change during the initial ground temperature measurements at the time of 1977-1981 is discussed in Section 6.3. Beaver Creek was the only community in the study area to show a statistically significant warming trend post-1976 when subjected to significance testing at a confidence level of 95 %. This significant MAAT increase of about 0.6˚C observed in Beaver Creek from 1980 to 2011 has resulted in one of the biggest ground temperature increases.

The most pronounced ground temperature increases were observed at the three borehole sites with the coldest MAGTs: R5, R6 and R8 (Figures 6.6, 6.7 and 6.8). Although warmer at shallow depths, R7 shows pronounced warming at depth. These sites are located at the northern end of the study area where MAATs are lower and there is less snowfall. Smith et al (2010) and Throop et al (2012) found a similar relationship at permafrost monitoring sites in northern Canada. Temperatures are able to propagate at these sites efficiently because the ground has less unfrozen moisture (French, 2007) when compared to the warmer borehole sites. The lower snow depths reduce buffering of the ground during winter in relation to the cold air temperatures.

The three borehole sites in warm permafrost (R3, R4 and R7; Figures 6.6, 6.7 and 6.8) show less of a ground temperature increase between 1977-1981 and 2011-2012. This is likely because the ground has higher unfrozen moisture contents. The amount of warming decreases due to the requirement of satisfying latent heat as unfrozen moisture increases (Burn, 2012).

Environmental change may also have played an important role in warming ground temperatures at permafrost sites in the study area. All the borehole sites were cleared of vegetation in the late 1970s before drilling, resulting in a reduction of shade and soil moisture supply for evaporation which are two significant site variables that reduce the ground surface

temperature in the summer (Osterkamp and Burn, 2003). The increase in MAAT at all permafrost sites in the study area was probably amplified, causing greater ground temperature rise (see Sections 6.4 and 6.5). Without proper modelling, it's not possible to say which is the more important.

6.3.2 Multi-Decadal Differences in Active Layer Thickness

Significant active layer thickening between August 1978 and August 2012 was observed at all the boreholes in permafrost in the study area (Figure 6.11). The changes were evaluated by comparing the frozen interface in the 1970s borehole logs to the inferred position of the 0˚C isotherm from the temperature measurements in August 2012 (Figure 6.11). The increase in thickening ranges from 6% at borehole R5 to 900% at borehole H2 (Figure 6.11).

The clearing of vegetation for drilling resulted in drainage change and post drilling surface settling and ponding around each borehole which has had a significant effect on active layer thickening. Heat conduction from the exposed black PVC pipes to the ground in summer has also had an important effect on active layer thickness at the borehole. Climate change alone cannot account for these large increases in active layer thickening. Probing results along the ERT surveys at each borehole site shows thinner active layers which support this interpretation. The exposed piping at the ground surface was therefore covered with a removable 4'' ABS cover for protection in summer 2011 which was spray-painted white to increase albedo and lower further energy transfer to the borehole (e.g. Smith et al., 2010; Lewkowicz et al., 2011).

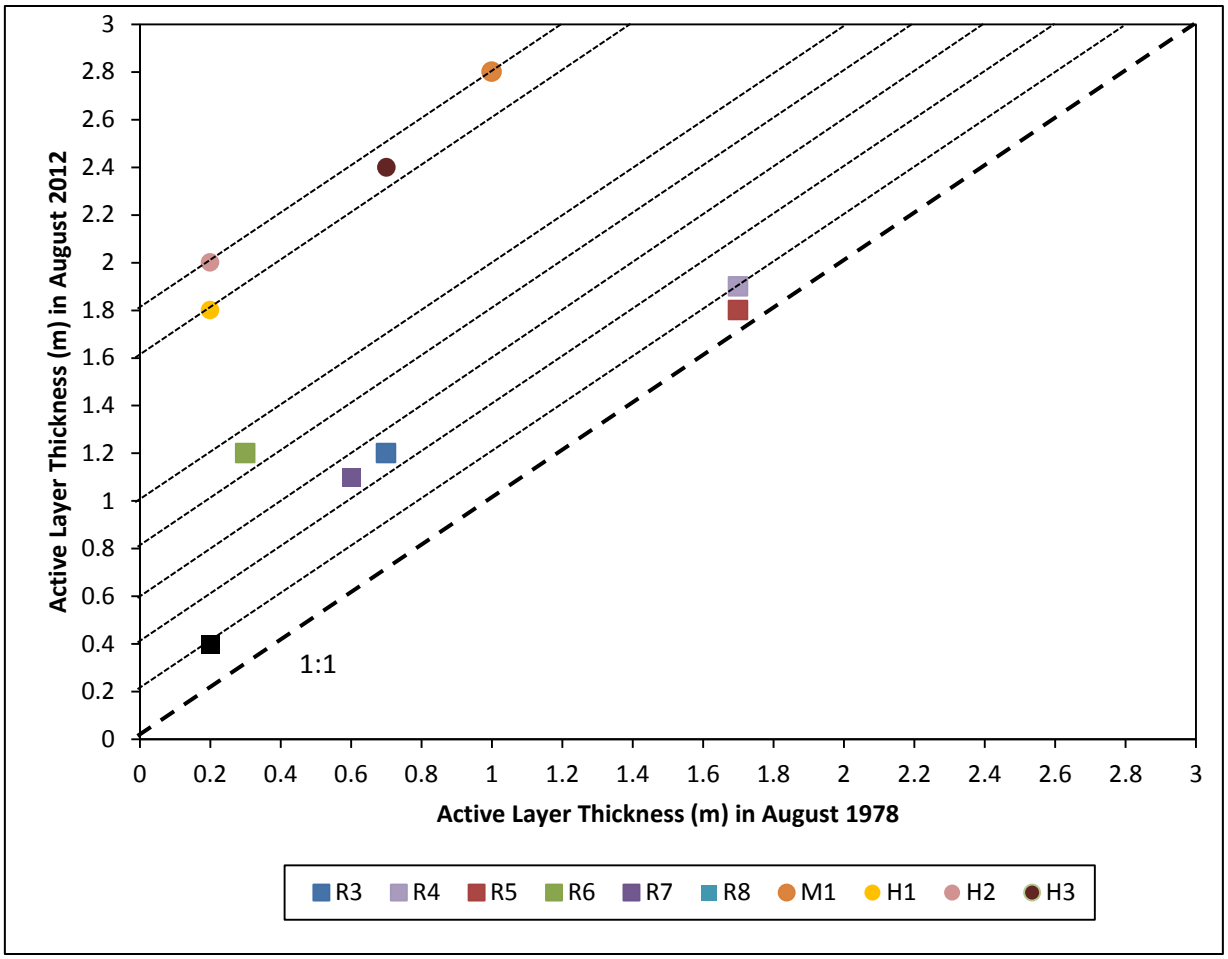

Figure 6.13: Relationship between the active layer thickness in August 1978 and August 2012 from all the boreholes, with the exception of R1 and R2 which are not in permafrost terrain. R-boreholes are represented by a square while the shallower manual temperature and HOBO instrumented boreholes are represented by a circle. Active layers from 1978 are taken from borehole log descriptions while active layers from 2012 were measured by linear interpolation of ground temperature measurements across the 0˚C isotherm. Frost probing depths were used in 2012 when there was a difference of more than 0.2 m with the interpolation results. Frost probing depths greater than the probe are represented as active layer depths of 1.2 m. Note that active layers were not necessarily measured at time of maximum thaw.

6.4 Limitations of the Study

This thesis was based on previously collected data and the re-location and instrumentation of abandoned boreholes to permit multi-decadal analysis of ground temperature change, and as a consequence, several limitations were encountered during the analyses.

1. Available information to relocate the boreholes was limited, making searches long and in many cases unsuccessful.
2. All re-located boreholes in permafrost were blocked by ice and had to be opened using a custom-made portable steaming rig. Finding a successful method to unblock the boreholes took a lot of time, thus limiting the number of boreholes that could be rehabilitated.
3. Some boreholes had collapsed and could not be unblocked.
4. Some borehole sites had not recovered from steaming before the start of thermal monitoring, limiting the length of usable data needed for a full annual record.
5. The equipment used at the sites and the methods of data collection during the initial manual temperature measurements taken between 1977-1981 were outside the control of this study.
6. It is possible that ground temperatures measured in the later years of the 1977-1981 thermal monitoring period may have already experienced warming from the step-like temperature increase of 1975-1976 as the boreholes are shallow.
7. Annual temperature waves were not sinusoidal, making it impossible to carry out original plans of mathematically calculating the thermal diffusivity, amplitude, D_{ZAA} and phase lag with equations 5 to 8 described in Section 2.6.
8. Climate stations could not be installed at each borehole site, limiting the interpretation of site specific air-to-permafrost interactions.
9. RBR logger failure due to animal damage at borehole R4 and logger failure at borehole R8 made it impossible to collect an annual thermal record at these sites.
10. ERT equipment malfunctions in summer 2011 meant that numerous surveys could not be used due to high modelled resistivity errors and that ERT surveys had to be re-done at most borehole sites in summer 2012.

6.5 Uncertainties

The limitations and errors associated with this research may have propagated in the results, causing uncertainties. The most important area of uncertainty is related to the removal of vegetation in the late 1970s during borehole drilling and to the step-like increase in MAAT that was observed in the study area between 1975 and 1975. The effect of these forcings on: 1978-1981 ground temperatures; 2011-2012 ground temperatures and; ground temperature change between 1978-1981 and 2011-2012 is summarized in Eq. (12), Eq. (13) and Eq. (14) respectively, where GT is the ground temperature.

1978-1981 GT = [(pre-1975 GT) + (effect of step like change) + (effect of vegetation clearance)] (12)

2011-2012 GT = [(1978-1981 GT) + (effect of gradual climate warming) + (effect of re-vegetation of site)] (13)

GT change between 1978-1981 and 2011-2012 = [(1978-1981 GT – 1975 GT) + (effect of gradual climate warming – effect of step-like change as of 1978-1981) + (effect of re-vegetation – effect of vegetation clearance)] (14)

The 1978-1981 ground temperatures reflect the cooler pre-1975 ground temperatures, the effect of the step like rise in air temperatures and the effect of vegetation clearance during drilling. However, it is uncertain how the ground temperatures reacted to this abrupt increase in MAAT. The earlier manual ground temperature measurements may still have been affected by the long term cooling trend while the measurements taken in the later years had probably already experienced ground temperature warming from the MAAT increase. The increase in ground temperatures due to climate change were also amplified by the removal of vegetation during borehole drilling.

The 2011-2012 ground temperatures reflect the 1978-1981 ground temperatures, the effects of gradual climate warming after the step-change and the effects of gradual re-vegetation. Vegetation had partially regrown when the most recent temperature measurements were taken in 2011 and 2012. Vegetation cover is an effective buffer in the summer, reducing the solar

radiation reaching the ground surface, consequently causing ground temperatures to be cooler than the air (Smith and Riseborough, 2002). Vegetation also plays an important role in trapping blowing snow in the winter, allowing a thicker snow cover to accumulate in some areas (Smith and Riseborough, 1996). In general, a thicker snowpack restricts heat loss from the ground to a greater extent during the coldest part of the year, thus limiting the magnitude of cooling (Goodrich, 1978; Smith and Riseborough, 2002).

The ground temperature change between 1978-1981 and 2011-2012 is impacted by the amount of change that had already occurred during initial temperature measurements, the aftermath effects of the step-like rise in air temperatures and gradual warming since as well as the relative effect of de-vegetation in the 1970s and re-vegetation since. It is most likely that the original manual ground temperatures had already been affected by warming from the step change in MAAT while re-vegetation has probably reduced the effects of recent warming. Although the degree at which this has affected ground temperatures is uncertain, the temperatures changes are likely less than they would have been had the boreholes been drilled 3 or 4 years earlier. Thus, ground temperature change should be greater under these assumptions. However, these assumptions cannot be properly tested without modelling.

Equilibrium TTOP was calculated in the study area using 5-year TDDa and FDDa means from the Burwash ECCS for the period preceding the 1975 step change, the period following the step change and the most recent period. The nt and nf used are representative values from 221 forested/shrubs monitoring sites in Yukon (Lewkowicz et al, 2012). The lower quartile (nt = 0.7) and upper quartile (nf = 0.5) produce results that are closest to the measured TTOP values and mean ground temperatures at 1 m depth in 2011-2012 in the study area (Table 6.2). Simulating a change in air temperature as the only forcing, the TTOP model shows that the largest change in the TTOP would have been due to the difference in climate between 1971-1975 and 1976-1980 period with an increase of 0.43˚C in the TTOP. This change resulted from the step-like increase in MAAT that occurred in 1975 and accounts for more than 95 % of the overall TTOP change due to only air temperature increase from the early 1970s to the most recent time. However, it appears likely that ground temperatures at or below the depth of zero annual amplitude would not have fully responded to this change by the time of the first set of measurements were made in the late 1970s. Consequently, significant change in ground temperatures took place post-1980

when the TTOP modelling suggests it should have been minimal. Another factor that likely played a role is the site disturbance associated with the initial drilling. This too may have been affecting the initial set of ground temperatures but its effects may not have been complete at the time. Numerical modelling would be needed to examine other variables affecting ground temperature change such as the clearing of vegetation and progressive re-vegetation. However, the results suggest that if climate change is responsible for the ground warming, most of the change can be attributed to the step-like MAAT increase that occurred between 1975-1976. The TTOP modelling indicates that the increase in air temperature between the two dates is not enough to account for the observed differences in ground temperatures.

Table 6.2: TTOP equilibrium model (Wright et al, 2003) using mean n_t and n_f values from 221 forested and shrubs field sites in Yukon (Lewkowicz et al, 2012). TTOP was calculated using Eq. (4). TDDa and FDDa used in the calculation are 5-year means from the period preceding the 1975 step change, the period following the step change and the most recent period using air temperatures from the Burwash ECCS. The Kt/Kf ratio of 0.3 used is for organic soils (Wright et al, 2003). Equilibrium TTOP values in the gray box more closely represent measured TTOP values and ground temperatures at 1 m depth in the study area.

Mean n-factors	$n_f = 0.2$ lower quartile	$n_f = 0.3$ mean	$n_f = 0.5$ upper quartile	Time Period
$n_t = 1.0$ upper quartile	0.55	0.27	-0.29	**1971-1975**
	0.81	0.60	0.17	**1976-1980**
	0.86	0.64	0.21	**2004-2008**
$n_t = 0.85$ mean	0.38	0.10	-0.46	**1971-1975**
	0.63	0.41	-0.01	**1976-1980**
	0.67	0.45	0.02	**2004-2008**
$n_t = 0.7$ lower quartile	0.22	-0.06	-0.62	**1971-1975**
	0.44	0.23	-0.19	**1976-1980**
	0.47	0.26	-0.17	**2004-2008**

Another area of uncertainty that may have propagated in the results is related to human error during the initial manual temperature measurements. Temperature measurements were obtained by manually lowering a single thermistor probe or a multithermistor cable in the borehole and by recording the ground temperatures once stabilized. Errors have resulted if the measurements were recorded before the thermistors reached equilibrium with the ground temperatures. If the multithermistor was not left in the borehole long enough before measurements were taken, higher than true temperatures would have been recorded in the summer while lower than true values would have been recorded in the winter.

6.6 Future Research

This thesis serves as a milestone in the current efforts to extend past and present permafrost monitoring along the Alaska Highway Corridor north of Whitehorse to the Alaskan border. Little work had been done since the late 1970s and early 1980s to understand the permafrost characteristics and geotechnical conditions in this important transportation and transmission corridor. Detailed descriptions of the research sites and methods used should allow this project to grow and thermal monitoring and geotechnical work to continue for future generations of permafrost researchers, thus contributing to the legacy of the International Polar Year.

Recommendations for research to be undertaken in the future include:

1. Continued thermal monitoring of RBR logger borehole sites and shallower HOBO logger borehole sites.
2. Rehabilitating and re-instrumenting the damaged borehole R4.
3. Installation of climate stations at each borehole site to characterise local micro-climates.
4. Installation of permanent ERT arrays for long-term geophysical monitoring and to explore seasonal cycling in electrical resistivities.
5. Conducting longer ERT surveys in an effort to determine the depth of permafrost at the borehole sites.
6. Re-locating, rehabilitating and instrumenting more boreholes from the original 1970s geotechnical drilling program.
7. Drilling new boreholes in areas where old ones cannot be re-located.

SECTION 7: CONCLUSION

7.0 CONCLUSION

The three main findings of this study are as follows:

(1) Permafrost appears to have warmed at 82 % of individual temperature sensors below 1 m depth in boreholes within the study area in 2011-2012 when compared to the same dates in 1977-1981. At permafrost sites alone, warming appears to have occurred at 90 % of measurement points and no negative temperature change was observed below 4.5 m. The ground temperatures from the few sensors indicating lower temperatures in 2011-2012 are in the range of potential error for the initial manual temperature measurements. Ground temperatures that were < 0˚C between 1977-1981 were still < 0˚C on the same dates in 2011-2012, with two exceptions; non-cryotic ground layers between 1977-1981 remain non-cryotic between 2011-2012; and no non-cryotic layers in the 1970s showed cryotic conditions in the most recent measurements. Most of the 1977-1981 manual temperature measurements were cooler than the absolute minimum temperatures measured during the annual thermal monitoring period of 2011-2012. Most sites show an overall ground temperature warming between 0.5-1.0˚C. The greatest warming was at the thawed borehole sites of R1 and R2 and at the cooler permafrost sites of boreholes R5, R6 and R8. Similar warming was observed at the deepest thermistor of borehole R7 while shallower depths did not warm much. The average ground temperature change at the deepest measurement depths for the boreholes in permafrost was 0.9˚C with a maximum change of 1.4˚C at R6 and a minimal change of 0.2˚C at R3. These depths are below or near the DZAA and represent real long-term change. The degree of warming was lower at borehole sites with MAGTs approaching 0˚C, probably because of the use of latent heat to increase unfrozen moisture as part of internal thaw of the permafrost (Burn, 2012).

(2) The ERT surveys showed that significant degradation of permafrost has occurred under the cleared cut-line used for geophysical work in the 1970s. Results indicate deepening of active layer and talik development at warmer permafrost sites and lower resistivity values but still frozen conditions at cooler permafrost sites such as borehole R8, suggesting an increase in unfrozen moisture content. Significant active layer thickening between 1977-

1981 and 2011-2012, ranging from 0.1 m to 1.8 m was also observed in the direct proximity of the boreholes.

(3) MAGTs below 1 m at permafrost sites in the study area range from -0.2˚C to -1.5˚C with permafrost thickness generally greater than 25 m. The absolute range in ground temperatures at depths of 1 m, 3 m and 5 m is greatest at cooler permafrost sites and smallest at permafrost sites with MAGTs near 0˚C. The permafrost at the study sites can be classified as sporadic discontinuous and extensive discontinuous and can probably survive under warmer climatic conditions as long as it remains protected by its ecosystem properties.

Changes in permafrost are attributed to a significant step-like increase in MAAT and the removal of vegetation for drilling in the 1970s. TTOP equilibrium modelling suggests that if climate change is responsible for the ground warming, most of the change can be attributed to this step change in air temperatures. However, the amount of climate change between the two dates is not enough to account for the observed differences in ground temperatures. The step rise occurred between 1975 and 1976 and caused an abrupt MAAT increase of 3.1˚C in Whitehorse, 2.8˚C in Haines Junction and Burwash Landing and, 2.1˚C in Beaver Creek (based on data from Environment Canada climate stations). This represented an important regime change in the study area from a long-term cooling phase to a long-term warming phase. Thereafter, temperatures warmed by 0.6˚C in Whitehorse between 1976-2011, 0.2˚C in Haines Junction between 1993-2006, 0.7˚C in Burwash Landing between 1976-2007 and cooled by 0.6˚C in Otter Falls between 1980-2006. However, these trends were not statistically significant when tested at a 95% confidence level. The only significant post-1976 warming trend was observed in Beaver Creek with a warming of 1.8˚C between 1980-2011, thus explaining one of the greatest ground temperature increases at the study sites. FDDa show high inter-annual variability along the study area while TDDa varies little on an annual basis. These trends indicate that winter is the most variable season spatially and temporally in the study area and the most responsive to recent climate change.

Overall, ground temperatures show limited increase when the 2011-2012 measurements are compared to those from the late 1970s. This is attributed to a combination of limited climate change, especially in the south of the study area, ground temperatures close to 0˚C, and the

gradual re-vegetation of sites. The limited change appears to match rates of ground warming observed elsewhere in northern Canada where permafrost temperatures are relatively warm (Smith et al., 2010). Greater ground warming has been observed further north in the continuous permafrost zone where ground temperatures are much colder and moisture is limited or absent (Throop et al., 2012).

REFERENCES

Anderson, DM., and Morgenstern, NR. (1973). Physics, chemistry and mechanics of frozen ground; A review, in Permafrost, The North American Contribution to the Second International Conference, Yakutsk, U.S.S.R., July 16-23, 1973, Proceedings: Washington, D.C., National Academy of Sciences, p. 257-288.

Anisimov, OA., and Nelson FE. (1997). Permafrost zonation and climate change: Results from transient general circulation models. *Climatic Change* **35**: 241-258.

Arctic Climate Impact Assessment (ACIA). (2005). Impacts of a Warming Arctic: Arctic Climate Impact Assessment. *Cambridge University Press*, Cambridge.

Arctic Monitoring and Assessment Program (AMAP). (2012). Arctic Climate Issues: Changes in Arctic Snow, Water, Ice and Permafrost, SWIPA 2011.

Baranov, IY. (1959). Geographical distribution of seasonally-frozen ground and permafrost. In: General Geocryology. V.A. Obruchev Institute of Permfrost Studies, Academy of Science, Moscow, Part 1, Chapter 7, 193-219. *National Research Council of Canada*, Ottawa, Technical Translation no.1121 (1364).

Bond, J. (2004). Late Wisconsinan McConnell glaciation of the Whitehorse map area (105D), Yukon. *In: Yukon Exploration and Geology 2003*, DS. Emond and LL. Lewis (eds.), Yukon Geological Survey, p. 73-88.

Bonnaventure, PP., and Lewkowicz, AG. (2012). Scenario-based climate change modelling for a regional permafrost probability model of the southern Yukon and northern British Columbia, Canada. *The Cryosphere*, **6**: 4517-4555

Bostock, HS. (1969). Kluane Lake, Yukon Territory; its drainage and allied problems. *Geological Survey of Canada*, Paper 69-28.

Brahney, J. (2007). Paleolimnology of Kluane Lake. *M.Sc. thesis*, Simon Fraser University, Burnaby, BC.

Brown, RJE., and Péwé TL. (1973). Distribution of permafrost in North America and its relationship to the environment: A review, 1963-1973. In Proceedings of the 2nd International Conference on Permafrost, Yakutsk, USSR, North American contribution. *National Academy of Science*, Washington, DC; 71-100.

Brown, RJE. (1978). Influence of climate and terrain on ground temperatures in the Continuous permafrost zone of northern Manitoba and Keewatin District, Canada, in *Proceedings, Third International Conference on Permafrost, July, Edmonton, Canada*. National Research Council of Canada, Ottawa, **1**: 15-21.

Burgess, M. (1982). Analysis of the ground thermal regime at Norman Wells and Fort Good Hope: 1971-1974; *M.Sc. thesis*, Carleton University, Ottawa, Ontario, 153p.

Burgess, MM., Judge, AS., and Taylor, AE. (1982). Yukon Ground Temperature Data Collection 1966 to August 1981; *Energy, Mines and Resources Canada*, Earth Physics Branch Open file **82**-1, E.M.R., Ottawa.

Burn, CR., and Smith, CAS. (1988). Observations of the 'thermal offset' in near-surface mean annual ground temperatures at several sites near Mayo, Yukon Territory, Canada. *Arctic* **41**: 99–104.

Burn, CR. (1991). Permafrost and ground ice conditions reported during recent geotechnical investigations in the Mayo District, Yukon Territory. *Permafrost and Periglacial Processes*, vol. **2**, p. 259-268.

Burn, CR. (1998). The active layer: two contrasting definitions. *Permafrost and Periglacial Processes* **9**: 411-416.

Burn, CR. (2004). The Thermal Regime of Cryosols. In Cryosols: permafrost-affected soils, JM Kimble (ed.). Springer-Verlag Berlin Heidelberg: Berlin, Germany; 391-413.

Burn, CR. (2012). Permafrost distribution and stability, in Changing Cold Environments: A Canadian Perspective, John Wiley and Sons, Ltd, Chichesten, uk. Doi: 10.1002/9781119950172. Ch7

Clague, JJ., Luckman, BH., Van Dorp, RD., Gilbert, R., Froese, D., Jensen, BJL., and Reyes, AV. (2006). Rapid changes in the level of Kluane Lake in Yukon Territory over the last millennium. *Quaternary Research* **66**: 342–355.

Cody, W. (1996). Flora of the Yukon Territory. *National Research Council Press*, Ottawa, Ontario, 643 p.

Christiansen, HH., Etzelmuller, B., Isaksen, K., Juliussen, H., Farbrot, H., Humlum, O,. ohansson, M., Ingeman-Nielsen, T., Kristensen, L., Hjort, J., Holmlund, P., Sannel, ABK., Sigsgaard, C., Åkerman, HJ., Foged, N., Blikra, LH., Pernosky, MA., and Odegård R. (2010). The thermal state of permafrost in the Nordic area during IPY 2007–2009. *Permafrost and Periglacial Processes*, **21**: 156–181.

Desrochers, DT. (1988). An investigation of snow and ground thermal regimes in the Schefferville area, northern Quebec. Ph.D. thesis. Department of Geography, McGill University, Montreal, Quebec.

Desrochers, DT., and Granberg, HB. (1988). Schefterville snow-ground interface temperatures. *In Senneset, K., ed. Permafrost. Fifth InternationaL Conference. Proceedings.* Volume 1. August 2-5, 1988. Trondheim, Tapir Publishers, 67-72.

Duk-Rodkin, A. (1999). Glacial limits map of Yukon Territory. Geological Survey of Canada, Open File 3694, Exploration and Geological Services Division, Yukon Region, Indian and Northern Affairs Canada, Geoscience Map 1999-2, scale 1:1 000 000.

Environment Canada (2012a). *Canadian Climate Data*. http://climate.weatheroffice.gc.ca/climateData/canada_e.html. [November 16, 2012]

Environment Canada (2012b). Canadian Climate Normals or Averages 1971-2000. http://climate.weatheroffice.gc.ca/climate_normals/index_e.html. [November 16, 2012]

French, HM. (2007). The periglacial environment. Third Edition. John Wiley & Sons, Ltd., West Sussex England.

French, HM., and Egorov IE. (1998). 20th century variations in the southern limit of permafrost near Thompson, Northern Manitoba, Canada. In Permafrost: Seventh International Conference, Yellowknife, Canada, Proceedings, Lewkowicz AG, Allard M (eds). Université Laval, Centre d'études nordiques: Quebec. *Nordicana* **55**, 297-304.

Fortier, R., Leblanc, A-M., Wenbing, Y. (2011). Impacts of permafrost degradation on a road embankment at Umiujaq in Nunavik (Quebec), Canada. *Canadian Geotechnical Journal*. **48**: 720-740.

Fortier, R., and Bolduc, M. (2008). Thaw settlement of degrading permafrost: a geohazard affecting the performance of man-made infrastructures at Umiujaq in Nunavik (Quebec). *Proceedings of the 4th Canadian Conference on Geohazrds: From Causes to Management*. Presse de l'Université Laval, Québec, 595 p.

Fuller, T., and Jackson, L. (2009). Quaternary Geology of the Yukon Territory. *Yukon Geological Survey*.

Fulton, RJ. (1989). Quaternary Geology of Canada and Greenland. Ottawa: *Geological Survey of Canada*; 839.

Gabrielse, H., Monger, JWH., Wheeler, JO., and Yorath, CJ. (1991). Part A. Morphogeological belts, tectonic assemblages and terranes, Chapter 2. *In:* Geology of the Cordilleran Orogen in Canada. H. Gabrielse and C.J. Yorath (eds.), *Geological Survey of Canada*, Geology of Canada, **4**: 15-28.

Goodrich, LE. (1978). Some results of a numerical study of ground thermal regimes, in *Proceedings, Third International Conference on Permafrost, July, Edmonton, Canada*. National Research Council of Canada, Ottawa, **1**: 29-34.

Goodrich, LE. (1982). The influence of snow cover on the ground thermal regime. *Canadian Geotechnical Journal* **19**: 421–432.

Gruber, S., King, L., Kohl, T., Herz, T., Haeberli, W., and Hoelzle, M. (2004). Interpretation of geothermal profiles perturbed by topography: the alpine permafrost boreholes at Stockhorn Plateau, Switzerland. *Permafrost and Periglacial Processes*, **15**: 349-357.

Harris, C. and Vonder Mühll, D. (2001): Permafrost and climate in Europe: climate change, mountain permafrost degradation and geotechnical hazard. In Visconti, G., Beniston, M., Iannorelli, E.D. and Barba, D., editors, *Global change in protected areas*. Dordrecht: Kluwer, 71–82.

Hauck, C., and Vonder Mühll, D. (1999): Using DC resistivity tomography to detect and characterise mountain permafrost. *Proceedings of the 61st European Association of Geoscientists and Engineers (EAGE) conference*. 7–11 June 1999, Helsinki, Finland, 2–15.

Hauck, C. (2002). Frozen ground monitoring using DC resistivity tomography. *Geophysical Research Letters* **29** (21).

Hauck C., Mühll, DV., and Maurer, H. (2003). Using DC resistivity tomography to detect and characterize mountain permafrost. *Geophysical Prospecting* **51**: 273-284.

Harris, C., and Vonder Mühll, D. (2001): Permafrost and climate in Europe: climate change, mountain permafrost degradation and geotechnical hazard. In Visconti, G., Beniston, M., Iannorelli, E.D. and Barba, D., editors, *Global change in protected areas*. Dordrecht: Kluwer, 71–82.

Hilbich, C., Hauck , C., Hoelzle, M., Scherler, M., Schudel, L., Völksch, I., Mühll, DV., and Mäusbacher, R. (2008). Monitoring mountain permafrost evolution using electrical resistivity tomography: a 7-year study of seasonal, annual, and long-term variations at Schilthron, Swiss Alps. *Journal of Geophysical Research* **113**: 12 pp.

Hilbich, C., Marescot, L., Hauck, C., Loke, MH., and Mäusbacher, R. (2009). Applicability of electrical resistivity tomography monitoring to coarse blocky and ice-rich permafrost landforms. *Permafrost and Periglacial Processes* **20**: 269-284.

Hilbich, C., Fuss, C., and Hauck, C. (2011). Automated time-lapse ERT for improved process analysis and monitoring of frozen ground, *Permafrost and Periglacial Processes* **22**(4), 306-319, DOI: 10.1002/ppp.732.

Heginbottom JR, Dubreuil MA, Harker PT. (1995). Canada Permafrost. (1:7,500,000 scale). *In The National Atlas of Canada*, 5th Edition, sheet MCR 4177. Ottawa: National Resources Canada.

Hulbert, LJ. (1997). Geology and metallogeny of the Kluane Range mafic-ultramafic belt, Yukon Territory, Canada: Eastern Wrangellia a new Ni-Cu-PGE metallogenic terrane; *Geological Survey of Canada Bulletin* **506**, 265 pp.

International Permafrost Association (IPA). (2011). Permafrost Distribution. Retrieved January 28, 2012 from: http://ipa.arcticportal.org/resources/what-is-permafrost.

IPCC. (2007). Climate Change 2007: Synthesis Report. Contribution of Working Groups I, II and III to the Fourth Assessment Report of the Intergovernmental Panel on Climate Change [Core Writing Team: RK Pachauri and A Reisinger (eds.)]. IPCC, Geneva, Switzerland, 104 pp.

Isaksen, K., Sollid, JL., Holmlund, P., and Harris, C. (2007). Recent warming of mountain permafrost in Svalbard and Scandinavia. *Journal of Geophysical Research*, 112.

Ishikawa, M. (2002). Thermal regimes and the snow-ground interface and their implications for permafrost investigation. *Geomorphology*, **52**: 105-120.

James, M. (2010). Historic change in permafrost distribution in northern British Columbia and southern Yukon Territory, Canada, *M.Sc. Thesis* University of Ottawa, Ottawa.

Jorgenson, MT., Racine, CH., Walters, JC., and Osterkamp, TE. (2001). Permafrost degradation and ecological changes associated with a warming climate in central Alaska. *Climatic Change*, **48**: 551-579.

Jorgenson, MT., Shur, YL., and Pullman, ER. (2006). Abrupt increase in permafrost degradation in Arctic Alaska. *Geophysical Research Letters*, **33**.

Judge, A. (1973). The prediction of Permafrost Thicknesses. *Canadian Geotechnical Journal*, **10**(1): 1-11.

Karunaratne, KC., and Burn, CR. (2003). Freezing n-factors in discontinuous permafrost terrain, Takhini River, Yukon Territory, Canada, in *Proceedings, Eighth International Conference on Permafrost, July 20-25,* Edited by M. Phillips, SM. Springman and LU. Arenson. University of Zurich, Switzerland: 519-524.

Karunaratne, KC. and Burn, CR. (2004). Relations between air and surface temperature in discontinuous permafrost terrain near Mayo, Yukon Territory. *Canadian Journal of Earth Sciences*, **41**: 1437-1451.

Klene, AE., Nelson, FE., Shiklomanov, NI., and Hinkel, KM. (2001). The N-Factor in Natural Landscapes: Variability of Air and Soil-Surface Temperatures, Kuparuk River Basin, Alaska, USA. *Arctic, Antarctic, and Alpine Research*, **33**, 2: 140-148.

Kneisel, C., Hauck, C., Fortier, R., and Moorman, B. (2008). Advances in Geophysical Methods for Permafrost Investigations. *Permafrost and Periglacial Processes* **19**: 157-178.

Kokelj, SV., Pisaric, MFJ., and Burn, CR. (2007). Cessationof ice-wedge development during the 20th century in spruce forests of eastern Mackenzie Delta, Northwest Territories, Canada, *Canadian Journal of Earth Sciences*, **44**: 1503-1515

Kudriavtsev, VA. (1954). The Temperature of Upper Horizons of Permafrost in the USSR. *USSR Academy of Sciences*: Moscow (In Russian).

Kudryavtsev, VA. (Editor). (1978). Obshcheye merzlotovedeniya (Geokriologiya) (General permafrost science) In Russian. Izd. 2, (Edu 2) Moskva (Moscow), Izdatel'stvo Moskovskogo Universiteta, (Moscow University Editions), 404 p.

Kuhry, P., Dorrepaal, E., Hugelius, G., Schuur, EAG., and Tarnocai, C. (2010). Potential remobilization of belowground permafrost carbon under future global warming. *Permafrost and Periglacial Processes* **21**: 208-214.

Kwong, Y.T. and Gan, TY. (1994). Northward migration of permafrost along the Mackenzie highway and climate warming. *Climate Change*, **26**: 399-419.

Ladanyi, B. (1995). Civil engineering concerns of climate warming in the Arctic. *Transactions of the Royal Society of Canada*. **6**, 7-20

Lachenbruch, AH., and Marshall, BV. (1986). Changing Climate: Geothermal Evidence From Permafrost in the Alaskan Arctic. *Science*, **234**: 689-696.

Laxton, NF., Burn, CR., and Smith., CAS. (1996). Productivity of Loessal Grasslands in the K Kluane Lake Region, Yukon Territory, and the Beringian-Production Paradox. *Arctic.* **49:** 2, 129-140.

Laxton, S. and Coates, J., (2011). Geophysical and borehole investigations of permafrost conditions associated with compromised infrastructure in Dawson and Ross River, Yukon. *In*: Yukon Exploration and Geology 2010, K.E. MacFarlane, L.H. Weston and C. Relf (eds.), *Yukon Geological Survey*, p. 135-148.

Lewkowicz, AG. (2008). Evaluation of miniature temperature-loggers to monitor snowpack evolution at mountain permafrost sites, northwestern Canada. *Permafrost and Periglacial Processes* **19**: 323-331.

Lewkowicz, AG., Etzelmuller, B., and Smith, SL. (2011). Characteristics of discontinuous permafrost based on ground temperature measurements and electrical resistivity tomography, southern Yukon, Canada. *Permafrost and Periglacial Processes*, **10**.1002/ppp.703

Lewkowicz, AG., Bonnaventure, PP., Smith, SL., and Kuntz, Z. (2012). Spatial and thermal characteristics of mountain permafrost, Northwest Canada. *Geografiska Annaler*: Series A, Physical Geography **94**(2): 195-213

Lepage, M., and Doré, G. (2010). Experimentation of mitigation techniques to reduce the effects of permafrost degradation on transportation infrastructures at Beaver Creek experimental road site (Alaska Highway, Yukon). 63rd Geotechnical conference, Calgary, Alberta.

Lipovsky, P., (2011). Long term monitoring of glacier dynamics, Lowell Glacier, *Yukon. Annual Progress Report. Yukon Geological Survey (YGS).*

Ling, F., and Zhang, T. (2003). Impact of the timing and duration of seasonal snow cover on the active layer and permafrost in the Alaskan Arctic, Permafrost and Periglacial Processes, **14**: 141-150.

Loke, MH. (1999). Electrical imaging for environmental and engineering studies: A practical guide to 2-D and 3-D surveys, Malaysia.

Loke, MH. (2011). Tutorial: 2-D and 3-D electrical imaging surveys.

MacIntosh, GD. (1997). Palaecology of Scottie Creek District, Beaver Creek, Yukon Territory: Life on the edge. *M.Sc Thesis*, University of Alaska, Fairbanks. 114 pp.

Mackay, JR. (1995). Active layer changes (1968–1993) following the forest-tundra fire near Inuvik, N.W.T. *Arctic and Alpine Research,* **27**: 323–336.

Mathews, WH., (1986). Physiography of the Canadian Cordillera. Geological Survey of Canada, Map 1701A. In: Geology of the Canadian Cordilleran Orogen in Canada. H. Gabrielse and CJ. Yorath (eds.), *Geological Survey of Canada*, Geology of Canada, **4**: 403-418.

Menounos, B., Osborn, G., Clague, JJ., Luckman, BH. (2009). Latest Pleistocene and Holocene glacier fluctuations in western Canada. *Quaternary Science Reviews* **28** (21-22): 2049-2074.

Miceli, C. (2012). Seasonal cycling in electrical resistivity at ten thin permafrost sites, southern Yukon and northern British Columbia. *M.Sc Thesis*, University of Ottawa. 216 pp.

Morse, PD., and Burn, CR. (2010). Ground temperature variation with snow, Kendall Island Bird Sanctuary, outer Mackenzie Delta, Northwest Territories. *GEO2010 conference*, Calgary, Alberta.

Muller, SW. (1943). Permafrost or permanently frozen ground and related engineering problems. *U.S. Engineers Office, Strategic Engineering Study*, Special Report, **62**: 136 p. (Reprinted in 1947, J.W. Edwards, Ann Arbor, Michigan, 231 p.)

Nicholson, FH., and Grandburg, HB. (1973). Permafrost and snowcover relationships near Schefferville, Proc, Second Intern Conf. Permafrost, North American Contribution, *U.S. Nat. Acad. Sc*, Washington, p. 151-158.

Nicholson, FH. (1978). Permafrost distribution and characteristics near Schefferville, Québec, *Proc 3rd Intern. Conf. Permafrost*, vol. **1**, p. 428-433.

NRCan. (2007). "Permafrost." Retrieved November 27, 2012, from http://www.nrcan.gc.ca/earth-sciences/climate-change/landscape-ecosystem/permafrost/230.

Onset Computer Corporation. (2013). "HOBO Micro Station Data Logger – H21-002." Retrieved 28/05/2013, from http://www.onsetcomp.com/products/data-loggers/h21-002.

Osterkamp, TE., and Romanovsky, VE. (1999). Evidence for Warming and Thawing of Discontinuous Permafrost in Alaska. *Permafrost and Periglacial Processes*, **10**: 17-37.

Osterkamp, TE., and Burn CR. (2003). Permafrost. *Elsevier Sciences Ltd*.

Osterkamp, TE. (2005). The recent warming of permafrost in Alaska. *Global and Planetary Change*, **49**: 187-202.

Outcalt, SI., Nelson, FE., and Hinkel, KM. (1990). The Zero-Curtain Effect: Heat and Mass Transfer Across an Isothermal Region in Freezing Soil. *Water Resources Research*, 26, 7: 1509-1516.

PDO INDEX (2013).Updated standardized values for the PDO index, derived as the leading PC of monthly SST anomalies in the North Pacific Ocean, poleward of 20N. Retrieved anuary 18, 2013 from http://jisao.washington.edu/pdo/PDO.latest

Philip, S., and Van Oldenborgh, GJ. (2006). Shifts in ENSO coupling processes under global warming. *Geophysical Research Letters* **33**, 11.

Pihlainen, JA. and Johnston, GH. (1963). Guide to a field description of permafrost for engineering purposes. *National Research Council of Canada, Associate Committee on Soil and Snow Mechanics,* technical memorandum 79.

Pullman, ER., Jorgenson, MT., and Shur, Y. (2007). Thaw Settlement in Soils of the Arctic Coastal Plain, Alaska. *Arctic, Antarctic and Alpine Research*, **39**, 3: 468-476.

Rampton, VN. (1969). Pleistocene geology of the Snag-Klutlan area, southwestern Yukon Territory, Canada. *Ph.D. Thesis,* University of Minnesota, 237 pp.

Rampton, V. (1971). Late Pleistocene Glatiations of the Snag-Klutlan Area, Yukon Territory. *Geological Society of America Bulletin* **82**: 959-978.

Rampton, VN., and Shearer, JM. (1978a). Bottom and sub-bottom conditions at Kluane Lake, Teslin River, and Nisutlin Bay pipe line crossings. Terrain Analysis Mapping Serv, Stittsville

RBR. (2012). "Products." Retrieved 22/11/2012, from http://www.rbr-global.com/products.

Reimchen, D., Doré, G., Fortier, D., Stanley, B., and Walsh, R. (2009). Cost and constructability of permafrost test sections along the alaska highway. In *2009 Annual Conference and Exhibition of the Transportation Association of Canada - Transportation in a Climate of Change*, Vancouver British Columbia.

Richie, JC. (1984). Past and present vegetation of the far northwest of Canada. *University of Toronto Press*, Toronto, Ontario, 251 p.

Riseborough, DW. (1990). Soil latent heat as a filter of the climate signal in permafrost, in *Proceedings, 5th Canadian Permafrost Conference*, Université Laval, Quebec City, Quebec, *Nordicana* **54**: 199-205.

Riseborough, DW., Shiklomanov, N., Etzelmuller, B., Gruber, S., and Marchenko, S. (2008). Recent Advances in Permafrost Modelling. *Permafrost and Periglacial Processes*. **19**: 137-156

Rowe, JS. (1972). Forest regions of Canada. Canadian Forestry Service Publication no. 1300, Publishing Division, Information Canada.

Romanovsky VE., and Osterkamp, TE. (1995). Interannual variations of the thermal regime of the active layer and near surface permafrost in Northern Alaska. *Permafrost and Periglacial Processes* **6**: 313–335.

Romanovsky, VE., Smith, SL., and Christiansen, HH. (2010). Permafrost Thermal State in the Polar Northern Hemisphere during the International Polar Year 2007–2009: a Synthesis. Permafrost and Periglacial Processes, **21**: 106-116.

Sartorelli, AN., and French, RB. (1982) Electromagnetic induction methods for mapping permafrost along northern pipeline corridors. *Proc. 4th Can. Permafrost Conf.*, Nat. Res. Counc. Canada, 283–298

Scudder, GGE. (1997). Environment of the Yukon. Department of Zoology, University of British Columbia.

Shur, YL., and Jorgenson, MT. (2007). Patterns of permafrost formation and degradation in relation to climate and ecosystems. Permafrost and Periglacial Processes **18**(1): 7-19.

Sloan, CE., and van Everdingen, RO. (1988). Region 28, Permafrost region, *in* Black, W., Rosenshein, JS., and Seaber, PR., eds., Hydrogeology: Boulder, Colorado, Geological Society of America, The Geology of North America, v. O-2.

Smith, MW., and Riseborough, DW. (1996). Permafrost monitoring and detection of climate change. *Permafrost and Periglacial Processes* **7**(4): 301-309.

Smith SL., and Burgess M. (1999). Mapping the sensitivity of Canadian permafrost to climate warming. In *Interactions between the cryosphere, climate and greenhouse gases, Birmingham, 18-30 July 1999*. International Association of Hydrological Sciences, Wallingford: UK; 71-78.

Smith, MW., and Riseborough, DW. (2002). Climate and the limits of permafrost: a zonal analysis. *Permafrost and Periglacial Processes* **13**(1): 1-15.

Smith, SL., Burgess, MM., Riseborough, DW., Nixon, FM. (2005). Recent trends from Canadian permafrost thermal monitoring network sites. *Permafrost and Periglacial Processes* **16**:19–30.

Smith, SL., Lewkowicz, AG., and Burn, CR. **(**2008) Thermal state of permafrost in Canada: a contribution to the International Polar Year. In *Ninth International Conference on Permafrost, Extended Abstracts*. Edited by D.L. Kane and K.M. Hinkel. Fairbanks Alaska. Institute of Northern Engineering, University of Alaska Fairbanks, pp. 295-296.

Smith, SL., Romanovsky, VE., Lewkowicz, AG., Burn, CR., Allard, M., Clow, GD., Yoshikawa, K., and Throop, J. (2010). Thermal state of permafrost in North America – A contribution to the International Polar Year, *Permafrost and Periglacial Processes*, **21**: 117-135.

Smith, SL., and Riseborough, DW. (2010). Modellin the thermal reponse of permafrost terrain to right-of-way disturbance and climate warming. Cold Regions Science and Technology, vol. 60, p. 92-103.

Schuur, EAG., Bockheim, J., Canadell, J., Euskirchen, E., Field, CB., Goryachkin, SV., Hagemann, S., Kuhry, P., Lafleur, P., Lee, H., Mazhitova, G., Nelson, FE., Rinke, A., Romanovsky, V., Shiklomanov, N., Tarnocai, C., Venevsky, S., Vogel, JG., and Zimov, SA. (2008). Vulnerability of permafrost carbon to climate change: implications for the global carbon cycle. *Bioscience* **58**: 701–714.

SOI Index (2013). Southern Oscillation Index monthly data 1876-2011. Retrieved January 18, 2013 from http://www.bom.gov.au/climate/current/soihtm1.shtml

Stocks, BJ., Mason, JA., Todd, JB., Bosch, EM., Wotton, BM., Amiro, BD., Flannigan, MD., Hirsch, KG., Logan, KA., Martell, DL., and Skinner, WR. (2002). Large forest fires in Canada, 1959-1997. *Journal of Geophysical Research* **107**: 8149, doi: 10.1029/2001JD000484.

Tarnocai, C., Canadell, JG., Schuur, EAG., Kuhry, P., Mazhitova, G., and Zimov, S. (2009). Soil organic carbon pools in the northern circumpolar permafrost region. *Global Biogeochemical Cycles* **23**: GB2023.

Taylor, AE. (1995). Field measurements of n-factors for natural forest areas, Mackenzie Valley, Northwest Territories, in *Current Research 1995-B, Geological Survey of Canada*: 89-98.

Taylor, AE., Burgess, MM., Judge, AS., and Allen, VS. (2000). Deep Ground Temperatures, in The Physical Environment of the Mackenzie Valley, Northwest Territories: a Baseline for the Assessment of Environmental Change, Edited by L.D. Dyke and G.R. Brooks. *Geological Survey of Canada, Bulletin* **547:** 105-109.

Throop, J., Lewkowicz, AG., et al. (2012). Climate and ground temperature relations at sites across the continuous and discontinuous permafrost zones, northern Canada. *Canadian Journal of Earth Sciences,* **49**(8): 865-875.

United Nations Environment Programme (UNEP). (2007). *Global Outlook for Snow and Ice*.

Van Everdingen, RO. (1978). Frost mounds at Bear Rock, near Fort Norman, N.W.T., 1975-1976. *Canadian Journal of Earth Sciences*, **15**(2): 263-276.

Vonder Mühll, D., Hauck, C. and Lehmann, F. (2000). Verification of geophysical models in Alpine permafrost by borehole information. *Annals of Glaciology* **31**, 300–306.

Vonder Mühll, D., Hauck, C., and Gubler, H. (2002). Mapping of mountain permafrost using geophysical methods. *Progress in Physical Geography* **26** (4): 643-660.

Wahl, HE., Fraser, DB., Harvey, RC., and Maxwell, JB. (1987). Climate of Yukon. *Environment Canada*, Ottawa; 1-321.

Williams, PJ. and Smith, MW. (1989). *The Frozen Earth: Fundamentals of Geocryology*. New York: Cambridge University Press.

Woo, M., Mollinga, M., and Smith, SL. (2007). Climate warming and active layer thaw in the boreal and tundra environments of the Mackenzie Valley. *Canadian Journal of Earth Sciences*, **44**: 733-743.

Wright, JF., Duchesne, C., and Côté, MM. (2003). Regional-scale Permafrost Mapping using the TTOP Ground Temperature Model. *Proceedings Eighth International Conference on Permafrost*: 1241-1246.

Wu, Q., Liu, Y., Zhang, J., and Tang, C. (2002). A Review of Recent Frozen Soil Engineering in Permafrost Regions along Qinghai-Tibet Highway, China*, Permafrost and Periglacial Processes* **13**: 199–205.

Yoshikawa K, Bolton WR, Romanovsky VE, Fukuda M, Hinzman LD. (2002). Impacts of wildfire on permafrost in the boreal forests of Interior Alaska. *Journal of Geophysical Research* **108**: 8148, doi:10.1029/2001JD000438.

Yukon Weather Centre Report. (2010). Internal Report YWC-10-110: *Climate Change in the Yukon*, Updated Observations.

Zhang, Y., Wallace, JM., and Battisti, BS. (1997). ENSO-like interdecadal variability: 1900-93. J. Climate, 10, 1004-1020.

Zoltai, SC. (1971) Southern limit of permafrost features in peat landforms, Manitoba and Saskatchewan. *Geological Association of Canada special paper*, **9**, 305310.

APPENDICES: Metadata for Appendices A-K

Appendix A: Site Locations and Dates of Investigation

Site Name

The original boreholes were drilled between 1978-1981 during an intensive geotechnical borehole drilling program and acquired by the Geological Survey of Canada (Burgess et al., 1982). The site names were changed in this thesis because this project is unique to university and government research and is not associated with the pipeline. "R" in the site name refers to deeper borehole sites (5 m to 8.75 m) where RBR loggers were installed, "H" refers to shallow borehole sites (2 m to 3.75 m) where HOBO Micro Station loggers were installed and "M" refers to a shallow borehole where only manual temperature measurements were taken. Boreholes are numbered sequentially from Whitehorse in the south-east to Beaver Creek in the north-west.

UTM Coordinates

The Zone, Easting and Northing fields make up the UTM coordinates (WGS 84 datum) of the sites we investigated. The UTM coordinates were taken with a Garmin eTrex Vista Cx with an accuracy ranging from ± 3 m to ± 15 m (Garmin, 2006). However, the upper end of the accuracy range should be considered more likely as the forest cover causes significant difficulty in satellite signals reaching the handheld GPS unit.

Date of Investigation

The dates of investigation are the dates that site investigation and/or field work took place in summer 2011 and 2012, in the format mm/dd/yy. All sites were visited multiple times during both field seasons.

Purpose

The purpose is the reason of site investigation and lists the field work that was conducted on any given date of investigation. This is elaborated in details in the methods section.

Appendix B: Time since Drilling Disturbance

The time since drilling in the 1970s was determined by counting the number of days between borehole drilling and manual temperature measurements. In some cases, only the month was given for the drilling date. The time since drilling disturbance in the 1970s and initial temperature measurements ranged from 63 days to more than 2 years. The time since borehole steaming and the start of logging in 2011 ranged from 1 day to 339 days. Site vegetation descriptions from the late 1970s and from 2011-2012 are also shown.

Appendix C: RBR and HOBO Logger Information

Borehole

The borehole names range from R1 to R8 where RBR loggers were installed in 2011 and from H1 to H3 where HOBO H21-002 Micro Station Loggers were installed in 2012.

Cable

This is the original thermistor cable length for RBR loggers before it was folded or cut. Lengths are either 10 m or 12m.

RBR Logger information

Information is given on the full name of the 8 RBR loggers, the serial number of the logger as well as the logger time/date, the start of logging and the end of logging. The sample period is 8:00 h for all loggers. Note that some of the loggers started logging before they were installed in the field. Dates of installation can be found in Appendix A. Individual borehole thermistor depths are also given with additional site specific details.

HOBO H21-002 Micro Station Logger information

Information is given on the full name of the 3 HOBO loggers, the serial number of the logger as well as the logger time/date, the start of logging and the end of logging. The sample period is 4:00 h for all loggers. Dates of installation can be found in Appendix A. Individual borehole thermistor depths and individual serial numbers are also given with additional site specific details. Note that borehole M1 was not instrumented with a HOBO logger.

Appendix D: Manual Ground Resistance Measurements and Temperature Conversions

Manual temperature measurements were made during summer 2011 at 4 shallow (2.0 m to 3.75 m) rehabilitated boreholes as described in Section 4. Original thermistor resistances (KOhm) at one minute intervals are given for 15 minutes for all depths below surface at 0.5 m increments. Temperatures were obtained using the following equation for the YSI thermistor: y= -0.0214x3 + 0.6809x2 - 9.1992x +39.347 (Accurate to ±0.02 for -5ºC to +7ºC). The degrees Celsius conversions are also given at one minute intervals for 15 minutes for all depths below surface at 0.5 m increments. Extrapolated equilibrium (30 minutes) temperatures are given for all depths as well as their specific logarithmic trend line equation. The forecasted ground temperatures at 30 minutes were used in Section 5.3. Manual ground temperature measurement information is given from borehole M1 to borehole H3 from a south-east to a north-west orientation along the study area.

Appendix E: Statistical Testing of Long-term Climate Data

Significant tests results (confidence limit of 95%) for 5-year running means are given for historical MAAT, total annual rainfall, total annual snowfall and total annual precipitation at Environment Canada weather stations in the study area. Records used for statistical testing include all available measurements taken before 1975 and all available measurements taken after 1975. The weather stations include; Whitehorse, Haines Junction, Otter Falls, Burwash and Beaver Creek. Significance test results given in the tables are; n (sample sizes), R^2 (coefficients of determination), slope coefficients, standard error of slope and the P-values.

Appendix F: RBR Instrumented Boreholes Original Temperature Measurements

This is the original 1978-1981 temperature measurements for the 8 RBR loggers installed boreholes (R1-R8) taken from the Yukon Ground Temperature Data Collection of the Earth Physics Branch, Energy, Mines and Resources Canada Open File 82-1 (Burgess et al., 1982). A summary of all depth-temperature logs is given for each borehole as well as drilling and manual temperature logging information. Original borehole names are used from a south-east to a north-west transect along the study area (79S-CS-5 (R1) to 78-A-8 (R8)).

Appendix G: HOBO Instrumented Boreholes Original Temperature Measurements

This is the original 1978-1981 temperature measurements for the shallower HOBO instrumented boreholes (M1-H3) taken from the Yukon Ground Temperature Data Collection of the Earth Physics Branch, Energy, Mines and Resources Canada Open File 82-1 (Burgess et al., 1982). Temperature measurements were not measured at borehole M1 and H1 during the 1970s. A summary of all depth-temperature logs is given for both borehole 78-B-25 (H2) and 78-A-39 (H3) as well as drilling and manual temperature logging information.

Appendix H: ERT Acquirement Settings

This is the acquirement settings used for the ERT surveys conducted in 2011 and 2012.

Appendix I: RBR Installed Boreholes Resistivity Pseudosections

Measured apparent resistivity pseudosections, calculated resistivity pseudosections and inverse resistivity sections are given for each the 8 RBR installed borehole field sites. ERT survey lengths are 160 m except borehole R1 which is 80 m in length and borehole R7 where a 40 m survey was also conducted to compliment the 160 m survey. The resistivity pseudosections are given from borehole R1 to borehole R8.

Appendix J: HOBO Installed Boreholes Resistivity Pseudosections

Measured apparent resistivity pseudosections, calculated resistivity pseudosections and inverse resistivity sections are given for each of the 4 shallower boreholes. Two 80 m ERT surveys were performed in cross-section with the borehole at the mid-point except for borehole H3 where only one 80 m survey was done. The resistivity pseudosections are given from borehole M1 to borehole H3.

Appendix K: 1970s Borehole Logs

These are the original borehole logs from the 1978-1981 geotechnical borehole drilling program which have been modified from the digital database. Information provided includes location, terrain type, sample-soil and ground ice information for all 8 RBR installed boreholes and for the 4 shallower boreholes. These logs were used in the interpretation of the ERT surveys in Section 5.

Terrain Type: These tables contain information on terrain type using notations from the Rampton System as described in Figure AP1:

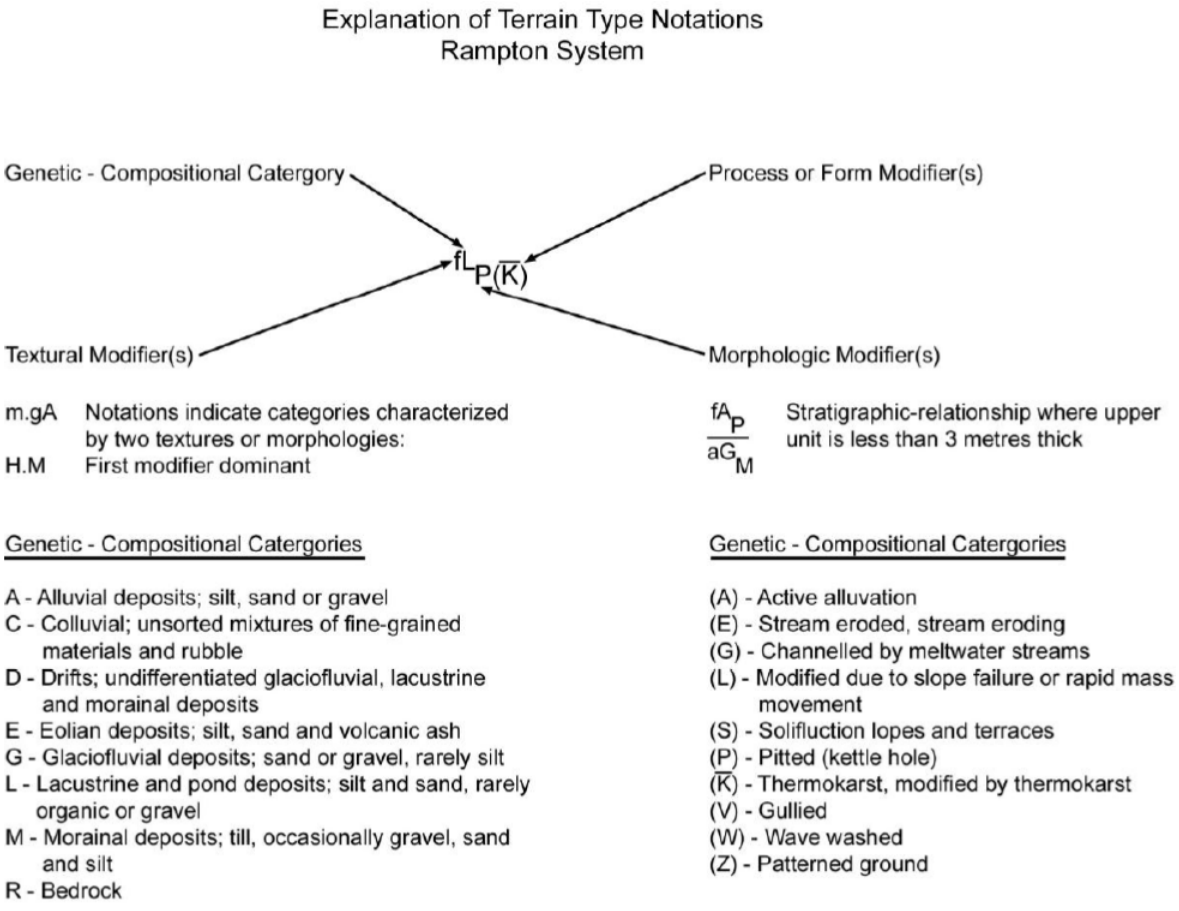

Figure AP 1: Explanation of terrain type notations from the Rampton System.

***Sample-Soil**:* These tables provides information on the borehole lithology.

Borehole – Original borehole name.

Top (m) - The depth of the top of the unit/interval for which the description applies.

Bottom (m) - The depth of the bottom of the unit/interval for which the description applies.

Soil Type - The material type.

Descriptions - The soil description for each unit/interval.

USC - Unified Soils Classification (USC) System code for the unit/interval (see Figure AP2). The code assignment is based on the information provided in the soil type and soil description fields.

Comments - Additional comments/description related to the unit/interval.

Ground Ice: These tables contains information on ground ice and permafrost characteristics.

Borehole – Original borehole name.

Record Seq - The position of the sample in the sequence.

Per Ice (%) - Estimate of the percentage of visible ice by volume.

Gr Ice Des - Ground ice description using coded classification based on Pihlainen and Johnston (1963). (Table AP1).

Fine-grained soils (more than half of material is smaller than #200 sieve size)	Silts and clays (liquid limit <50)		ML	Inorganic silts and very fine sands, rock flour silty sands of slight plasticity
			CL* W_L<30	Inorganic clays of low plasticity, gravelly, sandy, or silty clays, lean clays
			CI* 30<W_L<50	Inorganic clays of medium plasticity silty clays
			OL	Organic silts and organic silty clays of low plasticity
	Silts and clays (liquid limit >50)		MH	Inorganic silts, micaceous or diatomaceous, fine sandy or silty soils
			CH	Inorganic clays of high plasticity
			OH	Organic clays of high plasticity
	Highly organic soils		Pt	Peat and other highly organic soils
Major Divisions			Group Symbol	Typical names
Coarse-grained soils (more than half of material is larger than #200 sieve size)	Gravels (more than half of coarse fraction is larger than #4 sieve size)	Clean Gravels	GW	Well graded gravels, gravel-sand mixtures, <5% fines
			GP	Poorly graded gravels, gravel-sand mixtures, <5% fines
		Dirty Gravels	GM	Silty gravels, gravel-sand- silt mixtures >12%fines
			GC	Clayey gravels, gravel-sand-clay mixtures, >12% fines
	Sands (more than half of coarse fraction is smaller than #4 sieve size)	Clean Sands	SW	Well-graded sands, gravelly sands, <5% fines
			SP	Poorly-graded sands, or gravelly sands, <5% fines
		Dirty Sands	SM	Silty sands, sand-silt mixtures, >12% fines
			SC	Clayey sands, sand-clay mixtures, >12% fines

Figure AP2: Modified Unified Soil Classification (USC).

Table AP1: Ground ice description using coded classification based on Pihlainen and Johnston (1963).

Code	Ground Ice Description
Unfrozen	Material not frozen
Frozen	Material frozen - type unknown
FX	Material partially frozen - type unknown
N	Ice not visible
NF	Ice not visible - poorly bonded
NB	Ice not visible - well bonded
NBN	Ice not visible - well bonded - no excess ice
NBE	Ice not visible - well bonded - excess ice
V	Visible ice
VX	Visible ice - individual ice crystals or inclusions
VC	Visible ice - ice coating on particles
VR	Visible ice - random or irregular orientations
VS	Visible ice - stratified or oriented ice
ICE	Ice
Blank Space	Permafrost not recorded

Appendix A: Site Locations and Dates of Investigation

Table A1: Site information including GPS location, dates of investigation in 2011 and purpose of field visit (field work executed).

UTM Coordinates				Dates of investigation 2011	Purpose (Field Work Executed)
Site	Zone	Easting	Northing		
R1	08 V	448575	6740775	06/01/11 06/10/11 08/24/11 08/24/11 08/25/11	Borehole exploration DC Resistivity surveys (2x 80m) Borehole cased RBR Logger installed Fetched live RBR logger readings
R2	08 V	344168	6756453	05/30/11 06/30/11 06/30/11 08/14/11 08/15/11	Borehole exploration DC Resistivity surveys (2x 80m) Borehole cased RBR logger installed Fetched live RBR logger readings
R3	07 V	619134	6791170	06/02/11 08/16/11 08/16/11 08/16/11 08/28/11	Borehole exploration Borehole steaming Borehole cased RBR logger installed Fetched live RBR logger readings
R4	07 V	618414	6791821	06/02/11 08/19/11 08/19/11 08/24/11 08/28/11	Borehole exploration Borehole steaming Borehole cased RBR logger installed Fetched live RBR logger readings
R5	07 V	615815	6794364	06/02/11 08/17/11 08/19/11 08/19/11 08/24/11 08/28/11	Borehole exploration Borehole steaming Borehole steaming Borehole cased RBR logger installed Fetched live RBR logger readings
M1	07 V	596792	6809845	06/05/11 06/29/11 06/29/11 06/29/11 08/17/11	Borehole exploration Borehole steaming Borehole cased DC resistivity surveys (2x 80m) Manual temperature measurements
R6	07 V	589237	6820212	06/05/11 06/21/11 06/21/11 06/21/11 08/05/11 08/14/11	Borehole exploration Borehole steaming Borehole cased DC resistivity surveys (2x 80m) RBR logger installed Fetched live RBR logger readings

M2	07 V	581690	6829725	06/05/11 06/06/11 06/28/11 06/28/11 06/28/11 06/28/11 08/19/11	Borehole exploration Borehole exploration Borehole exploration Steaming/W-J-D Borehole cased DC resistivity surveys (2x 80m) Manual temperature measurements
M3	07 V	567345	6838370	06/05/11 06/25/11 06/25/11 06/26/11 06/26/11 08/21/11	Borehole exploration Borehole steaming DC resistivity surveys (2x 80m) W-J-D Borehole cased Manual temperature measurements
R7	07 V	561434	6842744	06/05/11 06/23/11 06/24/11 06/24/11 06/25/11 08/05/11 08/21/11 08/15/11	Borehole exploration Borehole steaming DC resistivity surveys (80m and 40m) Borehole steaming Borehole cased RBR logger installed Fetched live RBR logger readings Weather station installed
M4	07 V	561291	6842827	06/05/11 06/23/11 06/23/11 06/23/11 08/21/11	Borehole exploration Borehole steaming DC resistivity surveys (80m and 40m) Borehole cased Manual Temperature measurements
R8	07 V	512065	6906566	06/17/11 06/18/11 08/20/11 08/20/11 08/20/11	Borehole exploration Borehole steaming Borehole steaming Borehole cased RBR logger installed

Table A2: Site information including GPS location, dates of investigation in 2012 and purpose of field visit (field work executed).

UTM Coordinates				Dates of investigation 2012	Purpose (Field Work Executed)
Site	**Zone**	**Easting**	**Northing**		
R1	08 V	448575	6740775	06/04/12 08/21/12	Borehole RBR logger downloaded Borehole RBR logger downloaded
R2	08 V	344168	6756453	06/04/12 08/07/12 08/31/12	Borehole RBR logger downloaded DC resistivity survey (160 m) Borehole RBR logger downloaded
R3	07 V	619134	6791170	06/04/12 08/08/12 08/17/12	Borehole RBR logger downloaded DC resistivity survey (160 m) Borehole RBR logger downloaded

R4	07 V	618414	6791821	06/05/12 08/07/12	Borehole RBR logger downloaded (borehole was destroyed by a Bear and could not be fixed) DC resistivity survey (160 m)
R5	07 V	615815	6794364	06/05/12 08/08/12 08/20/12	Borehole RBR logger downloaded DC resistivity survey (160 m) Borehole RBR logger downloaded
M1	07 V	596792	6809845	08/16/12 08/16/12 08/17/12	Borehole instrumented with a HOBO Micro Station Frost Probing Fetched live HOBO Micro Station readings
R6	07 V	589237	6820212	06/05/12 08/06/12 08/17/12	Borehole RBR logger downloaded DC resistivity survey (160 m) Borehole RBR logger downloaded
M2	07 V	581690	6829725	08/16/12 08/16/12 08/17/12	Borehole instrumented with a HOBO Micro Station Frost Probing Fetched live HOBO Micro Station readings
M3	07 V	567345	6838370	08/16/12 08/16/12 08/17/12	Borehole instrumented with a HOBO Micro Station Frost Probing Fetched live HOBO Micro Station readings
R7	07 V	561434	6842744	06/06/12 06/06/12 08/05/12 08/16/12 08/16/12	Borehole RBR logger downloaded Weather station downloaded DC resistivity survey (160 m) Borehole RBR logger downloaded Weather station downloaded
M4	07 V	561291	6842827	08/16/12 08/16/12 08/17/12	Borehole instrumented with a HOBO Micro Station Frost Probing Fetched live HOBO Micro Station readings
R8	07 V	512065	6906566	06/06/12 06/06/12 08/05/12	Borehole RBR logger download failed RBR logger replaced and launched DC resistivity survey (160 m)

Appendix B: Time since Drilling Disturbance

Table B1: Time since drilling disturbance and ground temperature measurements for boreholes R1-R8. Vegetation changes since initial drilling disturbance in the 1970s are also described.

BH Site	1970s Borehole Drilling	1970s Manual Temperature Measurements Available	Time Since Drilling	Site Vegetation
R1	August 8-9, 1979	October 10, 1979; February 1, 1980; April 28, 1980; August 7, 1980; July 30, 1981	63 days; 176 days; 235 days; 385 days; 722 days	Already bared and exposed
R2	August 1978	November 26, 1978	At least 87 days	Cleared before drilling
R3	August 20, 1978	November 22, 1978; July 26, 1979	94 days; 340 days	Cleared before drilling
R4	August 1978	November 22, 1978	At least 83 days	Cleared before drilling
R5	August 19. 1978	November 22, 1978; July 26, 1979	95 days; 348 days	Cleared before drilling
R6	August 1978	November 23, 1978	At least 84 days	Cleared before drilling
R7	August 1978	November 23, 1978	At least 84 days	Cleared before drilling
R8	August 5, 1978	November 25, 1978; July 25, 1979	110 days; 355 days	Cleared before drilling
BH Site	**2011 Borehole Steaming**	**2011 start of Temperature logging**	**Time Since Steaming**	**Site Vegetation**
R1	Not steamed	August 24, 2011	Not steamed	Bared and exposed
R2	Not steamed	August 15, 2011	Not steamed	Exposed with scattered shrubs
R3	August 16, 2011	August 17, 2011	1 day	Regrown with shrubs and small spruce trees
R4	August 19, 2011	September 5, 2011	17 days	Regrown with shrubs and small spruce trees
R5	August 19, 2011	August 25, 2011	6 days	Clearance with shrubs and small spruce trees
R6	June 21, 2011	August 15, 2011	55 days	Clearance with shrubs and small spruce trees
R7	June 24, 2011	August 15, 2011	51 days	Regrown with spruce and birch
R8	August 20, 2011	July 25, 2012	339 days	Clearance with shrubs and small spruce trees

Appendix C: RBR and HOBO Loggers Information

Table C1: RBR Logger Information

Borehole	Cable	RBR Logger Information
R1	12m	**Logger:** RBR XR-420-T8 5.40 SERIAL # 012060 **Logger time/date:** 2011/Aug/24 16:35 **Start of Logging:** 2011/Aug/15 04:00 **End of Logging:** 2015/Dec/31 12:00 **Sampling period (h):** 8:00 **Depth of Thermistors (m):** 0.5 (air); 0; 0.5; 1.0; 2.0; 4.0; 6.5 **Notes:** Cable was cut below 6.5 m thermistor and tapped.
R2	10m	**Logger:** RBR XR-420-T8 5.61 SERIAL # 012401 **Logger time/date:** 2011/Aug/14 15:55 **Start of Logging:** 2011/Aug/14 16:00 **End of Logging:** 2013/Dec/31 12:00 **Sampling period (h):** 8:00 **Depth of Thermistors (m):** 0.75 (air); 0.25 (air); 0.25; 0.75; 1.75; 3.75; 6.25; 8.75 **Notes:** Thermistor at 6.25 m does not work.
R3	10m	**Logger:** RBR XR-T8 6.21 SERIAL # 014037 **Logger time/date:** 2011/Aug/16 14:43 **Start of Logging:** 2011/Aug/16 16:00 **End of Logging:** 2014/Dec/31 12:00 **Sampling period (h):** 8:00 **Depth of Thermistors (m):** 0.40 (air); 0.1; 0.6; 1.1; 2.1; 4.1; 6.6 **Notes:** Cable was cut below 6.6 m thermistor and tapped.
R4	12m	**Logger:** RBR XR-420-T8 5.61 SERIAL # 012403 **Logger time/date:** 2011/Aug/24 10:39 **Start of Logging:** 2011/Aug/15 04:00 **End of Logging:** 2015/Dec/31 12:00 **Sampling period (h):** 8:00 **Depth of Thermistors (m):** 0; 0.5; 1.0; 1.5; 2.5; 4.5; 5.0 **Notes:** Thermistor 7 (7.0 m) was folded back and tapped at 5.0 m and the cable was cut right below thermistor 7.
R5	12m	**Logger:** RBR XR-420 5.61 SERIAL # 013102 **Logger time/date:** 2011/Aug/24 11:44 **Start of Logging:** 2011/Aug/15 04:00 **End of Logging:** 2015/Dec/31 **Sampling period (h):** 8:00 **Depth of Thermistors (m):** 1.0; 1.5; 2.0; 2.5; 3.5; 5.5; 8.0 **Notes:** Thermistor 1 starts at 1.0 m to permit deeper readings. Cable was cut right below thermistor 7 (8.0 m). A puck logger (SERIAL # 975396) was installed with sensors at the ground surface (0 m) and 0.5 m on August 28, 2011. The logger failed and data could not be downloaded in August 2012.

R6	10m	**Logger:** RBR XR-T8 5.61 SERIAL # 014080 **Logger time/date:** 2011/Aug/5 12:40 **Start of Logging:** 2011/Aug/1 04:00 **End of Logging:** 2015/Dec/31 12:00 **Sampling period (h):** 8:00 **Depth of Thermistors (m):** 0.65; 1.15; 1.65; 2.15; 2.65; 3.15; 4.15; 5.15 **Notes:** Thermistors 7 and 8 were folded back. Thermistors at 1.65 m and 2.65 m failed on May 10, 2012.
R7	10m	**Logger:** RBR XR-420-T8 6.21 SERIAL # 013124 **Logger time/date:** 2011/Aug/06 16:08 **Start of Logging:** 2011/Aug/01 04:00 **End of Logging:** 2014/Dec/31 12:00 **Sampling period (h):** 8:00 **Depth of Thermistors (m):** 0; 0.5; 1.0; 1.5; 2.5; 4.5; 7.0 **Notes:** Cable was cut right after thermistor 7 (7.0 m) and tapped**.**
R8	12m	**Logger:** RBR XR-420-T8 5.61 SERIAL #: 013101 **Logger time/date:** 2011/Aug/20 14:50 **Start of Logging:** 2011/Aug/1 4:00 **End of Logging:** 2014/Dec/31 12:00 **Sampling period (h):** 8:00 **Depth of Thermistors (m):** 0.15; 0.65; 1.15; 1.65; 2.65; 4.65; 7.15 **Notes:** Cable was cut right after thermistor 7 (7.0 m) and tapped.

Table C2: HOBO Micro Station Logger Information

Borehole	HOBO H21-002 Micro Station Logger Information
M1	No logger installed
H1	**Logger:** HOBO H21-002 Micro Station SERIAL # 10068300 **Logger time/date:** 2012/Aug/16 13:53 **Start of Logging:** 2012/Aug/16 15:00 **End of Logging:** 2014/Dec/31 12:00 **Sampling period (h):** 4 **Depth of Thermistors (m):** 0.5 m (thermistor # 10067001); 1.0 m (thermistor # 10067004); 1.75 m (thermistor # 10067006); 2.87 (thermistor # 10067011). **Notes:** Each thermistor is connected to an individual cable for a total of 4 cables.
H2	**Logger:** HOBO H21-002 Micro Station SERIAL # 10068301 **Logger time/date:** 2012/Aug/16 16:25 **Start of Logging:** 2012/Aug/16 18:00 **End of Logging:** 2014/Dec/31 12:00 **Sampling period (h):** 4 **Depth of Thermistors (m):** 0.5 m (thermistor # 10066996); 1.0 m (thermistor # 10066998); 1.5 m (thermistor # 10067003); 2.0 (thermistor # 10067007). **Notes:** Each thermistor is connected to an individual cable for a total of 4 cables.
H3	**Logger:** HOBO H21-002 Micro Station SERIAL # 10068304 **Logger time/date:** 2012/Aug/16 17:43 **Start of Logging:** 2012/Aug/16 18:00 **End of Logging:** 2014/Dec/31 12:00 **Sampling period (h):** 4 **Depth of Thermistors (m):** 0.5 m (thermistor # 10066995); 1.0 m (thermistor # 10067005); 1.75 m (thermistor # 10067008); 2.39 (thermistor # 10070207). **Notes:** Each thermistor is connected to an individual cable for a total of 4 cables.

Appendix D: Manual Ground Resistance Measurements and Temperature Conversions

Table D1: Manual ground resistance measurements (KOhm) at borehole M1 on August 17, 2011.

Site	Depth below surface (m)	Ground Resistivity (KOhm) at one minute intervals				
		1	2	3	4	5
M1	0	6.23	6.37	6.42	6.43	6.43
M1	0.5	6.5	6.59	6.58	6.57	6.57
M1	1.0	6.58	6.6	6.62	6.62	6.62
M1	1.5	6.72	6.74	6.76	6.75	6.75
M1	2.5	6.85	6.88	6.9	6.92	6.93
M1	2.8	7.25	7.29	7.3	7.32	7.33
Site	**Depth below surface (m)**	**Ground Resistivity (KOhm) at one minute intervals**				
		6	**7**	**8**	**9**	**10**
M1	0	6.43	6.43	6.43	6.43	6.43
M1	0.5	6.57	6.57	6.57	6.57	6.57
M1	1.0	6.62	6.62	6.62	6.62	6.62
M1	1.5	6.75	6.75	6.75	6.75	6.75
M1	2.5	6.95	6.96	6.98	7	7
M1	2.8	7.33	7.34	7.34	7.34	7.34
Site	**Depth below surface (m)**	**Ground Resistivity (KOhm) at one minute intervals**				
		11	**12**	**13**	**14**	**15**
M1	0	6.43	6.43	6.43	6.43	6.43
M1	0.5	6.57	6.57	6.57	6.57	6.57
M1	1.0	6.62	6.62	6.62	6.62	6.62
M1	1.5	6.75	6.75	6.75	6.75	6.75
M1	2.5	7	7	7	7	7
M1	2.8	7.34	7.34	7.34	7.34	7.34

Table D2: Manual ground resistance measurements (KOhm) at borehole H1 on August 19, 2011.

Site	Depth below surface (m)	Ground Resistivity (KOhm) at one minute intervals				
		1	2	3	4	5
M2	0.2	4.65	5.1	5.32	5.52	5.68
M2	0.7	6.53	6.54	6.54	6.54	6.54
M2	1.2	6.74	6.9	7	7.07	7.13
M2	1.7	7.38	7.39	7.39	7.39	7.4
M2	2.7	7.45	7.47	7.48	7.44	7.49
M2	3.0	7.53	7.53	7.53	7.53	7.54
Site	**Depth below surface (m)**	**Ground Resistivity (KOhm) at one minute intervals**				
		6	**7**	**8**	**9**	**10**
M2	0.2	5.82	5.95	6.05	6.14	6.21
M2	0.7	6.55	6.55	6.55	6.55	6.55
M2	1.2	7.17	7.2	7.23	7.26	7.28
M2	1.7	7.4	7.4	7.41	7.41	7.41
M2	2.7	7.5	7.5	7.51	7.51	7.52
M2	3.0	7.54	7.54	7.54	7.54	7.54
Site	**Depth below surface (m)**	**Ground Resistivity (KOhm) at one minute intervals**				
		11	**12**	**13**	**14**	**15**
M2	0.2	6.27	6.32	6.37	6.4	6.42
M2	0.7	6.55	6.56	6.56	6.56	6.56
M2	1.2	7.29	7.31	7.32	7.33	7.33
M2	1.7	7.41	7.41	7.42	7.42	7.42
M2	2.7	7.52	7.52	7.53	7.53	7.53
M2	3.0	7.54	7.54	7.54	7.54	7.54

Table D3: Manual ground resistance measurements (KOhm) at borehole H2 on August 21, 2011.

Site	Depth below surface (m)	Ground Resistivity (KOhm) at one minute intervals				
		1	2	3	4	5
M3	0.2	6.49	6.51	6.52	6.53	6.54
M3	0.7	6.63	6.64	6.65	6.65	6.65
M3	1.2	6.76	6.82	6.86	6.88	6.88
M3	1.7	6.98	7.00	7.00	7.01	7.01
M3	2.0	7.14	7.17	7.2	7.21	7.22
Site	**Depth below surface (m)**	**Ground Resistivity (KOhm) at one minute intervals**				
		6	**7**	**8**	**9**	**10**
M3	0.2	6.54	6.54	6.55	6.55	6.55
M3	0.7	6.65	6.66	6.66	6.66	6.66
M3	1.2	6.88	6.88	6.89	6.89	6.89
M3	1.7	7.02	7.02	7.02	7.03	7.03
M3	2.0	7.23	7.24	7.25	7.25	7.25
Site	**Depth below surface (m)**	**Ground Resistivity (KOhm) at one minute intervals**				
		11	**12**	**13**	**14**	**15**
M3	0.2	6.55	6.56	6.56	6.56	6.56
M3	0.7	6.66	6.66	6.66	6.66	6.66
M3	1.2	6.89	6.89	6.89	6.89	6.89
M3	1.7	7.03	7.03	7.03	7.03	7.03
M3	2.0	7.25	7.25	7.26	7.26	7.26

Table D4: Manual ground resistance measurements (KOhm) at borehole H3 on August 21, 2011.

Site	Depth below surface (m)	Ground Resistivity (KOhm) at one minute intervals				
		1	2	3	4	5
M4	0.15m	5.3	5.5	5.56	5.87	5.94
M4	0.65m	6.32	6.33	6.35	6.36	6.36
M4	1.15m	6.54	6.62	6.66	6.69	6.72
M4	1.65m	6.92	6.98	7.02	7.05	7.07
M4	2.65m	7.22	7.25	7.27	7.29	7.3
M4	3.55m	7.41	7.42	7.43	7.43	7.43
Site	**Depth below surface (m)**	**Ground Resistivity (KOhm) at one minute intervals**				
		6	**7**	**8**	**9**	**10**
M4	0.15m	6	6.05	6.08	6.12	6.14
M4	0.65m	6.37	6.38	6.38	6.38	6.39
M4	1.15m	6.75	6.76	6.77	6.77	6.77
M4	1.65m	7.09	7.11	7.12	7.13	7.14
M4	2.65m	7.31	7.31	7.32	7.32	7.32
M4	3.55m	7.43	7.43	7.44	7.44	7.44
Site	**Depth below surface (m)**	**Ground Resistivity (KOhm) at one minute intervals**				
		11	**12**	**13**	**14**	**15**
M4	0.15m	6.16	6.18	6.2	6.21	6.22
M4	0.65m	6.39	6.39	6.39	6.39	6.39
M4	1.15m	6.78	6.78	6.78	6.79	6.79
M4	1.65m	7.14	7.14	7.14	7.15	7.15
M4	2.65m	7.33	7.33	7.33	7.34	7.34
M4	3.55m	7.44	7.44	7.44	7.44	7.44

Table D5: Temperature conversions for ground resistance measurements at borehole M1 on August 17, 2011. YSI thermistor calibrations from kilo-ohms to degrees Celsius are made using the following equation: y= -0.0214x3 + 0.6809x2 - 9.1992x +39.347 (Accurate to ±0.02 for -5ºC to +7ºC).

Site	Depth below surface (m)	Ground Temperature (ºC) at one minute intervals				
		1	2	3	4	5
M1	0	3.29	2.85	2.69	2.66	2.66
M1	0.5	2.44	2.17	2.20	2.23	2.23
M1	1.0	2.20	2.14	2.08	2.08	2.08
M1	1.5	1.78	1.72	1.67	1.69	1.69
M1	2.5	1.40	1.32	1.26	1.20	1.17
M1	2.8	0.29	0.18	0.15	0.10	0.07
Site	**Depth below surface (m)**	**Ground Temperature (ºC) at one minute intervals**				
		6	**7**	**8**	**9**	**10**
M1	0	2.66	2.66	2.66	2.66	2.66
M1	0.5	2.23	2.23	2.23	2.23	2.23
M1	1.0	2.08	2.08	2.08	2.08	2.08
M1	1.5	1.69	1.69	1.69	1.69	1.69
M1	2.5	1.12	1.09	1.03	0.98	0.98
M1	2.8	0.07	0.05	0.05	0.05	0.05
Site	**Depth below surface (m)**	**Ground Temperature (ºC) at one minute intervals**				
		11	**12**	**13**	**14**	**15**
M1	0	2.66	2.66	2.66	2.66	2.66
M1	0.5	2.23	2.23	2.23	2.23	2.23
M1	1.0	2.08	2.08	2.08	2.08	2.08
M1	1.5	1.69	1.69	1.69	1.69	1.69
M1	2.5	0.98	0.98	0.98	0.98	0.98
M1	2.8	0.05	0.05	0.05	0.05	0.05
Site	**Depth below surface (m)**	**30 minute forecast**	**LN equation for temperature forecasting (x) = 30**			
M1	0	2.00	y = -0.349ln(x) + 3.1829			
M1	0.5	2.03	y = -0.095ln(x) + 2.3552			
M1	1.0	1.92	y = -0.081ln(x) + 2.1936			
M1	1.5	1.57	y = -0.06ln(x) + 1.7691			
M1	2.5	0.81	y = -0.185ln(x) + 1.4377			
M1	2.8	-0.06	y = -0.092ln(x) + 0.2509			

Table D6: Temperature conversions for ground resistance measurements at borehole H1 on August 19, 2011. YSI thermistor calibrations from kilo-ohms to degrees Celsius are made using the following equation: y= -0.0214x3 + 0.6809x2 - 9.1992x +39.347 (Accurate to ±0.02 for -5ºC to +7ºC).

Site	Depth below surface (m)	Ground Temperature (ºC) at one minute intervals				
		1	2	3	4	5
M2	0.2	9.14	7.30	6.46	5.72	5.14
M2	0.7	2.35	2.32	2.32	2.32	2.32
M2	1.2	1.72	1.26	0.98	0.78	0.61
M2	1.7	-0.06	-0.09	-0.09	-0.09	-0.11
M2	2.7	-0.24	-0.30	-0.32	-0.22	-0.35
M2	3.0	-0.45	-0.45	-0.45	-0.45	-0.48
Site	**Depth below surface (m)**	**Ground Temperature (ºC) at one minute intervals**				
		6	**7**	**8**	**9**	**10**
M2	0.2	4.65	4.21	3.88	3.58	3.35
M2	0.7	2.29	2.29	2.29	2.29	2.29
M2	1.2	0.50	0.42	0.34	0.26	0.21
M2	1.7	-0.11	-0.11	-0.14	-0.14	-0.14
M2	2.7	-0.37	-0.37	-0.40	-0.40	-0.43
M2	3.0	-0.48	-0.48	-0.48	-0.48	-0.48
Site	**Depth below surface (m)**	**Ground Temperature (ºC) at one minute intervals**				
		11	**12**	**13**	**14**	**15**
M2	0.2	3.16	3.00	2.85	2.75	2.69
M2	0.7	2.29	2.26	2.26	2.26	2.26
M2	1.2	0.18	0.13	0.10	0.07	0.07
M2	1.7	-0.14	-0.14	-0.17	-0.17	-0.17
M2	2.7	-0.43	-0.43	-0.45	-0.45	-0.45
M2	3.0	-0.48	-0.48	-0.48	-0.48	-0.48
Site	**Depth below surface (m)**	**30 minute forecast**	**LN equation for temperature forecasting (x) = 30**			
M2	0.2	1.78	y = -1.907ln(x) + 8.2611			
M2	0.7	2.22	y = -0.043ln(x) + 2.3695			
M2	1.2	-0.19	y = -0.489ln(x) + 1.4686			
M2	1.7	-0.18	y = -0.04ln(x) - 0.0489			
M2	2.7	-0.50	y = -0.084ln(x) - 0.2167			
M2	3.0	-0.49	y = -0.012ln(x) - 0.4489			

Table D7: Temperature conversions for ground resistance measurements at borehole H2 on August 21, 2011. YSI thermistor calibrations from kilo-ohms to degrees Celsius are made using the following equation: y= -0.0214x3 + 0.6809x2 - 9.1992x +39.347 (Accurate to ±0.02 for -5ºC to +7ºC).

Site	Depth below surface (m)	Ground Temperature (ºC) at one minute intervals				
		1	2	3	4	5
M3	0.2	2.47	2.41	2.38	2.35	2.32
M3	0.7	2.05	2.02	1.99	1.99	1.99
M3	1.2	1.67	1.49	1.37	1.32	1.32
M3	1.7	1.03	0.98	0.98	0.95	0.95
M3	2.0	0.59	0.50	0.42	0.40	0.37
Site	**Depth below surface (m)**	**Ground Temperature (ºC) at one minute intervals**				
		6	**7**	**8**	**9**	**10**
M3	0.2	2.32	2.32	2.29	2.29	2.29
M3	0.7	1.99	1.96	1.96	1.96	1.96
M3	1.2	1.32	1.32	1.29	1.29	1.29
M3	1.7	0.92	0.92	0.92	0.89	0.89
M3	2.0	0.34	0.31	0.29	0.29	0.29
Site	**Depth below surface (m)**	**Ground Temperature (ºC) at one minute intervals**				
		11	**12**	**13**	**14**	**15**
M3	0.2	2.29	2.26	2.26	2.26	2.26
M3	0.7	1.96	1.96	1.96	1.96	1.96
M3	1.2	1.29	1.29	1.29	1.29	1.29
M3	1.7	0.89	0.89	0.89	0.89	0.89
M3	2.0	0.29	0.29	0.26	0.26	0.26
Site	**Depth below surface (m)**	**30 minute forecast**	**LN equation for temperature forecasting (x) = 30**			
M3	0.2	2.20	y = -0.077ln(x) + 2.4632			
M3	0.7	1.93	y = -0.033ln(x) + 2.0396			
M3	1.2	1.16	y = -0.119ln(x) + 1.5625			
M3	1.7	0.85	y = -0.053ln(x) + 1.0254			
M3	2.0	0.20	y = -0.099ln(x) + 0.5395			

Table D8: Temperature conversions for ground resistance measurements at borehole H3 on August 21, 2011. YSI thermistor calibrations from kilo-ohms to degrees Celsius are made using the following equation: y= -0.0214x3 + 0.6809x2 - 9.1992x +39.347 (Accurate to ±0.02 for -5ºC to +7ºC).

Site	Depth below surface (m)	Ground Temperature (ºC) at one minute intervals				
		1	2	3	4	5
M4	0.15m	6.53	5.79	5.57	4.48	4.24
M4	0.65m	3.00	2.97	2.91	2.88	2.88
M4	1.15m	2.32	2.08	1.96	1.87	1.78
M4	1.65m	1.20	1.03	0.92	0.84	0.78
M4	2.65m	0.37	0.29	0.23	0.18	0.15
M4	3.55m	-0.14	-0.17	-0.19	-0.19	-0.19
Site	**Depth below surface (m)**	**Ground Temperature (ºC) at one minute intervals**				
		6	**7**	**8**	**9**	**10**
M4	0.15m	4.04	3.88	3.78	3.65	3.58
M4	0.65m	2.85	2.81	2.81	2.81	2.78
M4	1.15m	1.69	1.67	1.64	1.64	1.64
M4	1.65m	0.73	0.67	0.64	0.61	0.59
M4	2.65m	0.13	0.13	0.10	0.10	0.10
M4	3.55m	-0.19	-0.19	-0.22	-0.22	-0.22
Site	**Depth below surface (m)**	**Ground Temperature (ºC) at one minute intervals**				
		11	**12**	**13**	**14**	**15**
M4	0.15m	3.51	3.45	3.39	3.35	3.32
M4	0.65m	2.78	2.78	2.78	2.78	2.78
M4	1.15m	1.61	1.61	1.61	1.58	1.58
M4	1.65m	0.59	0.59	0.59	0.56	0.56
M4	2.65m	0.07	0.07	0.07	0.05	0.05
M4	3.55m	-0.22	-0.22	-0.22	-0.22	-0.22
Site	**Depth below surface (m)**	**30 minute forecast**	**LN equation for temperature forecasting (x) = 30**			
M4	0.15m	2.69	y = -1.029ln(x) + 6.188			
M4	0.65m	2.70	y = -0.091ln(x) + 3.01			
M4	1.15m	1.40	y = -0.239ln(x) + 2.2142			
M4	1.65m	0.40	y = -0.219ln(x) + 1.1489			
M4	2.65m	-0.02	y = -0.109ln(x) + 0.3464			

Appendix E: Statistical Testing of Long-term Climate Data

Table E1: Significance test results of available MAAT data before 1975 at Environment Canada weather stations in the study area (confidence limit of 95%) (Environment Canada, 2012).

Station	Record	n	R^2	Slope Coefficient	Std. error of slope	P-value
Whitehorse	1943-1975	33	0.28	-0.066	0.019	0.002
Haines Junction	1945-1975	31	0.07	-0.029	0.020	0.150
Otter Falls	N/A	N/A	N/A	N/A	N/A	N/A
Burwash	-	-	-	-	-	-
Beaver Creek	-	-	-	-	-	-

Table E2: Significance test results of available MAAT data after 1975 at Environment Canada weather stations in the study area (confidence limit of 95%) (Environment Canada, 2012).

Station	Record	n	R^2	Slope Coefficient	Std. error of slope	P-value
Whitehorse	1976-2011	36	2.92E-03	0.017	0.016	0.301
Haines Junction	1993-2011	19	2.54E-03	0.010	0.048	0.838
Otter Falls	1980-2006	27	0.04	-0.025	0.025	0.327
Burwash	1976-2011	36	0.03	0.019	0.018	0.322
Beaver Creek	1980-2011	31	0.30	0.057	0.016	0.001

Table E3: Significance test results of available Thawing Degree Days (TDDa) at Environment Canada weather stations in the study area (confidence limit of 95%) (Environment Canada, 2012). Note that daily temperature means were not available for Otter Falls and Beaver Creek.

Station	Record	n	R^2	Slope Coefficient	Std. error of slope	P-value
Whitehorse	1943-1975	33	0.246	-6.747	2.158	0.004
	1976-2011	36	0.026	2.367	2.502	0.351
Haines Junction	1945-1975	31	0.005	0.920	2.217	0.682
Otter Falls	N/A	N/A	N/A	N/A	N/A	N/A
Burwash	1976-2007	32	0.028	2.289	2.496	0.367
Beaver Creek	N/A	N/A	N/A	N/A	N/A	N/A

Table E4: Significance test results of available Freezing Degree Days (FDDa) at Environment Canada weather stations in the study area (confidence limit of 95%) (Environment Canada, 2012). Note that daily temperature means were not available for Otter Falls and Beaver Creek.

Station	Record	n	R^2	Slope Coefficient	Std. error of slope	P-value
Whitehorse	1943-1975	33	0.214	18.530	6.469	0.007
	1976-2011	36	0.002	-1.491	5.561	0.790
Haines Junction	1945-1975	31	0.032	6.310	6.463	0.337
Otter Falls	N/A	N/A	N/A	N/A	N/A	N/A
Burwash	1976-2007	32	2.89E-05	-0.219	7.565	0.977
Beaver Creek	N/A	N/A	N/A	N/A	N/A	N/A

Table E5: Significance test results of available total annual rainfall data before 1975 at Environment Canada weather stations in the study area (confidence limit of 95%) (Environment Canada, 2012).

Station	Record	n	R^2	Slope Coefficient	Std. error of slope	P-value
Whitehorse	1943-1975	33	3.49E-03	0.277	0.841	0.744
Haines Junction	1945-1975	31	2.89E-03	-0.325	1.122	0.774
Otter Falls	N/A	N/A	N/A	N/A	N/A	N/A
Burwash	-	-	-	-	-	-
Beaver Creek	-	-	-	-	-	-

Table E6: Significance test results of available total annual rainfall data after 1975 at Environment Canada weather stations in the study area (confidence limit of 95%) (Environment Canada, 2012).

Station	Record	n	R^2	Slope Coefficient	Std. error of slope	P-value
Whitehorse	1976-2011	36	0.03	0.711	0.716	0.327
Haines Junction	1993-2006	14	5.33E-03	0.937	3.693	0.804
Otter Falls	1980-2006	27	1.02E-04	-0.068	1.344	0.960
Burwash	1976-2007	32	5.49E-03	0.372	0.914	0.687
Beaver Creek	1981-2006	25	0.02	1.857	2.491	0.464

Table E7: Significance test results of available total annual snowfall data before 1975 at Environment Canada weather stations in the study area (confidence limit of 95%) (Environment Canada, 2012).

Station	Record	n	R^2	Slope Coefficient	Std. error of slope	P-value
Whitehorse	1943-1975	33	0.16	1.447	0.600	0.022
Haines Junction	1945-1975	31	0.09	1.131	0.688	0.111
Otter Falls	N/A	N/A	N/A	N/A	N/A	N/A
Burwash	-	-	-	-	-	-
Beaver Creek	-	-	-	-	-	-

Table E8: Significance test results of available total annual snowfall data after 1975 at Environment Canada weather stations in the study area (confidence limit of 95%) (Environment Canada, 2012).

Station	Record	n	R^2	Slope Coefficient	Std. error of slope	P-value
Whitehorse	1976-2011	36	7.97E-04	-0.102	0.617	0.870
Haines Junction	1993-2006	14	0.03	-2.687	4.496	0.561
Otter Falls	1980-2006	27	0.03	-0.768	0.879	0.390
Burwash	1976-2007	32	0.05	0.575	0.480	0.240
Beaver Creek	1981-2006	25	0.03	-0.817	0.906	0.377

Table E9: Significance test results of available total annual precipitation data before 1975 at Environment Canada weather stations in the study area (confidence limit of 95%) (Environment Canada, 2012).

Station	Record	n	R^2	Slope Coefficient	Std. error of slope	P-value
Whitehorse	1943-1975	33	5.35E-03	0.392	0.962	0.686
Haines Junction	1945-1975	31	8.24E-04	0.229	1.480	0.878
Otter Falls	N/A	N/A	N/A	N/A	N/A	N/A
Burwash	-	-	-	-	-	-
Beaver Creek	-	-	-	-	-	-

Table E10: Significance test results of available total annual precipitation data after 1975 at Environment Canada weather stations in the study area (confidence limit of 95%) (Environment Canada, 2012).

Station	Record	n	R^2	Slope Coefficient	Std. error of slope	P-value
Whitehorse	1976-2011	36	0.04	0.857	0.753	0.263
Haines Junction	1993-2006	14	1.87E-03	-0.893	5.960	0.883
Otter Falls	1980-2006	27	5.87E-03	-0.650	1.692	0.704
Burwash	1976-2007	32	1.91E-03	0.225	0.938	0.812
Beaver Creek	1981-2006	25	4.20E-03	0.897	2.880	0.758

Appendix F: RBR Instrumented Boreholes Original Temperature Measurements

Figure F1: Original temperature measurements at borehole R1 (79S-CS-5).

EARTH PHYSICS BRANCH NO. 231 FOOTHILLS CS -2
DIRECTION DE LA PHYSIQUE DU GLOBE NO.

****

60 DEGREES 47.8 MINUTES NORTH
135 DEGREES 56.7 MINUTES WEST

60 DEGRES 47.8 MINUTES NORD
135 DEGRES 56.7 MINUTES OUEST

ELEVATION 686 METRES

SUMMARY OF DEPTH-TEMPERATURE LOGS

DIAGRAPHIES DONNANT LA TEMPERATURE EN FONCTION DE LA PROFONDEUR

Z(M)	DATE 79 10 26 T(C)	DATE 80 2 1 T(C)	DATE 80 4 28 T(C)	DATE 80 8 7 T(C)	DATE 81 7 30 T(C)
.6				9.21	
2.2	4.81	.60	-.77	3.07	1.54
3.7	3.30	1.26	-1.39	-2.74	-3.50
5.2	1.46	1.47	1.42	1.24	1.20
6.7	1.58	1.93	1.87	1.59	1.59
8.3				1.14	.87
9.8	1.47	1.43	1.39		
11.3	1.53	1.51	1.54	1.59	1.62
12.8	1.57	1.41	1.31	1.29	1.29
14.4	1.60	1.48	1.39	1.28	.78
15.9	1.55	1.52	1.51	1.50	1.45
17.4				1.32	.88
18.9	1.62	1.41	1.18	1.13	.87
20.5				1.26	
22.0	1.70	1.68	1.68	1.64	1.53
23.5				1.64	1.25
25.0	1.67	1.49	1.32	1.09	
26.6				1.77	1.63
28.1	1.87	1.85	1.84	1.83	1.80

TEMPERATURE RESULTS ARE OBTAINED FROM A MULTITHERMISTOR CABLE. FURTHER TEMPERATURE LOGS ARE EXPECTED FOR THIS HOLE.

TEMPERATURES OBTENUES A PARTIR D'UN CABLE A THERMISTORS MULTIPLES. ON PREVOIT ENTREPRENDRE D'AUTRES SONDAGES DE LA TEMPERATURE DE CE PUITS.

FOOTHILLS 79-CS-5, TAKHINI RIVER
-WELL SPUDDED 79 8 8
-DRILLING FOR 2 DAYS
-TOTAL DEPTH 30 METRES
-DRILLING STOPPED 79 8 9

FOOTHILLS 79-CS-5, TAKHINI RIVER
-DEMARRAGE DU PUITS LE 79 8 8
-FORAGE PENDANT 2 JOURS
-PROFONDEUR TOTALE 30 METRES
-FORAGE ARRETE LE 79 8 9

SITE IS A NATURAL CLEARING

Figure F2: Original temperature measurements at borehole R2 (78-A-71).

EARTH PHYSICS BRANCH NO. 226 ALCAN FOOTHILLS -12
DIRECTION DE LA PHYSIQUE DU GLOBE NO.

****

60 DEGREES 54.9 MINUTES NORTH
137 DEGREES 52.3 MINUTES WEST

60 DEGRES 54.9 MINUTES NORD
137 DEGRES 52.3 MINUTES OUEST

ELEVATION 840 METRES

SUMMARY OF DEPTH-TEMPERATURE LOGS

DIAGRAPHIES DONNANT LA TEMPERATURE EN FONCTION DE LA PROFONDEUR

DATE
78 11 26

Z(M)	T(C)
1.5	.23
3.0	.15
4.6	.17
6.1	.15
7.6	.16
9.8	.01

TEMPERATURE RESULTS ARE OBTAINED FROM SINGLE THERMISTOR LOGS.
LOGGING OF THIS HOLE IS COMPLETE.

TEMPERATURES OBTENUES A PARTIR DE SONDAGES AVEC UN THERMISTOR UNIQUE.
LE SONDAGE DE CE PUITS EST TERMINE.

FOOTHILLS 78-A-71
-DRILLED TO A TOTAL DEPTH OF 9 METRES

FOOTHILLS 78-A-71
-FORE A UNE PROFONDEUR TOTALE 9 METRES

DRILLED IN AUGUST 1978
SITE WAS CLEARED FOR DRILLING

Figure F3: Original temperature measurements at borehole R3 (78-A-64).

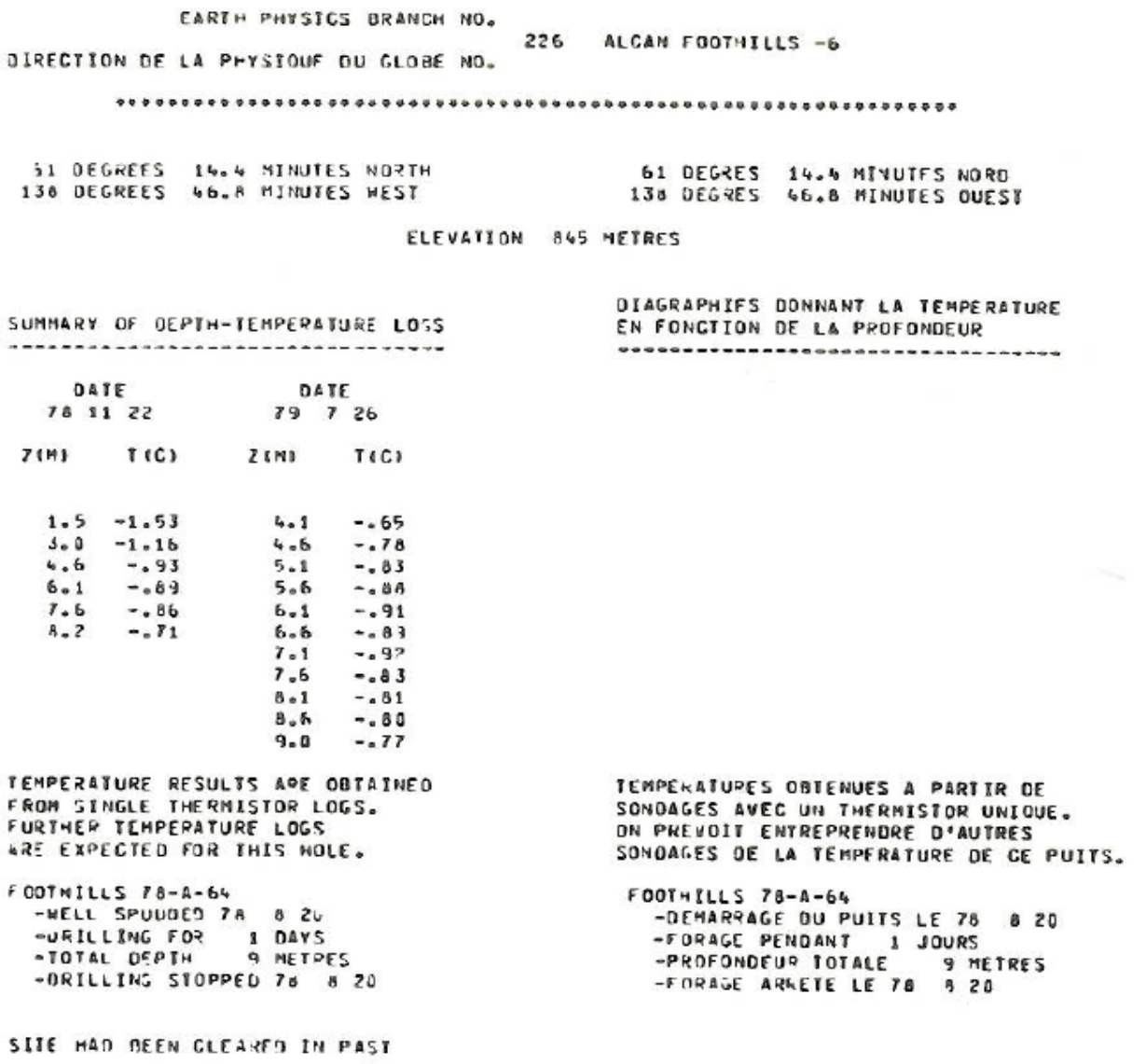

EARTH PHYSICS BRANCH NO. 226 ALCAN FOOTHILLS -6
DIRECTION DE LA PHYSIQUE DU GLOBE NO.

61 DEGREES 14.4 MINUTES NORTH
138 DEGREES 46.8 MINUTES WEST

61 DEGRES 14.4 MINUTES NORD
138 DEGRES 46.8 MINUTES OUEST

ELEVATION 845 METRES

SUMMARY OF DEPTH-TEMPERATURE LOGS

DIAGRAPHIES DONNANT LA TEMPERATURE EN FONCTION DE LA PROFONDEUR

DATE 78 11 22		DATE 79 7 26	
Z(M)	T(C)	Z(M)	T(C)
1.5	-1.53	4.1	-.65
3.0	-1.16	4.6	-.78
4.6	-.93	5.1	-.83
6.1	-.89	5.6	-.84
7.6	-.86	6.1	-.91
8.2	-.71	6.6	-.83
		7.1	-.92
		7.6	-.83
		8.1	-.81
		8.6	-.80
		9.0	-.77

TEMPERATURE RESULTS ARE OBTAINED FROM SINGLE THERMISTOR LOGS. FURTHER TEMPERATURE LOGS ARE EXPECTED FOR THIS HOLE.

TEMPERATURES OBTENUES A PARTIR DE SONDAGES AVEC UN THERMISTOR UNIQUE. ON PREVOIT ENTREPRENDRE D'AUTRES SONDAGES DE LA TEMPERATURE DE CE PUITS.

FOOTHILLS 78-A-64
-WELL SPUDDED 78 8 20
-DRILLING FOR 1 DAYS
-TOTAL DEPTH 9 METRES
-DRILLING STOPPED 78 8 20

FOOTHILLS 78-A-64
-DEMARRAGE DU PUITS LE 78 8 20
-FORAGE PENDANT 1 JOURS
-PROFONDEUR TOTALE 9 METRES
-FORAGE ARRETE LE 78 8 20

SITE HAD BEEN CLEARED IN PAST

Figure F4: Original temperature measurements at borehole R4 (78-A-63).

EARTH PHYSICS BRANCH NO. 226 ALCAN FOOTHILLS -11
DIRECTION DE LA PHYSIQUE DU GLOBE NO.

****

61 DEGREES 14.9 MINUTES NORTH
138 DEGREES 47.7 MINUTES WEST

61 DEGRES 14.9 MINUTES NORD
138 DEGRES 47.7 MINUTES OUEST

ELEVATION 823 METRES

SUMMARY OF DEPTH-TEMPERATURE LOGS

DIAGRAPHIES DONNANT LA TEMPERATURE EN FONCTION DE LA PROFONDEUR

DATE
78 11 22

ZEMI	T(C)
.3	-.77
1.5	-.23
3.0	-.59
4.0	-1.43
4.6	-1.51

TEMPERATURE RESULTS ARE OBTAINED FROM SINGLE THERMISTOR LOGS.
LOGGING OF THIS HOLE IS COMPLETE.

TEMPERATURES OBTENUES A PARTIR DE SONDAGES AVEC UN THERMISTOR UNIQUE.
LE SONDAGE DE CE PUITS EST TERMINE.

FOOTHILLS 78-A-63
-DRILLED TO A TOTAL DEPTH OF 5 METRES

FOOTHILLS 78-A-63
-FORE A UNE PROFONDEUR TOTALE 5 METRES

DRILLED IN AUGUST 1978
TOP 3 READINGS IN AIR
SITE WAS CLEARED FOR DRILLING

Figure F5: Original temperature measurements at borehole R5 (78-A-62).

EARTH PHYSICS BRANCH NO. 226 ALCAN FOOTHILLS -5
DIRECTION DE LA PHYSIQUE DU GLOBE NO.

****

51 DEGREES 16.1 MINUTES NORTH
138 DEGREES 50.3 MINUTES WEST

61 DEGRES 16.1 MINUTES NORD
138 DEGRES 50.3 MINUTES OUEST

ELEVATION 923 METRES

SUMMARY OF DEPTH-TEMPERATURE LOGS

DIAGRAPHIES DONNANT LA TEMPERATURE EN FONCTION DE LA PROFONDEUR

DATE 78 11 22		DATE 79 7 26	
Z(M)	T(C)	Z(M)	T(C)
1.5	-1.32	1.0	-.09
3.0	-1.23	1.5	-.56
4.6	-1.43	2.0	-.88
6.1	-1.57	2.5	-1.13
7.3	-1.63	3.0	-1.33
		3.5	-1.51
		4.0	-1.62
		4.5	-1.69
		5.0	-1.77
		5.5	-1.80
		6.0	-1.82
		6.5	-1.82
		7.0	-1.82
		7.5	-1.82
		8.0	-1.82
		8.5	-1.80
		9.0	-1.61

TEMPERATURE RESULTS ARE OBTAINED FROM SINGLE THERMISTOR LOGS. FURTHER TEMPERATURE LOGS ARE EXPECTED FOR THIS HOLE.

TEMPERATURES OBTENUES A PARTIR DE SONDAGES AVEC UN THERMISTOR UNIQUE. ON PREVOIT ENTREPRENDRE D'AUTRES SONDAGES DE LA TEMPERATURE DE CE PUITS.

FOOTHILLS 78-A-62
-WELL SPUDDED 78 8 19
-DRILLING FOR 1 DAYS
-TOTAL DEPTH 9 METRES
-DRILLING STOPPED 78 8 19

FOOTHILLS 78-A-62
-DEMARRAGE DU PUITS LE 78 8 19
-FORAGE PENDANT 1 JOURS
-PROFONDEUR TOTALE 9 METRES
-FORAGE ARRETE LE 78 8 19

SITE WAS CLEARED FOR DRILLING

Figure F6: Original temperature measurements at borehole R6 (78-A-51).

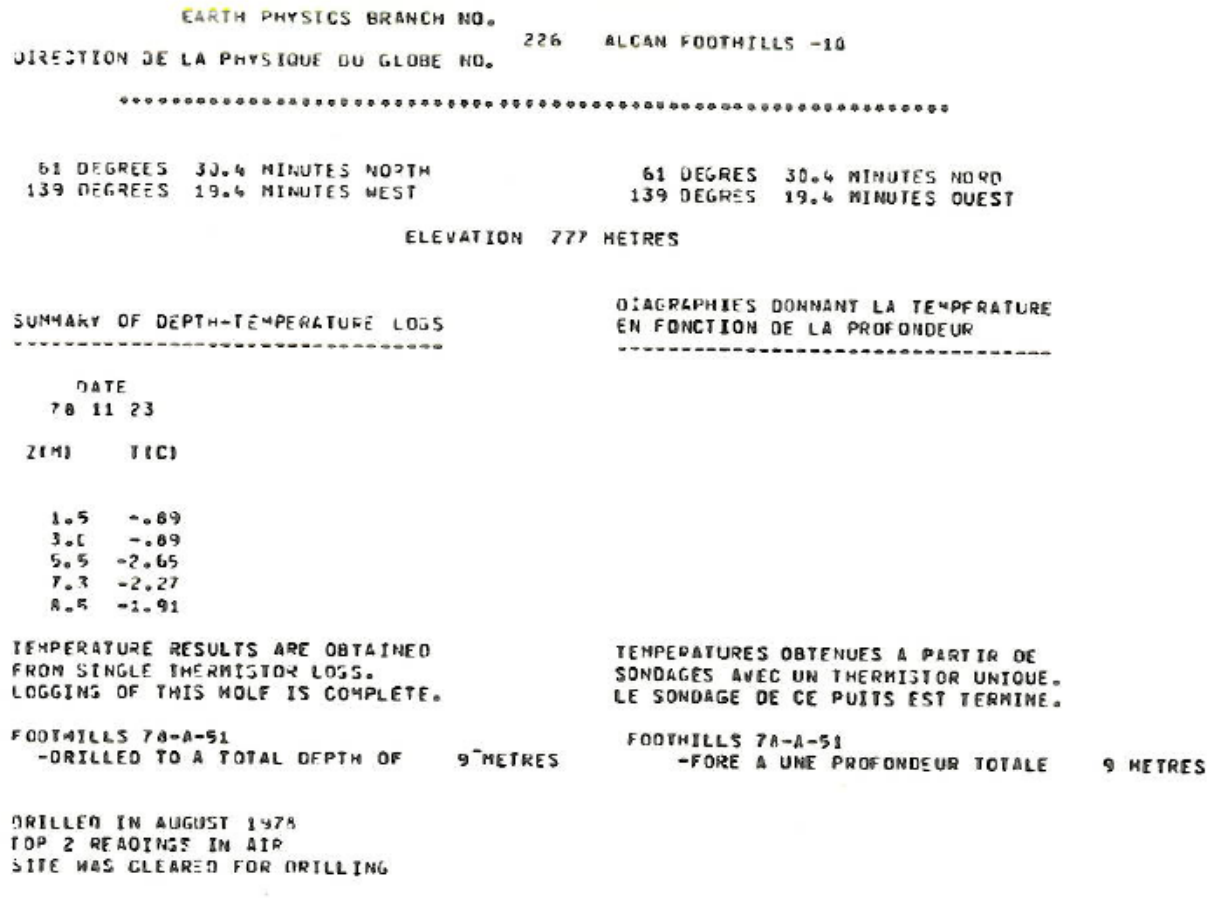

EARTH PHYSICS BRANCH NO. 226 ALCAN FOOTHILLS -10
DIRECTION DE LA PHYSIQUE DU GLOBE NO.

61 DEGREES 30.4 MINUTES NORTH
139 DEGREES 19.4 MINUTES WEST

61 DEGRES 30.4 MINUTES NORD
139 DEGRES 19.4 MINUTES OUEST

ELEVATION 777 METRES

SUMMARY OF DEPTH-TEMPERATURE LOGS

DIAGRAPHIES DONNANT LA TEMPERATURE EN FONCTION DE LA PROFONDEUR

DATE
78 11 23

Z(M)	T(C)
1.5	-.89
3.0	-.89
5.5	-2.65
7.3	-2.27
8.5	-1.91

TEMPERATURE RESULTS ARE OBTAINED FROM SINGLE THERMISTOR LOGS.
LOGGING OF THIS HOLE IS COMPLETE.

TEMPERATURES OBTENUES A PARTIR DE SONDAGES AVEC UN THERMISTOR UNIQUE.
LE SONDAGE DE CE PUITS EST TERMINE.

FOOTHILLS 78-A-51
-DRILLED TO A TOTAL DEPTH OF 9 METRES

FOOTHILLS 78-A-51
-FORE A UNE PROFONDEUR TOTALE 9 METRES

DRILLED IN AUGUST 1978
TOP 2 READINGS IN AIR
SITE WAS CLEARED FOR DRILLING

Figure F7: Original temperature measurements at borehole R7 (78-A-40).

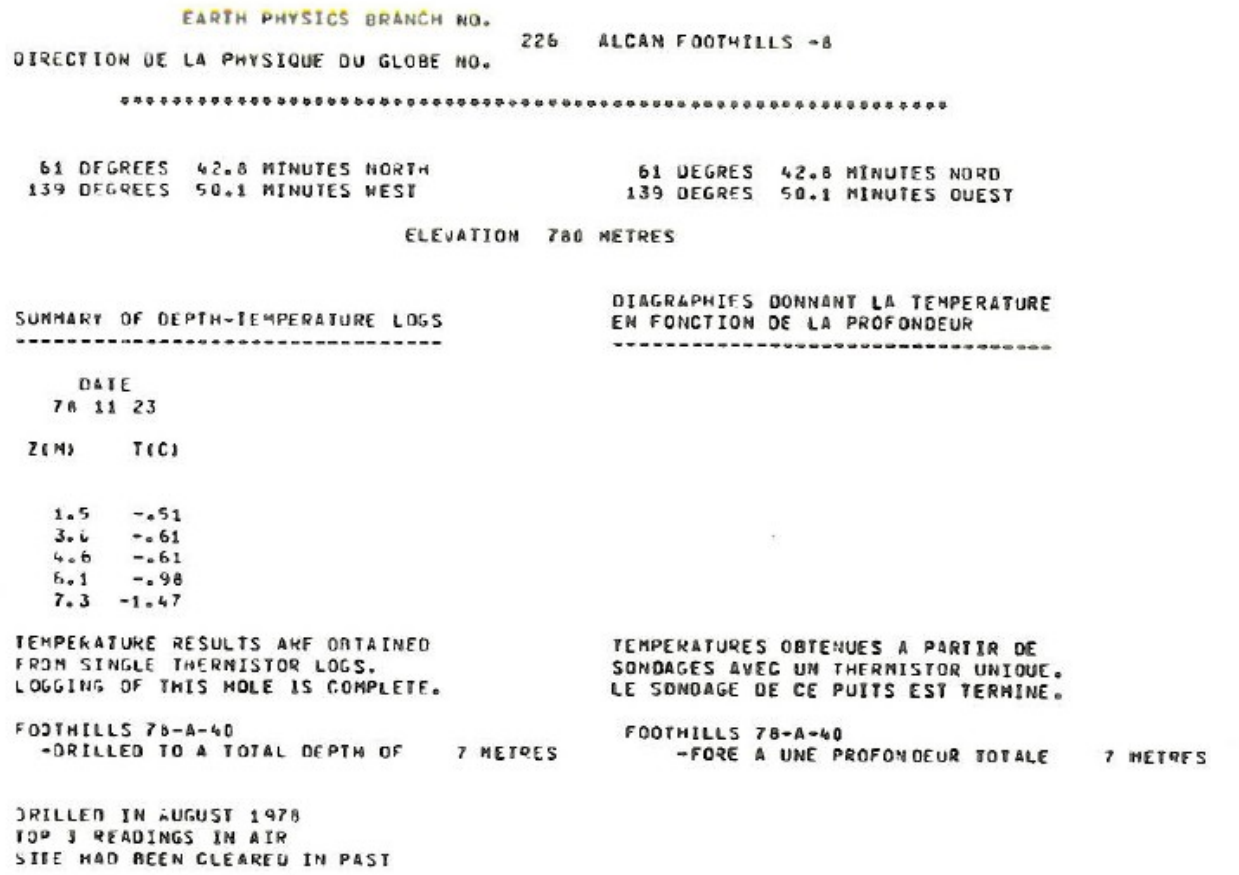

EARTH PHYSICS BRANCH NO. 226 ALCAN FOOTHILLS -8
DIRECTION DE LA PHYSIQUE DU GLOBE NO.

****

61 DEGREES 42.8 MINUTES NORTH
139 DEGREES 50.1 MINUTES WEST

61 DEGRES 42.8 MINUTES NORD
139 DEGRES 50.1 MINUTES OUEST

ELEVATION 780 METRES

SUMMARY OF DEPTH-TEMPERATURE LOGS

DIAGRAPHIES DONNANT LA TEMPERATURE EN FONCTION DE LA PROFONDEUR

DATE
78 11 23

Z(M)	T(C)
1.5	-.51
3.6	-.61
4.6	-.61
6.1	-.98
7.3	-1.47

TEMPERATURE RESULTS ARE OBTAINED FROM SINGLE THERMISTOR LOGS.
LOGGING OF THIS HOLE IS COMPLETE.

TEMPERATURES OBTENUES A PARTIR DE SONDAGES AVEC UN THERMISTOR UNIQUE.
LE SONDAGE DE CE PUITS EST TERMINE.

FOOTHILLS 78-A-40
-DRILLED TO A TOTAL DEPTH OF 7 METRES

FOOTHILLS 78-A-40
-FORE A UNE PROFONDEUR TOTALE 7 METRES

DRILLED IN AUGUST 1978
TOP 3 READINGS IN AIR
SITE HAD BEEN CLEARED IN PAST

Figure F8: Original temperature measurements at borehole R8 (78-A-8).

EARTH PHYSICS BRANCH NO. 226 ALCAN FOOTHILLS -2
DIRECTION DE LA PHYSIQUE DU GLOBE NO.

****

62 DEGREES 17.5 MINUTES NORTH
140 DEGREES 46.1 MINUTES WEST

62 DEGRES 17.5 MINUTES NORD
140 DEGRES 46.1 MINUTES OUEST

ELEVATION 747 METRES

SUMMARY OF DEPTH-TEMPERATURE LOGS

DIAGRAPHIES DONNANT LA TEMPERATURE EN FONCTION DE LA PROFONDEUR

DATE 78 11 25		DATE 79 7 25	
Z(M)	T(C)	Z(M)	T(C)
1.5	-2.39	.8	-.20
3.0	-1.77	1.3	-.73
4.6	-1.63	1.8	-1.08
6.1	-1.79	2.3	-1.42
7.0	-1.88	2.8	-1.66
		3.3	-1.83
		3.8	-1.94
		4.3	-2.01
		4.8	-2.07
		5.3	-2.11
		5.8	-2.12
		6.3	-2.13
		6.8	-2.12
		7.3	-2.11
		7.4	-2.09

TEMPERATURE RESULTS ARE OBTAINED FROM SINGLE THERMISTOR LOGS. FURTHER TEMPERATURE LOGS ARE EXPECTED FOR THIS HOLE.

TEMPERATURES OBTENUES A PARTIR DE SONDAGES AVEC UN THERMISTOR UNIQUE. ON PREVOIT ENTREPRENDRE D'AUTRES SONDAGES DE LA TEMPERATURE DE CE PUITS.

FOOTHILLS 78-A-8
-WELL SPUDDED 78 8 5
-DRILLING FOR 1 DAYS
-TOTAL DEPTH 8 METRES
-DRILLING STOPPED 78 8 5

FOOTHILLS 78-A-8
-DEMARRAGE DU PUITS LE 78 8 5
-FORAGE PENDANT 1 JOURS
-PROFONDEUR TOTALE 8 METRES
-FORAGE ARRETE LE 78 8 5

SITE WAS CLEARED FOR DRILLING

Appendix G: HOBO Instrumented Boreholes Original Temperature Measurements

Figure G1: Original temperature measurements at borehole H2 (78-B-25).

EARTH PHYSICS BRANCH NO. 226 ALCAN FOOTHILLS -9
DIRECTION DE LA PHYSIQUE DU GLOBE NO.

****

61 DEGREES 40.5 MINUTES NORTH
139 DEGREES 43.7 MINUTES WEST

61 DEGRES 40.5 MINUTES NORD
139 DEGRES 43.7 MINUTES OUEST

ELEVATION 716 METRES

SUMMARY OF DEPTH-TEMPERATURE LOGS

DIAGRAMMES DONNANT LA TEMPERATURE EN FONCTION DE LA PROFONDEUR

DATE
78 11 23

Z(M)	T(C)
1.5	-1.74
3.0	-1.23
4.6	-1.02
4.9	-1.02

TEMPERATURE RESULTS ARE OBTAINED FROM SINGLE THERMISTOR LOGS.
LOGGING OF THIS HOLE IS COMPLETE.

TEMPERATURES OBTENUES A PARTIR DE SONDAGES AVEC UN THERMISTOR UNIQUE.
LE SONDAGE DE CE PUITS EST TERMINE.

FOOTHILLS 78-B-25
-DRILLED TO A TOTAL DEPTH OF 5 METRES

FOOTHILLS 78-B-25
-FORE A UNE PROFONDEUR TOTALE 5 METRES

DRILLED IN AUGUST 1978
SITE WAS CLEARED FOR DRILLING

Figure G2: Original temperature measurements at borehole H3 (78-A-39).

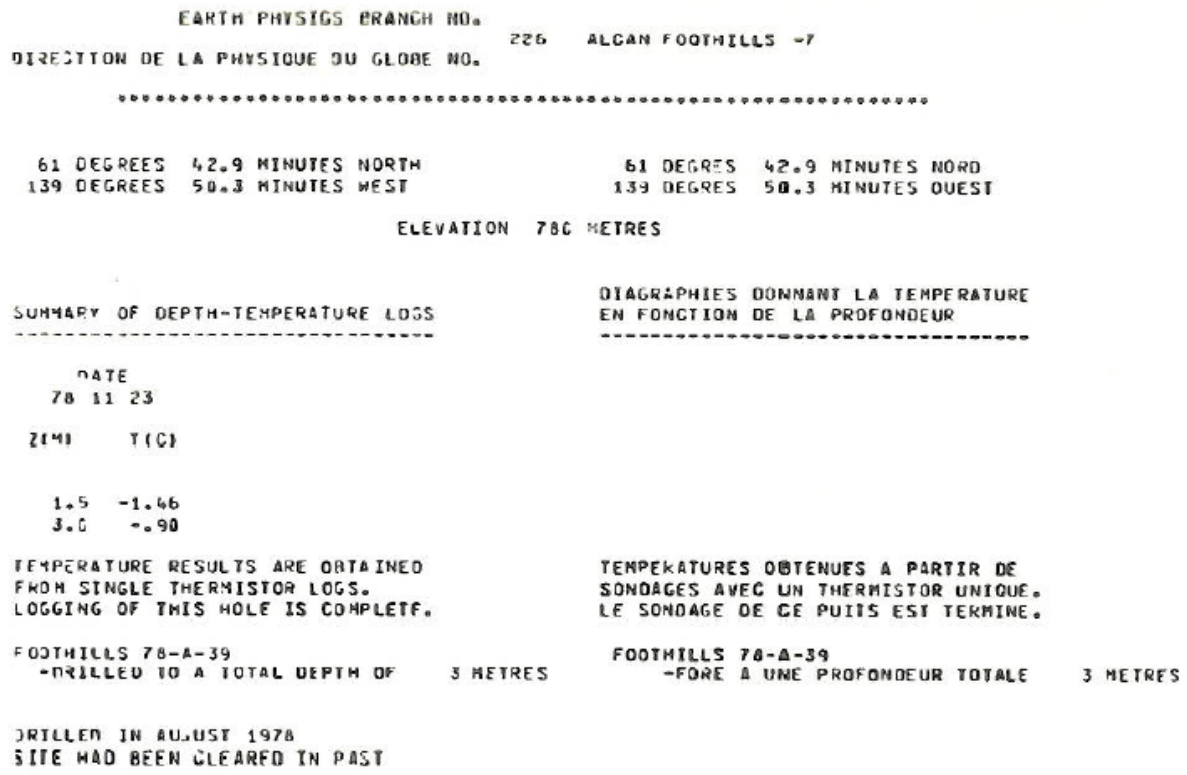

EARTH PHYSICS BRANCH NO. 226 ALCAN FOOTHILLS -7
DIRECTION DE LA PHYSIQUE DU GLOBE NO.

61 DEGREES 42.9 MINUTES NORTH
139 DEGREES 50.3 MINUTES WEST

61 DEGRES 42.9 MINUTES NORD
139 DEGRES 50.3 MINUTES OUEST

ELEVATION 780 METRES

SUMMARY OF DEPTH-TEMPERATURE LOGS

DIAGRAPHIES DONNANT LA TEMPERATURE EN FONCTION DE LA PROFONDEUR

DATE
78 11 23

Z(M)	T(C)
1.5	-1.46
3.0	-.90

TEMPERATURE RESULTS ARE OBTAINED FROM SINGLE THERMISTOR LOGS.
LOGGING OF THIS HOLE IS COMPLETE.

TEMPERATURES OBTENUES A PARTIR DE SONDAGES AVEC UN THERMISTOR UNIQUE.
LE SONDAGE DE CE PUITS EST TERMINE.

FOOTHILLS 78-A-39
-DRILLED TO A TOTAL DEPTH OF 3 METRES

FOOTHILLS 78-A-39
-FORE A UNE PROFONDEUR TOTALE 3 METRES

DRILLED IN AUGUST 1978
SITE HAD BEEN CLEARED IN PAST

Appendix H: ERT Acquirement Settings

Figure H1: ERT acquirement settings

- AGC_TimeSec: 0.060000
- Acq_DelaySec: 0.300000
- Acq_TimeSec: 0.600000
- AutoStack: 1
- BaseFreqHz: 60.000000
- CurrentLimitHighAmpere: 0.050000
- CurrentLimitLowAmpere: 0.005000
- DoInitialAGC: 0
- ElectrodeResistanceBadLimitHighOhm: 100000.000000
- ElectrodeResistanceBadLimitLowOhm: 50000.000000
- ElectrodeTest: 1
- ElectrodeTestCurrentAmpere: 0.020000
- ErrorLimit: 0.001000
- Fullwaveform: 0
- IPSP_TimeSec: 0.500000
- IP_MinOffTimeSec: 0.500000
- IP_OffTimeSec: 0.500000
- IP_WindowSecList: 0.01 0.02 0.02
- MarginLimitHigh: 1.200000
- MeasureMode: 2
- Measure_SNR: 0
- PowerLimitHighWatt: 100.000000
- PowerLimitLowWatt: 0.000000
- PowerLossLimitHighWatt: 30.000000
- SNR_TimeSec: 0.020000
- SP_TimeSec: 1.000000
- SampleRateHz: 1000.000000
- StackLimitsHigh: 2
- StackLimitsLow: 2
- StackNorm: 0
- VoltageLimitHighVolt: 600.000000
- VoltageLimitLowVolt: 0.000000

Appendix I: RBR Installed Boreholes Resistivity Pseudosections

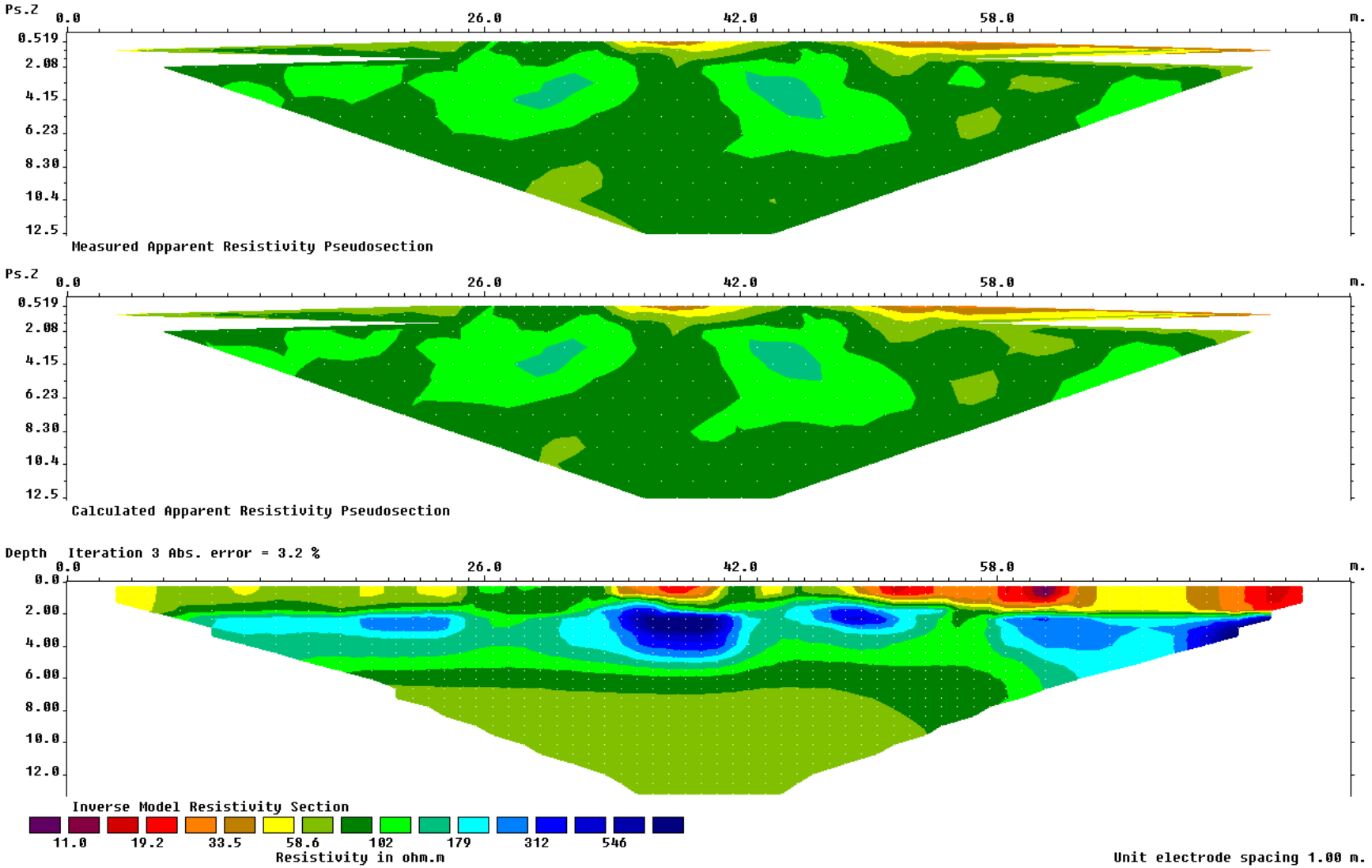

Figure I1: Borehole R1 June 10, 2011 NE-SW 80 m resistivity profile; measured apparent resistivity pseudosection, calculated apparent resistivity pseudosection and inverse model resistivity section.

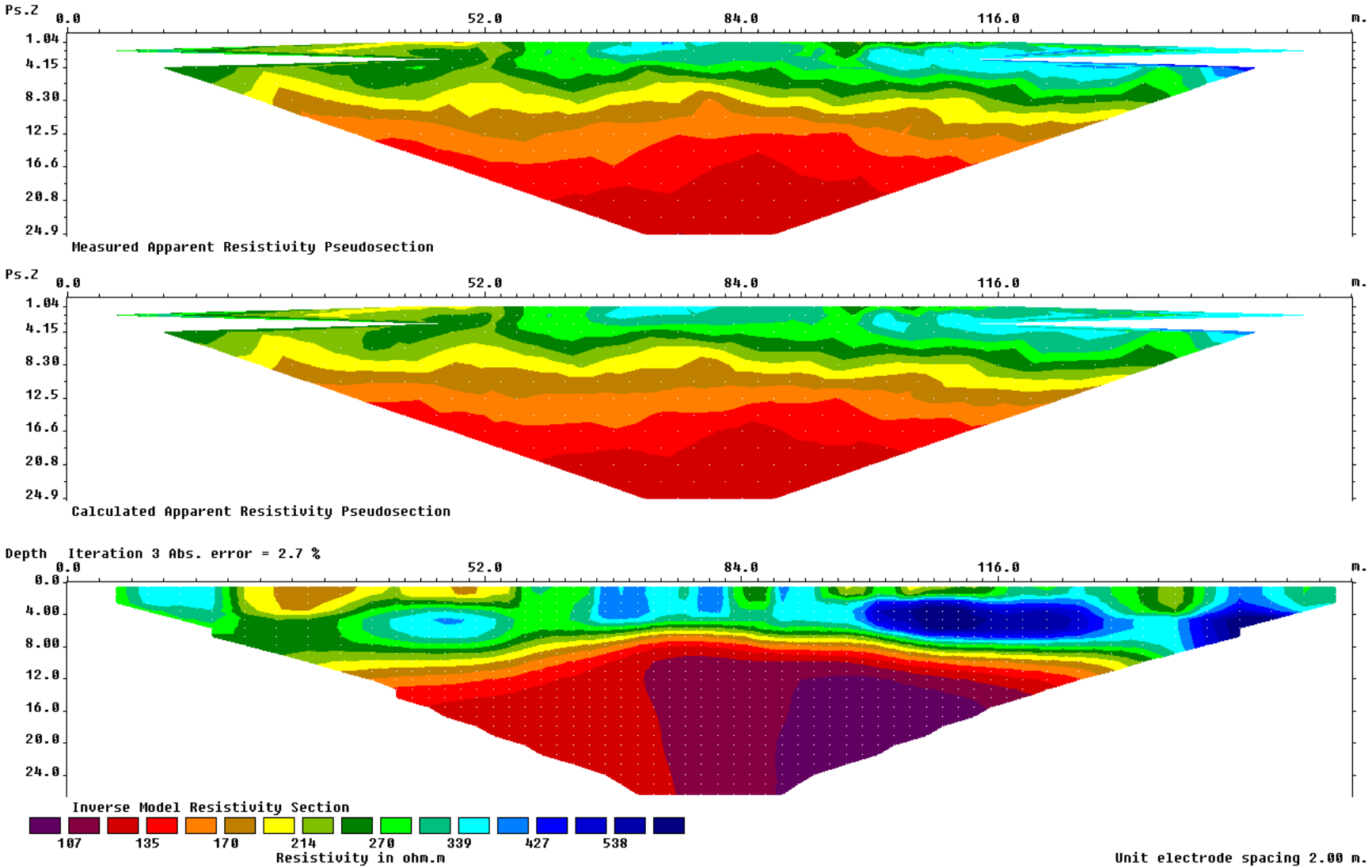

Figure I2: Borehole R2 August 7, 2012 NE-SW 160 m resistivity profile; measured apparent resistivity pseudosection, calculated apparent resistivity pseudosection and inverse model resistivity section.

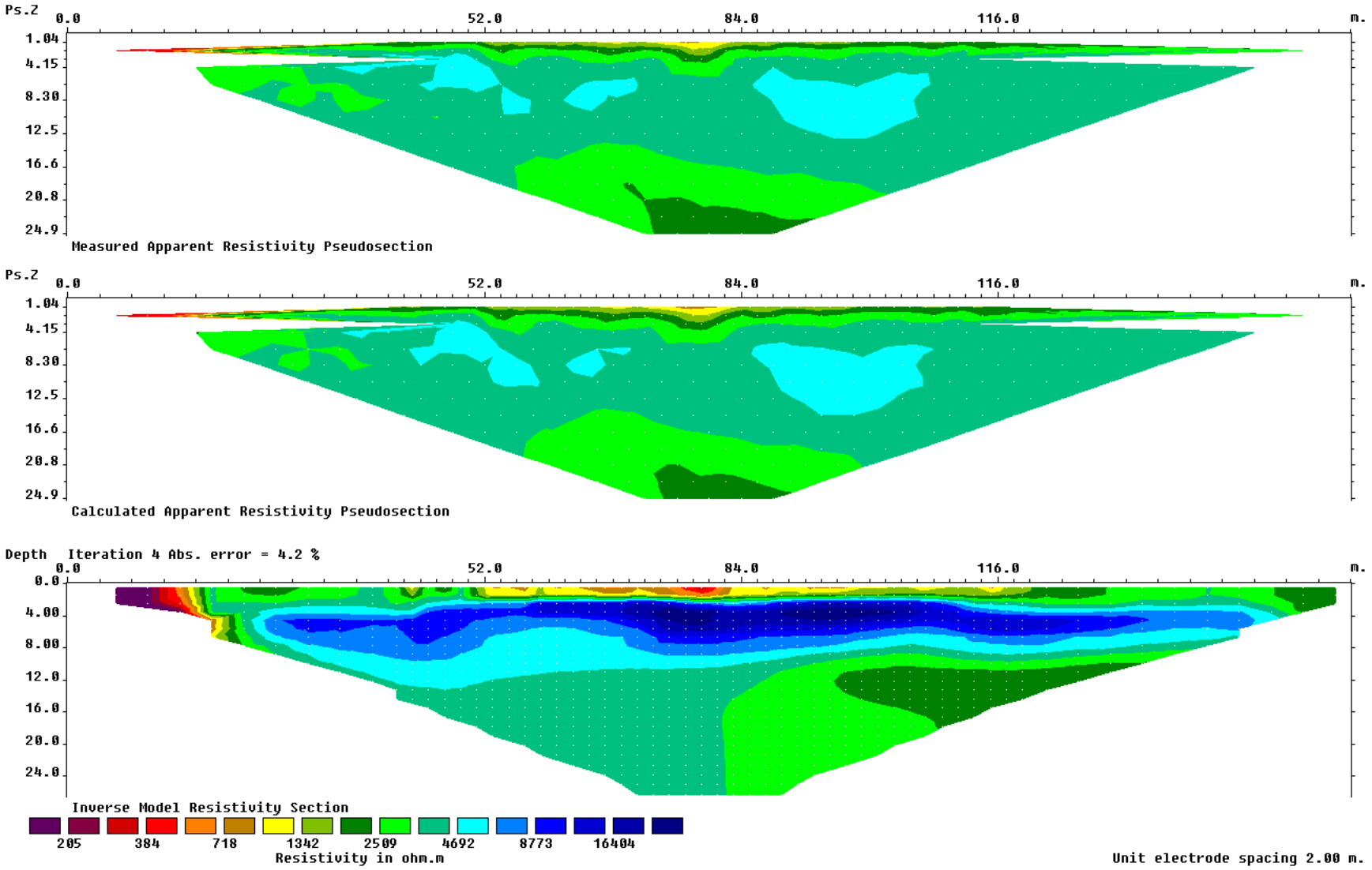

Figure I3: Borehole R3 August 8, 2012 NE-SW 160 m resistivity profile; measured apparent resistivity pseudosection, calculated apparent resistivity pseudosection and inverse model resistivity section.

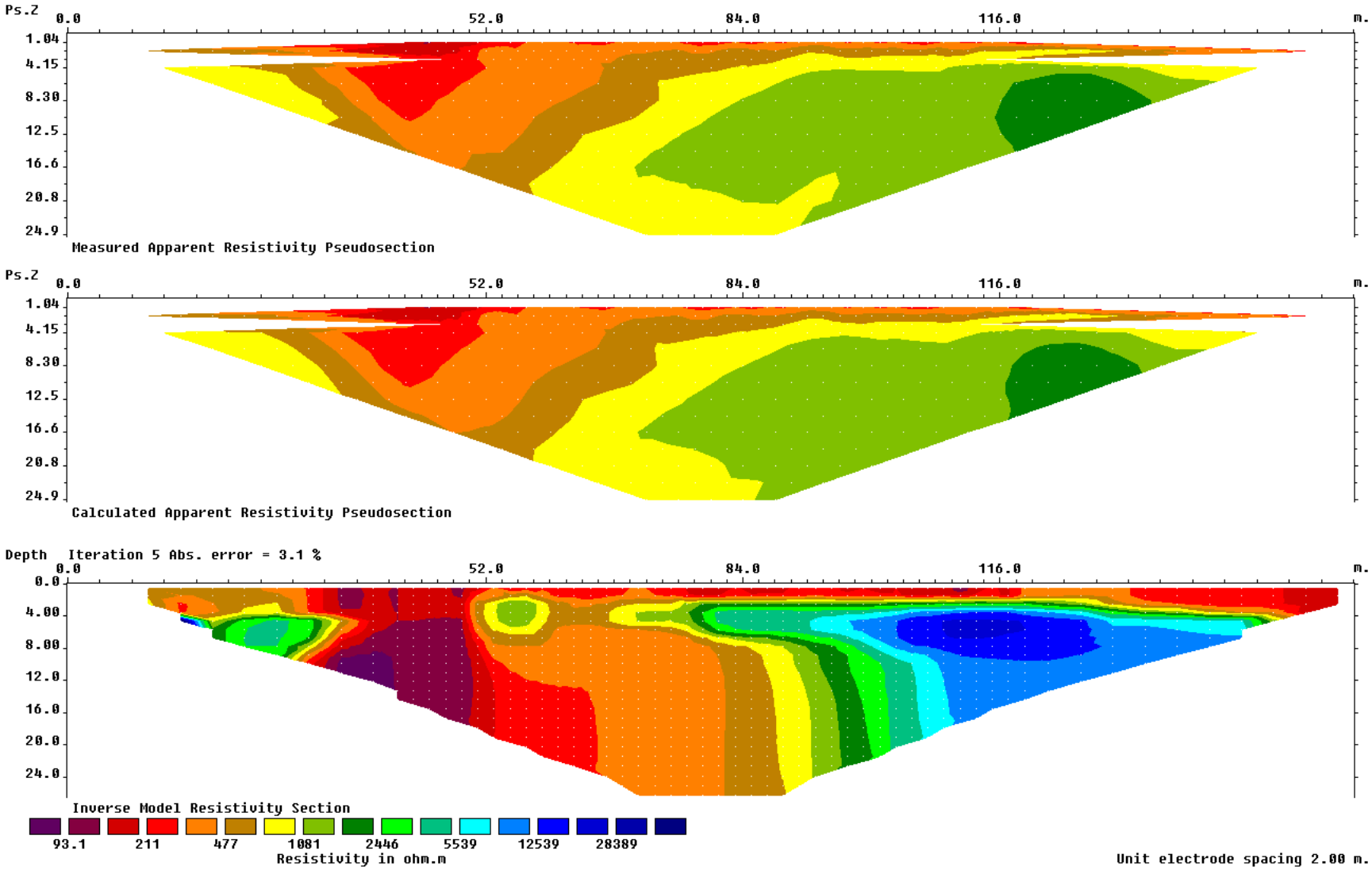

Figure I4: Borehole R4 August 7, 2012 NE-SW 160 m resistivity profile; measured apparent resistivity pseudosection, calculated apparent resistivity pseudosection and inverse model resistivity section.

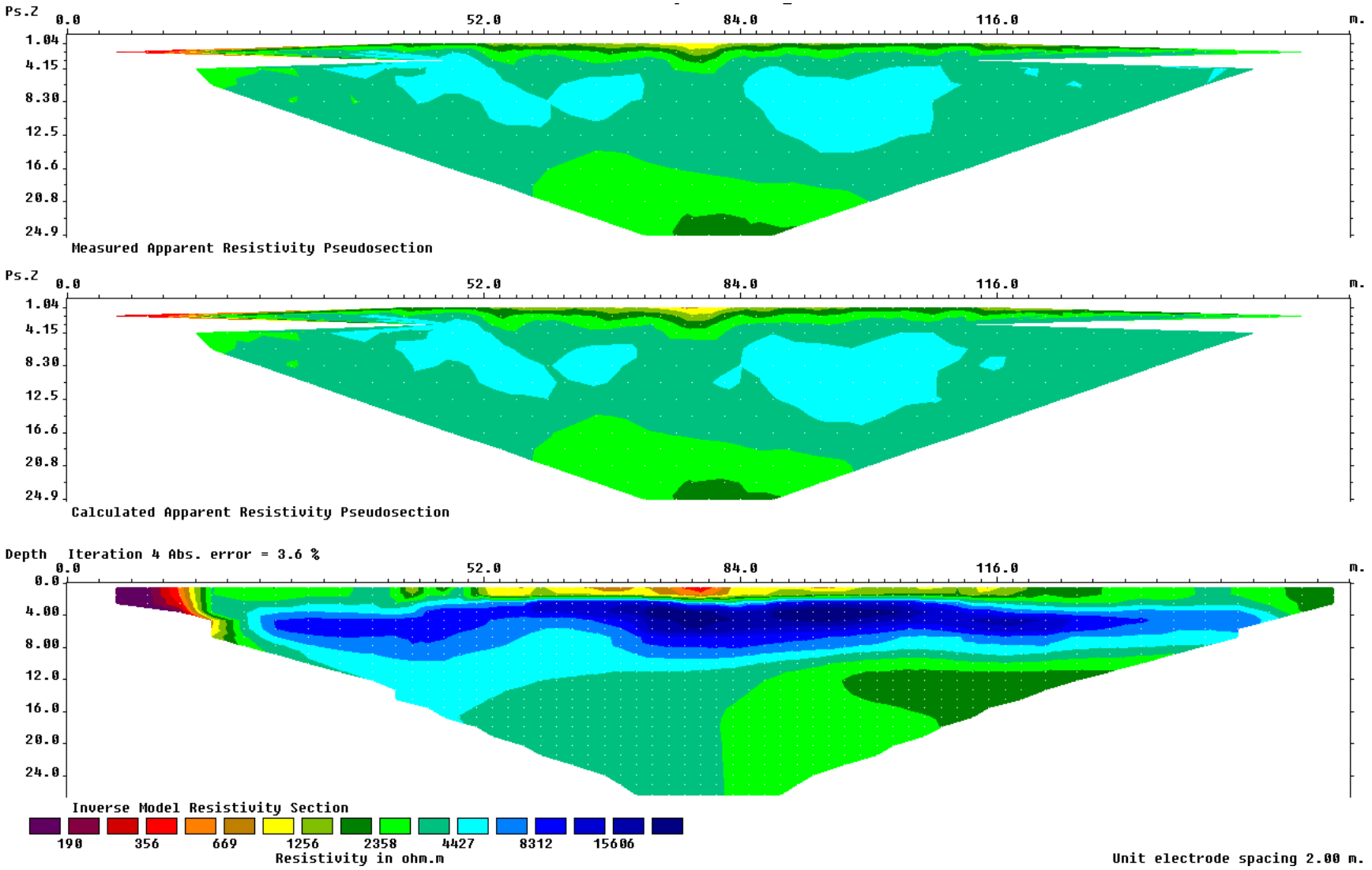

Figure I5: Borehole R5 August 9, 2012 NE-SW 160 m resistivity profile; measured apparent resistivity pseudosection, calculated apparent resistivity pseudosection and inverse model resistivity section.

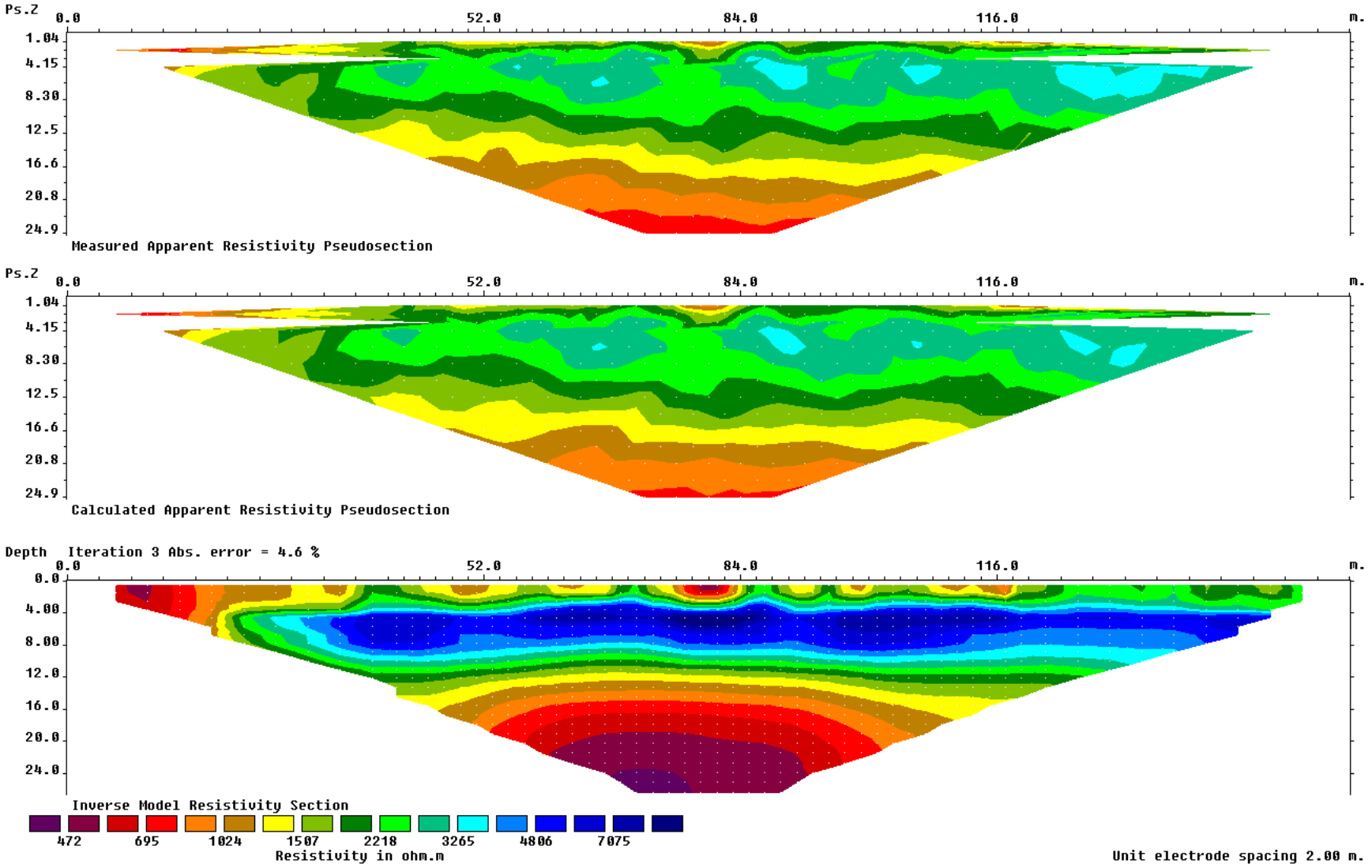

Figure I6: Borehole R6 August 7, 2012 NW-SE 160 m resistivity profile; measured apparent resistivity pseudosection, calculated apparent resistivity pseudosection and inverse model resistivity section.

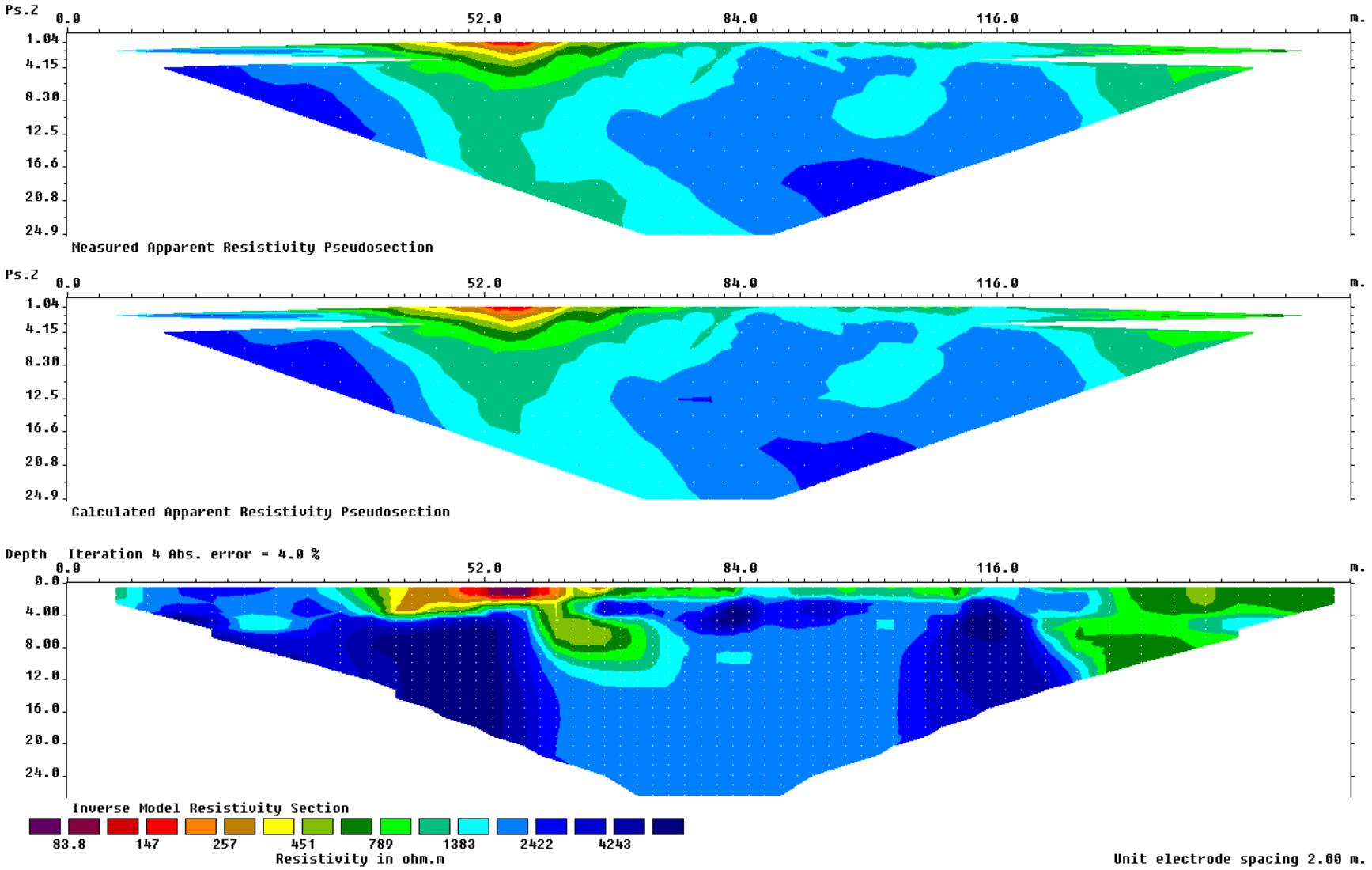

Figure I7: Borehole R7 August 5, 2012 SE-NW 160 m resistivity profile; measured apparent resistivity pseudosection, calculated apparent resistivity pseudosection and inverse model resistivity section.

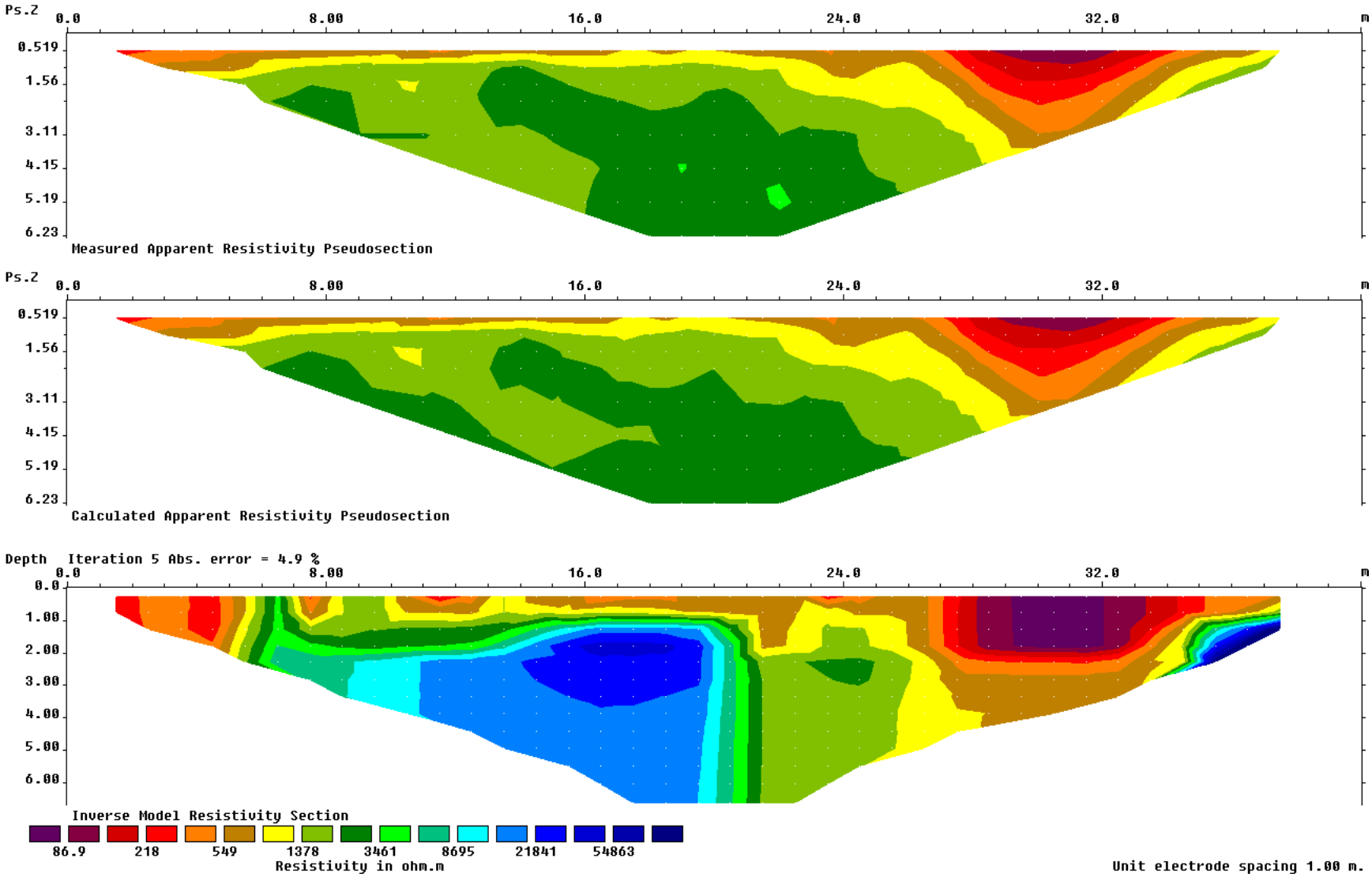

Figure I8: Borehole R7 June 24, 2011 NE-SW 40 m resistivity profile; measured apparent resistivity pseudosection, calculated apparent resistivity pseudosection and inverse model resistivity section.

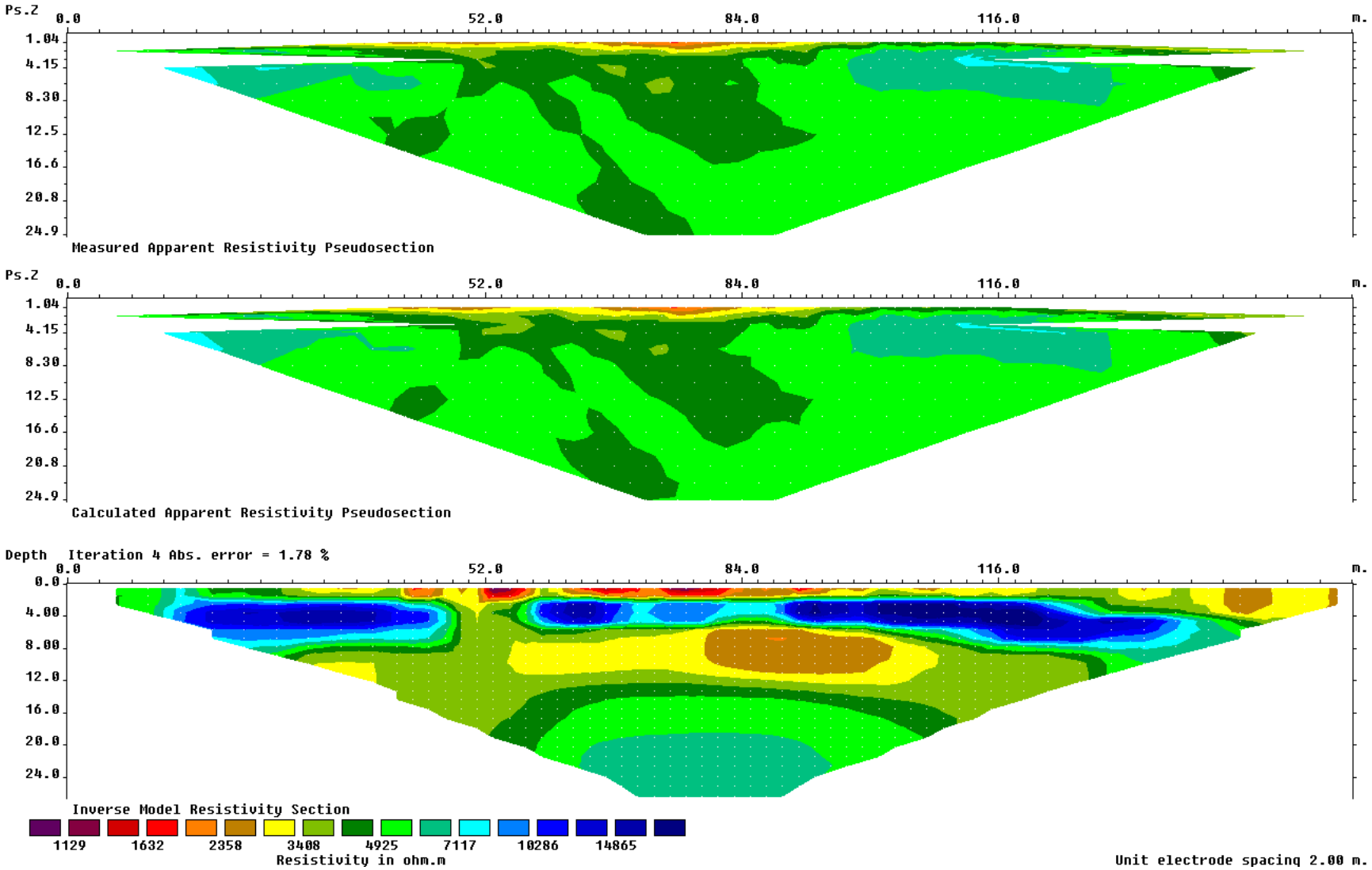

Figure I9: Borehole R8 August 5, 2012 SW-NE 160 m resistivity profile; measured apparent resistivity pseudosection, calculated apparent resistivity pseudosection and inverse model resistivity section.

Appendix J: HOBO Instrumented Boreholes Resistivity Pseudosections

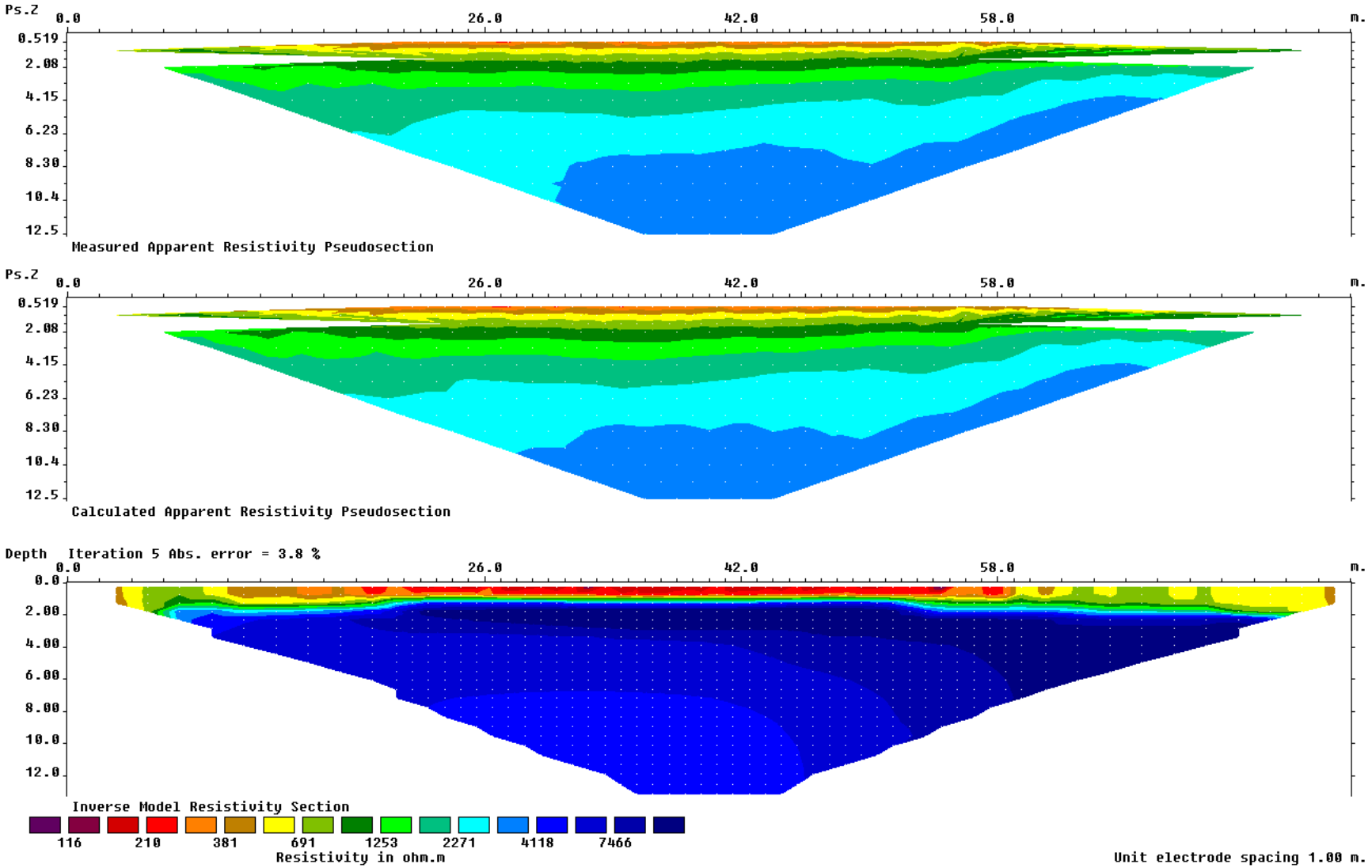

Figure J1: Borehole M1 June 29, 2011 SE-NW 80 m resistivity profile; measured apparent resistivity pseudosection, calculated apparent resistivity pseudosection and inverse model resistivity section.

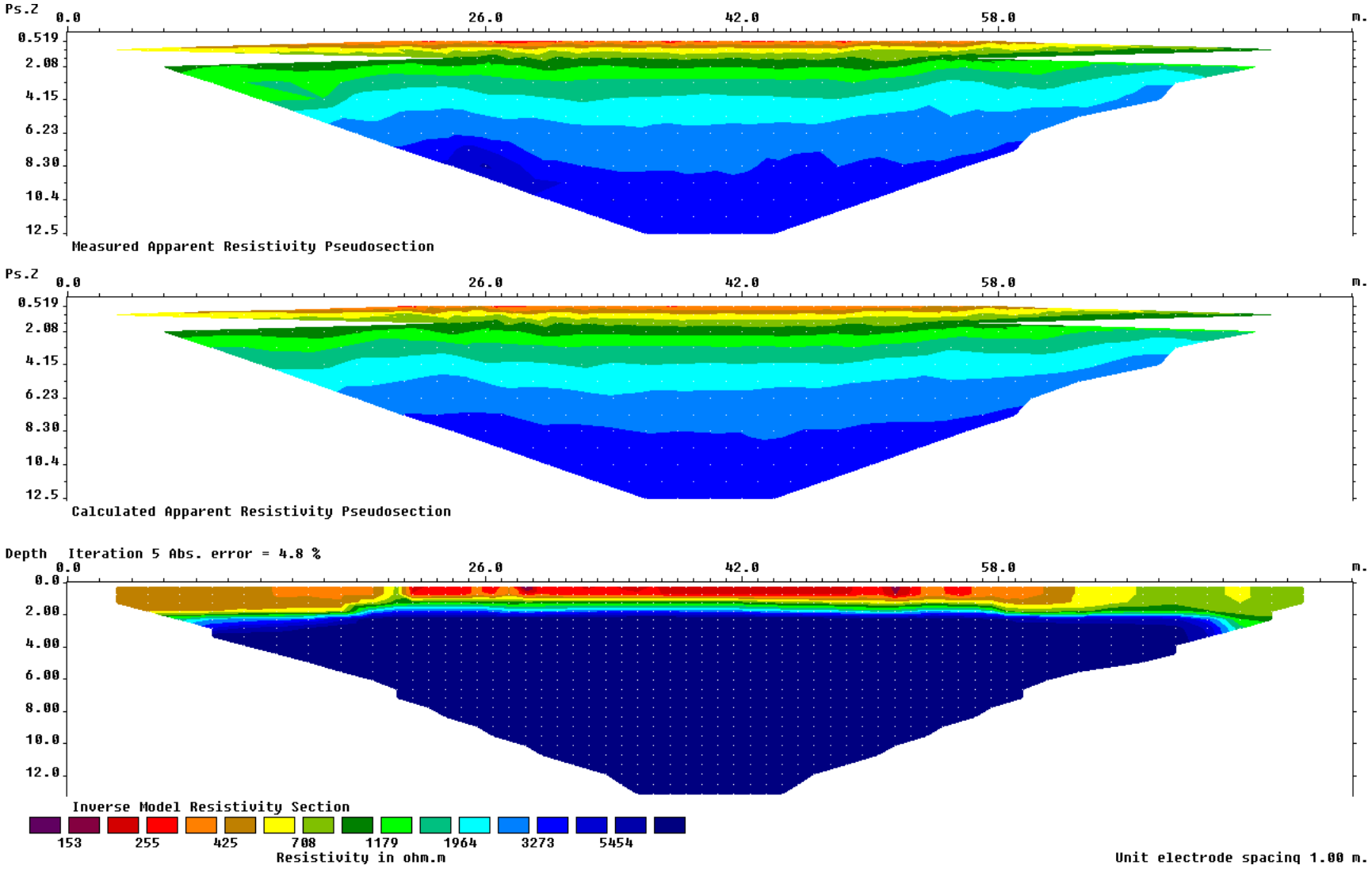

Figure J2: Borehole M1 June 29, 2011 NE-SW 80 m resistivity profile; measured apparent resistivity pseudosection, calculated apparent resistivity pseudosection and inverse model resistivity section.

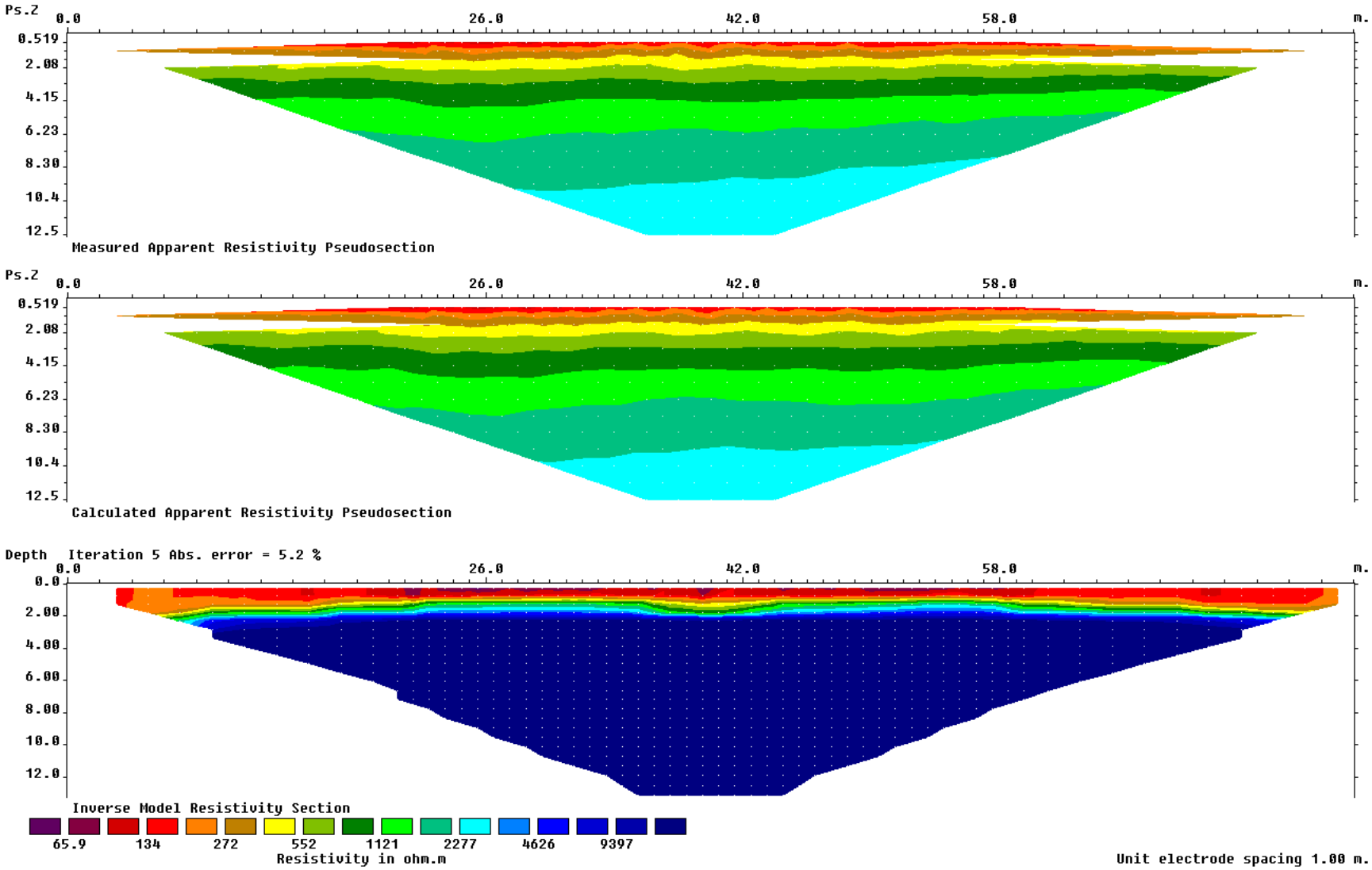

Figure J3: Borehole H1 June 28, 2011 SE-NW 80 m resistivity profile; measured apparent resistivity pseudosection, calculated apparent resistivity pseudosection and inverse model resistivity section.

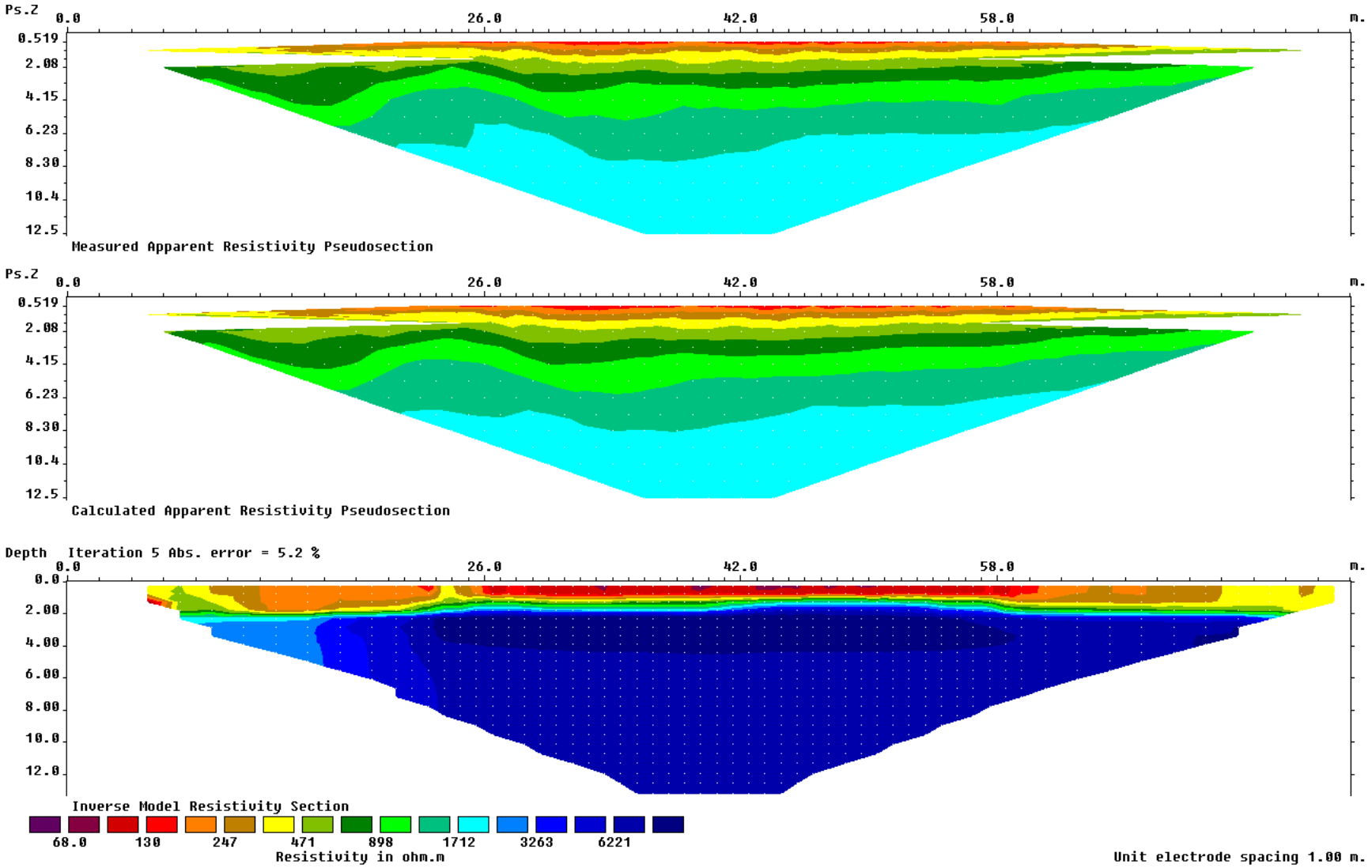

Figure J4: Borehole H1 June 28, 2011 NE-SW 80 m resistivity profile; measured apparent resistivity pseudosection, calculated apparent resistivity pseudosection and inverse model resistivity section.

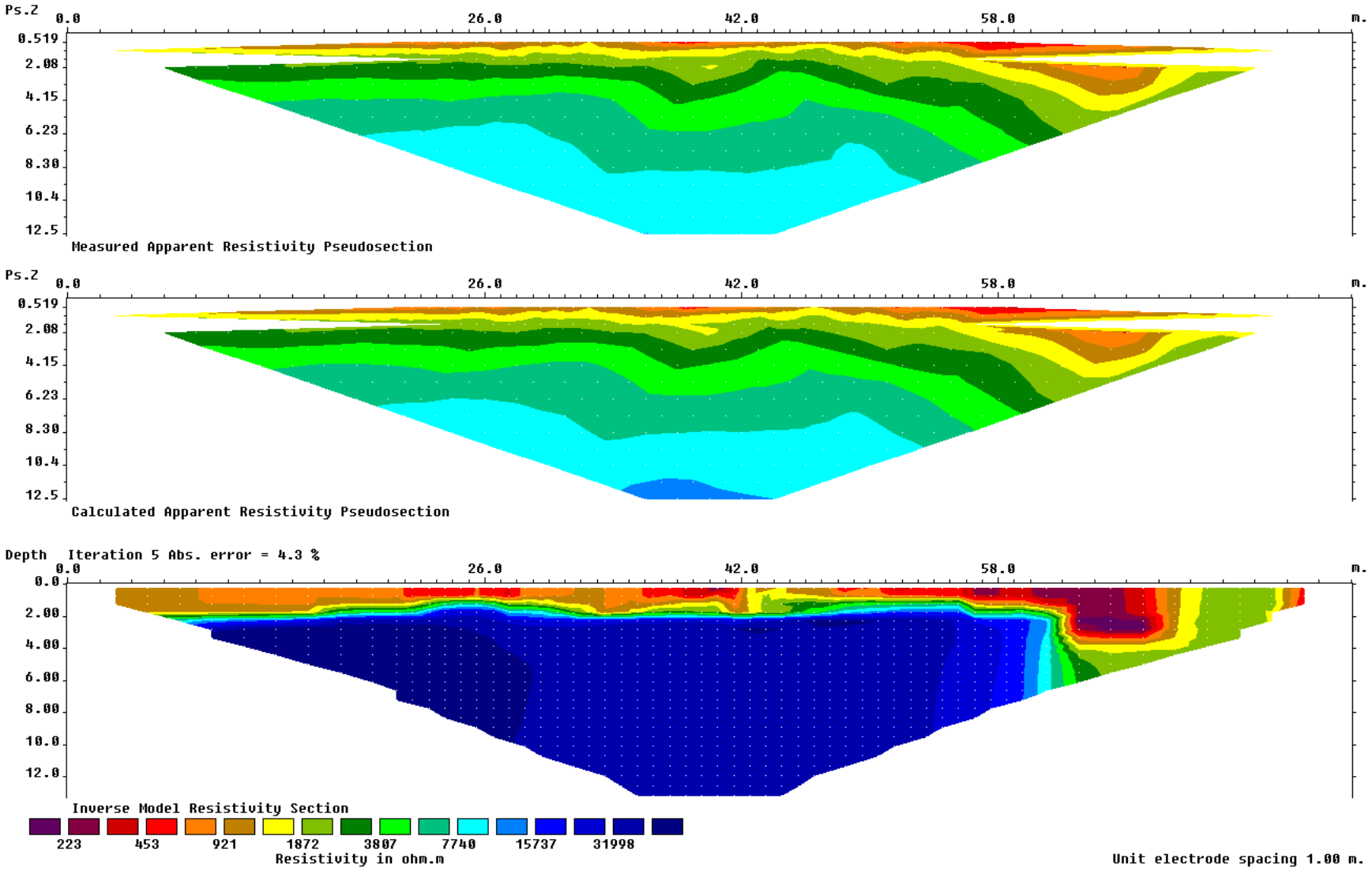

Figure J5: Borehole H2 June 25, 2011 SE-NW 80 m resistivity profile; measured apparent resistivity pseudosection, calculated apparent resistivity pseudosection and inverse model resistivity section.

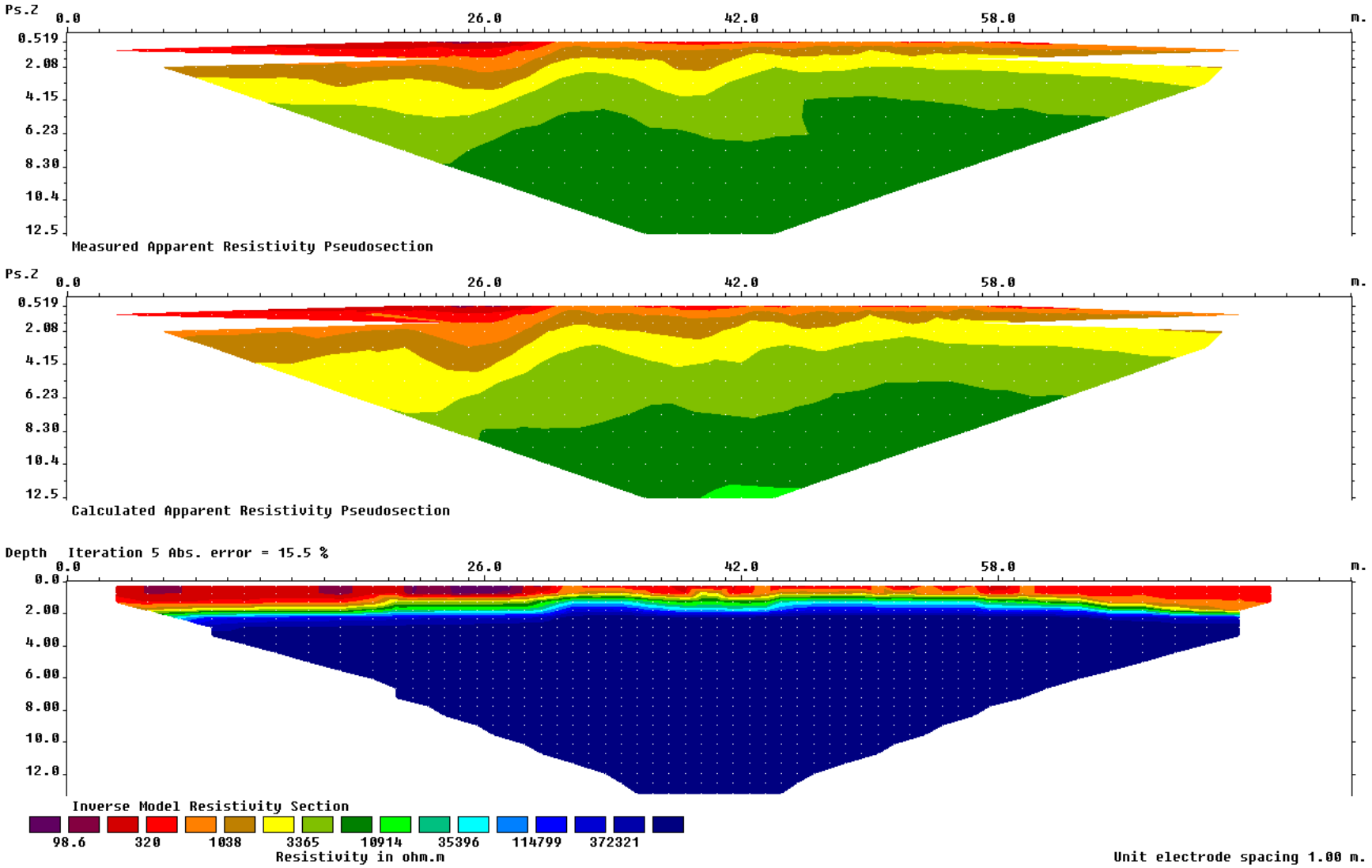

Figure J6: Borehole H2 June 25, 2011 NE-SW 80 m resistivity profile; measured apparent resistivity pseudosection, calculated apparent resistivity pseudosection and inverse model resistivity section.

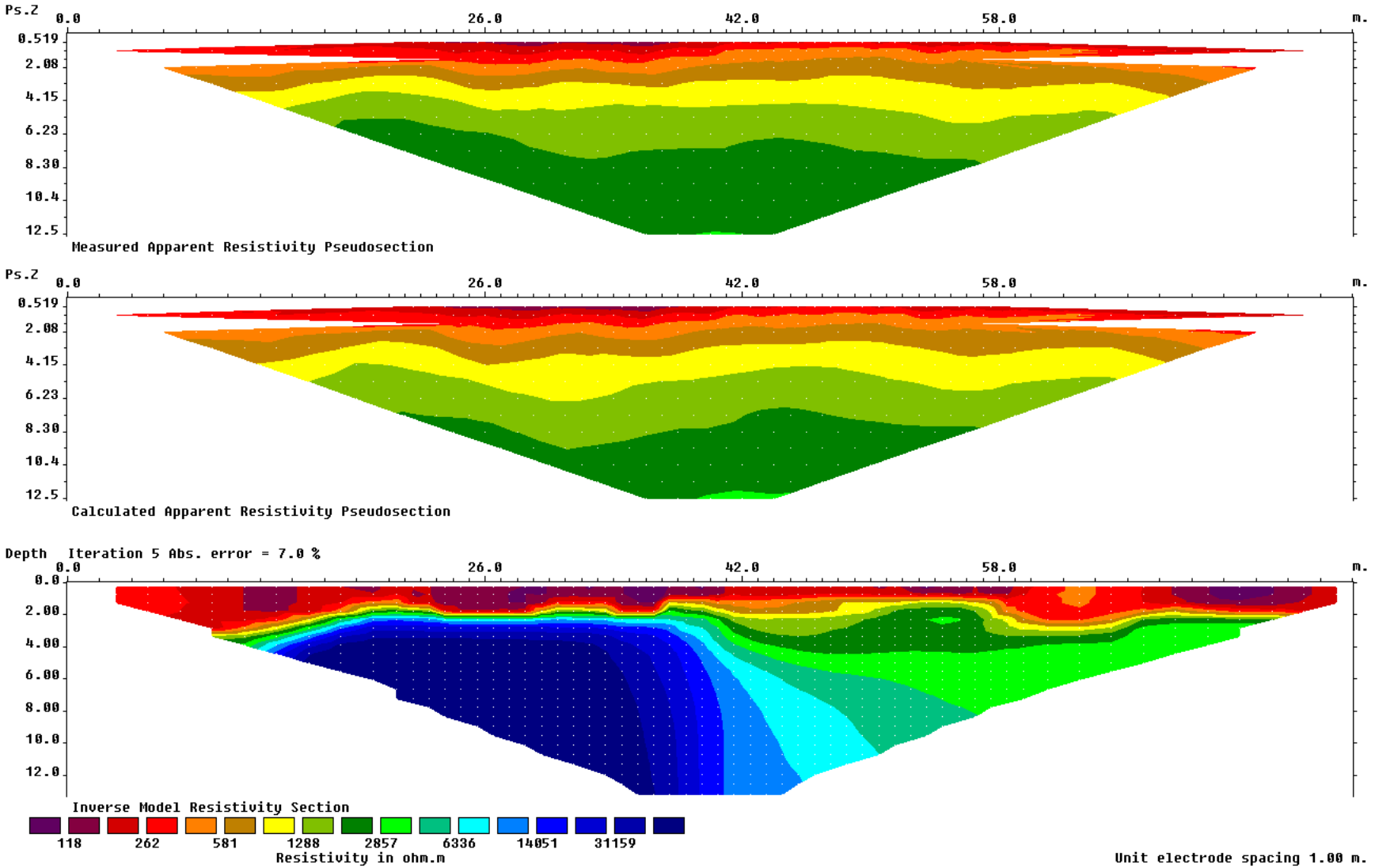

Figure J7: Borehole H3 June 23, 2011 SE-NW 80 m resistivity profile; measured apparent resistivity pseudosection, calculated apparent resistivity pseudosection and inverse model resistivity section.

Appendix K: 1970s Borehole Logs

Table K1: Terrain Type (RBR Instrumented Boreholes)

BOREHOLE	TerrainType	Reclassed
79S-CS5	cLp	Lacustrine
78-A-71	cLb/tMm	Lacustrine
78-A-64	fAa(a)	Alluvial
78-A-63	Ab/tMm	Alluvial
78-A-62	f/gAf	Alluvial
78-A-51	fEv/tMm	Eolian
78-A-40	f-vAa-p	Alluvial
78-A-8	fAp-a/Dm	Alluvial

Table K2: Terrain Type (HOBO Instrumented Boreholes)

BOREHOLE	TerrainType	Reclassed
78-A-57	f/gAf	Alluvial
78-A-46	f-vEv/tMm	Eolian
78-B-25	f-vEm	Eolian
78-A-39	f-vAa-p	Alluvial

Table K3: Sample-Soil Borehole Logs (RBR Instrumented Loggers)

BOREHOLE	TOP	BOTTOM	SOIL_TYPE	DESCRIPTIONS	USC	COMMENTS
79S-CS5	0	2.5	Clay	Silty, low plastic, occasional roots, brown, moist	CL	
79S-CS5	2.5	11.5	Clay	Medium plastic, grey, moist, thin layers to 2 cm thickness, dry partings, occasional high plastic layers. Brown to grey, fine sand partings, layers less than 1 mm thickness at 4.0 m. Light brown-grey to medium grey at 5.5 m. Light grey at 7.0 m. Damp at 8	CI	
79S-CS5	11.5	12	Clay	Silty, medium plastic, light grey-brown, damp	CI	
79S-CS5	12	12.7	Silt	Clayey, low plastic, light grey, moist	ML	
79S-CS5	12.7	14.2	Clay	Silty, medium plastic, light to medium grey, oxidized patches, moist	CI	
79S-CS5	14.2	15.7	Silt	Clayey, low plastic, occasional clay layer, light grey, damp	ML	
79S-CS5	15.7	17.8	Clay	Silty, medium plastic, grey, moist	CI	
79S-CS5	17.8	18.8	Silt	Clayey, low plastic, grey, occasional clay layers to 3 cm thickness	ML	
79S-CS5	18.8	30.25	Clay	Silty, medium plastic, grey, moist, occasional silt partings. Fine sand pocket, trace fine gravel at 21 m. Clayey silt layer 10 cm thick, low plastic at 29.9 m	CI	
79S-CS5	30.5			End	Botto m	Pneumatic peizometer installed tip at 18.3 m depth, E.M.R. thermistor installed to 29.6 m depth
78-A-71	0	1.2	Gravel	Fine to coarse grained some fine to medium grained sand, trace clay, cobbles to 12cm diameter, sub-angular to sub-rounded, brown	GW	

BOREHOLE	TOP	BOTTOM	SOIL_TYPE	DESCRIPTIONS	USC	COMMENTS
78-A-71	1.2	5.3	Clay	Silty, little to some coarse gravel, little sand, low plastic, oxidized pockets, grey moist (till-like)	CL	
78-A-71	0	1.2	Gravel	Fine to coarse grained some fine to medium grained sand, trace clay, cobbles to 12cm diameter, sub-angular to sub-rounded, brown	GW	
78-A-71	1.2	5.3	Clay	Silty, little to some coarse gravel, little sand, low plastic, oxidized pockets, grey moist (till-like)	CL	
78-A-71	0	1.2	Gravel	Fine to coarse grained some fine to medium grained sand, trace clay, cobbles to 12cm diameter, sub-angular to sub-rounded, brown	GW	
78-A-64	0	0.6	Peat	Moss cover to 0.2m depth	PT	CRREL to 1.2m
78-A-64	0.6	1.4	Clay	Silty, medium plastic, grey, occasional thin organic silt layers, low plastic	CL	
78-A-64	1.4	4.8	Sand	Low plastic silty clay, little sub-angular gravel sizes to 2.5cm diameter, grey (till-like)	SC	
78-A-64	4.8	9.2	Clay	Silty, little gravel, trace fine to medium sand, occasional cobble, gravel sizes to 4.0cm diameter, medium to high plastic, grey, rust pockets (till-like)	CI-CH	
78-A-64	9.2			End	Bottom	EMR pipe installed - tip at 9.1m
78-A-63	0.4	1.6	Clay	Silty, trace fine sand, low plastic with medium plastic clay lumps, brown, moist, and sand below 0.8m depth, grey-brown	CL	
78-A-63	1.6	5	Sand	Some clayey silt, little fine to coarse gravel (subrounded to subangular) occasional cobble to 7.5cm diameter, brown-grey, damp, and clayey silt, damp, gravel to 3cm diameter	SM	

BOREHOLE	TOP	BOTTOM	SOIL_TYPE	DESCRIPTIONS	USC	COMMENTS
78-A-63	5	5.9	Bedrock	Limestone, grey	BR	
78-A-63	5.9			End	Bottom	EMR pipe installed - tip at 4.6m
78-A-62	0	0.5	Organic Silt	Trace clay, low plastic, dark brown to black, organic inclusions, roots	OL	CRREL to 4.6m then vibration
78-A-62	0.5	1.8	Clay	Silty, little to some fine to medium sand, medium plastic, grey-brown	CI	
78-A-62	1.8	3.2	Silt	Sandy, trace clay, fine grained sand, numerous angular gravel sizes to 3.0cm diameter, low plastic, grey	ML	
78-A-62	3.2	3.8	Sand and Gravel	Little silt, trace clay, fine to coarse grained sand, gravel sizes to 3cm diameter, amgular to sub-rounded, non-plastic to low plastic, brown	SW-GW	
78-A-62	3.8	6.2	Sand	Fine to coarse grained, silty, trace clay, numerous gravel sizes to 3.0cm diameter, angular to sub-rounded, non-plastic to low plastic, brown	SM	
78-A-62	6.2	7.3	Clay	Silty, sandy, some gravel sizes to 2.5cm diameter, fine grained sand, sub-angular gravel, low plastic, brown rust pockets	CL	
78-A-62	7.3	9.2	Clay	Silty, sandy, occasional to numerous gravel sizes to 3cm diameter, fine grained sand, angular to sub-rounded gravel, medium plastic, brown, rust pockets	CI	
78-A-62	9.2			End	Bottom	EMR pipe installed - tip at 9.2m
78-A-51	0	0.1	Peat	Moss	PT	
78-A-51	0.1	0.2	Sand	Silt, grey-brown	SM	
78-A-51	0.2	0.3	Volcanic Ash	Silt	VA-ML	
78-A-51	0.3	0.8	Silt	Clayey, trace organics, low plastic	ML	

BOREHOLE	TOP	BOTTOM	SOIL_TYPE	DESCRIPTIONS	USC	COMMENTS
78-A-51	0.8	1.6	Clay	Silty, fine sandy, low plastic, brown	CL	
78-A-51	1.6	2.8	Clay	Silty, trace gravel to 3cm diameter, medium plastic, grey	CI	
78-A-51	2.8	3.8	Clay	Silty, some fine to coarse grained gravel, trace fine sand, high plastic (till-like)	CH	
78-A-51	3.8	4.6	Sand	Some clayey silt, some gravel and cobbles, red, oxidized	SM	
78-A-51	4.6	6	Clay	Silty, some subrounded to angular gravel, trace fine sand, medium plastic, moist, grey, 1cm thick ice lense at 4.8m (till-like)	CI	
78-A-51	6	7.3	Clay	Silty, some gravel, trace fine sand, medium plastic, dry, grey (till-like)	CH	
78-A-51	7.3	8.5	Clay	Silty, some gravel, trace fine sand, medium plastic, dry, grey	CI	
78-A-51	8.5			End	Botto m	EMR pipe installed - tip at 8.5m
78-A-40	0	0.3	Peat and Volcanic Ash	Roots, fine fibrous and medium grained sand	PT-VA	
78-A-40	0.3	0.9	Volcanic Ash and Sand	Medium grained, light brown	VA-SP	
78-A-40	0.9	2.1	Peat	Fine fibrous, occasional pieces of wood, rootlets, dark brown to black	PT	
78-A-40	2.1	2.8	Silt	Low plastic, medium grey	ML	
78-A-40	2.8	2.85	Peat	Woody, fine fibrous, dark brown	PT	
78-A-40	2.85	3.7	Silt	Clayey, non plastic, medium to dark grey	ML	
78-A-40	3.7	3.8	Peat	Little silt woody, brown grey	PT	
78-A-40	3.8	4.4	Silt	Trace organics, wood pieces, low plastic, light brown to grey	ML	
78-A-40	4.4	4.8	Peat	Organic Silt, wood pieces, light brown to black	PT	
78-A-40	4.8	5.8	Silt	Trace fine sand, low plastic, grey	ML	
78-A-40	5.8	6.15	Peat	Woody pieces, brown-grey	PT	

BOREHOLE	TOP	BOTTOM	SOIL_TYPE	DESCRIPTIONS	USC	COMMENTS
78-A-40	6.15	8.3	Silt	Non-plastic, little woody organics, grey	ML	
78-A-40	8.3			End	Bottom	EMR pipe installed-tip at 8.2m
78-A-8	0	0.3	Peat	Coarse fibrous, wet	PT	
78-A-8	0.3	0.5	Silt	Trace fine sand, tarce organics, non plastic, medium brown	ML	
78-A-8	0.5	0.7	Ice + Silt		Ice + Soil	
78-A-8	0.7	1	Silt	Trace organics, wood chips	ML	
78-A-8	1	1.1	Ice + Silt		Ice + Soil	
78-A-8	1.1	7.6	Silt	Little fine organics, wood chips, non plastic	ML	
78-A-8	7.6			End	Bottom	EMR pipe installed-tip at 7.6m

Table K4: Sample-Soil Borehole Logs (HOBO Instrumented Boreholes)

BOREHOLE	TOP	BOTTOM	SOIL_TYPE	DESCRIPTION	USC	COMMENTS
78-A-57	0	0.3	Peat	Fine fibrous, non-woody dark brown, saturated, roots, pieces of wood	PT	Auger to 9.5m
78-A-57	0.3	1.2	Organic Silt	Trace clay, low plastic, dark brown, damp to wet, rootlets	OL	Converted to CRREL
78-A-57	1.2	1.45	Silt	Clayey, little fine to coarse sand, little gravel sizes to 6.0cm diameter, low plastic, light grey	ML	
78-A-57	1.45	5.2	Gravel	Sandy, little silt, gravel sizes to 3.0cm diameter, sub-angular to sub-rounded, fine to coarse grained sand	GW	Converted to air circulation at 1.45m
78-A-57	5.2	5.7	Silt	Sandy, trace clay, fine grained sand, low plastic medium grey	ML	
78-A-57	5.7	6.55	Sand and Gravel	Little silt, fine to coarse sand, fine to coarse gravel, numerous cobble sizes	SW-GW	
78-A-57	6.55			End	Bottom	EMR pipe installed -tip at 2.7m
78-A-46	0	0.2	Peat	Moss cover	PT	
78-A-46	0.2	0.4	Volcanic Ash	Medium sand size	VA	
78-A-46	0.4	2	Organic Silt	Clayey, low plastic, grey (till-like)	OL	Convert to Vibration
78-A-46	2	3.2	Gravel	Some fine to coarse grained sand, little silt, isolated cobbles, gravel sizes to 5.0cm diameter, sub-amgular to sub-rounded	GM	
78-A-46	3.2	4.6	Clay	Sandy, silty, numerous gravel sizes to 4.0cm diameter, sub-rounded to sub-angular, occasional cobble, fine grained sand, low plastic, brown	CL	

78-A-46	4.6	6	Gravel	Medium to coarse grained sand, trace clayey silt, to 5cm diameter, sub-angular to sub-rounded	GP	
78-A-46	6	9	Sand	Fine to medium, some gravel, little silt, trace clay, gravel sizes to 3cm diameter, sub-angular and sub-rounded, brown	SM	
78-A-46	9			End	Bottom	EMR pipe installed -tip at 7.3m
78-B-25	0	0.2	Peat	Moss cover	PT	
78-B-25	0.2	0.4	Sand	Fine to grained, little silt, brown oxidized	SM	
78-B-25	0.4	2.7	Gravel	Some sand, little silt, grey	GM	
78-B-25	2.7	4.6	Sand	Fine to coarse grained, and gravel, trace silt	SW	
78-B-25	4.6	4.8	Silt	Sandy, trace clay, peat inclusions, low plastic, occasional subrounded pebbles to 2.5cm diameter	ML	
78-B-25	4.8	6.2	Gravel and Sand	Very silty, subangular, to 5cm diameter	GM	EMR pipe installed -tip at 6.2m
78-B-25	6.2			End	Bottom	
78-A-39	0	0.3	Peat	Roots, fibrous organics, silty, dark brown	PT	
78-A-39	0.3	0.9	Volcanic Ash	Medium grained sand, light grey, moist to wet	VA	
78-A-39	0.9	1.1	Peat	Woody, fibrous, dark brown	PT	
78-A-39	1.1	4.5	Clay	Silty, sandy, low plastic, trace woody organics, medium grey	CL	Converted to air circulation
78-A-39	4.5			End	Bottom	EMR pipe installation

Table K5: Ground Ice Borehole Logs (RBR Instrumented Boreholes)

BOREHOLE	TOP	BOTTOM	% ICE	Ground Ice Description
79S-CS5	0	30		Unfrozen
78-A-71	0.7	0.8		Unfrozen
78-A-71	1.3	1.4		Unfrozen
78-A-71	1.7	1.8		Unfrozen
78-A-71	2.6	2.75		Unfrozen
78-A-71	3.3	3.5		Unfrozen
78-A-71	4.2	4.3		Unfrozen
78-A-71	4.8	5		Unfrozen
78-A-71	5.6	5.7		Unfrozen
78-A-71	6.35	6.5		Unfrozen
78-A-71	7.2	7.3		Unfrozen
78-A-71	8	8.2		Unfrozen
78-A-71	8.8	9		Unfrozen
78-A-64	0.5	0.7		Unfrozen
78-A-64	1.7	1.8	1	Vx
78-A-64	2.4	2.5	1	Vx
78-A-64	3.4	3.5	1	Vx
78-A-64	4.2	4.3		Frozen
78-A-64	4.8	5		Frozen
78-A-64	5.8	5.9		Frozen
78-A-64	6.5	6.7		Frozen
78-A-64	7.5	7.6		Frozen
78-A-64	8	8.1		Frozen
78-A-64	9	9.1		Frozen
78-A-63	0	0.4		Unfrozen
78-A-63	0.4	0.8		Unfrozen
78-A-63	0.8	0.9		Unfrozen
78-A-63	0.9	1		Unfrozen
78-A-63	1	1.6		Unfrozen
78-A-63	1.6	1.8		Unfrozen
78-A-63	2.4	2.6	6	Unfrozen, Vs-Vx
78-A-63	4	4.2		Nbn
78-A-63	5.2	5.9		Nbn
78-A-62	0.4	0.5	10-20	Vs
78-A-62	0.75	1.2	40	Vx-Vr
78-A-62	2.3	2.5	20-30	Vx-Vr
78-A-62	2.8	3	15-20	Vs-Vx
78-A-62	3.25	3.35	20	Vr-Vx
78-A-62	4	4.3	20	Vr-Vx

BOREHOLE	TOP	BOTTOM	% ICE	Ground Ice Description
78-A-62	4.9	5	10-20	Vr-Vx
78-A-62	5.5	5.6	10-20	Vr-Vx
78-A-62	6.4	6.5	5-10	Vr-Vx
78-A-62	7.2	7.3	5-10	Vr-Vx
78-A-62	7.9	8	1-5	Vr-Vx
78-A-62	8.7	8.8	1-5	Vr-Vx
78-A-51	0.3	0.6	15-25	Vx
78-A-51	0.7	1		Nb
78-A-51	1.15	1.35		Nb
78-A-51	1.5	1.7	50-60	Vs
78-A-51	2.2	2.4	30-40	Vs
78-A-51	2.7	2.9	30-40	Vs
78-A-51	3.2	3.4	1-5	Vx-Vs
78-A-51	3.8	4	1-5	Vx-Vs
78-A-51	4.2	4.4	1-5	Vx-Vs
78-A-51	4.8	5	1-5	Vx-Vs
78-A-51	5.5	5.7	1-5	Vx-Vs
78-A-51	6.2	6.5		Frozen/Unfrozen
78-A-51	7	7.2		Frozen/Unfrozen
78-A-51	7.5	7.7		Frozen/Unfrozen
78-A-51	8.2	8.4		Frozen/Unfrozen
78-A-40	0	0.3		Unfrozen
78-A-40	0.3	0.6		Unfrozen
78-A-40	0.8	1.1	5-10	Vc
78-A-40	1.1	1.35	3	Vs
78-A-40	1.35	1.8	15	Vs
78-A-40	1.8	2.2	15	Vs
78-A-40	2.2	2.6	15	Vs
78-A-40	2.6	3.1	10-50	Vs, Vr-Vs
78-A-40	3.1	3.5	30	Vs
78-A-40	3.5	3.9	20	Vs
78-A-40	3.9	4.4	10-20	Vs
78-A-40	4.4	4.9	3-30	Vs
78-A-40	4.9	5.4	15	Vs
78-A-40	5.4	5.8	5	Vs
78-A-40	5.8	6.3	10-15	Vs
78-A-40	6.3	6.8	10	Vs
78-A-40	6.8	7.15	10	Vs
78-A-40	7.15	7.85	5	Vs
78-A-40	7.85	8.3	15	Vs

BOREHOLE	TOP	BOTTOM	% ICE	Ground Ice Description
78-A-8	0.2	0.6	20-95	Vs-Vr, Ice + Soil
78-A-8	0.6	1.1	10-95	Vs, Ice + Soil
78-A-8	1.1	1.7	15-60	Vs, Ice + Soil
78-A-8	1.7	2.1	15	Vs
78-A-8	2.1	2.3	2	Vs
78-A-8	2.3	2.8	2	Vs
78-A-8	2.8	3.2	1-2	Vs
78-A-8	3.2	3.6	1	Vs
78-A-8	3.6	3.9	20	Vs
78-A-8	3.9	4.3	20	Vs
78-A-8	4.3	4.7	3-20	Vs, Vr-Vs
78-A-8	4.7	5.5	40	Vs-Vr
78-A-8	5.5	5.9	10	Vs
78-A-8	5.9	6.3		Nbn
78-A-8	6.3	6.7		Nbn
78-A-8	6.7	6.8		Nbn
78-A-8	6.8	7.2		Nbn
78-A-8	7.2	7.6		Nbn

Table K6: Ground Ice Borehole Logs (HOBO Instrumented Boreholes)

BOREHOLE	TOP	BOTTOM	% ICE	Ground Ice Description
78-A-57	0	0.4		Unfrozen
78-A-57	0.4	0.95		Unfrozen
78-A-57	0.95	1.2	10-30	Vs
78-A-57	1.2	1.45	5-15	Vs-Vx
78-A-57	2.7	2.8	1-3	Vr-Vx
78-A-57	5.2	5.5		Nbe
78-A-46	0.4	0.6	5	Vx-Vs
78-A-46	1.1	1.3	5	Vx-Vs
78-A-46	2.2	2.4		Nbe
78-A-46	3.1	3.3	5	Vx
78-A-46	4	4.2	5	Vx
78-A-46	4.6	4.8	5	Vx
78-A-46	5.2	5.4	5	Vx
78-A-46	6	6.2		Nbn
78-A-46	6.4	6.6		Nbn
78-A-46	7.2	7.4		Nbn
78-A-46	7.9	8.1		Nbn
78-A-46	8.6	8.8		Nbn
78-B-25	0.5	0.7		Nbe
78-B-25	1	1.2		Nbe
78-B-25	1.2	1.4		Nbe
78-B-25	1.7	2	5-10	Vx
78-B-25	2.2	2.4	5-10	Vx
78-B-25	2.8	3	5-10	Vx
78-B-25	3.5	3.7	15-20	Vx-Vr
78-B-25	4.2	4.4	15-20	Vx-Vr
78-B-25	4.5	4.7	15-20	Vx-Vr
78-B-25	5.5	5.7	15-20	Vx-Vr
78-A-39	0	0.2		Unfrozen
78-A-39	0.4	0.6		Unfrozen
78-A-39	0.9	1.1	1	Vx
78-A-39	1.1	1.3	1	Vx
78-A-39	1.5	1.7	5	Vs
78-A-39	2.6	2.8	40	Vx
78-A-39	4.3	4.5	10	Vx